HABILITATION A DIRIGER DES RECHERCHES EN SCIENCES PHYSIQUES: Effective physical properties of heterogeneous materials and structures

THESIS · OCTOBER 2015

DOI: 10.13140/RG.2.1.1943.1126

1 AUTHOR:

Stefano Giordano

Université des Sciences et Technologies de …

83 PUBLICATIONS **713** CITATIONS

SEE PROFILE

UNIVERSITE DE LILLE 1

HABILITATION A DIRIGER DES RECHERCHES

EN SCIENCES PHYSIQUES

Effective physical properties of heterogeneous materials and structures

Propriétés physiques effectives des matériaux et structures hétérogènes

---

DOCUMENT DE SYNTHESE

PAR

Stefano GIORDANO

Soutenue le 01-10-2015 devant la commission d'examen composée de :

Rapporteur:	Mr. Renald BRENNER
Rapporteur:	Mr. Olivier CASTELNAU
Rapporteur:	Mr. Djimedo KONDO
Examinateur:	Mr. Guy BONNET
Examinateur:	Mr. Lionel BUCHAILLOT
Examinateur:	Mr. Fabrizio CLERI
Examinateur:	Mr. Vladimir PREOBRAZHENSKY
Garant de l'habilitation:	Mr. Philippe PERNOD

Io stimo più il trovar un vero, benché di cosa leggiera, che 'l disputar lungamente delle massime questioni senza conseguir verità nissuna.

I value more finding some truth, although on a light subject, than having long discussions about the greatest questions without achieving any truth.

J'apprécie plus de trouver une certaine vérité, même sur un sujet léger, que d'avoir de longues discussions sur les grandes questions sans obtenir aucune vérité.

Galileo Galilei
Galileo Galilei, Scritti Letterari, a cura di Alberto Chiari, Le Monnier, 1970.

Todas las demostraciones decepcionan, como todos los sueños realizados.
La incertidumbre es el clima del alma.

Toutes les démonstrations déçoivent, de même que tous les rêves réalisés.
L'incertitude est le climat de l'âme.

All demonstrations disappoint, like all dreams realized.
Uncertainty is the climate of the soul.

Nicolás Gómez Dávila
Escolios a un texto implícito, Bogotá, Instituto Colombiano de Cultura, 1977.

E mai che mi sia venuto in mente,
di essere più ubriaco di voi
di essere molto più ubriaco di voi.

An did never crossed my mind,
to be drunker than you
to be much drunker than you.

Et jamais l'idée ne m'a effleuré,
que j'étais plus ivre que vous
que j'étais beaucoup plus ivre que vous.

Fabrizio de André
Amico Fragile, Volume VIII, Produttori Associati, 1975.

Contents

Preamble

This document represents the summary of the research activities carried out during the period beginning with my doctorate and ending in early 2015.

I started my PhD in November 1996 at the University of Genoa (PhD Course in « Materials, Technology and Electronics Devices », XII Cycle, jointly promoted by the University of Trent, University of Genoa and Polytechnic in Turin) working on the determination of the electromagnetic effective properties of linear and nonlinear heterogeneous materials. In particular, I worked on some generalizations of the Maxwell theory for conducting dispersions, which represents the first milestone in the history of homogenization[1]. At the same time, thanks to the teaching of Prof. Bianco, I have undertaken the study of the statistical mechanics, at both classical and quantum level, which was not only useful to describe the probabilistic aspects of random microstructures in heterogeneous materials, but only to develop stochastic dynamic models with applications in microelectronics and bio-electromagnetism[2]. The use of the techniques based on the statistical theories is a crucial point of my activities, which I have continued to successfully capitalize in the years to come.

After the PhD defense I carried on the research activity at the University of Genoa, where I began to consider the problem of the determination of the mechanical properties of the heterogeneous materials. Indeed, from the methodological point of view, I realized that several techniques, useful to homogenize the response of electromagnetic composite structures, were applicable to mechanical problems as well. From the historical point of view, the works of Einstein on the viscosity of suspensions[3] and the works of Eshelby on the elasticity of composite structures[4] represent the crucial pioneering activities on the mechanical homogenization. I have therefore studied and applied the Eshelby theory, dealing with the behavior of an elastic ellipsoidal particle embedded into a different linear material. This theory, combined with the statistical effective medium theories already developed within the electromagnetic context, helped me to develop original homogenization schemes for the elastic response of heterogeneous structures with populations of randomly or pseudo-randomly oriented inhomogeneities. In other words, the performed analysis ranges from parallel spheroidal inclusions to completely random oriented inclusions. A unified theory covers all the angular distributions between the random and the parallel ones and is based on the definition of some new order parameters, which depend on the given angular distribution of particles.

---

[1] See James Clerk Maxwell, «A Treatise of Electricity and Magnetism», McMillan & Co, London, 1873, Chapter XI «Conduction through heteroheneous media», pages 360-373.

[2] The study of the effects of the electromagnetic field on the biological matter was a subject of wide interest within the Department of Biophysical and Electronic Engineering (of the University of Genoa) at that time.

[3] Albert Einstein, «A new determination of molecular dimensions», Ann. Phys. 19, 289–306 (1906). Corrections: Ann. Phys. 34, 591–592 (1911).

[4] John Douglas Eshelby, « The determination of the elastic field of an ellipsoidal inclusion and related problems», Proc. R. Soc. Lond. A 241, 376–396 (1957). John Douglas Eshelby, «The elastic field outside an ellipsoidal inclusion», Proc. R. Soc. Lond. A 252, 561–569 (1959).

In 2005 I moved to the Department of Physics of the University of Cagliari and I worked under a Research Contract on the subject: "Theories and concepts for the multi-scale modeling of the mechanical behavior in complex materials". Here I worked on some problems related to the mechanical behavior of composite media: the continuum mechanics of multi-fractured elastic materials, the application of the Kolossov-Muskelishvili method to the study of elastic inclusions at the nano-scale, the generalization of the Eshelby theory to the case of nonlinear inclusions (with the proof of existence and uniqueness based on variational methods).

Finally, I entered the CNRS in 2010 as senior researcher (CR1) within the Section 9, "Materials and structures engineering, solid mechanics, biomechanics , acoustics". During my first period as researcher at the IEMN UMR 8520 within the AIMAN-FILMS group and within the LIA LICS (former LEMAC), I worked on three different lines of research summed up as follows: 1) generalizations and applications of the Eshelby theory, homogenization techniques, 2) magnetoelectric multiferroic devices (combination of magnetoelectric and piezoelectric materials), 3) theoretical and numerical study of thermo-elastic behavior of polymers and chains of biological interest.

The first line of research concerns the analysis of the effective properties of heterogeneous materials (linear or non-linear, isotropic or anisotropic with physical behavior coupled or non-coupled). The Eshelby theory, as above said, allows to calculate the elastic fields inside and outside an elastic inhomogeneity inserted into a homogeneous matrix. When the inclusion and the matrix have a linear elastic behavior, and the medium is subjected to a uniform mechanical load, the stress and strain fields inside the inclusion are uniform. It is possible to calculate them analytically using elliptic integrals. In addition, it is possible to consider isotropic materials or anisotropic ones (with physical behavior coupled or non-coupled). This result is the basis of most effective medium approximations that determine the behavior of a heterogeneous environment in terms of the nature of the heterogeneities and their interactions. During my first period at IEMN, I developed different extensions of this methodology for solving the following problems: analysis of nonlinear particles and their scale effects, elastic particle with shape and size slightly different from those of the cavity which must receive it, effect of imperfect interfaces on the transport properties of heterogeneous media, degradation of the physical properties of a homogeneous medium containing a population of defects (e.g. fractures) having a defined density and, finally, development of some non-linear homogenization techniques for specific geometries.

The second line deals with the combination of the Eshelby theory with the Landau-Lifchitz-Gilbert formalism and the Langevin/Fokker-Planck methodology for analysing the behaviour of magnetoelastic (ferromagnetic) particles embedded in different matrices (e.g. piezoelectric). The Eshelby theory allows for the determination of all coupled fields within the particle, the Landau-Lifchitz-Gilbert equation describes the dynamics of the magnetization in single-domain ferromagnetic particles and, finally, the Langevin/Fokker-Planck methodology is able to take into account the thermal bath where the system is embedded and, therefore, to introduce the temperature in these systems. This research finds direct applications to the analysis of the stress-mediated magnetization switching in particles and the design of magnetoelectric memories[5]. Moreover, the introduction of the statistical mechanics in these systems permits to analyze the thermal effects on the stress-mediated switching and on the

[5] The design of a magnetoelectric memory called MELRAM and exploiting the stress-mediated switching has been recently developed at IEMN.

memory stability (i.e. the determination of the probability error). Possible future applications can be envisaged to describe memristive devices.

This activity represents my first collaboration with AIMAN-FILMS IEMN group and it facilitated my integration into the local scientific community. It represents only a first example of application of analytical methods (theory of elasticity, continuum mechanics and electromagnetism) to nanometric devices developed at IEMN. Indeed, the potentialities of these methods open several possibilities for analyzing the properties and responses (typically piezoelectric, magnetoelastic and electromagnetic) of real structures designed and built by this research group.

The third line of research is devoted to the theoretical and numerical study of the thermo-elastic behavior of polymers of biological interest. The thermoelasticity of a polymeric chain is studied with an uniform tension (generated by an applied force) or a non-uniform tension (generated by an external field). Analytical solutions, as well as molecular dynamics Monte Carlo simulations, are developed starting from two different classical models: the freely-jointed chain (FJC), and the worm-like chain (WLC). The analytic theory based on the statistical thermodynamics allows a rigorous mathematical treatment; however, the study of complex systems is based on Monte Carlo simulations. A study of the uniform tension of a chain is proposed, based on the statistical mechanics that controls the extension process. It is found that when the thermodynamic limit is not satisfied (limited number of monomers), different elastic behaviors can be observed by changing the boundary conditions (Helmholtz isometric ensemble or Gibbs isotension one), showing the fascinating complexity of the small systems thermodynamics. So, I studied the equivalence of the two ensembles when the number of monomers approaches infinity. The observed complexity is even more suggestive when we look at the behavior of bistable molecules whose domains have transitions between two stable states. This system can show cooperative or non-cooperative responses, according to the statistical ensemble considered. A second analysis is devoted to the study of the non-uniform tension of a macromolecule. The aim is to study the average configurational properties of the polymer and its variances, describing the fluctuations of the system.

In order to emphasize the general approach behind these works and the consistency of different developments made over the years, I chose to format this thesis as an original manuscript. It also allows to introduce standardized notations and to show a more synthetic vision of my activity. The document is structured as follows. A first chapter describes my curriculum vitae, where one can find, in particular, the pedagogical activity and the list of publications. A second chapter contains details on the scientific activity, concerning in particular the three lines of research previously introduced. The following chapter deals with the positioning of my research activity in the laboratory context. Finally, the fourth chapter introduces some points and perspectives for future researches.

A large number of people have helped me gain deeper understanding of the topics discussed in this dissertation, and hence have helped me to investigate them. Not being able to name them all, I limit myself to a few of them who, directly or indirectly, influenced my research activity.
First of all, I wish to thank my PhD advisor, Prof. Bruno Bianco, for his great humanity, for the helpful, stimulating and profound scientific discussions and for having introduced me to the world of the heterogeneous materials. Also from the University of Genoa, I wish to

acknowledge Prof. Alessandro Chiabrera [6] for the teaching of the '*balance between vision and pragmatism*' and all the PhD and post-doc colleagues I collaborated with (in no particular order: Elsa Moggia, Walter Rocchia, Simona Di Martino, Simona Bruna…).
Moreover, I am grateful to Prof. Luciano Colombo from the University of Cagliari for his extraordinary example of motivation and determination. All members of his group contributed to create a stimulating environment (in particular Alessandro Mattoni). A special thanks to Pier Luca Palla and Emiliano Cadelano for the friendship and for the inspiring and gratifying collaboration during their PhD activity.
Constant encouragement and support offered by all my colleagues of the AIMAN-FILM group at IEMN are also gratefully acknowledged: Vladislav Aleshin, Michael Baudoin, Yannick Dusch, Olivier Bou Matar, Marc Goueygou, Alain Merlen, Philippe Pernod, Vladimir Preobrazhensky, Abdelkrim Talbi, Nicolas Tiercelin, Farzam Zoueshtiaghand and the PhD or post-Doc students Adrien Bussonnière, Ilyesse Bihi, Théo Mathurin, Carmelo Magniez, Diwakar Seyyanur Venkatesan and other collaborators. Concerning my last research activity dealing with the thermo-elastic properties of polymers and chains of biological interest I am thankful to Fabio Manca for his friendship and for the crucial cooperation. I wish to thank Fabrizio Cleri, Pier Luca Palla (again) et Evelyne Lampin, members of the SDYNA group at IEMN, for the stimulating discussions and fruitful collaborations.
Finally, *last but not least*, I would like to express my sincere thanks to Philippe PERNOD (Supervisor of the HDR), Renald BRENNER, Olivier CASTELNAU, Djimedo KONDO (Referees), Guy BONNET, Lionel BUCHAILLOT, Fabrizio CLERI et Vladimir PREOBRAZHENSKY (Examiners) for the participation to the HDR committee. I am very honored for their interest in my work.
My wife Alessandra and my son Ernesto for the love and support without which these activities would have never carried out.

[6] Alessandro Chiabrera, born in 1940 and died in 1999. A permanent school of bioelectromagnetics was set up in 2003 and named « International School of Bioelectromagnetics Alessandro Chiabrera » for his important achievements in this field. The course is held each year in Erice (Sicily, Italy) at the Ettore Majorana Foundation and Centre for Scientific Culture.

Préambule

Ce document constitue la synthèse des travaux de recherches effectués pendant la période commençant avec mon doctorat et se terminant au début de 2015.

J'ai commencé mon doctorat en Novembre 1996 à l'Université de Gênes (Cours de doctorat en «Matériaux, technologies et dispositifs électroniques» , XIIe cycle, proposé conjointement par l'Université de Trent, l'Université de Gênes et le Polytechnique de Turin) travaillant sur la détermination des propriétés effectives électromagnétiques de matériaux hétérogènes linéaires et non linéaires. En particulier, j'ai travaillé sur quelques généralisations de la théorie de Maxwell pour les dispersions conductrices, qui représente la première pierre milliaire dans l'histoire de l'homogénéisation[7]. Dans le même temps, grâce à l'enseignement du professeur Bruno Bianco, j'ai entrepris l'étude de la mécanique statistique, aussi au niveau classique que quantique, qui n'était pas seulement utile pour décrire les aspects probabilistes de microstructures aléatoires dans des matériaux hétérogènes, mais également pour développer des modèles dynamiques stochastiques avec des applications en microélectronique et bio-électromagnétisme[8]. L'utilisation des techniques basées sur les théories statistiques est un point crucial de mes activités, que j'ai continué à exploiter avec succès dans les années qui suivirent.

Après la soutenance de thèse j'ai continué à développer l'activité de recherche à l'Université de Gênes, où j'ai commencé à considérer le problème de la détermination des propriétés mécaniques des matériaux hétérogènes. En effet, du point de vue méthodologique, j'avais réalisé que plusieurs techniques, utiles pour homogénéiser la réponse des structures composites électromagnétiques, étaient aussi bien applicables à des problèmes mécaniques. Du point de vue historique, les travaux d'Einstein sur la viscosité des suspensions[9] et les œuvres d'Eshelby sur l'élasticité des structures composites [10] représentent les activités pionnières et cruciales sur l'homogénéisation mécanique. J'ai donc étudié et appliqué la théorie d'Eshelby, concernant le comportement d'une particule ellipsoïdale élastique, encastrée dans un matériau linéaire différent. Cette théorie, combinée avec les théories statistiques de champ moyen, déjà développées dans le contexte électromagnétique, m'a aidé à développer des procédures d'homogénéisation originales pour déterminer la réponse élastique des structures hétérogènes avec des populations d'inhomogénéités orientées de façon aléatoire ou pseudo-aléatoire. En d'autres termes, l'analyse effectuée prend en considération tous les cas entre inclusions sphéroïdales parallèles et inclusions orientées de façon aléatoire. Une théorie unifiée couvre toutes les distributions angulaires et elle est basée sur la définition de certains nouveaux paramètres d'ordre, qui dépendent de la distribution angulaire de particules.

---

[7] Voir James Clerk Maxwell, « A Treatise of Electricity and Magnetism », McMillan & Co, London, 1873, Chapitre XI « Conduction through heteroheneous media », pages 360-373.

[8] L'étude des effets du champ électromagnétique sur la matière biologique était un sujet de vif intérêt au sein du Département de biophysique et génie électronique (de l'Université de Gênes) à l'époque.

[9] Albert Einstein, «A new determination of molecular dimensions», Ann. Phys. 19, 289–306 (1906). Corrections: Ann. Phys. 34, 591–592 (1911).

[10] John Douglas Eshelby, « The determination of the elastic field of an ellipsoidal inclusion and related problems», Proc. R. Soc. Lond. A 241, 376–396 (1957). John Douglas Eshelby, «The elastic field outside an ellipsoidal inclusion», Proc. R. Soc. Lond. A 252, 561–569 (1959).

En 2005, j'ai déménagé au Département de Physique de l'Université de Cagliari en vertu d'un contrat de recherche sur le sujet: « Théories et concepts pour la modélisation multi-échelle du comportement mécanique des matériaux complexes ». Ici, j'ai travaillé sur certains problèmes liés au comportement mécanique des matériaux composites: la mécanique des milieux continus élastiques multi-fracturés, l'application de la méthode de Kolossov-Muskelishvili à l'étude des inclusions élastiques à l'échelle nanométrique, la généralisation de la théorie Eshelby au problème des inclusions non linéaires (avec la preuve de l'existence et l'unicité basée sur des méthodes variationnelles).

Enfin, je suis entré au CNRS en 2010 en tant que chercheur CR1 au sein de la Section 9, «Ingénierie des matériaux et des structures, mécanique des solides, biomécanique, acoustique". Pendant ma première période d'activité comme chercheur avec l'affectation à l'unité IEMN UMR 8520 dans le groupe AIMAN-FILMS "Acoustique Impulsionnelle et Magnéto-Acoustique Non-linéaire / Fluides, Interfaces, Liquides et Microsystèmes" et au sein du LIA LICS, "Laboratoire International des phénomènes Critiques et Supercritiques", ex-LEMAC, "Laboratoire Européen en magnéto-acoustique nonlineaire", j'ai travaillé sur trois différentes lignes de recherche: 1) généralisations et applications de la théorie d'Eshelby, techniques d'homogénéisation, 2) dispositifs magnétoélectriques et multiferroïques (combinaison de matériaux magnétoélectriques et piézoélectriques), 3) étude théorique et numérique du comportement thermo-élastique des polymères d'intérêt biologique.

La première ligne de recherche concerne l'analyse des propriétés effectives des matériaux hétérogènes linéaires ou non-linéaires, isotropes ou anisotropes avec comportement physique couplé ou non-couplé. La théorie originale d'Eshelby, comme dit ci-dessus, permet de calculer les champs élastiques à l'intérieur et à l'extérieur d'une inhomogénéité élastique insérée dans une matrice homogène. Dans le cas où l'inclusion et la matrice ont un comportement linéaire élastique, et si le milieu est soumis à un chargement uniforme, les champs de déformation et de contrainte dans l'inclusion sont uniformes. Il est alors possible de les calculer analytiquement au moyen d'intégrales elliptiques. En outre, il est possible de prendre en considération les matériaux isotropes comme anisotropes (avec comportement physique couplé ou non-couplé). Ce résultat est le fondement de la plupart des approximations de milieux effectifs qui permettent de déterminer le comportement d'un milieu hétérogène tout en le considérant homogène mais avec des propriétés modifiées qui tiennent compte de la nature des hétérogénéités et de leurs interactions. Pendant ma première période d'activité, j'ai développé différentes extensions de cette méthodologie pour l'appliquer à la résolution des problèmes suivants: particules non linéaires et leurs effets d'échelle, particules élastiques de forme et dimensions légèrement différentes de celles des cavités qui doivent les accueillir, effets des interfaces imparfaites sur les propriétés de transport des milieux hétérogènes, dégradation des propriétés d'un milieu homogène contenant une population de défauts (fractures) ayant une densité définie et développement de quelques techniques d'homogénéisation non linéaires pour certaines géométries particulières.

La seconde ligne concerne la combinaison de la théorie Eshelby avec le formalisme de Landau-Lifchitz-Gilbert et la méthodologie de Langevin/Fokker-Planck pour analyser le comportement de particules magnéto-élastiques (ferromagnétiques) plongées dans différentes matrices (par exemple piézoélectriques). La théorie Eshelby permet la détermination de tous les champs couplés au sein de la particule, l'équation de Landau-Lifchitz-Gilbert décrit la dynamique de l'aimantation dans les particules ferromagnétiques avec un seul domaine et, enfin, la méthodologie de Langevin/Fokker-Planck est capable de prendre en compte le bain thermique où le système est intégré et, par conséquent, d'introduire la température dans ces

systèmes. Cette recherche trouve des applications directes à l'analyse de la commutation de l'aimantation induite par contrainte mécanique dans les particules et la conception de mémoires magnéto-électriques[11]. En outre, l'introduction de la mécanique statistique dans ces systèmes permet d'analyser les effets thermiques sur la commutation et sur la stabilité de la mémoire (c'est à dire la détermination de la probabilité d'erreur). De futures applications peuvent être envisagées pour décrire les dispositifs memristifs.

Cette activité représente ma première collaboration avec le groupe AIMAN-FILMS de l'IEMN et elle a contribué à faciliter mon intégration dans la communauté scientifique locale. Elle représente seulement un premier exemple d'application des méthodes analytiques (théorie de l'élasticité, mécanique et électromagnétisme des milieux continus) aux dispositifs développés à l'IEMN. En effet, les potentialités de ces méthodes ouvrent de nombreuses possibilités d'applications pour analyser les propriétés et les réponses (typiquement piézoélectriques, magnétoélastiques ou électromagnétiques) des structures réelles étudiées et réalisées par le groupe.

La troisième ligne de recherche est consacrée à l'étude théorique et numérique du comportement thermo-élastique des polymères d'intérêt biologique. On étudie la thermo-élasticité d'une molécule polymérique soumise soit à une traction uniforme (générée par une force appliquée) soit à une traction non uniforme (générée par un champ extérieur). Des solutions analytiques, ainsi que des simulations de dynamique moléculaire Monte Carlo, sont élaborées à partir de deux modèles classiques différents: freely-jointed chain (FJC) et worm-like chain (WLC). La théorie analytique, basée sur la thermodynamique statistique, permet un traitement mathématique rigoureux, tandis que l'étude des systèmes complexes est basée sur des simulations de Monte Carlo. Une étude de la traction uniforme d'une chaîne est proposée afin de comprendre la mécanique statistique qui contrôle le processus d'extension. On constate que, lorsque la limite thermodynamique n'est pas satisfaite (nombre de monomères limité), différents comportements élastiques sont observés en changeant les conditions aux limites (ensemble de Helmholtz iso-métrique ou ensemble de Gibbs iso-contrainte), montrant ainsi la fascinante intrication de la thermodynamique des petits systèmes (small systems thermodynamics). On a donc étudié l'équivalence de deux ensembles quand le nombre de monomères devient illimité. La complexité observée se révèle encore plus suggestive lorsque on regarde le comportement des molécules bistables dont les domaines présentent des transitions entre deux états stables. Ce système peut montrer une réponse coopérative ou non-coopérative à la force externe, en fonction de l'ensemble statistique considéré. Une deuxième analyse est consacrée à l'étude de la traction non uniforme d'une macromolécule. L'objectif est l'analyse des propriétés configurationnelles moyennes des polymères et des variances décrivant les fluctuations du système.

Afin de souligner l'approche générale de ces travaux et de la cohérence de différents développements réalisés au cours des années, j'ai choisi de formater cette thèse comme un manuscrit original. Celui-ci permet également de présenter au lecteur des notations uniformisées et d'avoir ainsi une vision plus synthétique. Le document est structuré comme suit. Un premier chapitre décrit mon curriculum vitae où l'on peut trouver, en particulier, l'activité pédagogique et la liste des publications. Un deuxième chapitre contient des détails sur l'activité scientifique, concernant en particulier les trois axes de recherche précédemment introduits. Le chapitre suivant traite le positionnement de mon activité de recherche dans le

[11] La conception d'une mémoire magnéto-électrique appelée MELRAM exploitant la commutation induite par stress mécanique a été récemment mis au point à l'IEMN.

contexte de laboratoire. Enfin, le quatrième chapitre présente quelques points concernant les perspectives pour les recherches futures .

Un grand nombre de personnes m'ont aidé à acquérir une meilleure compréhension des sujets abordés dans cette thèse, et donc m'ont aidé à les développer. N'étant pas en mesure de les nommer tous, je me limite à quelques-uns d'entre eux qui, directement ou indirectement, ont influencé mon activité de recherche.
Tout d'abord , je tiens à remercier mon directeur de thèse, le professeur Bruno Bianco, pour sa grande humanité, pour les discussions scientifiques utiles, stimulants et profondes et de m'avoir introduit dans le monde des matériaux hétérogènes. Également de l'Université de Gênes, je tiens à remercier le professeur Alessandro Chiabrera[12] pour l'enseignement de '*l'équilibre entre la vision et le pragmatisme*' et tous les collègues PhD et post-doc avec lesquels j'ai collaboré (sans ordre particulier : Elsa Moggia, Walter Rocchia, Simona Di Martino, Simona Bruna...).
En outre, je suis reconnaissant au professeur Luciano Colombo de l'Université de Cagliari pour son extraordinaire exemple de motivation et de détermination . Tous les membres de son groupe ont contribué à créer un environnement stimulant (Alessandro Mattoni en particulier). Un remerciement spécial à Pier Luca Palla et Emiliano Cadelano pour l'amitié et pour la collaboration inspirante et gratifiant au cours de leur activité de doctorat.
L'encouragement constant et le soutien offert par tous mes collègues du groupe AIMAN - FILM de l'IEMN sont également très appréciés: Vladislav Aleshin, Michael Baudoin, Yannick Dusch, Olivier Bou Matar, Marc Goueygou, Alain Merlen, Philippe Pernod, Vladimir Preobrazhensky, Abdelkrim Talbi, Nicolas Tiercelin, Farzam Zoueshtiagh et les thésards et post-doc Adrien Bussonnière, Ilyesse Bihi, Théo Mathurin, Carmelo Magniez, Diwakar Seyyanur Venkatesan et les autres collaborateurs. En ce qui concerne ma dernière activité de recherche portant sur les propriétés thermo-élastiques de polymères et des chaînes d'intérêt biologique je suis reconnaissant à Fabio Manca pour son amitié et pour la coopération productive et agréable. Je remercie Fabrizio Cleri , Pier Luca Palla (à nouveau) et Evelyne Lampin, membres du groupe SDYNA à l'IEMN, pour les discussions stimulantes et les collaborations fructueuses.
Enfin, *last but not least*, je tiens à remercier Philippe PERNOD (Garant de l'habilitation), Renald BRENNER, Olivier CASTELNAU, Djimedo KONDO (Rapporteurs), Guy BONNET, Lionel BUCHAILLOT, Fabrizio CLERI et Vladimir PREOBRAZHENSKY (Examinateurs) pour leur participation à mon jury d'habilitation. Je suis très honoré de leur intérêt pour mes travaux.
Ma femme Alessandra et mon fils Ernesto pour l'amour et le soutien sans lesquels ces activités n'auraient jamais été réalisées.

[12] Alessandro Chiabrera : né en 1940 e décédé en 1999. Une école permanente de bio-électromagnétisme a été créé en 2003 et nommé «International School of Bioelectromagnetics Alessandro Chiabrera» pour ses résultats importantes dans ce domaine. Le cours a lieu chaque année à Erice (Sicile, Italie) à la Fondation et Centre de Culture Scientifique Ettore Majorana.

1. Curriculum Vitae

Personal

Name and Surname	Stefano GIORDANO
Place and date of birth	Genoa (Italy), October, 14-1971
Nationality	Italian
Private Address	213, Rue Fénelon - 59260 Hellemmes - Lille
Telephone	Tel: (+33) 0954683737 Mobile: (+33) 0651914134
Work Address	Institut d'électronique, de microélectronique et de nanotechnologie (IEMN), UMR CNRS 8520 Laboratoire central, Cité scientifique Avenue Henri Poincaré, CS 60069, 59652 Villeneuve d'Ascq cedex
Telephone	fax: (+33) 03 20 19 79 84 tel: (+33) 03 20 19 79 58
Web	http://aiman.iemn.univ-lille1.fr http://www.giordanostefano.it
E-mail	Stefano.Giordano@iemn.univ-lille1.fr Stefano.Giordano@univ-lille1.fr

Summary

Entered the CNRS on 01/10/2010

61 papers in peer-reviewed journals or book chapters, 75 conference-congress presentations, 1 book

H-factor: 14 (http://scholar.google.fr/citations?user=2bjv5voAAAAJ&hl=fr)

Diplomas & Degrees

February, 18 - 2000	Final exam for obtaining the PhD title (University of Trento, Italy). Dissertation committee: PR. ERMANNO DI ZITTI (GENOVA-IT), PR. ANDREA NEVIANI (PADOVA-IT) et PR. GUIDO MASETTI (BOLOGNA-IT).
November 1996- - October 1999	**PhD Course** in 'Materials, Technology and Electronics Devices' XII Cycle with main office in the University of Trento (Italy). The activity is developed in the associated office in Genoa (Italy) at the Department of Biophysical and Electronic Engineering (DIBE) under the tutoring of the Prof. Bruno Bianco and in collaboration with Prof. Alessandro Chiabrera. Title of the thesis: "**Electromagnetic characterisation of linear and non linear heterogeneous media".** The work deals with the analysis of the physical properties (electrical, magnetic, thermal and so on) of heterogeneous media composed of a mixture of distinct homogeneous media **(homogenization**).
November 1996	Examination for the qualification to the exercise of the Engineer profession.
July 1996	University of Genoa: Master Degree in Electronic Engineering. Title of the thesis: "**Evolution equations for stochastic processes in classical and quantum mechanics**". Score: 110/110 cum laude. The methodology based on the Langevin and Fokker-Planck equations, useful to study stochastic systems, is analysed and applied to different physical problems. It has been developed a new form of the Schrödinger and Liouville-Von Neumann equations with external random forces. This work has been applied for developing a new formulation of friction and noise in mesoscopic quantum mechanics.
July 1990	Certificate for Technical Competence with specialisation in Industrial Electronics attained at the Institute 'Galileo Galilei' in Genoa. Score: 56/60

Research experience	
October 2010-current	Senior Researcher (CR1) at IEMN UMR CNRS 8520, Villeneuve d'Ascq (Group AIMAN). Member of the International Associated Laboratory LIA - LICS (ex-LEMAC).
October 2008-September 2010	Renewal of the two Years Research Contract (Assegno di Ricerca) on the subject: "**Theories and concepts for the multi-scale modelling of the mechanical behaviour in complex materials**" (Area: Physical Science FIS/03), Department of Physics, University of Cagliari. Application of the **Kolossov-Muskelishvili method** to the study of elastic inclusions at the nano-scale. Generalization of the **Eshelby theory** to the case of nonlinear inclusions (with the proof of existence and uniqueness based on **variational methods**) and inclusions with shape and size different from the hosting cavity. **Homogenization theories** for nonlinear elastic microstructures described by the **Landau coefficients.**
October 2006-September 2008	Two Years Research Contract (Assegno di Ricerca) on the subject: "**Theories and concepts for the multi-scale modelling of the mechanical behaviour in complex materials**" (Area: Physical Science FIS/03), Department of Physics, University of Cagliari, Responsible: Prof. Luciano Colombo. Analysis of the singular elastic fields around a **single crack** through a generalization of the Eshelby theory. Extension to the electric case. Development of **homogenization techniques for multi-fractured systems**. Development of a method for the analysis ellipsoidal inclusions with dielectric graded profile based on a system Riccati differential equations. Applications of the classical potential theory to the solution of the problem of the **anisotropic nonlinear ellipsoidal inclusion**.
September-October 2006	Research contract entitled "**Continuum mechanics of fractured elastic media**", Department of Physics, University of Cagliari, Responsible: Prof. Luciano Colombo.
October-November 2005	Research contract entitled "**Continuum mechanics analytical models for fracture phenomena in micro-cracked ceramic materials**" Department of Physics, University of Cagliari, and Responsible: Prof. Luciano Colombo.
October 2004-September 2005	Scientific collaboration with the University of Genoa: research activity in the field of the **composite materials characterization**.
September 2002-September2004	Two Years Research Contract (Assegno di Ricerca) on the subject: "**Electric and magnetic modelling of tissues and cells**", Department of Biophysics and Electronic Engineering, University of Genoa, Responsible: Prof. Bruno Bianco. Contract financed through the European Project RAMP 2001 (RISK ASSESSMENT FOR EXPOSURE OF NERVOUS SYSTEM CELLS TO MOBILE TELEPHONE EMF). Development of the Work-Package "**A numerical tool for computing electromagnetic field in-situ in arbitrarily shaped cellular structures**".
March 2001-August 2002	Scientific collaboration with the University of Genoa: research activity under a contract with TILAB (ex-CSELT, Turin-IT). Participation to the "National Research Program MIUR / CNR-ENEA".
February 2000-February 2001	Research contract with the University of Bradford (Prof. Peter EXCELL, now at the Glyndŵr University): "**Quantum modelling of protein binding sites under the effect of an exogenous electromagnetic field**".

Pedagogical activity

February 2015-

Quantum Physics course at "École Centrale de Lille" (32 hours, 20 students). Programme: analytical mechanics, Lagrange, Hamilton and Hamilton-Jacobi equations, electromagnetism, Bohr model, linear operators, postulates of the quantum mechanics, Schrodinger equation, continuity equation, Ehrenfest theorem, Heisenberg relation, classical limit, free particle, infinite potential well, tunnel effect, angular moment, hydrogen atom, harmonic oscillator and black body radiation.

June 2010-
May 2013

Co-direction (with Prof. Luciano Colombo, University of Cagliari, Italy) of the PhD thesis **THE ELASTIC BEHAVIOR OF POLYMER CHAINS: THEORY AND SIMULATIONS** of the PhD student Fabio MANCA. This thesis was framed within the Doctoral School of the University of Cagliari, Italy (Facoltà di Scienze Matematiche Fisiche e Naturali, Dipartimento di Fisica). However, the candidate has spent during his thesis, more than 2 years at the IEMN under my direct tutoring and in collaboration with Prof. Fabrizio CLERI, University Lille I. He defended his thesis on May 2013 at the University of Cagliari with an excellent evaluation.

October 2008-
September 2010

Co-direction of the PhD thesis of dr. Pier Luca PALLA (**MULTISCALE MODELING OF MECHANICAL BEHAVIOR IN NANOSTRUCTURED MATERIALS**) and dr. Emiliano CADELANO (**ELASTIC PROPERTIES OF GRAPHENE: A COMBINED CONTINUUM AND ATOMISTIC INVESTIGATION**) concerning the effective mechanical properties of linear and nonlinear nanostructures (nonlinear homogenization and classical molecular dynamics) and the mechanical properties of graphene (both in stretching and bending, with applications of differential geometry). Development of series of lectures (Elasticity theory, Electromagnetism, Constitutive equations of materials, Single electron devices) at the University of Cagliari-IT.

October 2006-
September 2008

Supervisor of the Master Degree thesis: "**PROPRIETA' ELETTROMAGNETICHE DI MATERIALI COMPOSITI LINEARI E NON LINEARI"** (Gianmarco ZANDA) and "**PROPRIETÀ MECCANICHE DI MATERIALI COMPOSITI MULTI-FRATTURATI"** (Ilenia SABA). Development of series of lectures (Fracture mechanics, Dislocations theory, Thermodynamics of elasticity and electromagnetism) at the University of Cagliari-IT. Author of the text-book "**Introduzione alla teoria della elasticità**" (Introduction to Elasticity Theory), published by Springer.

October 2000-
September 2005

Supervisor for the Master Degree thesis: "**INTERAZIONE TRA CAMPI ELETTROMAGNETICI ELF E POPOLAZIONI DI PROTISTI"** (Claudio BOZZO) and "**MODELLI A RISONANZA PARAMETRICA DELL'INTERAZIONE BIOELETTROMAGNETICA"** (Ivano MALLARINI). Member of the academy board for the courses 'Electromagnetic fields', 'Optical processing of signals', 'Bioelectromagnetism' and 'Environmental Electromagnetism and Bioelectromagnetic Interactions' at the University of Genoa. Development of series of lectures (electrostatics, magnetic field, waves, guided propagation, special relativity theory, geometrical optic, diffraction, angular spectrum, Fourier optics) at the University of Genoa-IT.

Languages

French, English and Italian (native)

Participation to projects

2005-2009: PON–EU/MIUR CYBERSAR: A CYBERINFRASTRUCTURE FOR SCIENCE AND TECHNOLOGY (ACTIVITY 07: COMPUTATIONAL HARD AND SOFTMATTER PHYSICS), UNIVERSITY OF CAGLIARI AND INFN, INAF, UNIVERSITY OF SASSARI (PROGETTO FINANZIATORE DEGLI ASSEGNI DI RICERCA 2006-2010).

2006-2008: External Research Network (6FP) of the Network of Excellence "Knowledge-based Multifunctional Materials".

2005-2008: Research project IndAM: Mathematical challenges in nanomechanics at the interface between atomistic and continuum models, University of Cagliari and SISSA, University of Brescia, Pavia, Udine, Roma, Pisa and Padova.

2002-2005: European Project RAMP 2001 (RISK ASSESSMENT FOR EXPOSURE OF NERVOUS SYSTEM CELLS TO MOBILE TELEPHONE EMF: FROM IN VITRO TO IN VIVO STUDIES), CONTRACT NUMBER: QLK4-CT-2001-00463, FP5 THEMATIC PROGRAMME: QUALITY OF LIFE AND MANAGEMENT OF LIVING RESOURCES.

2000-2003: Programma Nazionale di Ricerca MIUR / CNR-ENEA 2000-2004, Salvaguardia dell'Uomo e dell'Ambiente dalle Emissioni Elettromagnetiche.

1999-2001: RESEARCH CONTRACT N. 112/98/AI-L between TILAB (Telecom Laboratories, ex-CSELT, Torino) and ICEMB (Centro Interuniversitario per lo Studio delle Interazioni tra Campi Elettromagnetici e Biosistemi). Title: Attività di ricerca per la realizzazione di studi teorici e sperimentali sugli effetti biologici e meccanismi d'interazione dei campi elettromagnetici irradiati da apparati di comunicazione personali mobile.

Coordinated Projects

2011: Research and innovation project within the "Fondation Centrale Initiatives". Title: "Continuum approach for studying the static and dynamic behavior of piezo-magneto-elastic composite materials".

2009: Project "Large scale atomistic simulations of the mechanical properties in nanomaterials" submitted to and accepted by CASPUR under Standard HPC Grant 2009 (progetti di ricerca nel campo del calcolo ad alte prestazioni).

2000: Research project with the University of Bradford (Prof. Peter Excell): Models of interaction between electromagnetic fields and biological media based on the ligand binding process.

Computing Skills

Operating Systems	Ms-Dos, Windows (3.x, 95, NT, 98, 2000, XP), Linux, Unix
Mathematical and processing software	Matlab with Toolboxes, Maple VII, Mathematica Software for images processing (Photoshop etc.) High level experience in numerical calculus (matrices, differential equation symbolic calculus, images processing)
Languages	Fortran, Pascal, Basic, HTML, C
Others	Microsoft Office, Open Office, Latex, Internet etc.

Hobbies

Trekking, reading, travelling, jogging.

Military Service

Military Service absolved (Italy) from December 16-1997 to October 15-1998.

Areas of Expertise

Composite or Heterogeneous Materials

Application of the continuum mechanics and the electromagnetism to the determination of the effective physical properties (both linear and non-linear, coupled and uncoupled) of complex, heterogeneous or composite materials and structures (homogenization theories, effective medium theories).

Applications and generalizations of the Eshelby theory to linear/nonlinear, isotropic/anisotropic, coupled/uncoupled problems. This methodology allows to calculate the relevant quantities inside a given (ellipsoidal) inhomogeneity embedded in a host matrix, when the system is under the effects of external fields. This theory is the starting point of many effective medium theories. It can be used to investigate the elastic properties of micro-cracked materials (and/or fibro-reinforced) with a given orientational distribution of cracks (described by some order parameters). It also finds application in dilute (Maxwell-Garnett and Mori-Tanaka like models) or non-dilute dispersions of particles (iterative, multipoles and differential methods).

Homogenization theories for transport properties in composites with imperfect interfaces. Linear and nonlinear elastic properties of multilayered and functionally graded materials (with arbitrary physical coupling; e.g. artificial multiferroic).

Magnetoelectric & Multiferroic devices

Combination of the Eshelby theory with the Landau-Lifchitz-Gilbert equation and the Langevin/Fokker-Planck methodology for analysing the behaviour of magneto-elastic (ferromagnetic) particles embedded in different matrices (e.g. piezoelectric). The Eshelby theory allows the determination of all coupled field within the particle, the Landau-Lifchitz-Gilbert (LLG) equation describes the dynamics of the magnetization in single-domain ferromagnetic particles and, finally, the Langevin/Fokker-Planck methodology is able to take into account the thermal bath where the system is embedded and, therefore, to introduce the temperature in these systems. Applications to stress-mediated magnetization switching and magneto-electric memories. Analysis of the thermal effects on the stress-mediated switching and on the memory stability. Possible future applications to memristive devices.

Elasticity of polymeric chains

Thermo-elastic behaviour of polymer molecules with biological relevance (DNA, RNA, proteins, polysaccharides) analysed through the classical statistical mechanics. Applications to the thermo-elasticity of single polymer chains subjected to uniform stretching (generated by an applied force) or non-uniform stretching (generated by an external field). Generalizations of the freely-jointed chain (FJC) and the worm-like chain (WLC) models.

Analysis of the thermodynamic limit with different boundary conditions (Helmholtz or Gibbs ensemble): thermodynamics of small systems and ensemble equivalence in statistical mechanics. Investigations on bi-stable molecules with domains exhibiting conformational transitions between two stable states: from cooperative to non-cooperative response (application to the DNA stretching). Comparison with experimental results obtained with single-molecule experiments (atomic force microscopy, optical, magnetic and electromechanical tweezers, flow fields).

PUBLICATIONS

Articles in international journals

1) A. Chiabrera, B. Bianco, S. Bruna, S. Giordano, Bioelectromagnetics: the state of the science, Biology Forum 91 (1998), pp.233-246.

2) B. Bianco, A. Chiabrera, S. Giordano, D.C.-E.L.F. characterization of random mixtures of piecewise non-linear media, Bioelectromagnetics 21:145-149 (2000).

3) B. Bianco, E. Moggia, S. Giordano, W. Rocchia, A. Chiabrera, Friction and noise in quantum mechanics: a model for the interactions between a system and a thermal bath, Il Nuovo Cimento Vol.116 B, N.2, Febbraio 2001.

4) B. Bianco, S. Giordano, Electrical characterization of linear and non-linear random networks and mixtures, International Journal of Circuit Theory and Applications, Volume 31/2, 2003, pp.199-218. DOI: 10.1002/cta.217.

5) S. Giordano, Effective medium theory for dispersions of dielectric ellipsoids, Journal of Electrostatics, Vol. 58/1-2, 2003, pp. 59-76. DOI: 10.1016/S0304-3886(02)00199-7.

6) S. Giordano, Differential schemes for the elastic characterization of dispersions of randomly oriented ellipsoids, European Journal of Mechanics – A/Solids, 22 (2003) 885-902. DOI: 10.1016/S0997-7538(03)00091-3.

7) S. Giordano, Multipole analysis of a generic system of dielectric cylinders and application to fibrous materials, Journal of Electrostatics 63 (2005) 1-19. DOI: 10.1016/j.elstat.2004.06.007.

8) S. Giordano, Order and disorder in heterogeneous material microstructure: electric and elastic characterization of dispersions of pseudo oriented spheroids, International Journal of Engineering Science, 43 (2005) 1033–1058. DOI: 10.1016/j.ijengsci.2005.06.002.

9) S. Giordano, Disordered lattice networks: general theory and simulations, International Journal of Circuit Theory and Applications, 33 (2005) 519-540. DOI: 10.1002/cta.335.

10) S. Giordano, Walter Rocchia, Shape dependent effects of dielectrically nonlinear inclusions in heterogeneous media, Journal of Applied Physics 98, 104101 (2005) 1-10. DOI: 10.1063/1.2128689.

11) A. Amaroli, F. Trielli, B. Bianco, S. Giordano, E. Moggia and M.U. Delmonte Corrado, Effects of Time-Variant Extremely-Low-Frequency (ELF) Electromagnetic Fields (EMF) on Cholinesterase Activity in Dictyostelium discoideum, The Journal of Eukaryotic Microbiology, Vol. 52, Issue 2, Page 38S - March–April 2005. DOI: 10.1111/j.1550-7408.2005.05202003_6_1.x.

12) A. Amaroli, F. Trielli, B. Bianco, S. Giordano, E. Moggia and M.U. Delmonte Corrado, Effects of time-variant extremely low-frequency (ELF) electromagnetic fields (EMF) on cholinesterase activity in Dictyostelium discoideum (Protista), Chemico-Biological Interactions, Volumes 157-158, 15 December 2005, 355-356. DOI: 10.1016/j.cbi.2005.10.047.

13) S. Giordano, Equivalent permittivity tensor in anisotropic random media, Journal of Electrostatics, 64 (2006) 655-663. Doi:10.1016/j.elstat.2005.11.003.

14) A. Amaroli, F. Trielli, B. Bianco, S. Giordano, E. Moggia and M.Umberta Delmonte Corrado, Effects of 50 Hz magnetic field on Dictyostelium discoideum (Protista), Bioelectromagnetics 27: 528-534 (2006). DOI: 10.1002/bem.20240.

15) S. Giordano, W. Rocchia, Predicting the dielectric nonlinearity of anisotropic composite materials via tensorial analysis, 2006 Journal of Physics: Condensed Matter 18 10585-10599, Doi: 10.1088/0953-8984/18/47/006.

16) S. Giordano, Electrical behaviour of a single crack in a conductor and exponential laws for conductivity in micro cracked solids, International Journal of Applied Electromagnetics and Mechanics 26 (2007) 1–19.

17) S. Giordano, Two-dimensional disordered lattice networks with substrate, Physica A: Statistical Mechanics and its Applications, Volume 375, Issue 2 , 1 March 2007, Pages 726-740. Doi: 10.1016/j.physa.2006.09.026.

18) S. Giordano, Relation Between Microscopic and Macroscopic Mechanical Properties in Random Mixtures of Elastic Media, ASME, Engineering Materials and Technology, JULY 2007, Vol. 129 / 453. DOI: 10.1115/1.2400282

19) S. Giordano, L. Colombo, Effects of the orientational distribution of cracks in solids, Physical Review Letters 98, 055503 (2007). URL: http://link.aps.org/abstract/PRL/v98/e055503.
Doi: 10.1103/PhysRevLett.98.055503

20) S. Giordano and L. Colombo, Effects of the orientational distribution of cracks in isotropic solids, Engineering Fracture Mechanics, 74 (2007) 1983–2003, Doi:10.1016/j.engfracmech.2006.10.006.

21) S. Giordano and L. Colombo, Local elastic fields around cracks and their stress density of states, PHYSICAL REVIEW B 76, 174120 (2007). DOI: 10.1103/PhysRevB.76.174120.

22) S. Giordano and L. Colombo, Elastic properties of solids containing elliptic cracks, PHYSICAL REVIEW B 77, 054106 (2008). DOI: 10.1103/PhysRevB.77.054106.

23) P. Palla, S. Giordano, L. Colombo, Interfacial elastic properties of a-Si and c-Si, Physical Review B 78, 012105 (2008). DOI: 10.1103/PhysRevB.78.012105.

24) S. Giordano, P. L. Palla, Dielectric behavior of anisotropic inhomogeneities: interior and exterior points Eshelby tensors, Journal of Physics A: Mathematical and Theoretical 41 (2008) 415205 (24pp). Doi:10.1088/1751-8113/41/41/415205.

25) S. Giordano, L. Colombo, P. Palla, Nonlinear elastic Landau coefficients in heterogeneous materials, EuroPhysics Letters, 83 (2008) 66003. Doi: 10.1209/0295-5075/83/66003.

26) S. Giordano, P. L. Palla, L. Colombo, Effective permittivity of materials containing graded ellipsoidal inclusions, European Physics Journal B 66, 29–35 (2008).
DOI: http://dx.doi.org/10.1140/epjb/e2008-00382-7.

27) S. Giordano and Fausto Camboni, On some explicit results for the balanced generalized Polya urn, The Mathematical Scientist 33, 1-16 (2008), APPLIED PROBABILITY TRUST.

28) S. Giordano, P. L. Palla, L. Colombo, Nonlinear elasticity of composite materials: Landau coefficients in dispersions of spherical and cylindrical inclusions, European Physics Journal B 68, 89–101 (2009). DOI: http://dx.doi.org/10.1140/epjb/e2009-00063-1.

29) E. Cadelano, P. L. Palla, S. Giordano, L. Colombo, Nonlinear elasticity of monolayer graphene, Phys. Rev Lett. 102, 235502 (2009). DOI: 10.1103/PhysRevLett.102.235502. Also published in Virtual Journal of Nanoscale Science & Technology, STRUCTURAL PROPERTIES, Volume 19, Issue 25, June 22, 2009.

30) P. L. Palla, S. Giordano, L. Colombo, The role of interface elasticity in nanostructured silicon, Physical Review B, 80, 054105 (2009). DOI: 10.1103/PhysRevB.80.054105. Also published in the Virtual Journal of Nanoscale Science & Technology, SURFACE AND INTERFACE PROPERTIES, Volume 20, Issue 8, August 24, 2009.

31) S. Giordano, Dielectric and Elastic Characterization of Nonlinear Heterogeneous Materials. Materials (invited review paper published by Molecular Diversity Preservation International, ISSN 1996-1944) 2009, 2, 1417-1479. Doi: 10.3390/ma2041417.

32) Stefano Giordano, Order and disorder in the microstructure of dielectrically nonlinear heterogeneous materials, Journal of electrostatics 68, 2010, 227-236. DOI: http://dx.doi.org/10.1016/j.elstat.2010.01.004.

33) Emiliano Cadelano, Stefano Giordano, and Luciano Colombo, Interplay between bending and stretching in carbon nanoribbons, Phys. Rev. B 81, 144105 (2010). DOI: http://dx.doi.org/10.1103/PhysRevB.81.144105.

34) Pierluca Palla, Stefano Giordano, and Luciano Colombo, Lattice model describing scale effects in nonlinear elasticity of nanoinhomogeneities, Phys. Rev. B 81, 214113 (2010), also published in Vir. J. Nan. Sci. & Tech. / Volume 21 / Issue 26 / STRUCTURAL PROPERTIES.
DOI: http://dx.doi.org/10.1103/PhysRevB.81.214113.

35) Stefano Giordano, Maria Ilenia Saba, and Luciano Colombo, Elastic properties of multi-cracked composite materials, The European Physics Journal B 76, 261-269 (2010). DOI: http://dx.doi.org/10.1140/epjb/e2010-00174-6.

36) Emiliano Cadelano, Pier Luca Palla, Stefano Giordano and Luciano Colombo, Elastic properties of hydrogenated graphene, Physical Review B 82, 235414 (2010).
DOI: http://dx.doi.org/10.1103/PhysRevB.82.235414.

37) Luciano Colombo and Stefano Giordano, Nonlinear elasticity in nanostructured materials, Report on Progress in Physics 74, 116501 (2011). DOI: http://dx.doi.org/10.1088/0034-4885/74/11/116501.

38) Nicolas Tiercelin, Yannick Dusch, Alexey Klimov, Stefano Giordano, Vladimir Preobrazhensky, and Philippe Pernod, Room temperature magnetoelectric memory cell using stress-mediated magnetoelastic switching in nanostructured multilayers, APPLIED PHYSICS LETTERS 99, 192507 (2011).
DOI: http://dx.doi.org/10.1063/1.3660259.

39) Stefano Giordano, Pier Luca Palla, Emiliano Cadelano and Michele Brun, Elastic behaviour of inhomogeneities with size and shape different from their hosting cavities, Mechanics of Materials 44, 4 (2012).
DOI: http://dx.doi.org/10.1016/j.mechmat.2011.07.015.

40) Stefano Giordano and Pier Luca Palla, Conduction degradation in anisotropic multi-cracked materials, The European Physics Journal B 85, 59 (2012). DOI: http://dx.doi.org/10.1140/epjb/e2011-20814-5.

41) Fabio Manca, Stefano Giordano, Pier Luca Palla, Rinaldo Zucca, Fabrizio Cleri and Luciano Colombo, Elasticity of flexible and semiflexible polymers with extensible bonds in the Gibbs and Helmholtz ensembles, THE JOURNAL OF CHEMICAL PHYSICS 136, 154906 (2012). DOI: http://dx.doi.org/10.1063/1.4704607.

42) Stefano Giordano, Yannick Dusch, Nicolas Tiercelin, Philippe Pernod and Vladimir Preobrazhensky, Combined nanomechanical and nanomagnetic analysis of magnetoelectric memories, PHYSICAL REVIEW B 85, 155321 (2012). DOI: http://dx.doi.org/10.1103/PhysRevB.85.155321.

43) Fabio Manca, Stefano Giordano, Pier Luca Palla, Fabrizio Cleri and Luciano Colombo, Monte Carlo simulations of single polymer force-extension relations, Journal of Physics: Conference Series 383, 012016 (2012). DOI: http://dx.doi.org/10.1088/1742-6596/383/1/012016.

44) Yannick Dusch, Vasyl Rudenko, Nicolas Tiercelin, Stefano Giordano, Vladimir Preobrazhensky, and Philippe Pernod, Hysteretic magnetoresistance in stress controled magnetic memory device, Nanomaterials and nanostructures 2, 44 (2012). LINK: http://www.radiotec.ru/catalog.php?cat=jr18&art=11419.

45) Fabio Pavanello, Fabio Manca, Pier Luca Palla, and Stefano Giordano, Generalized interface models for transport phenomena: Unusual scale effects in composite nanomaterials, Journal of Applied Physics 112, 084306 (2012). DOI: http://dx.doi.org/10.1063/1.4759017.

46) Fabio Manca, Stefano Giordano, Pier Luca Palla, Fabrizio Cleri, and Luciano Colombo, Theory and Monte Carlo simulations for the stretching of flexible and semiflexible single polymer chains under external fields, Journal of Chemical Physics 137, 244907 (2012). DOI: http://dx.doi.org/10.1063/1.4772656.

47) Fabio Manca, Stefano Giordano, Pier Luca Palla, Fabrizio Cleri, and Luciano Colombo, Two-state theory of single-molecule stretching experiments, Physical Review E 87, 032705 (2013). DOI: http://dx.doi.org/10.1103/PhysRevE.87.032705.

48) Yannick Dusch, Nicolas Tiercelin, Alexey Klimov, Stefano Giordano, Vladimir Preobrazhensky, and Philippe Pernod Stress-mediated magnetoelectric memory effect with uni-axial TbCo2/FeCo multilayer on 011-cut PMN-PT ferroelectric relaxor, Journal of Applied Physics 113, 17C719 (2013). DOI: http://link.aip.org/link/doi/10.1063/1.4795440.

49) Fabio Pavanello and Stefano Giordano How imperfect interfaces affect the nonlinear transport properties in composite nanomaterials, Journal of Applied Physics 113, 154310 (2013). DOI: http://dx.doi.org/10.1063/1.4801889.

50) Stefano Giordano, Yannick Dusch, Nicolas Tiercelin, Philippe Pernod and Vladimir Preobrazhensky Stochastic magnetization dynamics in single domain particles, Eur. Phys. J. B 86, 249 (2013). DOI: http://dx.doi.org/10.1140/epjb/e2013-40128-x.

51) Stefano Giordano, Yannick Dusch, Nicolas Tiercelin, Philippe Pernod and Vladimir Preobrazhensky Thermal effects in magnetoelectric memories with stress-mediated switching, Journal of Physics D: Applied Physics 46, 325002 (2013). DOI: http://dx.doi.org/10.1088/0022-3727/46/32/325002.

52) Stefano Giordano, Analytical procedure for determining the linear and nonlinear effective properties of the elastic composite cylinder, International Journal of Solids and Structures 50, 4055-4069 (2013). DOI: http://dx.doi.org/10.1016/j.ijsolstr.2013.08.017.

53) Stefano Giordano, Explicit nonlinear homogenization for magneto-electro-elastic laminated materials, Mechanics Research Communications 55, 18-29 (2014). DOI: http://dx.doi.org/10.1016/j.mechrescom.2013.10.008.

54) Fabio Manca, Stefano Giordano, Pier Luca Palla, and Fabrizio Cleri On the equivalence of thermodynamics ensembles for flexible polymer chains, Physica A: Statistical Mechanics and its Applications 395, 154-170 (2014). DOI: http://dx.doi.org/10.1016/j.physa.2013.10.042.

55) S. Giordano, F. Manca, Analysis of heterogeneous structures described by the two-temperature model, International Journal of Heat and Mass Transfer 78, 189-202 (2014). DOI: http://dx.doi.org/10.1016/j.ijheatmasstransfer.2014.06.074.

56) Fabio Manca, Stefano Giordano, Pier Luca Palla, and Fabrizio Cleri, Scaling Shift in Multicracked Fiber Bundles, PHYSICAL REVIEW LETTERS 113, 255501 (2014). DOI: http://dx.doi.org/10.1103/PhysRevLett.113.255501.

Chapters in books or edited books

1) A. Chiabrera, B. Bianco, S. Giordano, S. Bruna, E. Moggia, J.J. Kaufman, Ligand Binding under RF EM exposure, in B. J. Klauenberg and D. Miklavcic (eds.), *Radio Frequency Radiation Dosimetry*, 429-447, Kluwer Academic Publishers (NETHERLANDS).

2) Pier Luca Palla, Mariella Ippolito, S. Giordano, Alessandro Mattoni and Luciano Colombo, Atomistic approach to nanomechanics: Concepts, methods, and (some) applications, Research Signpost 37/661 (2), Fort P.O., Trivandrum-695 023, Kerala, India, The Nanomechanics in Italy, 2007: 75-107 ISBN: 978-81-308-0237-4. Editor: Nicola Maria Pugno.

3) S. Giordano, P. L. Palla, Recent Advances in the Characterization of Composite Dielectric Structures, invited paper on the collection 'Dielectric Materials: Research, Technology and Applications' edited by Ai Huang, Nova Science Publishers, Inc., NY, 2009. ISBN: 978-1-60692-266-8.

4) S. Giordano, A. Mattoni, L. Colombo, Brittle fracture: from elasticity theory to atomistic simulations, REVIEWS IN COMPUTATIONAL CHEMISTRY, vol.27, pp.1-83, 2010.

5) N. Tiercelin, Y. Dusch, S. Giordano, A. Klimov, V. Preobrazhensky and P. Pernod, Strain Mediated Magnetoelectric Memory, to be published in "Nanomagnetic and spintronics devices and phenomena for energy-efficient computing", Editors J. Atulasimha and S. Bandyopadhyay, Wiley, New York. Scheduled to appear in 2015.

Books

1) Introduzione alla teoria della elasticità (Introduction à la théorie de l'élasticité), SPRINGER, UNITEXT, Colombo, Luciano et Giordano, Stefano, 2007, ISBN: 978-88-470-0697-3.

Congresses and conferences

1. B. Bianco, A. Bonfiglio, S. Giordano, E. Moggia, 'Caratterizzazione elettromagnetica di misture', XIII Riunione Annuale dei Ricercatori del Gruppo Nazionale di Elettrotecnica, Pisa, 19-21 Giugno 1997.

2. B. Bianco, A. Bonfiglio, S. Giordano, E. Moggia, 'Electromagnetic characterization of nonlinear mixtures', ICEAA International Conference on Electromagnetics in Advanced Applications, Torino, September 14-18, 1997.

3. S. Giordano, W. Rocchia, B. Bianco, A. Chiabrera, 'Quantum lifetimes and classical collision frequency of a ligand under e.m. exposure', Book of Abstract for the 1998 Annual Meeting of the Bioelectromagnetics Society (BEMS), June 7-11, St.Petersburg Beach, Florida, USA.

4. A. Chiabrera, B. Bianco, S. Giordano, S. Bruna, E. Moggia, J.J. Kaufman, 'Ligand Binding under RF EM exposure', Advanced Research Workshop on Radio Frequency Radiation Dosimetry and its Relationship to the Biological Effects of Electromagnetic Field, NATO, October 12-16, 1998.

5. A. Chiabrera, B. Bianco, S. Bruna, S. Giordano, 'Bioelectromagnetics: the state of the science' presented to the 'Meeting of Theoretical Biophysics', 23 Gennaio 1998, Dipartimento di Fisica, Università di Genova.

6. S. Giordano, B. Bianco, S. Bruna, A. Chiabrera, 'Influence of Basal Metabolism on ligand binding probability: a pre-requisite for bioelectromagnetic effects', 4th European Bioelectromagnetics Association (EBEA) Congress, Zagreb, November, 19-21, 1998.

7. A. Chiabrera, S. Bruna, B. Bianco, S. Giordano, 'Comparing the Zeeman-Stark and Langevin-Lorentz models for the effectiveness of electromagnetic fields on ligand-receptor binding', Book of Abstract for the 1999 Annual Meeting of the Bioelectromagnetics Society (BEMS), June 20-24, Long Beach, California, USA.

8. A. Chiabrera, B. Bianco, S. Giordano, S. Bruna, S. Di Martino, 'Modelling of Interaction Mechanism', Forum on Future European Research on Mobile Communications and Health, Cost 244bis Project, 19-20 April 1999, College of Chemistry and Physics (ENSCPB), University of Bordeaux, France.

9. B. Bianco, S. Giordano, S. Di Martino, E. Moggia, 'Electromagnetic dynamic behaviour of a polymeric film', ICEAA International Conference on Electromagnetics in Advanced Applications, Torino, 13-17 September 1999.

10. S. Giordano, 'Electrical field generated by a charged harmonic oscillator at thermodynamic equilibrium', WSES/MIUE/HNA International Conference on Mathematics and Computer in Physics, Florida Keys (Marathon), July 25-29, 1999.

11. S. Giordano, 'Relativistic Langevin and Fokker-Planck equations', WSES/MIUE/HNA International Conference on Mathematics and Computer in Physics, Florida Keys (Marathon), July 25-29, 1999.

12. S. Bruna, M. Liberti, S. Giordano, D. Perrone, A. Chiabrera, B. Bianco, G. D'Inzeo, 'Bioelectromagnetic models: an integrated approach to the study of interaction mechanism', Biological Effects, Health Consequences and Standards for Pulsed radio-frequency fields, Ettore Majorana Centre, Erice, Sicily, Italy, November 21-25, 1999.

13. S. Bruna, M. Liberti, S. Giordano, D. Perrone, B. Bianco, G. D'Inzeo, 'Interaction mechanisms in bioelectromagnetism: a new integrated approach', BEMS, Munich, Germany, June 11-16, 2000.

14. B. Bianco, E. Moggia, S. Di Martino, S. Bruna, S. Giordano, 'Bioelettromagnetismo: attività presso l'unità di Genova', XVI Riunione Nazionale di Elettrotecnica, Udine, 15-17 June 2000.

15. S. Bruna, M. Liberti, S. Giordano, D. Perrone, 'Modelli Bioelettromagnetici: un approccio integrato allo studio dei meccanismi di interazione', XIII RINEM, 25-28 September 2000, Como, Italy.

16. Profumo, Facelli, Passerini, S. Giordano, 'PSPICE implementation of a new electro-thermal model for high power diodes', World conference on industrial applications of electrical energy, 8-12 October 2000, Rome, Italy.

17. S. Bruna, M. Liberti, S. Giordano, E. Moggia, B. Bianco, G. D'Inzeo, 'Integrated Interaction models in bioelectromagnetism', Millenium Workshop, 17-20 October 2000, Heraklion, Crete, Greece (invited talk).

18. S. Bruna, M. Liberti, S. Giordano, E. Moggia, B. Bianco, G. D'Inzeo, 'A Zeeman-Stark/Markov Model Approach to Study the EM Exposure of a Potassium Channel', IEEE International Microwave Symposium 2001, Phoenix, Arizona 20-25 May 2001.

19. F. Apollonio, M. Liberti, S. Bruna, S. Giordano, L. Tarricone, B. Bianco, G. D'Inzeo, 'Modeling interaction between EM fields and cells', Workshop "Gli effetti dei campi elettromagnetici", Perugia, Villa Umbra, 15-16 Marzo 2001.

20. B. Bianco, S. Di Martino, S. Giordano, 'Cariche superficiali in conduttori percorsi da corrente', XVII Riunione Annuale dei Ricercatori di Elettrotecnica, Catania, 6-8 Settembre 2001.

21. B. Bianco, S. Giordano, 'Caratterizzazione elettromagnetica di mezzi eterogenei con proprietà periodiche', XVII Riunione Annuale dei Ricercatori di Elettrotecnica, Catania, 6-8 Settembre 2001.

22. S. Bruna, M. Liberti, S. Giordano, 'Bioelectromagntic models: an integrated approach to study the interaction mechanisms', Atti della Fondazione Giorgio Ronchi, Anno LVI, n.4-5, Luglio-Ottobre 2001.

23. B. Bianco, S. Giordano, E. Moggia, 'Microdosimetria dei Compartimenti Cellulari', Convegno Nazionale su Predizione dell'impatto ambientale dei sistemi elettromagnetici e valutazione dell'esposizione umana', Roma, 22-23 Aprile 2002.

24. B. Bianco, S. Giordano, S. Di Martino, E. Moggia, 'Verhulst populations dynamics: relation with entire functions', 4th International Workshop on Biosignal Interpretation, Villa Olmo, Como, Italy, 24-26 Giugno 2002.

25. B. Bianco, E. Moggia, S. Giordano, S. Di Martino, 'A discussion on thermal bath role in the framework of the interactions between weak electromagnetic fields and biosystems', URSI Conference, Maastricht, 17-24 Agosto 2002.

26. S. Giordano, "Caratterizzazione elettromeccanica di misture casuali lineari", XVIII Riunione Annuale dei Ricercatori di Elettrotecnica, Messina, 27-29 Giugno 2002.

27. F. Apollonio, M. Liberti, S. Giordano, E. Moggia, B. Bianco, G. D'Inzeo, "Interaction between electromagnetic fields from mobile communication systems and potassium channels: a modeling

approach", 2nd International Workshop on Biological Effects of EMFs, Rhodes, Greece, 7-11, October, 2002 (invited talk).

28. AMAROLI ANDREA, TRIELLI FRANCESCA, BIANCO BRUNO, GIORDANO STEFANO, MOGGIA ELSA, DELMONTE CORRADO MARIA UMBERTA, "Effects of exposure to time-variant low frequency electromagnetic fields on Dictyostelium discoideum", 4th European Congress of Protistology and 10th European Conference on Ciliate Biology, August 31st – September 5th, 2003, San Benedetto del Tronto (AP) Italy.

29. B. Bianco, S. Giordano, "ANALISI MULTIPOLARE PER SISTEMI DI CILINDRI DIELETTRICI E APPLICAZIONE A MATERIALI FIBROSI", XIX Riunione Nazionale dei Ricercatori di Elettrotecnica, ET2003 Perugia/Terni, 19-21 Giugno 2003.

30. B. Bianco, S. Giordano, "SCHEMI DIFFERENZIALI PER MISTURE DI ELLISSOIDI DIELETTRICI ORIENTATI CASUALMENTE", XIX Riunione Nazionale dei Ricercatori di Elettrotecnica, ET2003 Perugia/Terni, 19-21 Giugno 2003.

31. B. Bianco, S. Giordano, E. Moggia, "VALUTAZIONE DEL FATTORE DI MERITO E DEL CAMPO DI REAZIONE IN ESPOSITORI A BOBINE DI HELMHOLTZ", XIX Riunione Nazionale dei Ricercatori di Elettrotecnica, ET2003 Perugia/Terni, 19-21 Giugno 2003.

32. B. Bianco, S. Giordano, E. Moggia, I. Mallarini, "ON A NUMERICAL METHOD FOR THE ZEEMAN-STARK MODEL OF LIGAND BINDING UNDER EM EXPOSURE", EBEA2003, 6th International Congress of the European Bioelectromagnetics Association (EBEA), 13–15, November, 2003, Budapest, Hungary.

33. B. Bianco, M. Nervi, S. Di Martino, E. Moggia, S. Giordano, P. Girdinio, "A method for evaluating the electric field in biological samples at ELF/LF frequencies", EBEA2003, 6th International Congress of the European Bioelectromagnetics Association (EBEA), 13–15 November, 2003, Budapest, Hungary.

34. AMAROLI ANDREA, TRIELLI FRANCESCA, BIANCO BRUNO, GIORDANO STEFANO, MOGGIA ELSA, DELMONTE CORRADO MARIA UMBERTA, "TIME-VARYING ELF FIELDS EFFECTS ON A SINGLE-CELL DICTYOSTELIUM DISCOIDEUM (PROTISTA)", EBEA2003, 6th International Congress of the European Bioelectromagnetics Association (EBEA), 13–15, November, 2003, Budapest, Hungary.

35. B. Bianco, S. Giordano, E. Moggia, 'Metodologie per una microdosimetria in ambiente non lineare', Progetto MIUR / CNR-ENEA "Salvaguardia dell'uomo e dell'ambiente dalle emissioni elettromagnetiche", Convegno su "Interazione tra campi elettromagnetici e soggetti esposti", Roma, 1-2 aprile 2004.

36. B. Bianco, S. Giordano, E. Moggia, 'Analisi di misture non lineari tipo Maxwell-Garnett', XX Riunione annuale dei Ricercatori di Elettrotecnica ET2004, Università di Salerno, 16-19 giugno 2004, Salerno, Italy.

37. AMAROLI A., TRIELLI F., BIANCO B., GIORDANO S., MOGGIA E., DELMONTE CORRADO M. U. Effects of time-variant extremely-low-frequency (ELF) electromagnetic fields (EMF) on cholinesterase activity in Dictyostelium discoideum (Protista). VIII International Meeting of Cholinesterases, Perugia, September 26-30, 2004.

38. AMAROLI A., TRIELLI F., BIANCO B., GIORDANO S., MOGGIA E., DELMONTE CORRADO M. U., Effects of time-variant extremely-low-frequency (ELF) electromagnetic fields (EMF) on cholinesterase activity in Dictyostelium discoideum. XXIV Convegno della Società Italiana di Protozoologia, Ottobre 2004, Rapallo.

39. S. Giordano, W. Rocchia, Two dimensional random lattice networks: a model for heterogeneous films coupled to a substrate, MMD Meeting, Matter, Materials and Devices, Genova, June 22nd-25th, 2005.

40. S. Giordano, Teoria per griglie di resistenze (o impedenze) casuali interagenti con un substrato, XXI Riunione Annuale dei Ricercatori di Elettrotecnica, ET2005, 16-18 Giugno 2005, Roma, Italy.

41. S. Giordano and L. Colombo, Analysis of distributions of pseudo-oriented cracks in isotropic solids, Third International Conference on Multiscale Materials Modeling, September 18-22, 2006, Freiburg, Germany.

42. S. Giordano and L. Colombo, ELASTIC BEHAVIOR OF MICROSTRUCTURED SOLIDS CONTAINING A DISTRIBUTION OF CRACKS, Report SLACS, Cagliari, 2007.

43. S. Giordano and L. Colombo, CHARACTERIZATION OF MICROCRACKED SOLIDS WITH A GIVEN STATISTICAL ORIENTATION OF CRACKS, Fluctuations and Scaling in Materials, Statphys 23 Satellite Conference, Todi, Italy, 4th-7th July, 2007.

44. P. L. Palla, S. Giordano, L. Colombo, 'On the continuity of elastic fields at the interface between two materials: continuum vs. atomistic investigation', XIII Scuola Nazionale Scienza dei Materiali 'Materiali nanostrutturati nelle strategie di sviluppo', 30 Settembre - 9 Ottobre 2007 (Bressanone, sede estiva dell'Università di Padova).

45. Luciano Colombo, Stefano Giordano, Pierluca Palla, Emiliano Cadelano, Alessandro Mattoni, Mariella Ippolito, 'Nanomechanics@Cagliari: a multi-institutional and multi-disciplinary enterprise', EU-NoE "Knowledge-based Multicomponent Materials(KMM), Accademia dei Lincei - Roma, September 28, 2007.

46. S. Giordano, Luciano Colombo, 'Multiscale modeling of materials behavior', Italian Academy (APRE – Agenzia per la Promozione della Ricerca Europea), Centro Congressi Cavour di Roma, 27 Novembre 2007.

47. L. Colombo, S. Giordano, A. Mattoni, P. L. Palla, COMBINED ATOMISTIC AND CONTINUUM MODELLING OF NONLINEAR ELASTICITY IN NANOSTRUCTURED MATERIALS, 8th.World Congress on Computational Mechanics (WCCM8) and 5th European Congress on Computational Methods in Applied Sciences and Engineering (ECCOMAS 2008) June 30 –July 5, 2008, Venice, Italy.

48. P. L. Palla, S. Giordano, L. Colombo, Studio alla scala atomica delle proprieta' elastiche dell'interfaccia aSi/cSi, Conferenza Nazionale Italian e-Science 2008, IES08, 27-29 maggio 2008, Universita' degli di Studi di Napoli Federico II.

49. P. L. Palla, S. Giordano, L. Colombo, Molecular dynamics results showing continuum theory failure in describing the elastic behavior of nanoparticles embedded in Si-based systems, European Materials Research Society, Fall Meeting, 15-19 September 2008, Warsaw, Poland.

50. S. Giordano, I. Saba, L. Colombo DIFFERENTIAL METHODS IN MULTI-COMPONENT HETEROGENEOUS STRUCTURES: APPLICATION TO FIBRE-REINFORCING IN MICROCRACKED MATERIALS, International Conference on PROCESSING & MANUFACTURING OF ADVANCED MATERIALS Processing, Fabrication, Properties, Applications, August 25-29, 2009, Technical University-Berlin, Germany.

51. E. Cadelano, P. Palla, S. Giordano and L. Colombo LINEAR AND NONLINEAR STRETCHING ELASTICITY IN MONOLAYER GRAPHENE, International Conference on PROCESSING & MANUFACTURING OF ADVANCED MATERIALS Processing, Fabrication, Properties, Applications, August 25-29, 2009, Technical University-Berlin, Germany.

52. P. L. Palla, E. Cadelano, S. Giordano, L. Colombo, Elastic behavior of nanoparticles embedded in a homogeneous matrix: from continuum theory to molecular dynamics, IX CONVEGNO NAZIONALE MATERIALI NANOFASICI, 3-5 GIUGNO 2009, Palazzo Bellavista, Monteponi, Iglesias (CI).

53. E. Cadelano, P. L. Palla, S. Giordano, L. Colombo, Non linear stretching elasticity of graphene, IX CONVEGNO NAZIONALE MATERIALI NANOFASICI, 3-5 GIUGNO 2009, Palazzo Bellavista, Monteponi, Iglesias (CI).

54. E. Cadelano, P.L. Palla, S. Giordano and L. Colombo, Nonlinear elasticity of monolayer graphene, Workshop finale dei Progetti Grid PONRicerca2000-2006, Catania Dipartimento di Fisica e Astronomia Via S. Sofia 64, Aula Magna, 10-12 Febbraio 2009.

55. S. Giordano, E. Cadelano, P. L. Palla, L. Colombo, Elasticità lineare e non lineare di un foglio di grafene, VI CONVEGNO NAZIONALE MATERIALI MOLECOLARI AVANZATI PER FOTONICA ED ELETTRONICA, 25-27 Giugno 2009, VILLAGGIO TELIS, ARBATAX (TORTOLI).

56. P. L. Palla, S. Giordano, L. Colombo, Atomistic virtual laboratory for nonlinear nanomechanics: application to the Eshelby problem, 2009 MRS Fall Meeting, November 30 - December 4, Boston, MA.

57. E. Cadelano, P. L. Palla, S. Giordano, L. Colombo, Stretching and bending elasticity of graphene: a combined continuum/atomistic approach, 2009 MRS Fall Meeting, November 30 - December 4, Boston, MA.

58. Emiliano Cadelano, Pierluca Palla, Stefano Giordano, Luciano Colombo, Stretching and bending elasticity of graphene: a combined continuum/atomistic approach, IV European Conference on Computational Mechanics : Solids, Structures and Coupled Problems in Engineering, Paris, France, May 16-21, 2010, Palais des Congrès.

59. Stefano Giordano, Pier Luca Palla, Emiliano Cadelano, Luciano Colombo, Nonlinear features and scale-effects in the Eshelby configuration, SIMAI-2010 conference (Societa' Italiana di Matematica Applicata ed Industriale), Università di Cagliari, June 21, 2010 – June 25, 2010.

60. Luciano Colombo, Pier Luca Palla, Stefano Giordano, Elastic Behavior of Nano-Alloys and Nano-Graded Systems by a Hybrid Continuum/Atomistic Model, 9th World Congress on Computational Mechanics and 4th Asian Pacific Congress on Computational Mechanics 2010 - July 19-23, 2010 - Sydney, Australia.

61. Luciano Colombo, Emiliano Cadelano, Pierluca Palla, and Stefano Giordano, GRAPHITA 2011, A Multidisciplinary and Intersectorial European Workshop on Synthesis, Characterization and Technological Exploitation of Graphene CNR IMM-Bologna Università dell'Aquila 15-18 May 2011, Gran Sasso National Laboratories, Assergi - L'Aquila, Italy.

62. GIORDANO S., DUSCH Y., TIERCELIN N., TALBI A., BOU MATAR O., ALESHIN V., MERLEN A., PREOBRAZHENSKY V., PERNOD P., Magnetic particle embedded in a piezoelectric matrix : analysis and applications, Actes du 20ème Congrès Français de Mécanique, CFM 2011, Besançon, France, 28 août-2 septembre, 2011.

63. PERNOD P., PREOBRAZHENSKY V., TIERCELIN N., TALBI A., DUSCH Y., VIARD R., BOU MATAR O., MERLEN A., KLIMOV A., GIORDANO S., Magnetic & multiferroic nano-objects & nanostructures for micro-magneto-mechanical systems & functional electronics, Nano and Giga Challenges in Electronics, Photonics and Renewable Energy, Summer School, Moscow-Zelenograd, Russia, September 12-16, 2011.

64. MANCA F., GIORDANO S., PALLA P.L., CLERI F., COLOMBO L., Monte Carlo simulations of single polymer force-extension relations, 3rd Young Researcher Meeting in Rome, YRMR 2012, Rome, Italy, january 20, 2012.

65. MANCA F., GIORDANO S., PALLA P.L., CLERI F., COLOMBO L., Thermoelastic force-extension behavior of polymers with elastic bonds, 4th International Conference on Nano-Structures Self-Assembly, Nano-SEA 2012, Santa Margherita di Pula, Cagliari, Italy, june 25-29, 2012

66. GIORDANO S., DUSCH Y., TIERCELIN N., PERNOD P., PREOBRAZHENSKY V., The electro-magneto-elastic Eshelby tensor : applications to homogenization methods and nano-structures, Actes du Colloque National MECAMAT, Aussois, France, 23-27 janvier, 2012, 1-13

67. TIERCELIN N., DUSCH Y., KLIMOV A., GIORDANO S., PREOBRAZHENSKY V., PERNOD P., Magnetoelectric random access memory (MELRAM), International Conference on Functional Materials, ICFM 2013, Partenit, Crimea, Ukraine, september 29-october 5, 2013, paper EA-5O/2

68. DUSCH Y., TIERCELIN N., KLIMOV A., GIORDANO S., PREOBRAZHENSKY V., PERNOD P., Stress-mediated magnetoelectric memory effect with uni-axial TbCo2/FeCo multilayer on 011-cut PMN-PT ferroelectric relaxor, 12th Joint Magnetism and Magnetic Materials-Intermag Conference, MMM-Intermag 2013, Chicago, IL, USA, january 14-18, 2013.

69. TIERCELIN N., DUSCH Y., KLIMOV A., GIORDANO S., STOLZ A., PREOBRAZHENSKY V., PERNOD P., Application of PMN-PT ferroelectric relaxor for multiferroic random access memory cell, Proceedings of 3rd Joint IEEE International Symposium on the Applications of Ferroelectrics, ISAF 2013, Piezoresponse Force Microscopy and Nanoscale Phenomena in Polar Materials Workshop, PFM 2013, Prague, Czech Republic, july 21-25, 2013, paper ISAF2-E2-3.

70. TIERCELIN N., DUSCH Y., ZAKNOUNE M., DEBLOCK Y., STOLZ A., GIORDANO S., PREOBRAZHENSKY V., PERNOD P., Magnetoresistive structures and magnetic tunnel junctions with magnetoelastic materials on ferroelectric relaxors for magnetoelectric memories, International French-US Workshop : Toward Low Power Spintronic Devices, La Jolla, CA, USA, july 8-12, 2013, 53-53.

71. TIERCELIN N., DUSCH Y., GIORDANO S., KLIMOV A., ZAKHAROV D., PREOBRAZHENSKY V., PERNOD P. Unequivocal strain mediated magneto-electric memory, XXIII International Materials Research Congress, IMRC 2014, Cancún, Mexico, august 17-21, 2014, Symposium 7C - Interfaces, Structure, and Domains in Ferroic and Multiferroic Material Systems, abstract S7C-O013

72. PERRET G., MANCA F., GIORDANO S., PALLA P.L., LACORNERIE T., LARTIGAU E., KUMEMURA M., FUJITA H., CLERI F., COLLARD D. Méthodes expérimentales et théoriques dans la biomécanique de dégradation de l'ADN sous rayonnement pour le traitement optimisé des tumeurs, Actes des 17èmes Journées Nationales du Réseau Doctoral en Micro-Nanoélectronique, JNRDM 2014, Villeneuve d'Ascq, France, 26-28 mai, 2014, 5 pages

73. PAVANELLO F., MANCA F., PALLA P.L., LAMPIN E., CLERI F., GIORDANO S., Scale effects induced by imperfect interfaces in nanomaterials transport properties, European Materials Research Society Spring Meeting, E-MRS Spring 2014, Symposium E - Defect-induced effects in nanomaterials, Lille, France, may 26-30, 2014, paper P1.40

74. TIERCELIN N., DUSCH Y., ZAKHAROV D., ZAKNOUNE M., DEBLOCK Y., GIORDANO S., PREOBRAZHENSKY V., PERNOD P. Structures magnéto-élasto-résistives sur relaxeurs ferroélectriques pour mémoires magnétoélectriques, 1ères Journées Nationales du GdR OXYFUN « Oxydes fonctionnels : du matériau au dispositif », Autrans, France, 29 juin-2 juillet, 2014

75. MANCA F., GIORDANO S., PALLA P.L., PERRET G., LARTIGAU E., COLLARD D., FUJITA H., CLERI F., Theoretical study of the basic mechanisms of DNA damage by therapeutic radiation beams, European Materials Research Society Spring Meeting, E-MRS Spring 2014, Symposium N - Converging technology for nanobio-applications, Lille, France, may 26-30, 2014, paper PI.23

2.Scientific Research

The research activity mainly deals with three different topics briefly introduced below:

1. Determination of the effective properties of heterogeneous materials or composite structures (homogenization theories). This task can be accomplished for different micro-geometries and physical responses of the

constituents. From the point of view of the geometry we can take into consideration periodic structures, random or pseudo-random dispersions of particles, laminated or multi-laminated materials, functionally graded systems, polycrystalline phases or assemblies of grains and so on. On the other hand, from the point of view of the constitutive relations describing the physical responses of materials, we can consider linear or non linear behaviours, isotropic or anisotropic structures, and different physical properties (coupled or uncoupled): electric permittivity, magnetic permeability, electrical or thermal conductivity (in general transport properties), elastic moduli of mechanical structures and viscosities (shear and bulk) of fluids. From the historical point of view we remember the first study of Maxwell (J.C. Maxwell, A Treatise on Electricity and Magnetism, Clarendon Press, Oxford, 1881) concerning the permittivity of dispersions of spheres, the work of Einstein (Einstein, 1906. A new determination of molecular dimensions. Ann. Phys. (4) 19, 289–306. Corrections: Ann. Phys. 34 (1911), 591–592) dealing with the viscosity of fluids with rigid spheres and the more recent result of Eshelby (Eshelby, J.D., 1957. The determination of the elastic field of an ellipsoidal inclusion and related problems. Proc. R. Soc. Lond. A 241, 376–396, Eshelby, J.D., 1959. The elastic field outside an ellipsoidal inclusion. Proc. R. Soc. Lond. A 252, 561–569) describing the elastic behaviour of an ellipsoidal particle embedded in an elastic medium. More recent results concerns the cases with nonlinear and anisotropic particles, complex geometries and interface/surface effects.

2. Static/dynamic/thermal analysis of complex structures composed of magnetoelastic (typically ferromagnetic) and piezoelectric (typically ceramic) phases. The aim is that of combining the magneto-electric effect with mechanically mediated interactions in order to obtain device with desired functionalities. The possibility to realize these structures within the IEMN clean room, in collaboration with colleagues of the AIMAN group, allows to draw interesting comparison between theoretical and experimental results. A recent example is given by a stress-mediated magnetoelectric memory composed of a ferromagnetic particle embedded in a piezoelectric matrix. An external magnetic field is able to determine two stable states for the magnetization within the particle, corresponding to the stored bit. Moreover, the piezoelectric matrix, via mechanic coupling, can be used to switch the state of the memory, realizing a controlled commutation strategy. A complete analysis of these heterostructure has been performed through the following approaches: the Eshelby theory allows the determination of all coupled field within the particle (static response), the Landau-Lifchitz-Gilbert (LLG) equation (Landau L and Lifshitz E, 1935, On the Theory of the Dispersion of Magnetic Permeability in Ferromagnetic Bodies Phys. Z. Sowjetunion 8 153, Gilbert T L, 1955, A Lagrangian formulation of the gyromagnetic equation of the magnetic field Phys. Rev. 100 1243, abstract only, Gilbert T L, 2004, A phenomenological theory of damping in ferromagnetic materials IEEE Trans. Mag. 40 3443) describes the dynamics of the magnetization in single-domain ferromagnetic particles and, finally, the Langevin/Fokker-Planck methodology (Coffey W T and Kalmykov Y P, 2012, The Langevin equation, Singapore: World Scientific) is able to take into account the thermal bath where the system is embedded (determination of the error probability). Future efforts will be devoted to the development of memristor devices.

3. As third research line we investigate the thermo-elastic behaviour of single polymer chains under stretching. As a first analysis, we study how the force-extension curve of a model polymer chain is affected by the loading protocol, which can be typically defined as fixed-ends or fixed-force. Such macroscopic boundary conditions can be formulated within the Helmholtz and the Gibbs ensembles of the classical statistical mechanics (J. H. Weiner, *Statistical Mechanics of Elasticity,* Dover, New York, 2002). This approach is performed with flexible and semi-flexible polymer models, with and without extensible bonds (M. Rubinstein and R. H. Colby, *Polymer Physics,* Oxford University Press, New York, 2003). Extensible bonds are typically described by linear springs for simply comparing analytical and Metropolis Monte Carlo (MMC) numerical results (D. Frenkel and B. Smit, *Understanding Molecular Simulation,* Academic, San Diego, 1996, M. P. Allen and D. J. Tildesley, *Computer Simulations of Liquids,* Clarendon, Oxford, 1987). The introduction of different boundary conditions leads to the notion of thermodynamic limit. In particular, it is possible to prove (under precise hypotheses) that different experimental strategies used for stretching the polymer result in the same results when the number of monomers is large enough (thermodynamic limit). On the other hand, by MMC simulations we can show that for short chains the two ensembles are characterized by very different elastic behaviours. In all cases (FJC, WLC and their extensible versions) the convergence to the thermodynamic limit is described by suitable power laws with well defined scaling exponents. More specifically, such power laws can fit the MMC results with high accuracy and different polymer models have different scaling exponents. Moreover, it is important to consider the statistical mechanics of chain polymers composed of domains with two stable states (undergoing conformational transitions), subjected to a pulling force applied by a molecular-scale mechanical device. For short chain length, or

large stiffness of the device, the domain response is uncorrelated and originates the typical saw-tooth force-extension curve observed in many experiments. On the other hand, upon increasing chain length, or vanishing device stiffness, the response is cooperative and results in the plateau-like curve, also observed in other experiments (M. Rief, F. Oesterhelt, B. Heymann, and H. E. Gaub, Science 275, 28, 1997, M. Rief, M. Gautel, F. Oesterhelt, J. M. Fernandez, and H. E. Gaub, Science 276, 1109, 1997, S. M. Smith, Y. Cui, and C. Bustamante, Science 271, 795, 1996). Despite the simplicity of our models (described below), we are able to provide a unified picture for such apparently contrasting experimental situations.

A detailed description of the obtained results for each of the three research lines can be found in the following subsections.

2.1.Determination of the effective properties of heterogeneous materials or composite structures

In principle, any nanostructured material can be conceptualized as a distribution of nanoscale inhomogeneities, embedded within an otherwise homogeneous hosting matrix. This very general picture, in fact, embodies the specific case of an isolated nanoparticle (such as a buried quantum dot or a hard/soft elastic inclusion), the more general case of a dispersion of inhomogeneities (forming, for instance, a nanograined material or a nanograded interface) or even the case of a fiber-reinforced matrix or a texture of nanograins. The same model also applies to nanoporous systems, as well as to multicracked materials. While in the last two examples the inhomogeneities are indeed represented by void volumes, in the previous ones they rather correspond to a second-phase material with unlike physical properties with respect to the hosting matrix. Nanostructured materials play a major role in modern materials physics, both for the investigation on fundamental properties of condensed matter at the nanoscale (most of which are affected by the interplay between quantum mechanical features and confinement or length-scale issues) and for their large technological impact (basically due to the fact that their functional and structural properties can be tailored by varying the nanoparticles size and shape). Therefore, the theoretical development of techniques for studying the physical behaviour of embedded nanoparticles and their interactions is a crucial point for the modern material science and nanotechnology. Probably the most important result in the extensive literature on elastic composites is the Eshelby theorem on the response of a single isotropic ellipsoidal elastic particle in an isotropic elastic space subjected to a remote strain. Eshelby (Eshelby, J.D., 1957. The determination of the elastic field of an ellipsoidal inclusion and related problems. Proc. R. Soc. Lond. A 241, 376–396; Eshelby, J.D., 1959. The elastic field outside an ellipsoidal inclusion. Proc. R. Soc. Lond. A 252, 561–569) proved that an applied uniform strain results in a uniform strain within the ellipsoidal inhomogeneity. The so-called Eshelby tensor, involved in the strain calculation, depends on the geometry of the ellipsoid (i.e. on the ratios of semi-axes lengths) and on the elastic properties of the homogeneous hosting matrix. Some years later, a similar property was proved also for the elastic field of an anisotropic particle embedded in an anisotropic medium (Walpole, L.J., 1967. The elastic field of an inclusion in an anisotropic medium. Proc. R. Soc. Lond. Ser. A 300, 270–289). More recently the theory has been generalized for considering an arbitrarily anisotropic magneto-electro-elastic response (Huang, J.H., Chiu, Y.H., Liu, H.K., 1998. Magneto-electro-elastic Eshelby tensors for a piezoelectric-piezomagnetic composite reinforced by ellipsoidal inclusions. J. Appl. Phys. 83, 5364–5370). The present line of research mainly deals with other generalizations and applications of the Eshelby concept to complex materials with a nanoscale microstructure.

2.1.1.The linear and nonlinear dielectric homogenization of isotropic structures

(*S. Giordano, Effective medium theory for dispersions of dielectric ellipsoids, Journal of Electrostatics, Vol. 58/1-2, 2003, pp. 59-76, S. Giordano, Walter Rocchia, Shape dependent effects of dielectrically nonlinear inclusions in heterogeneous media, Journal of Applied Physics 98, 104101 (2005) 1-10*)

A widely dealt topic concerning the physical behavior of heterogeneous materials (mixtures) is that of calculating their permittivity starting from the knowledge of the permittivity of each medium composing the mixture as well as of the structural properties of the mixture itself (percentage of each medium, shapes and relative positions of the single parts of the various media). In literature we find a large number of approximate analytical expressions for the effective permittivity of composed media as a function of the permittivity of its homogeneous constituents and some stoichiometric parameter (L. K. H. Van Beek, *Progress in Dielectric*, Heywood, London, 7, 71,1967 and A. Lakhtakia, *Selected Papers on Linear Optical Composite Materials, SPIE,* 1996). Each of these relationships should yield correct results for a particular kind of microstructure or, in other words, for a well defined morphology of the composite material. From the historical point of view, we remember some theories describing a mixture composed by two linear isotropic components: one of the most famous is the Maxwell formula developed for a strongly diluted suspension of spheres (J. C. Maxwell, *A treatise on electricity and magnetism*, Clarendon Press,

Oxford, 1881); a similar methodology has been applied to the case of a mixture of parallel circular cylinders. An alternative model is provided by the differential scheme, which derives from the mixture characterization approach used by Bruggeman (D. A. G. Bruggeman, *Ann. Phys. Leipzig,* 24, 636, 1935). In this case the relations should maintain the validity also for less diluted suspensions. The first papers concerning mixtures of ellipsoids were written by Fricke (H. Fricke, *J. Phys. Chem*., 57, 934, 1953 and H. Fricke, *Phys. Rev*., 24, 575, 1924) dealing with the electrical characterization of inhomogeneous biological tissues containing spheroidal particles: he found out some explicit relationships that simply were an extension of the Maxwell formula to the case with ellipsoidal inclusions. In current literature Maxwell's relation for spheres and Fricke's expressions for ellipsoids are the so-called Maxwell-Garnett Effective Medium Theory results: both theories hold on under the hypothesis of the very low concentration of the dispersed component. In recent literature some applications of the Bruggeman procedure to mixtures of ellipsoids have been shown in connection with the problem of characterizing the dielectric response of water-saturated rocks (P. N. Sen, C. Scala, M. H. Cohen, *Geophysics*, 46, 781, 1981, K. S. Mendelson, M. H. Cohen, *Geophysics*, 47, 257, 1982, P. N. Sen, *Geophysics*, 49, 586, 1984). In these works the authors have shown that the Bruggeman method, applied to this specific problem, leads to results in good agreement with the empirical Archie's law (G. E. Archie, *Pet. Tech*., 5, 1, 1942), which describes the dependence of the dc conductivity of brine-saturated sedimentary rocks on porosity. In general, the electrical (thermal, elastic and so on) properties of composite materials are strongly microstructure dependent. The relationships between microstructure and properties may be used for designing and improving materials, or conversely, for interpreting experimental data in terms of micro-structural features. Ideally, the aim is to construct a theory that employs general micro-structural information to make some accurate property predictions. A simpler goal is the provision of property for different class of microstructures. A great number of works has been devoted to describe the relationship between microstructure and properties: a functional unifying approach has been applied to better understand the intrinsic mathematical properties of a general mixing formula (B. Bianco, M. Parodi, *J. Electr*., 15, 183, 1984). A fundamental result is given by the Hashin-Shtrikman's variational analysis (Z. Hashin, S. Shtrikman*, J. Appl. Phys*., 33, 3125, 1962 and S. Hashin, J. Shtrikman, *Mech. Phys. Solids*., 10, 335, 1962), which provides an upper and lower bound for composite materials, irrespective of the microstructure. In particular, for a two-phase material, these bounds are given by two expressions of the Maxwell-Fricke type. Finally, a method to find the relation between the spatial correlation function of the dispersed component and the final properties of the material is derived from the Brown (W. F. Brown, *J. Chem. Phys*., 23, 1514, 1955) and Torquato (S. Torquato, *J. Mech. Phys. Solids*, 45, 1421, 1997 and S. Torquato, *J. Mech. Phys. Solids*, 46, 1411, 1998) expansions.

Some other types of microstructures have been taken into consideration. For example, the problem of the mixture characterization has been exactly solved in the case of linear and nonlinear random mixtures, that is, materials for which the various components are isotropic, linear and mixed together as an ensemble of particles having random shapes and positions. This approach permits to apply the mixture theories to dielectric poly-crystals and random networks.

In this section, we describe some generalizations of the Maxwell-Garnett theory obtained by means of the differential scheme and by considering the nonlinear behavior of the materials forming the whole system. In particular, we briefly review the Maxwell-Garnett theory and we present some generalization based on the differential scheme (both for aligned and random oriented ellipsoids). Then, we cope with the problem of homogenizing a dispersion of nonlinear particle embedded in a linear matrix. We obtain the mixing rule for the hypersusceptibility of the material.

The theory for dispersion of aligned ellipsoids is based on the following result, which describes the behavior of a single ellipsoidal particle (ε_2) embedded in a homogeneous medium (ε_1). Let the axes of the ellipsoid be $a_x=a_1$, $a_y=a_2$ and $a_z=a_3$ (aligned with axes x, y, z of the reference frame) and let a uniform electrical field $\vec{E}_0 = \left(E_{0x}, E_{0y}, E_{0z}\right)$ applied to the structure. Then, a uniform electrical field appears inside the ellipsoid and it can be computed as follows. We define the function

$$R(s) = \sqrt{\left(s + a_x^{\,2}\right)\left(s + a_y^{\,2}\right)\left(s + a_z^{\,2}\right)} \quad (1)$$

and the depolarization factors along each axis

$$L_j = \frac{a_x a_y a_z}{2} \int_0^{+\infty} \frac{ds}{\left(s + a_j^{\,2}\right) R(s)} \quad (2)$$

We remark that $L_x+L_y+L_z=1$. Therefore, the electrical field inside the ellipsoid is given, in components, by

$$E_{sj} = \frac{E_{0j}}{1 + L_j \dfrac{\varepsilon_2 - \varepsilon_1}{\varepsilon_1}} \qquad (3)$$

This is the main result that plays an essential role in the further development of the theory. Now, we are ready to consider a dispersion of aligned ellipsoids (ε_2) embedded in a homogeneous medium (ε_1), see Fig. 1. Moreover, let c be the volume fraction of the embedded ellipsoids. To begin, we consider a diluted dispersion ($c<<1$) and thus we may evaluate the average value of the electrical field over the mixture volume by means of the following relationship

$$\langle E_j \rangle = cE_{sj} + (1 - c)E_{0j} \qquad (4)$$

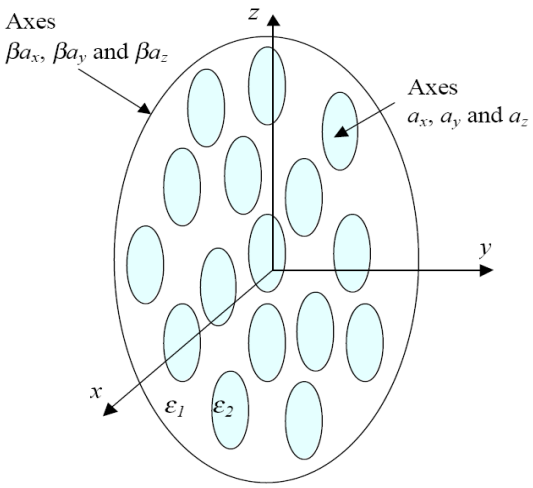

Figure 1. Structure of a dispersion of aligned ellipsoids. The external surface of the mixture is a greater ellipsoid with the same shape of the inclusions.

This means that we do not take into account the interactions among the inclusions because of the very low concentration: each little ellipsoid behaves as a single one in the whole space. Once more, to derive Eq. (4), we approximately take into account a uniform electrical field $\vec{E}_0 = (E_{0x}, E_{0y}, E_{0z})$ in the space outside the inclusions. To define the mixture we are going to characterize, we consider a greater ellipsoid, which contains all the other ones. This ellipsoid represents the external surface of the composite materials (see Fig. 1). As one can simply verify, the depolarization factors of this ellipsoid are the same of each inclusion contained in the mixture. Moreover, we may observe that the overall behavior of the mixture is anisotropic because of the alignment of the ellipsoidal particles. So, if we define the equivalent principal permittivity of the mixture along the axes x, y and z as $\varepsilon_{eff,x}$, $\varepsilon_{eff,y}$ and $\varepsilon_{eff,z}$, we may write down these expressions for the average value of the components of the electrical field inside the whole mixture

$$\langle E_j \rangle = \frac{E_{0j}}{1 + L_j \dfrac{\varepsilon_{eff,j} - \varepsilon_1}{\varepsilon_1}} \qquad (5)$$

These expressions are derived considering the whole mixture as a single inclusion in the space and then we have used the basic result given by Eq. (3). Now, by substituting Eq. (3) in Eq. (4) and by drawing a comparison with Eq. (5) we may find expressions for $\varepsilon_{eff,x}$, $\varepsilon_{eff,y}$ and $\varepsilon_{eff,z}$, which are the effective principal permittivities of the whole composite material

$$\varepsilon_{eff,j} = \varepsilon_1 + c(\varepsilon_2 - \varepsilon_1)\frac{1}{1 + (1 - c)L_j \dfrac{\varepsilon_2 - \varepsilon_1}{\varepsilon_1}} = \varepsilon_1 + c(\varepsilon_2 - \varepsilon_1)\frac{1}{1 + L_j \dfrac{\varepsilon_2 - \varepsilon_1}{\varepsilon_1}} + O(c^2) \qquad (6)$$

Each of the three independent relations, which appears in Eq. (2.6), may be recast in the unified form $\varepsilon=F(\varepsilon_1,\varepsilon_2,c)$ where ε represents $\varepsilon_{eff,x}$, $\varepsilon_{eff,y}$ or $\varepsilon_{eff,z}$. We use this very simple form to review the Bruggeman procedure (or differential scheme) that is the method to find a second mixture relationship considering a first theory describing the composite material (actually the function F). This second theory is usually more efficient than the first one, even if the mixture is not strongly diluted. In Bruggeman scheme the initially low concentration is gradually

increased by infinitesimal additions of the dispersed component. We start from $\varepsilon=F(\varepsilon_1,\varepsilon_2,c)$ for a mixture where c is the volume fraction of ellipsoids: we consider a unit volume of the mixture (1m^3) and we add a little volume dc_0 of inclusions. Therefore, we consider another mixture between a medium with permittivity ε (volume equals to 1 m^3) and a second medium (ε_2) with volume dc_0. In these conditions the volume fraction of the second medium will be $dc_0/(1+dc_0)\approx dc_0$. So, using the original relation for the mixture we can write: $\varepsilon+d\varepsilon=F(\varepsilon,\varepsilon_2,dc_0)$. In the final composite material, with the little added volume dc_0, the matrix (ε_1) will have effective volume *1-c* and the dispersed medium (ε_2) will have effective volume $c+dc_o$. The original volume fraction of the second medium is $c/1$ and the final one is $(c+dc_0)/(1+dc_0)$; so, it follows that the variation of the volume fraction of inclusions obtained by adding the little volume dc_0 is simply given by: $dc=(c+dc_0)/(1+dc_0)-c/1=dc_0(1-c)/(1+dc_0)\approx dc_0(1-c)$. Therefore, we have $\varepsilon+d\varepsilon=F(\varepsilon,\varepsilon_2,dc/(1-c))$. With a first order expansion we simply obtain: $\varepsilon+d\varepsilon=F(\varepsilon,\varepsilon_2,0)+\left.\frac{\partial F(\varepsilon,\varepsilon_2,c)}{\partial c}\right|_{c=0}\frac{dc}{1-c}$ and taking into account the obvious relation $\varepsilon=F(\varepsilon,\varepsilon_2,0)$ we obtain the differential equation: $\frac{d\varepsilon}{dc}=\frac{1}{1-c}\left.\frac{\partial F(\varepsilon,\varepsilon_2,c)}{\partial c}\right|_{c=0}$. This equation, when the function F is given, defines a new function, which should better describe the mixture when it is not strongly diluted. We may apply the method to the three expressions given in Eq. (6) obtaining a differential equation, which may be easily solved with the auxiliary conditions $\varepsilon_{eff,j}(c=0)=\varepsilon_1$

$$1-c=\frac{\varepsilon_2-\varepsilon_{eff,j}}{\varepsilon_2-\varepsilon_1}\left(\frac{\varepsilon_1}{\varepsilon_{eff,j}}\right)^{L_j}\quad(j=x,y,z)\qquad(7)$$

These are the final expressions, which characterize a dispersion of aligned ellipsoids, obtained by means of the Bruggeman approach.

We start now the characterization of dispersions of randomly oriented ellipsoids. To begin, we are interested in the electrical behavior of a single ellipsoidal inclusion (ε_2) arbitrarily oriented in the space and embedded in a homogeneous medium (ε_1). We define three unit vectors, which indicate the principal directions of the ellipsoids in the space: they are referred to as $\hat{n}_x,\hat{n}_y$ and $\hat{n}_z$ and they are aligned with the axes a_x, a_y and a_z of the ellipsoid, respectively. By using Eq. (3), we may compute the electrical field inside the inclusion, induced by a given external uniform electric field

$$\vec{E}_s=\frac{\left(\vec{E}_0\cdot\hat{n}_x\right)\hat{n}_x}{1+L_x\frac{\varepsilon_2-\varepsilon_1}{\varepsilon_1}}+\frac{\left(\vec{E}_0\cdot\hat{n}_y\right)\hat{n}_y}{1+L_y\frac{\varepsilon_2-\varepsilon_1}{\varepsilon_1}}+\frac{\left(\vec{E}_0\cdot\hat{n}_z\right)\hat{n}_z}{1+L_z\frac{\varepsilon_2-\varepsilon_1}{\varepsilon_1}}\qquad(8)$$

For the following derivation, we are interested in the average value of the electrical field inside the ellipsoid over all the possible orientations of the ellipsoid itself and then we have to compute the average value of the quantity $n_{j,k}$ $n_{j,q}$. Performing the integration over the unit sphere (by means of spherical coordinates) we obtain, after some straightforward computations, $\left\langle n_{j,k}n_{j,q}\right\rangle=\frac{1}{3}\delta_{k,q}$. Therefore, the average value of the electrical field (inside the randomly oriented inclusion), may be written as

$$\left\langle E_{s,q}\right\rangle=\frac{E_{0,q}}{3}\sum_{j}^{x,y,z}\frac{1}{1+L_j\frac{\varepsilon_2-\varepsilon_1}{\varepsilon_1}}\qquad(9)$$

Now, we are ready to consider a mixture of randomly oriented ellipsoids. In Fig. 2 one can find the structure of the composite material. We may define the volume of the mixture by means of a sphere which contains all the ellipsoidal inclusions and which represents the external surface of the heterogeneous material. Once more, let c be the volume fraction of the embedded ellipsoids. The average value of the electrical field over the mixture (inside the sphere) is approximately computed as follows

$$\left\langle\vec{E}\right\rangle=(1-c)\vec{E}_0+c\frac{\vec{E}_0}{3}\sum_{j}^{x,y,z}\frac{1}{1+L_j\frac{\varepsilon_2-\varepsilon_1}{\varepsilon_1}}\qquad(10)$$

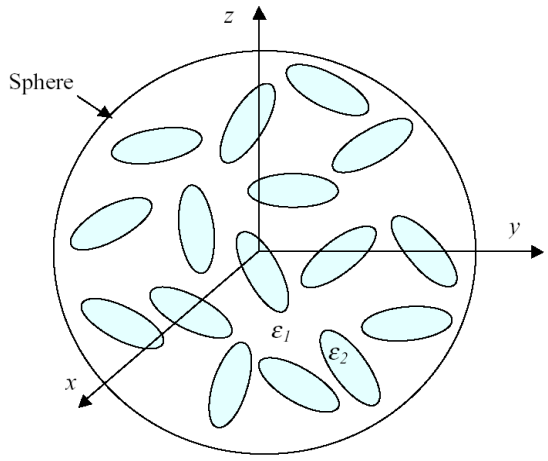

Figure 2. Structure of a dispersion of randomly oriented ellipsoids.

Then, we define ε as the effective permittivity of the whole mixture (which is isotropic because of the randomness of the orientations) by means of the relation $\langle \vec{D} \rangle = \varepsilon \langle \vec{E} \rangle$; to evaluate ε we may compute the average value of the displacement vector inside the random material. We also define V as the total volume of the mixture, V_e as the total volume of the embedded ellipsoids and V_o as the volume of the remaining space among the inclusions (so that $V=V_e \cup V_o$). The average value of $\vec{D}(\vec{r}) = \varepsilon(\vec{r})\vec{E}(\vec{r})$ is evaluated as

$$\begin{aligned}\langle \vec{D} \rangle &= \frac{1}{V}\int_V \varepsilon(\vec{r})\vec{E}(\vec{r})d\vec{r} = \frac{1}{V}\varepsilon_1 \int_{V_o} \vec{E}(\vec{r})d\vec{r} + \frac{1}{V}\varepsilon_2 \int_{V_e} \vec{E}(\vec{r})d\vec{r} = \\ &= \frac{1}{V}\varepsilon_1 \int_{V_o} \vec{E}(\vec{r})d\vec{r} + \frac{1}{V}\varepsilon_1 \int_{V_e} \vec{E}(\vec{r})d\vec{r} + \frac{1}{V}\varepsilon_2 \int_{V_e} \vec{E}(\vec{r})d\vec{r} - \frac{1}{V}\varepsilon_1 \int_{V_e} \vec{E}(\vec{r})d\vec{r} = \\ &= \varepsilon_1 \langle \vec{E} \rangle + c(\varepsilon_2 - \varepsilon_1)\langle \vec{E}_s \rangle\end{aligned} \quad (11)$$

By using previous expressions we may find a complete expression, which allows us to estimate the equivalent permittivity ε and its first order expansion with respect to the volume fraction c

$$\varepsilon = \varepsilon_1 + \frac{\frac{1}{3}c(\varepsilon_2 - \varepsilon_1)\sum_j^{x,y,z} \frac{\varepsilon_1}{\varepsilon_1 + L_j(\varepsilon_2 - \varepsilon_1)}}{1 + c\left[\frac{1}{3}\sum_j^{x,y,z} \frac{\varepsilon_1}{\varepsilon_1 + L_j(\varepsilon_2 - \varepsilon_1)} - 1\right]} = \varepsilon_1 + \frac{1}{3}c\varepsilon_1(\varepsilon_2 - \varepsilon_1)\sum_j^{x,y,z} \frac{1}{\varepsilon_1 + L_j(\varepsilon_2 - \varepsilon_1)} + O(c^2) \quad (12)$$

This result concerns the characterization of a very diluted dispersion of randomly oriented ellipsoids with given shape (i.e. with fixed depolarization factors L_j or eccentricities e and g). As before, to adapt this relationship to arbitrarily diluted composite materials we use the Bruggeman procedure, which leads to the following differential equation

$$\frac{d\varepsilon}{dc} = \frac{1}{1-c}\varepsilon(\varepsilon_2 - \varepsilon)\frac{1}{3}\sum_j^{x,y,z} \frac{1}{\varepsilon + L_j(\varepsilon_2 - \varepsilon)} \quad (13)$$

The solution of this equation depends on the values of the depolarization factors showing the relationship between the overall permittivity and the shape of the ellipsoidal inclusions. We search for the solution in two particular cases: a dispersion of ellipsoids of rotation and a dispersion of generally shaped ellipsoids. In the first case we have $L_x=L_y$ and $2L_x+L_z=1$ and thus only one factor completely defines the shape of the inclusions. The solution of Eq. (13) yields the final result

$$1 - c = \frac{\varepsilon_2 - \varepsilon}{\varepsilon_2 - \varepsilon_1}\left(\frac{\varepsilon_1}{\varepsilon}\right)^{\frac{3L(1-2L)}{2-3L}}\left[\frac{(1+3L)\varepsilon_1 + (2-3L)\varepsilon_2}{(1+3L)\varepsilon + (2-3L)\varepsilon_2}\right]^{\frac{2(3L-1)^2}{(2-3L)(1+3L)}} \quad (14)$$

where $L=L_x$ represents the depolarization factor along the directions orthogonal to the principal axes of each inclusion. To complete the study we analyze a mixture of ellipsoids with three independent axes. For such generally shaped ellipsoids the relation $L_x+L_y+L_z=1$ holds true and therefore we may use two factors (L_x and L_y) as parameters which completely define the shape of the inclusions. To simply integrate Eq. (13) we define the following quantities

$$\begin{cases} A = 3L_x^2 L_y + 3L_x L_y^2 - 3L_x L_y \\ B = L_x + L_y - 6L_x^2 L_y^2 - 8L_x L_y - 4L_x^3 L_y - 4L_x L_y^3 + \\ \quad + 11L_x^2 L_y + 11L_y^2 L_x - 3L_x^2 - 3L_y^2 + 4L_x^3 + 4L_y^3 - 2L_x^4 - 2L_y^4 \\ C = 4L_x^3 L_y + 4L_x L_y^3 - 2L_x L_y - 2L_x^2 L_y - 2L_y^2 L_x + 6L_x^2 L_y^2 + \\ \quad + 2L_x^2 + 2L_y^2 - 4L_x^3 - 4L_y^3 + 2L_x^4 + 2L_y^4 \\ D = L_x L_y - L_x - L_y + L_x^2 + L_y^2 \end{cases} \tag{15}$$

By means of a lengthy but straightforward integration we have found the solution as follows

$$1 - c = \frac{\varepsilon_2 - \varepsilon}{\varepsilon_2 - \varepsilon_1}\left(\frac{\varepsilon_1}{\varepsilon}\right)^{\frac{A}{D}}\left[\frac{(D-1)\varepsilon_1^2 - 2(D+1)\varepsilon_1\varepsilon_2 + D\varepsilon_2^2}{(D-1)\varepsilon^2 - 2(D+1)\varepsilon\varepsilon_2 + D\varepsilon_2^2}\right]^{\frac{B}{2D(D-1)}} \cdot$$

$$\cdot\left[\frac{\sqrt{1+3D}\,\varepsilon_2 + (D-1)\varepsilon - (D+1)\varepsilon_2}{\sqrt{1+3D}\,\varepsilon_2 + (D-1)\varepsilon_1 - (D+1)\varepsilon_2}\,\frac{\sqrt{1+3D}\,\varepsilon_2 - (D-1)\varepsilon_1 + (D+1)\varepsilon_2}{\sqrt{1+3D}\,\varepsilon_2 - (D-1)\varepsilon + (D+1)\varepsilon_2}\right]^{\frac{B(D+1)+C(D-1)}{2D(D-1)\sqrt{1+3D}}} \tag{16}$$

The complete model describes the equivalent permittivity as function of the following parameters: the permittivities of the two involved materials ε_2 and ε_1, the volume fraction c of the embedded ellipsoids and the characteristic eccentricities e and g. Finally, $\varepsilon = \varepsilon(\varepsilon_1, \varepsilon_2, c, e, g)$.

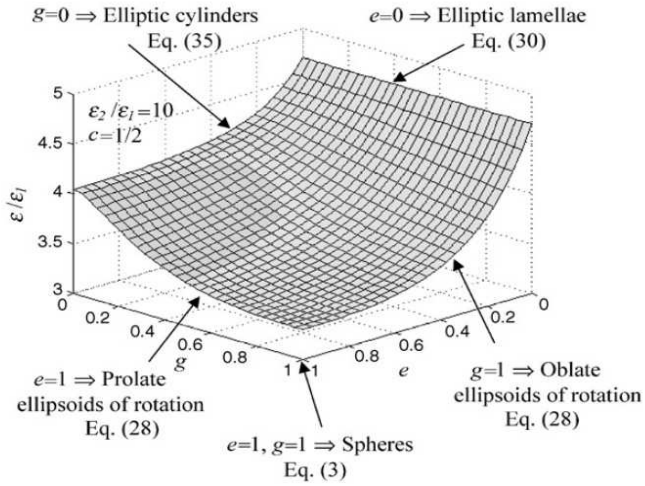

Figure 3. Results for a mixture of randomly oriented and generally shaped ellipsoids. The surface $\varepsilon/\varepsilon_1$ versus the eccentricities e and g is shown with the assumptions $\varepsilon_2/\varepsilon_1=10$ and $c=1/2$.

The irrational Eq. (16) has been numerically solved and a typical result is shown in Fig. 3 where one can deduce the effects of the shape of the inclusions on the effective macroscopic dielectric constant of the material. The limiting cases of interest have been clearly indicated.

When the above procedure is implemented for evaluating the aforesaid permittivity, a sensible dependence of the results on the shape of the inclusions (actually on the eccentricities) is shown. The closed form analysis of a dispersion of ellipsoids offers a simple but clear example of the dependence of the macroscopic behavior of composite materials on the microstructure or microscopic morphology. The results may suggest a hint for explaining why sometimes there are some inconsistencies between the standard mixture formulae and corresponding experiments: typically, standard formulae are based on the Maxwell relation for a mixture of spheres and do not take into account any different shapes of the inclusions, which may be present in actual heterogeneous

media.

In recent material science development, considerable attention has been devoted to electromagnetically nonlinear composite structures due to their applications, for instance, to integrated optical devices (such as optical switching and signal processing devices) . Many attempts have been made in order to take into account dielectric nonlinearity in the constitutive equations of the phases of a composite structure. A systematic perturbation expansion method was developed and employed to solve electrostatic and quasi-static boundary values problems of weakly nonlinear media (K. W. Yu, P. M. Hui, D. Stroud, *Phys. Rev. B,* 47, 14150, 1993). The results have been verified by means of numerical simulation (X. Zhang, D. Stroud, *Phys. Rev. B*, 49, 944, 1994). A lot of work has also been devoted to the analysis of the huge enhancing, caused by local field effects, of the effective cubic nonlinearity in random structures of poly-crystals (D. Stroud, *Phys. Rev. B*, 54, 3295, 1996, S. Barabash, D. Stroud, *J. Phys.: Cond. Matt*., 11, 10323, 1999, B. Liu, L. Gao, K. W. Yu, *Phys. Rev. B,* 72, 214208, 2005, M. N. Lakhtakia, A. Lakhtakia, Electromagnetics, 21, 129-138, 2001, T. G. Mackay, A. Lakhtakia, W. S. Weiglhofer, *Optics Communications*, 204, 219, 2002). Finally, the problems of second and third harmonic generation in random, dielectrically nonlinear composites have been tackled and fully general expressions for the equivalent second- and third-order hypersusceptibilities have been given in terms of the nonlinear behavior of the constituents (P. M. Hui, D. Stroud*, J. Appl. Phys.,* 82, 4740, 1997, P. M. Hui, P. Cheung, D. Stroud, J. Appl. Phys., 84, 3451, 1998).
In all of these cases, a linear medium has been considered containing spherical inclusions randomly located, or at most spheroidal inclusions having fixed orientation. In the following, we consider a dispersion of dielectrically nonlinear ellipsoidal particles randomly oriented in a linear matrix and we describe the results of a mathematical procedure able to perform the needed averages of the electric quantities over all orientations of the inclusions. A nonlinear isotropic and homogenous ellipsoid can be described from the electrical point of view by the constitutive equation $\vec{D} = \varepsilon(E)\vec{E}$, where $\vec{D}$ is the electric displacement inside the particle, $\vec{E}$ is the electric field and the function ε depends only on the modulus of $\vec{E}$.
We present a general solution to the problem of a nonlinear ellipsoidal particle embedded in a linear material. The theory is based on the following result derived for the linear case, which describes the behavior of one electrically linear ellipsoidal particle of permittivity ε_2 in a linear homogeneous medium of permittivity ε_1. As before, let the axes of the ellipsoid be a_x, a_y and a_z (aligned with axes x, y, z of ellipsoid reference frame) and let a uniform electric field $\vec{E}_0 = \left(E_{0x}, E_{0y}, E_{0z}\right)$ be applied to the structure. As above discussed, the electric field $\vec{E}_s = \left(E_{sx}, E_{sy}, E_{sz}\right)$ inside the ellipsoid is uniform and it can be expressed as follows

$$E_{si} = \frac{E_{0i}}{1 + L_i\left(\varepsilon_2/\varepsilon_1 - 1\right)} \quad (17)$$

The main result follows: the electric field inside the inclusion is uniform even in the nonlinear case and it may be calculated by means of the following system of equations

$$E_{si} = \frac{E_{0i}}{1 + L_i\left[\varepsilon\left(E_s\right)/\varepsilon_1 - 1\right]} \quad (18)$$

If a solution of Eq.(18) exists, due to self-consistency, all the boundary conditions are fulfilled and the problem is completely analogous to its linear counterpart, provided that $\varepsilon_2 = \varepsilon\left(E_s\right)$.
The principal aim is to extend these results, holding for a single inclusion, to a mixture of randomly oriented nonlinear ellipsoids in a linear homogeneous matrix. The permittivity of the inclusions is described by the isotropic nonlinear relation $\varepsilon(E) = \varepsilon_2 + \alpha E^2$ and the linear matrix has permittivity ε_1. The overall permittivity function of the dispersion is expected to be isotropic because of the random orientation of the particles and therefore it can be expanded in series with respect to the field modulus $\varepsilon(E) = \varepsilon_{eff} + \beta E^2 + \delta E^4 + \ldots$, where the parameters depend on various parameters of the mixture such as the eccentricities of the ellipsoids, the volume fraction c of the included phase, the permittivities ε_1, ε_2 and α. The homogenization procedure should provide the coefficients ε_{eff} and $\boldsymbol{\beta}$ in terms of the mentioned parameters. In the technical literature, the coefficients α and $\boldsymbol{\beta}$ of the first nonlinear term of the expanded constitutive equations for inclusions and mixture, respectively, are often called hyper-susceptibilities. The result is derived under the assumption of Kerr-like constitutive equation of the composite medium that is of the form $\varepsilon(E) = \varepsilon_{eff} + \beta E^2$, which neglects higher order terms.

To begin the analysis, we substitute $\varepsilon(E) = \varepsilon_2 + \alpha E^2$ holding for a single ellipsoid, in Eq.(18) describing the internal field and we obtain the solution

$$\vec{E}_s = \sum_i \left[\frac{\varepsilon_1 \vec{E}_0 \cdot \hat{n}_i}{b_i} - \frac{\alpha \varepsilon_1^{\,3} L_i \vec{E}_0 \cdot \hat{n}_i}{b_i^{\,2}} \sum_j \frac{\left(\vec{E}_0 \cdot \hat{n}_j\right)^2}{b_j^{\,2}} \right] \hat{n}_i \qquad (19)$$

where $b_i = (1 - L_i)\varepsilon_1 + L_i \varepsilon_2$. We observe that the first term represents the classical Lorentz field appearing in a dielectric linear ellipsoidal inclusion. The second term is the first nonlinear contribution, which is directly proportional to the inclusion hyper-susceptibility. The principal directions of each ellipsoid in space are referred to as $\hat{n}_x, \hat{n}_y$ and $\hat{n}_z$, and they correspond to the axes a_x, a_y and a_z of the ellipsoid.

We shall now average it over all the possible orientations of the particle. The result of the process is the following

$$\left\langle \vec{E}_s \right\rangle = \vec{E}_0 \left(\varepsilon_1 M - \alpha \varepsilon_1^{\,3} E_0^{\,2} N \right) \qquad (20)$$

where *M* and *N* depend on the linear term of the permittivities and on the geometry of the inclusions

$$M = \frac{1}{3} \sum_{i=1,2,3} \frac{1}{b_i} \qquad N = \frac{1}{15} \left[\sum_{i=1,2,3} \sum_{j=1,2,3} \frac{L_i}{b_i^{\,2} b_j^{\,2}} + 2 \sum_{i=1,2,3} \frac{L_i}{b_i^{\,4}} \right] \qquad (21)$$

We note that the average field inside the particle is aligned with the external field and thus the average behavior of the inclusion is isotropic. If we now consider a mixture with a volume fraction $c<<1$ of randomly oriented, nonlinear ellipsoids embedded in a homogeneous matrix with permittivity ε_1, we can evaluate a different kind of average, the one of the electric field over all of the space occupied by the mixture. It can be done via the following relationship $\left\langle \vec{E} \right\rangle = c \left\langle \vec{E}_s \right\rangle + (1 - c)\vec{E}_0$. This means that we do not take into account the interactions among the inclusions because of the very low concentration: each ellipsoid behaves as an isolated one. To evaluate the equivalent constitutive equation, we compute the average value of the displacement vector inside the random material

$$\left\langle \vec{D} \right\rangle = \varepsilon_1 \left\langle \vec{E} \right\rangle + c\varepsilon_1 (\varepsilon_2 - \varepsilon_1) M \vec{E}_0 + c\alpha \varepsilon_1^{\,4} P E_0^{\,2} \vec{E}_0 \qquad (22)$$

where *P* is defined as:

$$P = \frac{1}{15} \left[\sum_{i=1,2,3} \sum_{j=1,2,3} \frac{1}{b_i^{\,2} b_j^{\,2}} + 2 \sum_{i=1,2,3} \frac{1}{b_i^{\,4}} \right] \qquad (23)$$

From these results it follows that all the averaged vector quantities are aligned with $\vec{E}_0$, therefore, we can continue our computations with scalar quantities; moreover, from now on, we will leave out the average symbols $\langle \cdot \rangle$. The main equations may then be rewritten as

$$\begin{cases} E_s = \varepsilon_1 M E_0 - \alpha \varepsilon_1^{\,3} E_0^{\,3} N \\ E = c E_s + (1 - c) E_0 \\ D = \varepsilon_1 E + c\varepsilon_1 (\varepsilon_2 - \varepsilon_1) M E_0 + c\alpha \varepsilon_1^{\,4} P E_0^{\,3} \end{cases} \qquad (24)$$

By solving this system, we search for a relation between *D* and *E:* after straightforward calculations, the nonlinear constitutive equation for the composite medium has found in the form $\vec{D} = \varepsilon(E)\vec{E} = \left(\varepsilon_{eff} + \beta E^2\right)\vec{E}$, where

$$\varepsilon_{eff} = \varepsilon_1 + \frac{c\varepsilon_1 (\varepsilon_2 - \varepsilon_1) M}{(1 - c + c\varepsilon_1 M)} = \varepsilon_1 \frac{1 - c + c\varepsilon_2 M}{1 - c + c\varepsilon_1 M} \qquad (25)$$

$$\frac{\beta}{\alpha} = c\varepsilon_1^{\,4} \frac{P + c\left[(\varepsilon_2 - \varepsilon_1) MN + P(\varepsilon_1 M - 1)\right]}{(1 - c + c\varepsilon_1 M)^4} \qquad (26)$$

The already mentioned quantities *M*, *N* and *P*, depend only on geometrical factors (ellipsoid eccentricities) and on the linear terms of the permittivities. Eq. (25), giving the linear approximation for the permittivity, coincides with the Maxwell-Garnett formula for a dispersion of ellipsoids, Eq. (12). Moreover, Eq. (26) represents the mixture to inclusion hyper-susceptibility ratio.

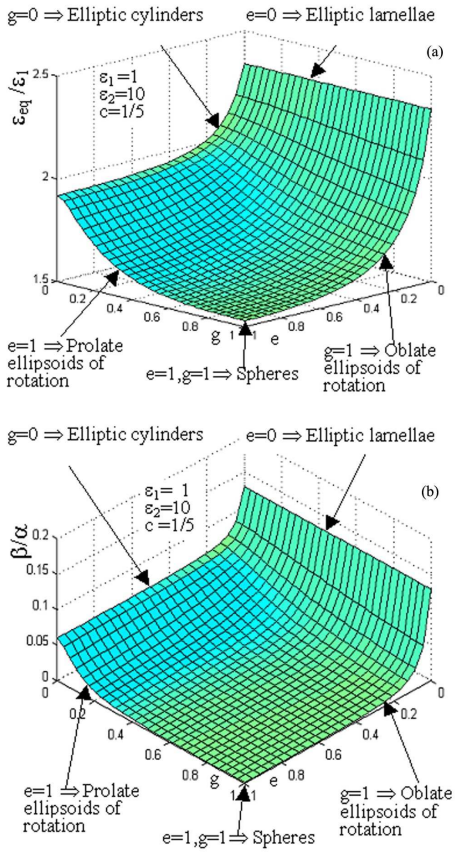

Figure 4. Plots of the surfaces $\varepsilon_{eq}/\varepsilon_1$ and β/α versus the eccentricities which define the shape of the particles with $\varepsilon_1=1$, $\varepsilon_2=10$ and $c=1/5$.

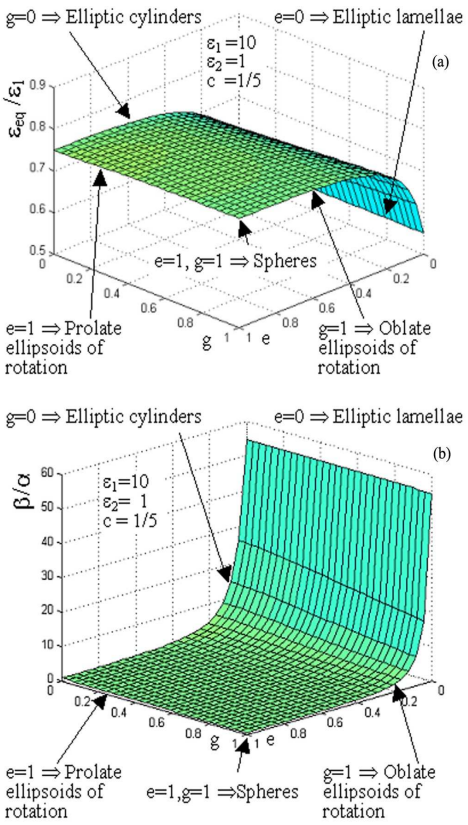

Figure 5. The same plots of Figure 4 with the assumptions $\varepsilon_1=10$, $\varepsilon_2=1$ and $c=1/5$. The amplification of the hyper-susceptibility assumes the greatest values when $\varepsilon_1>\varepsilon_2$ and we are dealing with elliptic lamellae.

The methodology was applied to examine the actual effects of particle nonsphericity on mixtures. In Fig. 4 and 5 we show plots of the properties of the overall mixture as a function of the eccentricities of the ellipsoids composing the mixture itself. In Fig. 4 one can see the plots of the effective quantities quantities versus the aspect ratios $0< e = a_x/a_y <1$ and $0< g = a_y/a_z <1$ defining the shape of the particles, derived from our results with $\varepsilon_1=1$, $\varepsilon_2=10$ and $c=1/5$. In Fig. 5 the same plots are derived with the following parameter values: $\varepsilon_1=10$, $\varepsilon_2=1$ and $c=1/5$. In both cases we may observe that the amplification of the hyper-susceptibility assumes the greatest values when dealing with planar nonlinear particles (elliptic lamellae). More surprisingly, hyper-susceptibility ratio tends to assume its highest values (greater than 50) when $\varepsilon_1>\varepsilon_2$.

2.1.2.Homogenization of random networks and mixtures

(*B. Bianco, A. Chiabrera, S. Giordano, D.C.-E.L.F. characterization of random mixtures of piecewise non-linear media, Bioelectromagnetics, 21, pp. 145-149, 2000, B. Bianco, S. Giordano, Electrical characterization of linear and non-linear random networks and mixtures, International Journal of Circuit Theory and Applications, Volume 31/2, 2003, pp. 199-218, S. Giordano, Disordered lattice networks: general theory and simulations, International Journal of Circuit Theory and Applications, 33, 2005, pp. 519-540, S. Giordano, Two-dimensional disordered lattice networks with substrate, Physica A: Statistical Mechanics and its Applications, Volume 375, Issue 2 , 1 March 2007, Pages 726-740*)

Disordered resistors networks have been, for many years, very useful tools to model transport phenomena in heterogeneous or composite physical systems. The first studies, from a general point of view, were developed by Kirkpatrick in the context of the isotropic transport and the percolation in random lattice (Kirkpatrick S. Classical transport in disordered media: Scaling and Effective-Medium Theories, Physical Review Letters 1971; 27, 1722-1725, Kirkpatrick S. Percolation and conduction. Reviews of Modern Physics 1973; 45, 574-588). In these works, the theoretical description of conduction was provided by a so-called effective medium theory. This theory, originally formulated to describe the conductivity of binary mixture, has been extended and adapted to treat disordered networks. Moreover, some attempts to generalise the theory to anisotropic random networks were made to clarify some general aspects of conduction in anisotropic materials (Bernasconi J., Conduction in anisotropic disordered systems: effective-medium theory. Physical Review B 1974; 9, 4575-4579). During the evolution of such theories many approaches have been used to obtain statistical information about the behaviour of heterogeneous systems. Theoretical circuit theory approaches have been adopted to obtain the electrical properties of statistical mixtures (Bianco B, Degani G. Conductivity of mixtures: exact calculation in a particular case. *Alta Frequenza* 1981; **2**L: 113-115, Bianco B, Parodi M, Degani G. A circuit approach for deriving the electrical properties of statistical mixtures. *Alta Frequenza* 1982; **2**LI: 80-85). More recently, the theories for linear random networks have been generalised to the case of non-linear random networks obtaining the equivalent non-linear behaviour of such heterogeneous systems (Bianco B, Chiabrera A, Giordano S. D.C. Characterisation of random mixtures of piecewise non-linear media. *Bioelectromagnetics* 2000; 21: 145-149, Bianco B, Giordano S. Electrical characterisation of linear and non-linear random networks and mixtures. International Journal of Circuit Theory and Applications 2003; 31, 199-218).

In all these cases the most considered topology is the simple two- or three-dimensional grid of resistors, which mimics the heterogeneity in two- or three-dimensional composite materials. Here, we devote our attention to a generalised topology where each node of the grid is connected to another external node (called substrate in the following) by means of a given resistors. In Fig. 1 one can find an example of such network for two-dimensional systems. The random character of the network may regard the resistors in the grid or the resistors towards the substrate or in the more complex case both of them. So, to obtain a general theory we develop our calculations for an arbitrary *n*-dimensional lattice with substrate. Moreover, the statistical distribution of the resistor values in the grid may follow different probability laws in the different directions of the grid. This possibility allows us to describe anisotropy of the system. In actual applications the most important particular cases for such a topology are the following: (i) the one-dimensional case, which corresponds to a classical ladder network, (ii) the two-dimensional anisotropic or isotropic case with or without substrate (useful to describe two-dimensional mixtures or films deposited on substrates with electric interaction), (iii) three-dimensional isotropic, transversely isotropic or completely anisotropic networks without substrate (in three-dimensional cases the substrate has not physical meaning, except for some theoretical applications).

The method applied to develop the general theory is based on two main steps: firstly an analysis of the homogeneous networks with substrate based on the lattice Green's functions is performed. This approach (Cserti J. Application of the lattice Green's function for calculating the resistance of an infinite network of resistors. Am. J. Phys. 2000; 68, 896-906, Delves RT, Joyce GS. Exact evaluation of the Green function for the anisotropic simple cubic lattice. J. Phys. A: Math. Gen. 2001; 34, 59-65) permits to obtain exact results about the electrical behaviour

of infinite regular lattice networks. The second step consists in applying an *ad hoc* averaging procedure based on the effective medium theory. This approach is a generaisation of the standard one in order to take into account the electrical interaction with the substrate. The application of the two steps allows us to find a strong conceptual connection between the lattice Green's function of the network and the problem of obtain the average behaviour of random grids. In other words, we may say that the lattice Green's functions introduced in this work are a very useful tool to develop effective medium theories for general topology networks. All the theoretical results have been verified by means of numerical Monte-Carlo simulations obtaining a remarkably good agreement between numerical and theoretical values. Finally, the general theory for such kind of networks has a strong application to the random walks theory of arbitrary dimensionality (Maassarani Z. Series expansions for lattice Green functions. J. Phys. A: Math. Gen. 2000; 33: 5675-5691, Hughes BD. *Random Walks and Random Environments*, vol. 1. Oxford University Press, 1965).

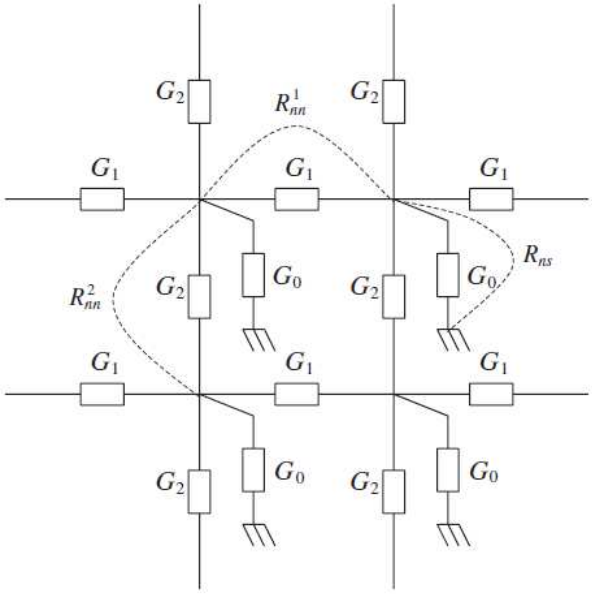

Fig. 1. Two-dimensional version of the general topology network used in this work. One can observe the anisotropy of the network and the definition of the characteristic node-node and node-substrate resistance.

To approach the problem of the general disordered resistance networks it is important to known, as preliminary information, the resistive behaviour of homogeneous infinite lattice networks. Therefore, we start by analysing the following general lattice topology: we take into consideration an anisotropic *n*-dimensional homogeneous grid. It means that we define different values for the conductances aligned along the different lattice directions. Homogeneous grid means that all the conductances in a given direction have the same value. In particular the value of all the conductances in direction *h* (*h*=1…*n*) will be indicated with G_h. Moreover, each node of the grid is connected with a substrate node (another external node not belonging to the grid) through a conductance G_0. For example, a two-dimensional version of the homogeneous network with substrate is represented in Fig. 1. Generally speaking, each node is connected to 2*n*+1 resistors: two resistors for each spatial lattice direction (one before and one after the node) and one resistor (G_0) towards the substrate. We represent the position of a given node with the integer coordinates $\bar{x} \in Z^n$ and we consider the associated electrical potential indicated as $V(\bar{x}) \; \forall \; \bar{x} \in Z^n$. As indicated before, in actual applications the most important particular cases for such a topology are the following: (i) the one-dimensional case, which corresponds to a classical ladder network, (ii) the two-dimensional anisotropic or isotropic case with or without substrate, (iii) three-dimensional isotropic, transversely isotropic or completely anisotropic networks without substrate. However, throughout all the paper, we will take into account the general *n*-dimensional anisotropic network with substrate in order to present a global theory, which describes and unifies all the lattice networks of practical interest.

To characterise such a network we take into consideration two arbitrary nodes *i* and *j* (represented by the lattice positions $\bar{x}^i$ and $\bar{x}^j$) and the common node *0* of the substrate. We suppose that two given currents I_i and I_j flow in terminal connected to the nodes $\bar{x}^i$ and $\bar{x}^j$, in order to define a two-port network. The current Kirchhoff law applied to the generic node $\bar{x}$ reads:

$$\sum_{i=1}^{n} G_i\left[2V(\bar{x}) - V(\bar{x} + \bar{e}_i) - V(\bar{x} - \bar{e}_i)\right] + G_0 V(\bar{x}) = I_i \delta\left(\bar{x}, \bar{x}^i\right) + I_j \delta\left(\bar{x}, \bar{x}^j\right) \qquad (1)$$

where $\delta\left(\bar{x}, \bar{y}\right)$ is the Kronecker's delta function ($\delta\left(\bar{x}, \bar{y}\right)=1$ if $\bar{x} = \bar{y}$ and $\delta\left(\bar{x}, \bar{y}\right)=0$ if $\bar{x} \neq \bar{y}$). We define the

following Fourier transform:

$$\Im\left[V(\bar{x})\right] = f(\bar{k}) = \sum_{\bar{x} \in Z^n} V(\bar{x})\, e^{-i\bar{k}\cdot\bar{x}} \qquad (2)$$

and we obtain the explicit solution in the transformed domain:

$$f(\bar{k}) = \frac{I_i e^{-i\bar{k}\cdot\bar{x}^i} + I_j e^{-i\bar{k}\cdot\bar{x}^j}}{\sum_{h=1}^{n} G_h\left[2 - e^{ik_h} - e^{-ik_h}\right] + G_0} \qquad (3)$$

The general expression for the inverse transform is given by:

$$V(\bar{x}) = \Im^{-1}\left[f(\bar{k})\right] = \frac{1}{(2\pi)^n}\int_{-\pi}^{+\pi}\cdots\int_{-\pi}^{+\pi} f(\bar{k})\, e^{i\bar{k}\cdot\bar{x}}\, d\bar{k} \qquad (4)$$

Therefore, we obtain, after some straightforward computations, the following integral expression for the electrical potential in an arbitrary node of the lattice network:

$$V(\bar{x}) = \frac{1}{(2\pi)^n}\int_{-\pi}^{+\pi}\cdots\int_{-\pi}^{+\pi} \frac{I_i e^{-i\bar{k}\cdot\bar{x}^i} + I_j e^{-i\bar{k}\cdot\bar{x}^j}}{\sum_{h=1}^{n} G_h\left[2 - e^{ik_h} - e^{-ik_h}\right] + G_0} e^{i\bar{k}\cdot\bar{x}}\, d\bar{k} \qquad (5)$$

This expression may be specialised to the two nodes of interest, by defining the potentials of the nodes $\bar{x}^i$ and $\bar{x}^j$, where the current generators have been connected. The potentials in these points are linearly related to the two current I_i and I_j by means of the impedance matrix $\tilde{Z}$

$$\begin{cases} V_i = V(\bar{x}_i) \\ V_j = V(\bar{x}_j) \end{cases} \Rightarrow \quad \begin{cases} V_i = \tilde{Z}_{ii} I_i + \tilde{Z}_{ij} I_j \\ V_j = \tilde{Z}_{ji} I_i + \tilde{Z}_{jj} I_j \end{cases} \qquad (6)$$

By drawing a comparison between Eq. (6) and Eq. (7) we may find out the explicit expressions for the impedance matrix elements:

$$\begin{cases} \tilde{Z}_{ii} = \tilde{Z}_{jj} = \dfrac{1}{(2\pi)^n}\displaystyle\int_{-\pi}^{+\pi}\cdots\int_{-\pi}^{+\pi} \frac{1}{\sum_{h=1}^{n} G_h\left[2 - e^{ik_h} - e^{-ik_h}\right] + G_0} d\bar{k} \\ \tilde{Z}_{ij} = \dfrac{1}{(2\pi)^n}\displaystyle\int_{-\pi}^{+\pi}\cdots\int_{-\pi}^{+\pi} \frac{e^{i\bar{k}\cdot\left(\bar{x}^i - \bar{x}^j\right)}}{\sum_{h=1}^{n} G_h\left[2 - e^{ik_h} - e^{-ik_h}\right] + G_0} d\bar{k} \\ \tilde{Z}_{ji} = \dfrac{1}{(2\pi)^n}\displaystyle\int_{-\pi}^{+\pi}\cdots\int_{-\pi}^{+\pi} \frac{e^{i\bar{k}\cdot\left(\bar{x}^j - \bar{x}^i\right)}}{\sum_{h=1}^{n} G_h\left[2 - e^{ik_h} - e^{-ik_h}\right] + G_0} d\bar{k} \end{cases} \qquad (7)$$

One can observe that the first formula in Eq. (8) represents the value of the resistance between a generic node of the lattice and the node corresponding to the substrate. Furthermore, it can be noticed that the value of this resistance is invariant to any permutations of the values $G_1, G_2 \ldots, G_n$.

It may be interesting to calculate the resistance between the nodes $\bar{x}^i$ and $\bar{x}^j$ if the node *0* of the substrate remains disconnected. We may calculate this resistance in the following way:

$$Z_{ij} = \frac{V_i - V_j}{I_i} = \frac{\tilde{Z}_{ii} I_i + \tilde{Z}_{ij} I_j - \left(\tilde{Z}_{ji} I_i + \tilde{Z}_{jj} I_j\right)}{I_i} = \frac{\tilde{Z}_{ii} I_i - \tilde{Z}_{ij} I_i - \tilde{Z}_{ji} I_i + \tilde{Z}_{jj} I_i}{I_i} = 2\tilde{Z}_{ii} - \tilde{Z}_{ij} - \tilde{Z}_{ji} \qquad (8)$$

By considering the relations given in Eq. (8) the node-node resistance can be written as follows:

$$Z_{ij} = \frac{1}{(2\pi)^n} \int_{-\pi}^{+\pi} \dots \int_{-\pi}^{+\pi} \frac{2 - e^{i\bar{k}\cdot(\bar{x}^i - \bar{x}^j)} - e^{-i\bar{k}\cdot(\bar{x}^i - \bar{x}^j)}}{\sum_{h=1}^{n} G_h\left[2 - e^{ik_h} - e^{-ik_h}\right] + G_0} d\bar{k} \qquad (9)$$

For various applications that will be explained in the following we suppose that the nodes $\bar{x}^i$ and $\bar{x}^j$ are two adjacent nodes along the direction *s* of the *n*-dimensional lattice. In this hypothesis we take into account, as main parameters of the lattice network, the node-substrate resistance and the node-node resistance between to adjacent nodes in direction *s* (see Fig.1):

$$R_{ns} = \frac{1}{\pi^n} \int_0^{+\pi} \dots \int_0^{+\pi} \frac{d\bar{k}}{2\sum_{h=1}^{n} G_h[1 - \cos k_h] + G_0}; \; R_{nn}^s = \frac{1}{\pi^n} \int_0^{+\pi} \dots \int_0^{+\pi} \frac{2[1 - \cos k_s]d\bar{k}}{2\sum_{h=1}^{n} G_h[1 - \cos k_h] + G_0} \qquad (10)$$

We present a method to reduce the multiple integrals described in Eq. (10) to single integrals performed on products of Bessel functions and exponential functions. This way of writing the resistance integrals is very useful for numerical application because of the fast convergence of such simple integrals. To begin we take into consideration the integrals that defines R_{ns}; the fraction that appears inside the integral may be developed by using the elementary property $\frac{1}{a} = \int_0^{\infty} e^{-at} dt, \quad a > 0$. Thus the expression may be rearranged as follows:

$$R_{ns} = \frac{1}{2\pi^n} \int_0^{+\pi} \dots \int_0^{+\pi} \frac{d\bar{k}}{\sum_{h=1}^{n} G_h[1 - \cos k_h] + \frac{G_0}{2}} = \frac{1}{2\pi^n} \int_0^{\infty} \int_0^{+\pi} \dots \int_0^{+\pi} e^{-\frac{G_0}{2}t} e^{-\sum_{h=1}^{n} G_h[1-\cos k_h]t} d\bar{k}dt \qquad (11)$$

The integrals over the variables k_1, $k_2 \dots k_n$ can be performed by using the following property of the Bessel functions $\pi I_0(\beta) = \int_0^{\pi} e^{\beta \cos x} dx$. Thus, the final form of the integral describing the node-substrate resistance is:

$$R_{ns} = \frac{1}{2} \int_0^{\infty} e^{-\frac{G_0}{2}t} e^{-\sum_{h=1}^{n} G_h t} I_0(G_1 t) I_0(G_2 t) \dots I_0(G_n t) dt \qquad (12)$$

The integral that represents the resistance R_{nn} may be developed, as before, obtaining the following expression:

$$R_{nn}^s = \frac{1}{\pi^n} \int_0^{+\pi} \dots \int_0^{+\pi} \frac{[1 - \cos k_s]d\bar{k}}{\sum_{h=1}^{n} G_h[1 - \cos k_h] + \frac{G_0}{2}} = \frac{1}{\pi^n} \int_0^{\infty} \int_0^{+\pi} \dots \int_0^{+\pi} [1 - \cos k_s] e^{-\frac{G_0}{2}t} e^{-\sum_{h=1}^{n} G_h[1-\cos k_h]} d\bar{k}dt \qquad (13)$$

At this point, we may use $\pi I_1(\beta) = \int_0^{\pi} \cos x \, e^{\beta \cos x} dx$ to obtain the second integral form

$$R_{nn}^s = \int_0^{\infty} e^{-\frac{G_0}{2}t} e^{-\sum_{h=1}^{n} G_h t} I_0(G_1 t) I_0(G_2 t) \dots [I_0(G_s t) - I_1(G_s t)] \dots I_0(G_n t) dt \qquad (14)$$

These forms of the resistance integrals may be very useful both for theoretical applications and for numerical procedures. A particular case of lattice is given by isotropic networks; in such case $G_1=G_2=\dots=G_n$ and Eqs. (12) and (14) can be written in a simplified form. Of course, we have $R_{nn}^s=R_{nn}$ for any values of *s*:

$$R_{ns} = \frac{1}{2} \int_0^{\infty} e^{-\frac{G_0}{2}t} e^{-nGt} I_0^n(Gt) dt; \; R_{nn} = \int_0^{\infty} e^{-\frac{G_0}{2}t} e^{-nGt} I_0^{n-1}(Gt)[I_0(Gt) - I_1(Gt)] dt \qquad (15)$$

Moreover, these relations can be elaborated eventually obtaining

$$\begin{cases} R_{ns} = \dfrac{1}{2G} \displaystyle\int_0^{\infty} e^{-\frac{G_0}{2G}x} e^{-nx} I_0^n(x) dx \\ R_{nn} = \dfrac{1}{nG}(1 - G_0 R_{ns}) \end{cases} \qquad (16)$$

In particular this result means that there is a direct relation between the node-node and the node-substrate resistance in isotropic lattice networks. In other words, when R_{ns} is calculated with the first integral we may compute R_{nn} directly by using the second relation in Eq. (16).

Moreover, with Eq. (16) we may analyse the behaviour of isotropic networks without substrate (G_0=0): in

particular, a well known problem in networks theory is the calculation of the impedance between adjacent nodes of infinite uniform n-dimensional resistive lattices. It is easy to observe that if $G_0=0$ the product G_0R_{ns} tends to zero and therefore, form Eq. (16) we obtain $R_{nn}=1/(nG)$, a well known result recently described, for example, in Osterberg PM, Inan AS. Impedance between adjacent nodes of infinite uniform D-dimensional resistive lattices. Am. J. Phys. 2004; 72, 972-973.

We shall refer ourselves to n-dimensional lattice networks with substrate and we define an anisotropic distribution of conductance values by introducing different probability densities $\rho_k(G)$ for the conductances aligned along the different lattice directions k (k=1…n). Moreover, the conductances of the substrate are distributed following a given probability density $\rho_0(G)$. All the conductance values (each direction and substrate) are independently distributed according to the probability densities upon described. In the effective medium theory the average effects of the random conductances in such a disordered network will be represented by an anisotropic effective network in which all the conductances in k direction have the same value $\overline{G}_k$ and all the conductances in the substrate have the same value $\overline{G}_0$. These effective conductances will be self consistently determined by the requirement that the fluctuating local potential in the random network should average to zero. This is the main idea, which allows us to build up the effective medium theory. Furthermore, for following purposes, we suppose to exactly know the functions $R_{nn}^k = R_{nn}^k\left(\overline{G}_0,\overline{G}_1,...,\overline{G}_n\right)\ \forall\ k$ and $R_{ns} = R_{ns}\left(\overline{G}_0,\overline{G}_1,...,\overline{G}_n\right)$ and to be able to compute them, almost numerically. They play a crucial role in determining the effective network equivalent to a random one. From now on, we suppose to know the effective network corresponding to a given random one, in order to understand the conceptual connection among them. In the effective network we change a single conductance $\overline{G}_k$, oriented along the direction k (k=1…n) or belonging to the substrate (k=0), back to its true value G_k. This procedure can be applied indifferently to a resistor in the lattice or a resistor in the substrate.

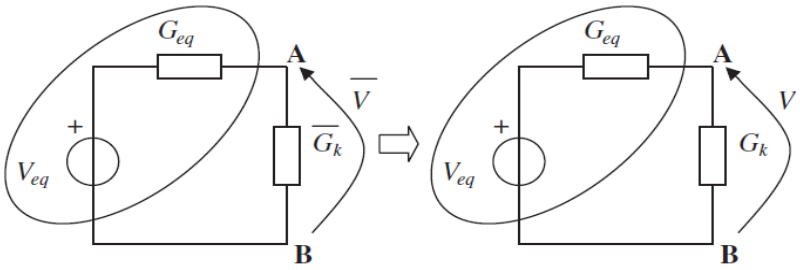

Fig. 2. Thevenin equivalent circuit between two adjacent arbitrary nodes of the lattice before and after the substitution of the effective conductance $\overline{G}_k$ with a particular random instance G_k.

In Fig. 2 one can find the graphical representation of such a substitution, where the Thevenin equivalent circuit of the remaining part of the effective network is indicated. Here, G_k is a particular instance for the conductance value and $\overline{G}_k$ is the corresponding effective value. Moreover, V_{eq} and G_{eq} are the parameters of the Thevenin equivalent circuit. The electrical potentials on the circuits described in Fig.2 can be evaluated as follows:

$$\overline{V} = V_{eq}\frac{G_{eq}}{G_{eq}+\overline{G}_k};\quad V = V_{eq}\frac{G_{eq}}{G_{eq}+G_k} \qquad (17)$$

So, the potential fluctuations due to the random character of the network are given by:

$$\Delta V = V-\overline{V} = V_{eq}\frac{G_{eq}}{G_{eq}+G_k}-\overline{V} = \overline{V}\frac{G_{eq}+\overline{G}_k}{G_{eq}}\frac{G_{eq}}{G_{eq}+G_k}-\overline{V} = \overline{V}\frac{\overline{G}_k-G_k}{G_{eq}+G_k} \qquad (18)$$

Now, we may observe a relationship between the Thevenin conductance G_{eq} and the values R_{nn} and R_{ns}. In fact, G_{eq} is the conductance between the nodes **A** and **B** of Fig.2 where we have eliminated the conductance $\overline{G}_k$. Thus, we may write down the relations

$$\begin{cases} k = 1..n \quad \Rightarrow \quad R_{nn}^k = \dfrac{1}{G_{eq}+\overline{G}_k} \quad \Rightarrow \quad G_{eq} = \dfrac{1}{R_{nn}^k}-\overline{G}_k \\ k = 0 \quad \Rightarrow \quad R_{ns} = \dfrac{1}{G_{eq}+\overline{G}_0} \quad \Rightarrow \quad G_{eq} = \dfrac{1}{R_{ns}}-\overline{G}_0 \end{cases} \qquad (19)$$

By substituting Eq. (25) into Eq. (24) we immediately obtain:

$$k = 1..n \Rightarrow \Delta V = \overline{V}\,\frac{\overline{G}_k - G_k}{1/R_{nn}^k - \overline{G}_k + G_k};\quad k = 0 \Rightarrow \Delta V = \overline{V}\,\frac{\overline{G}_0 - G_0}{1/R_{ns} - \overline{G}_0 + G_k} \qquad (20)$$

By imposing that the fluctuations of the potential average to zero, we have the homogenisation integral equations:

$$\begin{cases} \int_0^{+\infty} \rho_k(G)\,\dfrac{\overline{G}_k - G}{1/R_{nn}^k\left(\overline{G}_0,\overline{G}_1,...,\overline{G}_n\right) - \overline{G}_k + G}\,dG = 0 \quad \forall\, k = 1..n \\ \int_0^{+\infty} \rho_0(G)\,\dfrac{\overline{G}_0 - G}{1/R_{ns}\left(\overline{G}_0,\overline{G}_1,...,\overline{G}_n\right) - \overline{G}_0 + G}\,dG = 0 \end{cases} \qquad (21)$$

or, after some manipulations:

$$\begin{cases} \int_0^{+\infty} \rho_k(G)\,\dfrac{1}{1/R_{nn}^k\left(\overline{G}_0,\overline{G}_1,...,\overline{G}_n\right) - \overline{G}_k + G}\,dG = R_{nn}^k\left(\overline{G}_0,\overline{G}_1,...,\overline{G}_n\right) \quad \forall\, k = 1..n \\ \int_0^{+\infty} \rho_0(G)\,\dfrac{1}{1/R_{ns}\left(\overline{G}_0,\overline{G}_1,...,\overline{G}_n\right) - \overline{G}_0 + G}\,dG = R_{ns}\left(\overline{G}_0,\overline{G}_1,...,\overline{G}_n\right) \end{cases} \qquad (22)$$

These relations represent a system of n+1 equations with n+1 unknowns $\overline{G}_0,\overline{G}_1,...,\overline{G}_n$ that can be found when all the probability densities involved are given. The expressions for the resistance R_{nn} and R_{ns} in terms of the effective conductances $\overline{G}_0,\overline{G}_1,...,\overline{G}_n$ may be taken in various form: the starting multiple integral expressions or the simple integrals of Bessel functions. The simplest network is the isotropic one without substrate. In this case only one value is unknown $\overline{G} = \overline{G}_1 = ... = \overline{G}_n$; the substrate is absent and so $\overline{G}_0$ is not of interest. Moreover, only one probability density describes the distribution of resistors in the lattice. We use the property for isotropic networks without substrate $R_{nn}\left(\overline{G}\right) = 1/\left(n\overline{G}\right)$ and thus, we obtain the simplest homogenising result

$$\int_0^{+\infty} \rho(G)\,\frac{1}{(n-1)\overline{G} + G}\,dG = \frac{1}{n\overline{G}} \qquad (23)$$

This is a well-known result in the field of the isotropic random networks.

We show some exact results useful to calculate the resistance R_{nn} and R_{ns} in closed form or in terms of elliptic integrals. For two-dimensional structures the complete results are summarised below:

$$\begin{cases} R_{ns}(G_0,G_1,G_2) = \dfrac{r}{2\pi\sqrt{G_1G_2}}K(r) \\ R_{nn}^1(G_0,G_1,G_2) = \dfrac{1}{G_1}\left\{1 - \dfrac{2}{\pi}\left[K(r)E\left(\varepsilon,\sqrt{1-r^2}\right) - [K(r) - E(r)]F\left(\varepsilon,\sqrt{1-r^2}\right)\right]\right\} \\ R_{nn}^2(G_0,G_1,G_2) = \dfrac{1}{G_2}\left\{1 - \dfrac{2}{\pi}\left[K(r)E\left(\eta,\sqrt{1-r^2}\right) - [K(r) - E(r)]F\left(\eta,\sqrt{1-r^2}\right)\right]\right\} \end{cases} \qquad (24)$$

$$\varepsilon = \operatorname{arctg}\sqrt{\frac{4G_2 + G_0}{4G_1}},\quad \eta = \operatorname{arctg}\sqrt{\frac{4G_1 + G_0}{4G_2}},\quad r = 4\sqrt{\frac{G_1G_2}{(4G_1 + G_0)(4G_2 + G_0)}}$$

When the two-dimensional lattice is isotropic G=G_1=G_2 the following simplified expressions hold on

$$\begin{cases} R_{ns}(G_0,G,G) = \dfrac{2}{\pi(4G + G_0)}K\left(\dfrac{4G}{4G + G_0}\right) \\ R_{nn}(G_0,G,G) = \dfrac{1}{2G}\left\{1 - \dfrac{2G_0}{\pi(4G + G_0)}K\left(\dfrac{4G}{4G + G_0}\right)\right\} \end{cases} \qquad (25)$$

Furthermore, if the two-dimensional lattice network is without substrate (G_0=0) the exact formulas reduce to the following ones

$$R_{nn}^{1}(0,G_1,G_2) = \frac{2}{\pi G_1}\operatorname{arctg}\sqrt{\frac{G_1}{G_2}}; \quad R_{nn}^{2}(0,G_1,G_2) = \frac{2}{\pi G_2}\operatorname{arctg}\sqrt{\frac{G_2}{G_1}} \qquad (26)$$

Finally, for three-dimensional structures the results can be written in terms of integrals of elliptic functions

$$\begin{cases} R_{ns}(G_0,G_1,G_2,G_3) = \dfrac{1}{2\pi^2}\sqrt{\dfrac{G_s}{G_1G_2G_3}}\displaystyle\int_0^{+\pi} r_s(x)K[r_s(x)]\,dx \quad \forall\, s \\ R_{nn}^{s}(G_0,G_1,G_2,G_3) = \dfrac{1}{\pi^2}\sqrt{\dfrac{G_s}{G_1G_2G_3}}\displaystyle\int_0^{+\pi} (1-\cos x)\, r_s(x)K[r_s(x)]\,dx \end{cases} \qquad (27)$$

where the function $r_1(x)$ is given by:

$$r_1(x) = 4\sqrt{\frac{G_2G_3}{[4G_2+G_0+2G_1(1-\cos x)]\,[4G_3+G_0+2G_1(1-\cos x)]}} \qquad (28)$$

and the other ones $r_2(x)$ and $r_3(x)$ can be obtained by permuting the indices in the symbols G_1, G_2 and G_3.

We consider some examples of disordered two-dimensional lattices. A first series of simulations deal with the problem of the anisotropic percolation in two-dimensional systems. We consider a two-dimensional lattice grid without substrate with an anisotropic statistical distribution of the conductance values in the network. On the rows of the network (axis x) we assign conductances of value G_{ox} with probability 1-c_x and value zero with probability c_x. On the columns (axis y) we assign conductances with value G_{oy} with probability 1-c_y and value zero with probability c_y. After some straightforward manipulations, the system for the effective conductances $\overline{G}_x$ and $\overline{G}_y$ may be recast in the simple form:

$$\begin{cases} \operatorname{arctg}\sqrt{\dfrac{\overline{G}_x}{\overline{G}_y}} = \dfrac{\pi}{2}\dfrac{\overline{G}_x-(1-c_x)G_{ox}}{\overline{G}_x-G_{ox}} \\ \overline{G}_y = G_{oy}\dfrac{\overline{G}_x(1-c_y)+G_{ox}(c_x+c_y-1)}{\overline{G}_x-(1-c_x)G_{ox}} \end{cases} \qquad (29)$$

To perform the Monte-Carlo simulations we use the values G_{ox}=G_{oy}=1 and we analyse the behaviour of the system versus the volume fractions c_x and c_y. It is interesting to note that the percolation threshold for this system is given by c_x+c_y=1. In Fig. 3 the comparison between theoretical results (continuous lines) and simulations (triangles) is shown. Here the effective conductances in both spatial directions are plotted versus the first concentration c_x. A good agreement between theory and simulations has been obtained.

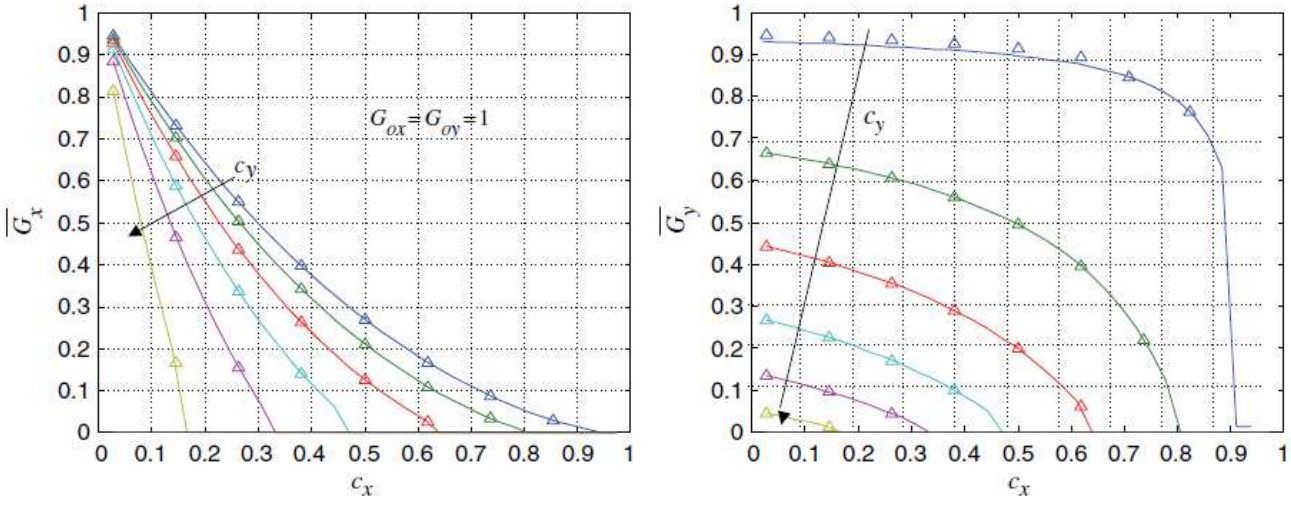

Fig. 3. Comparison between theoretical results (continuous lines) and simulations (triangles) for anisotropic percolation. The effective conductances in both spatial directions are plotted versus the first concentration c_x. Different curves represent different values of the other concentration c_y. In both plots from the top to the down the

curves correspond to the following values of c_y: 0.027-0.185-0.342-0.5-0.657-0.815.

Now, we devote our attention to two cases of two-dimensional networks with substrate that are very important for practical applications. The first case deals with a two dimensional isotropic grid where the conductances of the lattices are randomly placed and the conductances of the substrate are all fixed at a given value. Each conductance of the grid is placed into the network assuming the value G_1 with probability 1/2 and the value G_2 with probability 1/2. All the substrate conductances are fixed to the value G_0. The theory leads to the following equation for the unknown effective conductance $\overline{G}$ of the grid:

$$K\left(\frac{4\overline{G}}{4\overline{G}+G_0}\right)=\frac{\pi}{2}\frac{\left(G_1G_2-\overline{G}^2\right)\left(4\overline{G}+G_0\right)}{G_0\left(\overline{G}-G_1\right)\left(\overline{G}-G_2\right)} \tag{30}$$

This result is very interesting because the parameter G_0 modulates the kind of mean value $\overline{G}$ between G_1 and G_2; the extreme cases are the following: if G_0 is zero the value $\overline{G}$ corresponds to the *geometric mean* between G_1 and G_2, $\overline{G}=\sqrt{G_1G_2}$, and if G_0 tends to infinity the value $\overline{G}$ corresponds to the *arithmetic mean* between G_1 and G_2, $\overline{G}=\left(G_1+G_2\right)/2$. Simulations with G_1=1 and G_2=4 have been performed. A comparison between results obtained from Eq. (30) and Monte-Carlo simulations is shown in Fig. 4 where theoretical values of R_{ns} and numerical ones are shown versus values of G_0 between 1 and 100. A remarkably good fitting is evident.

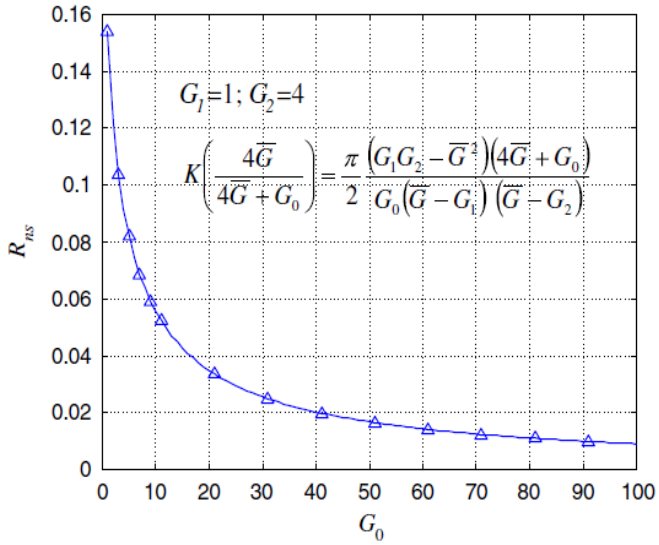

Fig. 4. Theoretical (continuous line) and Monte-Carlo results (triangles) for a two dimensional grid where the conductances of the lattices are randomly placed and the conductances of the substrate are all fixed at a given value. Each conductance of the grid is placed into the network assuming the value 1 with probability 1/2 and the value 4 with probability 1/2. All the substrate conductances are fixed to the value G_0. The node-substrate resistance R_{ns} of the network is represented versus the values of G_0.

The second case of two-dimensional lattices on substrate deals with a grid with fixed conductances in both directions and random conductances in the substrate. Each conductance of the substrate is placed into the network assuming the value G_1 with probability 1/2 and the value G_2 with probability 1/2. All the lattice conductances are fixed to the value G. As before, the theory leads to the following equation for the unknown effective conductance $\overline{G}_0$ of the grid

$$K\left(\frac{4G}{4G+\overline{G}_0}\right)=\frac{\pi}{2}\frac{\left(\overline{G}_0-\frac{G_1+G_2}{2}\right)\left(4G+\overline{G}_0\right)}{\left(\overline{G}_0-G_1\right)\left(\overline{G}_0-G_2\right)} \tag{31}$$

This result is similar to that given in Eq. (40) because the parameter G modulates the kind of mean value $\overline{G}_0$ between G_1 and G_2 also in this case; the extreme cases are the following: if G is zero the value $\overline{G}_0$ corresponds to the *harmonic mean* between G_1 and G_2, $\overline{G}_0 = 2G_1G_2/(G_1+G_2)$, and if G tends to infinity the value $\overline{G}_0$ corresponds to the *arithmetic mean* between G_1 and G_2, $\overline{G}_0 = (G_1+G_2)/2$. Finally, simulations with G_1=1 and G_2=4 have been performed. A comparison between theoretical results and Monte-Carlo simulations is shown in Fig. 5 where theoretical values of R_{ns} and numerical ones are shown versus values of G between 1 and 100. Once again, the theory is in very good agreement with numerical results. These cases have immediate applications to the analysis of heterogeneous films deposited on substrates with an electrical coupling. For sake of brevity we do not present here other comparisons with simulations; however the theory has been confirmed by means of many other numerical experiments.

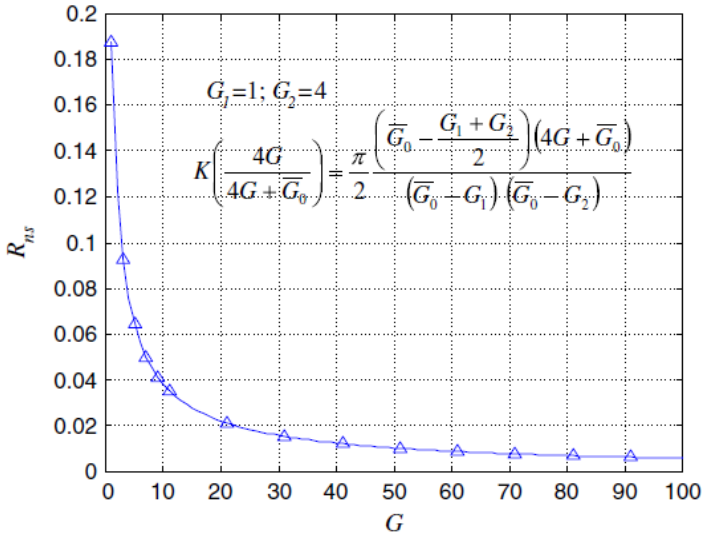

Fig. 5. Theoretical (continuous line) and Monte-Carlo results (triangles) for a two dimensional grid where the conductances of the lattices are fixed and the conductances of the substrate are randomly assigned. Each conductance toward the substrate is placed into the network assuming the value 1 with probability 1/2 and the value 4 with probability 1/2. All the grid conductances are fixed to the value G. The node-substrate resistance R_{ns} of the network is represented versus the values of G.

2.1.3.The dielectric homogenization of anisotropic structures

(*S. Giordano, Equivalent permittivity tensor in anisotropic random media, Journal of Electrostatics, 64 (2006) 655-663, S. Giordano, W. Rocchia, Predicting the dielectric nonlinearity of anisotropic composite materials via tensorial analysis, 2006 Journal of Physics: Condensed Matter 18 10585-10599, S. Giordano, P. L. Palla, Dielectric behavior of anisotropic inhomogeneities: interior and exterior points Eshelby tensors, Journal of Physics A: Mathematical and Theoretical 41, 2008, 415205*)

We analyse the dielectric behaviour of dispersions of anisotropic inclusions. In particular we take into account spherical anisotropic objects embedded in a homogeneous matrix. Because of the anisotropy of the embedded particles the most relevant aspect in the microstructure is the orientation of the spherical particles themselves. We take into account a partial orientational order described by an order parameter S, which has the following meaning. When S=0, the orientation of the particles is completely random, generating an overall isotropic medium. When S=1, all the particles are aligned along a given director allowing the formation of a uniaxial material. Finally, when S=-1/2, all the particles are lying randomly in planes perpendicular to the given director. In this work we take into account all the intermediate configurations between order and disorder with the aim to characterise a material with particles partially aligned. As we will explain later, the order parameter S can assume all the fractional values between –1/2 and 1. The three cases S=0, S=1 and S=-1/2 are simply presented as representative values on a continuum of values. We present, as result, the effective permittivity tensor of such a material depending on S. This analysis has immediate application to the field of the liquid crystals. Actually, our microstructure describes a material positionally disordered, but orientationally ordered, which corresponds to a nematic phase in liquid crystals. The level of ordering is reflected in the macroscopic properties. For example, from an optical point of

view, we may observe that the optical axis is given by the direction of orientation of the single crystals.

We first consider a single anisotropic sphere (characterised by its permittivity tensor $\boldsymbol{\varepsilon}$) embedded in an isotropic medium with permittivity ε_0. If we expose the system to a uniform electric field $\overline{E}_0$, a perturbation to this field appears both inside and outside the sphere. We are interested in the electric field which is present inside the sphere after the application of the external field. In an arbitrary reference frame, we may evaluate the internal electric field $\overline{E}_s$ and the internal electric displacement $\overline{D}_s$ as follows:

$$\overline{E}_s = 3\varepsilon_0\left[\boldsymbol{\varepsilon} + 2\varepsilon_0\mathbf{I}\right]^{-1}\overline{E}_0 \quad \text{and} \quad \overline{D}_s = 3\varepsilon_0\boldsymbol{\varepsilon}\left[\boldsymbol{\varepsilon} + 2\varepsilon_0\mathbf{I}\right]^{-1}\overline{E}_0 \qquad (1)$$

Here **I** represents the identity tensor of order three. These fields are uniform within the sphere volume, and determined by the exciting field and the anisotropic permittivity tensor. Note that the internal electrical field is not necessarily parallel to the external applied field. In this equation, the anisotropy is completely general. It covers not only uniaxial and biaxial materials, but also gyrotropic media in which the permittivity tensor contains an antisymmetric part. However, in the following we consider a symmetric permittivity tensor in order to apply diagonalisation by means of a suitable orthogonal matrix (rotation matrix **R**):

$$\boldsymbol{\varepsilon} = \mathbf{R}\begin{bmatrix}\varepsilon_x & 0 & 0\\ 0 & \varepsilon_y & 0\\ 0 & 0 & \varepsilon_z\end{bmatrix}\mathbf{R}^{-1} = \mathbf{R}\boldsymbol{\varepsilon}_d\mathbf{R}^{-1} \qquad (2)$$

where ε_x, ε_y, ε_z are the three principal permittivities of the anisotropic sphere; the rotation matrix **R** represents the angular position (orientation) of the sphere with respect to a reference frame with axis parallel to the principal directions of the permittivity tensor.
If we consider an arbitrary reference frame in the space, we may thus calculate the internal electric field and electric displacement using the following relations:

$$\overline{E}_s = 3\varepsilon_0\left[\mathbf{R}\boldsymbol{\varepsilon}_d\mathbf{R}^{-1} + 2\varepsilon_0\mathbf{I}\right]^{-1}\overline{E}_0 = 3\varepsilon_0\mathbf{R}\left[\boldsymbol{\varepsilon}_d + 2\varepsilon_0\mathbf{I}\right]^{-1}\mathbf{R}^{-1}\overline{E}_0 \qquad (3)$$

$$\overline{D}_s = 3\varepsilon_0\mathbf{R}\boldsymbol{\varepsilon}_d\mathbf{R}^{-1}\left[\mathbf{R}\boldsymbol{\varepsilon}_d\mathbf{R}^{-1} + 2\varepsilon_0\mathbf{I}\right]^{-1}\overline{E}_0 = 3\varepsilon_0\mathbf{R}\boldsymbol{\varepsilon}_d\left[\boldsymbol{\varepsilon}_d + 2\varepsilon_0\mathbf{I}\right]^{-1}\mathbf{R}^{-1}\overline{E}_0 \qquad (4)$$

In our scheme, the rotation matrix **R** is a random one describing the distribution of the orientations of the spheres embedded in the hosting isotropic medium. In order to simplify successive computations, we define this matrix: $\mathbf{A}_d = \left[\boldsymbol{\varepsilon}_d + 2\varepsilon_0\mathbf{I}\right]^{-1}$. It follows that the average values of the electric field and the displacement vectors (over the sphere dispositions) are given by the relationships:

$$\left\langle\overline{E}_s\right\rangle = 3\varepsilon_0\left\langle\mathbf{R}\mathbf{A}_d\mathbf{R}^{-1}\right\rangle\overline{E}_0 \text{ and } \left\langle\overline{D}_s\right\rangle = 3\varepsilon_0\left\langle\mathbf{R}\boldsymbol{\varepsilon}_d\mathbf{A}_d\mathbf{R}^{-1}\right\rangle\overline{E}_0 \qquad (5)$$

We may now define the statistical distribution of the orientations to calculate the above indicated average values. The entire material, that we wish to characterise, is positionally disordered, but partially orientationally ordered. This means that the centres of the spheres are randomly distributed inside the medium but the orientation of principal axis of the permittivity tensor of each particle follow some statistical rules. We consider a single anisotropic (in general biaxial) sphere with a reference frame aligned along the principal directions of the permittivity tensor. In this frame we consider a given unit vector $\overline{w}$, which helps to define the orientational order. Thus all the spheres are oriented, but do not generate a perfect alignment among all these directors. As we will explain later, we can define an order parameter (the average value of the second Legendre polynomial):

$$S = \left\langle\frac{3}{2}\cos^2\vartheta - \frac{1}{2}\right\rangle_\vartheta \qquad (6)$$

where ϑ is the angle each particle (each unit vector $\overline{w}$) makes with the preferential direction given by the ξ-axis of a global reference frame (the symbol $\langle\ \rangle_\vartheta$ represents the average value over theangle ϑ). The meaning of this parameter can be described as follows. If S=1, the alignment is perfect (ϑ =0), if S=0 the alignment is completely random and if S=-1/2 all the particles (the corresponding unit vectors $\overline{w}$) are lying randomly in planes perpendicular to the director (ϑ =π/2). We take into account all the intermediate configurations between order and disorder with the aim to characterise a material with particles partially aligned with an arbitrary degree of order (see Fig. 1 for some examples of degree of order in the entire composite material).
Once the direction of orientation is taken for a single sphere, it may be arbitrarily (randomly) rotated along the director. This means that we subdivide the complete rotation process in two elementary steps:

-First, we create non-perfect alignment by randomly fixing the angle ϑ (ϑ =0 means perfect alignment);
-Secondly, we randomly rotate the sphere around the director, in order to establish a single preferential direction in the behaviour of the entire medium.

A very long analysis allows to prove that the average electric field inside an embedded sphere is given by (for the given unit vector $\overline{w}$ we define the associated anti-symmetric matrix **w**):

$$\left\langle \overline{E}_s \right\rangle = 3\varepsilon_0 S\left[\mathbf{A}_d + \mathbf{A}_d\mathbf{w}^2 + \mathbf{w}^2\mathbf{A}_d - \frac{1}{2}\mathbf{w}\mathbf{A}_d\mathbf{w} + \frac{3}{2}\mathbf{w}^2\mathbf{A}_d\mathbf{w}^2 \right]\overline{E}_0 + \varepsilon_0(1-S)\mathrm{tr}\left(\mathbf{A}_d\right)\overline{E}_0 \quad (7)$$

A similar relation holds on for the electrical displacement with $\boldsymbol{\varepsilon}_d\mathbf{A}_d$ substituted for $\mathbf{A}_d$.

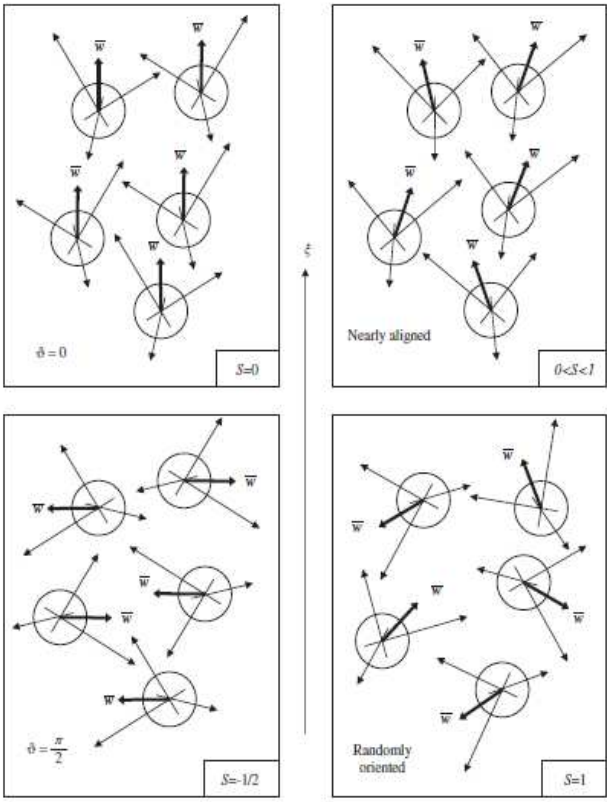

Fig. 1. Structure of a dispersion of pseudo-oriented anisotropic spheres. One can find some orientational distributions ranging from order to disorder. The two-phase material is described by the electric response of each phase, by the state of order and by the volume fraction of the inclusions.

The statistical distribution of orientations generates an overall material that is uniaxial from a macroscopic point of view, and the principal axis is given by the director $\overline{w}$. Therefore, we are interested in the average value of the electric field and the electric displacement when the applied field $\overline{E}_0$ is parallel or perpendicular to the unit vector $\overline{w}$. The result is

$$\overline{E}_0 \,//\, \overline{w} \Rightarrow \begin{cases} \left\langle \overline{E}_s \right\rangle = \varepsilon_0 \sum_j \dfrac{3Sw_j^{\,2} + 1 - S}{\varepsilon_j + 2\varepsilon_0}\overline{E}_0 = \alpha_{//}\overline{E}_0 \\ \left\langle \overline{D}_s \right\rangle = \varepsilon_0 \sum_j \dfrac{\varepsilon_j\left(3Sw_j^{\,2} + 1 - S\right)}{\varepsilon_j + 2\varepsilon_0}\overline{E}_0 = \beta_{//}\overline{E}_0 \end{cases} \quad (8)$$

$$\overline{E}_0 \perp \overline{w} \Rightarrow \begin{cases} \left\langle \overline{E}_s \right\rangle = \varepsilon_0 \sum_j \dfrac{\frac{3}{2}S\left(1 - w_j^{\,2}\right) + 1 - S}{\varepsilon_j + 2\varepsilon_0}\overline{E}_0 = \alpha_{\perp}\overline{E}_0 \\ \left\langle \overline{D}_s \right\rangle = \varepsilon_0 \sum_j \dfrac{\varepsilon_j\left[\frac{3}{2}S\left(1 - w_j^{\,2}\right) + 1 - S\right]}{\varepsilon_j + 2\varepsilon_0}\overline{E}_0 = \beta_{\perp}\overline{E}_0 \end{cases} \quad (9)$$

Until now, we have analysed the average electric behaviour of a single spherical particle embedded in a random medium with a given statistical orientation in both principal directions, e.g. parallel and perpendicular to $\overline{w}$. We now consider a random medium where many particles, as described above (see Fig. 1), are embedded in an isotropic matrix having permittivity ε_0. The volume fraction of the dispersed phase will be indicated by c, where $0<c<1$, and we consider diluted dispersion. This means that we do not take into account the interactions among the inclusions because of the very low concentration of spheres. The following considerations are valid both in the direction along $\overline{w}$ and in the directions orthogonal to $\overline{w}$. Specifically, we define ε ($\varepsilon_{//}$ or $\varepsilon_{\perp}$) as the equivalent permittivity of the entire mixture by means of the relation $\langle \overline{D} \rangle = \varepsilon \langle \overline{E} \rangle$. To evaluate ε, we may compute the average value of the electric field and of displacement vector inside the random material. We also define V as the total volume of the mixture, V_e as the total volume of the embedded spheres, and V_o as the volume of the remaining space among the inclusions (so that $V=V_e \cup V_o$). The average value of the electric field is assumed to be the following $\langle \overline{E} \rangle = c\langle \overline{E}_s \rangle + (1-c)\overline{E}_0 = (c\alpha + 1 - c)\overline{E}_0$. This is the sole approximation introduced in this analysis and it corresponds to the classic approximation adopted to derive the standard Maxwell mixing formula. The average value of $\overline{D}(\bar{r}) = \varepsilon(\bar{r})\overline{E}(\bar{r})$ is evaluated as follows:

$$\langle \overline{D} \rangle = \frac{1}{V}\int_V \varepsilon(\bar{r})\overline{E}(\bar{r})d\bar{r} = \frac{1}{V}\varepsilon_0 \int_{V_o} \overline{E}(\bar{r})d\bar{r} + \frac{1}{V}\int_{V_e} \overline{D}(\bar{r})d\bar{r} =$$

$$= \frac{1}{V}\varepsilon_0 \int_{V_o} \overline{E}(\bar{r})d\bar{r} + \frac{1}{V}\varepsilon_0 \int_{V_e} \overline{E}(\bar{r})d\bar{r} + \frac{1}{V}\int_{V_e} \overline{D}(\bar{r})d\bar{r} - \frac{1}{V}\varepsilon_0 \int_{V_e} \overline{E}(\bar{r})d\bar{r} = \quad (10)$$

$$= \varepsilon_0\langle \overline{E} \rangle + c\langle \overline{D}_s \rangle - c\varepsilon_0\langle \overline{E}_s \rangle = \varepsilon_0\langle \overline{E} \rangle + c(\beta - \varepsilon_0\alpha)\overline{E}_0$$

We may now find a complete expression that allows us to estimate the equivalent permittivity ε in the given direction and its first order expansion with respect to the volume fraction c:

$$\varepsilon = \varepsilon_0 + c\frac{\beta - \varepsilon_0\alpha}{1 - c + c\alpha} \cong \varepsilon_0 + c(\beta - \varepsilon_0\alpha) \qquad (11)$$

Hence, we characterise the heterogeneous material along the director $\overline{w}$:

$$\varepsilon_{//} = \varepsilon_0 + c\frac{\varepsilon_0\sum_j \frac{(\varepsilon_j - \varepsilon_0)(3Sw_j^2 + 1 - S)}{\varepsilon_j + 2\varepsilon_0}}{1 - c + c\varepsilon_0\sum_j \frac{3Sw_j^2 + 1 - S}{\varepsilon_j + 2\varepsilon_0}} \cong \varepsilon_0\left[1 + c\sum_j \frac{(\varepsilon_j - \varepsilon_0)(3Sw_j^2 + 1 - S)}{\varepsilon_j + 2\varepsilon_0}\right] \qquad (12)$$

Similarly, we find the permittivity in the directions orthogonal to $\overline{w}$:

$$\varepsilon_{\perp} = \varepsilon_0 + c\frac{\varepsilon_0\sum_j \frac{(\varepsilon_j - \varepsilon_0)\left[\frac{3}{2}S(1 - w_j^2) + 1 - S\right]}{\varepsilon_j + 2\varepsilon_0}}{1 - c + c\varepsilon_0\sum_j \frac{\frac{3}{2}S(1 - w_j^2) + 1 - S}{\varepsilon_j + 2\varepsilon_0}} \cong \varepsilon_0\left[1 + c\sum_j \frac{(\varepsilon_j - \varepsilon_0)\left[\frac{3}{2}S(1 - w_j^2) + 1 - S\right]}{\varepsilon_j + 2\varepsilon_0}\right] \qquad (13)$$

Results often useful in practical applications are obtained by letting $\varepsilon_x=\varepsilon_y$ (uniaxial particles) partially aligned along the optical axis given by $w_x=0$, $w_y=0$ and $w_z=1$. This case corresponds, for example, to a nematic liquid crystal where each uniaxial molecule is modelled by a spherical anisotropic particle. In any case, if we apply the general solutions to the present case we may obtain the final relationships:

$$\varepsilon_{//} = \varepsilon_0 + c\frac{\varepsilon_0\left[2\frac{\varepsilon_x - \varepsilon_0}{\varepsilon_x + 2\varepsilon_0}(1 - S) + \frac{\varepsilon_z - \varepsilon_0}{\varepsilon_z + 2\varepsilon_0}(1 + 2S)\right]}{1 - c + c\varepsilon_0\left[2\frac{1 - S}{\varepsilon_x + 2\varepsilon_0} + \frac{1 + 2S}{\varepsilon_z + 2\varepsilon_0}\right]} =$$

$$\cong \varepsilon_0\left[1 + 2c\frac{\varepsilon_x - \varepsilon_0}{\varepsilon_x + 2\varepsilon_0}(1 - S) + c\frac{\varepsilon_z - \varepsilon_0}{\varepsilon_z + 2\varepsilon_0}(1 + 2S)\right] \qquad (14)$$

$$\varepsilon_{\perp} = \varepsilon_0 + c\frac{\varepsilon_0\left[2\frac{\varepsilon_x-\varepsilon_0}{\varepsilon_x+2\varepsilon_0}\left(1+\frac{1}{2}S\right)+\frac{\varepsilon_z-\varepsilon_0}{\varepsilon_z+2\varepsilon_0}(1-S)\right]}{1-c+c\varepsilon_0\left[2\frac{1+S/2}{\varepsilon_x+2\varepsilon_0}+\frac{1-S}{\varepsilon_z+2\varepsilon_0}\right]} = \cong \varepsilon_0\left[1+2c\frac{\varepsilon_x-\varepsilon_0}{\varepsilon_x+2\varepsilon_0}\left(1+\frac{1}{2}S\right)+c\frac{\varepsilon_z-\varepsilon_0}{\varepsilon_z+2\varepsilon_0}(1-S)\right] \quad (15)$$

These particular results are in perfect agreement with those obtained in T. Nagatani, 'Effective permittivity in random anisotropic media', J. Appl. Phys. 51 (1980) 4944-4949, which uses a complicated statistical technique from the standpoint of statistical continuum mechanics. Figure 2 shows plots of the equivalent permittivities $\varepsilon_{//}$ and $\varepsilon_{\perp}$ versus the order parameter S for the case -1/2<S<1 using the parameters: w_x=0, w_y=0, w_z=1, ε_x=15, ε_y=15, ε_z=3 and ε_0=1. Six curves are presented for $\varepsilon_{//}$ and for $\varepsilon_{\perp}$ which correspond to six different values of the volume fraction c starting from c=0 and reaching the limiting value c=1. One can observe the validity of the relation $\varepsilon_{\perp}(S=1) = \varepsilon_{//}(S=-1/2)$.

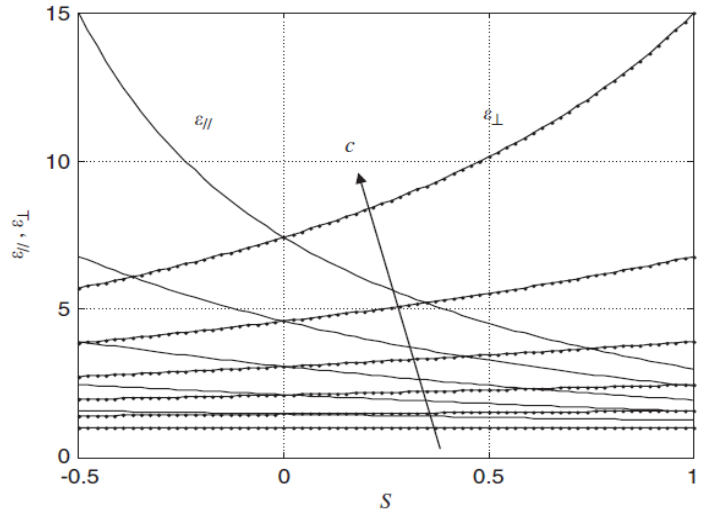

Fig. 2. Plots of the equivalent permittivities $\varepsilon_{//}$ and $\varepsilon_{\perp}$ versus the order parameter S (-1/2<S<1) with the values: w_x=0, w_y=0, w_z=1, ε_x=15, ε_y=15, ε_z=3 and ε_0=1. Six curves are presented, and they correspond to six different values of the volume fraction c starting from c=0 and reaching the limiting value c=1.

We present now a variation of the Maxwell-Garnett approach that provides explicit, analytical results applicable to mixtures where the host is a linear isotropic material and the randomly dispersed inclusions are made of nonlinear anisotropic spheres. The random orientation of all the spherical grains results in an overall nonlinear but still isotropic behaviour of the composite. We express the dielectric behaviour up to the third-order hypersusceptibility in terms of the electrical constitutive tensors of the grains. Our method is based on the exact field calculation inside a single inclusion, followed by an averaging process and it only assumes the dilute limit.

Let's first introduce anisotropy; a linear anisotropic sphere is characterised by its constant permittivity tensor ε (constitutive equation $\mathbf{D}_s = \varepsilon\mathbf{E}_s$, where $\mathbf{E}_s$ and $\mathbf{D}_s$ are electric field and displacement, respectively, inside the inclusion). The sphere is embedded in an isotropic medium with scalar permittivity ε_0 and it is subjected to a uniform electric field $\mathbf{E}_0$. The electric field inside the sphere, due to the application of $\mathbf{E}_0$, is uniform and given by $\mathbf{E}_s = 3\varepsilon_0\left[\varepsilon+2\varepsilon_0 I\right]^{-1}\mathbf{E}_0$. As expected, the internal electric field may be not aligned with $\mathbf{E}_0$. This relationship can be extended to the case of nonlinear media described by the constitutive equation $\mathbf{D}_s = \varepsilon(\mathbf{E}_s)\mathbf{E}_s$, where the permittivity tensor $\varepsilon(\mathbf{E}_s)$ depends arbitrarily on the internal electric field $\mathbf{E}_s = 3\varepsilon_0\left[\varepsilon(\mathbf{E}_s)+2\varepsilon_0 I\right]^{-1}\mathbf{E}_0$. Actually, this relation implicitly determines the unknown electric field $\mathbf{E}_s$. This is true since the electric field fulfilling this relation satisfies both Maxwell's laws and the boundary conditions at the inclusion surface as its linear counterpart does when $\varepsilon = \varepsilon(\mathbf{E}_s)$. This very simple property has several

interesting consequences. It is worth saying that any kind of anisotropy can be modelled through the procedure here presented, including uniaxial, biaxial and also gyrotropic media, in which the permittivity tensor contains an antisymmetric part. However, in the following, we consider a symmetric permittivity tensor in order to exploit diagonalization by means of a suitable orthogonal matrix; this is done for sake of simplicity in the exposition and it does not restrict the generality of the presented approach. Let's consider the following expansion of the permittivity tensor:

$$\varepsilon_{ij}\left(\mathbf{E}_s\right) = \varepsilon^{0}_{ij} + \eta_{ijk}E_k + \chi_{ijkh}E_kE_h\,. \qquad (16)$$

Here E_k represents the k-th component of $\mathbf{E}_S$ in an arbitrary basis. The tensors appearing in Eq. (16) have some well-known symmetry rules, which descend from the existence of a thermodynamic potential (the Gibbs free energy) for the crystal: the first order linear permittivity tensor ε^{0}_{ij} is symmetric in the subscripts i and j. The second order hypersusceptibility tensor η_{ijk} is symmetric in the subscripts j and k (18 independent entries). The third order hypersusceptibility tensor χ_{ijkh} is invariant on any permutation of the three last subscripts j, k and h (30 independent entries). These properties, named internal symmetries, can be synthesised as follows:

$$\begin{gathered}\varepsilon^{0}_{ij} = \varepsilon^{0}_{ji}, \qquad \eta_{ijk} = \eta_{ikj}, \\ \chi_{ijkh} = \chi_{ijhk} = \chi_{ikjh} = \chi_{ihjk} = \chi_{ikhj} = \chi_{ihkj}\end{gathered}\,. \qquad (17)$$

Other symmetry rules are fulfilled when the tensors refer to a material belonging to one of the 32 admissible crystal classes. A long calculation provides the explicit form for the electric field inside a nonlinear anisotropic sphere:

$$\begin{aligned}E_i = {} & \frac{3\varepsilon_0}{\varepsilon_j + 2\varepsilon_0}E_{0j}\delta_{ij} - \frac{9\varepsilon_0^{\,2}\eta_{ijk}}{(\varepsilon_i + 2\varepsilon_0)(\varepsilon_j + 2\varepsilon_0)(\varepsilon_k + 2\varepsilon_0)}E_{0j}E_{0k} + \\ & + \frac{\left(2\dfrac{\eta_{ijq}\eta_{qkh}}{\varepsilon_q + 2\varepsilon_0} - \chi_{ijkh}\right)27\varepsilon_0^{\,3}}{(\varepsilon_i + 2\varepsilon_0)(\varepsilon_j + 2\varepsilon_0)(\varepsilon_k + 2\varepsilon_0)(\varepsilon_h + 2\varepsilon_0)}E_{0j}E_{0k}E_{0h}\end{aligned}\,. \qquad (18)$$

Here we have considered the diagonal linear permittivity $\varepsilon^{0}_{ij} = \varepsilon_i\delta_{ij}$. Equation (3) is exact up to the third order in the external electric field and represents a strong generalization of the Lorentz field. So far, we have used a fixed coordinate system, corresponding to the principal directions of the permittivity tensor of the sphere. Now, we'll consider an arbitrary reference frame in order to compute the average value of the internal electric field when the sphere is randomly oriented in the space. Let $\mathbf{n}_1, \mathbf{n}_2$ and $\mathbf{n}_3$ be unit vectors determining the principal directions of the sphere in space, the vectorial expression of the internal electric field is given by:

$$\mathbf{E}_s = \left\{ a_j\delta_{ij}\left(\mathbf{E}_0\mathbf{n}_j\right) + b_{ijk}\left(\mathbf{E}_0\mathbf{n}_j\right)\left(\mathbf{E}_0\mathbf{n}_k\right) + c_{ijkh}\left(\mathbf{E}_0\mathbf{n}_j\right)\left(\mathbf{E}_0\mathbf{n}_k\right)\left(\mathbf{E}_0\mathbf{n}_h\right)\right\}\mathbf{n}_i\,, \qquad (19)$$

where the coefficients a, b and c can be easily identified through Eq.(18). We now want to average $\mathbf{E}_s$ over all the possible orientations of the sphere in the space:

$$\left\langle E_r\right\rangle = a_j\delta_{ij}E_{0l}\left\langle n_{jl}n_{ir}\right\rangle + b_{ijk}E_{0l}E_{0s}\left\langle n_{jl}n_{ks}n_{ir}\right\rangle + c_{ijkh}E_{0l}E_{0s}E_{0t}\left\langle n_{jl}n_{ks}n_{ht}n_{ir}\right\rangle, \qquad (20)$$

where n_{jk} is the k-th component of the unit vector $\mathbf{n}_j$. The result is

$$\left\langle \mathbf{E}_s\right\rangle = \alpha\,\mathbf{E}_0 + \beta\,E_0^2\mathbf{E}_0\,, \qquad (21)$$

where we have defined the following averaging parameters, and made explicit every summation process:

$$\begin{cases}\alpha = \displaystyle\sum_i \frac{\varepsilon_0}{\varepsilon_i + 2\varepsilon_0} \\ \beta = \displaystyle\sum_{i,k}\frac{9\varepsilon_0^{\,3}}{5(\varepsilon_i + 2\varepsilon_0)^2(\varepsilon_k + 2\varepsilon_0)^2}\left(2\sum_q\frac{\eta_{iiq}\eta_{qkk}}{\varepsilon_q + 2\varepsilon_0} - 3\chi_{iikk} + 4\sum_q\frac{\eta_{ikq}\eta_{qik}}{\varepsilon_q + 2\varepsilon_0}\right)\end{cases}. \qquad (22)$$

It is important to observe that the second order term vanishes; this is coherent with the random orientation hypothesis. If we now consider a mixture with a volume fraction $c<<1$ of randomly oriented, dielectrically anisotropic and nonlinear spheres embedded in a homogeneous matrix with permittivity ε_0, we can evaluate a

different kind of average, the space average of the electric field E and the electric displacement D over all of the volume occupied by the mixture. We have:

$$\begin{cases} E_s = \alpha E_0 + \beta E_0^3 \\ E = cE_s + (1-c)E_0 \\ D = \varepsilon_0 E + 3c\varepsilon_0 E_0 - 3c\varepsilon_0 E_s \end{cases} . \qquad (23)$$

By solving the system in Eq.(23), we search for a relation between D and E characterizing the nonlinear mixture. The result is

$$D = \varepsilon_0 \frac{1+2c-2c\alpha}{1-c+c\alpha} E - \frac{3c\beta\varepsilon_0 E^3}{(1-c+c\alpha)^4} . \qquad (24)$$

As we will show later on, this expression is a generalisation of the standard Maxwell mixing formula for linear isotropic spheres in linear isotropic matrix. It can be written in the simple isotropic form $D = \varepsilon_{eq} E + \chi_{eq} E^3$ where:

$$\begin{cases} \varepsilon_{eq} = \varepsilon_0 \dfrac{1+2c-2c\alpha}{1-c+c\alpha} = \varepsilon_0 \dfrac{1+2c-2c\sum_i \frac{\varepsilon_0}{\varepsilon_i+2\varepsilon_0}}{1-c+c\sum_i \frac{\varepsilon_0}{\varepsilon_i+2\varepsilon_0}} \\ \chi_{eq} = -\dfrac{3c\beta\varepsilon_0}{(1-c+c\alpha)^4} = -\dfrac{27c\varepsilon_0^4}{\left(1-c+c\sum_j \frac{\varepsilon_0}{\varepsilon_j+2\varepsilon_0}\right)^4} \sum_{i,k} \dfrac{\left(2\sum_q \frac{\eta_{iiq}\eta_{qkk}}{\varepsilon_q+2\varepsilon_0} - 3\chi_{iikk} + 4\sum_q \frac{\eta_{ikq}\eta_{qik}}{\varepsilon_q+2\varepsilon_0}\right)}{5(\varepsilon_i+2\varepsilon_0)^2(\varepsilon_k+2\varepsilon_0)^2} \end{cases} \qquad (25)$$

Summarizing, we have expressed the equivalent linear permittivity and the equivalent Kerr third-order hypersusceptibility in terms of the parameters of the composite material: the volume fraction c, the host linear permittivity ε_0 and the characteristic tensors ε, η and χ. The linear and nonlinear macroscopic quantities describing the isotropic mixture must be invariant with respect to the framework adopted. We have shown that the equivalent permittivity ε_{eq} and the equivalent hypersusceptibility χ_{eq} are two actual invariants of the system.

The aim of the following discussion is to introduce a methodology to cope with the completely anisotropic ellipsoidal inclusion/inhomogeneity problem. In particular we show explicit expressions for the electric field both inside and outside the ellipsoidal particle. We follow an approach that is widely utilized in similar problems within the elasticity theory. The problem of an inhomogeneity in heterogeneous elastic materials has been completely solved by Eshelby in the case of isotropic environment by means of a very elegant mathematical procedure. Here, we follow that line of thought but we apply it to anisotropic dielectric composite systems. It is interesting to remark the strong analogy between electrostatics and elastostatics: in Tab. 1 we draw a comparison among all the corresponding elastic and electric quantities for the reader interested in such a similarity.

Tab. 1. Comparison among the most important quantities and equations in electrostatics and elasticity theory.

Electric quantities			Elastic quantities		
Electric field	E_i	$E_i = -\dfrac{\partial V}{\partial x_i}$	Elastic strain	$\varepsilon_{s,ij}$	$\varepsilon_{s,ij} = \dfrac{1}{2}\left(\dfrac{\partial u_i}{\partial x_j} + \dfrac{\partial u_j}{\partial x_i}\right)$
Electric potential	V		Elastic displacement	u_i	
Electric displacement	D_i		Stress tensor	T_{ij}	
Maxwell equation	$\dfrac{\partial D_i}{\partial x_i} = 0$		Balance of forces	$\dfrac{\partial T_{ij}}{\partial x_i} = 0$	
Permittivity tensor	ε_{ij}		Stiffness tensor	C_{ijkh}	
Constitutive equation	$D_i = \varepsilon_{ij} E_j$		Constitutive equation	$T_{ij} = C_{ijkh}\varepsilon_{s,kh}$	

The electric equations are written in absence of free charges and the elastostatic relations are written in absence of external forces: the analogy holds on when all the sources are absent or remotely applied. An important preliminary issue for the following purposes is the determination of the electric Green function for an anisotropic environment. Therefore, we have to solve the basilar equation of the electrostatics, as described in Tab. 1, with an impulsive source corresponding to a charged point Q. It means that we have to solve the following differential problem

$$\vec{\nabla} \cdot \left[\vec{\vec{\varepsilon}} \vec{\nabla} V(\vec{r}) \right] = -Q\delta(\vec{r}) \quad \text{or} \quad \varepsilon_{kl} \frac{\partial}{\partial x_k} \frac{\partial}{\partial x_l} V(\vec{r}) = -Q\delta(\vec{r}) \tag{26}$$

with an arbitrary permittivity tensor $\vec{\vec{\varepsilon}}$ having elements ε_{kl}. The result is

$$V(\vec{r}) = \frac{Q}{4\pi \sqrt{\det \vec{\vec{\varepsilon}} \left[\vec{r}^T \vec{\vec{\varepsilon}}^{-1} \vec{r} \right]}} \tag{27}$$

Therefore, all the electrostatic results concerning a generic potential $V_{TOT}(\vec{r})$ in the anisotropic environment can be obtained with a convolution integral between the above Green function and the total effective spatial charge distribution $\rho_{TOT}(\vec{r})$

$$V_{TOT}(\vec{r}) = \frac{1}{4\pi \sqrt{\det \vec{\vec{\varepsilon}}}} \int_{\Re^3} \frac{\rho_{TOT}(\vec{x}) d\vec{x}}{\sqrt{(\vec{r} - \vec{x})^T \vec{\vec{\varepsilon}}^{-1} (\vec{r} - \vec{x})}} \tag{28}$$

This is true because of the linearity and of the space invariant property of the original partial differential equation analyzed.

We define a certain region of the space as an *inclusion* when the constitutive equation, in that zone, assumes the form $\vec{D} = \vec{\vec{\varepsilon}} \left(\vec{E} - \vec{E}^* \right)$ where $\vec{E}^*(\vec{r})$ is an assigned vector function of the position $\vec{r}$, which is named *eigenfield*. We remark that the concept of inclusion is determined by the presence of a given eigenfield, which modifies the constitutive equation as above discussed, but it is not connected with the permittivity tensor $\vec{\vec{\varepsilon}}$, which remains homogeneous in the entire space. The eigenfield, defined in some region of the space, acts as a sort of source of electric field and its effects can be studied as follows. If the free charge distribution is absent in this region we may use the Gauss equation $\vec{\nabla} \cdot \vec{D} = 0$ obtaining $\vec{\nabla} \cdot \left[\vec{\vec{\varepsilon}} \left(\vec{E} - \vec{E}^* \right) \right] = 0$ or, equivalently, $\vec{\nabla} \cdot \left[\vec{\vec{\varepsilon}} \vec{E} \right] = \vec{\nabla} \cdot \left[\vec{\vec{\varepsilon}} \vec{E}^* \right]$. Now, we can introduce the electric potential in the standard way, writing the relation $\vec{\nabla} \cdot \left[\vec{\vec{\varepsilon}} \vec{\nabla} V(\vec{r}) \right] = -\vec{\nabla} \cdot \left[\vec{\vec{\varepsilon}} \vec{E}^* \right]$ or, similarly, the generalized Poisson equation $\vec{\nabla} \cdot \left[\vec{\vec{\varepsilon}} \vec{\nabla} V(\vec{r}) \right] = -\rho^*$ where $\rho^* = \vec{\nabla} \cdot \left[\vec{\vec{\varepsilon}} \vec{E}^* \right]$ is the charge distribution equivalent to the eigenfield. In this context the introduction of the concepts of eigenfield and inclusion has not a given direct physical meaning but it is a physical-mathematical expedient very useful to solve some problems in the electrostatics of the inhomogeneities, as we will show later on. So, we want to analyze the effects of the presence of a given inclusion (described by its eigenfield) on the electrical quantities. To begin, we suppose that the eigenfield is defined in the whole three-dimensional space and, therefore, we may solve the generalized Poisson equation by means of the Green function introduced in the previous section

$$V_{TOT}(\vec{r}) = \frac{1}{4\pi \sqrt{\det \vec{\vec{\varepsilon}}}} \int_{\Re^3} \frac{\vec{\nabla} \cdot \left[\vec{\vec{\varepsilon}} \vec{E}^*(\vec{x}) \right] d\vec{x}}{\sqrt{(\vec{r} - \vec{x})^T \vec{\vec{\varepsilon}}^{-1} (\vec{r} - \vec{x})}} = \frac{1}{4\pi \sqrt{\det \vec{\vec{\varepsilon}}}} \int_{\Re^3} \frac{\frac{\partial}{\partial x_l} \left[\varepsilon_{lk} E_k^*(\vec{x}) \right] d\vec{x}}{\sqrt{(\vec{r} - \vec{x})^T \vec{\vec{\varepsilon}}^{-1} (\vec{r} - \vec{x})}} \tag{29}$$

Now, we can use a sort of integration by part, holding on for multiple integrals, which can be written, in its general formulation, as follows

$$\int_{\Re^3} \vartheta(\vec{x}) \frac{\partial \lambda(\vec{x})}{\partial x_l} d\vec{x} = -\int_{\Re^3} \lambda(\vec{x}) \frac{\partial \vartheta(\vec{x})}{\partial x_l} d\vec{x} \tag{30}$$

where $\vartheta(\vec{x})$ and $\lambda(\vec{x})$ are two given functions with sufficiently regular behavior at infinity (this property is an immediate consequence of the divergence theorem). The application of this relation simply leads to

$$V_{TOT}(\vec{r}) = -\frac{1}{4\pi \sqrt{\det \vec{\vec{\varepsilon}}}} \int_{\Re^3} \varepsilon_{lk} E_k^*(\vec{x}) \frac{\partial}{\partial x_l} \left(\frac{1}{\sqrt{(\vec{r} - \vec{x})^T \vec{\vec{\varepsilon}}^{-1} (\vec{r} - \vec{x})}} \right) d\vec{x} \tag{31}$$

Moreover, it easy to recognize the validity of the expression

$$\frac{\partial}{\partial x_l}\frac{1}{\sqrt{(\vec{r}-\vec{x})^T\vec{\vec{\varepsilon}}^{-1}(\vec{r}-\vec{x})}} = -\frac{\partial}{\partial r_l}\frac{1}{\sqrt{(\vec{r}-\vec{x})^T\vec{\vec{\varepsilon}}^{-1}(\vec{r}-\vec{x})}} \qquad (32)$$

and therefore we can put Eq. (29) in the following final form

$$V_{TOT}(\vec{r}) = \frac{1}{4\pi\sqrt{\det\vec{\vec{\varepsilon}}}}\int_{\Re^3}\varepsilon_{lk}E_k^*(\vec{x})\frac{\partial}{\partial r_l}\left(\frac{1}{\sqrt{(\vec{r}-\vec{x})^T\vec{\vec{\varepsilon}}^{-1}(\vec{r}-\vec{x})}}\right)d\vec{x} \qquad (33)$$

If the eigenfield $E_k^*(\vec{x})$ is constant in a limited region V of the space we can say that we are dealing with a *uniform* or *homogeneous inclusion V* and the relative electric potential over the entire space become

$$V_{TOT}(\vec{r}) = \frac{1}{4\pi\sqrt{\det\vec{\vec{\varepsilon}}}}\varepsilon_{lk}E_k^*\frac{\partial}{\partial r_l}\int_V\frac{d\vec{x}}{\sqrt{(\vec{r}-\vec{x})^T\vec{\vec{\varepsilon}}^{-1}(\vec{r}-\vec{x})}} \qquad (34)$$

We define the *anisotropic harmonic potential* of an arbitrary region V as

$$\psi_V(\vec{r}) = \int_V\frac{d\vec{x}}{\sqrt{(\vec{r}-\vec{x})^T\vec{\vec{\varepsilon}}^{-1}(\vec{r}-\vec{x})}} \qquad (35)$$

So, Eq. (34) can be written

$$V_{TOT}(\vec{r}) = \frac{1}{4\pi\sqrt{\det\vec{\vec{\varepsilon}}}}\varepsilon_{lk}E_k^*\frac{\partial\psi_V(\vec{r})}{\partial r_l} \qquad (36)$$

Moreover, we define the *isotropic harmonic potential* of a region Ω as

$$\Phi_\Omega(\vec{q}) = \int_\Omega\frac{d\vec{y}}{\sqrt{(\vec{q}-\vec{y})^T(\vec{q}-\vec{y})}} \qquad (37)$$

In electrostatics and more generally in physics and mathematics many useful properties are well known for the isotropic harmonic potential: in order to utilize these properties in our context, it could be interesting to obtain a relation between the anisotropic and the isotropic potentials. To this aim, we undertake the following reasoning starting from the diagonalization $\vec{\vec{\varepsilon}} = \vec{\vec{R}}^T\vec{\vec{\Delta}}\,\vec{\vec{R}}$ for the permittivity tensor

$$\psi_V(\vec{r}) = \int_V\frac{d\vec{x}}{\sqrt{(\vec{r}-\vec{x})^T\vec{\vec{R}}^T\vec{\vec{\Delta}}^{-1}\vec{\vec{R}}(\vec{r}-\vec{x})}} = \int_V\frac{d\vec{x}}{\sqrt{\left[\vec{\vec{\Delta}}^{-1/2}\vec{\vec{R}}(\vec{r}-\vec{x})\right]^T\left[\vec{\vec{\Delta}}^{-1/2}\vec{\vec{R}}(\vec{r}-\vec{x})\right]}} \qquad (38)$$

By using the substitution $\vec{y} = \vec{\vec{\Delta}}^{-1/2}\vec{\vec{R}}\vec{x}$, which leads to $d\vec{x} = \sqrt{\det\vec{\vec{\varepsilon}}}\,d\vec{y}$, we obtain

$$\psi_V(\vec{r}) = \sqrt{\det\vec{\vec{\varepsilon}}}\int_{\vec{\vec{\Delta}}^{-1/2}\vec{\vec{R}}V}\frac{d\vec{y}}{\left\|\vec{\vec{\Delta}}^{-1/2}\vec{\vec{R}}\vec{r}-\vec{y}\right\|} = \sqrt{\det\vec{\vec{\varepsilon}}}\,\Phi_{\vec{\vec{\Delta}}^{-1/2}\vec{\vec{R}}V}\left(\vec{\vec{\Delta}}^{-1/2}\vec{\vec{R}}\vec{r}\right) \qquad (39)$$

where the symbol $\vec{\vec{\Delta}}^{-1/2}\vec{\vec{R}}V$ represents the deformation of the volume V under the effect of the linear operator $\vec{\vec{\Delta}}^{-1/2}\vec{\vec{R}}$. A very simple property of the isotropic harmonic potential is the following

$$\Phi_\Omega\left(\vec{\vec{R}}\vec{q}\right) = \Phi_{\vec{\vec{R}}^T\Omega}(\vec{q}) \qquad (40)$$

holding on for any orthogonal rotation matrix $\vec{\vec{R}}$. Now, we can apply the property obtaining

$$\begin{aligned}\psi_V(\vec{r}) &= \sqrt{\det\vec{\vec{\varepsilon}}}\,\Phi_{\vec{\vec{\Delta}}^{-1/2}\vec{\vec{R}}V}\left(\vec{\vec{\Delta}}^{-1/2}\vec{\vec{R}}\vec{r}\right) = \sqrt{\det\vec{\vec{\varepsilon}}}\,\Phi_{\vec{\vec{\Delta}}^{-1/2}\vec{\vec{R}}V}\left(\underbrace{\vec{\vec{R}}\vec{\vec{R}}^T}_{\vec{\vec{I}}}\vec{\vec{\Delta}}^{-1/2}\vec{\vec{R}}\vec{r}\right) = \\ &= \sqrt{\det\vec{\vec{\varepsilon}}}\,\Phi_{\vec{\vec{R}}^T\vec{\vec{\Delta}}^{-1/2}\vec{\vec{R}}V}\left(\vec{\vec{R}}^T\vec{\vec{\Delta}}^{-1/2}\vec{\vec{R}}\vec{r}\right) = \sqrt{\det\vec{\vec{\varepsilon}}}\,\Phi_{\sqrt{\vec{\vec{\varepsilon}}}^{-1}V}\left(\sqrt{\vec{\vec{\varepsilon}}}^{-1}\vec{r}\right)\end{aligned} \qquad (41)$$

This equation is the researched relationship between the anisotropic and the isotropic potentials. Finally, we obtain the following general relation for the electric potential generated, in the whole anisotropic space, by a uniform eigenfield

$$V_{TOT}(\vec{r}) = \frac{1}{4\pi}\varepsilon_{lk}E_k^*\frac{\partial}{\partial r_l}\Phi_{\sqrt{\vec{\vec{\varepsilon}}}^{-1}V}\left(\sqrt{\vec{\vec{\varepsilon}}}^{-1}\vec{r}\right) \qquad (42)$$

written in terms of the isotropic harmonic potential (but related to the region $\sqrt{\vec{\varepsilon}}^{-1}V$ and calculate in the argument $\sqrt{\vec{\varepsilon}}^{-1}\vec{r}$). This result will play a crucial role in the development of the theory.

We wish to specialize this result for an inclusion with an ellipsoidal shape. So, we assume that the region V is described by

$$V:\ \sum_{i=1}^{3}\frac{r_i^2}{a_i^2}\le 1 \qquad \text{or} \qquad V:\ \vec{r}^T\vec{a}^{-2}\vec{r}\le 1 \qquad (43)$$

where a_1, a_2 and a_3 are the semi-axis of the ellipsoid aligned with the reference frame and we have defined a diagonal matrix $\vec{a}$ with the diagonal elements equal to a_1, a_2 and a_3. In order to develop Eq. (42) we may better characterize the region $\sqrt{\vec{\varepsilon}}^{-1}V$. If a point $\vec{y}$ belongs to $\sqrt{\vec{\varepsilon}}^{-1}V$ we can write $\vec{y}=\sqrt{\vec{\varepsilon}}^{-1}\vec{r}$ where $\vec{r}\in V$; so, by considering the inverse relation $\vec{r}=\sqrt{\vec{\varepsilon}}\vec{y}$, and substituting it in Eq. (43), we obtain a useful description for $\sqrt{\vec{\varepsilon}}^{-1}V$

$$\sqrt{\vec{\varepsilon}}^{-1}V:\quad \vec{y}^T\left(\sqrt{\vec{\varepsilon}}\vec{a}^{-2}\sqrt{\vec{\varepsilon}}\right)\vec{y}\le 1 \qquad (44)$$

So, the region $\sqrt{\vec{\varepsilon}}^{-1}V$ is again ellipsoidal but the ellipsoid is not aligned to the axes of the reference frame and it is described by the tensor $\sqrt{\vec{\varepsilon}}\vec{a}^{-2}\sqrt{\vec{\varepsilon}}$. Therefore, it is not diagonal but symmetric and positive definite and always diagonalizable by means of suitable rotation matrix $\vec{P}$

$$\sqrt{\vec{\varepsilon}}\vec{a}^{-2}\sqrt{\vec{\varepsilon}}=\vec{P}^T\vec{b}^{-2}\vec{P} \qquad (45)$$

where $\vec{b}$ is a diagonal matrix containing the three semi-axis b_1, b_2 and b_3 of the rotated ellipsoid $\sqrt{\vec{\varepsilon}}^{-1}V$; of course, these three values are the eigenvalues of the tensor $\sqrt{\vec{\varepsilon}}\vec{a}^{-2}\sqrt{\vec{\varepsilon}}$. Moreover, it is important to observe that the rotation matrix $\vec{P}$, which diagonalizes $\sqrt{\vec{\varepsilon}}\vec{a}^{-2}\sqrt{\vec{\varepsilon}}$, is different from the previously introduced rotation matrix $\vec{R}$, which instead diagonalizes the permittivity tensor $\vec{\varepsilon}$. Anyway, a point $\vec{y}$ belongs to $\sqrt{\vec{\varepsilon}}^{-1}V$ if $\vec{y}^T\left(\vec{P}^T\vec{b}^{-2}\vec{P}\right)\vec{y}\le 1$ or, similarly, if $\left(\vec{P}\vec{y}\right)^T\vec{b}^{-2}\left(\vec{P}\vec{y}\right)\le 1$; hence, we define a point $\vec{z}=\vec{P}\vec{y}$ belonging to the domain $V'=\vec{P}\sqrt{\vec{\varepsilon}}^{-1}V$. So, the point $\vec{z}$ belongs to V' if and only if $\vec{z}^T\vec{b}^{-2}\vec{z}\le 1$. Therefore, since $V'=\vec{P}\sqrt{\vec{\varepsilon}}^{-1}V$, we can write $\sqrt{\vec{\varepsilon}}^{-1}V=\vec{P}^TV'$ where V' is the ellipsoid $\vec{z}^T\vec{b}^{-2}\vec{z}\le 1$ aligned with the reference frame under consideration. At the end of these considerations we may transform the isotropic potential appearing in Eq. (42) as follows

$$\Phi_{\sqrt{\vec{\varepsilon}}^{-1}V}\left(\sqrt{\vec{\varepsilon}}^{-1}\vec{r}\right)=\Phi_{\vec{P}^TV'}\left(\sqrt{\vec{\varepsilon}}^{-1}\vec{r}\right)=\Phi_{V'}\left(\vec{P}\sqrt{\vec{\varepsilon}}^{-1}\vec{r}\right) \qquad (46)$$

Finally the electric potential generated, in the whole anisotropic space, by a uniform ellipsoidal eigenfield is given by

$$V_{TOT}(\vec{r})=\frac{1}{4\pi}\varepsilon_{lk}E_k^*\frac{\partial}{\partial r_l}\Phi_{V'}\left(\vec{P}\sqrt{\vec{\varepsilon}}^{-1}\vec{r}\right) \qquad (47)$$

We remember that $\vec{P}$ and $\vec{b}$ are defined by the diagonalization $\sqrt{\vec{\varepsilon}}\vec{a}^{-2}\sqrt{\vec{\varepsilon}}=\vec{P}^T\vec{b}^{-2}\vec{P}$ and the region V' is defined by all the points $\vec{z}$ satisfying $\vec{z}^T\vec{b}^{-2}\vec{z}\le 1$. The final result given in Eq. (47) is the most important result in order to write the electric potential $V_{TOT}(\vec{r})$ in closed form: in fact, now, the isotropic electric potential $\Phi_{V'}$ is written in terms of an ellipsoidal region aligned to the reference frame.

Now, we find an explicit expression for the electric field generated inside the inclusion in terms of the uniform eigenfield above defined. We need to use a well-known important property of the isotropic harmonic potential: the isotropic harmonic potential generated by a unitary density in a given volume V' is defined by

$$\Phi_{V'}(\vec{z})=\int_{V'}\frac{d\vec{p}}{\left\|\vec{z}-\vec{p}\right\|} \qquad (48)$$

where V' is the region $\vec{z}^T\vec{b}^{-2}\vec{z}\le 1$, and it can be represented by means of the following integral

$$\Phi_{V'}(\vec{z}) = \pi b_1 b_2 b_3 \int_0^{+\infty} \frac{1 - f(\vec{z},s)}{R(s)} ds \qquad (49)$$

Here the functions $f(\vec{z},s)$ and $R(s)$ are defined as follows

$$f(\vec{z},s) = \sum_{i=1}^{3} \frac{z_i^2}{b_i^2 + s}; \qquad R(s) = \sqrt{(b_1^2 + s)(b_2^2 + s)(b_3^2 + s)} \qquad (50)$$

Such an integral representation can be utilized in Eq. (47) as follows

$$V_{TOT}(\vec{r}) = \frac{1}{4\pi} \varepsilon_{lk} E_k^* \frac{\partial}{\partial r_l} \left[\pi b_1 b_2 b_3 \int_0^{+\infty} \frac{1 - f(\vec{z},s)}{R(s)} ds \right]_{\vec{z} = \vec{P}\sqrt{\vec{\varepsilon}}^{-1}\vec{r}} \qquad (51)$$

The electric field can be calculated differentiating the previous relation with respect to the position vector $\vec{r}$. After a long calculation we have

$$\vec{E} = \left\{ \frac{\det(\vec{a})}{2} \int_0^{+\infty} \frac{\left(\vec{a}^2 + s\vec{\varepsilon}\right)^{-1}\vec{\varepsilon}}{\sqrt{\det\left(\vec{a}^2 + s\vec{\varepsilon}\right)}} ds \right\} \vec{E}^* \qquad (52)$$

We have find the uniform electric field $\vec{E}$ generated inside a uniform ellipsoidal inclusion ($\vec{a}$) in an anisotropic environment ($\vec{\varepsilon}$) in terms of the eigenfield $\vec{E}^*$.
Similarly, we search for an explicit expression for the electric field generated outside the inclusion in terms of the uniform eigenfield. Again, we need to use another important property of the isotropic harmonic potential. It can be represented by means of the following integral, in the region outside V'

$$\Phi_{V'}(\vec{z}) = \pi b_1 b_2 b_3 \int_{\eta(\vec{z})}^{+\infty} \frac{1 - f(\vec{z},s)}{R(s)} ds \qquad (53)$$

where the functions $f(\vec{z},s)$ and $R(s)$ are defined in Eq. (50) and the quantity $\eta(\vec{z})$ satisfies the relation $f(\vec{z},\eta(\vec{z})) = 1$. The resulting electric field for $\vec{r} \in \Re^3 \setminus V$ is given by

$$E_j(\vec{r}) = -\frac{\varepsilon_{lk} E_k^*}{4\pi} \frac{\partial}{\partial r_j} \frac{\partial}{\partial r_l} \left[\Phi_{V'}(\vec{z})\right]_{\vec{z} = \vec{P}\sqrt{\vec{\varepsilon}}^{-1}\vec{r}} \qquad (54)$$

A long derivation allows us to obtain:

$$\vec{E}(\vec{r}) = \left\{ \frac{1}{2}\det(\vec{a}) \int_{\eta}^{+\infty} \frac{\left(\vec{a}^2 + s\vec{\varepsilon}\right)^{-1}\vec{\varepsilon}}{\sqrt{\det\left(\vec{a}^2 + s\vec{\varepsilon}\right)}} ds - \frac{\det(\vec{a})}{\sqrt{\det\left(\vec{a}^2 + \eta\vec{\varepsilon}\right)}} \frac{\left[\left(\vec{a}^2 + \eta\vec{\varepsilon}\right)^{-1}\vec{r}\right]\left[\vec{\varepsilon}\left(\vec{a}^2 + \eta\vec{\varepsilon}\right)^{-1}\vec{r}\right]^T}{\left[\left(\vec{a}^2 + \eta\vec{\varepsilon}\right)^{-1}\vec{r}\right]^T\left[\vec{\varepsilon}\left(\vec{a}^2 + \eta\vec{\varepsilon}\right)^{-1}\vec{r}\right]} \right\} \vec{E}^* \qquad (55)$$

where the function η is implicitly defined by $\vec{r}^T\left(\vec{a}^2 + \eta\vec{\varepsilon}\right)^{-1}\vec{r} = 1$ and the overall behavior of the electric field is simply governed by the main tensors $\vec{\varepsilon}$ and $\vec{a}$, as expected.
We have completely solved the problem of a homogeneous ellipsoidal inclusion in an anisotropic environment. This solution can be summarized as follows. Both the Eq. (52) for the internal field and the Eq. (55) for the external one define a tensor (in brackets) which acts on the eigenfield to give the effective electric field in the corresponding region. By adopting a terminology taken from the elasticity theory we may call such tensors the internal electric Eshelby tensor and the external electric Eshelby tensor. Their complete expressions follow

$$\vec{S} = \frac{\det(\vec{a})}{2} \int_0^{+\infty} \frac{\left(\vec{a}^2 + s\vec{\varepsilon}\right)^{-1}\vec{\varepsilon}}{\sqrt{\det\left(\vec{a}^2 + s\vec{\varepsilon}\right)}} ds \qquad (56)$$

$$\vec{S}^{\infty}(\vec{r}) = \frac{\det(\vec{a})}{2} \int_{\eta}^{+\infty} \frac{\left(\vec{a}^2 + s\vec{\varepsilon}\right)^{-1}\vec{\varepsilon}}{\sqrt{\det\left(\vec{a}^2 + s\vec{\varepsilon}\right)}} ds - \frac{\det(\vec{a})}{\sqrt{\det\left(\vec{a}^2 + \eta\vec{\varepsilon}\right)}} \frac{\left[\left(\vec{a}^2 + \eta\vec{\varepsilon}\right)^{-1}\vec{r}\right]\left[\vec{\varepsilon}\left(\vec{a}^2 + \eta\vec{\varepsilon}\right)^{-1}\vec{r}\right]^T}{\left[\left(\vec{a}^2 + \eta\vec{\varepsilon}\right)^{-1}\vec{r}\right]^T\left[\vec{\varepsilon}\left(\vec{a}^2 + \eta\vec{\varepsilon}\right)^{-1}\vec{r}\right]} \qquad (57)$$

Such definitions allow us to put the final equations for the electric field in the very simple form

$$\begin{cases} \vec{E} = \vec{\vec{S}}\vec{E}^* & \text{if} \quad \vec{r} \in V \\ \vec{E}(\vec{r}) = \vec{\vec{S}}^{\infty}(\vec{r})\vec{E}^* & \text{if} \quad \vec{r} \in \Re^3 \setminus V \end{cases} \tag{58}$$

Now, we show that the problem of an electrostatic inclusion, as stated above, is extremely useful to solve the problem of a given anisotropic inhomogeneity placed in an anisotropic matrix. We will show an equivalence principle that reduces the analysis of the behavior of a inhomogeneity to that of an inclusion. Let's start by considering an ellipsoidal inhomogeneity with permittivity tensor $\vec{\vec{\varepsilon}}_i$ embedded in a anisotropic environment with permittivity $\vec{\vec{\varepsilon}}$. We suppose that the whole structure is subjected to an external uniform electric field (remotely applied) $\vec{E}^{\infty}$ (of course we have $\vec{D}^{\infty} = \vec{\vec{\varepsilon}}\vec{E}^{\infty}$). We are searching for the perturbation to this uniform field induced by the presence of the inhomogeneity. The equivalence principle, which we are going to illustrate, has been summarized in Fig. 3.

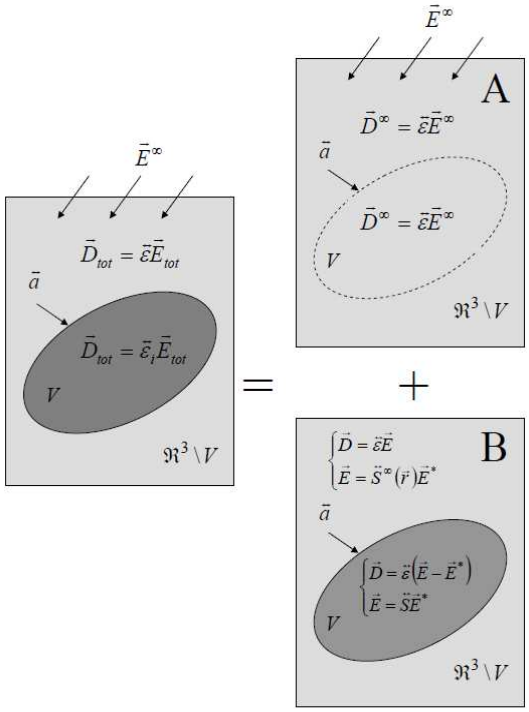

Fig. 3. Scheme of the equivalence principle between the inhomogeneity problem and the problem A (homogeneous medium) superimposed to the problem B.

The actual presence of an inhomogeneity can be described by the superimposition of the effects generated by two different situations A and B. The first situation is very simple because it considers the effects of the remote field $\vec{E}^{\infty}$ in an homogeneous matrix without the inhomogeneity. In such a case, we simply observe that the displacement vector $\vec{D}^{\infty} = \vec{\vec{\varepsilon}}\vec{E}^{\infty}$ remains uniform in the entire space. The situation B corresponds to an inclusion scheme where the eigenfield $\vec{E}^*$ is still unknown and it can be determined by imposing the equivalence between the original problem and the superimposition A+B. We define as $\vec{D}_{tot}$ and $\vec{E}_{tot}$ the electric quantities in the initial inhomogeneity problem; as above said the fields $\vec{D}^{\infty}$ and $\vec{E}^{\infty}$ correspond to the remote applied field and completely describe the situation A; finally, the problem B is described by the electric variables $\vec{D}$ and $\vec{E}$. Therefore, in any points of the space we have the superimposition $\vec{D}_{tot} = \vec{D}^{\infty} + \vec{D}$ and $\vec{E}_{tot} = \vec{E}^{\infty} + \vec{E}$. Hence, inside the ellipsoid we obtain

$$\vec{\vec{\varepsilon}}_i\vec{E}_{tot} = \vec{\vec{\varepsilon}}\vec{E}^{\infty} + \vec{\vec{\varepsilon}}\left(\vec{E} - \vec{E}^*\right) \quad \text{and} \quad \vec{E}_{tot} = \vec{E}^{\infty} + \vec{E} \tag{59}$$

These relationships, which must be verified in the internal region, allow us to calculate the exact value of the eigenfield $\vec{E}^*$ that assure the equivalence between the initial problem and the model A+B. Since $\vec{E} = \vec{\vec{S}}\vec{E}^*$ for $\vec{r} \in V$, we may write

$$\vec{\vec{\varepsilon}}_i\vec{E}_{tot} = \vec{\vec{\varepsilon}}\vec{E}^{\infty} + \vec{\vec{\varepsilon}}\left(\vec{\vec{S}} - \vec{\vec{I}}\right)\vec{E}^* \quad \text{and} \quad \vec{E}_{tot} = \vec{E}^{\infty} + \vec{\vec{S}}\vec{E}^* \tag{60}$$

By substituting the second relation in the first one we have

$$\vec{\vec{\varepsilon}}_i\left(\vec{E}^{\infty} + \vec{\vec{S}}\vec{E}^{*}\right) = \vec{\vec{\varepsilon}}\vec{E}^{\infty} + \vec{\vec{\varepsilon}}\left(\vec{\vec{S}} - \vec{\vec{I}}\right)\vec{E}^{*} \qquad (61)$$

This is an equation in the eigenfield $\vec{E}^{*}$ that can be easily solved by obtaining

$$\vec{E}^{*} = \left[\left(\vec{\vec{I}} - \vec{\vec{\varepsilon}}^{-1}\vec{\vec{\varepsilon}}_i\right)^{-1} - \vec{\vec{S}}\right]^{-1}\vec{E}^{\infty} \qquad (62)$$

This is the value of the eigenfield that ensures the validity of the equivalence principle. Moreover, it is important to calculate the total electric field $\vec{E}_{tot}$ induced inside the inhomogeneity. We simply derive $\vec{E}^{*} = \vec{\vec{S}}^{-1}\left(\vec{E}_{tot} - \vec{E}^{\infty}\right)$ and, therefore, we have

$$\vec{\vec{\varepsilon}}_i\vec{E}_{tot} = \vec{\vec{\varepsilon}}\vec{E}^{\infty} + \vec{\vec{\varepsilon}}\left(\vec{\vec{S}} - \vec{\vec{I}}\right)\vec{\vec{S}}^{-1}\left(\vec{E}_{tot} - \vec{E}^{\infty}\right) \qquad (63)$$

This equation in the unknown $\vec{E}_{tot}$ can be solved with straightforward algebraic calculations, arriving at the solution

$$\vec{E}_{tot} = \left[\vec{\vec{I}} - \vec{\vec{S}}\left(\vec{\vec{I}} - \vec{\vec{\varepsilon}}^{-1}\vec{\vec{\varepsilon}}_i\right)\right]^{-1}\vec{E}^{\infty} \quad (\vec{r} \in V) \qquad (64)$$

This is the internal electric field induced in the ellipsoid: this is a uniform vector field since all the quantities involved are constants.

Now, we can consider the external region: here the superimposition $\vec{E}_{tot} = \vec{E}^{\infty} + \vec{E}$ simply leads to the relation $\vec{E}_{tot}(\vec{r}) = \vec{E}^{\infty} + \vec{\vec{S}}^{\infty}(\vec{r})\vec{E}^{*}$, which, by considering the eigenfield obtained, leads immediately to the final result

$$\vec{E}_{tot}(\vec{r}) = \left\{\vec{\vec{I}} + \vec{\vec{S}}^{\infty}(\vec{r})\left[\left(\vec{\vec{I}} - \vec{\vec{\varepsilon}}^{-1}\vec{\vec{\varepsilon}}_i\right)^{-1} - \vec{\vec{S}}\right]^{-1}\right\}\vec{E}^{\infty} \quad (\vec{r} \in \Re^3 \setminus V) \qquad (65)$$

These results have been generalized to the nonlinear case and have been largely applied to determine the effective response of anisotropic particulate materials (S. Giordano, P. L. Palla, Dielectric behavior of anisotropic inhomogeneities: interior and exterior points Eshelby tensors, Journal of Physics A: Mathematical and Theoretical 41, 2008, 415205).

2.1.4.Functionally graded ellipsoidal dielectric particles

(*S. Giordano, P. L. Palla, L. Colombo, Effective permittivity of materials containing graded ellipsoidal inclusions, The European Physics Journal B 66, 29-35,2008; S. Giordano, P. Palla, Recent Advances in the Characterization of Composite Dielectric Structures, in Dielectric Materials: Research, Technology and Applications edited by Ai Huang, Nova Science Publishers, Inc., NY, 2009*)

The physical response of materials with spatial gradients in composition and structure is of considerable interest in disciplines as diverse as tribology, geology, microelectronics, optoelectronics, biomechanics, fracture mechanics, and nanotechnology. The damage and failure resistance of surfaces to normal and sliding contact or impact can be changed substantially through such gradients. Also in dielectric structures, graded composites and metamaterials have attracted much attention because their effective properties have advantages over traditional homogeneous composite materials (J. B. Pendry, D. Schurig, D. R. Smith, *Science*, **312**, 1780, 2006, N. M. Litchintser, I. R. Gabitov, A. I. Maimistov, V. M. Shalaev, *Progr. Optics*, **51**, 1, 2008, A. Sihvola, *Metamaterials*, **1**, 2, 2007).

Gradations in microstructure and/or porosity are commonly seen in biological structures such as bamboo, plant stems, and bone, where the strongest elements are located in regions that experience the highest stresses. Gradual changes in the elastic properties of sands, soils, and rocks beneath Earth's surface influence the settlement and stability of structural foundations, plate tectonics, and the ease of drilling into the ground. Graded transitions in composition, either continuous or in fine, discrete steps, across an interface between two dissimilar materials (such as a metal and a ceramic), can be used to redistribute thermal stresses or electric fields, to reduce stress concentrations at the intersection between an interface and a free surface and to improve interfacial bonding between dissimilar material.

The typical experiment utilized to define the response of a graded material is the indentation (S. Suresh, *Science*, **292**, 2447, 2001), which defines the force-penetration curve for an indenter applied on the free surface of the medium. The shape of the gradation inside the material may strongly influence the force-penetration curve and, therefore, the mechanical behavior of the complex material.

With currently available materials synthesis and processing capabilities, engineered gradations in properties, over nanometer to macroscopic length scales, offer appealing prospects for the design of damage-, fracture-, and wear-resistant surfaces in applications as diverse as magnetic storage media, microelectronics, bioimplants for humans, load-bearing engineering structures, protective coatings, and nano- and micro-electromechanical systems.

In the field of dielectric composites there have been a number of attempts, both analytical and experimental, to

study the responses of functionally graded materials under specific electric loads and for different microstructures. Moreover, the responses of composites made of functionalized inclusions can be useful and interesting. Various different attempts have been made to treat the composite materials of graded inclusions (L. Dong, G. Q. Gu, K. W. Yu, *Phys. Rev. B,* **67**, 224205, 2003; En-Bo Wei, Y.M. Poon, K.W. Yu*, Phys. Lett. A*, **350**, 159, 2006; G.Q. Gu, K. W. Yu, *J. Appl. Phys*., **94-5**, 3376, 2003). In this section we present a complete theory for dealing with graded ellipsoidal particles: in particular we prove an equivalence theorem between a graded dielectric ellipsoid (with gradation along a family of internal confocal ellipsoids) and an anisotropic homogeneous ellipsoid. In particular we describe a procedure to obtain the three principal permittivities of the effective ellipsoid when the gradation profile is given.

The analysis of a coated particle is the most important preliminary issue in order to deal with functionally graded inclusions. We consider the structure represented in Fig. 1 where a dielectric coated particle is taken into consideration. The core is made of an anisotropic material with principal directions of the permittivity tensor aligned with the geometrical principal directions of the internal ellipsoid (semi-axes a_{c1}, a_{c2}, a_{c3}): the principal permittivities are ε_{3k} for k=1,2,3. The shell is occupied by an isotropic material with permittivity ε_2 (semi-axes a_{s1}, a_{s2}, a_{s3}). Finally, the external homogeneous media is isotropic with permittivity ε_1. The two ellipsoids are confocal (i.e. they have the same foci). The following family of confocal ellipsoids is very useful

$$\frac{x_1^2}{a_{s1}^2+\xi}+\frac{x_2^2}{a_{s2}^2+\xi}+\frac{x_3^2}{a_{s3}^2+\xi}=1 \qquad (1)$$

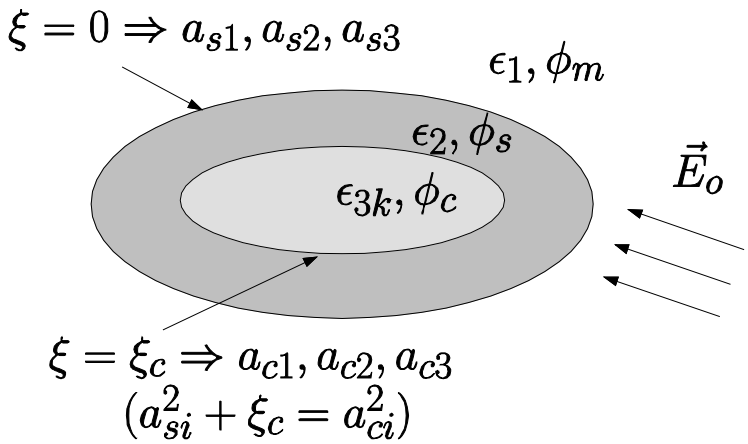

Figure 1. Coated dielectric ellipsoidal particle with external shell (s) and with internal core (c) in a given matrix (m).

If ξ=0 Eq. (1) describes the external shell (semi-axes a_{s1}, a_{s2}, a_{s3}); if $\xi=\xi_c$ it describes the surface of the internal core (semi-axes a_{c1}, a_{c2}, a_{c3}). Therefore, we have $a_{si}^2+\xi_c=a_{ci}^2$, which is a relationship among the internal semi-axes and the external ones. We assume that the external semi-axes are ordered as follows: $0<a_{s3}<a_{s2}<a_{s1}$. So, inside the particle we always have $-a_{s3}^2<\xi<0$. A given value of ξ in this range represents an ellipsoid placed inside the composite particle. It is also useful to introduce the volume fraction of the core into the whole inclusion, $c=(a_{c1}a_{c2}a_{c3})/(a_{s1}a_{s2}a_{s3})$. We prove the following property.

Theorem 1: *under the effects of a uniform field, the inclusion composed by an anisotropic core of permittivities ε_{3k} (for k=1,2,3) with volume fraction c and by an isotropic confocal shell of permittivity ε_2 (see Fig. 1) is exactly equivalent to an anisotropic homogeneous ellipsoid with principal permittivities*

$$\varepsilon_{eff,k}=\varepsilon_2\frac{\left[(\varepsilon_{3k}-\varepsilon_2)L_{ck}+\varepsilon_2\right]+c(\varepsilon_{3k}-\varepsilon_2)(1-L_{sk})}{\left[(\varepsilon_{3k}-\varepsilon_2)L_{ck}+\varepsilon_2\right]-c(\varepsilon_{3k}-\varepsilon_2)L_{sk}} \qquad (2)$$

where L_{ck} and L_{sk} are the depolarization factors of the core and of the shell, respectively.

Proof: we consider the structure represented in Fig. 1 under the effect of an externally applied uniform electric field $\vec{E}_o=E_{ok}\vec{e}_k$. We suppose that the solution for the electric potential in the three zones of the space (core, shell and matrix) can be represented as

$$\begin{aligned}
\phi_c &= C_k x_k && \text{if} \quad -a_{s3}^2 < \xi < \xi_c \\
\phi_s &= S_k x_k + T_k x_k \int_{\xi}^{+\infty} \frac{dt}{R(t)\left(a_{sk}^2 + t\right)} && \text{if} \quad \xi_c < \xi < 0 \\
\phi_m &= -E_{ok} x_k + Q_k x_k \int_{\xi}^{+\infty} \frac{dt}{R(t)\left(a_{sk}^2 + t\right)} && \text{if} \quad \xi > 0
\end{aligned} \tag{3}$$

where the sum over k is implied, $R(t)=(a_{s1}^2+t)^{1/2}\,(a_{s2}^2+t)^{1/2}(a_{s3}^2+t)^{1/2}$ and the variable ξ is defined by Eq. (1). The coefficients C_k, S_k, T_k and Q_k can be found with the boundary conditions for the electric potential, which are

$$\begin{aligned}
\phi_c &= \phi_s && \text{if} \quad \xi = \xi_c \\
\phi_s &= \phi_m && \text{if} \quad \xi = 0 \\
\varepsilon_{3k} \frac{\partial \phi_c}{\partial x_k} n_k &= \varepsilon_2 \frac{\partial \phi_s}{\partial n} && \text{if} \quad \xi = \xi_c \\
\varepsilon_2 \frac{\partial \phi_s}{\partial n} &= \varepsilon_1 \frac{\partial \phi_m}{\partial n} && \text{if} \quad \xi = 0
\end{aligned} \tag{4}$$

The long development of such conditions leads to the system

$$\begin{cases}
C_k = S_k + \dfrac{2}{a_{c1}a_{c2}a_{c3}} L_{ck} T_k \\
S_k + \dfrac{2}{a_{s1}a_{s2}a_{s3}} L_{sk} T_k = -E_{ok} + \dfrac{2}{a_{s1}a_{s2}a_{s3}} L_{sk} Q_k \\
\varepsilon_{3k} C_k = \varepsilon_2 \left[S_k + \dfrac{2}{a_{c1}a_{c2}a_{c3}} \left(L_{ck} - 1\right) T_k \right] \\
\varepsilon_2 \left[S_k + \dfrac{2}{a_{s1}a_{s2}a_{s3}} \left(L_{sk} - 1\right) T_k \right] = \varepsilon_1 \left[-E_{ok} + \dfrac{2}{a_{s1}a_{s2}a_{s3}} \left(L_{sk} - 1\right) Q_k \right]
\end{cases} \tag{5}$$

The solutions follow after straightforward algebra

$$\begin{cases}
C_k = \dfrac{\varepsilon_1 \varepsilon_2 a_{s1}a_{s2}a_{s3}}{a_{c1}a_{c2}a_{c3}(\varepsilon_{3k} - \varepsilon_2)(\varepsilon_2 - \varepsilon_1) L_{sk}(L_{sk} - 1) - a_{s1}a_{s2}a_{s3}\left[(\varepsilon_2 - \varepsilon_1)L_{sk} + \varepsilon_1\right]\left[(\varepsilon_{3k} - \varepsilon_2)L_{ck} + \varepsilon_2\right]} E_{ok} \\
S_k = \dfrac{\varepsilon_1 a_{s1}a_{s2}a_{s3}\left[(\varepsilon_{3k} - \varepsilon_2)L_{ck} + \varepsilon_2\right]}{a_{c1}a_{c2}a_{c3}(\varepsilon_{3k} - \varepsilon_2)(\varepsilon_2 - \varepsilon_1) L_{sk}(L_{sk} - 1) - a_{s1}a_{s2}a_{s3}\left[(\varepsilon_2 - \varepsilon_1)L_{sk} + \varepsilon_1\right]\left[(\varepsilon_{3k} - \varepsilon_2)L_{ck} + \varepsilon_2\right]} E_{ok} \\
T_k = -\dfrac{1}{2} \dfrac{\varepsilon_1 a_{s1}a_{s2}a_{s3}a_{c1}a_{c2}a_{c3}(\varepsilon_{3k} - \varepsilon_2)}{a_{c1}a_{c2}a_{c3}(\varepsilon_{3k} - \varepsilon_2)(\varepsilon_2 - \varepsilon_1) L_{sk}(L_{sk} - 1) - a_{s1}a_{s2}a_{s3}\left[(\varepsilon_2 - \varepsilon_1)L_{sk} + \varepsilon_1\right]\left[(\varepsilon_{3k} - \varepsilon_2)L_{ck} + \varepsilon_2\right]} E_{ok} \\
Q_k = \dfrac{a_{s1}a_{s2}a_{s3}}{2} \dfrac{a_{c1}a_{c2}a_{c3}(\varepsilon_{3k} - \varepsilon_2)\left[(\varepsilon_2 - \varepsilon_1)L_{sk} - \varepsilon_2\right] - a_{s1}a_{s2}a_{s3}(\varepsilon_2 - \varepsilon_1)\left[(\varepsilon_{3k} - \varepsilon_2)L_{ck} + \varepsilon_2\right]}{a_{c1}a_{c2}a_{c3}(\varepsilon_{3k} - \varepsilon_2)(\varepsilon_2 - \varepsilon_1) L_{sk}(L_{sk} - 1) - a_{s1}a_{s2}a_{s3}\left[(\varepsilon_2 - \varepsilon_1)L_{sk} + \varepsilon_1\right]\left[(\varepsilon_{3k} - \varepsilon_2)L_{ck} + \varepsilon_2\right]} E_{ok}
\end{cases} \tag{6}$$

It is important to observe that the external field is completely controlled by the coefficients Q_k. In order to analyze the special case of an anisotropic ellipsoid without external shell, in Eq. (6) for Q_k, we consider the following substitutions: $\varepsilon_{3k} \to \varepsilon_{eff,k}$, $a_{ci}=a_{si}$ for $i=1,2,3$, $L_{cj}=L_{sj}$ for $j=1,2,3$. In this case the shell disappears and the result is

$$Q_k = \frac{a_{s1}a_{s2}a_{s3}}{2}\frac{\varepsilon_{eff,k} - \varepsilon_1}{\left(\varepsilon_{eff,k} - \varepsilon_1\right) L_{sk} + \varepsilon_1} E_{ok} \qquad (7)$$

These coefficients describe the external field for an anisotropic ellipsoid of semi-axes a_{si} and permittivities $\varepsilon_{eff,k}$ placed in a matrix with dielectric constant ε_1. By drawing a comparison between Q_k given in Eq. (6) and Q_k given in Eq. (7) we obtain an equation for the effective permittivities of the composite inclusion

$$\frac{c(\varepsilon_{3k} - \varepsilon_2)[(\varepsilon_2 - \varepsilon_1)L_{sk} - \varepsilon_2] - (\varepsilon_2 - \varepsilon_1)[(\varepsilon_{3k} - \varepsilon_2)L_{ck} + \varepsilon_2]}{c(\varepsilon_{3k} - \varepsilon_2)(\varepsilon_2 - \varepsilon_1)L_{sk}(L_{sk} - 1) - [(\varepsilon_2 - \varepsilon_1)L_{sk} + \varepsilon_1][(\varepsilon_{3k} - \varepsilon_2)L_{ck} + \varepsilon_2]} = \frac{\varepsilon_{eff,k} - \varepsilon_1}{\left(\varepsilon_{eff,k} - \varepsilon_1\right) L_{sk} + \varepsilon_1} \qquad (8)$$

Finally, by solving the above equation for $\varepsilon_{eff,k}$ we obtain the expression shown in Eq. (2). We remark that the result given in Eq. (2) does not depend on ε_1 and depends only on the internal properties of the particle. QED.
The previous theorem allows us to consider functionally graded particle with arbitrary permittivity profile $\varepsilon(\xi)$ for $-a_{s3}^2<\xi<0$. The following result solves the problem of homogenizing graded dielectric inclusions.

Theorem 2: *under the effects of a uniform field, the functionally graded ellipsoidal particle with permittivity profile $\varepsilon(\xi)$ (in the entire range $-a_{s3}^2<V<0$, the variable ξ being defined in Eq. (1)) is exactly equivalent to an homogeneous anisotropic ellipsoid with principal permittivities defined by $\varepsilon_k(0)$ where the functions $\varepsilon_k(\xi)$ are solutions of the following differential Riccati equations (k=1,2,3)*

$$\begin{cases} \dfrac{d\varepsilon_k(\xi)}{d\xi} = -\dfrac{[\varepsilon_k(\xi) - \varepsilon(\xi)]^2}{2\varepsilon(\xi)\left(a_{sk}^2 + \xi\right)} - \dfrac{1}{R(\xi)}\dfrac{dR(\xi)}{d\xi}[\varepsilon_k(\xi) - \varepsilon(\xi)] \\ \varepsilon_k\left(-a_{s3}^2\right) = \varepsilon\left(-a_{s3}^2\right) \end{cases} \qquad (9)$$

We recall that $R(\xi)=(a_{s1}^2+\xi)^{1/2}(a_{s2}^2+\xi)^{1/2}(a_{s3}^2+\xi)^{1/2}$. The values $\varepsilon_k(s)$ (for a given s in the entire range $-a_{s3}^2<s<0$) represent the effective principal permittivities of the ellipsoid defined by the bounds $-a_{s3}^2<\xi<s$.

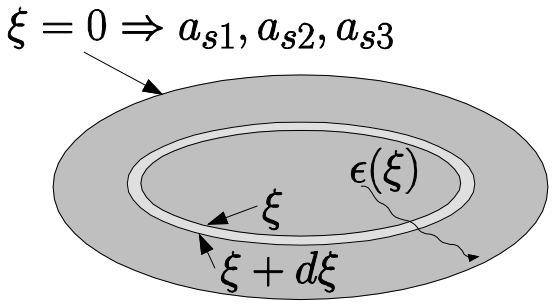

Figure 2. Functionally graded inclusion. An infinitesimal ellipsoidal layer ($\xi,\xi+d\xi$) is considered.

Proof: we take into consideration Fig.2, where an infinitesimal ellipsoidal layer ($\xi,\xi+d\xi$) is represented. We suppose that the region ($-a_{s3}^2$, ξ) has been homogenized by obtaining the effective principal permittivities $\varepsilon_k(\xi)$ (anisotropic core). The infinitesimal ellipsoidal layer ($\xi,\xi+d\xi$) is characterized by the actual permittivity $\varepsilon(\xi)$ (isotropic shell). Now, we obtain the effective principal permittivities $\varepsilon_k(\xi+d\xi)$ of the larger region ($-a_{s3}^2$, $\xi+d\xi$) by utilizing the theorem 1

$$\varepsilon_k(\xi + d\xi) = \varepsilon(\xi)\frac{(\varepsilon_k(\xi) - \varepsilon(\xi))L_k(\xi) + \varepsilon(\xi) + c(\varepsilon_k(\xi) - \varepsilon(\xi))(1 - L_k(\xi + d\xi))}{(\varepsilon_k(\xi) - \varepsilon(\xi))L_k(\xi) + \varepsilon(\xi) - c(\varepsilon_k(\xi) - \varepsilon(\xi))L_k(\xi + d\xi)} \qquad (10)$$

where the volume fraction c is given (up to the first order in $d\xi$) by

$$c = \frac{R(\xi)}{R(\xi + d\xi)} = \frac{R(\xi)}{R(\xi) + \dfrac{dR(\xi)}{d\xi}d\xi} = \frac{1}{1 + \dfrac{1}{R(\xi)}\dfrac{dR(\xi)}{d\xi}d\xi} = 1 - \frac{1}{R(\xi)}\frac{dR(\xi)}{d\xi}d\xi \qquad (11)$$

and the depolarization factors of the ellipsoid defined by ξ are

$$L_k(\xi) = \frac{R(\xi)}{2}\int_0^{+\infty} \frac{ds}{R(\xi + s)\left(a_{sk}^2 + \xi + s\right)} \qquad (12)$$

From Eq. (5.11) we may build the difference quotient for the variable $\varepsilon_k(\xi)$

$$\frac{\varepsilon_k(\xi + d\xi) - \varepsilon_k(\xi)}{d\xi} = \frac{\varepsilon(\xi)}{d\xi}\frac{(\varepsilon_k(\xi) - \varepsilon(\xi))L_k(\xi) + \varepsilon(\xi) + c(\varepsilon_k(\xi) - \varepsilon(\xi))(1 - L_k(\xi + d\xi))}{(\varepsilon_k(\xi) - \varepsilon(\xi))L_k(\xi) + \varepsilon(\xi) - c(\varepsilon_k(\xi) - \varepsilon(\xi))L_k(\xi + d\xi)} - \frac{\varepsilon_k(\xi)}{d\xi} \qquad (13)$$

By performing the limit for $d\xi \to 0$ and by using Eq. (11) we obtain the first form of the differential equation

$$\frac{d\varepsilon_k}{d\xi} = \frac{(\varepsilon_k - \varepsilon)\left[(\varepsilon_k - \varepsilon)\frac{dL_k}{d\xi} - \frac{1}{R}\frac{dR}{d\xi}((\varepsilon_k - \varepsilon)L_k + \varepsilon)\right]}{\varepsilon} \qquad (14)$$

Now, the derivative of L_k, given in Eq. (12), can be found as

$$\frac{dL_k(\xi)}{d\xi} = \frac{1}{R(\xi)}\frac{dR(\xi)}{d\xi}L_k(\xi) - \frac{1}{2\left(a_{sk}^2 + \xi\right)} \qquad (15)$$

Finally, the substitution of Eq. (15) in Eq. (14) allows us to obtain the final result shown in Eq. (9). QED.

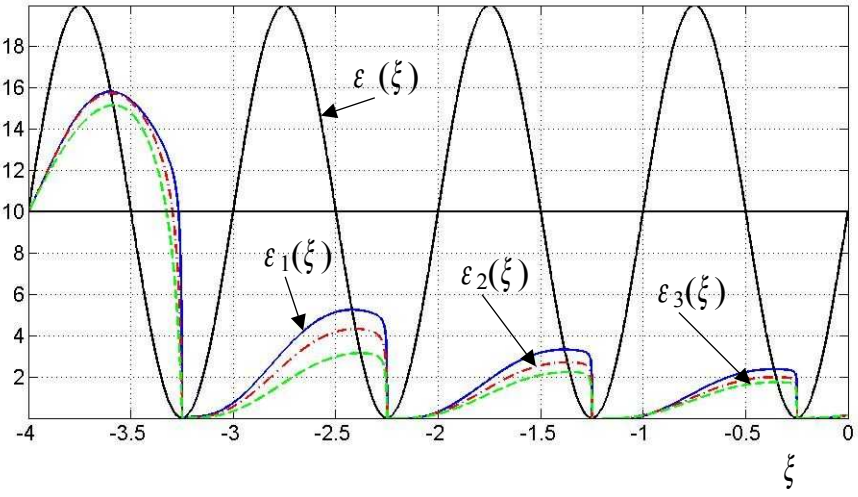

Figure 3. Example of application of the Riccati differential equations: semi-axes a_{s1}=3, a_{s2}=2.2, a_{s3}=2; permittivity profile $\varepsilon(\xi)=10+10\sin[8\pi(a_{s3}^2+\xi)/ a_{s3}^2]$ in arbitrary units (blue continuous line: $\varepsilon_1(\xi)$, red dashed-dotted line: $\varepsilon_2(\xi)$, green dashed line: $\varepsilon_3(\xi)$).

This theorem, being proved for an arbitrarily shaped ellipsoid, can be also applied to specific geometries like spheres or cylinders (with applications to simple dispersions and to fibrous materials). We show in Fig.3 an example of solution of the Riccati differential equations for a periodic profile of the permittivity $\varepsilon(\xi)$. Adopted parameters: semi-axes a_{s1}=3, a_{s2}=2.2, a_{s3}=2; permittivity profile $\varepsilon(\xi)=10+10\sin[8\pi(a_{s3}^2+\xi)/ a_{s3}^2]$ in arbitrary units.
We move now to the case of a population of functionally graded ellipsoidal particles. We assume that each particle has a given permittivity profile $\varepsilon(\xi)$. We consider that all the particles are embedded in a given matrix. Each of these particles can be substituted by an homogeneous anisotropic inclusion with principal permittivities given by the Riccati equations. These values can be obtained with the first part of the homogenization procedure, i.e. with the integration of Eq.(9). The second part of the homogenizing theory consists in finding the effective dielectric constant of the entire dispersion. Any generalization of the Maxwell-Garnett theory may be used in order to take

into account the anisotropic character of the particles. This idea is commonly referred to as multiscale approach: a paradigm effectively coupling different methods and thus providing a unique theoretical device able to pass physical information across different scales. In our case the multiscale two-steps homogenization first solves the problem inside each graded particle and then copes with the overall dispersion of inclusions.
In such a discussion, for simplicity, we have considered only static permittivities but we point out that our methodology can be also applied to the case of frequency dependent permittivities. For example it is possible to consider Drude-like dielectric constant with ξ-dependent plasma frequency and/or ξ-dependent damping coefficient. The graded Drude dielectric function is indeed very useful to analyze the properties of metal-dielectric composites.

2.1.5.Homogenization methods for linear elastic materials
(S. Giordano, Differential schemes for the elastic characterization of dispersions of randomly oriented ellipsoids, European Journal of Mechanics – A/Solids, 22, 2003, 885-902, S. Giordano, Relation Between Microscopic and Macroscopic Mechanical Properties in Random Mixtures of Elastic Media, ASME, Engineering Materials and Technology, JULY 2007, Vol. 129 / 453)

Dealing with elastic characterisation of dispersions (L. J. Walpole, 1981, Elastic behaviour of composite materials: theoretical foundations, Advanced in Applied Mechanics, 11, 169-242) the most famous and studied elastic mixture theory regards a composite material formed by spherical inclusions embedded in a solid matrix. An exact result exists for such a material composed by a very dilute concentration of spherical inclusions (with bulk modulus k_2 and shear modulus μ_2) dispersed in a solid matrix (with moduli k_1 and μ_1). This result is attributed to numerous authors (Z. Hashin, 1983, Analysis of composite materials – a survey, J. Appl. Mech., 50, 481-505). To adapt the dilute formulas to the case of any finite volume fraction a great number of proposals have been made and they appear in technical literature. The electric mixture characterisation approach used by Bruggeman is also used in micro-mechanical theories applying a similar philosophy (R. McLaughlin, 1977, A study of the differential scheme for composite materials, Int. J. Eng. Sci., 15, 237-244, N. Norris, 1985, A differential scheme for the effective moduli of composites, Mechanics of Materials, 4, 1-16. and M. Avellaneda, 1987, Iterated homogenisation, differential effective medium theory and applications, Communications on Pure and Applied Mathematics, 40, 527-554): let's suppose that the effective moduli of a composite medium are known to be k and μ. Now, if a small additional volume of inclusions is embedded in the matrix, the change in the elastic moduli is approximated to be that which arise if an infinitesimal volume of inclusions were added to a uniform, homogeneous matrix with moduli k and μ. This leads, in the simpler and most studied case, to a pair of coupled differential equations: these equations may be numerically solved and the results generate the so-called differential effective medium theory. We characterise a dispersion of randomly oriented elastic ellipsoids embedded in a given solid matrix. We will obtain a theory for very diluted dispersions and we will apply the Bruggeman procedure to generalise it to higher values of the volume fraction of the inclusions. The bonding at the interfaces remains intact in our models when the whole mixture is placed in an equilibrated state of infinitesimal elastic strain by external loads or constraints. In the present case, the boundary conditions require that both the vector displacement and the stress tensor be continuous across any interfaces. Each separate homogeneous region is characterised by its stiffness tensor, which describes the stress-strain relation. If both materials are linear and homogeneous this relation is given by:

$$T_{ij} = L^s_{ijkl} E_{kl} \qquad s = 1,2 \qquad (1)$$

where **T** is the stress tensor, **E** is the strain tensor and **L** is the constant stiffness tensor, which depends on the medium considered. For isotropic media this latter is written, for example in terms of the bulk and shear constants, as follows:

$$L^s_{ijkl} = k_s \delta_{ij}\delta_{kl} + 2\mu_s \left(\delta_{ik}\delta_{jl} - \frac{1}{3}\delta_{ij}\delta_{kl} \right) \qquad s = 1,2 \qquad (2)$$

where k_s and μ_s are the bulk and shear moduli of the s-th medium (s=1,2) and δ_{nm} is the Kronecker's delta. We start with some definitions used to simplify the problem. Instead of describing the strain with the complete symmetric tensor we adopt the Voigt notation based on a vector representation. So doing, the stress-strain relations became $\hat{\mathbf{T}} = \hat{\mathbf{L}}^1\hat{\mathbf{E}}$ in the matrix and $\hat{\mathbf{T}} = \hat{\mathbf{L}}^2\hat{\mathbf{E}}$ inside each inclusion. At this point, to begin the strain computation we take into consideration a single ellipsoidal isotropic inclusion (medium 2) embedded in a isotropic matrix (medium 1); we suppose that the matrix is placed in an equilibrated state of infinitesimal constant elastic strain by external loads and then the inclusion is added to the matrix reaching a corresponding state of strain, which is well described by the Eshelby (J. D. Eshelby, 1957, The determination of the elastic field of an ellipsoidal inclusion and related problems, Proc. R. Soc. London, Ser. A, 241, 376-396, J. D. Eshelby, 1959, The elastic field outside an ellipsoidal inclusion, Proc. R. Soc. London, Ser. A, 252, 561-569) theory. In particular we consider an ellipsoid with axes a_1,

a_2, a_3 aligned with the axes $x_1=x$, $x_2=y$, $x_3=z$ of the reference frame with the assumption $a_1>a_2>a_3>0$ and we define two eccentricities, which describe the shape of the inclusion: $0< e = a_3/a_2 <1$ and $0< g = a_2/a_1 <1$. Accordingly with the Eshelby theory (extensively described in T. Mura, 1987, *Micromechanics of defects in solids*, Kluwer Academic Publishers, Dordrecht) the relationship between the original external strain and the induced internal strain is given by:

$$\hat{\mathbf{E}}_i = \left\{ \mathbf{I} - \hat{\mathbf{S}} \left[\mathbf{I} - \left(\hat{\mathbf{L}}^1 \right)^{-1} \hat{\mathbf{L}}^2 \right] \right\}^{-1} \hat{\mathbf{E}}_0 = \hat{\mathbf{A}} \hat{\mathbf{E}}_0 \qquad (3)$$

where $\mathbf{I}$ is the identity matrix with size 6x6, $\hat{\mathbf{E}}_i$ is the internal strain, $\hat{\mathbf{E}}_0$ is the original external strain, $\hat{\mathbf{L}}^1$ and $\hat{\mathbf{L}}^2$ are the stiffness tensor of the matrix and the inclusion respectively and $\hat{\mathbf{S}}$ is the Eshelby tensor, which depends on the eccentricities e and g of the ellipsoid and on the Poisson ratio of the matrix. We remember that Eq. (3) is written taking into account a particular reference frame with axes aligned to the three principal directions of the embedded ellipsoid. In these condition matrix $\hat{\mathbf{A}}$ has the following mathematical form:

$$\hat{\mathbf{A}} = \begin{bmatrix} A_{1111} & A_{1122} & A_{1133} & 0 & 0 & 0 \\ A_{2211} & A_{2222} & A_{2233} & 0 & 0 & 0 \\ A_{3311} & A_{3322} & A_{3333} & 0 & 0 & 0 \\ 0 & 0 & 0 & A_{1212} & 0 & 0 \\ 0 & 0 & 0 & 0 & A_{2323} & 0 \\ 0 & 0 & 0 & 0 & 0 & A_{1313} \end{bmatrix} \qquad (4)$$

With the aim of analysing the behaviour of a mixture of randomly oriented ellipsoids, we need to evaluate the average value of the internal strain inside the ellipsoid over all its possible orientations or rotations in the space. To perform this averaging over all the rotations we name the original reference frame with the letter B and we consider another generic reference frame that is named with the letter F.

The relation between these bases B and F is described by means of a generic rotation matrix $\mathbf{R}(\psi,\theta,\varphi)$ where ψ, θ and φ are the Euler angles; we may consider this matrix as the product of three elementary rotations along the axes z, x and z respectively:

$$\mathbf{R}(\psi,\theta,\varphi) = \begin{bmatrix} \cos\psi & -\operatorname{sen}\psi & 0 \\ \operatorname{sen}\psi & \cos\psi & 0 \\ 0 & 0 & 1 \end{bmatrix} \cdot \begin{bmatrix} 1 & 0 & 0 \\ 0 & \cos\theta & -\operatorname{sen}\theta \\ 0 & \operatorname{sen}\theta & \cos\theta \end{bmatrix} \cdot \begin{bmatrix} \cos\varphi & -\operatorname{sen}\varphi & 0 \\ \operatorname{sen}\varphi & \cos\varphi & 0 \\ 0 & 0 & 1 \end{bmatrix} \qquad (5)$$

Therefore the following relations hold on between the different frames: $\mathbf{E}_i^B = \mathbf{R}\,\mathbf{E}_i^F\,\mathbf{R}^T$ for the internal strain and $\mathbf{E}_0^B = \mathbf{R}\,\mathbf{E}_0^F\,\mathbf{R}^T$ for the bulk strain (here the subscript T means transposed). These expressions have been written with standard notation for the strain. They may be converted in our notation defining a matrix $\hat{\mathbf{M}}(\psi,\theta,\varphi)$, 6x6 sized, which acts as a rotation matrix on our strain vectors: so, we may write $\hat{\mathbf{E}}_i^{\,B} = \hat{\mathbf{M}}\hat{\mathbf{E}}_i^{\,F}$ inside the ellipsoid and $\hat{\mathbf{E}}_0^{\,B} = \hat{\mathbf{M}}\hat{\mathbf{E}}_0^{\,F}$ outside it. The entries of the matrix $\hat{\mathbf{M}}$ are completely defined by the comparison between the relations $\mathbf{E}_i^B = \mathbf{R}\,\mathbf{E}_i^F\,\mathbf{R}^T$ and $\hat{\mathbf{E}}_i^{\,B} = \hat{\mathbf{M}}\hat{\mathbf{E}}_i^{\,F}$ and by considering the notation adopted for the strain. Eq. (3) is written on the frame B and therefore it actually reads $\hat{\mathbf{E}}_i^{\,B} = \hat{\mathbf{A}}\hat{\mathbf{E}}_0^{\,B}$; this latter may be reformulated on the generic frame F simply obtaining:

$$\hat{\mathbf{E}}_i^{\,F} = \left\{ \hat{\mathbf{M}}(\Psi,\theta,\varphi)^{-1}\,\hat{\mathbf{A}}\hat{\mathbf{M}}(\Psi,\theta,\varphi) \right\} \hat{\mathbf{E}}_0^{\,F} \qquad (6)$$

Finally, the average value of the strain inside the inclusion may be computed by means of the following integration over all the possible rotations:

$$\left\langle \hat{\mathbf{E}}_i \right\rangle = \frac{1}{8\pi^2} \int_0^{2\pi}\int_0^{2\pi}\int_0^{\pi} \left\{ \hat{\mathbf{M}}(\Psi,\theta,\varphi)^{-1}\,\hat{\mathbf{A}}\hat{\mathbf{M}}(\Psi,\theta,\varphi) \right\} \operatorname{sen}\theta \; d\theta \; d\varphi \; d\Psi \, \hat{\mathbf{E}}_0 \qquad (7)$$

By means of a very long but straightforward integration we have obtained an explicit relation between the external strain $\hat{\mathbf{E}}_0$ ($=\hat{\mathbf{E}}_0^{\,F}$) and the average value $\left\langle \hat{\mathbf{E}}_i \right\rangle$ inside the randomly oriented ellipsoid:

$$\left\langle \hat{\mathbf{E}}_i \right\rangle = \begin{bmatrix} \alpha & \beta & \beta & 0 & 0 & 0 \\ \beta & \alpha & \beta & 0 & 0 & 0 \\ \beta & \beta & \alpha & 0 & 0 & 0 \\ 0 & 0 & 0 & \alpha - \beta & 0 & 0 \\ 0 & 0 & 0 & 0 & \alpha - \beta & 0 \\ 0 & 0 & 0 & 0 & 0 & \alpha - \beta \end{bmatrix} \hat{\mathbf{E}}_0 = \hat{\mathbf{B}}\hat{\mathbf{E}}_0 \quad (8)$$

where α and β depend only on the coefficients A_{ijkl}:

$$\begin{cases} \alpha = \frac{1}{5}A_{1111} + \frac{1}{5}A_{2222} + \frac{1}{5}A_{3333} + \frac{2}{15}A_{1313} + \frac{2}{15}A_{2323} + \frac{2}{15}A_{1313} + \\ \quad + \frac{1}{15}A_{1122} + \frac{1}{15}A_{1133} + \frac{1}{15}A_{2211} + \frac{1}{15}A_{2233} + \frac{1}{15}A_{3311} + \frac{1}{15}A_{3322} \\ \\ \beta = \frac{1}{15}A_{1111} + \frac{1}{15}A_{2222} + \frac{1}{15}A_{3333} - \frac{1}{15}A_{1313} - \frac{1}{15}A_{2323} - \frac{1}{15}A_{1313} + \\ \quad + \frac{2}{15}A_{1122} + \frac{2}{15}A_{1133} + \frac{2}{15}A_{2211} + \frac{2}{15}A_{2233} + \frac{2}{15}A_{3311} + \frac{2}{15}A_{3322} \end{cases} \quad (9)$$

We may say that the matrix $\hat{\mathbf{B}}$ represents the average value of $\hat{\mathbf{A}}$ over all the possible rotations of the inclusion. From now on, we have to deal with an ensemble of inclusions randomly oriented and distributed in the solid matrix. To begin the analysis of the behaviour of the overall structure, first of all, we consider an extremely low value of the volume fraction of the dispersed component so that we may neglect the interactions among the inclusions. Therefore, each ellipsoidal particle behaves as a single one in the whole space. We define c as the volume fraction of the inclusions. Because of the low value of c we may compute the average value of the elastic strain over the whole heterogeneous material by means of the relation:

$$\left\langle \hat{\mathbf{E}} \right\rangle = (1-c)\hat{\mathbf{E}}_0 + c\left\langle \hat{\mathbf{E}}_i \right\rangle = \left[(1-c)\mathbf{I} + c\hat{\mathbf{B}}\right]\hat{\mathbf{E}}_0 \quad (10)$$

where we have considered the strain outside the inclusions approximately constant and identical to the bulk strain $\hat{\mathbf{E}}_0$. Moreover, we define $\hat{\mathbf{L}}_{eq}$ as the equivalent stiffness tensor of the whole mixture (which is isotropic because of the randomness of the orientations of the inclusions) by means of the relation $\left\langle \hat{\mathbf{T}} \right\rangle = \hat{\mathbf{L}}_{eq}\left\langle \hat{\mathbf{E}} \right\rangle$; to evaluate $\hat{\mathbf{L}}_{eq}$ we compute the average value $\left\langle \hat{\mathbf{T}} \right\rangle$ of the stress inside the random material. The average value of $\hat{\mathbf{T}}$ over the volume of the whole material is eventually obtained as follows

$$\left\langle \hat{\mathbf{T}} \right\rangle = \hat{\mathbf{L}}^1\left\langle \hat{\mathbf{E}} \right\rangle + c\left(\hat{\mathbf{L}}^2 - \hat{\mathbf{L}}^1\right)\left\langle \hat{\mathbf{E}}_i \right\rangle = \hat{\mathbf{L}}^1\left\langle \hat{\mathbf{E}} \right\rangle + c\left(\hat{\mathbf{L}}^2 - \hat{\mathbf{L}}^1\right)\hat{\mathbf{B}}\hat{\mathbf{E}}_0 \quad (11)$$

Drawing a comparison between Eq. (10) and (11) we may find a complete expression, which allows us to estimate the equivalent stiffness tensor $\hat{\mathbf{L}}_{eq}$:

$$\hat{\mathbf{L}}_{eq} = \hat{\mathbf{L}}^1 + c\left(\hat{\mathbf{L}}^2 - \hat{\mathbf{L}}^1\right)\hat{\mathbf{B}}\left[(1-c)\mathbf{I} + c\hat{\mathbf{B}}\right]^{-1} \quad (12)$$

We observe that $\hat{\mathbf{L}}_{eq}$ corresponds to an isotropic material described by the following bulk and shear moduli:

$$k_{eq} = \frac{k_1(1-c) + ck_2(\alpha + 2\beta)}{1 - c + c(\alpha + 2\beta)} = k_1 + (\alpha + 2\beta)(k_2 - k_1)c + O(c^2)$$

$$\mu_{eq} = \frac{\mu_1(1-c) + c\mu_2(\alpha - \beta)}{1 - c + c(\alpha - \beta)} = \mu_1 + (\alpha - \beta)(\mu_2 - \mu_1)c + O(c^2) \quad (13)$$

By introducing particular values of the characteristic eccentricities we may find out explicit relations for dispersions of spheres (e=1, g=1), randomly oriented circular cylinder (e=1, g=0) and randomly oriented planar inclusions (slabs or sheets with e=0, g=1). For spheres we have:

$$
\begin{aligned}
k_{eq} &= \frac{k_1(4\mu_1 + 3k_2) + 4c\mu_1(k_2 - k_1)}{4\mu_1 + 3k_2 - 3c(k_2 - k_1)} = \\
&= k_1 + \frac{4\mu_1 + 3k_1}{4\mu_1 + 3k_2}(k_2 - k_1)c + O(c^2) \\
\mu_{eq} &= \mu_1 \frac{[(1-c)\mu_1 + c\mu_2](9k_1 + 8\mu_1) + 6\mu_2(k_1 + 2\mu_1)}{\mu_1(9k_1 + 8\mu_1) + 6[(1-c)\mu_2 + c\mu_1](k_1 + 2\mu_1)} = \\
&= \mu_1 + \frac{5\mu_1(4\mu_1 + 3k_1)(\mu_2 - \mu_1)}{\mu_1(9k_1 + 8\mu_1) + 6\mu_2(k_1 + 2\mu_1)}c + O(c^2)
\end{aligned}
\tag{14}
$$

For cylinders:

$$
\begin{aligned}
k_{eq} &= k_1 + \frac{\mu_2 + 3\mu_1 + 3k_1}{\mu_2 + 3\mu_1 + 3k_2}(k_2 - k_1)c + O(c^2) \\
\mu_{eq} &= \mu_1 + \frac{1}{5}\frac{(\mu_2 - \mu_1)\left\{\begin{array}{l} 64\mu_1^4 + 84k_1\mu_1^3 + 63\mu_1^3k_2 + 184\mu_1^3\mu_2 + 156\mu_1^2k_2\mu_2 + \\ + 72\mu_1^2\mu_2^2 + 120k_1\mu_1^2\mu_2 + 81k_1\mu_1^2k_2 + 36k_1\mu_2^2\mu_1 + \\ + 90k_1k_2\mu_1\mu_2 + 21k_2\mu_1\mu_2^2 + 9k_1k_2\mu_2^2 \end{array}\right\}}{(\mu_1 + \mu_2)(\mu_2 + 3k_2 + 3\mu_1)(3\mu_1k_1 + \mu_1^2 + 3k_1\mu_2 + 7\mu_1\mu_2)}c + O(c^2)
\end{aligned}
\tag{15}
$$

For planar inclusions:

$$
\begin{aligned}
k_{eq} &= \frac{k_1(4\mu_2 + 3k_2) + 4c\mu_2(k_2 - k_1)}{4\mu_2 + 3k_2 - 3c(k_2 - k_1)} = \\
&= k_1 + \frac{4\mu_2 + 3k_1}{4\mu_2 + 3k_2}(k_2 - k_1)c + O(c^2) \\
\mu_{eq} &= \mu_2 \frac{5\mu_1(4\mu_2 + 3k_2) + c(\mu_2 - \mu_1)(9k_2 + 8\mu_2)}{5\mu_2(4\mu_2 + 3k_2) - 6c(\mu_2 - \mu_1)(k_2 + 2\mu_2)} = \\
&= \mu_1 + \frac{1}{5}\frac{(9k_2\mu_2 + 8\mu_2^2 + 12\mu_1\mu_2 + 6\mu_1k_2)(\mu_2 - \mu_1)}{\mu_2(3k_2 + 4\mu_2)}c + O(c^2)
\end{aligned}
\tag{16}
$$

Other interesting limiting cases concern void particles (porous materials) and rigid particles (reinforced materials). Spherical pores:

$$
\begin{aligned}
\nu_{eq} &= \frac{5\nu_1^2c - 3c + 2c\nu_1 - 14\nu_1 + 10\nu_1^2}{15\nu_1^2c - 13c + 2c\nu_1 - 14 + 10\nu_1} = \nu_1 - \frac{3}{2}\frac{(1 - 5\nu_1)(1 - \nu_1^2)}{5\nu_1 - 7}c + O(c^2) \\
E_{eq} &= \frac{2(1-c)(5\nu_1 - 7)E_1}{15\nu_1^2c - 13c + 2c\nu_1 - 14 + 10\nu_1} = E_1 - \frac{3}{2}\frac{E_1(5\nu_1 + 9)(\nu_1 - 1)}{5\nu_1 - 7}c + O(c^2)
\end{aligned}
\tag{17}
$$

If the spherical inclusions are completely rigid the strain inside the inclusion must be zero and therefore we let $\mu_2 \to \infty$: this condition completely describes a solid with no elastic deformations allowed. Letting $\mu_2 \to \infty$ we observe that the equation for the bulk modulus remains unchanged and the other one, for the shear modulus becomes $\mu_{eq} = \mu_1 + 5\mu_1(4\mu_1 + 3k_1)c/6k_1 + O(c^2)$. For instance, in this first order approximation, if we let $k_1 \to \infty$ we obtain the very simple relation $\mu_{eq} = \mu_1(1 + 5/2c) + O(c^2)$ which describes a mixture of inelastic spheres in a matrix with $k_1 \to \infty$. This is the elastic version of the well-known Einstein result (Einstein, 1906, A new determination of molecular dimensions, Annalen der Physik 4, 19, 289-306, Corrections 1911, *ibid.*, 34, 591-592) for the viscosity of a dispersion of rigid spheres in a viscous incompressible fluid (in fluid theory $k_1 \to \infty$ means incompressibility of the liquid and μ behaves as the viscosity): if very small rigid spheres are suspended in a liquid, the viscosity is thereby increased by a fraction which is equal to 5/2 times the total volume of the spheres suspended in a unit volume, provided that this total volume is very small. Anyway, converting our relations to Young modulus and Poisson ratio, we obtain the results for spherical rigid inclusions:

$$\nu_{eq} = \frac{c\left(10\nu_1^2 - 11\nu_1 + 3\right) + \left(8\nu_1 - 10\nu_1^2\right)}{30\nu_1^2 c + 13c - 41c\nu_1 + 8 - 10\nu_1} = \nu_1 + \frac{3}{2}\frac{(1-5\nu_1)(1-2\nu_1)(\nu_1-1)}{5\nu_1 - 4}c + O\left(c^2\right) \qquad (18)$$

$$E_{eq} = E_1 \frac{2\left(7 - 19\nu_1 + 10\nu_1^2\right)c^2 + \left(23 - 50\nu_1 + 35\nu_1^2\right)c + \left(8 - 2\nu_1 - 10\nu_1^2\right)}{\left(-13 + 28\nu_1 + 11\nu_1^2 - 30\nu_1^3\right)c^2 + \left(5 - 26\nu_1 - \nu_1^2 + 30\nu_1^3\right)c + \left(8 - 2\nu_1 - 10\nu_1^2\right)} =$$

$$= E_1 + 3E_1 \frac{(\nu_1 - 1)\left(5\nu_1^2 - \nu_1 + 3\right)}{(\nu_1 + 1)(5\nu_1 - 4)}c + O\left(c^2\right)$$

Cylindrical pores:

$$\nu_{eq} = \frac{3c\nu_1 + 8c\nu_1^2 - 5c - 15\nu_1}{16\nu_1^2 c - 20c - 4c\nu_1 - 15} = \nu_1 + \frac{1}{15}(1+\nu_1)\left(16\nu_1^2 - 28\nu_1 + 5\right)c + O\left(c^2\right) \qquad (19)$$

$$E_{eq} = \frac{15(1-c)E_1}{15 + 20c + 4c\nu_1 - 16c\nu_1^2} = E_1 + \frac{1}{15}E_1\left(16\nu_1^2 - 4\nu_1 - 35\right)c + O\left(c^2\right)$$

If the cylindrical inclusions become rigid the whole structure remains blocked by the network of rigid rods independently on the elasticity of the matrix medium (this is true because of the infinite length of the inelastic cylinders).

An interesting case is given by considering the vacuum as matrix: we obtain a random three dimensional grid of elastic rods embedded in air. The corresponding simple relationships follow

$$\nu_{eq} = \frac{1}{2}\frac{2c\nu_2 - 3c + 3}{6 - 5c} = \frac{1}{4} + \frac{1}{6}\left(\nu_2 - \frac{1}{4}\right)c + O\left(c^2\right) \qquad (20)$$

$$E_{eq} = \frac{cE_2}{6 - 5c} = \frac{1}{6}E_2\, c + O\left(c^2\right)$$

This means that the Poisson ratio of this random grid is approximately equals to ¼ for very small radius of the elastic cylinders.

From now on, we will describe mixtures formed by infinite two-dimensional planes randomly embedded in a given homogeneous matrix. If the second medium (planar inclusions) is the vacuum the sheets generates a not connected elastic matrix and the equivalent Young modulus of the whole medium vanishes. If the planar inclusions become rigid the whole structure remains blocked by the network of rigid sheets independently on the elasticity of the matrix medium. However, the other two following cases are more interesting: if we let E_1=0 we are considering the vacuum as matrix and therefore we obtain a random three dimensional grid of elastic sheets embedded in air. The corresponding equivalent moduli follow

$$\nu_{eq} = \frac{3 + 5\nu_2^2 c - 3c + 2c\nu_2 + 12\nu_2 - 15\nu_2^2}{15\nu_2^2 c - 15\nu_2^2 + 2c\nu_2 - 12\nu_2 - 13c + 27} = \frac{5\nu_2 + 1}{5\nu_2 + 9} + \frac{2}{3}\frac{(5\nu_2 - 7)(5\nu_2 - 1)(\nu_2 + 1)}{(5\nu_2 + 9)^2(\nu_2 - 1)}c + O\left(c^2\right) \qquad (21)$$

$$E_{eq} = \frac{2c(7 - 5\nu_2)E_2}{15\nu_2^2 c - 15\nu_2^2 + 2c\nu_2 - 12\nu_2 - 13c + 27} = \frac{2}{3}\frac{c(7 - 5\nu_2)E_2}{(5\nu_2 + 9)(1 - \nu_2)} + O\left(c^2\right)$$

Finally, the last case considered deals with a rigid matrix $E_1 \to \infty$: the randomly oriented elastic sheets separate rigid parts of the matrix (that remains not connected). In other words, we may think to a random filling of rigid stones separated or cemented by an elastic medium or paste. The analysis leads to the explicit expressions

$$\nu_{eq} = \frac{10\nu_2^2 c + 3\nu_2 - 11c\nu_2 + 3c - 3}{30\nu_2^2 c - 30\nu_2^2 - 41c\nu_2 + 51\nu_2 + 13c - 21} = \frac{1}{7 - 10\nu_2} - \frac{2}{3}\frac{(5\nu_2 - 4)(2\nu_2 - 1)(5\nu_2 - 1)}{(10\nu_2 - 7)^2(\nu_2 - 1)}c + O\left(c^2\right) \qquad (22)$$

$$E_{eq} = \frac{\left(5c\nu_2 - 15\nu_2 - 7c + 15\right)\left(2c - 4c\nu_2 - 3 + 3\nu_2\right)E_2}{(\nu_2 + 1)\left(30\nu_2^2 c - 30\nu_2^2 - 41c\nu_2 + 51\nu_2 + 13c - 21\right)c} =$$

$$= \frac{15}{c}\frac{(\nu_2 - 1)E_2}{(10\nu_2 - 7)(\nu_2 + 1)} - 2\frac{\left(50\nu_2^2 - 70\nu_2 + 27\right)E_2}{(10\nu_2 - 7)^2(\nu_2 + 1)} - \frac{4}{3}\frac{(2\nu_2 - 1)(5\nu_2 - 4)(5\nu_2 - 1)^2 E_2}{(10\nu_2 - 7)^3(\nu_2 + 1)(\nu_2 - 1)}c + O\left(c^2\right)$$

In the present case, if the volume fraction of the planar elastic sheets vanishes, the whole structure becomes rigid and thus the Young modulus diverges to infinity.

For the sake of simplicity, the relationships above described may be recast in the following unified form, for a given shape of the inclusions embedded in the elastic matrix:

$$\begin{cases} k_{eq} = F(k_1, k_2, \mu_1, \mu_2, c) \\ \mu_{eq} = G(k_1, k_2, \mu_1, \mu_2, c) \end{cases} \tag{23}$$

The Bruggeman procedure is a method to find a second set of mixture relationships considering a first theory describing the composite material (actually functions F and G). This second theory is usually more efficient than the first one even if the mixture is not strongly diluted. In Bruggeman scheme the initially low concentration is gradually increased by infinitesimal additions of the dispersed component. By applying this technique we obtain the following system of ordinary differential equations:

$$\begin{cases} \dfrac{dk_{eq}}{dc} = \dfrac{1}{1-c} \left. \dfrac{\partial F}{\partial c} \right|_* \\ \dfrac{d\mu_{eq}}{dc} = \dfrac{1}{1-c} \left. \dfrac{\partial G}{\partial c} \right|_* \end{cases} \tag{24}$$

This system, when two functions F and G are given, defines a new couple of functions, which should better describe the mixture even if it is not strongly diluted. The application of this Bruggeman approach to Eq. (13) allows us to write down the differential system:

$$\begin{cases} \dfrac{dk_{eq}}{dc} = \dfrac{(\alpha + 2\beta)(k_2 - k_{eq})}{1-c} \\ \dfrac{d\mu_{eq}}{dc} = \dfrac{(\alpha - \beta)(\mu_2 - \mu_{eq})}{1-c} \end{cases} \tag{25}$$

where α and β are calculated with $k_1=k_{eq}$ and $\mu_1=\mu_{eq}$. We remember that the coefficients α *and* β depend on $k_1=k_{eq}$, k_2, $\mu_1=\mu_{eq}$, μ_2, e, g and thus the differential scheme takes into consideration the actual shape of the inclusions.

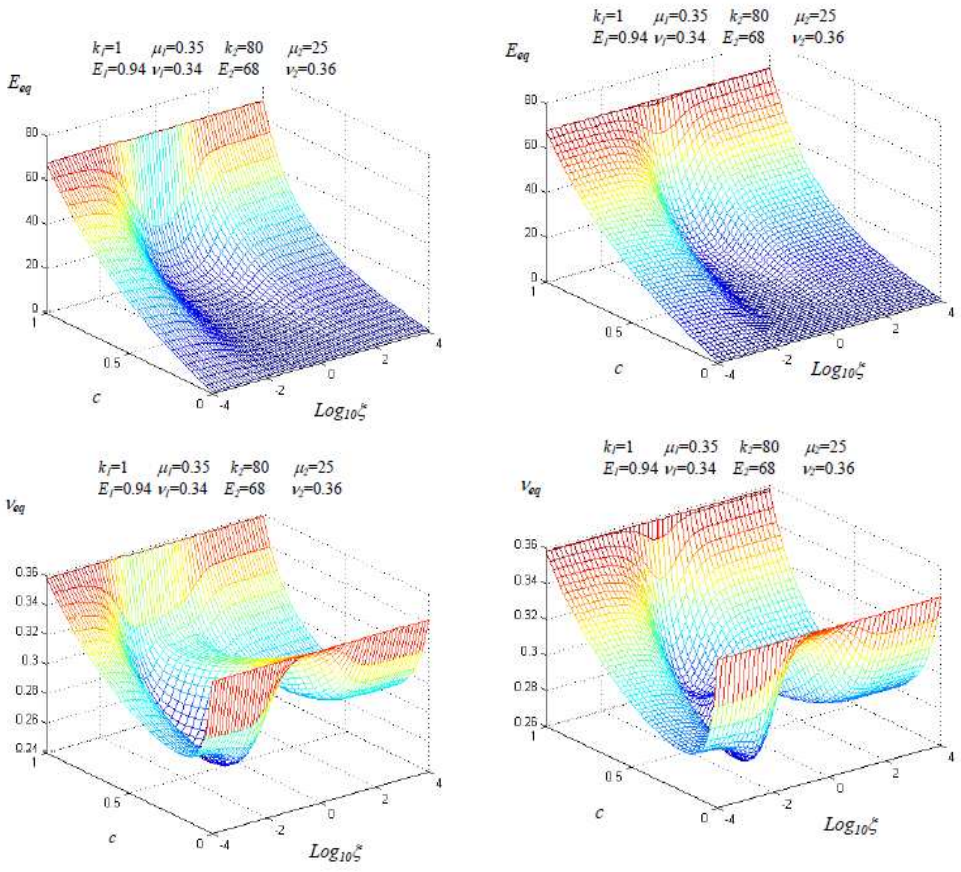

Fig 1. Results obtained for a mixture of ellipsoids of rotation described by the first procedure, holding on for very diluted dispersions (left). Results obtained by means of the differential scheme applied to a mixture of ellipsoids of rotation (right). The elastic constants are plotted versus the eccentricity and the volume fraction.

A comparison between the strongly diluted characterisation, explained in the first section of the work, and the differential scheme has been shown in Figs. 1. We defined ξ as the ratio between the length of the two different axes of the ellipsoids: $\xi>1$ for prolate ellipsoids (of ovary or elongated form) and $\xi<1$ for oblate ellipsoids (of planetary or flattened form). Therefore, in Fig.1, we have plotted the behaviour of the elastic moduli versus the volume fraction c of the inclusions and the decimal logarithm of the parameter ξ. The larger quantitative differences between the two approaches are exhibited in the zone of spheroidal particles $\log_{10\xi}=0$. From now on, we try to apply this method to obtain some explicit expressions for different classes of heterogeneous materials. Dealing with dispersions of spheres, we may obtain the following results in closed form. If we are considering the mixture of porous spheres we can apply the differential procedure, obtaining the explicit relations:

$$\begin{cases} \left(\dfrac{1-5\nu_{eq}}{1-5\nu_1}\right)^{\frac{5}{6}}\left(\dfrac{1-\nu_1}{1-\nu_{eq}}\right)^{\frac{1}{6}}\left(\dfrac{1+\nu_1}{1+\nu_{eq}}\right)^{\frac{2}{3}} = 1-c \\ \\ E_{eq} = E_1\left(\dfrac{1-5\nu_{eq}}{1-5\nu_1}\right)^{\frac{5}{3}}\left(\dfrac{1+\nu_1}{1+\nu_{eq}}\right)^{\frac{2}{3}} \end{cases} \tag{26}$$

The same procedure may be worked out for the mixture with rigid spheres. Once again, the differential scheme may be solved by means of straightforward integration of rational functions, obtaining:

$$\begin{cases} \left(\dfrac{1-5\nu_{eq}}{1-5\nu_1}\right)^{\frac{5}{6}}\left(\dfrac{1-\nu_1}{1-\nu_{eq}}\right)^{\frac{1}{6}}\left(\dfrac{1-2\nu_1}{1-2\nu_{eq}}\right)^{\frac{2}{3}} = 1-c \\ \\ E_{eq} = E_1\dfrac{1+\nu_{eq}}{1+\nu_1}\left(\dfrac{1-2\nu_{eq}}{1-2\nu_1}\right)^{\frac{5}{3}}\left(\dfrac{1-5\nu_1}{1-5\nu_{eq}}\right)^{\frac{5}{3}} \end{cases} \tag{27}$$

In each system, once the first irrational equation is (numerically) solved with respect to the effective Poisson ratio, the Young modulus of the structure is directly given by the second expression. These relationships exhibit the following properties. For porous materials (with spherical pores) we obtain two fixed points for the Poisson ratio: if $\nu_1=-1$ we have $\nu_{eq}=-1$ and if $\nu_1=1/5$ we have $\nu_{eq}=1/5$ for all pores concentrations. Although the equivalent Young's modulus cannot be analytically independent on the Poisson's ratio ν_1 of the matrix, it is numerically so over the restricted range $0<\nu_1<1/2$. Once more, two fixed points also exist for dispersions of rigid spheres: if $\nu_1=1/2$ we have $\nu_{eq}=1/2$ and if $\nu_1=1/5$ we have $\nu_{eq}=1/5$ for all inclusions concentrations. Moreover, the equivalent Young's modulus of the dispersion of inelastic spheres is a monotonically increasing function of the concentration c of the spheres and diverges to infinity when $c=1$; the obtained Young's modulus is practically independent on the Poisson's ratio ν_1 of the matrix for $0<\nu_1<1/2$. In both models for $c=1$ the equivalent Poisson's ratio converges to the fixed non-zero value $\nu_0=1/5$ irrespective of the matrix Poisson's ratio.

For instance, we draw some comparisons between Eq. (26) and experimental results. Measurements on the compressibility ($1/k_{eq}$) of a porous glass over a wide range of porosities have been performed (J. B. Walsh, W. F. Brace, A. W. England, 1965, Effect of porosity on compressibility of glass, J. Am. Ceram. Soc., 48, 605-608). Bulk and shear moduli of the pure glass were measured to be $k_1=46.3$ GPa and $\mu_1=30.5$ GPa, respectively. Standard conversions among different elastic moduli allow us to draw a comparison between bulk modulus experimentally measured and computed by Eq. (26), as one can see in Fig. 2. Moreover, the Young's modulus of the polycrystalline monoclinic Gd_2O_3 has been studied (J. A. Haglund, O. Hunter, 1973, Elastic properties of polycrystalline monoclinic Gd_2O_3, J. Am. Ceram. Soc., 56, 327-330). Poisson's ratio and Young's modulus of the pure oxide were measured to be: $E=150$ GPa and $\nu=0.29$. In Fig. 2 a comparison is drawn between the experimental data and the results given by Eq. (26).

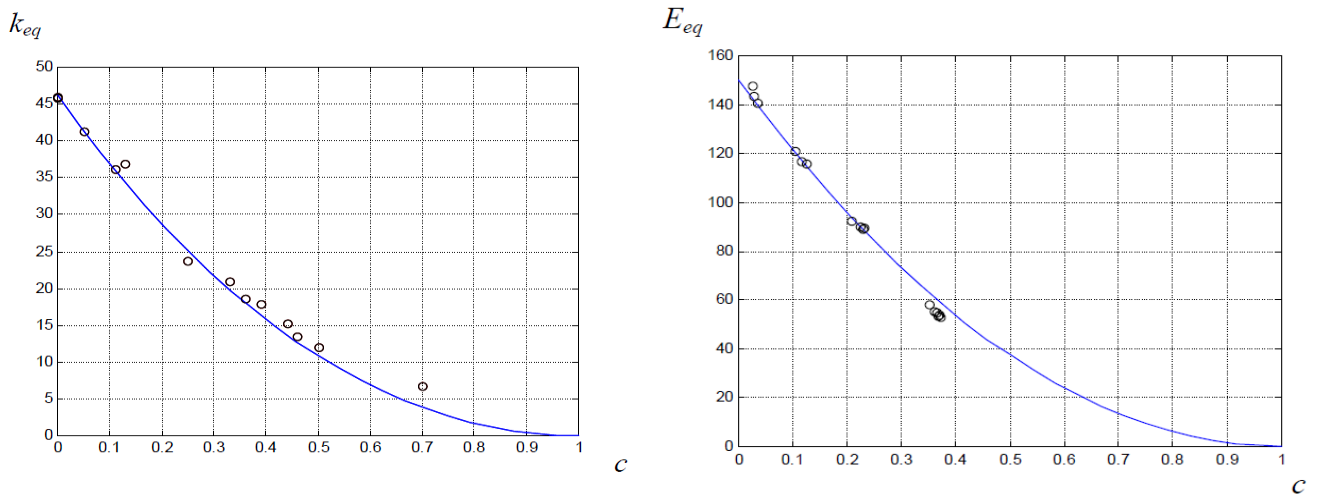

Fig. 2. Bulk modulus k_{eq} in GPa of porous P-311 glass (circles) measured at room temperature compared with data obtained by Eq. (26) (solid line) for different values of the porosity c (left). Measured Young's modulus E_{eq} (in GPa) of porous oxide Gd_2O_3 (circles) versus porosity c (right) compared with the solution of Eq. (26) (solid line).

We show now some results concerning the linear random mixtures (perfectly random microstructure). Roughly speaking, a random (or statistical) mixture is a material composed of little particles, having completely haphazard sizes, positions and shapes; each particle is entirely composed of one of some given homogeneous isotropic materials. This definition has a clear intuitive meaning, though it does not withstand an accurate criticism. Each separate homogeneous region has its characteristic stiffness tensor, which describes the stress-strain relation. If the materials are linear, isotropic and homogeneous this relation is given by $T_{ij} = L^s_{ijkl} E_{kl}, \quad s = 1,2,...,N$ where T is the stress tensor, E is the strain tensor and L is the constant stiffness tensor, which depends on the medium considered. For isotropic media this latter is written in terms of k_s and μ_s, which are the bulk and shear moduli of the s-th medium. We know that for a dispersion of spheres we have

$$\begin{cases} k = k_1 + \dfrac{4\mu_1 + 3k_1}{4\mu_1 + 3k_2}(k_2 - k_1)c + O(c^2) \\ \\ \mu = \mu_1 + \dfrac{5\mu_1(4\mu_1 + 3k_1)(\mu_2 - \mu_1)}{\mu_1(9k_1 + 8\mu_1) + 6\mu_2(k_1 + 2\mu_1)}c + O(c^2) \end{cases} \tag{28}$$

This is the exact result for a material composed by a very dilute concentration of spherical inclusions (medium 2 with moduli k_2 and μ_2 and volume fraction c) dispersed in a solid matrix (medium 1 with moduli k_1 and μ_1 and volume fraction 1-c). A similar result holds on for the two dimensional case (circles in the plane):

$$\begin{cases} k = k_1 + \dfrac{\mu_1 + k_1}{\mu_1 + k_2}(k_2 - k_1)c + O(c^2) \\ \\ \mu = \mu_1 + \dfrac{2\mu_1(\mu_1 + k_1)(\mu_2 - \mu_1)}{\mu_1(k_1 + \mu_2) + \mu_2(k_1 + \mu_1)}c + O(c^2) \end{cases} \tag{29}$$

It should be noted that the bulk modulus k, in Eq. (29), is not the same as the customarily used three-dimensional bulk modulus; however, for the plane strain conditions they are related by the formula: $k_{2D} = k_{3D} + \frac{1}{3}\mu_{3D}$.

Moreover, we remember that the shear modulus has the same definition in two or three-dimensions: $\mu_{2D} = \mu_{3D}$. We omit the indication *2D* or *3D* adopting the convention that k represents k_{2D} in all two-dimensional relationships. In the sequel, these results will be used to derive some exact properties of two-phase random mixtures, that is, materials for which the components are isotropic, linear and mixed together as an ensemble of particles having random shapes and positions. We consider the case of a random mixture (either two-dimensional or three-

dimensional) composed by two media with concentrations $c_1 = 1 - c$ and $c_2 = c$ respectively. We assume by hypothesis that the only structural information on the mixture is the volume fraction of the second medium, since either medium is composed of particles completely randomised in size, position and shape. In this problem we may not distinguish between the matrix and the inclusions. For example, in a polycrystalline media, each crystal may be treated as an inclusion embedded in the remaining crystals and hence, all crystals have the same significance. So, there is complete symmetry in treating each crystal as an inclusion. Therefore, the concept of a matrix with embedded inclusions is no longer relevant. Nevertheless, it is possible to use Eqs. (28) and (29), in order to find some properties of a random mixture. For such a mixture we may use relations of this kind for the average moduli: $k = F(k_1, k_2, \mu_1, \mu_2, c)$ and $\mu = G(k_1, k_2, \mu_1, \mu_2, c)$. Functions F and G completely define the overall behaviour of the random two-phase mixture and they are, for the moment, unknown in structure. This statement is actually a definition of random mixture: a mixture composed by parts so randomised, as above said, that the only significant structural information is merely the volume fraction c of the second medium (1- c for the first medium). This definition is heuristically useful to calculate average parameters, as it is shown in the sequel. We search for some mathematical properties of functions F and G, which may be used in the following derivations to find out their complete analytical structure. Let us examine the situation for very low values of c; we may think that a low value of c is reached when the structure contains only a single very small element of the second medium embedded in the matrix of the first medium. In this limiting case, Eqs. (28) and (29), obtained for diluted suspensions of spheres, hold on even for random mixture: i.e., the very small concentration behaviour of functions F and G must be the same of that exhibited by Eqs. (28) and (29). More precisely, we think of a single embedded sphere with infinitesimal volume (or radius): this very small sphere represents a single point defect in the solid matrix and then it describes a random mixture with a single very small element of the second medium. Therefore, we may write down the derivatives of the functions F and G with respect to the volume fraction c, calculated for c=0. In the three-dimensional case we have:

$$\begin{cases} \left.\dfrac{\partial F}{\partial c}\right|_{c=0} = \dfrac{4\mu_1 + 3k_1}{4\mu_1 + 3k_2}(k_2 - k_1) \\ \\ \left.\dfrac{\partial G}{\partial c}\right|_{c=0} = \dfrac{5\mu_1(4\mu_1 + 3k_1)(\mu_2 - \mu_1)}{\mu_1(9k_1 + 8\mu_1) + 6\mu_2(k_1 + 2\mu_1)} \end{cases} \tag{30}$$

Similarly, for the two dimensional case:

$$\begin{cases} \left.\dfrac{\partial F}{\partial c}\right|_{c=0} = \dfrac{\mu_1 + k_1}{\mu_1 + k_2}(k_2 - k_1) \\ \\ \left.\dfrac{\partial G}{\partial c}\right|_{c=0} = \dfrac{2\mu_1(\mu_1 + k_1)(\mu_2 - \mu_1)}{\mu_1(k_1 + \mu_2) + \mu_2(k_1 + \mu_1)} \end{cases} \tag{31}$$

By using these expressions, we may solve the complete problem of a random mixture composed of N homogeneous media, having volume fractions $c_1, c_2, \ldots, c_N$ (Σc_i=1, i=1..N) and moduli (k_1, μ_1), (k_2, μ_2),…,(k_N, μ_N) respectively. We consider these assumptions on the statistical composition of the random heterogeneous material: we subdivide the whole medium in many smaller pieces having completely random shape and position; each of this part is homogeneous and has moduli (k_j, μ_j) with probability c_j. The values of the moduli in a given little piece are statistically independent on the values assigned in the other pieces. This means, by using the law of large numbers, that the stoichiometric coefficient of the j-th components is c_j. In other words, the density probability of the values of the elastic moduli in a given piece of material has the form $W(k,\mu) = \sum_{j=1}^{N} c_j \delta(k - k_j)\delta(\mu - \mu_j)$. These values are statistically independent for different parts of the whole material. This is the definition of the N-phase elastic random medium used to obtain the following results. Note that all the constituents have the same significance to define the whole heterogeneous material. It is only the volume fractions that are of concern.

Now, we are ready to consider a generic mixture with N different media. Each medium, in the generic mixture, has moduli k_i and μ_i and volume concentration c_i (i=1..N); k and μ are the equivalent moduli of the mixture. If we add to the mixture a little volume dc with moduli k_j and μ_j we create a new heterogeneous material formed by the original mixture (moduli k and μ) and a volume with moduli k_j and μ_j; this new mixture can be analysed considering it as a

two component one; therefore, its moduli, referred to as k_j' and μ_j', are given by:

$$\begin{cases} k_j' = F\left(k, k_j, \mu, \mu_j, \dfrac{dc}{1+dc}\right) \cong F\left(k, k_j, \mu, \mu_j, dc\right) \\ \mu_j' = G\left(k, k_j, \mu, \mu_j, \dfrac{dc}{1+dc}\right) \cong G\left(k, k_j, \mu, \mu_j, dc\right) \end{cases} \tag{32}$$

Let us suppose that the procedure of adding a volume *dc* is made for each medium (j=1,2…N), giving a probability c_j to the case of moduli (k_j, μ_j). The average moduli are clearly the very same k and μ of the original mixture, hence one may state that:

$$\begin{cases} k = \sum_{j=1}^{N} k_j' c_j = \sum_{j=1}^{N} F\left(k, k_j, \mu, \mu_j, dc\right) c_j = \sum_{j=1}^{N} \left[F\left(k, k_j, \mu, \mu_j, 0\right) + \left. \dfrac{\partial F\left(k, k_j, \mu, \mu_j, c\right)}{\partial c} \right|_{c=0} dc \right] c_j \\ \mu = \sum_{j=1}^{N} \mu_j' c_j = \sum_{j=1}^{N} G\left(k, k_j, \mu, \mu_j, dc\right) c_j = \sum_{j=1}^{N} \left[G\left(k, k_j, \mu, \mu_j, 0\right) + \left. \dfrac{\partial G\left(k, k_j, \mu, \mu_j, c\right)}{\partial c} \right|_{c=0} dc \right] c_j \end{cases} \tag{33}$$

By using the relations $F\left(k, k_j, \mu, \mu_j, 0\right) = k$, $G\left(k, k_j, \mu, \mu_j, 0\right) = \mu$ and $\sum_{j=1}^{N} c_j = 1$, we obtain, after some straightforward calculations:

$$\begin{cases} \sum_{j=1}^{N} \left. \dfrac{\partial F\left(k, k_j, \mu, \mu_j, c\right)}{\partial c} \right|_{c=0} c_j = 0 \\ \sum_{j=1}^{N} \left. \dfrac{\partial G\left(k, k_j, \mu, \mu_j, c\right)}{\partial c} \right|_{c=0} c_j = 0 \end{cases} \tag{34}$$

For the three dimensional case we obtain:

$$\begin{cases} \dfrac{1}{3k + 4\mu} = \sum_{j=1}^{N} \dfrac{c_j}{3k_j + 4\mu} \\ \dfrac{1}{5\mu\left(3k + 4\mu\right)} = \sum_{j=1}^{N} \dfrac{c_j}{3k\left(2\mu_j + 3\mu\right) + 4\mu\left(2\mu + 3\mu_j\right)} \end{cases} \tag{35}$$

For the two-dimensional one:

$$\begin{cases} \dfrac{1}{k + \mu} = \sum_{j=1}^{N} \dfrac{c_j}{k_j + \mu} \\ \dfrac{1}{2\mu\left(k + \mu\right)} = \sum_{j=1}^{N} \dfrac{c_j}{k\left(\mu_j + \mu\right) + 2\mu_j\mu} \end{cases} \tag{36}$$

Such expressions represent the explicit relation among the microscopic properties of the material and the macroscopic ones, which can be measured on a large region of medium. We may observe that each component intervenes in the same way, to define the whole structure of the formulas, exhibiting the complete symmetry among the constituents of the random medium.

When all constituents of an elastic composite have the same shear modulus μ, Hill has shown that the effective modulus k, in three-dimensional structures, is given by the exact formula (Hill, R., Elastic properties of reinforced solids: Some theoretical principles, *J. Mech. Phys. Solids* 11, 1963, 357-372):

$$\frac{1}{3k + 4\mu} = \left\langle \frac{1}{3k(\mathbf{x}) + 4\mu} \right\rangle \tag{37}$$

where $\langle f(\mathbf{x}) \rangle$ represents the average value of the function $f(\mathbf{x})$ over the entire mixture volume. This result is true for any microstructure and may be also formulated for two dimensional mixtures:

$$\frac{1}{k+\mu} = \left\langle \frac{1}{k(\mathbf{x})+\mu} \right\rangle \qquad (38)$$

Both these exact results, being independent on the microstructure, in particular, should be correct in the case of random mixtures. In effect, they are in complete agreement with our results, as can be easily verified.

We consider an isotropic planar random elastic medium. It is incompressible at each point (infinite bulk modulus) and it is formed by a mixture between two media with shear moduli μ_1 and μ_2 and infinite bulk modulus. The duality theorem (Berdichevski, V.L., *Variational principles in mechanics of continuum media*, Nauka, Moscow, 1983) can be stated as follows. We may write the effective shear modulus μ as a function $h(\mu_1, \mu_2)$ of the shear moduli of the phases and it exactly satisfies the phase interchange relation:

$$h(\mu_1,\mu_2)h(\mu_2,\mu_1) = \mu_1\mu_2 \qquad (39)$$

In particular, if the composite is phase interchange invariant, i.e. $h(\mu_1,\mu_2) = h(\mu_2,\mu_1)$, like a two-dimensional checkerboard or like a two-phase two-dimensional equal fraction random mixture, then Eq. (39) implies the following formula (Lurie, K.A. and Cherkaev, A.V., G-closure of some particular sets of admissible material characteristics for the problem of bending of the thin elastic plates, *J. Opt. Theory Appl.* 42/2, 1984, 305-316)

$$\mu = \sqrt{\mu_1\mu_2} \qquad (40)$$

By using the translation method (Cherkaev, A.V., Lurie, K.A. and Milton, G.W., Invariant properties of the stress in plane elasticity and equivalence classes of composites', *Proc. Roy. Soc. London, Ser. A* **438,** 1992, 519-529, Milton, G.W., On characterising the set of possible effective tensors of composites: the variational method and the translation method, *Communs Pure Appl. Math.* **43,** 1990, 63-125) they generalised this result to two-dimensional structures composed of compressible media having the same bulk modulus and they found that the effective shear modulus μ of the mixture is given by:

$$\mu = \frac{k}{-1+\sqrt{\dfrac{(k+\mu_1)(k+\mu_2)}{\mu_1\mu_2}}} \qquad (41)$$

where k, μ_1 and μ_2 are the common planar bulk and two shear moduli of the components. One can observe that Eq. (41), in the limiting case of $k \to \infty$, reduces to Eq. (40) as expected.

Now, we can simply show that our Eq. (36) yields the same results. To describe a phase interchange invariant structure we consider a two-phase two-dimensional random mixture with $c_1=c_2=1/2$ and we suppose $k_1=k_2=k$. Also in this case, it is not difficult to prove that our theory yields results in agreement with those available in literature.

The proposed approach may be applied also to the elastic characterisation of porous materials when the voids (zero stiffness inclusions) are randomly distributed and have random shape. From a general point of view we expect the equivalent Young's modulus E and the Poisson's ratio v to depend on properties of the solid matrix E_1 and v_1. Therefore, the final mixing rules should appear as $E=E_1 f(c,v_1)$ and $v=g(c,v_1)$. Here c is the voids volume fraction (porosity) and the mathematical structure of the dimensionless functions f and g depend on the microstructure of the pores.

We begin the analysis with two-dimensional random porous structures; so, the theory is applied with a zero stiffness phase ($k_2=0$ and $\mu_2=0$). Equation (36) has two possible solutions, one equals to zero and another different from zero: since it is reasonable to assume that the shear modulus be a non-negative, continuous function of c, the true solution is given by the following relationship:

$$\mu = \begin{cases} \dfrac{\mu_1 k_1(1-3c)}{k_1(1-c)+2c\mu_1} & if \quad c \le \dfrac{1}{3} \\ 0 \quad if \quad c > 1/3 \end{cases} \qquad (42)$$

Therefore, for two-dimensional structure, we observe a percolation threshold given by $c_0=1/3$. Similarly, we find out the expression for the two-dimensional bulk modulus as follows:

$$k = \begin{cases} \dfrac{\mu_1 k_1(1-3c)}{\mu_1(1-2c)+ck_1} & if \quad c \le \dfrac{1}{3} \\ 0 \quad if \quad c > 1/3 \end{cases} \qquad (43)$$

In terms of the Young's modulus and the Poisson's ratio we have

$$E = \begin{cases} E_1(1 - 3c) & if \quad c \le 1/3 \\ 0 & if \quad c > 1/3 \end{cases} \tag{44}$$

$$\nu = \begin{cases} c + \nu_1(1 - 3c) & if \quad c \le 1/3 \\ 1/3 & if \quad c > 1/3 \end{cases} \tag{45}$$

These relations exhibit two general properties: the Young's modulus is independent on the solid Poisson's ratio and the equivalent Poisson's ratio converges to the fixed point v_0=1/3 when $c \to c_0$=1/3. The value c_0=1/3 corresponds to the two-dimensional percolation threshold.

Now, we may analyse the three-dimensional case: we have to solve Eq. (35) considering k_2=0 and μ_2=0. As before, assuming that the shear modulus is a non-negative, continuous function of the porosity, the correct solution is given by the following relationship:

$$\mu = \begin{cases} \frac{1}{4}\mu_1(2 - 5c) - \frac{3}{16}k_1(3 - c) + \frac{1}{16}R & if \quad c \le \frac{1}{2} \\ 0 & if \quad c > 1/2 \end{cases} \tag{46}$$

Here we have defined the quantity R as follows:

$$R = \sqrt{16\mu_1^2(2 - 5c)^2 + 24k_1\mu_1(2 + c)(3 - 5c) + 9k_1^2(3 - c)^2} \tag{47}$$

The bulk modulus may be similarly developed obtaining the final expression:

$$k = \begin{cases} k_1(1 - c)\dfrac{4\mu_1(2 - 5c) - 3k_1(3 - c) + R}{4\mu_1(2 - 5c) - 3k_1(3 - 5c) + R} & if \quad c \le \frac{1}{2} \\ 0 & if \quad c > 1/2 \end{cases} \tag{48}$$

Finally, we are interested in the elastic behaviour, described in terms of the Young's modulus and the Poisson's ratio; we obtain

$$E = \begin{cases} \dfrac{3E_1(1 - c)}{1 - 2\nu_1}\dfrac{1 - 9c + (21c - 11)\nu_1 + Q}{17 - 21c + (5 + 9c)\nu_1 + Q} & if \quad c \le \frac{1}{2} \\ 0 & if \quad c > 1/2 \end{cases} \tag{49}$$

$$\nu = \begin{cases} \dfrac{7 - 3c + (19 - 33c)\nu_1 - Q}{17 - 21c + (5 + 9c)\nu_1 + Q} & if \quad c \le \frac{1}{2} \\ 1/5 & if \quad c > 1/2 \end{cases} \tag{50}$$

where we have defined the quantity Q:

$$Q = \sqrt{\nu_1^2(441c^2 - 270c + 25) - 14\nu_1(9c - 5)(3c - 1) + (81c^2 - 114c + 49)} \tag{51}$$

The Young's modulus exhibits a behaviour analytically depending on the solid matrix Poisson's ratio; however, in the range $0<\nu_1<1/2$ the values of the equivalent Young's modulus are quite independent on ν_1. Moreover, this approach shows a convergent behaviour of the equivalent Poisson's ratio to the value ν=1/5 when the porosity assume the value c_0=1/2, which represents the three-dimensional percolation threshold. In Fig. 3 one can find the behaviour of the Young's modulus and the Poisson's ratio for a random porous material, both in two- and three-dimensional cases.

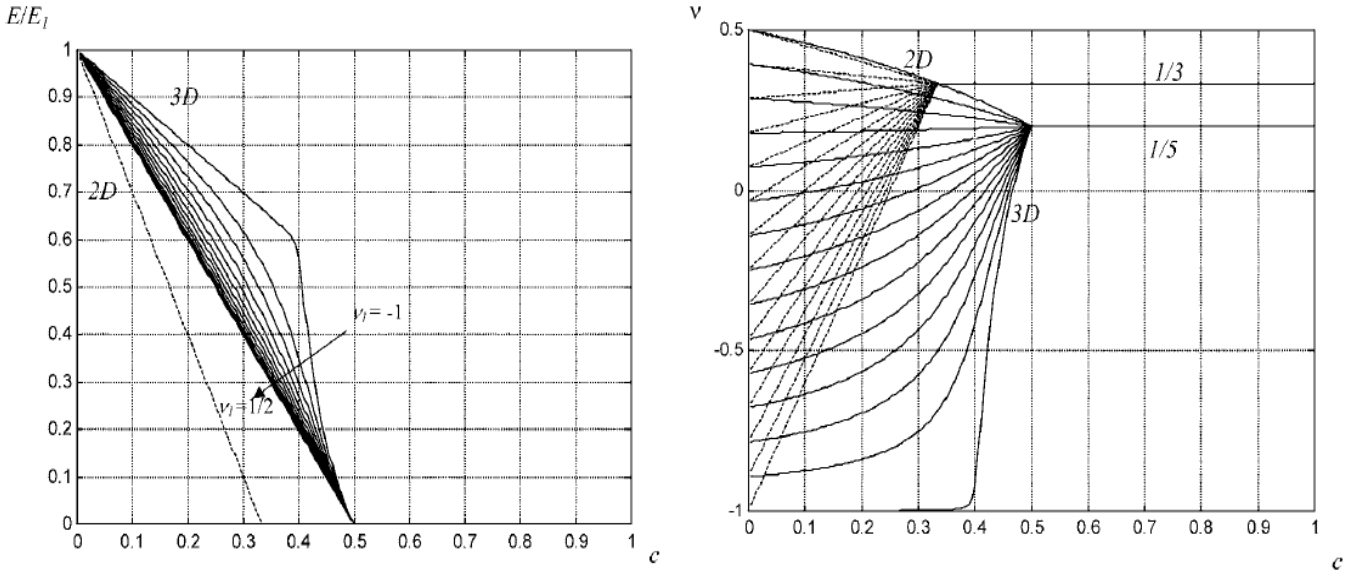

Fig.3. Young's modulus and Poisson's ratio for a random porous material versus the elastic moduli of the pure matrix and the porosity. Dashed lines correspond to the two-dimensional case, continuous lines correspond to the three-dimensional case.

Ceramic materials give some examples of porous materials that are well described by the present theory. In this field one of the most common procedures is sintering. During sintering a ceramic material is heated in a furnace or ovenlike device, where it is exposed to high temperatures. The sintering process has been used to produce ceramics with different porosity and the corresponding elasticity modulus has been measured in many different cases. We draw a comparison between four types of ceramic oxides and the theory here outlined. In Fig. 4a the properties of holmium oxide, Ho_2O_3 (holmia, diamonds), and that of ytterbium oxide, Yb_2O_3 (ytterbia, plus) are represented. Moreover, in Fig. 4b the properties of yttrium oxide, Y_2O_3 (yttria, triangles), and that of samarium oxide, Sm_2O_3 (samaria, circles) are reported. The plots correspond to the values of the Young's modulus measured and calculated by means of the theory. A good agreement is quite evident.

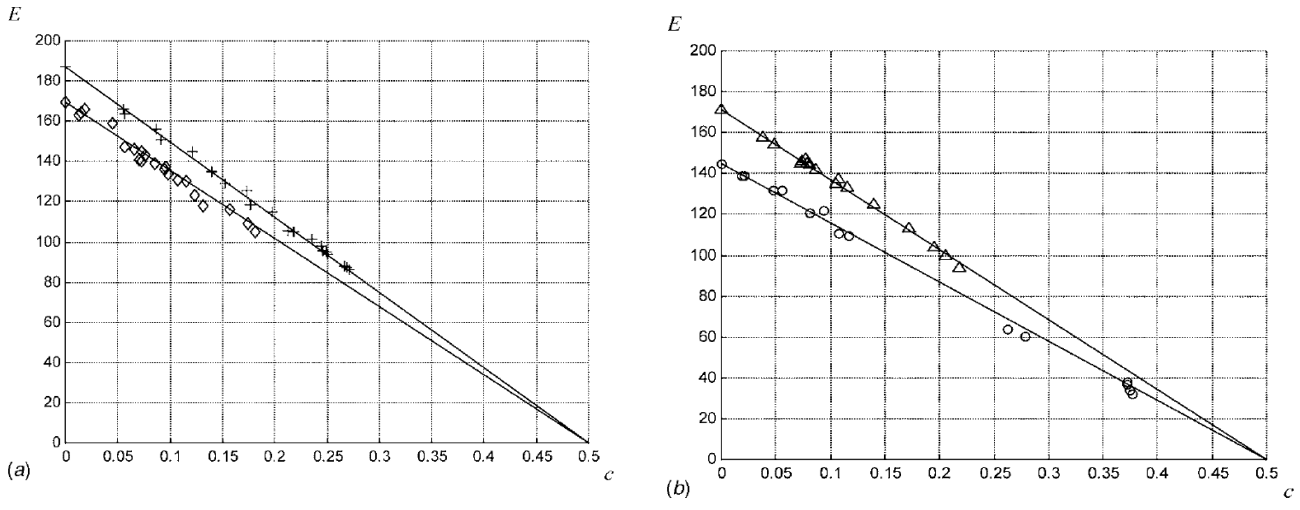

Fig. 4 Young's modulus of different ceramic oxides. In (a) the properties of holmium oxide, Ho_2O_3 (holmia, diamonds), and those of ytterbium oxide, Yb_2O_3 (ytterbia, plus) are represented. Moreover, in (b) the properties of yttrium oxide, Y_2O_3 (yttria, triangles), and those of samarium oxide, Sm_2O_3 (samaria, circles) are reported.

2.1.6.Effects of distributions of cracks in solids

(*S. Giordano, L. Colombo, Effects of the orientational distribution of cracks in solids, Physical Review Letters 98, 055503, 2007, S. Giordano and L. Colombo, Effects of the orientational distribution of cracks in isotropic solids, Engineering Fracture Mechanics, 74, 2007, 1983–2003, S. Giordano and L. Colombo, Local elastic fields around cracks and their stress density of states, Phys. Rev. B 76, 174120, 2007, S. Giordano and L. Colombo, Elastic properties of solids containing elliptic cracks, Phys. Rev. B 77, 054106, 2008, Stefano Giordano, Maria Ilenia Saba, and Luciano Colombo, Elastic properties of multi-cracked composite materials, The European Physics Journal B 76, 261-269, 2010, S. Giordano, A. Mattoni, L. Colombo, Brittle fracture: from elasticity theory to atomistic simulations, REVIEWS IN COMPUTATIONAL CHEMISTRY, vol.27, pp.1-83, 2010*)

We derive a theory for the elastic characterization of multi-cracked solids based on a homogenization technique. We consider a material containing a two-dimensional arbitrary distribution of parallel slit cracks which is elastically equivalent to a crystal with orthorhombic symmetry. We obtain explicit expressions for the macroscopic elastic stiffness tensor which is found to depend upon both the density of cracks and their angular distribution, here described by a suitable order parameter. For the isotropic case we find that the degradation depends exponentially on the crack density.

The macroscopic degradation of brittle materials is governed by the generation of cracks and by their mutual interactions. While linear elastic fracture mechanics (LEFM) provides the basic understanding of the failure instability for a single crack, the overall mechanical behavior actually depends upon the positional and orientational distribution of an assembly of cracks. The basic result of LEFM is represented by the Griffith theory (A. A. Griffith, Philos. Trans. R. Soc. London A 221, 163, 1920): upon loading a single crack with length $l > l_c$ will further grow (eventually producing materials failure), while if $l < l_c$ it will remain stable. Here the critical length l_c is inversely proportional to the square of the tensile stress applied to the material.

When considering the overall materials behavior, a key conceptual issue consists in evaluating the *effective elastic properties* (e.g. the stiffness tensor) that determine the mechanical performance of the system containing a given distribution of cracks. Firstly, we observe that a solid body with a two-dimensional arbitrary orientational distribution of parallel slit cracks is ultimately equivalent to a crystal with orthorhombic symmetry and then we explicitly derive its stiffness tensor. Moreover, we demonstrate that the angular distribution of cracks can be described by a sole order parameter, which takes into account all of the microscopic features reflected macroscopically. Finally, by developing an iterated homogenization procedure we show that the Young modulus of such a solid exponentially decays with the density of cracks. The elementary object of our model is an ellipsoidal void with an infinitesimally-thick minor axis, so as to mimic the flat shape of a crack. Treating the crack as a void and oblate ellipsoid of vanishing eccentricity is very convenient since we develop our arguments by taking profit from general results holding for ellipsoidal inclusions. We consider an ellipsoid with semi-axes a_x, a_y and a_z ($a_x > a_y > a_z > 0$) aligned, respectively, along the x, y and z axes of a given cartesian frame of reference. If one of the principal axes of the ellipsoidal void, say a_x, becomes very large and the minor axis a_z becomes negligibly small, then the ellipsoid reduces to a slit-like crack with half length $a_y=b$ (see Fig. 1).

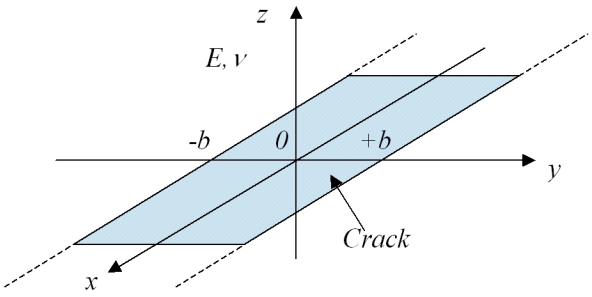

Fig. 1. Geometrical representation of a slit-crack aligned along the x-axis. The half-length of the crack is b. The host matrix has Young modulus E and Poisson's ratio ν.

Hence we considered a void with infinite a_x, and finite a_y and a_z. In other words the void is an elliptic cylinder aligned with the x-axes. We define the aspect ratio as $e = a_z/a_y$. The actual slit-like crack geometry is then described by the limit $a_z \to 0$ or, equivalently, $e \to 0$. The present Letter is addressed to investigating a multi-cracked solid with a given distribution of cracks. Therefore, a number of slit-cracks are randomly placed within the plane z-y. We may

consider different cases as described in Fig. 2, ranging from distributions with cracks parallel to a given direction (Figs.2a,d), to cracks uniformly oriented in space (Fig.2c), to cracks preferentially oriented in some direction (Fig.2b). This latter configuration represents the intermediate distribution between the liming cases of full order (Figs.2a,d) and complete disorder (Fig.2c). The angular distribution of cracks is described by an order parameter P (see below), while the host solid matrix is characterized by the Young modulus E and by the Poisson ratio ν. The present theory holds for any $E > 0$ and $-1<\nu<1/2$.

Let us consider at first the case of a single crack created into the host solid which, in turn, was previously accommodated in a state of constant elastic strain due to some external load. The resulting state of strain of the cracked solid is well described by the Eshelby theory. In its most general formulation, the Eshelby theory provides the elastic behavior of an ellipsoidal inclusion embedded into a matrix. The most important feature is that the internal stress and strain fields are constant if the external strain is constant. Such internal elastic fields can be calculated from the external applied ones by means of the so-called Eshelby tensor. It depends only on geometrical factors of the ellipsoidal inclusion and on the Poisson ratio ν of the host matrix. So, the Eshelby tensor contains all the physical information needed to predict the mechanical interaction between the inclusion and the matrix under external load. For voids or cavities the relationship between the original applied strain $\boldsymbol{\varepsilon}_0$ and the induced internal strain $\boldsymbol{\varepsilon}_i$ is given by $\boldsymbol{\varepsilon}_i=\{\mathbf{I}-\mathbf{S}\}^{-1}\boldsymbol{\varepsilon}_0$ where $\mathbf{I}$ is the identity tensor and $\mathbf{S}$ is the Eshelby tensor. If we consider a void shaped as the elliptic cylinder described above, the Eshelby tensor becomes simply dependent on the aspect ratio $e = a_z/a_y$ and on the Poisson ratio ν of the matrix. We used this result for a single crack as defined in Fig.1, although arbitrarily rotated around the x-axis of an angle θ. The angle θ has the role of a random variable symmetrically distributed over the range $(-\pi/2, \pi/2)$. We now define the order parameter $P=\langle\sin^2\theta\rangle$ which completely describes the state of order ($\theta=0$ or $\pi/2$) and disorder ($0<\theta<\pi/2$) of the distribution of cracks. It is easy to recognize that P assumes special values for particular angular distributions of cracks as indicated in Fig. 2. So, we computed the average value (hereafter indicated by $\langle\bullet\rangle$ squares) of the internal strain $\langle\boldsymbol{\varepsilon}_i\rangle$ over all the possible orientations: $\langle\boldsymbol{\varepsilon}_i\rangle=\langle\{\mathbf{I}-\mathbf{S}\}^{-1}\boldsymbol{\varepsilon}_0\rangle=\langle\{\mathbf{I}-\mathbf{S}\}^{-1}\rangle\boldsymbol{\varepsilon}_0=\mathbf{C}\boldsymbol{\varepsilon}_0$ where $\mathbf{C}$ is the averaged Wu's tensor (K.Z. Markov, L. Preziozi, Eds., *Heterogeneous Media: Micromechanics, Modeling, Methods, and Simulations,* Birkhauser, Boston, 2000) depending only on e, ν and P.

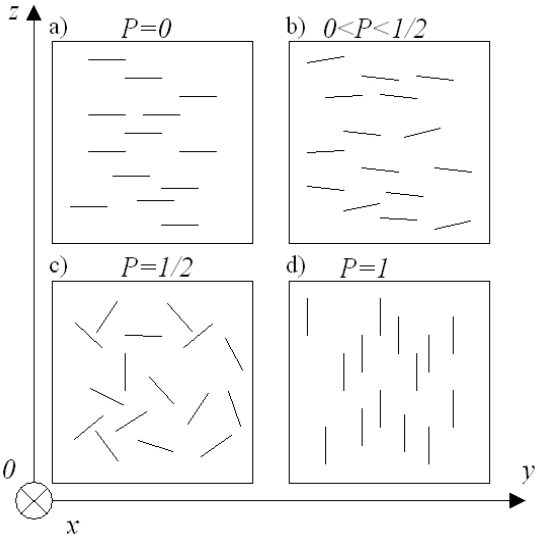

Fig. 2. Structure of a multi-cracked solid with slit-cracks along the x-axis. The order parameter P clearly indicates the state of order (panels a and d) or disorder (panel c).

We move now to the case of an actual distribution of several cracks: we consider a region of the plane z-y having area A and containing N elliptic inclusions with aspect ratio e (equivalent to slit-cracks in the limit $e\to0$), and an angular distribution characterized by the order parameter P (see Fig. 2). The volume fraction c of the inclusions is given by N times the area $\pi a_z a_y$ of the elliptic base, divided by total area A of the region of interest, so that $c = \pi a_z a_y N/A$. Since $a_y = b$ and $e = a_z/a_y$, we easily obtain the result $c = \pi e b^2 N/A$. Moreover, we can define the new characteristic quantity $\alpha = \pi b^2 N/A$: it is dimensionless and it effectively represents the crack density. Hence, we may write $c = \alpha e$. We need now to compute the average value of the strain $\langle\boldsymbol{\varepsilon}\rangle$ and of the stress $\langle\mathbf{T}\rangle$ over the whole region of interest (i.e. area A). To begin, we work under the hypothesis of low cracks density so that the cracks are not interacting with each other. Therefore, we approximate the average value of the strain outside the cracks with the external applied strain $\boldsymbol{\varepsilon}_0$ (this is strictly true for a single crack exposed to a given external load) and

we get $\langle\boldsymbol{\varepsilon}\rangle=c\langle\boldsymbol{\varepsilon}_i\rangle+(1-c)\boldsymbol{\varepsilon}_0$. By recalling the definition of the tensor $\mathbf{C}$, we finally obtain the sole approximated relation introduced in the present model, namely:

$$\langle\boldsymbol{\varepsilon}\rangle=[(1-c)\mathbf{I}+c\mathbf{C}]\boldsymbol{\varepsilon}_0 \qquad (1)$$

On the other hand, an exact result can be obtained for the stress:

$$\langle\mathbf{T}\rangle=\mathbf{L}[\langle\boldsymbol{\varepsilon}\rangle-c\mathbf{C}\boldsymbol{\varepsilon}_0] \qquad (2)$$

where $\mathbf{L}$ is the stiffness tensor of the homogeneous (i.e. non-cracked) matrix and $\langle\boldsymbol{\varepsilon}\rangle$ is given by eq. (1). We define the *effective* stiffness tensor $\mathbf{L}_{eff}$ of the cracked body trough the relation $\langle\mathbf{T}\rangle=\mathbf{L}_{eff}\langle\boldsymbol{\varepsilon}\rangle$. By means of eqs. (1) and (2) we obtain $\mathbf{L}_{eff}=\mathbf{L}\left\{\mathbf{I}-\mathbf{G}[\mathbf{I}+\mathbf{G}]^{-1}\right\}$ where $\mathbf{G}=\lim_{e\to 0} c\mathbf{C}$ and it depends on α, ν and P. This crucial step is performed under the limiting condition $e\to 0$ in order to take into account the actual planar geometry of the cracks.

It is evident by the micro-geometry of the system that the solid is elastically anisotropic: along the x-axes we find the alignment of slit-cracks, while along the y and z axes we get different elastic behaviours because of the given orientation of the cracks. However, the three different behaviors along the three axes lead to an orthorhombic anisotropy for the whole system, so that

$$\mathbf{L}_{\text{eff}}=\begin{bmatrix} L_{1111} & L_{1122} & L_{3311} & 0 & 0 & 0 \\ L_{1122} & L_{2222} & L_{2233} & 0 & 0 & 0 \\ L_{3311} & L_{2233} & L_{3333} & 0 & 0 & 0 \\ 0 & 0 & 0 & L_{1212} & 0 & 0 \\ 0 & 0 & 0 & 0 & L_{2323} & 0 \\ 0 & 0 & 0 & 0 & 0 & L_{3131} \end{bmatrix} \qquad (3)$$

where the relation $\langle T_{ij}\rangle=L_{ijkl}\langle\varepsilon_{kl}\rangle$ characterizes the multi-cracked solid. Here L_{ijkh} are the entries of $\mathbf{L}_{eff}$ (corresponding to nine independent parameters). We can write the closed form expressions for the stiffness tensor entries in terms of the E, ν as well as in terms of the parameters P and α described above:

$$\begin{aligned} L_{1111} &= [4\alpha^2 P(1-P)(1+\nu)(1-\nu)^2 \\ &\quad + 2(1-\nu)\alpha + 1 - \nu]D^{-1}E \\ L_{2222} &= (1-\nu)[1+2(1-P)\alpha]D^{-1}E \\ L_{3333} &= (1-\nu)[1+2\alpha P]D^{-1}E \end{aligned} \qquad (4)$$

$$L_{1122} = \nu[1+2(1-P)(1-\nu)\alpha]D^{-1}E$$

$$L_{2233} = \nu D^{-1}E \qquad L_{3311} = \nu[1+2P(1-\nu)\alpha]D^{-1}E \qquad (5)$$

$$\begin{aligned} L_{1212} &= \{(1+\alpha P)(1+\nu)\}^{-1}E \\ L_{2323} &= \{[1+(1-\nu)\alpha](1+\nu)\}^{-1}E \\ L_{3131} &= \{[1+\alpha(1-P)](1+\nu)\}^{-1}E \end{aligned} \qquad (6)$$

where $D=[4\alpha^2P(1-P)(1-\nu)^2+2(1-\nu)^2\alpha+1-2\nu](1+\nu)$.

Eqs. (4-6) represent the complete characterization of a solid with a given distribution of slit-cracks under the sole hypothesis of low cracks density. When the slit-cracks are uniformly random oriented in the y-z plane the overall multi-cracked material is transversely isotropic (along the x-axis) and the corresponding stiffness tensor is given by eqs. (4-6) with P=1/2. As it is well known, the number of independent entries in the stiffness tensor decreases from nine to five moving from orthorhombic anisotropy to transverse isotropy. Typically, in two-dimensional elasticity a transversely isotropic medium may be used under the conditions of plane stress or plane strain (and it appears as an isotropic material with effective moduli E_{eff} and ν_{eff}.). Starting from eqs. (4-6) (with P=1/2) we may apply the iterated homogenization method that allows us to remove the hypothesis of low cracks density. The principles of this technique are here summarized: let's suppose that the effective moduli of a multi-cracked medium are known

to be E_{eff} and ν_{eff}. Therefore, if a small number of cracks ΔN is added to the matrix, the change in the elastic moduli is the same as in an uniform, homogeneous matrix with moduli E_{eff} and ν_{eff}.. When the number of additional cracks ΔN assumes the role of an infinitesimal quantity, the iterated homogenization method converges to the differential effective medium theory. Eventually, this approach leads to the following results under plane stress conditions:

$$E_{\text{eff}} = \frac{E}{\sqrt{\nu^2 + (1-\nu^2)e^{2\alpha}}} \qquad \nu_{\text{eff}} = \frac{\nu}{\sqrt{\nu^2 + (1-\nu^2)e^{2\alpha}}} \tag{7}$$

A similar procedure can be followed for the plane strain case, obtaining the effective elastic moduli as follows:

$$E_{\text{eff}} = E\frac{2\nu + (1-\nu)e^{\alpha}}{[\nu + (1-\nu)e^{\alpha}]^2(1+\nu)} \qquad \nu_{\text{eff}} = \frac{\nu}{\nu + (1-\nu)e^{\alpha}} \tag{8}$$

It is important to observe that our solutions (given by eq. (7) for plane stress and by eq. (8) for plane strain) depend exponentially on the cracks density. In Fig. 3 these results have been represented versus the parameter α. A comparison between the plane stress and the plane strain cases has been drawn both for positive and negative Poisson's ratio.

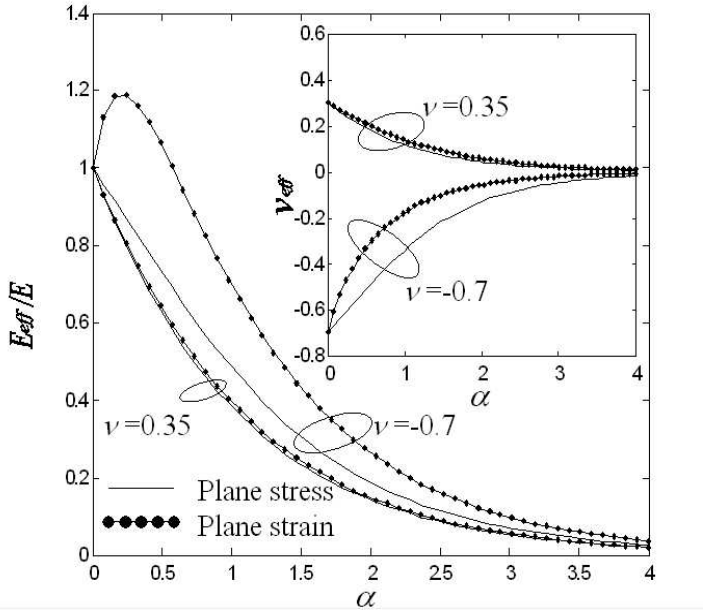

Fig. 3. Effective Young modulus and Poisson ratio for a multi-cracked solid under plane stress and plane strain conditions. The plots have been derived for two different homogeneous matrix having ν =0.35 and ν =-0.7.

An interesting unconventional behavior of the effective Young modulus of the multi-cracked solid has been found for negative Poisson ratio under plane strain condition. When -1< ν <-1/2 we obtain, for low values of α, an effective Young modulus greater than the Young modulus of the original elastic matrix. More precisely, the effective Young modulus in such a case has a maximum for $\alpha = \ln(-3\nu/(1-\nu))$ which can be approximated as $\alpha = -(1+2\nu)/(1-\nu)$ when α is small enough. This effect is shown in Fig. 3 where a value ν =–0.7 is assumed. This effect is not present under plane stress conditions. The unusual behavior observed in plane strain conditions can be attributed to the specific meaning of the Young modulus in such a case: the elastically loaded plain-strain system has fewer degrees of freedom than the system in plane-stress, because of the peculiar boundary conditions needed to avoid the appearing of out-of-plane strain in the solid. This means that, when one measures the Young modulus on a given direction in plane strain conditions, some other forces must be applied in the orthogonal directions in order to fulfill the plain strain state, generating a very special set of loading.
An interesting experimental verification of this theory have been recently performed (Travis, Q. and Mobasher, B., 2010, Correlation of Elastic Modulus and Permeability in Concrete Subjected to Elevated Temperatures, J. Mater.

Civ. Eng., 22, 735–740). The laboratory testing of concrete has shown that elevated temperatures cause air permeability index (API) increase and elastic modulus *E* decrease. Indeed, the API response typically spans several orders of magnitude making it a sensitive indicator of elastic modulus reduction. The crack density α introduced in eqs.(7) and (8) has been written in terms of the change in overall air permeability due to damage, denoted Δk_h (m/s) through a constant Ω

$$\alpha = \frac{1}{2}\sqrt{\frac{\Delta k_h / \Omega}{\sqrt[3]{\nu_{air} g}}} \qquad (9)$$

This constant Ω depends on several factors, as properly described in the above quoted paper. Moreover, ν_{air} represents the air kinematic viscosity and *g* the gravitational acceleration. It is useful to define the dimensionless air permeability $\Delta K_h = \frac{\Delta k_h}{\sqrt[3]{\nu_{air} g}}$, so that we have $\alpha = \frac{1}{2}\sqrt{\frac{\Delta K_h}{\Omega}}$. Our eqs.(7) and (8) for the Young modulus degradation can be written in terms of the dimensionless air permeability, by obtaining two equations for the plane stress and plane strain conditions, respectively

$$\Delta K_h = \Omega\left[\ln\sqrt{\frac{1-\nu^2(E/E_0)^2}{(1-\nu^2)(E/E_0)^2}}\right]^2 \quad \text{(plane stress)} \qquad (10)$$

$$\Delta K_h = \Omega\left[\ln\left(\frac{E_0/E}{2(1+\nu)} - \nu + \frac{1}{\sqrt{1+\nu}}\sqrt{\frac{(E_0/E)^2}{4(1+\nu)} + \nu\frac{E_0}{E}}\right) - \ln(1-\nu)\right]^2 \quad \text{(plane strain)}$$

Moreover, for many materials, such as concrete, ν^2 is much less than 1. For small ν^2, eq.(10) simplifies to the surprisingly simple relation for both conditions

$$\Delta K_h = \Omega[\ln(E/E_0)]^2 \qquad (11)$$

The proposed model was compared with several API and dynamic elastic modulus measurements as reported in the experimental work by Recalde 2005 and field data measured by Dilek and Leming 2007 and Dilek and Leming 2008. Since the present model is specific to relative elastic modulus changes, it is therefore assumed that the derived equations may be applied, without correction, to the dynamic elastic modulus ratio as well. In Figs.4 and 5 one can find the comparison between eq.(11) and the experimental results; the good agreement is very good in a large range of variation of the Young modulus.

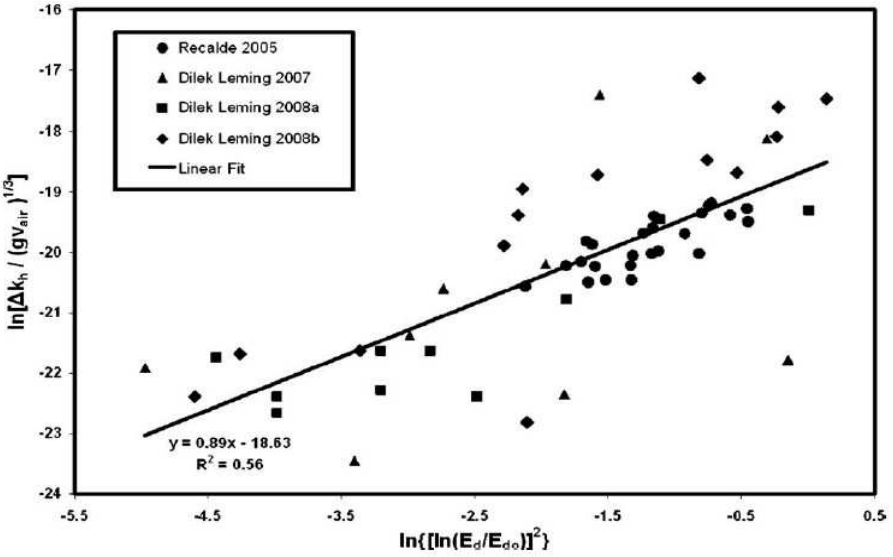

Fig.4 Nondimensional permeability versus the Young modulus in bi-logarithmic scale.

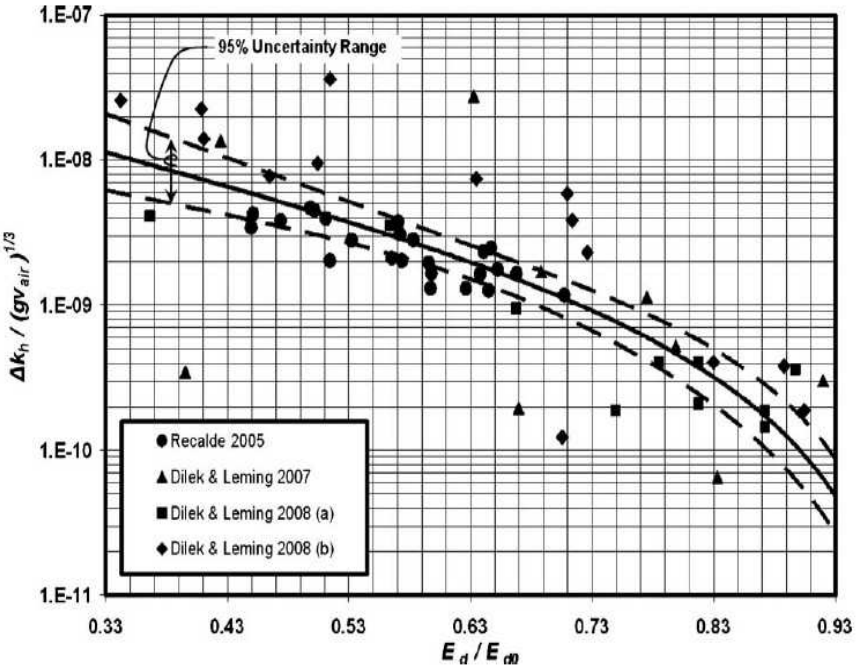

Fig.5. Dimensionless permeability versus the Young modulus in linear scale.

In the following, we describe some results concerning the behavior of the elastic fields around a crack in two three-dimensional configurations: the slit and the circular (penny-shaped) crack. These canonical problems contain almost all features related to the stress and strain fields of interest in linear elastic fracture mechanics. We start with the slit crack (see Fig. 6) in a three-dimensional environment under the applied stress $T_{22} = \sigma$, where σ represents the tensile stress applied in Mode I along the x_2 direction, as represented in Fig. 6 on the right. The corresponding displacement field has been calculated by means of a methodology based on the Eshelby theory.

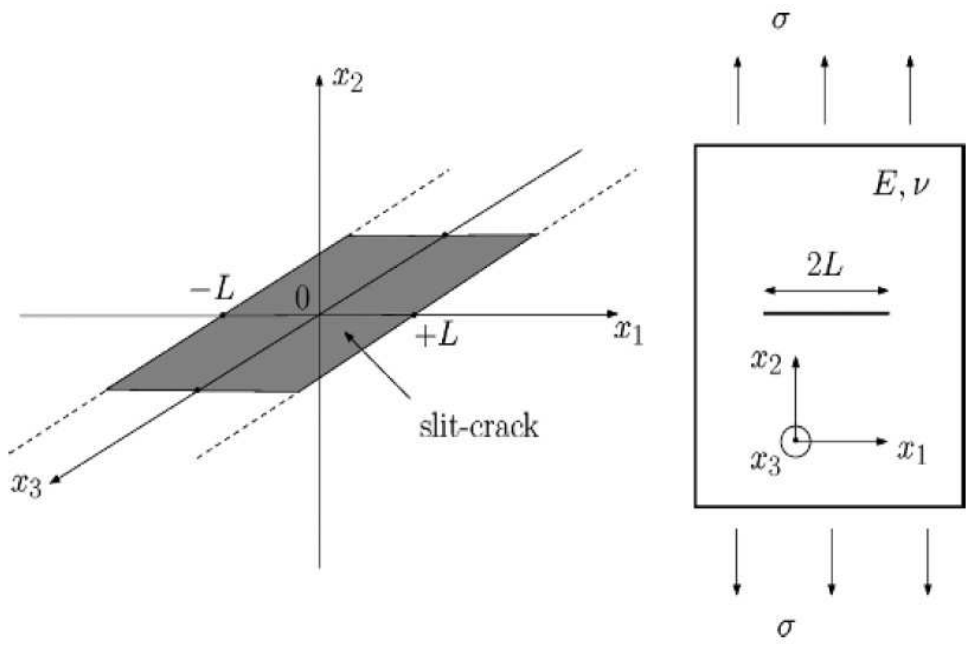

Fig.6. Left panel: geometry of a slit crack lying in the (x_1, x_3) plane. Right panel: elastic medium (with Young modulus E and Poisson ratio ν) containing a slit crack (with length 2L) under uniaxial stress (along x_2).

We get the following result:

$$u_1 = -\frac{\sigma x_1 (1+\nu)}{E}\left[\frac{1-2\nu^2}{1+\nu} - \frac{\beta}{\alpha}\sqrt{\frac{\eta}{L^2+\eta}}\right]$$
$$u_2 = \frac{\sigma x_2 (1+\nu)}{E}\left[\frac{\nu(1+2\nu)}{1+\nu} + \frac{\beta}{\alpha}\sqrt{\frac{L^2+\eta}{\eta}}\right] \qquad (12)$$
$$u_3 = -\frac{\sigma\nu x_3}{E}$$

Recall that the slit-crack is aligned along the x_3 axis, and the two surfaces of the crack lie on the plane (x_1, x_3); it follows that the component u_3 is not affected by the presence of the slit crack. The parameters introduced are listed as follows

$$\alpha = x_1^2\eta^2 + x_2^2(L^2+\eta)^2$$
$$\beta = (1-2\nu)\left(x_1^2+x_2^2\right)\eta^2 + 2(1-\nu)x_2^2L^4 + (3-4\nu)x_2^2L^2\eta \qquad (13)$$
$$\eta = \frac{1}{2}\left(x_1^2+x_2^2-L^2\right) + \frac{1}{2}\sqrt{\left(x_1^2+x_2^2+L^2\right)^2 - 4L^2x_1^2}$$

Eqs.(12) and (13) are important because they describe in a very compact form the displacement field in the whole space, and they contain, as particular cases, all standard LEFM results. Eqs. (12) and (13) can be used in several ways to analyze the behavior of a crack. For example, it is easy to calculate the strain or the stress tensor just in some regions of interest by using the constitutive relation of the matrix. Here, we do not report the expressions for strain and stress because they are very complicated and do not add any conceptual content to the present discussion. Rather, we focus on the T_{22} component of the stress. It is interesting to note the two singularities appearing at the crack tips, showing the typical intensification of the stress. When $x_2 = 0$, we indeed obtain the well-known result

$$T_{22} = \frac{|x_1|\sigma}{\sqrt{x_1^2-L^2}} \qquad (14)$$

This result is important because it naturally drives to the concept of stress intensity factor by obtaining

$$K_I = \lim_{x\to L} T_{yy}(x,0)\sqrt{2\pi(x-L)} = \sigma\sqrt{\pi L} \qquad (15)$$

We now can consider the circular or penny-shaped crack shown in Fig. 7. In this case, we assume that the external forces are characterized by a tensile stress $T_{33} = \sigma$. To describe the resulting three-dimensional displacement field, it is useful to introduce a system of polar cylindrical coordinates (ρ,ϑ,x_3), where $x_1 = \rho\cos(\vartheta)$ and $x_2 = \rho\sin(\vartheta)$. For the symmetry of our system, the final results will not depend on the angle ϑ.

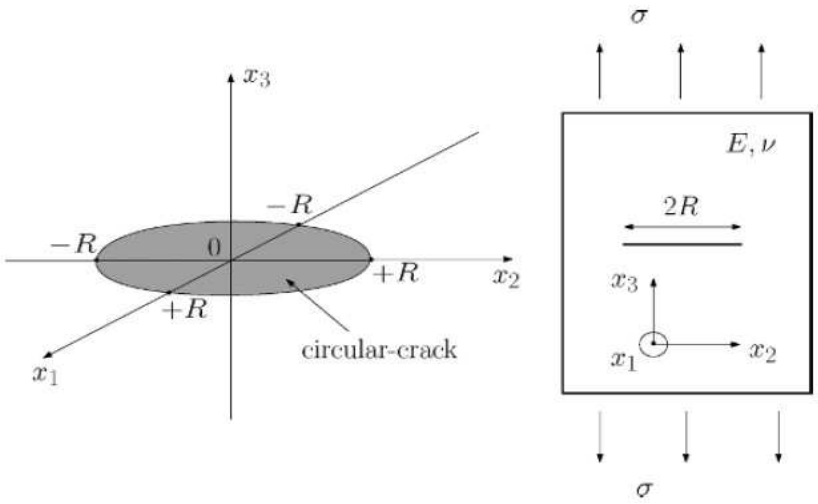

Fig. 7. Left panel: geometry of a circular crack lying in the (x_1,x_2) plane. Right panel: elastic medium (with Young modulus E and Poisson ratio ν) containing a circular crack (with radius R) under uniaxial stress σ (along x_3).

The explicit result describing the total displacement u_ρ and u_3 is given as follows:

$$u_\rho = -\frac{\sigma\rho\,(1+\nu)}{2E}\left[(1-2\nu)\left(\frac{(1+2\nu)\,(1-\nu)}{(1-2\nu)\,(1+\nu)} - \frac{2}{\pi}\arctan\frac{\sqrt{\eta}}{R}\right) - \frac{2}{\pi}\frac{\beta}{\alpha}\frac{R\sqrt{\eta}}{R^2+\eta}\right]$$

$$u_3 = \frac{\sigma x_3\,(1+\nu)}{E}\left[(1-2\nu)\left(\frac{\nu\,(1+2\nu)}{(1+\nu)\,(1-2\nu)} + \frac{2}{\pi}\arctan\frac{\sqrt{\eta}}{R}\right) + \frac{2}{\pi}\frac{\beta - x_3{}^2R^2(R^2+\eta)}{\alpha}\frac{R}{\sqrt{\eta}}\right] \quad (16)$$

where the variable u_ρ represents the radial displacement and ρ is the radius. We also have introduced the axial displacement u_3 and the following definitions:

$$\alpha = \rho^2\eta^2 + x_3^2(R^2+\eta)^2$$

$$\beta = (1-2\nu)\,(x_3^2+\rho^2)\eta^2 + 4\,(1-\nu)\,\eta x_3^2R^2 + (3-2\nu)\,x_3^2R^4 \quad (17)$$

$$\eta = \frac{1}{2}\left(x_3^2+\rho^2-R^2\right) + \frac{1}{2}\sqrt{\left(x_3^2+\rho^2+R^2\right)^2 - 4R^2\rho^2}$$

The stress T_{33} along the direction of the Mode I loading can be calculated by deriving the displacement and by using the constitutive equation. It interesting to observe that for ρ=R and x_3 = 0 (i.e., on the circumference of the crack), we have a singularity describing the stress intensification on the circular crack front. The quantity T_{33} can be specialized on the plane of the circular crack x_3 =0 and for external radius ρ>R, obtaining the following result

$$T_{33}(\rho) = \frac{2\sigma}{\pi}\left[\frac{R}{\sqrt{\rho^2-R^2}} + \arctan\frac{\sqrt{\rho^2-R^2}}{R}\right] \quad (18)$$

This relation represents the analogue of the slit-crack formula (see Eq.(14)), for a circular crack. Similarly, we can evaluate the stress intensity factor. For the circular crack, the distance from the border of the crack is given by ρ-R, and the stress intensity factor is calculated as follows

$$K_I = \lim_{\rho \to R,\, x_3 \to 0} \sqrt{2\pi(\rho - R)}\, T_{33} = \frac{2\sqrt{R}}{\sqrt{\pi}}\sigma \qquad (19)$$

To conclude, we point out that the stress intensity factor depends on the geometry of the system under consideration.

2.1.7.The nonlinear elastic behaviour of inhomogeneities

(*S. Giordano, L. Colombo, P. L. Palla, Nonlinear elastic Landau coefficients in heterogeneous materials, EuroPhysics Letters 83, 2008, 66003, S. Giordano, P. L. Palla, L. Colombo, Nonlinear elasticity of composite materials: Landau coefficients in dispersions of spherical and cylindrical inclusions, The European Physics Journal B 68, 89-101, Stefano Giordano, Dielectric and Elastic Characterization of Nonlinear Heterogeneous Materials, Materials 2009, 2, 1417-1479, 2009, L. Colombo and S. Giordano, Nonlinear elasticity in nanostructured materials, Rep. Prog. Phys., 74, 11, 2011, 116501-1-35*)

The central problem in predicting the elasticity of heterogeneous materials (like, e.g., composite or nanostructured systems, mixtures, multi-defected or multi-cracked media) consists in the evaluation of their effective macroscopic elastic properties, still taking into account the actual microscale material features. This leads to the concept of homogenization, a coarse-graining approach addressed to determine the relationship between the microstructure and the effective elastic behavior. Homogenization has been successfully developed for linear elastic properties (see previous Sections). However, in heterogeneous or composite materials the nonlinear regime has been investigated only under specific conditions. Nevertheless, the general nonlinear elastic features are relevant in many materials science problems. For instance, transient elastography has shown its efficiency to map the linear and nonlinear properties of soft tissues and it is nowadays used as diagnostic technique (Catheline S., Gennisson J.-L. and Fink M., J. Acoust. Soc. Am., 114 ,2003, 3087, Catheline S., Gennisson J.-L., Tanter M. and Fink M., Phys. Rev. Lett., 91, 2003, 164301). In fact, it has been verified that malignant lesions tend to exhibit nonlinear elastic behavior contrary to normal tissues or to benignant lesions. This point is explained by observing that malignant lesions alter the structure of the cellular network enhancing the nonlinear properties. The pathological nonlinear zones can be profitably described by the so-called Landau coefficients (see below), making feasible their localization through noninvasive imaging techniques (ultrasound and/or magnetic resonance) (Sinkus R. et al., IEEE Trans. UFFC, 53, 2006, 2009). Another relevant example is offered by the engineering of semiconductor quantum dots, embedded in a confining solid matrix. The quantum dots growth, ordering and orientation (occuring during processing) are largely affected by elastic phenomena, even beyond the linear regime (Holy' V. et al., Phys. Rev. Lett., 83, 1999, 356, Schmidbauer M. et al., Phys. Rev. Lett., 96, 2006, 066108). Finally, many problems of fracture mechanics in composite materials do contain nonlinear features like, e.g., the interaction between the stress fields generated by a moving crack and a fiber (or, more generally, an inclusion) (Mattoni A., Colombo L. and Cleri F., Phys. Rev. B, 70, 2004, 094108).

We proved that the elastic fields within a generic nonlinear and anisotropic inhomogeneity embedded in a (linear and anisotropic) matrix are uniform. We apply this general result to the specific case of a dispersion of isotropic nonlinear spheres and we obtain a universal mixing scheme for the Landau coefficients. Nonlinearity can be introduced in the theory of elasticity by means of the exact relation for the Lagrangian strain (geometrical nonlinearity) and/or through a nonlinear stress-strain constitutive relation (non-Hookean physical nonlinearity). In this analysis, we adopt the physical nonlinearity standpoint, whereas the geometrical linearity is everywhere assumed: therefore, the balance equations are based on the small-strain tensor and on the symmetric Cauchy stress tensor, and on an arbitrary (nonlinear) stress-strain relation. The general property we are looking for sets out from the Eshelby theory, which solves the elasticity equations for a single anisotropic linear ellipsoid (stiffness $C^{(2)}$) embedded into an anisotropic linear matrix (stiffness $C^{(1)}$). Upon uniform remote loading, it is proved that the strain field inside the ellipsoid is uniform and assumes the value

$$\hat{\epsilon}^s = \{\hat{I} - \hat{\mathcal{S}}[\hat{I} - (\hat{\mathcal{C}}^{(1)})^{-1}\hat{\mathcal{C}}^{(2)}]\}^{-1}\hat{\epsilon}^{\infty}, \quad (1)$$

where the Eshelby tensor S depends only on the geometry and on $C^{(1)}$. We can generalize this result to the case where the inhomogeneity is nonlinear, i.e. $C^{(2)}$ is any strain-dependent anisotropic stiffness tensor. The energy balance is described by the Green formulation: for a given state of deformation, the stress power is absorbed into a strain energy function *U*, leading to the constitutive equation $\hat{T} = \partial U(\hat{\varepsilon})/\partial \hat{\varepsilon}$, equivalent to $\hat{T} = \hat{C}^{(2)}(\hat{\varepsilon})\hat{\varepsilon}$. The strain energy function can be identified with the internal energy per unit volume in an isentropic process, or with the Helmholtz free-energy per unit volume in an isothermal process. In the present generalization nonlinear features are described by an arbitrary free-energy function *U*. In order to cope with this problem, we suppose to have found a solution for the equation

$$\hat{\epsilon}^s = \{\hat{I} - \hat{\mathcal{S}}[\hat{I} - (\hat{\mathcal{C}}^{(1)})^{-1}\hat{\mathcal{C}}^{(2)}(\hat{\epsilon}^s)]\}^{-1}\hat{\epsilon}^{\infty}, \quad (2)$$

obtained from eq. (1) through the substitution $\hat{C}^{(2)} \rightarrow \hat{C}^{(2)}(\hat{\varepsilon})$. If such a solution $\hat{\varepsilon} = \hat{\varepsilon}^*$ exists, it means that the nonlinear inhomogeneity could be replaced by a linear one with constant stiffness $\hat{C}^{(2)} = \hat{C}^{(2)}(\hat{\varepsilon})$, without modifications of the elastic fields at any point. Therefore, if a solution exists, then eq. (2) exactly describes, through self-consistency, the elastic behavior of the nonlinear anisotropic inclusion. This is not a trivial result: for instance, such a generalization of eq. (1) is not valid if a nonlinear behavior is assumed for material 1 (matrix). The existence and unicity of a solution for eq. (2) can be exactly proved under the sole hypothesis of convexity for the strain energy function *U*. We rearrange eq. (2) as follows:

$$\begin{aligned}
[\hat{I} - \hat{\mathcal{S}}]\hat{\epsilon}^s + \hat{\mathcal{S}}(\hat{\mathcal{C}}^{(1)})^{-1}\frac{\partial U(\hat{\epsilon}^s)}{\partial \hat{\epsilon}^s} &= \hat{\epsilon}^{\infty}, \\
\hat{\mathcal{C}}^{(1)}[\hat{\mathcal{S}}^{-1} - \hat{I}]\hat{\epsilon}^s - \hat{\mathcal{C}}^{(1)}\hat{\mathcal{S}}^{-1}\hat{\epsilon}^{\infty} + \frac{\partial U(\hat{\epsilon}^s)}{\partial \hat{\epsilon}^s} &= 0, \qquad (3) \\
\frac{\partial}{\partial \hat{\epsilon}}\left\{\frac{1}{2}\hat{\epsilon}\hat{\mathcal{C}}^{(1)}[\hat{\mathcal{S}}^{-1} - \hat{I}]\hat{\epsilon} - \hat{\epsilon}\hat{\mathcal{C}}^{(1)}\hat{\mathcal{S}}^{-1}\hat{\epsilon}^{\infty} + U(\hat{\epsilon})\right\} &= 0.
\end{aligned}$$

Now, the first term represents a symmetric (because of the Betti reciprocal theorem) and positive definite (because of the minimum-potential-energy principle) quadratic form, while the second term is a linear function. Therefore, the sum of these two terms is a convex functional with relative minimum at $\left[\hat{I} - \hat{S}\right]\hat{\varepsilon}^{\infty}$. If U is a convex functional (with U(0) = 0) as well, the brackets in eq. (3) contain the sum of two convex terms: they result in an overall convex functional with a minimal extremum at $\hat{\varepsilon} = \hat{\varepsilon}^*$. Therefore, a unique solution of eq. (2) exists under the convexity assumption for U. We have obtained an important new property of an arbitrary inhomogeneity: if the linear elastic matrix is subjected to remote uniform loading, then the stress and strain fields inside the embedded inhomogeneity
will be uniform, independently of the (nonlinear and anisotropic) constitutive relation for the inhomogeneity itself. The general result stated in eq. (2) can be applied to fully homogenize any dispersion of arbitrarily nonlinear and anisotropic ellipsoidal inclusions. Let us now consider a more specific dispersion of nonlinear spherical isotropic inclusions. The density is described by the volume fraction c, defined as the ratio between the total volume of the embedded spheres and the total volume of the heterogeneous material (see fig. 1). The matrix is described by the bulk and shear moduli K_1 and μ_1. To model the spherical inclusions, we adopt the most general isotropic nonlinear constitutive equation expanded up to the second order in the strain components: it follows that the function *U* can only depend upon the principal invariants of the strain tensor. Therefore, by expanding *U* up to the third order in the strain components, we obtain

$$\begin{aligned}
U(\hat{\epsilon}) = {} & \mu_2 \mathrm{Tr}(\hat{\epsilon}^2) + \frac{1}{2}\left(K_2 - \frac{2}{3}\mu_2\right)[\mathrm{Tr}(\hat{\epsilon})]^2 \qquad (4) \\
& + \frac{A}{3}\mathrm{Tr}(\hat{\epsilon}^3) + B\mathrm{Tr}(\hat{\epsilon})\mathrm{Tr}(\hat{\epsilon}^2) + \frac{C}{3}[\mathrm{Tr}(\hat{\epsilon})]^3
\end{aligned}$$

and deriving the stress, we get

$$\begin{aligned}
\hat{T} = {} & 2\mu_2\hat{\epsilon} + \left(K_2 - \frac{2}{3}\mu_2\right)\mathrm{Tr}(\hat{\epsilon})\hat{I} \qquad (5) \\
& + A\hat{\epsilon}^2 + B\{\mathrm{Tr}(\hat{\epsilon}^2)\hat{I} + 2\hat{\epsilon}\mathrm{Tr}(\hat{\epsilon})\} + C[\mathrm{Tr}(\hat{\epsilon})]^2\hat{I}
\end{aligned}$$

for the material corresponding to the spherical inclusions. The parameters A,B, and C are the Landau moduli (Landau L. D. and Lifschitz E. M., Theory of Elasticity, Butterworth Heinemann, Oxford, 1986) and they represent the deviation from the standard linearity. It can be proved that

$$\begin{aligned} L\hat{\epsilon}^s &+ M\mathrm{Tr}\left(\hat{\epsilon}^s\right)\hat{I} + N\left(\hat{\epsilon}^s\right)^2 + O\hat{\epsilon}^s\mathrm{Tr}\left(\hat{\epsilon}^s\right) \\ &+ P\mathrm{Tr}[(\hat{\epsilon}^s)^2]\hat{I} + Q\left[\mathrm{Tr}\left(\hat{\epsilon}^s\right)\right]^2\hat{I} = \hat{\epsilon}^\infty, \end{aligned} \tag{6}$$

defining the explicit relation between the internal strain and the remote deformation, for a single nonlinear spherical inhomogeneity. The parameters follow

$$\begin{aligned} L &= 1 + \frac{6}{5}\frac{K_1 + 2\mu_1}{3K_1 + 4\mu_1}\left(\frac{\mu_2}{\mu_1} - 1\right), \\ M &= \frac{5K_2 - K_1\left(3 + 2\frac{\mu_2}{\mu_1}\right) - 4\left(\mu_2 - \mu_1\right)}{5\left(3K_1 + 4\mu_1\right)}, \\ N &= \frac{3}{5}\frac{A}{\mu_1}\frac{K_1 + 2\mu_1}{3K_1 + 4\mu_1}, \\ O &= \frac{6}{5}\frac{B}{\mu_1}\frac{K_1 + 2\mu_1}{3K_1 + 4\mu_1}, \\ P &= \frac{1}{15\left(3K_1 + 4\mu_1\right)}\left[15B - A\left(1 + 3\frac{K_1}{\mu_1}\right)\right], \\ Q &= \frac{1}{15\left(3K_1 + 4\mu_1\right)}\left[15C - 2B\left(1 + 3\frac{K_1}{\mu_1}\right)\right] \end{aligned} \tag{7}$$

Let us now move to the actual case of a dilute dispersion of spheres (see fig. 1). Under the hypothesis of a small c, the average value of the strain and of the stress in the overall system can be easily determined. These average fields combined through eq. (6), determine the effective constitutive equation for the heterogeneous system. Basically, it is written as eq. (5) where, however, the effective linear and nonlinear elastic moduli μ_{eff}, Keff, A_{eff}, B_{eff} and C_{eff} must be introduced. As for the linear elastic coefficients, we obtain

$$\begin{aligned} \mu_{eff} &= \mu_1 + c\frac{\mu_2 - \mu_1}{c + (1-c)\left[1 + \frac{6}{5}\left(\frac{\mu_2}{\mu_1} - 1\right)\frac{K_1 + 2\mu_1}{3K_1 + 4\mu_1}\right]}, \\ K_{eff} &= K_1 + \frac{\left(3K_1 + 4\mu_1\right)\left(K_2 - K_1\right)c}{3K_2 + 4\mu_1 - 3c(K_2 - K_1)}. \end{aligned} \tag{8}$$

We observe that K_{eff} and μ_{eff} only depend upon their linear counterparts for materials 1 and 2. Interesting enough, the effective Landau coefficients show a more complicated structure

$$A_{eff} = c\frac{A}{L'^2} - 2c\frac{N'(\mu_2-\mu_1)}{L'^3},$$

$$B_{eff} = 2c\frac{(N'M' - L'P')(\mu_2-\mu_1)}{L'^3(L'+3M')} - c\frac{(N'+3P')\left[K_2-K_1-\frac{2}{3}(\mu_2-\mu_1)\right]}{L'^2(L'+3M')} + c\frac{B}{L'^2}. \quad (9)$$

$$\begin{aligned} C_{eff} = {} & \frac{1}{9}\frac{c(9C+9B+A)}{(L'+3M')^2} + \frac{1}{9}\frac{c(A-3B)}{L'^2} \\ & + \frac{1}{9}\frac{c(4N'+6O')(\mu_2-\mu_1)}{L'^2(L'+3M')} - \frac{2}{9}\frac{c(3B+A)}{L'(L'+3M')} \\ & + \frac{1}{9}\frac{c(3N'+9P')(K_2-K_1)}{L'^2(L'+3M')} - \frac{4}{9}\frac{N'(\mu_2-\mu_1)c}{L'^3} \\ & - \frac{1}{3}\frac{c(9Q'+3O'+3P'+N')(K_2-K_1)}{(L'+3M')^3}, \end{aligned}$$

where we have introduced the parameters $L'=c+(1-c)L$, $M'=(1-c)M$, $N'=(1-c)N$, $O'=(1-c)O$, $P'=(1-c)P$, and $Q'=(1-c)Q$. We note that eq. (9) holds even in the limiting case of c= 1, falling beyond the adopted hypothesis of small volume fraction. This scheme describes a complex scenario frequently found in material physics problems, where possible strong amplifications of the nonlinearities may arise in some given conditions. We considered a mixture of nonlinear spheres with Landau coefficients *A, B* and *C* as indicated in Fig.1 (left) embedded in a linear matrix. The new nonlinear theory is able to predict the effective nonlinear properties of the composite as described in Fig.1 (right).

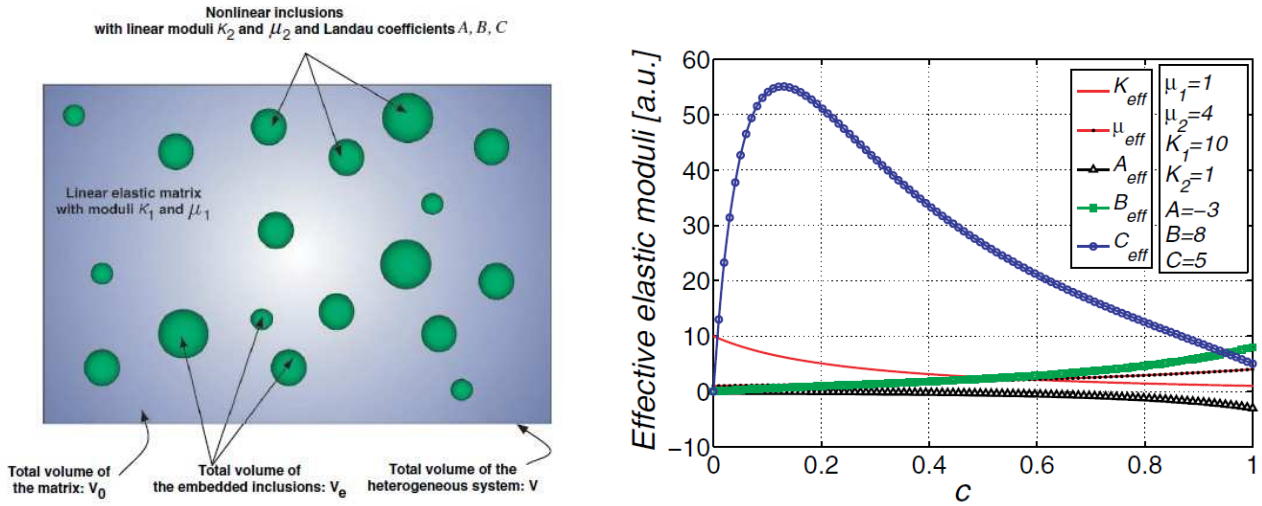

Fig.1. (left) Scheme of a dispersion of nonlinear spheres (described by the Landau coefficients) embedded in a linear matrix. (right) Linear and nonlinear effective moduli of the complex structure in terms of the volume fraction c of the spheres.

The enhancement of C_{eff} shown in Fig.1 (right) is remarkable; we underline that such an intriguing feature is obtained for any set of parameters, provided that the matrix is much more incompressible than the inclusions. We point out that this feature occurs well within the range of validity of the present theory, namely for small values of *c*. More in general, the enhancement of Landau moduli suggests that the nonlinear effective properties can be strongly affected by the linear moduli of the constituents of the heterogeneous material. For example, the ratio C_{eff}/C is sensibly modulated by the ratio K_1/K_2. In conclusion, we have developed a complete homogenization the-

ory for a dilute dispersion of nonlinear spheres into a linear matrix. A fully analytical set of equations describing the effective elastic behaviour is worked out. The present theoretical device is properly suited to recognize complex unusual nonlinear mixing phenomena exhibited by a heterogeneous material.

We are interested in studying the nonlinear phenomena combined with the scale effects induced by the possible small size of the particles embedded in the matrix. To do this we build a numerical techniques based on a lattice and on specific interactions potentials. To do this, we aim at replacing over-rich interatomic potentials, as typically used in molecular dynamics simulations, by suitable simplified *constitutive force fields*, paradigmatically accounting for any given elastic behavior and fully exploiting the atomistic features of condensed matter (but still conceiving the continuum description of the relevant elastic phenomena). We will develop this notion for two-dimensional elastic problems. The reason for that is twofold: on the one hand, the typical boundary conditions considered for several three-dimensional nanostructures actually lead to effective two-dimensional mathematical settings; on the other hand, the elasticity of two-dimensional atomic sheets is an important topic since the developement of graphene and related materials. In particular, we will adopt a triangular two-dimensional lattice, since it is the only structure which always exhibits an isotropic linear elastic behavior and, therefore, allows us to perform a thorough comparison between atomistic and continuum results.

If we take into consideration a system of N interacting particles, the potential energy U_p is a function of the vector distances $\{\vec{r}_{\alpha\beta}\}_{\alpha,\beta=1,N}$ between each pair of atoms. For further convenience, we cast U_p in the form of the following power series

$$U_p = U_0 + \sum K^{ij}_{\alpha\beta\gamma\delta}\ \ r_{\alpha\beta,i}\, r_{\gamma\delta,j} + \sum K^{ijk}_{\alpha\beta\gamma\delta\zeta\eta}\ \ r_{\alpha\beta,i}\, r_{\gamma\delta,j}\, r_{\zeta\eta,k} + \ldots \tag{10}$$

where $r_{\alpha\beta,i}$ ($i = x, y, z$) is the i-th coordinate of the vector distance between the atom α and the atom β, while U_0, $K^{ij}_{\alpha\beta\gamma\delta}$, $K^{ijk}_{\alpha\beta\gamma\delta\zeta\eta}$, ... and so on are constants. This function must show a minimum at equilibrium: in the following, we will indicate such a reference configuration as $\{\vec{r}^{\,0}_{\alpha\beta}\}_{\alpha,\beta=1,N}$, defined but for an arbitrary roto-traslation of the particles system. For sake of simplicity, the formal expansion given in Eq.(10) will be arrested at the third-order term in the interatomic distance vectors.

If the system is subjected to a uniform strain field $\hat{\varepsilon}$, the vector distance between the atom α and the atom β is given by $\vec{r}_{\alpha\beta} = \vec{r}^{\,0}_{\alpha\beta} + \hat{\varepsilon}\,\vec{r}^{\,0}_{\alpha\beta}$ and the corresponding strain energy density is

$$U(\hat{\varepsilon}) = \frac{1}{V_0} U_p(\{\vec{r}^{\,0}_{\alpha\beta} + \hat{\varepsilon}\,\vec{r}^{\,0}_{\alpha\beta}\}_{\alpha,\beta=1,N}) \tag{11}$$

where V_0 is the volume of the reference (unstrained) configuration. By using previous equations and by expanding $U(\hat{\varepsilon})$ in powers of $\hat{\varepsilon}$, it is easy to prove that the linear and nonlinear elastic constants must be a linear functions of the parameters $K^{ij}_{\alpha\beta\gamma\delta}$ and $K^{ijk}_{\alpha\beta\gamma\delta\zeta\eta}$. Therefore, it is possible to obtain any elastic behavior by properly setting the K-parameters of the lattice model.

As a useful example, we consider a simple constitutive force field given by harmonic springs between neighboring atoms placed at $\vec{r}_\alpha$ and $\vec{r}_\beta$. The corresponding pair elastic potential energy is

$$U^{2b}_h(r_{\alpha\beta};\kappa_h) = \frac{1}{2}\kappa_h(r_{\alpha\beta} - r_0)^2 \tag{12}$$

where $r_{\alpha\beta} = |\vec{r}_{\alpha\beta}| = |\vec{r}_\alpha - \vec{r}_\beta|$, κ_h is the spring constant, and r_0 is the equilibrium distance. The subscript h stands for *harmonic*. The term U^{2b} is intended to mimic bond-stretching interactions. If we expand Eq.(12) in the form of Eq.(10), all the coefficients $K^{ij}_{\alpha\beta\gamma\delta}$, $K^{ijk}_{\alpha\beta\gamma\delta\zeta\eta}$,... will be simply proportional to the spring constant κ_h. If the system is subjected to a displacement field $\vec{u}$, so that $\vec{r}_{\alpha\beta} = \vec{r}^{\,0}_{\alpha\beta} + \Delta\vec{u}_{\alpha\beta}$ being $\Delta\vec{u}_{\alpha\beta} = \vec{u}(\vec{r}^{\,0}_\alpha) - \vec{u}(\vec{r}^{\,0}_\beta)$, the potential energy for the $\alpha - \beta$ pair is

$$U^{2b}_h = \frac{1}{2}\kappa_h(|\vec{r}^{\,0}_{\alpha\beta} + \Delta\vec{u}_{\alpha\beta}| - r_0)^2 \tag{13}$$

We can expand this function in powers of $\vec{u}$, eventually obtaining

$$U^{2b}_h = \frac{1}{2}\kappa_h\left(\vec{n}_{\alpha\beta}\cdot\Delta\vec{u}_{\alpha\beta}\right)^2 + O(u^3) \tag{14}$$

where $\vec{n}_{\alpha\beta} = \dfrac{\vec{r}^{\,0}_{\alpha\beta}}{r_0}$. If the displacement field corresponds to a uniform strain $\hat{\varepsilon}$, it can be expressed as $\Delta\vec{u}_{\alpha\beta} = \hat{\varepsilon}\,\vec{r}^{\,0}_{\alpha\beta}$ and Eq.(14) assumes the form

$$U_h^{2b} = \frac{1}{2}\kappa_h\left(\vec{n}_{\alpha\beta}\cdot\hat{\varepsilon}\,\vec{r}^{\,0}_{\alpha\beta}\right)^2 + \mathsf{O}(\varepsilon^3) \tag{15}$$

We can easily verify that the linear elastic moduli are proportional to the potential parameter κ_h. Moreover, we can see that, through the $\mathsf{O}(\varepsilon^3)$ term in Eq.(15), the harmonic interaction affects also the nonlinear behavior, i.e. the nonlinear elastic constants will be proportional to κ_h as well. Therefore, if we are interested to model a purely linear elastic regime, we can use just the second order term in Eq.(14), by obtaining a corresponding ideal linear elastic constitutive model. We name such a linearized potential energy a *linearized spring*, assuming the form

$$U_l^{2b}(r_{\alpha\beta};\kappa_l) = \mathsf{L}_{\mathsf{IN}}\left[\frac{1}{2}\kappa_l\left(r_{\alpha\beta} - r_0\right)^2\right] = \frac{1}{2}\kappa_l\left(\vec{n}_{\alpha\beta}\cdot\Delta\vec{u}_{\alpha\beta}\right)^2 \tag{16}$$

where we have introduced a spring constant κ_l (l stands for *linear*) and the linearization operator L_{IN}.
A similar analysis can be performed on the following 3-body harmonic potential energy

$$U_h^{3b}(\theta_{\alpha\beta\gamma};\gamma_h) = \frac{1}{2}\frac{\gamma_h}{r_0^2}(\cos\theta_{\alpha\beta\gamma} - \cos\theta_0)^2 \tag{17}$$

which is intended to mimic bond-bending interactions. In Eq.(17) $\cos\theta_{\alpha\beta\gamma} = \dfrac{\vec{r}_{\alpha\beta}\cdot\vec{r}_{\alpha\gamma}}{|\vec{r}_{\alpha\beta}||\vec{r}_{\alpha\gamma}|}$ and θ_0 is the equilibrium angle of the 3-body interaction. In this case we get

$$\begin{aligned} U_h^{3b} &= \frac{1}{2}\frac{\gamma_h}{r_0^4}\left[\vec{n}_{\alpha\beta}\cdot\Delta\vec{u}_{\alpha\gamma} + \vec{n}_{\alpha\gamma}\cdot\Delta\vec{u}_{\alpha\beta}\right. \\ &\left. - \cos\theta_0\left(\vec{n}_{\alpha\beta}\cdot\Delta\vec{u}_{\alpha\beta} + \vec{n}_{\alpha\gamma}\cdot\Delta\vec{u}_{\alpha\gamma}\right)\right]^2 + \mathsf{O}(u^3) \end{aligned} \tag{18}$$

Similarly to the bond-stretching case, the 3-body harmonic interaction introduces both a linear and a nonlinear contribution to the strain energy density. Therefore, a purely linear elastic constitutive model can be obtained by introducing the following *linearized bond-bending energy*

$$\begin{aligned} U_l^{3b}(\theta_{\alpha\beta\gamma};\gamma_l) &= \mathsf{L}_{\mathsf{IN}}\left[\frac{1}{2}\frac{\gamma_l}{r_0^2}\left(\cos\theta - \cos\theta_0\right)^2\right] \\ &= \frac{1}{2}\frac{\gamma_l}{r_0^4}\left[\vec{n}_{\alpha\beta}\cdot\Delta\vec{u}_{\alpha\gamma} + \vec{n}_{\alpha\gamma}\cdot\Delta\vec{u}_{\alpha\beta} - \cos\theta_0\left(\vec{n}_{\alpha\beta}\cdot\Delta\vec{u}_{\alpha\beta} + \vec{n}_{\alpha\gamma}\cdot\Delta\vec{u}_{\alpha\gamma}\right)\right]^2 \end{aligned} \tag{19}$$

The potential energy terms given in Eqs.(12) and (16) and in Eqs.(17) and (19) are additive and their sum actually describes the resulting elastic behavior of the system of particles.
In order to generalize this conceptual scheme we introduce two *anharmonic* terms (for two body and three body interaction, respectively) as

$$U_a^{2b}(r_{\alpha\beta};\kappa_a) = \frac{1}{3}\frac{\kappa_a}{r_0}\left(r_{\alpha\beta} - r_0\right)^3 \tag{20}$$

$$U_a^{3b}(\theta_{\alpha\beta\gamma};\gamma_a) = \frac{1}{3}\frac{\gamma_a}{r_0^2}\left(\cos\theta_{\alpha\beta\gamma} - \cos\theta_0\right)^3 \tag{21}$$

The final resulting potential energy is therefore written as

$$\begin{aligned} U_p &= U_0 + \frac{1}{2}\sum_{\alpha\beta}\left[U_l^{2b}(r_{\alpha\beta};\kappa_l) + U_h^{2b}(r_{\alpha\beta};\kappa_h) + U_a^{2b}(r_{\alpha\beta};\kappa_a)\right] \\ &+ \sum_{\alpha\beta\gamma}\left[U_l^{3b}(\theta_{\alpha\beta\gamma};\gamma_l) + U_h^{3b}(\theta_{\alpha\beta\gamma};\gamma_h) + U_a^{3b}(\theta_{\alpha\beta\gamma};\gamma_a)\right] \end{aligned} \tag{22}$$

where nonlinear features are described through the harmonic and the anharmonic contributions in the constitutive model. Interesting enough, Eq.(22) can be applied to any kind of lattice.
By considering a two-dimensional nonlinear isotropic material, the strain energy density must depend only on the

invariants of the tensor $\hat{\varepsilon}$, i.e. it must hold that $U(\hat{\varepsilon}) = U\left(Tr(\hat{\varepsilon}), Tr(\hat{\varepsilon}^2)\right)$. By limiting nonlinear features to the third order, we can write

$$U(\hat{\varepsilon}) = \frac{\lambda}{2} Tr(\hat{\varepsilon})^2 + \mu \; Tr(\hat{\varepsilon}^2) + \mathrm{e}\, Tr(\hat{\varepsilon}) Tr(\hat{\varepsilon}^2) + \mathrm{f}\; Tr(\hat{\varepsilon})^3 \tag{23}$$

where λ and μ are the Lamé constants describing the linear elasticity of the system, while the nonlinear behavior is modeled by the two coefficients e and f. The Lamé constants can be expressed in terms of the two-dimensional Young modulus E_{2D} and the Poisson ratio ν_{2D} (plane strain conditions) or, equivalently, in terms of the stiffness tensor components as

$$\lambda = \frac{\nu_{2D} E_{2D}}{1 - \nu_{2D}^2} = C_{12} \tag{24}$$

$$\mu = \frac{E_{2D}}{2(1 + \nu_{2D})} = \frac{C_{11} - C_{12}}{2} = C_{44} \tag{25}$$

We remark that, since the system is isotropic, the Cauchy relation $2C_{44} = C_{11} - C_{12}$ is always fulfilled. Moreover, the coefficients e and f can be expressed in terms of the standard third order elastic moduli through the following relations

$$\mathrm{e} = \frac{1}{4}(C_{111} - C_{112}) \qquad \mathrm{f} = \frac{1}{4}\left(C_{112} - \frac{1}{3} C_{111}\right) \tag{26}$$

In conclusion, in the case of a fully isotropic medium the nonlinear elasticity is modeled by two independent elastic constants, namely e and f (or, equivalently, C_{111} and C_{112}).

The above system is not related to any crystalline symmetry group since all of them are characterized by an anisotropic nonlinear elastic behavior. Nevertheless, such a fully isotropic model describes the paradigmatic Eshelby configuration. From the atomistic point of view, the most similar crystal class is corresponding to a triangular planar lattice, which exhibits an isotropic behavior in the linear elastic regime at least. Therefore, we will develop our atomistic model for such a lattice.

Since the strain energy function is invariant under a rotation of $\pi/3$ about the principal axis (normal to the lattice plane), there exist two linear moduli and three nonlinear independent elastic coefficients hereafter named Λ_1, Λ_2 and Λ_3. It can be easily proved that

$$\begin{aligned} U(\hat{\varepsilon}) = {} & \frac{\lambda}{2}[Tr(\hat{\varepsilon})]^2 + \mu \; Tr(\hat{\varepsilon}^2) + \Lambda_1(\varepsilon_{xx} - \varepsilon_{yy})[(\varepsilon_{xx} - \varepsilon_{yy})^2 - 12\varepsilon_{xy}^2] \\ & + \frac{1}{2}\Lambda_2 Tr(\hat{\varepsilon})[2\, Tr(\hat{\varepsilon}^2) - Tr(\hat{\varepsilon})^2] + \frac{1}{2}\Lambda_3 Tr(\hat{\varepsilon})^3 \end{aligned} \tag{27}$$

where

$$\begin{aligned} & \Lambda_1 = \frac{1}{12}(C_{111} - C_{222}) \quad \Lambda_2 = \frac{1}{4}(C_{222} - C_{112}) \\ & \Lambda_3 = \frac{1}{12}(2C_{111} - C_{222} + 3C_{112}) \end{aligned} \tag{28}$$

The triangular lattice shows a linear isotropic elastic behavior (described by the Lamé coefficients λ and μ) and an anisotropic nonlinear elastic one (described by three independent elastic moduli Λ_1, Λ_2 and Λ_3). Only in the special case with $C_{111} = C_{222}$ we obtain a fully isotropic system, even in the nonlinear regime. In such an isotropic case we get $\Lambda_2 = \mathrm{e}$ and $\Lambda_3 - \Lambda_2 = 2\mathrm{f}$, where e and f are the nonlinear elastic constants defined in Eq.(23).

In order to build a constitutive force field for a two-dimensional triangular lattice with any possible linear and nonlinear features, we assume that the corresponding potential energy is composed by two-body (U^{2b}) and three-body (U^{3b}) terms: this is the minimal formulation required to describe bond-stretching and bond-bending phenomena. Consistently, for a mono-component triangular lattice the linear and nonlinear elastic moduli are reported in Table 1, after a cumbersome algebra. This Table must be used as follows: each elastic constant (or modulus) appearing in the first column is determined by adding all the entries in the corresponding row associated to the different constitutive force field terms. For example, the first elastic constant is given by

$C_{11} = \frac{3\sqrt{3}}{4}(\kappa_l + \kappa_h) + \frac{9\sqrt{3}}{8}(\gamma_l + \gamma_h)$. We also remark that the isotropy condition $C_{44} = (C_{11} - C_{12})/2$ is always satisfied.

Table 1: Contributions to the linear and nonlinear stiffness tensor components (C_{ij} and C_{ijk}) and to the elastic moduli (λ, μ, Λ_1, Λ_2 and Λ_3) of the constitutive force field terms (U_β^α with $\alpha = 2b$ or $3b$ and $\beta = l$, h or a) in the case of a planar triangular lattice.

	$U_l^{2b}(r;\kappa_l)$	$U_l^{3b}(\theta;\gamma_l)$	$U_h^{2b}(r;\kappa_h)$	$U_h^{3b}(\theta;\gamma_h)$	$U_a^{2b}(r;\kappa_a)$	$U_a^{3b}(\theta;\gamma_a)$
C_{11}	$+\frac{3\sqrt{3}}{4}\kappa_l$	$+\frac{9\sqrt{3}}{8}\gamma_l$	$+\frac{3\sqrt{3}}{4}\kappa_h$	$+\frac{9\sqrt{3}}{8}\gamma_h$	0	0
C_{12}	$+\frac{\sqrt{3}}{4}\kappa_l$	$-\frac{9\sqrt{3}}{8}\gamma_l$	$+\frac{\sqrt{3}}{4}\kappa_h$	$-\frac{9\sqrt{3}}{8}\gamma_h$	0	0
C_{111}	0	0	$+\frac{9\sqrt{3}}{16}\kappa_h$	$-\frac{189\sqrt{3}}{32}\gamma_h$	$+\frac{9\sqrt{3}}{8}\kappa_a$	$+\frac{27\sqrt{3}}{32}\gamma_a$
C_{222}	0	0	$+\frac{3\sqrt{3}}{16}\kappa_h$	$-\frac{27\sqrt{3}}{32}\gamma_h$	$+\frac{11\sqrt{3}}{8}\kappa_a$	$-\frac{27\sqrt{3}}{32}\gamma_a$
C_{112}	0	0	$-\frac{5\sqrt{3}}{16}\kappa_h$	$+\frac{117\sqrt{3}}{32}\gamma_h$	$+\frac{3\sqrt{3}}{8}\kappa_a$	$-\frac{27\sqrt{3}}{32}\gamma_a$
λ	$+\frac{\sqrt{3}}{4}\kappa_l$	$-\frac{9\sqrt{3}}{8}\gamma_l$	$+\frac{\sqrt{3}}{4}\kappa_h$	$-\frac{9\sqrt{3}}{8}\gamma_h$	0	0
μ	$+\frac{\sqrt{3}}{4}\kappa_l$	$+\frac{9\sqrt{3}}{8}\gamma_l$	$+\frac{\sqrt{3}}{4}\kappa_h$	$+\frac{9\sqrt{3}}{8}\gamma_h$	0	0
Λ_1	0	0	$+\frac{\sqrt{3}}{32}\kappa_h$	$-\frac{27\sqrt{3}}{64}\gamma_h$	$-\frac{\sqrt{3}}{48}\kappa_a$	$+\frac{9\sqrt{3}}{64}\gamma_a$
Λ_2	0	0	$+\frac{\sqrt{3}}{8}\kappa_h$	$-\frac{36\sqrt{3}}{32}\gamma_h$	$+\frac{\sqrt{3}}{4}\kappa_a$	0
Λ_3	0	0	0	0	$+\frac{\sqrt{3}}{6}\kappa_a$	0

We can also calculate the explicit form of the Poisson ratio

$$\nu_{2D} = \frac{1}{3} - \frac{4(\gamma_l + \gamma_h)}{2(\kappa_l + \kappa_h) + 3(\gamma_l + \gamma_h)} \tag{29}$$

and Young modulus

$$E_{2D} = \frac{2\sqrt{3}}{3}(\kappa_l + \kappa_h)\left[\frac{(\kappa_l + \kappa_h) + \frac{9}{2}(\gamma_l + \gamma_h)}{(\kappa_l + \kappa_h) + \frac{3}{2}(\gamma_l + \gamma_h)}\right] \tag{30}$$

Eq.(29) confirms the well-known result that the Poisson ratio of a system subjected to only two-body interactions is $\nu_{2D} = 1/3$. Moreover, it is interesting to observe that both ν_{2D} and E_{2D} depend only on the sums $\kappa_l + \kappa_h$ and $\gamma_l + \gamma_h$, which, therefore, govern the linear elastic behavior of our system.

Starting from the results given in Table 1, we can also obtain the potential parameters for any observed (or just guessed) elastic behavior. To this aim, we first note that we have five elastic constants and six force field parameters: therefore, we have to solve an indeterminate system of simultaneous equations with five unknowns and six equations. The simpler solution is given by fixing the value of one parameter: for example, we choose to fix the

value $\gamma_a = 0$, which cancel out the effects of the anharmonic three-body interaction, and we eventually obtain

$$\begin{aligned}
\kappa_l &= \frac{\sqrt{3}}{3}C_{11} + \frac{\sqrt{3}}{3}C_{12} + \frac{38\sqrt{3}}{9}C_{111} - 5\sqrt{3}C_{222} + \frac{17\sqrt{3}}{3}C_{112} \\
\gamma_l &= \frac{2\sqrt{3}}{27}C_{11} - \frac{2\sqrt{3}}{9}C_{12} + \frac{32\sqrt{3}}{81}C_{111} - \frac{4\sqrt{3}}{9}C_{222} + \frac{4\sqrt{3}}{9}C_{112} \\
\kappa_h &= -\frac{38\sqrt{3}}{9}C_{111} + 5\sqrt{3}C_{222} - \frac{17\sqrt{3}}{3}C_{112} \\
\gamma_h &= -\frac{32\sqrt{3}}{81}C_{111} + \frac{4\sqrt{3}}{9}C_{222} - \frac{4\sqrt{3}}{9}C_{112} \\
\kappa_a &= \frac{\sqrt{3}}{3}C_{111} - \frac{\sqrt{3}}{6}C_{222} + \frac{\sqrt{3}}{2}C_{112}
\end{aligned} \tag{31}$$

These relations provide the design or the determination of the force field parameters, given the macroscopic elastic behavior, provided that it is respectively guessed or assigned.

Isolated inhomogeneity: continuum picture. The Eshelby theory provides a fundamental result, namely: the strain field within both a linear or a nonlinear inhomogeneity is uniform (when the matrix is linear). We apply such results to a two-dimensional case with a circular inhomogeneity with linear Lamé coefficients by $\mu^{(2)}$ and $\lambda^{(2)}$ and nonlinear constants e and f. On the other hand, the linear matrix is described by the moduli $\mu^{(1)}$ and $\lambda^{(1)}$; $\hat{\varepsilon}^{(2)}$ and $\hat{\varepsilon}^{\infty}$ represent the strain within the inhomogeneity and the remotely applied strain, respectively. It is possible to obtain the implicit equation for the internal field $\hat{\varepsilon}^{(2)}$ as

$$\begin{aligned}
\hat{\varepsilon}^{\infty} &= A\hat{\varepsilon}^{(2)} + BTr(\hat{\varepsilon}^{(2)})\hat{I} + CTr(\hat{\varepsilon}^{(2)})\hat{\varepsilon}^{(2)} \\
&+ DTr\left[(\hat{\varepsilon}^{(2)})^2\right]\hat{I} + ETr^2\left(\hat{\varepsilon}^{(2)}\right)\hat{I}
\end{aligned} \tag{32}$$

where

$$\begin{aligned}
A &= 1 - \frac{\lambda^{(1)} + 3\mu^{(1)}}{2(\lambda^{(1)} + 2\mu^{(1)})}\left(1 - \frac{\mu^{(2)})}{\mu^{(1)})}\right) \\
B &= \frac{2(\lambda^{(2)} - \lambda^{(1)}) + \left(1 - \dfrac{\mu^{(2)}}{\mu^{(1)}}\right)\left(\lambda^{(1)} + \mu^{(1)}\right)}{4(\lambda^{(1)} + 2\mu^{(1)})} \\
C &= \frac{1}{2\mu^{(1)}}\frac{\lambda^{(1)} + 3\mu^{(1)}}{\lambda^{(1)} + 2\mu^{(1)}}\mathrm{e} \\
D &= \frac{1}{2}\frac{\mathrm{e}}{\lambda^{(1)} + 2\mu^{(1)}} \\
E &= \frac{1}{2}\frac{3\mathrm{f}}{\lambda^{(1)} + 2\mu^{(1)}} - \frac{\lambda^{(1)} + \mu^{(1)}}{4\mu^{(1)}}\frac{\mathrm{e}}{\lambda^{(1)} + 2\mu^{(1)}}
\end{aligned} \tag{33}$$

are constant parameters. We eventually get the expression of the internal strain field as

$$\begin{aligned}
\hat{\varepsilon}^{(2)} &= \frac{\hat{\varepsilon}^{\infty}}{A} - \frac{B}{A(A+2B)}Tr(\hat{\varepsilon}^{\infty})\hat{I} + \frac{2B(A+B)(C+D) - EA^2}{A^2(A+2B)^3}Tr^2\left(\hat{\varepsilon}^{\infty}\right)\hat{I} \\
&- \frac{1}{A^2(A+2B)}\left(CTr(\hat{\varepsilon}^{\infty})\hat{\varepsilon}^{\infty} + DTr\left[(\hat{\varepsilon}^{\infty})^2\right]\hat{I}\right)
\end{aligned} \tag{34}$$

The applied homogeneous uniaxial elongation is described by the strain tensor

$$\hat{\varepsilon}^{\infty} = \begin{pmatrix} \varepsilon & 0 \\ 0 & 0 \end{pmatrix} \tag{35}$$

where ε is a scalar parameter describing the intensity of the uniaxial deformation.

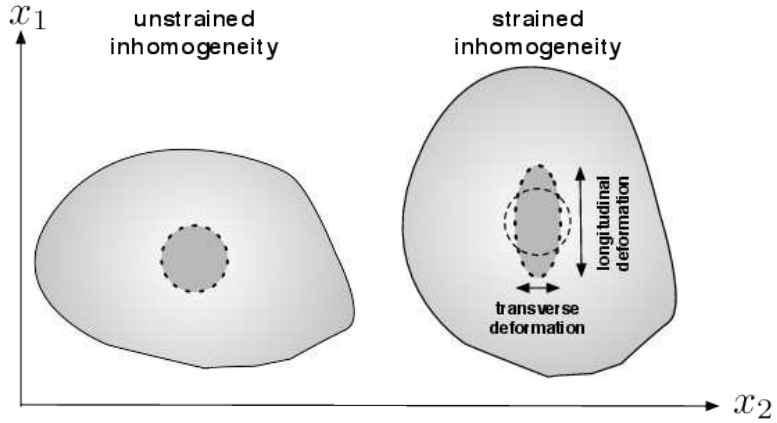

Figure 2: A matrix/inhomogeneity system under uniaxial loading along the x_1 direction. The resulting transverse and longitudinal deformation of the inhomogeneity is shown, while the corresponding strain tensor components are defined in the text.

Eq.(34) assumes the form

$$\hat{\varepsilon}^{(2)} = \begin{pmatrix} \varepsilon_l & 0 \\ 0 & \varepsilon_t \end{pmatrix} = \begin{pmatrix} L^I\varepsilon + L^{II}\varepsilon^2 & 0 \\ 0 & T^I\varepsilon + T^{II}\varepsilon^2 \end{pmatrix} \tag{36}$$

where we have introduced the simplified notation $\varepsilon_l = L^I\varepsilon + L^{II}\varepsilon^2$ and $\varepsilon_t = T^I\varepsilon + T^{II}\varepsilon^2$ to indicate the fractional elongations along the longitudinal and the transverse directions, respectively (see Fig.2). Both ε_l and ε_t are quadratic functions of the remotely applied strain ε and the four corresponding coefficients (L^I and T^I for the linear response and L^{II} and T^{II} for the nonlinear one) are the key quantities of this elastic problem. They are straightforwardly calculated as

$$L^I = \frac{A+B}{A(A+2B)} \tag{37}$$

$$T^I = \frac{-B}{A(A+2B)} \tag{38}$$

$$L^{II} = \frac{-(C+D)(A^2+2AB+2B^2)-EA^2}{A^2(A+2B)^3} \tag{39}$$

$$T^{II} = -\frac{A^2(D+E)+2B(A+B)(D-C)}{A^2(A+2B)^3} \tag{40}$$

If the inhomogeneity is linear (i.e. $\mathrm{e}=0$ and $\mathrm{f}=0$), then we get $L^{II}=0$ and $T^{II}=0$ and the original linear Eshelby result (2D) is recovered.

Isolated inhomogeneity: atomistic picture. The atomistic counterpart of the isolated inhomogeneity is developed within the constitutive force field framework introduced above. We set two different elastic media: a fully isotropic linear material with $C_{111}=C_{222}=C_{112}=0$ and an isotropic nonlinear one with $C_{111}=C_{222}$. The linear material is described by the set of parameters $\kappa_l = K$, $\kappa_h = 0$, $\kappa_a = 0$ and $\gamma_i = 0$ for any $i = l,h,a$, where K is a constant governing the elastic stiffness. The resulting elastic behavior is thus given by the following moduli

$$C_{11}^l = \frac{3\sqrt{3}}{4}K, C_{12}^l = \frac{\sqrt{3}}{4}K, C_{111}^l = 0, C_{222}^l = 0, C_{112}^l = 0 \tag{41}$$

The nonlinear material is described by setting $\kappa_l = 0$, $\kappa_h = K$, $\kappa_a = \frac{3}{2}K$ and $\gamma_i = 0$ for any $i = l,h,a$. Interactions are therefore composed by an *harmonic* term (affecting both the linear as the nonlinear elastic behavior) and by an *anharmonic* term (affecting only the nonlinear features), tailored to obtain an isotropic behavior. The resulting elastic moduli are

$$C_{11}^{nl} = \frac{3\sqrt{3}}{4}K, C_{12}^{nl} = \frac{\sqrt{3}}{4}K$$

$$C^{nl}_{111} = \frac{9}{4}\sqrt{3}K, C^{nl}_{222} = \frac{9}{4}\sqrt{3}K, C^{nl}_{112} = \frac{\sqrt{3}}{4}K \qquad (42)$$

We have chosen the same equilibrium distance $r_0 = 3.4$ Å and the same crystallographic orientation for both the inhomogeneity and matrix materials. So doing, we avoid the formation of disordered interfaces, which can appear in more complicated structures; here, we are interested in drawing a comparison with the continuum Eshelby theory which do not contain any information about features induced by possible lattice mismatch. The interaction between atoms belonging to the different phases has been described by a *linearized* spring with a constant given by the geometric mean of the stiffness of the two adjacent materials (Lorentz-Berthelot rule).
The system has been analysed for different values of the *elastic contrast* between the matrix and the inhomogeneity, defined as $\log_2(K_{mat}/K_{inc})$, where K_{mat} and K_{inc} are the elastic stiffness parameters of the matrix and inhomogeneity, respectively, entering in Eqs.(41) and (42). A positive (negative) contrast means that the matrix is stiffer (softer) than the inhomogeneity. Moreover, all the simulations are been repeated for several values of the radius R of the inhomogeneity in order to study the scale effects. In the present simulations we have described the embedded inhomogeneity by a simulation cell which is a square box of length 120 nm. The system has been relaxed through dumped dynamics in order to allow for the relaxation of the internal degrees of freedom.

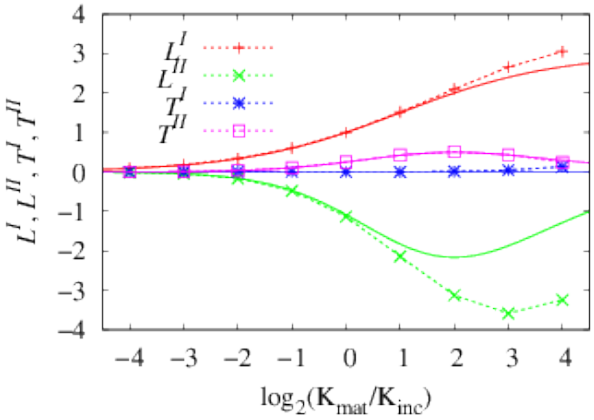

Figure 3: Longitudinal (L^I and L^{II}) and transverse (T^I and T^{II}) coefficients for an isolated nonlinear inhomogeneity. The solid lines represent the results of the continuum Eshelby theory. Dashed lines with + and × (□ and ∗) symbols represent the atomic result for the longitudinal (transverse) coefficients.

Nonlinear inhomogeneity in a linear matrix. We have modeled the inhomogeneity by the nonlinear isotropic elastic model represented by Eq.(42) setting $K = K_{inc}$. The matrix is described, in turn, by a linear material with $K = K_{mat}$ (see Eq.(41)). The inhomogeneity radius is $R = 10$ Å and the resulting internal strain field was found to be uniform.
In Fig.3 we report the longitudinal and transverse coefficients for several values of the elastic contrast. As for the linear L^I and T^I coefficients, atomistic data slightly differ from the continuum prediction when the contrast is positive (i.e. when the inhomogeneity is softer than the hosting matrix) , while for negative contrast a perfect agreement between the two approaches is observed. As for the nonlinear L^{II} and T^{II} coefficient, we found once again a perfect agreement between atomistic and Eshelby results under the condition that the inhomogeneity is stiffer than the matrix (negative values of the contrast). On the other hand, atomistic effects are present in the case of positive contrast. We observe that the atomistic transverse nonlinear coefficient is equal to the corresponding continuum one for any value of the contrast. At variance, sizeable discrepancies have been found for the longitudinal coefficient. The disagreement between the continuum theory predictions and the atomistic results has been further investigated by varying the radius of the inhomogeneity. We have found that the two different pictures reconcile by increasing the radius of the inhomogeneity, as shown in Fig.4.

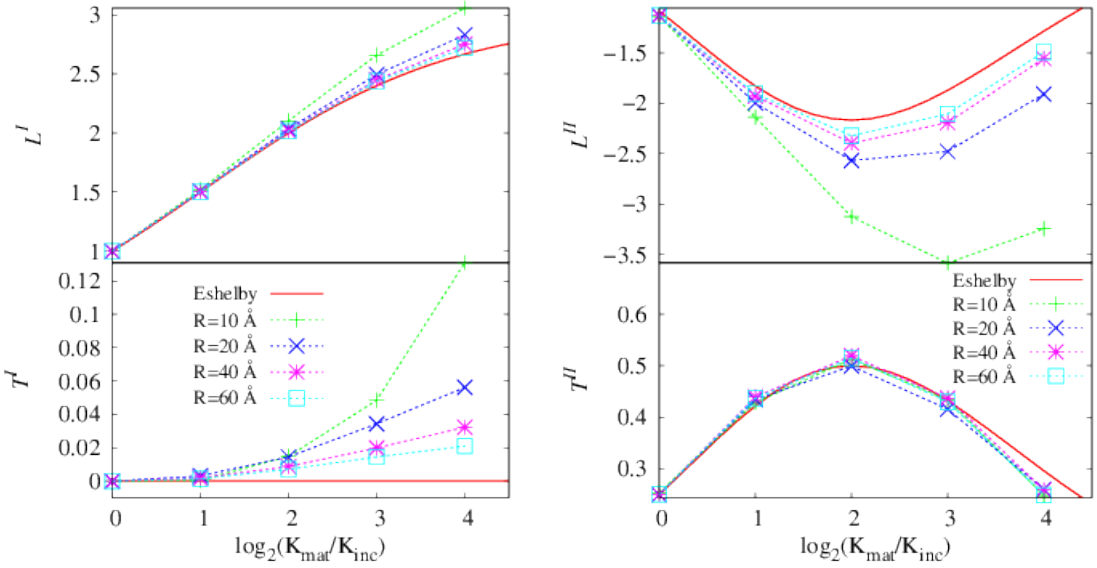

Figure 4: Coefficients L^I, T^I, L^{II} and T^{II} as a function of the elastic contrast, calculated for increasing values of the inhomogeneity radius R. The solid lines represent the Eshelby predictions, while dashed lines with symbols represent the atomistic results.

This result suggests that L-coefficients could be indeed affected by the actual dimension of the inhomogeneity. It is therefore worth investigating how the longitudinal linear L^I and nonlinear L^{II} coefficients vary as a function of R. As shown in Fig.5 atomistic data are nicely fitted by a simple power law as

$$\frac{L^I(R)}{L^I(\infty)} = 1 + \frac{a}{R^\alpha} \quad and \quad \frac{L^{II}(R)}{L^{II}(\infty)} = 1 + \frac{b}{R^\beta} \tag{43}$$

where a, b, α and β are fitting parameters. The numerical fits provide the same scaling exponent ($\beta = \alpha$) with value 1.11 for the linear and nonlinear coefficients. It is important to remark that the values of these scaling exponents are independent on the elastic contrast, as shown in Fig.5. The above result suggests that the linear and nonlinear behaviors of our lattice system belong to the same universality class. In such a case with $\alpha = \beta$, the overall internal displacement ε_l fulfills a similar simple power law $\varepsilon_l(\varepsilon; R) = \varepsilon_l(\varepsilon; \infty) + \Delta(\varepsilon) R^{-\alpha}$ where $\Delta(\varepsilon) = aL^I(\infty)\varepsilon + bL^{II}(\infty)\varepsilon^2$. As a consequence of such a scaling behavior, the measurement or the computation of the $\varepsilon_l(\varepsilon; \widetilde{R})$ curve for a given value of $\widetilde{R}$, allows for the direct knowledge of the same curve for an arbitrary radius R, being the latter simply proportional to the former

$$\frac{\varepsilon_l(\varepsilon; R) - \varepsilon_l(\varepsilon; \infty)}{\varepsilon_l(\varepsilon; \widetilde{R}) - \varepsilon_l(\varepsilon; \infty)} = \left(\frac{R}{\widetilde{R}} \right)^{-\alpha} \tag{44}$$

In other words, because of the relation $\beta = \alpha$, inhomogeneities with different radii exhibit responses to the external load which differ only for a constant scale factor $(R/\widetilde{R})^{-\alpha}$ independently on the magnitude ε of the applied strain. These conclusions have been proved by varying the radius oh the inhomogeneity within the range 5 Å - 60 Å.

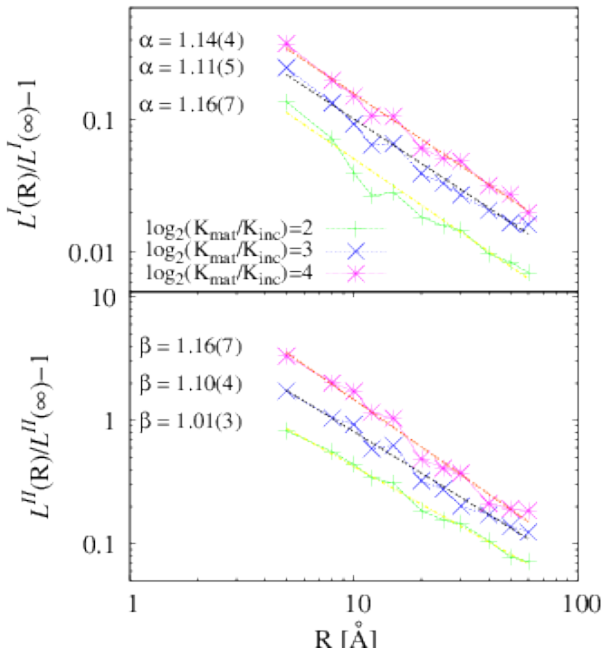

Figure 5: Fitting of Eq.(43) for different elastic contrast between the matrix and the inhomogeneity.

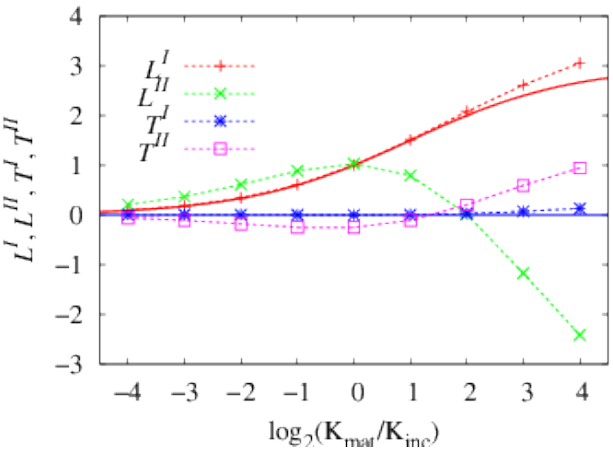

Figure 6: Linear (L^I and T^I) and nonlinear (L^{II} and T^{II}) coefficients for a linear inohomogeneity embedded in a nonlinear matrix. The solid lines represent the linear results of the continuum Eshelby theory for L^I and T^I. Dashed lines with + and × (□ and ∗) symbols represent the atomic result for the longitudinal (transverse) coefficients.

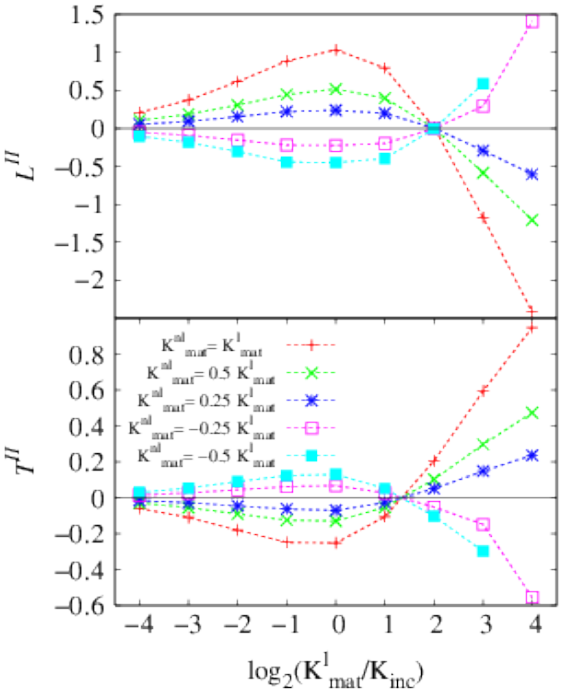

Figure 7: Atomistic results for the nonlinear coefficients L^{II} (top) and T^{II} (bottom) versus the elastic contrast $\log_2(K^l_{mat}/K_{inc})$ for different values of the nonlinearity ratio K^{nl}_{mat}/K^l_{mat} in the matrix.

Linear inhomogeneity in a nonlinear matrix. We now consider the case of a linear inhomogeneity embedded into a nonlinear matrix. The elastic behavior of the inhomogeneity is described by the Eq.(41) with $K = K_{inc}$, while the matrix is modeled according to Eq.(42) with $K = K_{mat}$.

In Fig.6 we report the longitudinal and transverse coefficients for several values of the elastic contrast. Even in this case the internal strain field is found to be uniform, although this result is not anticipated by the Eshelby theory. When the matrix is nonlinear it is remarkable to observe that two values of contrast exist which cancel out the second order nonlinear effects in the longitudinal and transverse direction, respectively (see Fig.6).

A continuum theory solution of this case is not available. Therefore, we further analyze the elastic behavior of the inhomogeneity/matrix system by varying the nonlinearity of the matrix. To this aim, we have set $\kappa_l = K$, $\kappa_h = K'$ and $\kappa_a = \frac{3}{2}K'$ within the nonlinear matrix, where K and K' are constants, so to get

$$C^{nl}_{11} = \frac{3\sqrt{3}}{4}K^l_{mat},\ C^{nl}_{12} = \frac{\sqrt{3}}{4}K^l_{mat}$$

$$C^{nl}_{111} = \frac{9}{4}\sqrt{3}K^{nl}_{mat},\ C^{nl}_{222} = \frac{9}{4}\sqrt{3}K^{nl}_{mat},\ C^{nl}_{112} = \frac{\sqrt{3}}{4}K^{nl}_{mat} \qquad (45)$$

where $K^l_{mat} = K + K'$ and $K^{nl}_{mat} = K'$ directly affect the linear and nonlinear behavior, respectively. By varing the value of K^{nl}_{mat} with respect to K^l_{mat}, we can emphasize the nonlinear regime. In Fig.7 we report the atomistic results for the nonlinear coefficients L^{II} (top) and T^{II} (bottom) versus the (linear) elastic contrast for different values of nonlinearity ratio K^{nl}_{mat}/K^l_{mat} in the matrix. We have not reported the results for the linear coefficients L^I and T^I since they are not affected by the nonlinear features of both inhomogeneity and matrix; indeed, they assume the very same values reported in Fig.6. It is interesting to underline that the longitudinal coefficient L^{II} vanishes for a given linear contrast for any possible value of the nonlinear parameter K^{nl}_{mat} of the matrix. The same phenomenon has been observed for the transverse coefficient T^{II}.

Nonlinear inhomogeneity in a nonlinear matrix. We finally consider the case of a nonlinear inhomogeneity embedded into a nonlinear matrix. We start by considering both media as described in Eq.(42) with $K = K_{inc}$ and $K = K_{mat}$, respectively in the inhomogeneity and matrix. In Fig.8 we report the longitudinal and transverse coefficients for several values of the elastic contrast. In this case the zero contrast value corresponds to a nonlinear but homogeneous material (without inhomogeneity). Therefore, we obtained $L^{II} = T^{II} = 0$ and $L^{I} = 1$ for $K_{mat} = K_{inc}$, as expected.

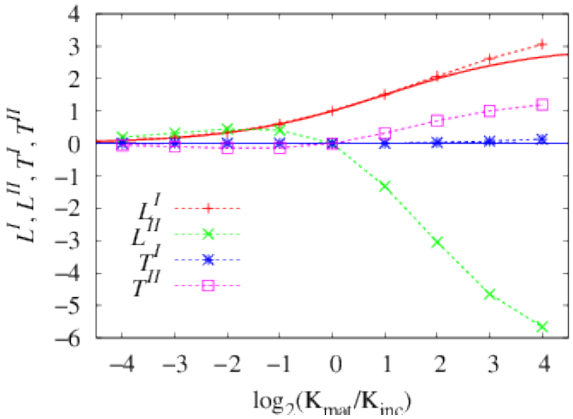

Figure 8: Linear (L^I and T^I) and nonlinear (L^{II} and T^{II}) coefficients for a nonlinear inhomogeneity embedded in a nonlinear matrix. The solid lines represent the linear results of the continuum Eshelby theory. Dashed lines with + and × (□ and ∗) symbols represent the atomic result for the longitudinal (transverse) coefficients.

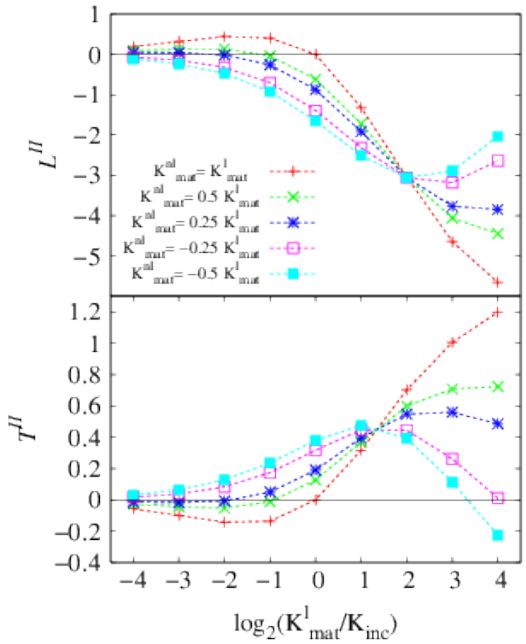

Figure 9: Atomistic results for the nonlinear coefficients L^{II} (top) and T^{II} (bottom) versus the (linear) elastic contrast $\log_2(K^l_{mat}/K_{inc})$ for different values of the K^{nl}_{mat}/K^l_{mat} ratio in the matrix.

Since, as in the previous case, this configuration is hardly affordable by continuum theory, we performed a more detailed analysis by investigating several nonlinear hosting matrices, all modeled by Eq.(45) but characterized by a different ratio K^{nl}_{mat}/K^l_{mat} between the nonlinear and the linear stiffness coefficients. We have instead set the behavior of the inhomogeneity according to Eq.(42), with $K = K_{inc}$. In Fig.9 we show the atomistic results for the nonlinear coefficients L^{II} (top) and T^{II} (bottom) versus the elastic contrast for different values of the K^{nl}_{mat}/K^l_{mat}

ratio. We have not reported the results for the linear coefficients L^I and T^I since they are not affected by the nonlinear features of both inhomogeneity and matrix; indeed, they assume the very same values reported in Fig.8. Interesting enough, we observe that there is a value of the (linear) elastic contrast $\log_2(K^l_{mat}/K_{inc})$ which generates a constant value of L^{II} (see Fig.9, top) for any nonlinearity of the matrix. This result indicates that, in such a specific condition, the nonlinear effects of the matrix are quenched. The same behavior is also observed for the transverse coefficient T^{II} (see Fig.9, bottom).

The elastic behaviour of inhomogeneities with size and shape different from their hosting cavities. We also considered a generalization of the Eshelby theory concerning the elastic behaviour of prestrained or prestressed inhomogeneities. The Eshelby theory, in its original version, deals with a configuration where both the ellipsoidal particle and the surrounding matrix are in elastostatic equilibrium if no external loads are applied to the system. Here, we considered slightly different shapes and sizes for the particle and the hosting cavity (whose surfaces are firmly bonded together) and, therefore, we observed a given state of strain (or stress) even without externally applied loads. We developed a complete procedure able to determine the uniform elastic field induced in an arbitrarily prestrained particle subjected to arbitrary remote loadings. An interesting example of application is given by composite materials and structures at the nano-scale. In Fig.10 (left) one can find the atomistic structure of an interface between a matrix and a cylindrical nano-inhomogeneity: the effects of the lattice mismatch between cylinder and cavity are evident in the region close to the interface. That zone is in fact characterized by a disorder (with atoms density larger than the pure crystal phase), which generates a quite uniform hydrostatic compression within the particle. This effect can be simply modelled through the insertion of a particle with radius larger than the matrix cavity. A very similar situation is found when the particle exhibits a thermal coefficient different from the matrix one. In Fig. 10 (right) one can find the results for a circular inclusion with and without externally applied stress (Stefano Giordano, Pier Luca Palla, Emiliano Cadelano and Michele Brun, Elastic behaviour of inhomogeneities with size and shape different from their hosting cavities, Mechanics of Materials 44, 4, 2012).

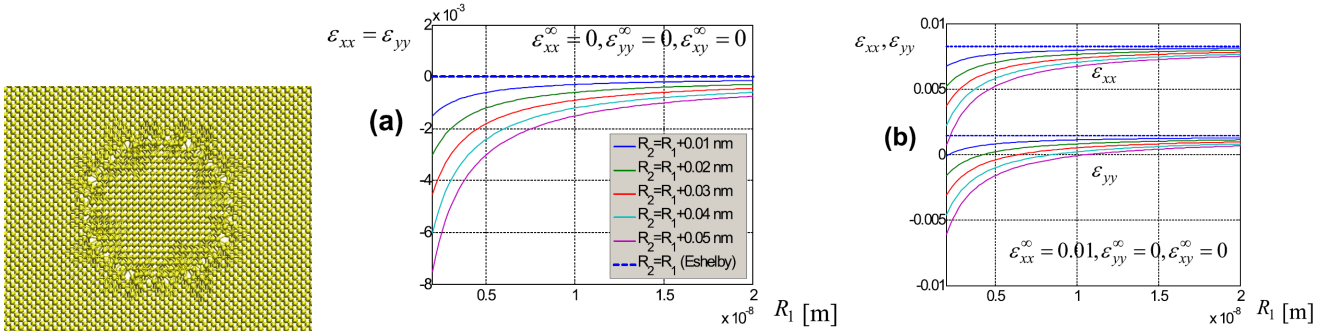

Fig. 10. (left) Example of an atomistically resolved prestrained cylindrical inhomogeneity. (right) Internal components along x and y of the strain tensor for a prestrained cylindrical inhomogeneity (stiffness C_2 and radius R_2) embedded into a homogeneous matrix (stiffness C_1 and cavity with radius R_1). Results without external load (a) and the effects of a remotely applied deformation (b).

2.1.8.Nonlinear elasticity of two-dimensional atomic sheets

(*Emiliano Cadelano, Pier Luca Palla, Stefano Giordano, and Luciano Colombo, Nonlinear Elasticity of Monolayer Graphene, Physical Review Letters, 102, 235502, 2009, Emiliano Cadelano, Pier Luca Palla, Stefano Giordano and Luciano Colombo, Elastic properties of hydrogenated graphene, Physical Review B 82, 235414, 2010, Emiliano Cadelano, Stefano Giordano, and Luciano Colombo, Interplay between bending and stretching in carbon nanoribbons, Phys. Rev. B 81, 144105, 2010, Luciano Colombo and Stefano Giordano, Nonlinear elasticity in nanostructured materials, Report on Progress in Physics 74, 116501, 2011*)

Monolayer crystals, as thin as a single atomic sheet, represent a versatile source of novel two-dimensional materials with intriguing physical properties, possibly useful in many front-end technologies such as nano-/opto-electronics, energetics and nanomechanics. The experimental search, synthesis and characterization of such low-dimensional materials, as well as the theoretical investigation of their properties, is a very active and lively field of modern nanoscience. Above all, graphene (i.e. a two-dimensional hexagonal lattice of carbon atoms) is playing a role of paramount importance, due to its unique electronic, transport and mechanical properties (Wu Y H, Yu T and Shen Z X 2010 Two-dimensional carbon nanostructures: fundamental properties, synthesis, characterization, and

potential applications *J. Appl. Phys.* 108 071301, Gomez-Navarro C, Burghard M and Kern K 2008 Elastic properties of chemically derived single graphene sheets *Nano Lett.* 8 2045–9). In this section, we precisely focus on graphene and its hydrogenated counterparts (also referred to as graphanes) by investigating their linear and nonlinear elastic features.

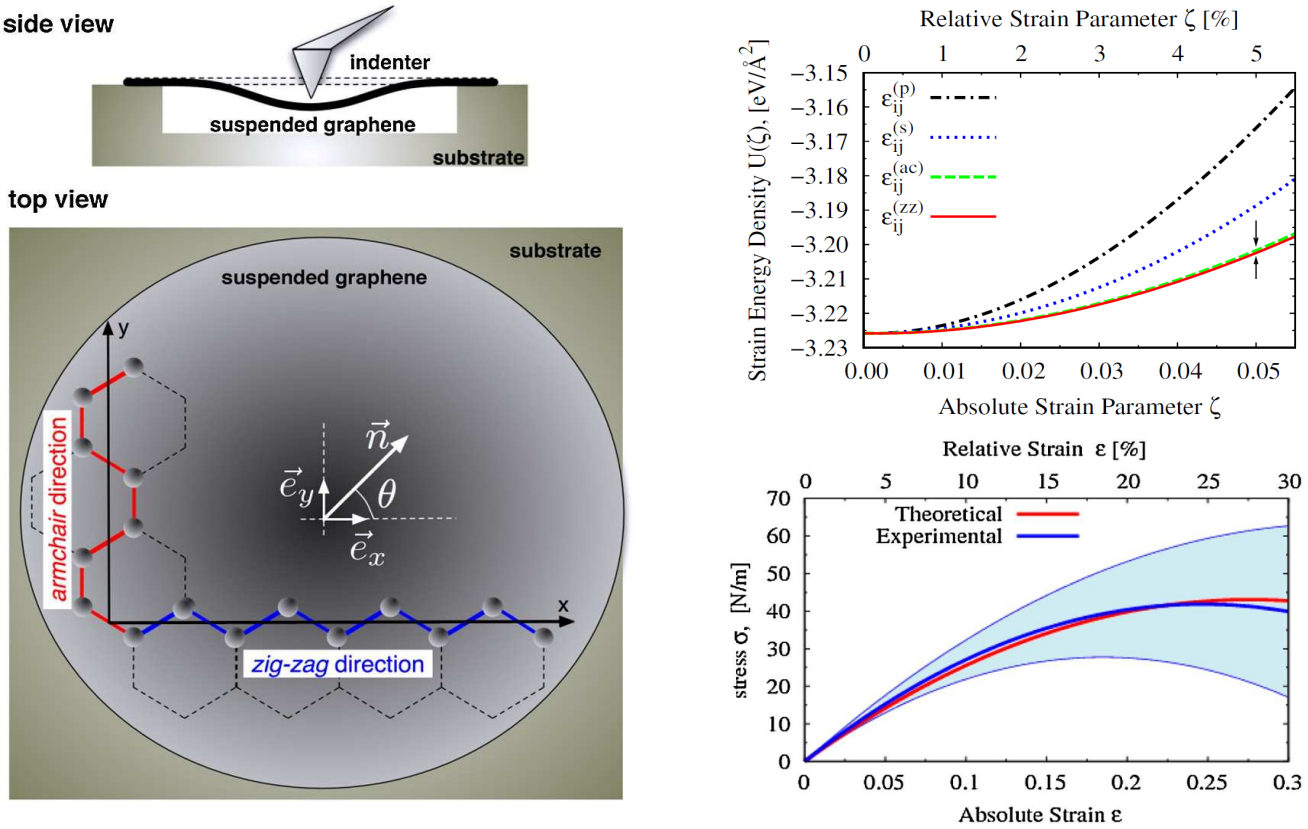

FIG. 1 On the left we have the graphenc structure. Top: scheme of the indentation of a suspended monolayer graphene (side view). Bottom: definition of zigzag and armchair directions (top view). On the right we have some results. Top: strain energy density U, obtained by TB-AS, as a function of the strain parameter corresponding to the four homogeneous deformations summarized in Table I. Bottom: theoretical (present work) and experimental (see C. Lee et al., Science 321, 385, 2008) stress-strain curves, as defined in the main text. Shaded area represents the experimental error.

We start by analysing the nonlinear elasticity of graphene. The graphene atomic scaffold is sketched in Figure 1, together with its two nonequivalent high-symmetry 'armchair' and 'zigzag' directions. By the general principles of continuum (small strain) elasticity, we can straightforwardly write down the formal expression, up to third order in strain, for the graphene strain energy density U

$$
\begin{aligned}
2U = {} & \frac{E}{1+\nu}\mathrm{Tr}\left(\hat{\epsilon}^2\right) + \frac{E\nu}{1-\nu^2}\left(\mathrm{Tr}\hat{\epsilon}\right)^2 + \frac{1}{3}C_{111}\epsilon_{xx}^3 + \frac{1}{3}C_{222}\epsilon_{yy}^3 \\
& + C_{112}\epsilon_{xx}^2\epsilon_{yy} + (C_{111} - C_{222} + C_{112})\epsilon_{xx}\epsilon_{yy}^2 \\
& + (3C_{222} - 2C_{111} - C_{112})\epsilon_{xx}\epsilon_{xy}^2 \\
& + (2C_{111} - C_{222} - C_{112})\epsilon_{yy}\epsilon_{xy}^2 .
\end{aligned}
\qquad \textbf{(1)}
$$

The elastic properties of graphene have been recently determined by atomic force microscope nanoindentation (C. Lee et al., Science 321, 385, 2008), measuring the deformation of a free-standing monolayer as sketched in Fig. 1. In particular, the experimental force-deformation relation has been expressed as a phenomenological nonlinear scalar relation between the applied stress and the observed strain $\sigma=E\varepsilon+D\varepsilon^2$ where E and D are, respectively, the Young modulus and an effective nonlinear (third-order) elastic modulus of the wo-dimensional carbon sheet. The reported experimental values are E =340 $\pm$ 40 N/m and D= 690 $\pm$ 120 N/m. While the first result is consistent with previous existing data, the above value for D represents so far the only available information about the

nonlinear elasticity of a one-atom thick carbon sheet. Although nonlinear features are summarized in $\sigma=E\varepsilon+D\varepsilon^2$ by one effective parameter D, continuum elasticity theory predicts the existence of three independent third-order parameters C_{ijk} for graphene, as reported in Eq.(1). In other words, while $\sigma=E\varepsilon+D\varepsilon^2$ represents a valuable effective relation for the interpretation of a complex experiment, a more rigorous theoretical picture must be worked out in order to properly define all the nonlinear elastic constants of graphene and to understand the physical meaning of D. This corresponds to the content of the present section where we investigate the constitutive nonlinear stress-strain relation of graphene, by combining continuum elasticity and tightbinding atomistic simulation (TB-AS).

We begin by considering very simple in-plane deformations, namely, (i) a uniaxial deformation ζ along the zigzag direction, corresponding to a strain tensor $\varepsilon^{(zz)}_{ij}= \zeta\delta_{ix}\delta_{jx}$; (ii) a uniaxial deformation ζ along the armchair direction, corresponding to a strain tensor $\varepsilon^{(ac)}_{ij}= \zeta\delta_{iy}\delta_{jy}$; (iii) a hydrostatic planar deformation ζ , corresponding to the strain tensor $\varepsilon^{(p)}_{ij}= \zeta\delta_{ij}$ and, finally, (iv) a shear deformation ζ , corresponding to an in-plane strain tensor $\varepsilon^{(s)}_{ij}= \zeta(\delta_{ix}\delta_{jy} + \delta_{iy}\delta_{jx})$. The continuum picture is now blended to atomistics and, therefore, the energy versus strain curves needed to determine elastic moduli have been calculated atomistically by a suitable tight-binding (TB) model for a periodically repeated square cell containing as many as 400 carbon atoms (see Fig.1, right-top). For any given applied deformation, full relaxation of the internal degrees of freedom of the simulation cell was performed by zero temperature damped dynamics, until interatomic forces were not larger than a given threshold. For these deformations the elastic energy of strained graphene can be written in terms of just the single deformation parameter ζ , as follows

$$U(\zeta) = U_0 + \tfrac{1}{2}U^{(2)}\zeta^2 + \tfrac{1}{6}U^{(3)}\zeta^3 + O(\zeta^4), \qquad (2)$$

where U_0 is the energy of the unstrained configuration. Since the expansion coefficients $U^{(2)}$ and $U^{(3)}$ are related to elastic moduli as summarized in table 1, a straightforward fit of equation (2) can provide the full set of linear and nonlinear moduli. The present TB calculation provides a (two-dimensional) Young's modulus value E = 312 N/m which is in reasonable agreement with the literature, while Poisson's ratio value ν = 0.31 is found to be larger than most of the ab initio results. This disagreement is clearly due to the empirical character of the adopted TB model. It is, however, important to note that the nonlinear elastic features discussed below only weakly depend upon ν: as a matter of fact, by varying its value within the set of values found in the literature, we observed a variation of the effective moduli smaller than 10%. The same fitting of the $U = U(\zeta)$ curve has determined the full set of TOECs as well, which were $C_{111} = -1689.2$, $C_{222} = -1487.7$ and $C_{112} = -484.1$ in units of N/m. We note that C_{111} is different from C_{222}, i.e. a monolayer graphene is isotropic in the linear elasticity approximation (as indeed confirmed by the analysis of the above shear deformation), while it is anisotropic whenever nonlinear features are properly taken into account.

Uniform strain	$U^{(2)}$	$U^{(3)}$
$\hat{\epsilon}^{(zz)} = \begin{pmatrix} \zeta & 0 \\ 0 & 0 \end{pmatrix}$	$\frac{E}{1-\nu^2}$	C_{111}
$\hat{\epsilon}^{(ac)} = \begin{pmatrix} 0 & 0 \\ 0 & \zeta \end{pmatrix}$	$\frac{E}{1-\nu^2}$	C_{222}
$\hat{\epsilon}^{(p)} = \begin{pmatrix} \zeta & 0 \\ 0 & \zeta \end{pmatrix}$	$\frac{2E}{1-\nu}$	$4C_{111} - 2C_{222} + 6C_{112}$
$\hat{\epsilon}^{(s)} = \begin{pmatrix} 0 & \zeta \\ \zeta & 0 \end{pmatrix}$	$\frac{2E}{1+\nu}$	0

Table I. Relationship among the energy expansion coefficients $U_{(2)}$ and $U_{(3)}$ of equation (2) and the elastic moduli of graphene for four in-plane deformations.

In order to compare our predictions with experimental data, we preliminarily observe that, for any uniaxial deformation along n (see fig. 1) the stress field is described by in-plane components $T_{xx} = \sigma_n \cos^2\theta$, $T_{xy} = \sigma_n \cos\theta \sin\theta$ and $T_{yy} = \sigma_n \sin^2\theta$. Similarly, we can find the relative variation of length $\varepsilon_n = n \cdot \varepsilon\, n$ along the direction defined by n. By combining these results, we can elaborate the effective stress-strain relation along the arbitrary direction n in a very simple form

$$\sigma_{\vec{n}} = E\epsilon_{\vec{n}} + D_{\vec{n}}\epsilon_{\vec{n}}^2, \qquad (3)$$

where we have introduced the effective two-dimensional nonlinear modulus

$$D_{\vec{n}} = \tfrac{3}{2}(1-\nu)^3\Lambda_3 + \frac{3}{2}(1-\nu)(1+\nu)^2\Lambda_2 \\ +3(2\cos^2\theta - 1)(16\cos^4\theta - 16\cos^2\theta + 1)(1+\nu)^3\Lambda_1 \tag{4}$$

describing the overall nonlinear behavior of the carbon sheet where the Λ-parameters are given below

$$\Lambda_1 = \tfrac{1}{12}(C_{111} - C_{222}), \qquad \Lambda_2 = \tfrac{1}{4}(C_{222} - C_{112}), \qquad \Lambda_3 = \tfrac{1}{12}(2C_{111} - C_{222} + 3C_{112}). \tag{5}$$

If we set n along x (i.e. $\theta = 0$), we obtain the nonlinear modulus $D^{(zz)}$ for stretching along the zigzag direction

$$D^{(zz)} = 3(1+\nu)^3\Lambda_1 + \tfrac{3}{2}(1-\nu)(1+\nu)^2\Lambda_2 + \tfrac{3}{2}(1-\nu)^3\Lambda_3 \tag{6}$$

while, by setting n along y (i.e. $\theta = \pi/2$),we obtain the nonlinear modulus $D^{(ac)}$ for stretching along the armchair direction

$$D^{(ac)} = -3(1+\nu)^3\Lambda_1 + \tfrac{3}{2}(1-\nu)(1+\nu)^2\Lambda_2 + \tfrac{3}{2}(1-\nu)^3\Lambda_3. \tag{7}$$

In order to perform a meaningful comparison with experimental data, we need to average the expression of D_n over θ: as a matter of fact, the stress–strain was obtained by nanoindentation of a suspended monolayer graphene sample, a situation generating a strain field with radial symmetry. This procedure leads to

$$\langle D_{\vec{n}} \rangle = \frac{1}{2\pi}\int_0^{2\pi} D_{\vec{n}}\,\mathrm{d}\theta = \frac{D^{(zz)} + D^{(ac)}}{2} \\ = \frac{3}{2}(1-\nu)\left[(1+\nu)^2\Lambda_2 + (1-\nu)^2\Lambda_3\right]. \tag{8}$$

We will consistently assume that the experimentally determined nonlinear modulus of graphene actually corresponds to the average value of the moduli for the zigzag and armchair directions. Using the TB values for TOECs, we easily obtain $D^{(zz)} = -696.2$, $D^{(ac)} = -469.6$ and $\langle D_n \rangle = -582.9$ in units N/m. While the negative values for $D^{(zz)}$) and $D^{(ac)}$ indicate that, if the nonlinear behavior of graphene is softening hyperelastic, the value for D_n is indeed very close to the experimentally reported value $D = -690$N/m (C. Lee et al., Science 321, 385, 2008), thus proving the reliability of the followed procedure. This is convincingly confirmed by figure 1 where the theoretical and experimental graphene stress–strain curves are compared: the agreement is indeed remarkable. We can also determine the failure stress (maximum of the stress–strain curve) $\sigma_f = -E^2/4\langle D_n \rangle$, corresponding to a predicted failure stress as high as 42.4N/m. This result is once again in excellent agreement with the experimental value 42±4N/m, reported in literature (C. Lee et al., Science 321, 385, 2008). These values correspond to the failure strength of a two-dimensional system. In order to draw a comparison with bulk materials, we define an effective three-dimensional failure stress $\sigma_f^{3D} = \sigma_f / d$, where d is taken as the interlayer spacing in graphite. By considering $d = 0.335$ nm, we obtain $\sigma_f^{3D} = 130$ GPa. This very high value, exceeding that of most materials (even including multi-walled nanotubes), motivates the use of one-atom thick carbon layers as possible reinforcement in advanced composites.

We describe now the nonlinear elasticity of graphane. Graphane is the hydrogenated form of graphene; it consists of a two-dimensional, periodic, and covalently bonded hydrocarbon with a C:H ratio of 1 (Sofo J O, Chaudhari A S, and Barber G D 2007 Graphane: a two-dimensional hydrocarbon *Phys. Rev.* B **75** 153401, Boukhvalov D W, Katsnelson M I, and Lichtenstein A I 2008, Hydrogen on graphene: electronic structure, total energy, structural distortions and magnetism from first-principles calculations *Phys. Rev.* B **77** 035427). Since hydrogen atoms can bind to carbon atoms on both the top and bottom side, there are three possible decoration schemes, shown in Fig. 2, generating an equal number of inequivalent conformers: chair (C-), boat (B-) and washboard (W-) graphane. They all fulfil the characterizing conditions of: (i) 1:1 ratio between carbon and hydrogen atoms; (ii) in-plane

translational invariance. The striking difference of graphane with respect to its mother structure graphene is that hydrogenation causes a change in the orbital hybridization which is now *sp*3-like. The actual values of elastic moduli are likely to be affected by this major change in chemical bonding. Furthermore, some graphane conformers are not isotropic, at variance with graphene which is so (in the linear approximation): hydrogenation is expected to dramatically affect the overall mechanical behavior of the system by introducing an anisotropic dependence of its response to an external load.

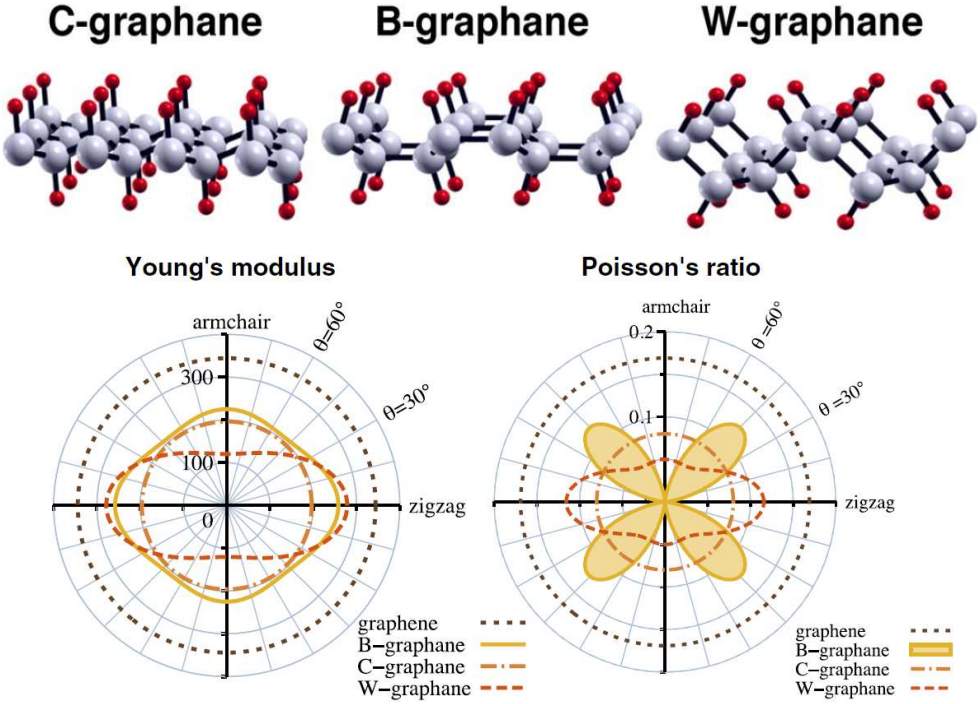

Fig.2. Top. Atomic architecture of the graphane conformers. Gray (red) spheres represent carbon (hydrogen). Bottom. Polar diagram for Young's modulus E (left) in units N/m and Poisson's ratio (right) of graphene and all graphane conformers. The angle θ identifies the extension direction with respect to the zigzag one. Isotropic (anisotropic) behavior is associated with a circular (non-circular) shape of the polar plot. The special case of B-graphane (as for the Poisson ratio) is highlighted by shading.

While C-graphane has trigonal symmetry (and, therefore, is elastically isotropic in linear regime as hexagonal graphene), the remaining B- and W-conformers show an orthorhombic symmetry, which causes an anisotropic linear elastic behavior. Accordingly, the linear elastic energy density (per unit of area) accumulated upon strain can be expressed as

$$U_{trigo} = \frac{1}{2} C_{11}\left(\varepsilon_{xx}^2 + \varepsilon_{yy}^2 + 2\varepsilon_{xy}^2\right) + C_{12}\left(\varepsilon_{xx}\varepsilon_{yy} - \varepsilon_{xy}^2\right) \tag{9}$$

for the istropic structures and as

$$U_{ortho} = \frac{1}{2} C_{11}\varepsilon_{xx}^2 + \frac{1}{2} C_{22}\varepsilon_{yy}^2 + C_{12}\varepsilon_{xx}\varepsilon_{yy} + 2C_{44}\varepsilon_{xy}^2 \tag{10}$$

for the anisotropic ones. Elastic constants are defined as usual and it must be understood that the small strain tensor is calculated with reference to the planar displacement $\vec{u} = (u_x, u_y)$. It is important to remark that U_{trigo} can be obtained from U_{ortho} by simply imposing the isotropy condition $C_{11} = C_{22}$ and the Cauchy relation $2C_{44} = C_{11} - C_{12}$, holding for both the hexagonal and trigonal symmetry. We will take profit of this by focussing just on the elastic behavior of a system described by Eq.(10); when needed, the general results so obtained will be applied to the isotropic structures by fully exploiting the above conditions. The constitutive in-plane stress-strain equations are straightforwardly derived from Eq.(10): $T_{xx} = C_{11}\varepsilon_{xx} + C_{12}\varepsilon_{yy}$, $T_{yy} = C_{22}\varepsilon_{yy} + C_{12}\varepsilon_{xx}$ and $T_{xy} = 2C_{44}\varepsilon_{xy}$.

We now suppose to apply to whichever conformer an axial tension σ along the arbitrary direction

$\vec{n} = \cos\theta \vec{e}_x + \sin\theta \vec{e}_y$, where the angle θ identifies the extension direction with respect to the zigzag one (see Fig.1, still holding for graphane). By following a standard procedure, we easily get both the longitudinal component

$$\varepsilon_l = \sigma \left[\frac{C_{11}}{\Delta} s^4 + \frac{C_{22}}{\Delta} c^4 + \left(\frac{1}{C_{44}} - 2\frac{C_{12}}{\Delta} \right) c^2 s^2 \right] \tag{11}$$

and the transverse component

$$\varepsilon_t = \sigma \left[\left(\frac{C_{11} + C_{22}}{\Delta} - \frac{1}{C_{44}} \right) c^2 s^2 - \frac{C_{12}}{\Delta} \left(c^4 + s^4 \right) \right] \tag{12}$$

of the resulting small strain tensor along (i.e. longitudinal) or normally to (i.e. transverse) the direction $\vec{n}$ (we set $\Delta = C_{11}C_{22} - C_{12}^2$, $c = \cos\theta$, and $s = \sin\theta$). By means of Eqs.(11) and (12) we can evaluate, respectively, the θ-dependent Young modulus

$$E(\theta) = \sigma / \varepsilon_l = \frac{\Delta}{C_{11} s^4 + C_{22} c^4 + \left(\frac{\Delta}{C_{44}} - 2C_{12} \right) c^2 s^2} \tag{13}$$

and the θ-dependent Poisson ratio

$$\nu(\theta) = -\varepsilon_t / \varepsilon_l = -\frac{\left(C_{11} + C_{22} - \frac{\Delta}{C_{44}} \right) c^2 s^2 - C_{12} \left(c^4 + s^4 \right)}{C_{11} s^4 + C_{22} c^4 + \left(\frac{\Delta}{C_{44}} - 2C_{12} \right) c^2 s^2} \tag{14}$$

Following the same path as for graphene, $E(\theta)$ and $\nu(\theta)$ can be directly obtained by the linear elastic constants C_{ij}, suitably computed through energy-vs-strain curves for homogeneous in-plane deformations. Table 2 summarizes the numerical results obtained by Density Functional Theory (DFT) as implemented in the Quantum ESPRESSO package. We used such an ab initio total energy method since no quantitatively reliable TB or empirical potential models are available for the elasticity of those hydrocarbons here investigated.

	Graphene	C-graphane	B-graphane	W-graphane
C_{11}	354	248	258	280
C_{22}			225	121
C_{12}	60	20	−1.7	14
C_{44}			93	81

Table 2. Graphene and graphane independent elastic constants (units of N/m). For graphene and C-graphane $C_{11} = C_{22}$ *and* $2C_{44} = C_{11} - C_{12}$.

We focus on an important new qualitative feature characterizing some graphane conformers, namely: their elastic moduli could depend upon the loading direction. This is shown in Fig.1 (bottom) where we report the polar plots for both the Young modulus (left) and the Poisson ratio (right). It is apparent that graphene and C-graphane are, as expected, characterized by linear elastic moduli independent of θ. On the other hand, it is found that W- and B-graphane are indeed elastically anisotropic, W- being much more anisotropic than the B-conformer. Furthermore, it is provided evidence that the Poisson ratio in whichever graphane conformer is much smaller than in pristine graphene. Finally, an intriguing unconventional behavior is observed in Fig.1 for B-graphane, namely: for extensions along to the zigzag and armchair directions, the corresponding Poisson value is vanishingly small.

The intriguing elastic behavior of graphane hydrocarbons is further confirmed by their nonlinear features. The strain energy function U_{trigo} for C-graphane is straightforwardly provided by continuum up to the third order in the strain

$$U_{trigo} = \frac{1}{2}C_{11}\left(\varepsilon_{xx}^{2} + \varepsilon_{yy}^{2} + 2\varepsilon_{xy}^{2}\right) + C_{12}\left(\varepsilon_{xx}\varepsilon_{yy} - \varepsilon_{xy}^{2}\right)$$
$$+ \frac{1}{6}C_{111}\left(\varepsilon_{xx}^{3} + \varepsilon_{yy}^{3}\right) + \frac{1}{2}C_{112}\left(\varepsilon_{xx}^{2}\varepsilon_{yy} + \varepsilon_{xx}\varepsilon_{yy}^{2}\right)$$
$$+ 2C_{144}\left(\varepsilon_{xx}\varepsilon_{xy}^{2} + \varepsilon_{yy}\varepsilon_{xy}^{2}\right) + C_{114}\left(\varepsilon_{xx}^{2}\varepsilon_{xy} + \varepsilon_{yy}^{2}\varepsilon_{xy}\right)$$
$$+ 2C_{124}\varepsilon_{xx}\varepsilon_{xy}\varepsilon_{yy} + \frac{4}{3}C_{444}\varepsilon_{xy}^{3} \qquad (15)$$

Although for such a trigonal symmetry $C_{111} = C_{222}$, $C_{112} = C_{122}$ and $C_{144} = C_{244}$, still the overall nonlinear elastic response is truly anisotropic since not all the relevant isotropic conditions are fulfilled. Similarly, the strain energy function U_{ortho} for the B- and W-graphane is given by

$$U_{ortho} = \frac{1}{2}C_{11}\varepsilon_{xx}^{2} + \frac{1}{2}C_{22}\varepsilon_{yy}^{2} + 2C_{44}\varepsilon_{xy}^{2} + C_{12}\varepsilon_{xx}\varepsilon_{yy}$$
$$+ \frac{1}{6}C_{111}\varepsilon_{xx}^{3} + \frac{1}{6}C_{222}\varepsilon_{yy}^{3} + \frac{1}{2}C_{112}\varepsilon_{xx}^{2}\varepsilon_{yy}$$
$$+ \frac{1}{2}C_{122}\varepsilon_{xx}\varepsilon_{yy}^{2} + 2C_{144}\varepsilon_{xx}\varepsilon_{xy}^{2} + 2C_{244}\varepsilon_{yy}\varepsilon_{xy}^{2} \qquad (16)$$

Eqs.(15) and (16) can be obtained by using the standard tables of the tensor symmetries, found in many crystallography textbooks (see for instance Nye J F 1985 *Physical Properties of Crystals,* Oxford: Oxford University Press and Huntington H B 1958 *The Elastic Constants of Crystals,* New York: Academic). Following our usual protocol, U_{trigo} and U_{ortho} can be computed through energy-vs-strain curves corresponding to suitable homogeneous in-plane deformations described by just the single parameter ζ

$$U(\zeta) = U_0 + \frac{1}{2}U^{(2)}\zeta^{2} + \frac{1}{6}U^{(3)}\zeta^{3} + O(\zeta^{4}) \qquad (17)$$

Since the expansion coefficients $U^{(2)}$ and $U^{(3)}$ are related to elastic constants, as summarized in Table 3 (left) for the C-graphane and in Table 3 (right) for the B- and W-graphane, a straightforward fit of Eq.(17) can provide the full set of third-order elastic constants which are indeed reported in Table 4. We also report the graphene moduli for sake of comparison (these latter are obtained through the ab initio method and can be also compared with the corresponding tight binding results of the previous Section on graphene).

Uniform strain	$U^{(2)}$	$U^{(3)}$
$\begin{pmatrix}\zeta & 0\\ 0 & 0\end{pmatrix}$	C_{11}	C_{111}
$\begin{pmatrix}\zeta & 0\\ 0 & \zeta\end{pmatrix}$	$2(C_{11}+C_{12})$	$2C_{111}+6C_{112}$
$\begin{pmatrix}0 & \zeta\\ \zeta & 0\end{pmatrix}$	$2(C_{11}-C_{12})$	$8C_{444}$
$\begin{pmatrix}\zeta & \zeta\\ \zeta & 0\end{pmatrix}$	$3C_{11}-2C_{12}$	$C_{111}+12C_{144}+6C_{114}+8C_{444}$
$\begin{pmatrix}0 & \zeta\\ \zeta & -\zeta\end{pmatrix}$	$3C_{11}-2C_{12}$	$-C_{111}-12C_{144}+6C_{114}+8C_{444}$
$\begin{pmatrix}\zeta & \zeta\\ \zeta & -\zeta\end{pmatrix}$	$4(C_{11}-C_{12})$	$12C_{114}-12C_{124}+8C_{444}$

Uniform strain	$U^{(2)}$	$U^{(3)}$
$\begin{pmatrix}\zeta & 0\\ 0 & 0\end{pmatrix}$	C_{11}	C_{111}
$\begin{pmatrix}0 & 0\\ 0 & \zeta\end{pmatrix}$	C_{22}	C_{222}
$\begin{pmatrix}\zeta & 0\\ 0 & \zeta\end{pmatrix}$	$C_{11}+C_{22}+2C_{12}$	$C_{111}+C_{222}+3C_{112}+3C_{122}$
$\begin{pmatrix}0 & \zeta\\ \zeta & 0\end{pmatrix}$	$4C_{44}$	0
$\begin{pmatrix}\zeta & \zeta\\ \zeta & 0\end{pmatrix}$	$C_{11}+4C_{44}$	$C_{111}+12C_{144}$
$\begin{pmatrix}0 & \zeta\\ \zeta & \zeta\end{pmatrix}$	$C_{22}+4C_{44}$	$C_{222}+12C_{244}$
$\begin{pmatrix}\zeta & 0\\ 0 & -\zeta\end{pmatrix}$	$C_{11}+C_{22}-2C_{12}$	$C_{111}-C_{222}-3C_{112}+3C_{122}$

Table 3. Left. Strain fields applied to compute the linear (C_{ij}) and nonlinear (C_{ijk}) elastic constants of C-graphane. The relation between such constants and the fitting terms $U^{(2)}$ and $U^{(3)}$ of Eq.(17) is reported as well. Right. Strain fields applied to compute the linear (C_{ij}) and nonlinear (C_{ijk}) elastic constants of the B- and W-graphane. The relation between such constants and the fitting terms $U^{(2)}$ and $U^{(3)}$ of Eq.(17) is reported as well.

We note that $C_{111} < C_{222}$ for graphene and $C_{222} > C_{111}$ for B-graphane or, equivalently, graphene and B-graphane are characterized by an inverted anisotropy. On the contrary, W-graphane has the same anisotropy of graphene ($C_{111} < C_{222}$), but a larger $|C_{111} - C_{222}|$ difference. This means that the different distribution of hydrogen atoms can induce strong qualitative variations for the nonlinear elastic behavior of the different conformers. We remark that necessarily $C_{444} = 0$ in B- and W-graphane because of the orthorhombic symmetry. On the other hand, this nonlinear shear modulus could assume any value for the trigonal lattice. Interesting enough, we have verified that $C_{444} = 0$ also for C-graphane. This is due to the additional (with respect to the trigonal symmetry) mirror symmetry of C-graphane.

	Graphene	C-graphane	B-graphane	W-graphane
C_{111}	-1910 ± 11	-1385 ± 18	-1609 ± 31	-1756 ± 33
C_{222}	-1764 ± 3		-1827 ± 7	-487 ± 85
C_{112}	-341 ± 35	-195 ± 41	-20 ± 14	-75 ± 54
C_{122}			-55 ± 22	-296 ± 36
C_{124}		-411 ± 17		
C_{114}		530 ± 12		
C_{144}		568 ± 7	-161 ± 4	-143 ± 17
C_{244}			-159 ± 3	-287 ± 10
C_{444}		0.0 ± 10^{-5}		

Table 4. Graphene and graphane independent nonlinear elastic constants (units of Nm^{-1}).

Similarly to the case of graphene, an effective direction-dependent nonlinear stress-strain relation can be derived also for the three graphane conformers, having the same form given in Eq.(3) with $E = E(\theta)$ taken from Eq.(13). The nonlinear elastic modulus $D_{\vec{n}}^{(trigo)}$ for the C-graphane (as well as for any trigonal 2D lattice) is given by

$$\begin{aligned} D_{\vec{n}}^{(trigo)} = & \frac{1}{2}[\nu(1-\nu)(C_{111} - 3C_{112}) \\ & + (1-\nu)(1+\nu^2)C_{111} \\ & + 6cs(1+\nu)(1+\nu^2)C_{114} - 12cs(1+\nu)\nu C_{124} \\ & + 3c^2s^2(1-\nu)(1+\nu^2)(-C_{111} + 4C_{144} + C_{112}) \\ & + 4c^3s^3(1+\nu)(1+\nu^2)(-3C_{114} + 2C_{444} + 3C_{124}) \\ & + 8c^3s^3(1+\nu)\nu(-6C_{114} + 5C_{444} + 6C_{124})] \end{aligned} \quad (18)$$

while the corresponding modulus $D_{\vec{n}}^{(ortho)}$ for B- and W-graphane is

$$\begin{aligned} D_{\vec{n}}^{(ortho)} = & \frac{1}{2\Delta^3 E_{\vec{n}}^3}[C_{111}(C_{22}c^2 - C_{12}s^2)^3 \\ & + C_{222}(C_{11}s^2 - C_{12}c^2)^3 \\ & + 3C_{112}(C_{11}s^2 - C_{12}c^2)(C_{22}c^2 - C_{12}s^2)^2 \\ & + 3C_{122}(C_{22}c^2 - C_{12}c^2)(C_{11}s^2 - C_{12}c^2)^2 \\ & - 3C_{166}c^2s^2(C_{22}c^2 - C_{12}s^2)(\Delta/C_{44})^2 \\ & - 3C_{266}c^2s^2(C_{11}s^2 - C_{12}c^2)(\Delta/C_{44})^2] \end{aligned} \quad (19)$$

They are shown in Fig.3 as function of θ .

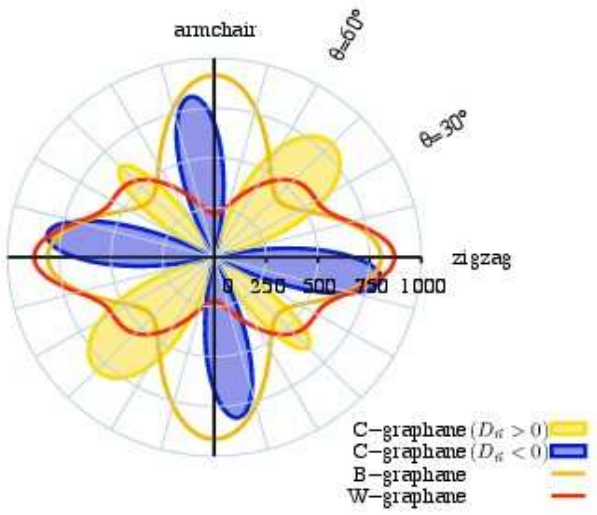

Fig. 3: Polar representation of the nonlinear elastic moduli $D_{\vec{n}}$ of the three graphane conformers. In the B- and W-graphane cases, $D_{\vec{n}} \equiv D$ are everywhere negative (softening hyperelesticity), while in the C-graphene one the $D_{\vec{n}}$ alternates negative and positive values (hardening hyperelesticity).

Since all $C_{ijk} < 0$, as shown in Tab.4, $D_{\vec{n}}^{(ortho)}$ are negative for stretching along any direction and, correspondingly, B- and W-graphane are characterized by an hyperelastic softening behavior. The trigonal C-graphane behaves in a very different way instead. Since the C_{114} and C_{144} are positive, an hyperelastic hardening behavior in the angular sectors $5/12\pi + k\pi < \theta < 1/12 + k\pi$ and $8/12\pi + k\pi < \theta < 10/12 + k\pi$ is in fact predicted. We can conclude that C-graphane admits both softening and hardening hyperelasticity, depending on the direction of the applied strain. This unusual nonlinear property makes graphane a very intriguing material with potentially large technological impact in nanomechanics.

2.1.9.Generalized interface models for transport phenomena

(Fabio Pavanello, Fabio Manca, Pier Luca Palla, and Stefano Giordano, Generalized interface models for transport phenomena: Unusual scale effects in composite nanomaterials, Journal of Applied Physics 112, 084306, 2012; Fabio Pavanello and Stefano Giordano How imperfect interfaces affect the nonlinear transport properties in composite nanomaterials, Journal of Applied Physics 113, 154310, 2013)

The effective transport properties of heterogeneous nanoscale materials and structures are affected by several geometrical and physical factors. Among them the presence of imperfect interfaces plays a central role being often at the origin of the scale effects. To describe real contacts between different phases some classical schemes have been introduced in literature, namely the low and the high conducting interface models. Here, we introduce a generalized formalism, which is able to take into account the properties of both previous schemes and, at the same time, it implements more complex behaviors, already observed in recent investigations. We apply our models to the calculation of the effective conductivity in a paradigmatic structure composed of a dispersion of particles. In particular we describe the conductivity dependence upon the size of the inclusions finding an unusual non-monotone scale effect with a pronounced peak at a given particle size. We introduce some intrinsic length scales governing the universal scaling laws.
One of the central problems in material science is to evaluate the effective electric, magnetic, elastic and thermal properties governing the physical behavior of heterogeneous materials (S. Torquato, *Random Heterogeneous Materials,* Springer-Verlag, New York, 2002; G. W. Milton, *The Theory of Composites,* Cambridge University Press, Cambridge, 2002). In recent years, with the progressive miniaturization of structures and devices, possible size effects have attracted an ever increasing interest. One crucial property that usually drives the scale effects in structured materials is the complexity of interfaces between different phases. Typically, in the macroscopic modeling, the interfaces are assumed to be perfect. In the context of the electrical conduction it means that the potential V and the normal component of the current density $\vec{J}$ are continuous across any interface: $\llbracket V \rrbracket = 0$ and $\vec{J} \cdot \vec{n} = 0$, where the symbol $\llbracket f \rrbracket$ represents the jump of the function f across the interface. This approximation turns out to be valid in the case of small surface/volume ratio. However, in many real cases of technological

interest, e.g. nanocomposites, it is important to take into consideration the specific properties of the contacts among the constituents. To this aim, two effective interface models have been so far introduced for describing two extreme situations in a zero thickness formulation. Moreover, other models are based of an explicit interphase of finite thickness and, therefore, they typically consider a three-phase heterogeneous material composed of the inclusions, the interphase medium and the matrix.

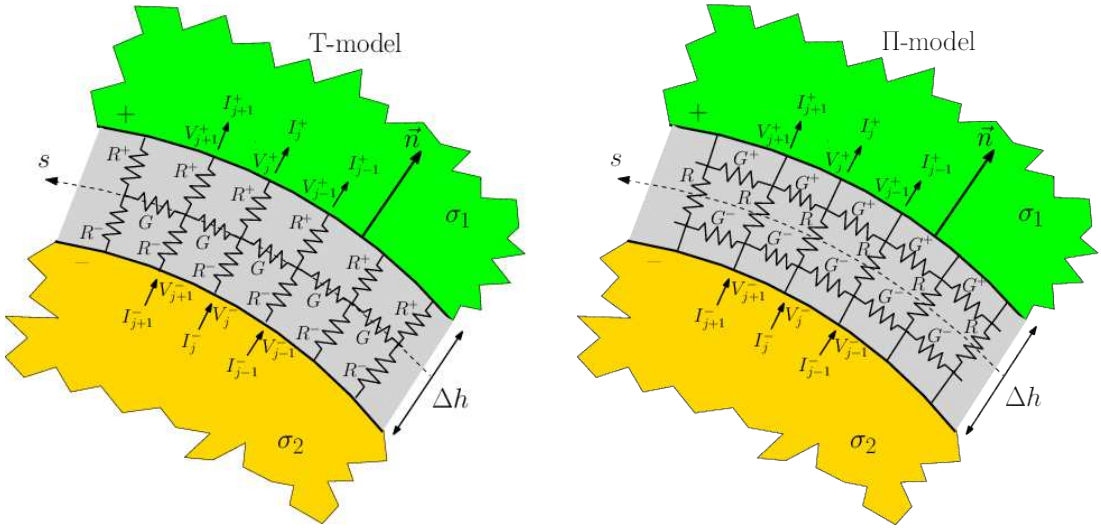

Fig.1 Schemes of the dual anisotropic imperfect interfaces (T-model and Π -model) between two homogeneous media with conductivities σ_1 and σ_2.

The first zero thickness model is called *low conducting interface* and it is based on the Kapitza resistance, introduced in the context of the thermal conduction.[8] According to this approach $\vec{J} \cdot \vec{n} = 0$, while the potential suffers a jump proportional to the local flux, $V = -r\vec{J} \cdot \vec{n}$, where r is the Kapitza-like resistance. The second model, called *high conducting interface*, concerns the case of an interphase of very high conductivity with vanishing thickness. In this situation $V = 0$, while the normal component of the current density is proportional to the surface Laplacian of the potential, $\vec{J} \cdot \vec{n} = g\nabla_S^2 V$, where g represents the interphase conductance. Several investigations on heterogeneous materials with low (Y. Benveniste and T. Miloh, Int. J. Eng. Sci. **24**, 1537, 1986; Y. Benveniste, J. Appl. Phys. **61**, 2840, 1987; D. P. H. Hasselman and L. F. Johnson, J. Compos. Mater. **21**, 508, 1987; S. Torquato and M. D. Rintoul, Phys. Rev. Lett. **75**, 4067, 1995; R. Lipton and B. Vernescu, Proc. R. Soc. London, Ser. A **452**, 329, 1996; R. Lipton and B. Vernescu, J. Appl. Phys. **79**, 8964, 1996; H. Cheng and S. Torquato, Proc. R. Soc. London, Ser. **A453**, 145, 1997; C.-W. Nan, R. Birringer, D. R. Clarke, and H. Gleiter, J. Appl.Phys. **81**, 6692, 1997; Z. Hashin, J. Appl. Phys. **89**, 2261, 2001; H. L. Duan, B. L. Karihaloo, Phys. Rev. B **75**, 064206, 2007; H. Le Quang, Q.-C. He, G. Bonnet, Phil. Mag. **91**, 3358, 2011) or high (R. Lipton, SIAM J. Appl. Math. **57**, 347, 1997; R. Lipton, J. Mech. Phys. Solids **45**, 361, 1997; T. Miloh and Y. Benveniste, Proc. R. Soc. London, Ser. **A455**, 2687, 1999; J. Yvonnet, Q.-C. He, and C. Toulemonde, Compos. Sci. Technol. **68**, 2818, 2008; H. Le Quang, G. Bonnet, Q.-C. He, Phys. Rev. B **81**, 064203, 2010) conducting interfaces can be found in literature.

In many cases, the behavior of complex interfaces cannot be simply described through the low or high conducting model. In fact, these schemes account for a single interlayer with an extreme (high or low) value of the conductivity, while real interface typically exhibit a complex or multilayered structure. To overcome this difficulty we introduce a generalized anisotropic interface formalism, which consider both the normal resistance (similarly to the Kapitza case) and the tangential conductance (as in the high conducting interface model). The term anisotropic refers to the fact that the normal resistance and the tangential conductance are completely independent, describing a different behavior in the two directions. As discussed below, in order to integrate both the normal and tangential features, two dual schemes are possible, as shown in Fig.1. They exploit the classical T and Π electric lattice structures. By means of this approach we take into account all situations comprised between the low and high conducting interface models, which can be seen as limiting cases of the present theory. In our schemes both the potential and the normal component of the current density are discontinuous at the interface. The richness of the proposed models allows us to effectively describe the behavior of real imperfect/multilayered/structured interfaces, which can be found in several heterogeneous materials of technological interest and, in particular, for those displaying a complex nanoscale structure.

At first, we have applied the generalized interfaces to model a single particle embedded in a different matrix (inhomogeneity). One of the most important technique used to study this system is based on the Eshelby formalism. A relevant universal property states that the field induced in cylindrical or spherical particles with zero-thickness low or high conducting interfaces is uniform if the externally applied field is so. It is true for both isotropic constituents and anisotropic ones. In the present work, we show that the uniformity property of the internal field for spheres and cylinders is preserved also for our generalized interface models. Moreover, to extend the validity of the Eshelby approach, we propose a method which is able to determine the field within and around a single particle even if the externally applied field is not uniform.
The previous results have been applied to determine the overall conductivity (through an effective medium theory) of a dispersion of particles with imperfect interfaces. We have verified that, in contrast to perfectly bonded inclusions, the effective properties depend upon the size of the inhomogeneities. Interestingly enough, while in the case of low or high conducting interfaces the scale effects are described by monotone scaling laws, the present generalized models show non-monotone scale effects with a sizeable peak of the transport properties. This point can be considered as a specific signature of the complex resistive/conductive behavior of the interface. A description of this intriguing behavior has been made through different intrinsic length scales governing the universal scaling laws. Typical material science problems where these interface models can be profitably applied are the following: tailoring of composites with semiconductor whiskers; thermal optimization of metal/dielectric interfaces and change materials through nanoclusters of stable oxides; analysis of thermal and electric conductivity of carbon-based nanostructures; size effects understanding in SiC/epoxy (or similar) nanocomposites.
Throughout all the section we develop the formalism with the terminology of the electrical transport, but all results can be applied to the analogous situations of thermal conduction, antiplane elasticity, magnetic permeability and electric permittivity as well.

To begin, we introduce a simple lattice network taking into account the normal resistors R^+ and R^- and the tangential conductance G (see Fig.1, T-model). This structure is able to consider both the anisotropy (along the normal and tangential directions) and the different behavior of the normal conductivity on the two sides of the interface. For the moment we consider a curvilinear interface between two different materials of a planar structure (2D geometry). The generalization to the arbitrary three-dimensional case will be made straightforwardly. By a direct application of the Kirchhoff circuit laws we obtain two equalities describing the voltage jump and current jump across the interface (the definition of the relevant quantities is shown in Fig.1)

$$V_j^+ - V_j^- = - R^+ I_j^+ - R^- I_j^- , \tag{1}$$

$$I_j^+ - I_j^- = GR^+ \left(I_{j-1}^+ - 2I_j^+ + I_{j+1}^+ \right) + G\left(V_{j-1}^+ - 2V_j^+ + V_{j+1}^+ \right). \tag{2}$$

In the limit of a continuous zero-thickness interface we easily obtain from Eqs.(1) and (2) the relations for the interface in the form

$$V = - r^+ \left(\vec{J} \cdot \vec{n} \right)^+ - r^- \left(\vec{J} \cdot \vec{n} \right)^- , \tag{3}$$

$$\vec{J} \cdot \vec{n} = gr^+ \frac{\partial^2}{\partial s^2} \left(\vec{J} \cdot \vec{n} \right)^+ + g \frac{\partial^2}{\partial s^2} V^+ . \tag{4}$$

The parameters r^-, r^+ and g are the suitably rescaled counterparts of R^-, R^+ and G (r^- and r^+ are measured in Ω m^2 and g in Ω^{-1}). In previous expressions, the partial derivatives are performed with respect to the variable s, which represents the curvilinear abscissa along the arbitrarily curved interface on the plane. As usual, in the three-dimensional case the operator $\partial^2/\partial s^2$ must be substituted with the surface Laplacian ∇_S^2, which is introduced and discussed in Appendix A. We can observe that the present approach reproduces the *low conducting interface* model if $g = 0$ (with a Kapitza resistance $r = r^- + r^+$) and the *high conducting interface* model if $r^- = r^+ = 0$.

The low conducting model is characterized by a sequence of normal resistances $R = R^+ + R^-$ (T-model with $G = 0$). If we consider Δs as the step along the curvilinear abscissa s and Δz as the step along the direction perpendicular to the plane represented in Fig.1 we have $R = \frac{1}{\sigma_\perp} \frac{\Delta h}{\Delta s \Delta z}$ where $\sigma_\perp$ is the normal conductivity of the interphase of thickness Δh. The Kapitza resistance is therefore given by $r = R \Delta S$ where $\Delta S = \Delta s \Delta z$ is the area

element associated to $\vec{J}\cdot\vec{n}$; we finally obtain $r=\lim_{\Delta h\to 0,\sigma_\perp\to 0}\frac{\Delta h}{\sigma_\perp}$. Similarly, the high conducting model is characterized by a series of tangential conductances G (T-model with $R^-=R^+=0$). It is simple to observe that $G=\sigma_P\frac{\Delta h\Delta z}{\Delta s}$ where σ_P is the tangential conductivity of the interphase. The specific conductivity is therefore given by $g=G\frac{\Delta s^2}{\Delta S}$ (where $\Delta S=\Delta s\Delta z$) and we obtain the result $g=\lim_{\Delta h\to 0,\sigma_P\to\infty}\sigma_P\Delta h$. So, we have a direct link between the interphase properties (Δh, $\sigma_\perp$, σ_P) and the models parameters (r, g) for the high and low conducting interfaces. We observe that when we consider an anisotropic single layer interphase (which is uniaxial or transversely isotropic with normal conductivity $\sigma_\perp$ and tangential conductivity σ_P), the only component $\sigma_\perp$ is relevant for the low conducting model and the only component σ_P is relevant for the high conducting interface.

Of course, if both relations $g=0$ and $r^-=r^+=0$ are satisfied in the T-model, then the ideal interface is simply obtained. It is not difficult to prove that this model is completely equivalent to a series of three different ideal sheets (multi-layered interface) A, B and C: an external low conducting phase with Kapitza resistance $r^+=\lim_{\Delta h^{(A)}\to 0,\sigma_\perp^{(A)}\to 0}\frac{\Delta h^{(A)}}{\sigma_\perp^{(A)}}$, a halfway high conducting phase with specific conductance $g=\lim_{\Delta h^{(B)}\to 0,\sigma_P^{(B)}\to\infty}\sigma_P^{(B)}\Delta h^{(B)}$ and, finally, an internal low conducting phase with Kapitza resistance $r^-=\lim_{\Delta h^{(C)}\to 0,\sigma_\perp^{(C)}\to 0}\frac{\Delta h^{(C)}}{\sigma_\perp^{(C)}}$. The three layers are characterized by thickness $\Delta h^{(A)}$, $\Delta h^{(B)}$, $\Delta h^{(C)}$ (with $\Delta h=\Delta h^{(A)}+\Delta h^{(B)}+\Delta h^{(C)}$) and conductivities $\sigma_\perp^{(A)}$, $\sigma_P^{(B)}$, $\sigma_\perp^{(C)}$. So, we have built an example of interpretation of the model parameters with a concrete physical multilayered structure.

A dual model can be introduced by considering the second structure depicted in Fig.1 (Π-model). A procedure similar to the previous one leads to the following interface equations

$$V=-r\left(\vec{J}\cdot\vec{n}\right)^+ + rg^+\frac{\partial^2}{\partial s^2}V^+, \tag{5}$$

$$\vec{J}\cdot\vec{n}=g^+\frac{\partial^2}{\partial s^2}V^+ + g^-\frac{\partial^2}{\partial s^2}V^-, \tag{6}$$

where the parameters r, g^+ and g^- are the suitably rescaled counterparts of R, G^+ and G^-, appearing in Fig.1, right. As before, the operator $\partial^2/\partial s^2$ must be substituted with the surface Laplacian ∇_S^2 for the 3D case. We can prove that also the Π-model is exactly equivalent to a series of three different ideal sheets: an external high conducting phase with conductance $g^+=\lim_{\Delta h^{(A)}\to 0,\sigma_P^{(A)}\to\infty}\sigma_P^{(A)}\Delta h^{(A)}$, a halfway low conducting phase with Kapitza resistance $r=\lim_{\Delta h^{(B)}\to 0,\sigma_\perp^{(B)}\to 0}\frac{\Delta h^{(B)}}{\sigma_\perp^{(B)}}$ and, finally, an internal high conducting phase with conductivity $g^-=\lim_{\Delta h^{(C)}\to 0,\sigma_P^{(C)}\to\infty}\sigma_P^{(C)}\Delta h^{(C)}$. As before, the layers are characterized by thickness $\Delta h^{(A)}$, $\Delta h^{(B)}$, $\Delta h^{(C)}$ and conductivities $\sigma_P^{(A)}$, $\sigma_\perp^{(B)}$, $\sigma_P^{(C)}$. It is important to remark that the interpretation of the model through three adjacent layers (for both the T and Π structures) it is not restrictive; in fact, the proposed schemes can be also used to effectively represent different imperfect interfaces with all parameters fitted in order to mimic their correct behavior. We also underline that some more complete models have been proposed in literature (see, e.g., the recent Gu and He interface (S.T. Gu, Q.C. He, J. Mech. Phys. Sol. **59**, 1413, 2011), which also degenerates to the high or low conducting models and it is able to take into account all the coupling among the electric, magnetic and elastic fields); here, we have proposed our schemes with the idea to find a compromise between the complexity and the possibility to analytically solve the problem for paradigmatic composite structures. The proposed models are dual from both the geometrical point of view, as shown by the T and Π lattice structures, and the physical point of view, as discussed below through the results for the composite materials.

We consider now a single circular (in 2D) or spherical (in 3D) particle with conductivity σ_2 embedded into a matrix with conductivity σ_1 (see Fig.2): we suppose that the interface between the constituents is described by Eqs.(3) and (4) (T-model) and we determine the effect of an arbitrary externally applied field. Since we are dealing with two isotropic phases, in order to solve the problem we can directly apply the original idea of Maxwell, which is based on the following steps. Firstly, we observe that the electrical potential must be an harmonic function both inside and outside the particle: therefore, it can be straightforwardly expanded in trigonometric series (in 2D) and in series of spherical harmonics (in 3D). Secondly, we can substitute such expansions in the interface conditions, by obtaining a set of equations for the unknown coefficients, completely describing the potential both inside and outside the inhomogeneity.

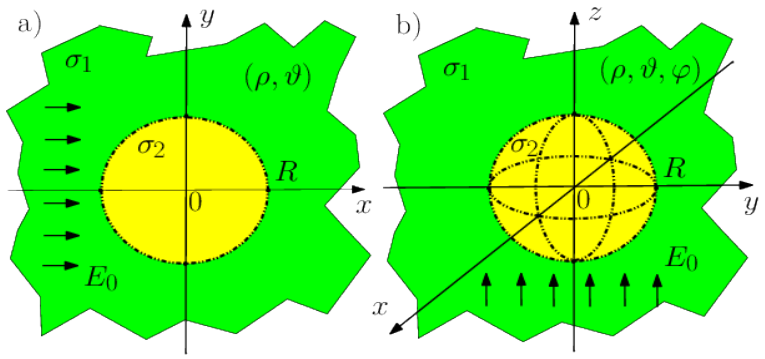

Figure 2: (Color online) Scheme of a single circular (a) or spherical (b) particle with conductivity σ_2 embedded into a matrix with conductivity σ_1. The interface between the two phases is described by either Eqs.(3) and (4) or Eqs.(5) and (6).

To accomplish this last step we must determine the surface Laplacian of the series expansions: to do this we remember that the trigonometric functions and the spherical harmonics are eigenfunctions of the ∇_S^2 operator with certain eigenvalues described in Appendix A. The complete procedure, which is valid for any externally applied field, is described in Appendix B for the 2D case and in Appendix C for the 3D case. Here, we are interested in the particular case with an uniform applied electric field E_0, corresponding to a potential $V_0 = -\rho \cos\vartheta E_0$ (see Fig.2). The perturbation induced by the inhomogeneity with imperfect contact has been eventually found as

$$for\ \rho < R \Rightarrow\ V = -\rho \cos\vartheta E_0 \left(\frac{d\sigma_1}{\mathsf{C}} \right), \tag{7}$$

$$for\ \rho > R \Rightarrow\ V = -\rho \cos\vartheta E_0 \left(1 + \frac{R^d}{\rho^d} \frac{\mathsf{B}}{\mathsf{C}} \right), \tag{8}$$

where $d = 2$ for the circle, $d = 3$ for the sphere and the parameters B and C are defined as follows

$$\mathsf{B} = \sigma_1 - \sigma_2 + \frac{r^+ + r^-}{R} \sigma_1 \sigma_2 - (d-1) \frac{g}{R} \left[1 - r^+ \frac{\sigma_1}{R} \right] \left[1 + r^- \frac{\sigma_2}{R} \right], \tag{9}$$

$$\mathsf{C} = (d-1)\sigma_1 + \sigma_2 + (d-1) \frac{r^+ + r^-}{R} \sigma_1 \sigma_2 + (d-1) \frac{g}{R} \left[1 + (d-1) r^+ \frac{\sigma_1}{R} \right] \left[1 + r^- \frac{\sigma_2}{R} \right]. \tag{10}$$

We can observe that the electric quantities both inside and outside the particle, in contrast to the case with perfect interfaces, depend on R. So, the previous result can be used for analysing the scale effects induced by the imperfect contact. From Eq.(7) it is easy to identify the induced internal field as $E_{int}/E_0 = d\sigma_1/\mathsf{C}$. A first scaling law for $R \to \infty$ can be obtained by introducing the classical Lorentz field for a particle with a perfect interface $E_{lor} = E_{int}|_{r^+ = r^- = 0, g = 0}$; we can easily prove that

$$\frac{E_{int}}{E_{lor}} - 1 = -\frac{(d-1)\sigma_1}{(d-1)\sigma_1 + \sigma_2}\frac{\ell^- + \ell^+ + \mathsf{L}}{R} + O\left(\frac{1}{R^2}\right), \tag{11}$$

where we have introduced the following intrinsic length scales

$$\ell^- = \sigma_2 r^-, \ell^+ = \sigma_2 r^+, \mathsf{L} = \frac{g}{\sigma_1}, \tag{12}$$

which automatically emerge from the analysis and completely control all the scaling laws. Eq.(11) means that the internal field approaches the Lorentz field for large radius of the particle, i.e. the effects of the contact imperfection are vanishingly small for $R \to \infty$.

We discuss now the scaling laws obtained for $R \to 0$. A long but straightforward analysis leads to

$$\frac{E_{int}}{E_0} = \frac{d\sigma_2}{(d-1)^2\sigma_1}\frac{R^3}{\ell^-\ell^+\mathsf{L}} + O\left(R^4\right), \tag{13}$$

$$\left.\frac{E_{int}}{E_0}\right|_{g=0} = \frac{d}{(d-1)}\frac{R}{\ell^- + \ell^+} + O\left(R^2\right), \tag{14}$$

$$\left.\frac{E_{int}}{E_0}\right|_{r^+=r^-=0} = \frac{d}{(d-1)}\frac{R}{\mathsf{L}} + O\left(R^2\right). \tag{15}$$

In any case the internal field converges to zero for very small particles. It is interesting to observe that the internal field for the T-model follows a scaling law with a power of three, while the low and high conductivity models follow a law with a scaling exponent equal to one. It can be seen in Fig.3 where $log_{10}(E_{int}/E_0)$ is represented versus $log_{10}R$. The blue curves (with squares) and the black ones (without symbols) describe the generic interface ($g \neq 0$, $r^+ \neq 0$, $r^- \neq 0$) and show a slope +3 for small R, which is in agreement with Eq.(13). On the other hand, green curves (with triangles) and red ones (with circles) correspond to the high and the low conductivity interface, respectively: they all exhibit a slope +1 for small R as predicted by Eqs.(14) and (15). We also note that all curves in Fig.3 converge to the Lorentz field for $R \to \infty$, as described by Eq.(11).

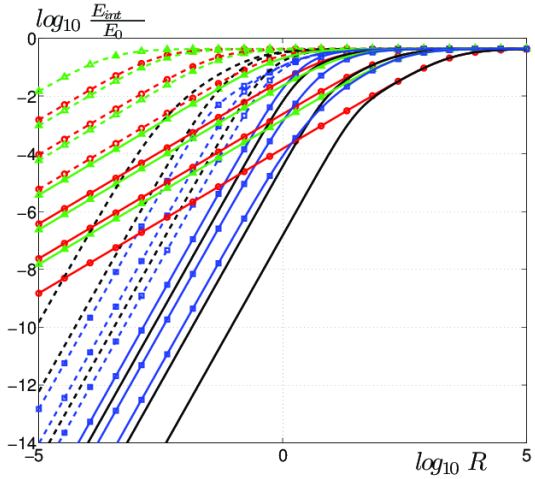

Figure 3: (Color online) Plot of $log_{10}(E_{int}/E_0)$ versus $log_{10}R$ for the T-model. Green curves with triangles: high conductivity model with a varying g in $\Omega = \{0.001, 0.016, 0.25, 4, 64, 1000\}$. Red curves with circles: low conductivity model with a varying $r^+ = r^-$ in Ω. Blue curves with squares: general model with $r^+ = r^- = 1$ and g varying in Ω. Black curves without symbols: general model with $g = 1$ and $r^+ = r^-$ varying in Ω. Everywhere, the dashed lines correspond to the values < 1 of the varying quantity. Parameters adopted in a.u.: $\sigma_1 = 1$, $\sigma_2 = 5$, $d = 3$, $c = 0.3$.

Now, we take into consideration the Π-model described by Eqs.(5) and (6). The perturbation to the electric potential generated by the inhomogeneity is described again by Eqs.(7) and (8) but with new coefficients B and C given below

$$\mathsf{B} = \sigma_1 - \sigma_2 + \frac{r}{R}\sigma_1\sigma_2 - (d-1)^2\frac{g^- g^+ r}{R^3} - \frac{(d-1)}{R}\left\{ g^-\left[1 - r\frac{\sigma_1}{R}\right] + g^+\left[1 + r\frac{\sigma_2}{R}\right]\right\}, \tag{16}$$

$$\mathsf{C} = (d-1)\sigma_1 + \sigma_2 + (d-1)\frac{r}{R}\sigma_1\sigma_2 + (d-1)^2\frac{g^- g^+ r}{R^3} + \frac{(d-1)}{R}\left\{ g^-\left[1 + (d-1)r\frac{\sigma_1}{R}\right] + g^+\left[1 + r\frac{\sigma_2}{R}\right]\right\}. \tag{17}$$

With regards to the scaling law for $R \to \infty$, it is possible to prove that Eq.(11) must be substituted with

$$\frac{E_{int}}{E_{lor}} - 1 = -\frac{(d-1)\sigma_1}{(d-1)\sigma_1 + \sigma_2}\frac{\ell + \mathsf{L}^+ + \mathsf{L}^-}{R} + O\left(\frac{1}{R^2}\right), \tag{18}$$

where we have introduced the dual intrinsic length scales

$$\ell = \sigma_2 r, \mathsf{L}^+ = \frac{g^+}{\sigma_1}, \mathsf{L}^- = \frac{g^-}{\sigma_1}. \tag{19}$$

As expected, also in this case the internal field approaches the Lorentz field for large radius of the particle. On the other hand, for $R \to 0$, Eqs.(13)-(15) become as follows

$$\frac{E_{int}}{E_0} = \frac{d\sigma_2}{(d-1)^2\sigma_1}\frac{R^3}{\ell\mathsf{L}^+\mathsf{L}^-} + O\left(R^4\right), \tag{20}$$

$$\left.\frac{E_{int}}{E_0}\right|_{g^+ = g^- = 0} = \frac{d}{(d-1)}\frac{R}{\ell} + O\left(R^2\right), \tag{21}$$

$$\left.\frac{E_{int}}{E_0}\right|_{r=0} = \frac{d}{(d-1)}\frac{R}{\mathsf{L}^+ + \mathsf{L}^-} + O\left(R^2\right). \tag{22}$$

As before, the internal field converges to zero for very small particles (with different scaling exponents, as above described).

To analyse the effects of imperfect interfaces on a composite material we consider a dispersion of cylindrical or spherical particles of conductivity σ_2 in a matrix with conductivity σ_1. When the interfaces are described by Eqs. (3) and (4) (T-model) we can generalize the Maxwell approach or, equivalently, the Mori-Tanaka scheme by obtaining the following effective conductivity for a composite with a volume fraction c of the dispersed particles

$$\frac{\sigma_{eff}}{\sigma_1} = \frac{1}{1 + \dfrac{cd\mathsf{B}}{(1-c)\mathsf{C} + c[\mathsf{C} - (d-1)\mathsf{B}]}}, \tag{23}$$

where B and C are given in Eqs.(9) and (10). For interfaces described by the low conductivity model we obtain $\sigma_{low} = \sigma_{eff}\big|_{g=0}$, which is in perfect agreement with recent investigations; on the other hand, when the high conductivity model is accounted for we have $\sigma_{high} = \sigma_{eff}\big|_{r^+ = r^- = 0}$, which corresponds to some known results. Moreover, when we consider a perfect contact between the constituents we obtain the celebrated Maxwell formula

$$\frac{\sigma_{max}}{\sigma_1} = \frac{1}{1 + \dfrac{dc(\sigma_1 - \sigma_2)}{(1-c)[(d-1)\sigma_1 + \sigma_2] + cd\sigma_2}}. \tag{24}$$

The first important scaling law concerns the situation with a large radius of the particles: in this case, as above said, the size effects disappear and the effective conductivity converges to the Maxwell one as follows

$$\frac{\sigma_{eff}}{\sigma_{max}} - 1 = \frac{cd^2\sigma_1^2}{\mathsf{G}}\frac{\mathsf{H}}{R} + O\left(\frac{1}{R^2}\right), \tag{25}$$

where we have defined

$$\mathsf{H} = (d-1)\mathsf{L} - \frac{\sigma_2}{\sigma_1}(\ell^+ + \ell^-), \tag{26}$$

$$\mathsf{G} = \left[(d+c-1)\sigma_1 + (1-c)\sigma_2\right] \times \left[(d-1)(1-c)\sigma_1 + (cd-c+1)\sigma_2\right]. \tag{27}$$

The parameter H represents the overall length scale of this process and it is a linear combination of the terms defined in Eq.(12). This result can be simply compared with recent achievements concerning the cases with low and high conductivity interfaces. Indeed, we find a perfect agreement if $\ell^+ = \ell^- = 0$ or $\mathsf{L} = 0$.

Other interesting scaling laws can be found for $R \to 0$. To analyse this case we define the conductivity σ_0, which represents a Maxwell dispersion with $\sigma_2 \to 0$ (dispersion of voids), and the conductivity σ_∞, which characterizes a Maxwell dispersion with $\sigma_2 \to \infty$ (dispersion of superconducting particles):

$$\frac{\sigma_0}{\sigma_1} = \frac{(1-c)(d-1)}{d+c-1}; \frac{\sigma_\infty}{\sigma_1} = \frac{1-c+cd}{1-c}. \tag{28}$$

First of all we observe that if $r^+ \neq 0$ we have $\sigma_{eff} \to \sigma_0$ with the scaling law

$$\frac{\sigma_{eff}}{\sigma_0} - 1 = \frac{cd^2\sigma_2}{(d-1)(1-c)(d-1+c)\sigma_1}\frac{R}{\ell^+} + O\left(R^2\right).$$

Similarly, if $r^- \neq 0$ with $r^+ = 0$ and $g = 0$ we obtain $\sigma_{eff} \to \sigma_0$ with the scaling law

$$\frac{\sigma_{eff}}{\sigma_0} - 1 = \frac{cd^2\sigma_2}{(d-1)(1-c)(d-1+c)\sigma_1}\frac{R}{\ell^-} + O\left(R^2\right).$$

So, for the general T-model and for the low conducting interface we have $\sigma_{eff} \to \sigma_0$ (when $R \to 0$) with a scaling exponent equals to one. On the other hand, for $g \neq 0$ and $r^+ = 0$ we prove the convergence $\sigma_{eff} \to \sigma_\infty$ with a scaling law

$$\frac{\sigma_{eff}}{\sigma_\infty} - 1 = -\frac{cd^2}{(d-1)(1-c)(cd-c+1)}\frac{R}{\mathsf{L}} + O\left(R^2\right).$$

It means that the high conductivity model leads to $\sigma_{eff} \to \sigma_\infty$ for $R \to 0$.

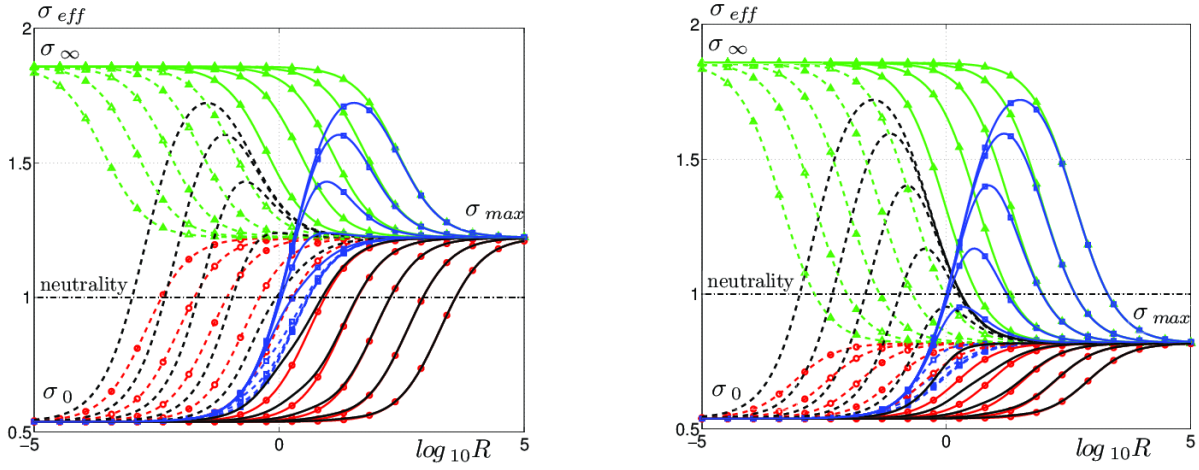

Figure 4: (Color online) Plot of σ_{eff} versus $\log_{10}R$ for the T-model. We adopted the following parameters (in a.u.): $\sigma_1 = 1$, $\sigma_2 = 2$ (left) and $\sigma_1 = 1$, $\sigma_2 = 1/2$ (right). Everywhere we used $d = 2$, $c = 0.3$. Green curves with triangles: high conductivity model ($r^+ = r^- = 0$) with a varying g in $\Omega = \left\{10^{-3+2(j-1)/3}, j = 1...10\right\}$. Red curves with circles: low conductivity model ($g = 0$) with a varying $r^+ = r^-$ in Ω. Blue curves with squares: T-model with $r^+ = r^- = 1$ and g varying in Ω. Black curves without symbols: T-model with $g = 1$ and $r^+ = r^-$ varying in Ω. Everywhere, the dashed lines correspond to values < 1 of the varying quantity.

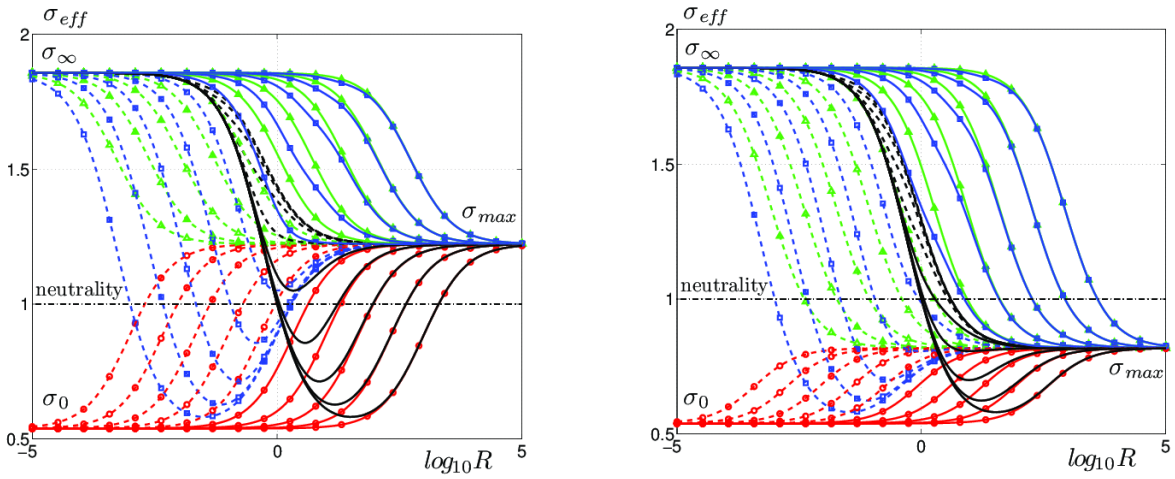

Figure 5: (Color online) Plot of σ_{eff} *versus* $log_{10}R$ *for the* Π *-model. We adopted the following parameters (in a.u.):* $\sigma_1 = 1$, $\sigma_2 = 2$ *(left) and* $\sigma_1 = 1$, $\sigma_2 = 1/2$ *(right). Everywhere we used* $d = 2$, $c = 0.3$. *Green curves with triangles: high conductivity model (*$r = 0$*) with a varying* $g^- = g^+$ *in* $\Omega = \{10^{-3+2(j-1)/3}, j = 1...10\}$. *Red curves with circles: low conductivity model (*$g^+ = g^- = 0$*) with a varying* r *in* Ω. *Blue curves with squares:* Π *-model with* $r = 1$ *and* $g^+ = g^-$ *varying in* Ω. *Black curves without symbols:* Π *-model with* $g^+ = g^- = 1$ *and* r *varying in* Ω. *Everywhere, the dashed lines correspond to values* < 1 *of the varying quantity.*

This complex scenario is summarized in Fig.4 where σ_{eff} is shown versus $log_{10}R$. Even at constant volume fraction c, significant size effects on the effective conductivity are evident for a variable radius R. In Fig.2 (left) we have reported the results for $\sigma_2/\sigma_1 = 2$ and in Fig.2 (right) for $\sigma_2/\sigma_1 = 0.5$. In both cases we have shown the neutrality axis at which the effective conductivity σ_{eff} equals the matrix conductivity σ_1, making the inclusions effectively hidden. We can observe that σ_{eff} is a monotonically decreasing function of R (from σ_∞ to σ_{max}) for the high conductivity model (green curves with triangles), while it is a monotonically increasing function of R (from σ_0 to σ_{max}) for the low conductivity model (red lines with circles). So, the neutrality condition ($\mathsf{B} = 0$) can be satisfied by the low conductivity model for $\sigma_2 > \sigma_1$ ($\sigma_2 - \sigma_1 = r\sigma_1\sigma_2/R$, see Fig.4, left) and by the high conductivity model for $\sigma_2 < \sigma_1$ ($\sigma_1 - \sigma_2 = g(d-1)/R$, see Fig.4, right). On the other hand, the blue and black lines concern the case of the general T-model and they exhibit a non monotone behavior starting from σ_0 and arriving at σ_{max}. It is interesting to note that, with the general T-model, it is possible to satisfy the neutrality condition for both the cases $\sigma_2 > \sigma_1$ and $\sigma_2 < \sigma_1$. The condition leading to neutrality in this case (T-model) is

$$g = \frac{\sigma_1 - \sigma_2 + \dfrac{r^+ + r^-}{R}\sigma_1\sigma_2}{(d-1)\dfrac{1}{R}\left[1 - r^+\dfrac{\sigma_1}{R}\right]\left[1 + r^-\dfrac{\sigma_2}{R}\right]}, \tag{29}$$

which is represented in Fig.4 by the intersections of blue and black curves with the neutrality axis.
As for the dual Π -model, we can affirm that the generalized Maxwell theory given in Eq.(23) is still valid but the coefficients B and C must be taken from Eqs.(16) and (17), respectively. For a large radius of the particle we have the scaling law identical to Eq.(25) where G is given by Eq.(27) and H by the following expression

$$\mathsf{H} = (d-1)(\mathsf{L}^+ + \mathsf{L}^-) - \frac{\sigma_2}{\sigma_1}\ell. \tag{30}$$

It represents the overall length scale of the Π -model and it is indeed a linear combination of the terms defined in

Eq.(19). We also report the scaling laws for $R \to 0$. If $g^+ \neq 0$ we have that $\sigma_{eff} \to \sigma_\infty$ with the scaling law

$$\frac{\sigma_{eff}}{\sigma_\infty} - 1 = - \frac{cd^2}{(d-1)(1-c)(cd-c+1)} \frac{R}{L^+} + O\left(R^2\right).$$

Similarly, if $g^- \neq 0$ with $r = 0$ and $g^+ = 0$ we obtain $\sigma_{eff} \to \sigma_\infty$ with the scaling law

$$\frac{\sigma_{eff}}{\sigma_\infty} - 1 = - \frac{cd^2}{(d-1)(1-c)(cd-c+1)} \frac{R}{L^-} + O\left(R^2\right).$$

So, for the general Π-model and for the high conducting interface we have $\sigma_{eff} \to \sigma_\infty$ (when $R \to 0$) with a scaling exponent equals to one. On the other hand, for $r \neq 0$ and $g^+ = 0$ we prove the convergence $\sigma_{eff} \to \sigma_0$ with a scaling law

$$\frac{\sigma_{eff}}{\sigma_0} - 1 = \frac{cd^2\sigma_2}{(d-1)(1-c)(d-1+c)\sigma_1} \frac{R}{\ell} + O\left(R^2\right).$$

It means that, as expected, the low conductivity model leads to $\sigma_{eff} \to \sigma_0$ for $R \to 0$.

In Fig.5 the results for the Π-model are shown: the effective conductivity is represented versus the radius R of the particles. In Fig.5 (left) we have the case with $\sigma_2/\sigma_1 = 2$ and in Fig.5 (right) we show the results for $\sigma_2/\sigma_1 = 0.5$. All previous scaling laws are confirmed and clearly indicated. By drawing a comparison between Fig.4 and Fig.5 we can point out the dual character of the proposed models: the T-model behaves similarly to the low conducting interface with regards to the limiting cases $R \to 0$ and $R \to \infty$ but it shows a specific additional upwards peak describing the competition of the scale effects with the presence of the tangential conductances g. Conversely, the Π-model behaves similarly to the high conducting interface with regards to the limiting cases $R \to 0$ and $R \to \infty$ but it shows a specific additional downwards peak describing the competition of the scale effects with the presence of the normal resistances r. As before, also in the case of the Π-model, we can satisfy the neutrality condition for both the contrast situations $\sigma_2/\sigma_1 > 1$ and $\sigma_2/\sigma_1 < 1$. The condition leading to neutrality in this case (Π-model) is

$$r = \frac{\sigma_1 - \sigma_2 - \dfrac{g^+ + g^-}{R}(d-1)}{(d-1)^2 \dfrac{g^+ + g^-}{R^3} - \dfrac{d-1}{R^2}(g^-\sigma_1 - g^+\sigma_2) - \dfrac{\sigma_1\sigma_2}{R}}, \tag{31}$$

and it is satisfied in Fig.5 at the intersection points between the blue or blacks curves and the neutrality axis.

By means of this analysis we can assert that the T and Π models exhibit an interesting complex behavior which is able to reproduce many properties of real interfaces appearing in different nano-systems. As an example we can compare our results with those recently obtained for a dispersion of SiC particles (with radius between 5 and 15Å) in a polymeric (epoxy) matrix (S. Yu, S. Yang, and M. Cho, J. Appl. Phys. **110**, 124302, 2011). By means of a multiscale combination of the non-equilibrium molecular dynamics and a micromechanics bridging model, the thermal conductivity has been studied in terms of the particles radius. The result is in perfect qualitative agreement with our T-model and a maximum value of the conductivity was obtained for a given radius. To obtain such a result the Kapitza resistance and a specific interphase describing the bonding of the polymers to the monocrystalline SiC particles have been considered. Our T-model is able to describe the overall response of the structured/multilayered interface through the simple conditions given in Eqs.(3) and (4) imposing the jumps of the physical fields over the zero-thickness interface. Therefore, the proposed models perfectly implement the multiscale paradigm by introducing the effective properties of a given interface behavior.

We have taken into consideration the possible scale effects induced by imperfect interfaces between the constituents of an heterogeneous system. To this aim we introduced two generalised schemes, namely the T and Π structures, which can be seen as natural combinations of the so-called low and high conducting interface models. One important property discussed concerns the uniformity of the physical fields in circular or spherical particles with T or Π imperfect interfaces. This point extends well known theorems proving the uniformity in different conditions and opens the possibility to study the behavior of new interfaces in anisotropic, elliptic and ellipsoidal particles, which are standard problems in the theory of inhomogeneities. The results for a single inclusion were applied to the analysis of the effective properties of dispersions. In particular we studied the scale effects and we found interesting behaviors, which generalize those observed with low and high conductivity interfaces. We indeed

observed a specific peak of the effective conductivity in correspondence to a critical radius of the dispersed particles: it corresponds to the competition between the tendency to attain the Maxwell conductivity limit for a large radius and the conduction properties of the interface, which tend to increase or decrease the overall conductivity, depending on the specific parameters. This is exactly the trend observed in recent analysis of imperfect interfaces in nanocomposites (hard particles in polymeric matrix or similar mixtures). To conclude, we have analysed the neutrality properties of the T and Π models: contrarily to the low and high conducting interface, we have proved that it is possible to satisfy the neutrality condition for any contrast σ_2/σ_1 between the conductivities of the involved phases. So, Eqs.(29) and (31) are the updated versions of the neutrality criteria, representing the generalizations of some findings, published in recent literature. We remark that all the achievements of the present paper can be also used in dynamic regime if we consider a wavelength λ of the propagating waves that is much larger than the radius R of the particles. In this case we are working in the so-called quasi-static regime and any inhomogeneity feels a nearly static applied field.

Appendix:

A: The surface Laplacian

The surface Laplacian operator is defined as

$$\nabla_S^2 f = \frac{1}{\sqrt{g}} \frac{\partial}{\partial \alpha_i} \left\{ \sqrt{g} g^{ij} \frac{\partial f}{\partial \alpha_j} \right\}, \tag{32}$$

where g_{ij} are the components of the metric tensor (the first fundamental form) of the Riemannian manifold (the surface) $\vec{r} = \vec{r}(\alpha_1, \alpha_2)$. It means that $g_{ij} = \frac{\partial \vec{r}}{\partial \alpha_i} \cdot \frac{\partial \vec{r}}{\partial \alpha_j}$ and the dual components g^{ij} are obtained by inverting the matrix g_{ij}. The quantity g is the determinant of g_{ij}. Typically, in differential geometry of two-dimensional surfaces we adopt the symbols $g_{11} = E$, $g_{12} = g_{21} = F$ and $g_{22} = G$; so, for an orthogonal system of coordinate lines $F = 0$ and Eq.(32) reduces to

$$\nabla_S^2 f = \frac{1}{\sqrt{EG}} \left\{ \frac{\partial}{\partial \alpha_1} \left[\sqrt{\frac{G}{E}} \frac{\partial f}{\partial \alpha_1} \right] + \frac{\partial}{\partial \alpha_2} \left[\sqrt{\frac{E}{G}} \frac{\partial f}{\partial \alpha_2} \right] \right\}. \tag{33}$$

For a planar circle $\vec{r} = (R\cos\vartheta\ ,\ R\sin\vartheta)$ we simply have

$$\nabla_S^2 f = \frac{\partial^2 f}{\partial s^2} = \frac{1}{R^2} \frac{\partial^2 f}{\partial \vartheta^2}, \tag{34}$$

and the following property is evident

$$\nabla_S^2 e^{in\vartheta} = -\frac{1}{R^2} n^2 e^{in\vartheta}. \tag{35}$$

It means that the trigonometric functions $\cos n\vartheta$ and $\sin n\vartheta$ are eigenfunctions of the Laplacian operator with eigenvalues $-\frac{1}{R^2} n^2$.

For a spherical surface $\vec{r} = (R\cos\varphi\ \sin\vartheta\ ,\ R\sin\varphi\ \sin\vartheta\ ,\ R\cos\vartheta)$ it is possible to obtain

$$\nabla_S^2 f = \frac{1}{R^2} \left\{ \frac{1}{\sin\vartheta} \frac{\partial}{\partial \vartheta} \left[\sin\vartheta \frac{\partial f}{\partial \vartheta} \right] + \frac{1}{\sin^2\vartheta} \frac{\partial^2 f}{\partial \varphi^2} \right\}, \tag{36}$$

and we can prove that

$$\nabla_S^2 Y_{nm}(\vartheta, \varphi) = -\frac{1}{R^2} n(n+1) Y_{nm}(\vartheta, \varphi). \tag{37}$$

It means that the spherical harmonics $Y_{nm}(\vartheta, \varphi)$ are eigenfunctions of the surface Laplacian operator with eigenvalues $-\frac{1}{R^2} n(n+1)$. They are defined (for $n \geq 0$, $-n \leq m \leq n$) as

$$Y_{nm}(\vartheta,\varphi)=\sqrt{\frac{2n+1}{4\pi}\frac{(n-m)!}{(n+m)!}}P_n^m(\cos\vartheta)e^{im\varphi}, \tag{38}$$

where $P_n^m(\xi)$ are the associated Legendre polynomials

$$P_n^m(\xi)=(-1)^m\left(1-\xi^2\right)^{\frac{m}{2}}\frac{1}{2^n n!}\frac{d^{n+m}}{d\xi^{n+m}}\left(\xi^2-1\right)^n. \tag{39}$$

B: Two-dimensional geometry: the circle

We suppose to consider a circular inhomogeneity of radius R (conductivity σ_2) in the plane (x,y) with conductivity σ_1. We consider an arbitrary applied (or pre-existing) potential $V_0(x,y)$ and we search for the perturbation induced by the inhomogeneity. Since the electric potential must be harmonic both inside and outside the interface, we have

$$V=V_0+\sum_{n=0}^{+\infty}\rho^n\left(A_n\cos n\vartheta+B_n\sin n\vartheta\right),\rho<R, \tag{40}$$
$$V=V_0+\sum_{n=0}^{+\infty}\rho^{-n}\left(\widetilde{A}_n\cos n\vartheta+\widetilde{B}_n\sin n\vartheta\right),\rho>R,$$

where (ρ,ϑ) are the standard polar coordinates. The potential V_0 and its derivatives $\frac{\partial V_0}{\partial\rho}$ can be expanded in Fourier series for $\rho=R$

$$V_0(R,\vartheta)=\sum_{n=0}^{+\infty}\left(C_n\cos n\vartheta+D_n\sin n\vartheta\right), \tag{41}$$
$$\frac{\partial V_0}{\partial\rho}(R,\vartheta)=\sum_{n=0}^{+\infty}\left(F_n\cos n\vartheta+G_n\sin n\vartheta\right).$$

By substituting Eq.(40) in the anisotropic interface model (Eqs.(3) and (4)) and by using Eqs.(35) and (41), we obtain a set of equations for A_n and $\widetilde{A}_n$

$$R^{-n}\widetilde{A}_n-R^nA_n=r^+\sigma_1\left(F_n-nR^{-n-1}\widetilde{A}_n\right)$$
$$+r^-\sigma_2\left(F_n+nR^{n-1}A_n\right), \tag{42}$$
$$\sigma_2\left(F_n+nR^{n-1}A_n\right)-\sigma_1\left(F_n-nR^{-n-1}\widetilde{A}_n\right)$$
$$=gr^+\sigma_1R^{-2}n^2\left(F_n-nR^{-n-1}\widetilde{A}_n\right)$$
$$-gR^{-2}n^2\left(C_n+R^{-n}\widetilde{A}_n\right), \tag{43}$$

and a similar one for the unknowns B_n and $\widetilde{B}_n$, not reported here for brevity. These systems can be easily solved obtaining the electrical potential in the whole plane. In the particular case of a uniform applied field $V_0=-xE_0=-\rho\cos\vartheta E_0$ only the coefficients A_1 and $\widetilde{A}_1$ are different from zero and we obtain Eqs.(7) and (8) for $d=2$. A similar procedure (not reported here for brevity) can be followed to analyse the properties of the Π-model described by Eqs.(5) and (6).

C: Three-dimensional geometry: the sphere

We consider now a spherical inhomogeneity of radius R (conductivity σ_2) in a matrix with conductivity σ_1. As before, we assume an arbitrary applied potential $V_0(x,y,z)$ and we study the effects of the embedded particle. The final electric potential can be expanded as follows

$$V=V_0+\sum_{n=0}^{+\infty}\sum_{m=-n}^{+n}B_{nm}\rho^nY_{nm}(\vartheta,\varphi),\rho<R, \tag{44}$$
$$V=V_0+\sum_{n=0}^{+\infty}\sum_{m=-n}^{+n}C_{nm}\rho^{-n-1}Y_{nm}(\vartheta,\varphi),\rho>R,$$

where we have introduced the spherical coordinates $(\rho, \vartheta, \varphi)$. The potential V_0 and its derivatives $\frac{\partial V_0}{\partial \rho}$ can be expanded in a series of spherical harmonics for $\rho = R$

$$V_0(R,\vartheta,\varphi) = \sum_{n=0}^{+\infty} \sum_{m=-n}^{+n} \beta_{nm} Y_{nm}(\vartheta,\varphi), \tag{45}$$

$$\frac{\partial V_0}{\partial \rho}(R,\vartheta,\varphi) = \sum_{n=0}^{+\infty} \sum_{m=-n}^{+n} \alpha_{nm} Y_{nm}(\vartheta,\varphi).$$

By substituting Eq.(44) in the anisotropic interface model (Eqs.(3) and (4)) and by using Eqs.(37) and (45), we obtain a set of equations for B_{nm} and C_{nm}

$$\begin{aligned} & R^{-n-1} C_{nm} - R^n B_{nm} \\ & = r^+ \sigma_1 \left[\alpha_{nm} - (n+1) R^{-n-2} C_{nm}\right] \\ & + r^- \sigma_2 \left[\alpha_{nm} + n R^{n-1} B_{nm}\right], \end{aligned} \tag{46}$$

$$\begin{aligned} & \sigma_2 \left[\alpha_{nm} + n R^{n-1} B_{nm}\right] \\ & - \sigma_1 \left[\alpha_{nm} - (n+1) R^{-n-2} C_{nm}\right] \\ & = g r^+ \sigma_1 R^{-2} n(n+1) \left[\alpha_{nm} - (n+1) R^{-n-2} C_{nm}\right] \\ & - g R^{-2} n(n+1) \left[\beta_{nm} + R^{-n-1} C_{nm}\right]. \end{aligned} \tag{47}$$

It is now possible to find B_{nm} and C_{nm} obtaining the electrical potential in the whole space. In the particular case of a uniform applied field $V_0 = -zE_0 = -\rho \cos\vartheta E_0$ only the coefficients B_{10} and C_{10} are different from zero and we obtain Eqs.(7) and (8) for $d = 3$. We remark that a similar procedure can be followed for studying the dual interface described by Eqs.(5) and (6).

2.1.10.Degradation of transport properties in multi-cracked materials

(*S. Giordano and P.L. Palla, Conduction degradation in anisotropic multi-cracked materials, Eur. Phys. J. B (2012) 85: 59*)

Recently, it has been observed that the macroscopic degradation of materials with a large number of cracks is governed by different laws depending on the orientational statistical distribution of the cracks within the host matrix. More precisely, two different specific decays of the effective elastic constants have been observed for dispersions of uniformly random oriented cracks and parallel cracks. As a matter of fact, there are indications that a uniformly random oriented population of cracks leads to an exponential degradation of the elastic response in terms of the crack density while a population of parallel cracks leads to a power-law decay of the effective response. This scenario clearly indicates the need for a more detailed understanding of the degradation behaviour of multi-cracked materials. In fact, a model of general validity which explain the degradation behaviour versus the orientational distribution of cracks is not available in literature. We analysed the conduction properties of a multicracked material with an arbitrary statistical orientation of defects (ranging from parallel to random distributions). Our approach is based on a two-step procedure: firstly, we obtain an exact result describing the electric field behaviour within an elliptic inhomogeneity embedded in an anisotropic two-dimensional conductor. Basically, the solution for the inhomogeneity has been obtained by the so-called equivalence principle which is formulated by an inclusion scheme described by a suitable eigenfield. The important point of the present development lies in the combination of the anisotropy and the two-dimensionality of the system, which allow us to obtain a new closed form expression for the polarisation tensor of the particle. The elliptic geometry allows us to use such a result to model a crack: if one of the principal axes of the ellipse becomes negligibly small, then the ellipse reduces to a thin crack. In Fig. 1 one can find the scheme of an elliptic inhomogeneity with conductivity tensor different from that of the matrix. We suppose to apply a uniform electric field to the structure and we can determine the internal field distribution. We then prove that the internal field is always uniform and we explicitly obtain the solution. To conclude, the combination of equations shown in Fig. 1 solves the problem of determining the electric field inside the inhomogeneity in term of the remotely applied field.

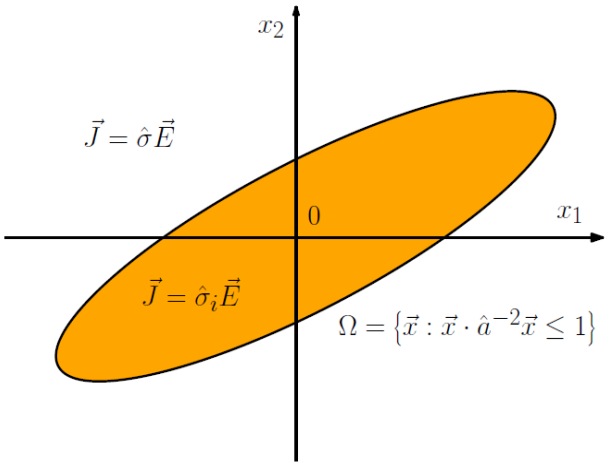

$$\boldsymbol{E}_{tot} = \left[\hat{I} - \hat{\mathcal{S}}\left(\hat{I} - \hat{\sigma}^{-1}\hat{\sigma}_i\right)\right]^{-1} \boldsymbol{E}^{\infty}$$

$$\hat{\mathcal{S}} = \frac{\hat{a}^{-2}\hat{\sigma} + \hat{I}\sqrt{\det\left(\hat{a}^{-2}\hat{\sigma}\right)}}{\mathrm{tr}\left(\hat{a}^{-2}\hat{\sigma}\right) + 2\sqrt{\det\left(\hat{a}^{-2}\hat{\sigma}\right)}}$$

Fig. 1. Schematic representation of the matrix/inhomogeneity system defined by the different conductivity tensors outside and inside the ellipse defined by the tensor a. The results on the right represent the relation between the externally applied and the intern electric field and the explicit expression for the corresponding Eshelby tensor.

As second step, we adopt an *ad hoc* iterative technique considering an increasing number of cracks, leading to a specific system of nonlinear differential equations for the effective conductivities of a multi-cracked material. By combining the anisotropic character of the system with the iterative scheme, we confirm the two different degradation behaviours of the effective conductivity for parallel and random geometries, already observed in literature. Interestingly enough, we have obtained the complete description of the system for all the orientational distribution comprised between the two above limiting cases: in other words, we have obtained an unified formalism ranging from the power law decay to the exponential law decay.

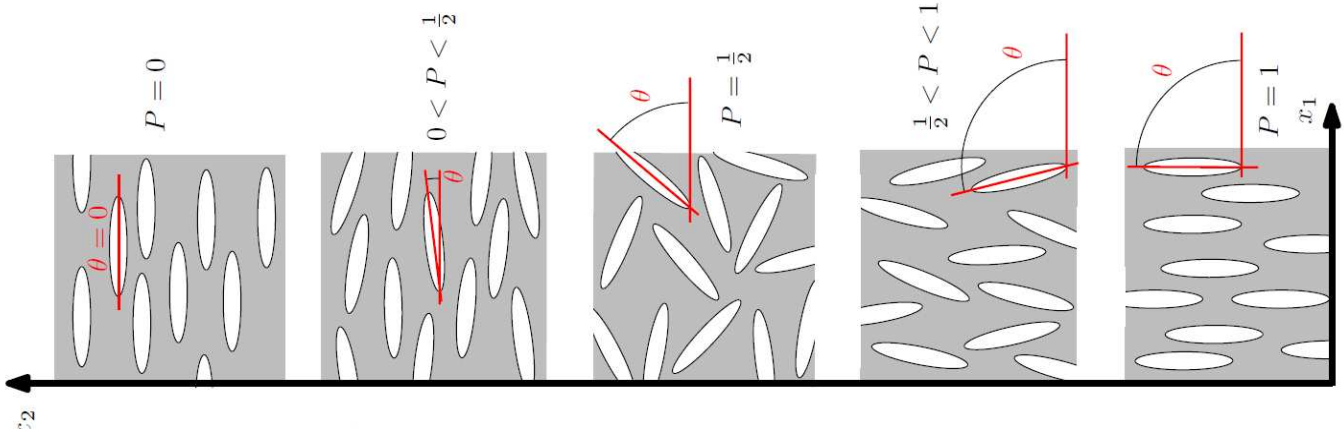

Fig. 6. Schematic representation of several dispersions of cracks in the anisotropic conductor with given conductivity. Each sample is characterized by a different order parameter P, corresponding to a particular orientational distribution of cracks.

We consider a region *S* containing *N* voids (i.e. cracks) with the major half-axis equal to *a*. These defects are oriented in the plane with an order parameter *P* defined in Fig.2. The results presented in Fig.1 are very useful to exploit the iterated homogenization method, that allows us to generalize the results to very large crack density values. It is important to remark that the application of the iterative or differential technique to the multi-cracked conductor is possible only through the knowledge of the exact response of one single defect in an anisotropic environment; in fact, when a given crack is added to a given existing distribution of cracks, it feels an anisotropic environment generated by the not uniform (for example parallel cracks or crack nearly aligned in a given direction) random orientation of the cracks themselves. It happens even if the original not cracked material is perfectly isotropic. If the matrix conductivity tensor is σ = diag(σ_{10}, σ_{20}) then the effective conductivity tensor will be of the similar form σ_{eff} = diag(σ_1, σ_2). The final expressions can be eventually written as

$$\sigma_1 = \sigma_{10} \frac{4 \frac{1-P}{\left(1+\frac{\sigma_{10}}{\sigma_{20}}\right)P-1} \frac{\sqrt{\frac{\sigma_{10}}{\sigma_{20}}}-\sqrt{\frac{1-P}{P}}}{\sqrt{\frac{\sigma_{10}}{\sigma_{20}}}+\sqrt{\frac{1-P}{P}}} e^{-\pi a^2 \frac{N}{S}\sqrt{P(1-P)}}}{\left[1-\frac{\sqrt{\frac{\sigma_{10}}{\sigma_{20}}}-\sqrt{\frac{1-P}{P}}}{\sqrt{\frac{\sigma_{10}}{\sigma_{20}}}+\sqrt{\frac{1-P}{P}}} e^{-\pi a^2 \frac{N}{S}\sqrt{P(1-P)}}\right]^2} \tag{1}$$

$$\sigma_2 = \sigma_{20} \frac{4 \frac{P}{\frac{\sigma_{20}}{\sigma_{10}}-P\left(1+\frac{\sigma_{20}}{\sigma_{10}}\right)} \frac{\sqrt{\frac{\sigma_{20}}{\sigma_{10}}}-\sqrt{\frac{P}{1-P}}}{\sqrt{\frac{\sigma_{20}}{\sigma_{10}}}+\sqrt{\frac{P}{1-P}}} e^{-\pi a^2 \frac{N}{S}\sqrt{P(1-P)}}}{\left[1-\frac{\sqrt{\frac{\sigma_{20}}{\sigma_{10}}}-\sqrt{\frac{P}{1-P}}}{\sqrt{\frac{\sigma_{20}}{\sigma_{10}}}+\sqrt{\frac{P}{1-P}}} e^{-\pi a^2 \frac{N}{S}\sqrt{P(1-P)}}\right]^2} \tag{2}$$

By means of these complete solutions it is possible to obtain the behaviour of several limiting cases. In particular, we observe that the degradation of the conductivity with a parallel dispersion of cracks (in the direction orthogonal to the cracks) follows a power law of the form $\log \sigma_{1,2} \sim -\log N$ or, equivalently, $\sigma_{1,2} \sim 1/N^2$. On other hand, the disordered case leads to the exponential law $\log \sigma_{1,2} \sim -N$ or, equivalently, $\sigma_{1,2} \sim \exp(-N/N_0)$, with a given N_0. We have indeed proved that the model is able to explain the degradation process of a multi-cracked material for different orientational distribution of the cracks within the host matrix. In particular it predicts an exponential law for randomly oriented cracks and a power law for parallel cracks, as observed in recent literature.

2.1.11.Nonlinear homogenization of heterogeneous structures

(*Stefano Giordano, Analytical procedure for determining the linear and nonlinear effective properties of the elastic composite cylinder, International Journal of Solids and Structures 50, 4055-4069, 2013*)

In this section we take into consideration a specific structure with two different nonlinear phases: a cylinder composed of a nonlinear core (or inhomogeneity) embedded into a nonlinear shell (or matrix). We introduce a homogenization technique for the linear elastic moduli (second order elastic constants) and for the nonlinar elastic moduli, which are called Landau coefficients (third order elastic constants). The proposed procedure is based on two main steps: firstly, we develop a nonlinear perturbation method which is able to turn the initial nonlinear elastic problem into a couple of linear problems, which are simpler and analytically solvable. Then, we are able to prove that only the solution of the first linear problem is needed for determining the linear and nonlinear effective properties of the heterogeneous structure. The second step consists in the exact solution of such a linear problem (within the two-dimensional elasticity) by means of the the Kolossov-Muskhelishvili elastic potentials (Muskhelishvili, N. I., 1953. Some basic problems in the mathematical theory of elasticity. Noordhoff, Groningen, Holland). As final result we obtain the exact closed forms for the linear and nonlinear effective elastic moduli, which are valid for any volume fraction of the core embedded in the external shell.

Analytical results for coated fibers and composite cylinders are important for several applications in material science. In spite of the development of refined techniques for analysing the linear properties of composite cylinders and fibrous structures, many applications to real materials need to deal with nonlinear features and their mixing laws. For example, multi-shell nanowires are candidates for future electronic and photonic devices. Indeed, electronic confinement in two and three dimensions have been realized through quantum wires and quantum dots, respectively (Johnson, H.T., Freund, L.B., 2001. The influence of strain on confined electronic states in semiconductor quantum structures. Int. J. Solids Struct. 38, 1045-1062). The quantitative knowledge of stress and strain distributions in these nonlinear structures are essential for characterizing and tailoring their optoelectronic properties. A second example of great importance in material science concerns the use of single-walled and multi-walled nanotubes in reinforced composites (Seidel, G.D., Lagoudas, D.C., 2006. Micromechanical analysis of the effective elastic properties of carbon nanotube reinforced composites. Mechanics of Materials 38, 884-907). The effective properties of these structures can be analysed through the composite cylinder approach, where the nonlinear features must be taken into consideration.
We consider a nonlinear elastic problem for an arbitrary region Ω with boundary $\partial\Omega$ and unit normal vector $\vec{n}$ (see Fig.1 for details). Under the hypothesis of small deformations we can introduce the displacement field $\vec{u}(\vec{x})$, the infinitesimal strain tensor $\hat{\varepsilon}(\vec{x})$ and the Cauchy stress tensor $\hat{T}(\vec{x})$. The standard definition of the strain tensor follows

$$\varepsilon_{ij} = \frac{1}{2}\left(\frac{\partial u_i}{\partial x_j} + \frac{\partial u_j}{\partial x_i} \right) \tag{1}$$

and the balance laws for the linear and angular momentum are given below (for the static case without body forces)

$$\frac{\partial T_{ji}}{\partial x_i} = 0, \; T_{ij} = T_{ji} \tag{2}$$

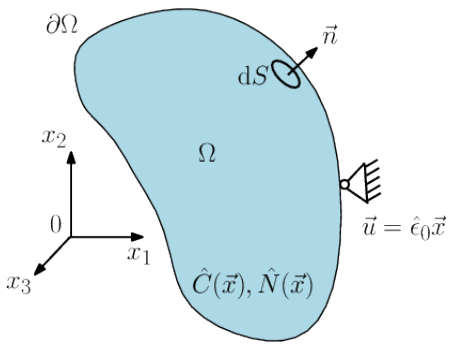

Figure 1: Definition of a nonlinear elastic problem for a region Ω with prescribed displacement on the boundary $\partial\Omega$. The constitutive relation is controlled by $\hat{C}$, which describes the linear elasticity (tensor of the second order elastic constants, SOEC), while $\hat{N}$ represents the nonlinear response (tensor the third order elastic constants, TOEC). The unit vector $\vec{n}$ is normal to the external surface $\partial\Omega$ and it is associated with the area element dS.

These laws hold for all materials, regardless of their constitution. However, in order to obtain a complete system of equations we need to introduce the constitutive equations, which characterize the actual elastic behaviour of the investigated system. Here, we are interested in an heterogeneous nonlinear behaviour in Ω and, therefore, we assume the following constitutive equation

$$T_{ij}(\vec{x}) = C_{ijkh}(\vec{x})\varepsilon_{kh}(\vec{x}) + \lambda N_{ijkhlm}(\vec{x})\varepsilon_{kh}(\vec{x})\varepsilon_{lm}(\vec{x}) \tag{3}$$

or, equivalently, in compact tensor notation $\hat{T}(\vec{x}) = \hat{C}(\vec{x})\hat{\varepsilon}(\vec{x}) + \lambda \hat{N}(\vec{x})\hat{\varepsilon}(\vec{x})\hat{\varepsilon}(\vec{x})$ where $\hat{C}$ describes the linear elasticity (the C_{ijkh} are the second order elastic constants, SOEC) while $\hat{N}$ describes the nonlinear elasticity (the N_{ijkhlm} are the third order elastic constants, TOEC). Both $\hat{C}$ and $\hat{N}$ are heterogeneous tensors over Ω. The tensor $\hat{N}$ measures the first deviation from the linearity. It can be noticed that the tensor $\hat{C}$ has 21 independent entries, while the second order tensor $\hat{N}$ has 56 independent components. Tables for the values of C_{ijkh} and N_{ijkhlm} can be found in literature for different crystal symmetries. Moreover, these values can be obtained by experimental procedures and by computational techniques, such as molecular dynamics or first-principles calculations. In order to apply a perturbation method we have introduced in Eq.(3) a small parameter λ. The general nonlinear problem in the region Ω is described by the combination of Eqs.(1), (2) and (3) with the boundary condition $\vec{u} = \hat{\varepsilon}_0\vec{x}$ on $\partial\Omega$ where $\hat{\varepsilon}_0$ is a constant strain tensor (prescribed displacement on $\partial\Omega$). The formulated problem has a series of important properties which are thoroughly discussed in the following.

Firstly, we observe that if the system is homogeneous (i.e. $\hat{C}(\vec{x}) = \hat{C}$ and $\hat{N}(\vec{x}) = \hat{N} \forall\ \vec{x} \in \Omega$), then the solution is given by $\hat{\varepsilon}(\vec{x}) = \hat{\varepsilon}_0 \forall\ \vec{x} \in \Omega$. In fact, the uniform strain $\hat{\varepsilon}_0$ in Ω satisfies the boundary conditions and leads to an uniform stress, compatible with the balance equations stated in Eq.(2).

As second property, we remember that for arbitrarily heterogeneous structures, the average value of the strain tensor over the region Ω is equal to $\hat{\varepsilon}_0$, regardless of the constitutive equation. So, we have

$$\langle \varepsilon_{ij} \rangle = \frac{1}{V}\int_\Omega \varepsilon_{ij}(\vec{x})d\vec{x} = \varepsilon_{0,ij} \tag{4}$$

where $V = mes(\Omega)$. This property is sometimes called average-strain theorem (Qu, J., Cherkaoui, M., 2006. Fundamentals of micromechanics of solids. John Wiley & Sons, Inc., Hoboken, New Jersey). We can now define the effective linear and nonlinear elastic tensors of the heterogeneous structure through the determination of the average value of the stress tensor over the region Ω. Since $\langle \hat{\varepsilon} \rangle = \hat{\varepsilon}_0$ we can write

$$\langle \hat{T} \rangle = \hat{C}_{eff}\hat{\varepsilon}_0 + \lambda \hat{N}_{eff}\hat{\varepsilon}_0\hat{\varepsilon}_0 + o(\lambda) \tag{5}$$

where we have neglected the terms with the third power of the strain and higher. Eq.(5) represents an operative definition of the effective response based on the evaluation of the average stress in the structure.

This result comes from the fact that the stress is a homogeneous function of degree 1 and 2 of the applied average strain for the linear and nonlinear part, respectively.
The effective parameters $\hat{C}_{eff}$ and $\hat{N}_{eff}$ can be alternatively defined through the determination of the average value of the tensor contraction $\hat{T} : \hat{\varepsilon} = T_{ij}\varepsilon_{ij}$. In fact, they can be introduced through the following relation

$$\left\langle \hat{T} : \hat{\varepsilon} \right\rangle = \hat{\varepsilon}_0 : \hat{C}_{eff}\hat{\varepsilon}_0 + \lambda\, \hat{\varepsilon}_0 : \hat{N}_{eff}\hat{\varepsilon}_0\hat{\varepsilon}_0 + o(\lambda) \tag{6}$$

which represents, differently from Eq.(5), an operative definition of the effective response based on the evaluation of the average value of $\hat{T} : \hat{\varepsilon}$ in the heterogeneous structure. The definitions of the effective behavior given in Eqs.(5) and (6) are mathematically equivalent. This point can be verified by using the following result

$$\left\langle T_{ij}\varepsilon_{ij} \right\rangle = \left\langle \hat{T} \right\rangle : \hat{\varepsilon}_0 \tag{7}$$

It represents the so-called Hill's lemma. It is evident that the substitution of Eq.(5) in Eq.(7) leads to Eq.(6), proving the equivalence of the different definitions of the effective properties.
In order to apply a perturbation technique, we consider λ as a small parameter and we search a solution of the general problem in the form

$$\vec{u} = \vec{u}^{L} + \lambda\, \vec{u}^{NL} + o(\lambda) \tag{8}$$

$$\hat{\varepsilon} = \hat{\varepsilon}^{L} + \lambda\, \hat{\varepsilon}^{NL} + o(\lambda) \tag{9}$$

$$\hat{T} = \hat{T}^{L} + \lambda\, \hat{T}^{NL} + o(\lambda) \tag{10}$$

By using the constitutive equation (see Eq.(3)) we have

$$\begin{aligned} \hat{T} &= \hat{C}\hat{\varepsilon} + \lambda\, \hat{N}\hat{\varepsilon}\hat{\varepsilon} \\ &= \hat{C}\hat{\varepsilon}^{L} + \lambda \left(\hat{C}\hat{\varepsilon}^{NL} + \hat{N}\hat{\varepsilon}^{L}\hat{\varepsilon}^{L} \right) + o(\lambda) \end{aligned} \tag{11}$$

and by applying the linear momentum balance equation we simply obtain

$$\vec{\nabla} \cdot \left(\hat{C}\hat{\varepsilon}^{L} \right) + \lambda\, \vec{\nabla} \cdot \left(\hat{C}\hat{\varepsilon}^{NL} + \hat{N}\hat{\varepsilon}^{L}\hat{\varepsilon}^{L} \right) + o(\lambda) = 0 \;\forall\; \lambda \tag{12}$$

Therefore, for the arbitrariness of λ, we obtain the standard linear problem of the elasticity theory

$$\begin{cases} \vec{\nabla} \cdot \left(\hat{C}\hat{\varepsilon}^{L} \right) = 0 \\ \hat{\varepsilon}^{L} = \dfrac{1}{2}\left(\vec{\nabla}\, \vec{u}^{L} + \vec{\nabla}^{T} \vec{u}^{L} \right) \\ \vec{u}^{L} = \hat{\varepsilon}_0 \vec{x} \quad on \quad \partial\Omega \end{cases} \tag{13}$$

and the associated problem which describes the first deviation from the linearity

$$\begin{cases} \vec{\nabla} \cdot \left(\hat{C}\hat{\varepsilon}^{NL} \right) = -\vec{\nabla} \cdot \left(\hat{N}\hat{\varepsilon}^{L}\hat{\varepsilon}^{L} \right) \\ \hat{\varepsilon}^{NL} = \dfrac{1}{2}\left(\vec{\nabla}\, \vec{u}^{NL} + \vec{\nabla}^{T} \vec{u}^{NL} \right) \\ \vec{u}^{NL} = 0 \quad on \quad \partial\Omega \end{cases} \tag{14}$$

The initial nonlinear problem has been split in two simpler linear problems. The first one is the standard linear elasticity problem and the second one is a linear problem with a distribution of body forces, depending on the solution of the first problem. The solution of these problems allows us to describe the elastic fields within the heterogeneous structure. This method could be also generalized in order to consider more terms in the series expansion: it would lead to a hierarchy of Lamé equations describing the behaviour of the displacement expansion terms. We attempt an alternative approach useful to calculate directly the elastic effective properties of the composite body (at least the SOEC and the TOEC).

We consider again the tensor contraction $\hat{T} : \hat{\varepsilon}$ and we expand it in series of λ (by using Eqs.(9) and (11))

$$\left\langle \hat{T} : \hat{\varepsilon} \right\rangle = \left\langle \hat{\varepsilon}^{L} : \hat{C}\hat{\varepsilon}^{L} \right\rangle + \lambda \left\langle 2\hat{\varepsilon}^{L} : \hat{C}\hat{\varepsilon}^{NL} + \hat{\varepsilon}^{L} : \hat{N}\hat{\varepsilon}^{L}\hat{\varepsilon}^{L} \right\rangle + o(\lambda) \tag{15}$$

We can now prove that $\left\langle \hat{\varepsilon}^{L} : \hat{C}\hat{\varepsilon}^{NL} \right\rangle = 0$ as follows. To begin we observe that

$$\left\langle \hat{\varepsilon}^{L} : \hat{C}\hat{\varepsilon}^{NL} \right\rangle = \frac{1}{V}\int_{\Omega} C_{ijkl} \frac{\partial u_i^L}{\partial x_j} \frac{\partial u_k^{NL}}{\partial x_l} d\vec{x} \tag{16}$$

because of the symmetries of the linear elastic tensor. Therefore we have

$$\left\langle \hat{\varepsilon}^{L} : \hat{C}\hat{\varepsilon}^{NL} \right\rangle = \frac{1}{V}\int_{\Omega} \frac{\partial}{\partial x_l}\left(C_{ijkl} \frac{\partial u_i^L}{\partial x_j} u_k^{NL} \right) d\vec{x} - \frac{1}{V}\int_{\Omega} \frac{\partial}{\partial x_l}\left(C_{ijkl} \frac{\partial u_i^L}{\partial x_j} \right) u_k^{NL} d\vec{x} \tag{17}$$

The second integral is zero since $\partial T_{kl}^L / \partial x_l = 0$ and we obtain

$$\left\langle \hat{\varepsilon}^{L} : \hat{C}\hat{\varepsilon}^{NL} \right\rangle = \frac{1}{V}\int_{\partial\Omega} C_{ijkl} \frac{\partial u_i^L}{\partial x_j} u_k^{NL} n_l dS = 0 \tag{18}$$

since $\vec{u}^{NL} = 0 \; on \; \partial\Omega$. To conclude, starting with Eq.(15) we have obtained the result

$$\left\langle \hat{T} : \hat{\varepsilon} \right\rangle = \left\langle \hat{\varepsilon}^{L} : \hat{C}\hat{\varepsilon}^{L} \right\rangle + \lambda \left\langle \hat{\varepsilon}^{L} : \hat{N}\hat{\varepsilon}^{L}\hat{\varepsilon}^{L} \right\rangle + o(\lambda) \tag{19}$$

Drawing a comparison with Eq.(6) we obtain the main achievements of the present Section

$$\hat{\varepsilon}_0 : \hat{C}_{eff}\hat{\varepsilon}_0 = \left\langle \hat{\varepsilon}^{L} : \hat{C}\hat{\varepsilon}^{L} \right\rangle \tag{20}$$

$$\hat{\varepsilon}_0 : \hat{N}_{eff}\hat{\varepsilon}_0\hat{\varepsilon}_0 = \left\langle \hat{\varepsilon}^{L} : \hat{N}\hat{\varepsilon}^{L}\hat{\varepsilon}^{L} \right\rangle \tag{21}$$

In previous expressions $\hat{\varepsilon}^{L}(\vec{x})$ is the solution of the linear problem stated in Eq.(13) with the boundary condition defined by the constant strain $\hat{\varepsilon}_0$. Therefore, linear and nonlinear effective properties (i.e., SOEC and TOEC) depend only on the linear solution of the proposed problem. We remark that Eqs.(20) and (21) are exact results, not affected by any kind of approximation. In fact, the approximation introduced by the perturbation technique concerns the number of terms retained in the series expansions, being each term exactly evaluated. Moreover, we remark that the knowledge of the linear solution $\hat{\varepsilon}^{L}$ is adequate only to obtain the second order and the third order effective elastic constants, but it is not sufficient for determining the higher order effective behaviors. Evidently, in such a case it is necessary to consider also the nonlinear solution $\hat{\varepsilon}^{NL}$ and the further terms of the series expansion. To conclude, our methodology is based on the following idea: by selecting different suitable homogeneous deformations $\hat{\varepsilon}_0$ and by solving the correspondent linear problem given in Eq.(13), we can efficiently apply Eqs.(20) and (21) and we can find all the components of the effective tensors $\hat{C}_{eff}$ and $\hat{N}_{eff}$. In the following, we apply Eqs.(20) and (21) to an isotropic nonlinear composite cylinder under plane-strain conditions.

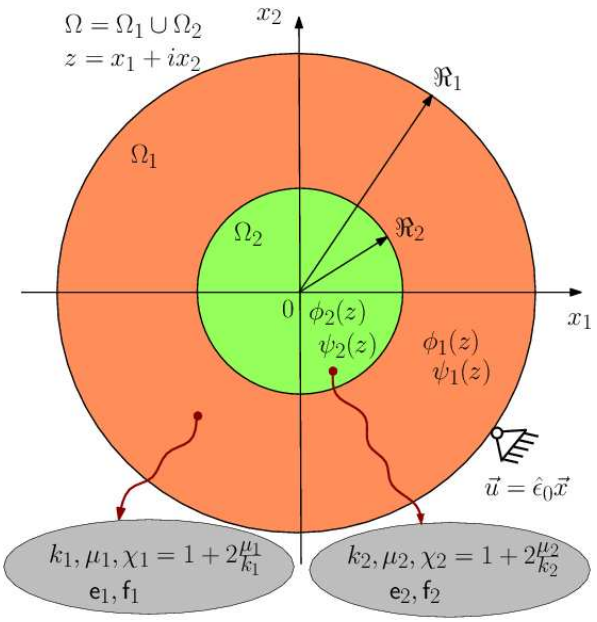

Figure 2: Schematic representation of the cross-section of the composite cylinder shown in Fig.0. The whole planar region Ω *has been subdivided into the shell* Ω_1 *(with parameters* k_1, μ_1, χ_1, e_1 *and* f_1*) and the core* Ω_2 *(with parameters* k_2, μ_2, χ_2, e_2 *and* f_2*). We will adopt the complex variable method for the two-dimensional elasticity based on the couple of Kolossov-Muskhelishvili potentials* $\phi_\alpha(z)$ *and* $\psi_\alpha(z)$ *(for* $\alpha = 1,2$*), where the complex number* $z = x_1 + ix_2$ *represents the position on the plane.*

We are interested in applying the previous procedure to the case of a composite cylinder composed by a nonlinear core embedded in a nonlinear external shell. We suppose to analyse the plane strain behavior of this heterogeneous structure on a plane perpendicular to the axis of the cylinder (see Fig.2). To begin we define the linear and nonlinear elastic behavior of both components. We consider each phase ($\alpha = 1,2$) described by the Green approach (Atkin, R. J., Fox N., 2005. An Introduction to the Theory of Elasticity. Dover, New York) and we formulate the corresponding energy balance: for a given state of deformation, the stress power is absorbed into a strain energy function $U_\alpha(\hat{\varepsilon})$, leading to the constitutive equation $\hat{T} = \partial U_\alpha(\hat{\varepsilon})/\partial\hat{\varepsilon}$. As well known, the strain energy function can be identified with the internal energy per unit volume in an isentropic process, or with the Helmholtz free-energy per unit volume in an isothermal process. To model core and shell materials, we adopt the most general isotropic nonlinear constitutive stress-strain relation of the two-dimensional elasticity, expanded up to the second order in the strain components: it follows that the function $U_\alpha(\hat{\varepsilon})$ can only depend upon the principal invariants of the strain tensor, i.e. $U_\alpha(\hat{\varepsilon}) = U_\alpha\left(Tr(\hat{\varepsilon}), Tr(\hat{\varepsilon}^2)\right)$. Therefore, by expanding $U_\alpha(\hat{\varepsilon})$ up to the third order in the strain components, we obtain

$$U_\alpha(\hat{\varepsilon}) = \mu_\alpha Tr(\hat{\varepsilon}^2) + \frac{1}{2}(k_\alpha - \mu_\alpha)Tr^2(\hat{\varepsilon}) + e_\alpha Tr(\hat{\varepsilon})Tr(\hat{\varepsilon}^2) + f_\alpha Tr^3(\hat{\varepsilon}) \quad (22)$$

and deriving the stress, we get

$$\hat{T} = 2\mu_\alpha\hat{\varepsilon} + (k_\alpha - \mu_\alpha)Tr(\hat{\varepsilon})\hat{I} + 2e_\alpha Tr(\hat{\varepsilon})\hat{\varepsilon} + e_\alpha Tr(\hat{\varepsilon}^2)\hat{I} + 3f_\alpha Tr^2(\hat{\varepsilon})\hat{I} \quad (23)$$

for the materials corresponding to the shell ($\alpha = 1$) and to the core ($\alpha = 2$). We remark that in Eqs.(22) and (23) tensors $\hat{\varepsilon}$ and $\hat{T}$ are represented by matrices 2x2 (planar geometry). The parameters e_α and f_α are the so-called (two-dimensional) Landau moduli and they represent the first deviation from the standard linearity (they are the TOEC in our system). On the other hand, k_α and μ_α represent the linear elastic moduli or,

equivalently, the SOEC. Parameters k_α represent the two-dimensional bulk moduli and therefore they are related with the standard three-dimensional bulk moduli K_α through the relations $k_\alpha = K_\alpha + (1/3)\mu_\alpha$ (for $\alpha = 1,2$). On the other hand, the shear moduli μ_α assume the same value both in the two-dimensional and three-dimensional geometries and, therefore, there is no possible ambiguity. Of course, we assume that the technological assembling processes are able to generate a quite perfect core-shell interface. In fact, it is well known that the behavior of composite materials (in particular at the nanoscale) is deeply affected by interface features occurring at the boundary between different phases. In the following, we search for the overall behavior of the cylinder, which is described by the effective constitutive equation deduced from Eq.(5)

$$\begin{aligned}\langle \hat{T} \rangle &= 2\mu_{eff}\langle \hat{\varepsilon} \rangle + (k_{eff} - \mu_{eff}) Tr(\langle \hat{\varepsilon} \rangle)\hat{I} \\ &+ 2\mathrm{e}_{eff} Tr\left(\langle \hat{\varepsilon} \rangle\right)\langle \hat{\varepsilon} \rangle + \mathrm{e}_{eff} Tr\left(\langle \hat{\varepsilon} \rangle^2\right)\hat{I} \\ &+ 3\mathrm{f}_{eff} Tr^2\left(\langle \hat{\varepsilon} \rangle\right)\hat{I} + o\left(\langle \hat{\varepsilon} \rangle^2\right)\end{aligned} \tag{24}$$

where we have defined the effective linear moduli k_{eff} and μ_{eff} and the effective nonlinear coefficients e_{eff} and f_{eff}. The effective constitutive relation given in Eq.(24) has the same form of Eq.(23) which is valid for each phase, except for the possible higher order terms, which will be neglected in the following developments. All the linear (k_{eff} and μ_{eff}) and nonlinear (e_{eff} and f_{eff}) effective elastic parameters will be found as function of the parameters of the two phases and the volume fraction $c = \Re_2^2/\Re_1^2$ of the core (with radius $\Re_2$) embedded in the shell (with radius $\Re_1$).

In order to solve the linear counterpart of our problem, we use the complex variable method for the two-dimensional elasticity. We assume that the elastic state of a given homogeneous region Ω_α ($\alpha = 1,2$) is exactly described by two holomorphic functions $\phi_\alpha(z)$ and $\psi_\alpha(z)$, where z represents the position on the plane (see Fig.2 for details). The Kolossov-Muskhelishvili equations allow for the determination of the elastic fields in each region

$$u_1^\alpha + i\,u_2^\alpha = \frac{1}{2\mu_\alpha}\left[\chi_\alpha \phi_\alpha(z) - z\,\overline{\phi'_\alpha(z)} - \overline{\psi_\alpha(z)}\right] \tag{25}$$

$$T_{11}^\alpha + T_{22}^\alpha = 2\left[\phi'_\alpha(z) + \overline{\phi'_\alpha(z)}\right] \tag{26}$$

$$T_{22}^\alpha - T_{11}^\alpha + 2\,i\,T_{12}^{(\alpha)} = 2\left[\bar{z}\phi''_\alpha(z) + \psi''_\alpha(z)\right] \tag{27}$$

where $\overline{f}$ is the conjugate of f while f' and f'' indicate the first and the second derivative of the analytic function f, respectively. Functions $\phi_1(z)$ and $\psi_1(z)$ are defined for $\Re_2 < |z| < \Re_1$, while $\phi_2(z)$ and $\psi_2(z)$ are defined for $|z| < \Re_2$. Moreover, the parameter χ_α introduced in Eq.(25) is given by $\chi_\alpha = 3 - 4\nu_\alpha$ (plane strain conditions) where the Poisson ratio can be written as $\nu_\alpha = (k_\alpha - \mu_\alpha)/(2k_\alpha)$.

The solution of the elastic problem can be obtained by imposing the perfect bonding at the interface and the prescribed displacement on the external boundary. These conditions can be expressed in terms of the elastic potentials

$$\frac{1}{2\mu_1}\left[\chi_1\phi_1 - z\,\overline{\phi'_1} - \overline{\psi_1}\right] = \frac{1}{2\mu_2}\left[\chi_2\phi_2 - z\,\overline{\phi'_2} - \overline{\psi_2}\right] \tag{28}$$

$$\phi_1 + z\,\overline{\phi'_1} + \overline{\psi_1} = \phi_2 + z\,\overline{\phi'_2} + \overline{\psi_2} \tag{29}$$

for $z = \Re_2 e^{i\theta}$, and

$$\frac{1}{2\mu_1}\left[\chi_1\phi_1 - z\,\overline{\phi'_1} - \overline{\psi_1}\right] = \sum_{k=-\infty}^{+\infty} g_k e^{ik\theta} \tag{30}$$

for $z = \Re_1 e^{i\theta}$. Here, we have developed the prescribed displacement in Fourier series with coefficients g_k. The potentials $\phi_2(z)$ and $\psi_2(z)$ can be represented by Taylor series and $\phi_1(z)$ and $\psi_1(z)$ by Laurent series

$$\phi_2(z) = \sum_{k=0}^{+\infty} a_k z^k, \psi_2(z) = \sum_{k=0}^{+\infty} b_k z^k \tag{31}$$

$$\phi_1(z) = \sum_{k=-\infty}^{+\infty} c_k z^k, \psi_1(z) = \sum_{k=-\infty}^{+\infty} d_k z^k \tag{32}$$

The analysis of the problem proves that the following simplified representations are sufficient to solve the problem

$$\psi_1(z) = d_{-3}\frac{1}{z^3} + d_{-1}\frac{1}{z} + d_1 z \tag{33}$$

$$\phi_1(z) = c_{-1}\frac{1}{z} + c_1 z + c_3 z^3 \tag{34}$$

$$\psi_2(z) = b_1 z \tag{35}$$

$$\phi_2(z) = a_1 z + a_3 z^3 \tag{36}$$

First of all we solve the system for obtaining the coefficients c_1, a_1 and d_{-1}

$$a_1 = \frac{(\chi_1 + 1)Tr(\hat{\varepsilon}_0)}{\frac{1}{\mu_2}(2c + \chi_1 - 1)(\chi_2 - 1) + \frac{1}{\mu_1}2(1-c)(\chi_1 - 1)} \tag{37}$$

$$c_1 = \frac{\left[2 + \frac{\mu_1}{\mu_2}(\chi_2 - 1)\right]Tr(\hat{\varepsilon}_0)}{\frac{1}{\mu_2}(2c + \chi_1 - 1)(\chi_2 - 1) + \frac{1}{\mu_1}2(1-c)(\chi_1 - 1)} \tag{38}$$

$$d_{-1} = \frac{\left[(\chi_1 - 1) - \frac{\mu_1}{\mu_2}(\chi_2 - 1)\right]2c\Re_1^2 Tr(\hat{\varepsilon}_0)}{\frac{1}{\mu_2}(2c + \chi_1 - 1)(\chi_2 - 1) + \frac{1}{\mu_1}2(1-c)(\chi_1 - 1)} \tag{39}$$

The two unknowns c_{-1} and c_3 are then given by

$$c_{-1} = \frac{-\left(\frac{1}{\mu_1} - \frac{1}{\mu_2}\right)\mu_1(\varepsilon_{0,11} + 2i\varepsilon_{0,12} - \varepsilon_{0,22})\Re_2^2}{\frac{3}{\alpha}\left(\frac{1}{\mu_1} + \frac{\chi_2}{\mu_2}\right)\left(\frac{1}{\mu_1} - \frac{1}{\mu_2}\right)\left(1 - \frac{1}{c}\right)^2 + \beta} \tag{40}$$

$$c_3 = -\bar{c}_{-1}\frac{1}{\alpha\Re_2^4}\left(\frac{1}{\mu_1} + \frac{\chi_2}{\mu_2}\right)\left(1 - \frac{1}{c}\right) \tag{41}$$

where

$$\alpha = \left(\frac{\chi_1}{\mu_1} - \frac{\chi_2}{\mu_2}\right) - \frac{1}{c^3}\chi_1\left(\frac{1}{\mu_1} + \frac{\chi_2}{\mu_2}\right) \tag{42}$$

$$\beta = \left(\frac{\chi_1}{\mu_1} + \frac{1}{\mu_2}\right) - c\chi_1\left(\frac{1}{\mu_1} - \frac{1}{\mu_2}\right) \tag{43}$$

Finally, the other coefficients can be eventually found as

$$d_{-3} = \chi_1\bar{c}_3\Re_1^6 + c_{-1}\Re_1^2 \tag{44}$$

$$d_1 = \chi_1\bar{c}_{-1}\Re_1^{-2} - 3c_3\Re_1^2 + \\ - \mu_1(\varepsilon_{0,11} - 2i\varepsilon_{0,12} - \varepsilon_{0,22}) \tag{45}$$

$$a_3 = c_3\left(1 + \chi_1\frac{1}{c^3}\right) - \bar{c}_{-1}\frac{1}{\Re_2^4}\left(1 - \frac{1}{c}\right) \tag{46}$$

$$b_1 = \bar{c}_{-1}\left[\frac{1}{\Re_2^2}\left(4 - \frac{3}{c}\right) + \frac{\chi_1}{\Re_1^2}\right] - 3c_3\left(\Re_1^2 + \frac{\chi_1\Re_2^2}{c^3}\right)$$
$$- \mu_1\left(\varepsilon_{0,11} - 2i\varepsilon_{0,12} - \varepsilon_{0,22}\right) \tag{47}$$

At this point we want to apply the nonlinear perturbation technique to the composite cylinder system. To this aim we take into consideration the following linear isotropic operator described by the space varying linear moduli $\mu(\vec{x})$ and $k(\vec{x})$

$$\hat{C}(\vec{x})\hat{\varepsilon}(\vec{x}) = 2\mu(\vec{x})\hat{\varepsilon}(\vec{x}) + [k(\vec{x}) - \mu(\vec{x})]Tr[\hat{\varepsilon}(\vec{x})]\hat{I} \tag{48}$$

Similarly, we consider the following nonlinear isotropic operator controlled by the space varying nonlinear coefficients $\mathrm{e}(\vec{x})$ and $\mathrm{f}(\vec{x})$

$$\hat{N}(\vec{x})\hat{\varepsilon}(\vec{x})\hat{\varepsilon}(\vec{x}) = 2\mathrm{e}(\vec{x})Tr[\hat{\varepsilon}(\vec{x})]\hat{\varepsilon}(\vec{x}) + \mathrm{e}(\vec{x})Tr\left\{[\hat{\varepsilon}(\vec{x})]^2\right\}\hat{I}$$
$$+ 3\mathrm{f}(\vec{x})Tr^2[\hat{\varepsilon}(\vec{x})]\hat{I} \tag{49}$$

We determine the following scalar quantities for an arbitrary strain tensor field $\hat{\varepsilon}(\vec{x})$

$$\hat{\varepsilon}(\vec{x}) : \hat{C}(\vec{x})\hat{\varepsilon}(\vec{x}) = [k(\vec{x}) + \mu(\vec{x})]Tr^2[\hat{\varepsilon}(\vec{x})]$$
$$- 4\mu(\vec{x})Det[\hat{\varepsilon}(\vec{x})] \tag{50}$$

$$\hat{\varepsilon}(\vec{x}) : \hat{N}(\vec{x})\hat{\varepsilon}(\vec{x})\hat{\varepsilon}(\vec{x}) = 3[\mathrm{e}(\vec{x}) + \mathrm{f}(\vec{x})]Tr^3[\hat{\varepsilon}(\vec{x})]$$
$$- 6\mathrm{e}(\vec{x})Tr[\hat{\varepsilon}(\vec{x})]Det[\hat{\varepsilon}(\vec{x})] \tag{51}$$

In Eqs.(50) and (51) we used the standard relation $Tr\left\{[\hat{\varepsilon}(\vec{x})]^2\right\} = Tr^2[\hat{\varepsilon}(\vec{x})] - 2Det[\hat{\varepsilon}(\vec{x})]$ for two-dimensional matrices. Equations (50) and (51) must be evaluated with $\hat{\varepsilon}(\vec{x}) = \hat{\varepsilon}_0$, $\hat{C}(\vec{x}) = \hat{C}_{eff}$ and $\hat{N}(\vec{x}) = \hat{N}_{eff}$ for obtaining the left hand sides of Eqs.(20) and (21), and with $\hat{\varepsilon}(\vec{x}) = \hat{\varepsilon}^L$, $\hat{C}(\vec{x}) = \left\{\hat{C}_1 \; if \; \vec{x} \in \Omega_1, \hat{C}_2 \; if \; \vec{x} \in \Omega_2\right\}$ and $\hat{N}(\vec{x}) = \left\{\hat{N}_1 \; if \; \vec{x} \in \Omega_1, \hat{N}_2 \; if \; \vec{x} \in \Omega_2\right\}$ for obtaining the right hand sides of the same equations. The distribution of the linear part of the strain ($\hat{\varepsilon}^L$) within our heterogeneous structure is easily determined with previous results: in fact, it is sufficient to consider the solutions and to substitute them in the displacement expression given in Eq.(25). By differentiating this last equation (see Eq.(1)), we easily find the strain tensor $\hat{\varepsilon}^L$ within the regions Ω_1 and Ω_2, which is the main quantity exploited to obtain the linear and nonlinear effective elastic properties. It is important to remark that the $\hat{\varepsilon}^L$ depends only on the strain $\hat{\varepsilon}_0$ applied on the boundary of radius $\Re_1$ (prescribed displacement).

For simplifying the formalism, we therefore introduce the scalar quantities $\mathrm{S}_C = \int_\Omega \hat{\varepsilon}^L : \hat{C}\hat{\varepsilon}^L d\vec{x}$ and $\mathrm{S}_N = \int_\Omega \hat{\varepsilon}^L : \hat{N}\hat{\varepsilon}^L\hat{\varepsilon}^L d\vec{x}$, which are functions of the applied strain

$$\mathrm{S}_C(\hat{\varepsilon}_0) = (k_1 + \mu_1)\int_{\Omega_1}\left\{Tr[\hat{\varepsilon}^L(\vec{x})]\right\}^2 d\vec{x} \tag{52}$$
$$- 4\mu_1\int_{\Omega_1} Det[\hat{\varepsilon}^L(\vec{x})]d\vec{x}$$
$$+ (k_2 + \mu_2)\int_{\Omega_2}\left\{Tr[\hat{\varepsilon}^L(\vec{x})]\right\}^2 d\vec{x}$$
$$- 4\mu_2\int_{\Omega_2} Det[\hat{\varepsilon}^L(\vec{x})]d\vec{x}$$

$$
\begin{aligned}
S_N(\hat{\varepsilon}_0) &= 3(e_1 + f_1)\int_{\Omega_1} Tr^3[\hat{\varepsilon}^L(\vec{x})]d\vec{x} \\
&- 6e_1\int_{\Omega_1} Tr[\hat{\varepsilon}^L(\vec{x})]Det[\hat{\varepsilon}^L(\vec{x})]d\vec{x} \\
&+ 3(e_2 + f_2)\int_{\Omega_2} Tr^3[\hat{\varepsilon}^L(\vec{x})]d\vec{x} \\
&- 6e_2\int_{\Omega_2} Tr[\hat{\varepsilon}^L(\vec{x})]Det[\hat{\varepsilon}^L(\vec{x})]d\vec{x}
\end{aligned}
\tag{53}
$$

All integrals in previous expressions can be calculated in closed form through the straightforward introduction of the cylindrical coordinates. However, we do not report here the complete results which are rather complicated and do not add relevant information to our development. Instead, we apply Eqs.(52) and (53) for determining the effective behavior.

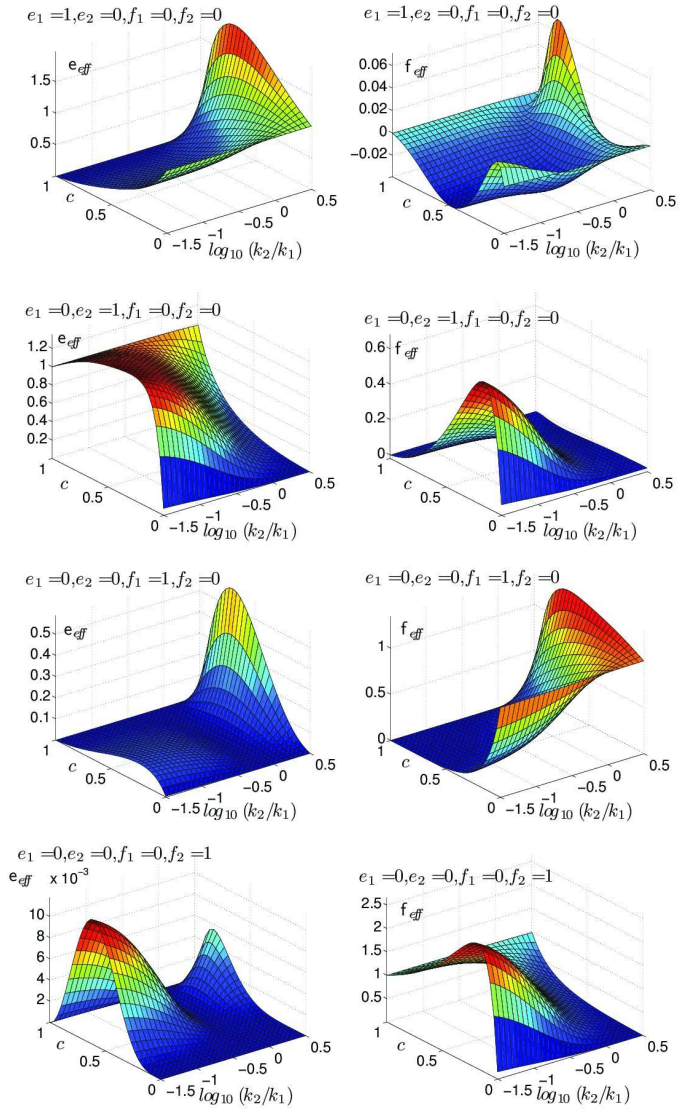

Figure 3: Nonlinear effective elastic moduli in terms of the volume fraction c *of the internal core and the compressibility contrast* $\log_{10}(k_2/k_1)$. *We have adopted the parameters* $k_1 = 1$, $\nu_1 = 0.33$, $\nu_2 = 0.3$. *Four couples of plots for* e_{eff} *and* f_{eff} *correspond to the nonlinear parameter of the structure (* $e_1 = 1, e_2 = 0, f_1 = 0, f_2 = 0$*),* $(e_1 = 0, e_2 = 1, f_1 = 0, f_2 = 0)$*,* $(e_1 = 0, e_2 = 0, f_1 = 1, f_2 = 0)$ *and (* $e_1 = 0, e_2 = 0, f_1 = 0, f_2 = 1$*). It is therefore possible to observe the effects of any nonlinearity source separately.*

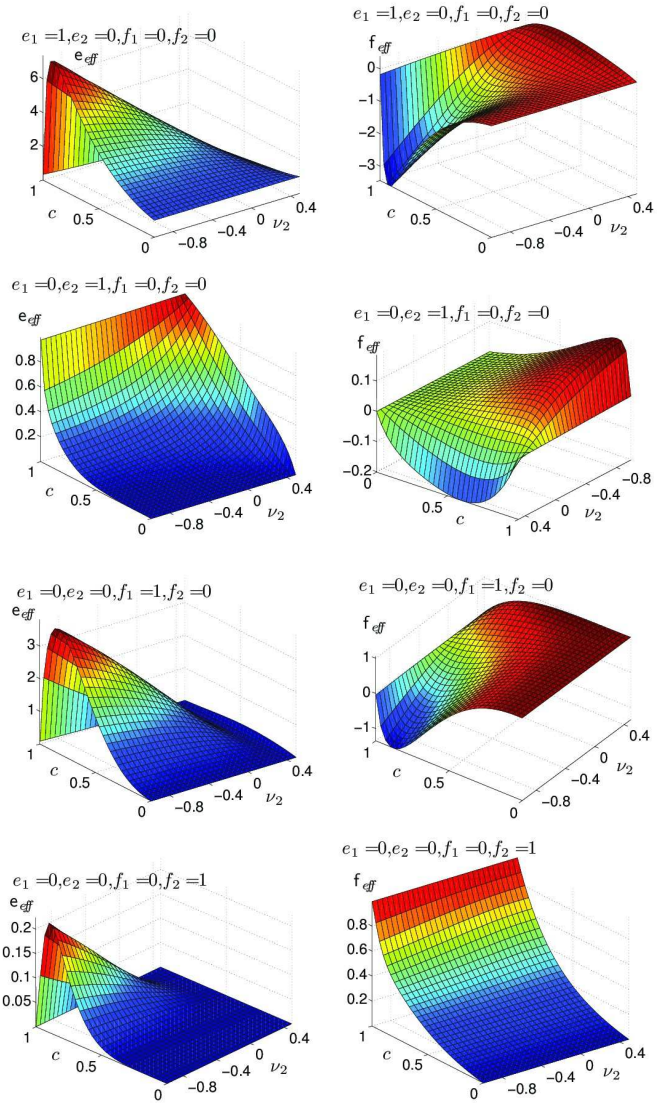

Figure 4: Nonlinear effective elastic moduli in terms of the volume fraction c *and the Poisson ratio* ν_2 *of the embedded inhomogeneity (or core). We have adopted the parameters* $k_1 = 1$, $\nu_1 = 0.33$, $k_2 = 2$. *Four couples of plots for* e_{eff} *and* f_{eff} *correspond to the nonlinear parameter of the structure (* $e_1 = 1, e_2 = 0, f_1 = 0, f_2 = 0$*), (*$e_1 = 0, e_2 = 1, f_1 = 0, f_2 = 0$*), (*$e_1 = 0, e_2 = 0, f_1 = 1, f_2 = 0$*) and (*$e_1 = 0, e_2 = 0, f_1 = 0, f_2 = 1$*). It is therefore possible to observe the effects of any nonlinearity source separately.*

We adopt suitable homogeneous in-plane deformations and we obtain the effective linear moduli

$$\mu_{eff} = \frac{1}{4\pi \Re_1^2} \mathrm{S}_C\left(\begin{bmatrix} 0 & 1 \\ 1 & 0 \end{bmatrix}\right) \tag{54}$$

$$k_{eff} = \frac{1}{\pi \Re_1^2}\left\{ \mathrm{S}_C\left(\begin{bmatrix} 1 & 0 \\ 0 & 0 \end{bmatrix}\right) - \frac{1}{4}\mathrm{S}_C\left(\begin{bmatrix} 0 & 1 \\ 1 & 0 \end{bmatrix}\right)\right\} \tag{55}$$

and the effective nonlinear coefficients

$$\mathrm{e}_{eff} = \frac{1}{3\pi \Re_1^2}\left\{ 2\mathrm{S}_N\left(\begin{bmatrix} 1 & 0 \\ 0 & 0 \end{bmatrix}\right) - \frac{1}{4}\mathrm{S}_N\left(\begin{bmatrix} 1 & 0 \\ 0 & 1 \end{bmatrix}\right)\right\} \tag{56}$$

$$\mathrm{f}_{eff} = \frac{1}{3\pi \Re_1^2}\left\{ \frac{1}{4}\mathrm{S}_N\left(\begin{bmatrix} 1 & 0 \\ 0 & 0 \end{bmatrix}\right) - \mathrm{S}_C\left(\begin{bmatrix} 1 & 0 \\ 0 & 1 \end{bmatrix}\right)\right\} \tag{57}$$

Since the expression for $\mathrm{S}_C(\hat{\varepsilon}_0)$ depends only on the linear elastic parameters, we observe that the effective linear moduli depend only on the linear elastic moduli of the components, as expected. On the other hand, it is evident that the effective nonlinear moduli depend both on the linear and nonlinear responses of the different phases composing the structure. It is interesting to observe that the whole procedure can be implemented both numerically, with standard software techniques, and analytically in symbolic computation environments.

We show now a numerical application of these results. We are interested in better understanding the effects of the nonlinear parameters $\mathrm{e}_1, \mathrm{f}_1$, e_2 and f_2 on the effective nonlinear properties of the overall composite cylinder. In Fig.3 we can observe the behavior of e_{eff} and f_{eff} in terms of the volume fraction c of the internal core and the compressibility contrast $\log_{10}(k_2/k_1)$. We have adopted the parameters $k_1 = 1$, $\nu_1 = 0.33$, $\nu_2 = 0.3$. Four couples of plots for e_{eff} and f_{eff} correspond to the following nonlinear parameter of the structure: ($\mathrm{e}_1 = 1, \mathrm{e}_2 = 0, \mathrm{f}_1 = 0, \mathrm{f}_2 = 0$), ($\mathrm{e}_1 = 0, \mathrm{e}_2 = 1, \mathrm{f}_1 = 0, \mathrm{f}_2 = 0$), ($\mathrm{e}_1 = 0, \mathrm{e}_2 = 0, \mathrm{f}_1 = 1, \mathrm{f}_2 = 0$) and ($\mathrm{e}_1 = 0, \mathrm{e}_2 = 0, \mathrm{f}_1 = 0, \mathrm{f}_2 = 1$). It means that in each case we have considered only one source of nonlinearity in order to isolate its effects, produced on the effective nonlinear behavior. We can notice a very complex scenario from which we can deduce some general trends: (i) each of the nonlinearity $\mathrm{e}_1, \mathrm{f}_1$, e_2 and f_2 generates both e_{eff} and f_{eff} as final effective result; (ii) when the nonlinear behavior is concentrated in the matrix we observe a strong intensification of the effective nonlinearities for a positive contrast $\log_{10}(k_2/k_1)$ (i.e. $k_2 >> k_1$); (iii) conversely, when the nonlinear behavior is concentrated in the core we observe a strong intensification of the effective nonlinearities for a negative contrast $\log_{10}(k_2/k_1)$ (i.e. $k_2 = k_1$). Moreover, in Fig.4 we can find the results of a second analysis conducted to obtain the nonlinear effective elastic moduli in terms of the volume fraction c and the Poisson ratio ν_2 of the embedded inhomogeneity (or core). We have adopted the parameters $k_1 = 1$, $\nu_1 = 0.33$, $k_2 = 2$. As before, four couples of plots for e_{eff} and f_{eff} correspond to the nonlinear parameter of the structure ($\mathrm{e}_1 = 1, \mathrm{e}_2 = 0, \mathrm{f}_1 = 0, \mathrm{f}_2 = 0$), ($\mathrm{e}_1 = 0, \mathrm{e}_2 = 1, \mathrm{f}_1 = 0, \mathrm{f}_2 = 0$), ($\mathrm{e}_1 = 0, \mathrm{e}_2 = 0, \mathrm{f}_1 = 1, \mathrm{f}_2 = 0$) and ($\mathrm{e}_1 = 0, \mathrm{e}_2 = 0, \mathrm{f}_1 = 0, \mathrm{f}_2 = 1$). Also in this case we observe a very intriguing and complex mixing behavior of the nonlinear features. In particular we note that, when the nonlinearity is confined within the external shell, the nonlinear parameter e_{eff} exhibits a strong positive amplification effect for a negative Poisson ratio ν_2 of the core and, on the other hand, the nonlinear parameter f_{eff} exhibits a negative amplification effect for a negative Poisson ratio of the core. Moreover, when $\mathrm{e}_2 = 1$ we have a quite constant e_{eff} for different values of ν_2 and two intensification effects of f_{eff} (i.e. a negative peak for positive ν_2 and a positive peak for negative ν_2). Finally, when $\mathrm{f}_2 = 1$ we have a quite constant f_{eff} for different values of ν_2 and an intensification effect of e_{eff} (i.e. a positive peak for negative ν_2).

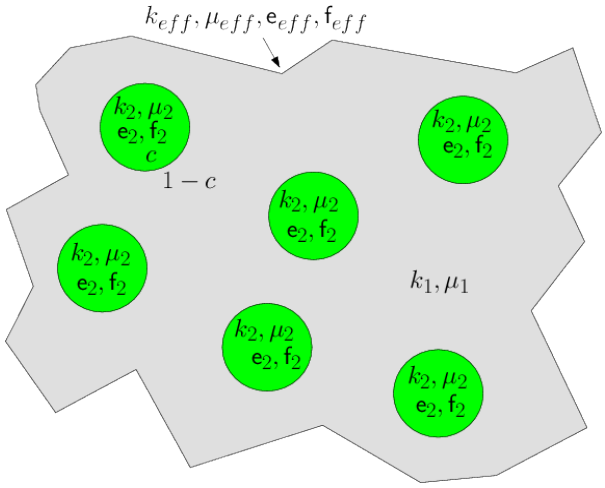

Figure 5: Scheme of a dispersion of nonlinear circular inhomogeneities (with linear moduli μ_2 *and* k_2 *and nonlinear constants* e_2 *and* f_2*) embedded into a linear matrix with elastic moduli* μ_1 *and* k_1*.*

Here, we want to study the relations between the present general theory and previous homogenization schemes. To this aim, we briefly introduce an earlier result concerning the two-dimensional homogenization of a dispersion of circular nonlinear inhomogeneities embedded in a linear isotropic plane. The structure of this composite material is depicted in Fig.5. The circular inhomogeneities are randomly and isotropically embedded into a linear matrix with elastic moduli μ_1 and k_1 (k_1 is always the two-dimensional version of the bulk modulus). To begin, we suppose that the volume fraction c of the embedded phase is small (dilute dispersion). If we identify the linear coefficients of the inhomogeneities by μ_2 and k_2 and their nonlinear constants by e_2 and f_2, then the stress-strain relation is given by Eq.(23) with $\alpha = 2$.
The constitutive equation of the whole system is expressed in terms of the effective linear and nonlinear elastic moduli as in Eq.(24). In this case the effective linear elastic moduli are given by

$$\mu_{eff} = \mu_1 + c\frac{\mu_2 - \mu_1}{c + (1-c)\left[1 + \frac{1}{2}\left(\frac{\mu_2}{\mu_1} - 1\right)\frac{k_1 + 2\mu_1}{k_1 + \mu_1}\right]} \tag{58}$$

$$k_{eff} = k_1 + c\frac{k_2 - k_1}{c + (1-c)\frac{\mu_1 + k_2}{\mu_1 + k_1}} \tag{59}$$

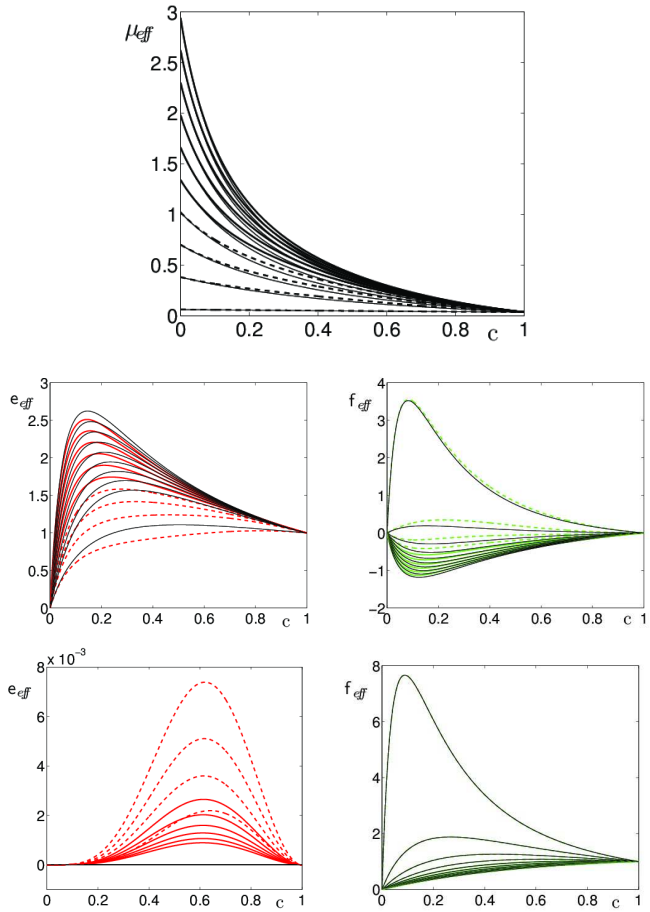

Figure 6: Results for the composite structure with the linear matrix (inhomogeneity softer than the matrix): comparison of the general theory given in Eqs.(54)-(57) (coloured lines, dashed for positive matrix Poisson ratio and solid for negative matrix Poisson ratio) with the old theory given in Eqs.(58)-(61) (thin black lines). The first plot represents the linear result for μ_{eff} *; the two couples of nonlinear results for* e_{eff} *and* f_{eff} *correspond to* $\mathrm{e}_2 = 1, \mathrm{f}_2 = 0$ *and* $\mathrm{e}_2 = 0, \mathrm{f}_2 = 1$*, respectively. All effective parameters have been represented versus the volume fraction* c*. We have adopted the parameters* $k_1 = 1$*,* $0 < \mu_1 < 3k_1$ *(or equivalently* $-1 < \nu_1 < 1/2$*) sampled through 10 equispaced values,* $k_2 = 0.1$*,* $\nu_2 = 0.33$*.*

and the effective nonlinear elastic moduli by

$$\mathrm{e}_{eff} = \frac{\mathrm{e}_2 c}{\mathrm{L}^2}\left(1 - \frac{1-c}{\mathrm{L}+2\mathrm{M}}\frac{k_2 - k_1}{\mu_1 + k_1}\right) \tag{60}$$

$$\begin{aligned}\mathrm{f}_{eff} = &-\frac{c(1-c)(k_2-k_1)(\mathrm{e}_2+2\mathrm{f}_2)}{2(k_1+\mu_1)(\mathrm{L}+2\mathrm{M})^3} \\ &-\frac{\mathrm{e}_2 c}{6\mathrm{L}^2} + \frac{c(\mathrm{e}_2+2\mathrm{f}_2)}{2(\mathrm{L}+2\mathrm{M})^2} - \frac{\mathrm{e}_2 c}{3\mathrm{L}(\mathrm{L}+2\mathrm{M})} \\ &+\frac{\mathrm{e}_2 c(1-c)\left[\mu_1(k_2-k_1)+(k_1+2\mu_1)(\mu_2-\mu_1)\right]}{6\mu_1(k_1+\mu_1)\mathrm{L}^2(\mathrm{L}+2\mathrm{M})}\end{aligned} \tag{61}$$

where we have defined the coefficients

$$\mathsf{L} = c + (1 - c)\left[1 + \frac{1}{2}\frac{k_1 + 2\mu_1}{k_1 + \mu_1}\left(\frac{\mu_2}{\mu_1} - 1\right)\right] \tag{62}$$

$$\mathsf{M} = (1 - c)\frac{1}{4(k_1 + \mu_1)} \times \left[2k_2 - k_1\left(1 + \frac{\mu_2}{\mu_1}\right) - 2(\mu_2 - \mu_1)\right] \tag{63}$$

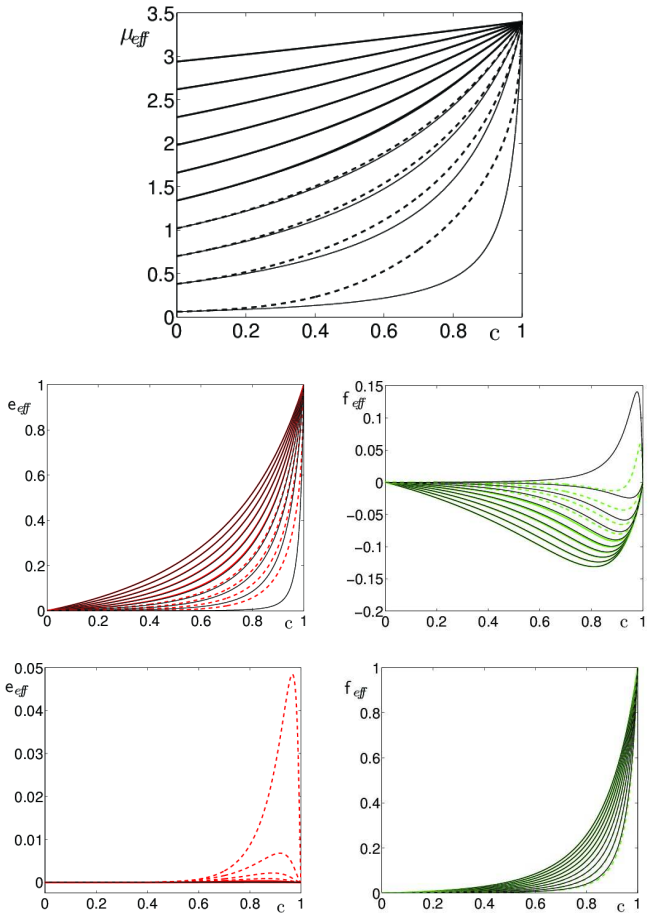

Figure 7: Results for the composite structure with the linear matrix (inhomogeneity harder than the matrix): comparison of the general theory given in Eqs.(54)-(57) (coloured lines, dashed for positive matrix Poisson ratio and solid for negative matrix Poisson ratio) with the old theory given in Eqs.(58)-(61) (thin black lines). The first plot represents the linear result for μ_{eff} *; the two couples of nonlinear results for* e_{eff} *and* f_{eff} *correspond to* $\mathrm{e}_2 = 1, \mathrm{f}_2 = 0$ *and* $\mathrm{e}_2 = 0, \mathrm{f}_2 = 1$*, respectively. We have adopted the parameters* $k_1 = 1$*,* $0 < \mu_1 < 3k_1$ *(or equivalently* $-1 < \nu_1 < 1/2$*) sampled through 10 equispaced values corresponding to lines in figures,* $k_2 = 10$*,* $\nu_2 = 0.33$*.*

It is important also to consider the first order development of previous expressions with respect to the volume fraction c. We straightforwardly obtain

$$\mu_{eff} = \mu_1 + \frac{2\mu_1(\mu_2 - \mu_1)(k_1 + \mu_1)}{k_1\mu_2 + 2\mu_1\mu_2 + k_1\mu_1}c + o(c^2) \tag{64}$$

$$k_{eff} = k_1 + \frac{(k_2 - k_1)(k_1 + \mu_1)}{\mu_1 + k_2}c + o(c^2) \tag{65}$$

Similarly, for the effective nonlinear elastic moduli we get

$$\mathrm{f}_{eff} = \frac{(k_1 + \mu_1)^3(\Xi_e \mathrm{e}_2 + \Xi_f \mathrm{f}_2)}{2(k_1\mu_2 + 2\mu_1\mu_2 + k_1\mu_1)^2(\mu_1 + k_2)^3} c + o(c^2) \tag{66}$$

$$\mathrm{e}_{eff} = \frac{4(k_1 + \mu_1)^3 \mu_1^2}{(k_1\mu_2 + 2\mu_1\mu_2 + k_1\mu_1)^2(\mu_1 + k_2)} \mathrm{e}_2 c + o(c^2) \tag{67}$$

where the coefficients Ξ_e and Ξ_f introduced in Eq.(66) are given by

$$\Xi_e = [k_1(\mu_1 + \mu_2) + 2\mu_1\mu_2]^2 - 4\mu_1^2(k_2 + \mu_1)^2 \tag{68}$$

$$\Xi_f = 2(k_1\mu_2 + 2\mu_1\mu_2 + k_1\mu_1)^2 \tag{69}$$

We draw a first comparison by analysing the first order expansions (for low values of the volume fraction c) of the general theory obtained in the present paper. The proposed nonlinear homogenization scheme yields the following results: from the linear point of view, by using Eqs.(54) and (55) we obtain, for diluted structures ($c<<1$), the same expressions given in Eqs.(64) and (65). On the other hand, for the nonlinear part we can use Eqs.(56) and (57) and, therefore, we have the possibility to consider the nonlinear behavior of the matrix, not accounted for in Eqs.(66) and (67). Their form becomes

$$\mathrm{f}_{eff} = \mathrm{f}_1 + \frac{\frac{1}{2}(\mathsf{A}\mathrm{e}_1 + \mathsf{B}\mathrm{f}_1 + \mathsf{C}\mathrm{e}_2 + \mathsf{D}\mathrm{f}_2)c}{(k_1\mu_2 + 2\mu_1\mu_2 + k_1\mu_1)^2(\mu_1 + k_2)^3} + o(c^2) \tag{70}$$

$$\mathrm{e}_{eff} = \mathrm{e}_1 + \frac{(\mathsf{E}\mathrm{e}_1 + \mathsf{F}\mathrm{f}_1 + \mathsf{G}\mathrm{e}_2)c}{(k_1\mu_2 + 2\mu_1\mu_2 + k_1\mu_1)^2(\mu_1 + k_2)} + o(c^2) \tag{71}$$

where the coefficients $\mathsf{A},\mathsf{B},\mathsf{C},\mathsf{D},\mathsf{E},\mathsf{F}$ and G are not reported here for the sake of brevity. When the matrix is linear we have the coincidence of Eqs.(66) and (67) with Eqs.(70) and (71). In fact, in this case we have $\mathrm{e}_1 = \mathrm{f}_1 = 0$ and the following relation are satisfied: $\mathsf{C} = (k_1 + \mu_1)^3 \Xi_e$, $\mathsf{D} = (k_1 + \mu_1)^3 \Xi_f$ and $\mathsf{G} = 4\mu_1^2(k_1 + \mu_1)^3$.

A first general property can be therefore stated as follows. The two following results are exactly coincident: (i) the first order expansions of the effective medium theory for a dispersion of non linear inhomogeneity in a linear matrix; (ii) the first order expansions of the exact effective results for a composite cylinder (with a linear shell). We infer that the results obtained in the present paper for a composite cylinder can be also applied to the case of dispersions (at least for the dilute situation). The important point is that now we are able to take into consideration both the possible nonlinearity of the matrix and the nonlinear behavior of the embedded cylinders. To better explain this issue we show in Figs.6 and 7 a comparison between the new results stated in Eqs.(54)-(57) (coloured lines) with the old theory given in Eqs.(58)-(61) (thin black lines). Clearly, in order to draw a coherent comparison we have adopted a linear matrix in our general solution described by Eqs.(54)-(57). We have presented the effective nonlinear parameter on the complete range $0 < c < 1$ of the volume fraction for three different compressibility contrasts: $k_2 = 0.1k_1$ in Fig.6, and $k_2 = 10k_1$ in Fig.7. We deduce a good agreement between the theories, except for e_{eff} when $\mathrm{e}_2 = 0$. In fact, in this case with $\mathrm{e}_2 = 0$ the old theory provides $\mathrm{e}_{eff} = 0$ while the new formalism gives a result different from zero because of the strong coupling among the different nonlinear properties. However, we remark that the values of e_{eff} with $\mathrm{e}_2 = 0$ are quite negligible also when calculated with the complete theory. In general, the small differences between the new predictions given in Eqs.(54)-(57) and the former theory resumed in Eqs.(58)-(61) can be explained as follows. New expressions are exact (up to the second order of nonlinearity) for the composite cylinder geometry and, therefore, they can not perfectly represent the random and isotropic distribution of fibers. On the other hand, the former result is an approximation specifically developed for the random structure. It is rather interesting to observe a good concordance between the different approaches.

2.2 Analysis of heterostructures composed of magnetoelastic and piezoelectric phases

Magneto-electro-elastic and multiferroic heterostructures have become one of the hottest topics of condensed matter physics in recent years (R. Ramesh and N. A. Spaldin, Nat. Mater. 6, 21, 2007; C.W. Nan,M. I. Bichurin, S. Dong, D. Viehland, and G. Srinivasan, J. Appl. Phys. 103, 031101, 2008). The coexistence of electric, magnetic, and elastic subsystems brings out novel physical phenomena and offers possibilities for new devices, such as sensors, actuators, transducers, and memories. Of paramount interest is the cross coupling between the magnetic and electric orders. In fact, the magnetic field control of electric polarization and the electric field control of magnetization have been observed in different materials (T. Kimura, T. Goto, H. Shintani, K. Ishizaka, T. Arima, and Y. Tokura, Nature, London, 426, 55, 2003; V. Garcia, M. Bibes, L. Bocher, S.Valencia, F. Kronast, A.Crassous, X. Moya, S. Enouz-Vedrenne, A. Gloter, D. Imhoff, C. Deranlot, N. D. Mathur, S. Fusil, K. Bouzehouane, and A. Barthélémy, Science 327, 106, 2010). However, because of the weak magnetoelectric coupling of most single-phase systems, the introduction of composites, such as ferromagnetic-ferroelectric heterostructures, offers a promising route for obtaining strong cross couplings. In these structures, the coupling between polarization and magnetization is mechanically mediated through the magnetostrictive and the piezoelectric properties of the components. Typically, the heterogeneous structure is multilayered or composed of a ferromagnetic nanoparticle in contact with or embedded into a ferroelectric substrate or matrix. The determination of the exact distribution of the elastic fields in the structure is crucial for quantifying the coupling between the ferroic phases. Therefore the nanomechanical techniques, e.g., based on the multiphysics Eshelby theory, are of primary importance and must be combined with ferromagnetic and/or ferroelectric models in order to obtain the whole picture of the heterostructures behaviour. One of the most important reasons for considering multiferroic materials and structures comes from the global demand for low-power devices. In fact, it is generally accepted that the factor limiting the down scaling and the high integration level in standard semiconductor electronics is the power dissipation. The energy needed for switching the state of a bit in a standard electronic device is equal to at least $Nk_BT\ln(1/p)$, where N is the numbers of electrons (weakly or non interacting carriers) involved in the process, k_B is the Boltzmann constant, T is the temperature and p is the bit error probability. On the other hand, if the information is encoded in the magnetization state of a monodomain ferromagnet (with M strongly interacting spins), the switching process dissipates an energy equal to about $k_BT\ln(1/p)$, independently of the number M of spins. Because of this remarkable result, ferromagnetic and multiferroic nanolayers and nanoparticles are attracting increasing attention for computing architectures and for systems based on energy harvesting techniques. In particular, mechanically induced rotation of magnetization consumes extremely low energies and is very appropriate for nanomagnetic logic (N. D'Souza, J. Atulasimha, and S. Bandyopadhyay, J. Phys. D: Appl. Phys. 44, 265001, 2011; N. A. Pertsev and H. Kohlstedt, Nanotechnology 21, 475202, 2010). Among all the above mentioned applications, multiferroic or magnetoelectric random access memories (RAM) are paradigmatic examples promising nonvolatile magnetic storage and low power consumption. In these devices, the information is stored in different magnetization states of a ferromagnetic phase and the switching is controlled by electric and/or elastic actions. Within the IEMN central laboratory a new structure has been proposed for a stress-mediated magnetoelectric memory element. This line of research has therefore dealt with the analytical/numerical static/dynamic and thermal analysis of this device.

2.2.1.Static/dynamic nanomechanical and nanomagnetic analysis of magnetoelectric memories

(*Stefano Giordano, Yannick Dusch, Nicolas Tiercelin, Philippe Pernod and Vladimir Preobrazhensky, Combined nanomechanical and nanomagnetic analysis of magnetoelectric memories, PHYSICAL REVIEW B 85, 155321, 2012, Yannick Dusch, Vasyl Rudenko, Nicolas Tiercelin, Stefano Giordano, Vladimir Preobrazhensky, and Philippe Pernod, Hysteretic magnetoresistance in stress controled magnetic memory devices, Nanomaterials and nanostructures 2, 44, 2012, Nicolas Tiercelin, Yannick Dusch, Alexey Klimov, Stefano Giordano, Vladimir Preobrazhensky, and Philippe Pernod, Room temperature magnetoelectric memory cell using stress-mediated magnetoelastic switching in nanostructured multilayers, APPLIED PHYSICS LETTERS 99, 192507, 2011*)

Numerous efforts are made in order to develop the next generation of random access memories, possibly non volatile, having low power consumption and high integration density. Recently, the different existing approaches and technologies have been compared and discussed: one promising solution is based on

nonlinear magnetostrictive (ferromagnetic) particles embedded in a piezoelectric matrix. In this activity, we have outlined a procedure able to evaluate all the physical field in the system represented in Fig. 1, where the magnetization orientation inside the particle can be controlled through ad hoc externally applied fields. In particular, a bi-stable behaviour (controlled by the applied electric field) can be obtained and it could be useful for applications to memory cells design.

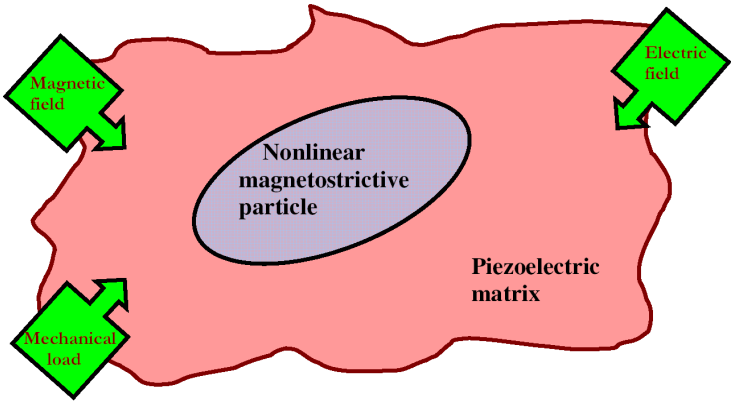

Fig. 1. Structure of the system under investigation: a nonlinear magnetostrictive particle embedded in a piezoelectric matrix. The externally applied electric, magnetic and mechanical fields are indicated and they can possibly control the magnetization orientation inside the particle.

To begin, we take into consideration a particle which exhibits ferromagnetic behaviour. We suppose that the size of the particle is small enough to assure that the particle can be treated as a single ferromagnetic domain. It means that, in any case, inside the inhomogeneity an uniform magnetization appears and it is given by $\vec{M} = M_s \vec{\gamma}$ where M_s is the constant intensity of the magnetization (saturation depending on the material under consideration) and $\vec{\gamma} = (\gamma_1, \gamma_2, \gamma_3)$ is the unknown unit vector fixing the direction of the magnetization. The principal aim of the following procedure is that of determining the orientation $\vec{\gamma}$ in terms of the externally applied fields and of the boundary conditions. It can be obtained by minimizing the energy function of the single domain particle, as follows

$$w(\vec{\gamma}) = -\mu_0 \underbrace{M_s \vec{\gamma}}_{\vec{M}} \cdot \vec{H} + \varphi(\vec{\gamma}) - \hat{T} : \hat{\varepsilon}_\mu(\vec{\gamma}) \tag{1}$$

the first term represents the magnetic interaction energy where $\vec{H}$ is the local magnetic field measured inside the particle: this is the Zeemann term and it describes the influence of the magnetic field on the orientation of the magnetization. The second term $\varphi(\vec{\gamma})$ represents the anisotropic energy depending on the crystal class of the material. These directions are connected to the crystallographic structure and the magneto-crystalline energy is minimum when $\vec{\gamma}$ is parallel to the easy axis. The third term represents the elastic interaction energy where $\hat{T}$ is the local stress tensor measured inside the particle and $\hat{\varepsilon}_\mu(\vec{\gamma})$ is the strain tensor induced by the magnetization. Both $\hat{T}$ and $\hat{\varepsilon}_\mu(\vec{\gamma})$ are uniform within the single domain particle. Moreover, the local magnetic field and stress tensor inside the particle depend on the environment where the particle is embedded and on the external fields applied to the structure. To conclude we can state the constitutive equations of the particle in the following way. For the magnetic point of view we have $\vec{B} = \mu_0(\vec{H} + \vec{M}) = \mu_0[\vec{H} + M_s\vec{\gamma}(\vec{H}, \hat{T})]$ where $\vec{B}$ is the magnetic induction. For the elastic point of view we have $\hat{T} = \hat{L}_2\{\hat{\varepsilon}_0 - \hat{\varepsilon}_\mu[\vec{\gamma}]\} = \hat{L}_2\{\hat{\varepsilon}_0 - \hat{\varepsilon}_\mu[\vec{\gamma}(\vec{H}, \hat{T})]\}$ where $\hat{\varepsilon}_0$ is the local strain tensor and $\hat{L}_2$ is the stiffness tensor of the particle. As above stated, the magnetic field $\vec{H}$ entering the energy in Eq.(1) is the local (internal) magnetic field and, therefore, it is important to obtain its relationships with the externally applied magnetic field $\vec{H}^\infty$. To this aim we can utilize a recent results which is valid for an arbitrary nonlinear and anisotropic ellipsoidal particle embedded in a linear but anisotropic matrix. Finally, after straightforward calculations, we obtain the following result: the local magnetic field can be explicitly written in terms of the remotely

applied magnetic field and of the internal magnetization orientation $\vec{H} = \vec{H}\left(\vec{H}^{\infty}, \vec{\gamma}\right)$. On the other hand, the coupling with the external electric and elastic fields is mediated by the piezoelectric matrix, where the particle is embedded. As result of the application of the electro-elastic Eshelby theory we can obtain the local elastic stress in terms of the external elastic and electric fields and of the magnetization direction through a function $\hat{T} = \hat{T}\left(\hat{\varepsilon}^{\infty}, \vec{E}^{\infty}, \vec{\gamma}\right)$ which is available in closed form. We can also exploit these dependences as

$$\begin{aligned} \vec{H} &= \vec{H}\left(\vec{H}^{\infty}, \vec{\gamma}\right) = \hat{A}\vec{H}^{\infty} + \hat{B}\vec{\gamma} \\ \hat{T} &= \hat{T}\left(\hat{\varepsilon}^{\infty}, \vec{E}^{\infty}, \vec{\gamma}\right) = \hat{C}\hat{\varepsilon}^{\infty} + \hat{D}\vec{E}^{\infty} + \hat{F}\left[\hat{\varepsilon}_{\mu}(\vec{\gamma}) - \hat{\varepsilon}_{\mu}(\vec{\gamma}_0)\right] \end{aligned} \tag{2}$$

where the tensors $\hat{A}, \hat{B}, \hat{C}, \hat{D}$ and $\hat{F}$ can be obtained through the procedures previously outlined. We can define a new energy function $\tilde{w}$ as follows

$$\tilde{w} = -\mu_0 M_s \vec{\gamma} \cdot \hat{A}\vec{H}^{\infty} - \frac{1}{2}\mu_0 M_s \vec{\gamma} \cdot \hat{B}\vec{\gamma} + \varphi(\vec{\gamma}) - \hat{C}\hat{\varepsilon}^{\infty} : \hat{\varepsilon}_{\mu}(\vec{\gamma}) - \hat{D}\vec{E}^{\infty} : \hat{\varepsilon}_{\mu}(\vec{\gamma}) - \frac{1}{2}\hat{F}\hat{\varepsilon}_{\mu}(\vec{\gamma}) : \hat{\varepsilon}_{\mu}(\vec{\gamma}) + \hat{F}\hat{\varepsilon}_{\mu}(\vec{\gamma}_0) : \hat{\varepsilon}_{\mu}(\vec{\gamma}) \tag{3}$$

which is much more convenient since it leads to the final magnetization orientation directly in terms of the external fields applied to the structure. In other words, the minimum of the energy function $\tilde{w}$ represents the real orientation of the magnetization when all the external field are fixed.

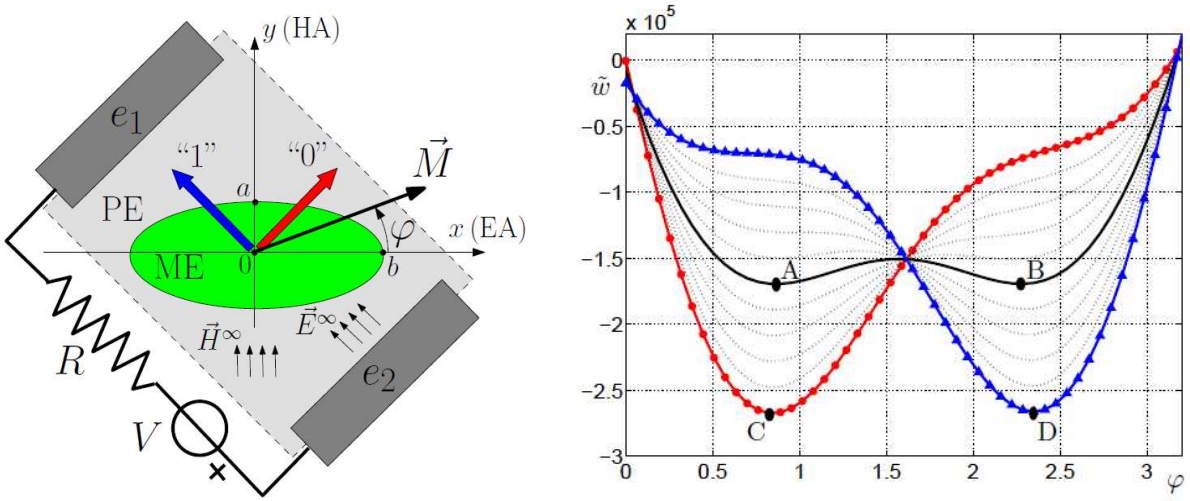

Fig.2. (left) Scheme of the magnetoelastic (ME) particle embedded in the piezoelectric (PE) matrix. The easy axis (EA) and the hard axis (HA) of the particle are aligned with the reference frame (x,y). The resulting two stable positions for the magnetization vector correspond to the values "0" and "1" of the stored bit. (right) Curves $\tilde{w}$ [J/m^3] for different values of the applied voltage ranging from -0.5V (blue line with triangles) to 0.5V (red line with circles). The solid black line corresponds to 0V and shows the two stable points A and B.

In our specific case we adopt a external magnetic field along the y axis (see Fig.2 left): the competition of this latter with the uniaxial anisotropy of the magneto elastic particle (along the x axis) generates two stable position corresponding to the possible states of the memory. These two positions appear around $\varphi = \pi/4$ and $\varphi = 3\pi/4$ with a magnetic field of 50A/m (it can be proved by minimizing Eq.(3)). In Fig.2 (right) one can find the plot of the energy function with magnetization direction (cos φ, sin φ, 0) (on the plane z = 0) in terms of the angle φ. The solid black line corresponds to the case without electric field and the bistable behaviour is identified by the couple of minima A and B. The external electric field and the piezo-electric matrix represent the system used for switching the state of the memory. We assume that the matrix is polarized along the direction $\varphi = 3\pi/4$. In Fig.2 (right) one can also find the plot of the energy function for different values of the applied voltage: it ranges from 0.5V (red line with circles) to -0.5V (blue line with triangles). It is evident by the profile of the energy function that the electric field is able to switch the state of the memory without the knowledge of the stored bit. Given the size of the magnetic, the magnetic system is assumed to be monodomain. Therefore, the dynamics of the magnetization direction is described by the Landau-Lifshitz-Gilbert (LLG) equation

$$\frac{d\vec{\gamma}}{dt} = -\frac{\mathcal{G}}{M_s(1+\alpha^2)}\left[\vec{\gamma}\wedge\frac{\partial\tilde{w}}{\partial\vec{\gamma}} - \alpha\vec{\gamma}\wedge\left(\vec{\gamma}\wedge\frac{\partial\tilde{w}}{\partial\vec{\gamma}}\right)\right] \tag{4}$$

The results are shown in Fig.3. Here, the results of the integration of Eq. (4) are shown for two different values of the applied voltage: ±0.3 V (which means E = ±2.3 × 10^6 V/m) and ±0.5 V (which means E = ±3.85 × 10^6 V/m). A complete cycle with the two switching phases is represented and reveals two important properties: (i) the transition times are always in the sub-nanosecond scale (<0.4 ns) and (ii) such times decrease with larger applied voltages. While in the static analysis of the system we have described the commutation strategy on the plane, in the actual dynamic case, the complex behaviour is the result of the interplay between the in-plane and the out-of-plane motion of the vector $\gamma(t)$. This point becomes evident by the observation of the component γ_z in the second panel of Fig.3. Interestingly enough, we observe that the values of the stress are inverted passing from the point A to the point B (see Fig.2) because of the symmetry of the system. Nevertheless, such a geometrical symmetry does not lead to the same dynamical features of the switching phases B-C and A-D (see Fig.3). In fact, the phase B-C is characterized by a compression inducing a planar anisotropy from the magnetic point of view. On the other hand, the phase A-D is characterized by a traction inducing an axial anisotropy for the magnetization. To conclude, we discuss the results of the energetic analysis of the system. The dissipated energy during switching processes derives from the charge/discharge of the effective capacitor and from the damped precession of the magnetization: the total energy amount for a switching phase corresponds to 3 × 10^{-17}J with the applied voltage of ±0.3 V and to 8 × 10^{-17}J with ±0.5 V. These values are strongly competitive when compared with most nonvolatile memory technologies. . In fact, some values of the switching energy are as follows: 0.02pJ for the spin transfer torque RAM (STTRAM), 2pJ for the ferroelectric RAM (FRAM), 2pJ for the copper bridge RAM (CBRAM), 2pJ for the dynamicRAM (DRAM), and 10pJ for the carbon nanotube RAM (NRAM). Moreover, the thermal stability can be assured by the energy barrier between the states A and B corresponding to 1.7 × 10^{-18}J 400k_BT. This value of the energy barrier is sufficiently high to inhibit spontaneous magnetization flipping due to thermal effects. To conclude, dynamics of the magnetization switching between orthogonal positions was studied using the Eshelby theory combined with the LLG equation.

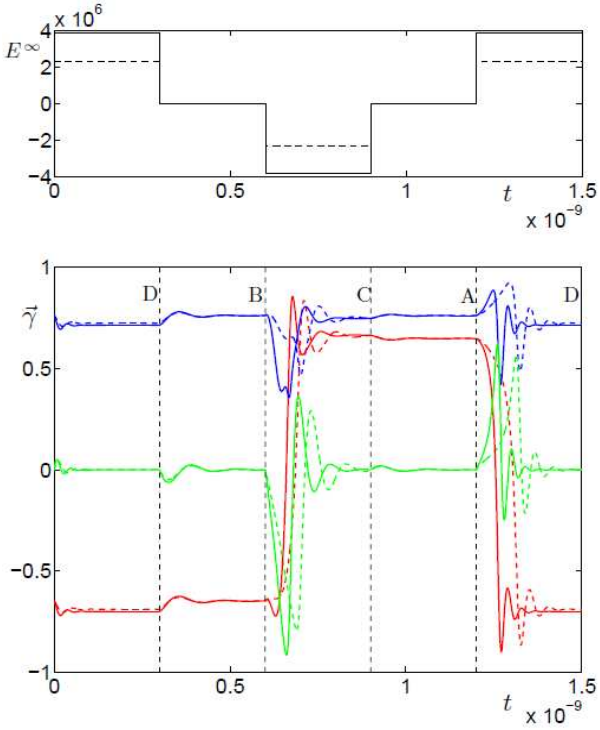

Fig.3. Time behaviour of the imposed electric field and the corresponding evolution of the magnetization direction (x red, y blue and z green) for a voltage equals to ±0.5V (solid lines) and ±0.3V (dashed lines). A complete cycle with the two switching phases is represented and reveals two important properties: (i) the transition times are always <0.3nsec and (ii) such times decrease with larger applied voltages.

2.2.2.Thermal analysis of magnetoelectric memories

(*Stefano Giordano, Yannick Dusch, Nicolas Tiercelin, Philippe Pernod and Vladimir Preobrazhensky, Thermal effects in magnetoelectric memories with stress-mediated switching, Journal of Physics D: Applied Physics 46, 325002, 2013, Stefano Giordano, Yannick Dusch, Nicolas Tiercelin, Philippe Pernod and Vladimir Preobrazhensky, Stochastic magnetization dynamics in single domain particles, Eur. Phys. J. B 86, 249, 2013*)

The static and dynamic behaviour of the memory element has been described in the previous section where, however, the temperature effects were neglected. Here, we illustrate the analysis of the dynamical response of this heterostructure at finite temperature and, in particular, we determine the switching time, the error probability and the energy dissipation associated to the process of writing a bit. These important quantities have been studied in terms of the ratio k_BT/v, describing the compromise between temperature and particle size. As an important result we develop a procedure for determining the maximum admissible value of the ratio k_BT/v. It means that we are able to find the maximum operating temperature if the size of the nanoparticle is fixed or, conversely, the minimum volume of the nanomagnet when the temperature is imposed. In order to consider the temperature effects, the Landau-Lifshitz-Gilbert (LLG) equation has been generalized by means of the Brown formalism, i.e. by introducing a random field acting on the magnetization (Brown W F 1959 Relaxational Behavior of Fine Magnetic Particles J. Appl. Phys. 30 S130; Brown W F 1963 Thermal Fluctuations of a Single-Domain Particle J. Appl. Phys. 34 1319; Brown W F 1963 Thermal Fluctuations of a Single-Domain Particle Phys. Rev. 130 1677; Brown W F 1979 Thermal fluctuation of fine ferromagnetic particles IEEE Trans. Magn. 15 1196). This approach leads to a stochastic Langevin equation or, equivalently, to a Fokker-Planck equation describing the time evolution of the density probability of the magnetization direction (Risken H 1989 The Fokker-Planck equation, Berlin: Springer Verlag). The numerical solution of the Langevin LLG stochastic equation allows us to obtain a complete picture on the dynamic behaviour (i.e. the commutation strategy) of the system at finite temperature. In particular, these results are useful to design the device in agreement with the desired balance between operating temperature and particle size. In order to introduce thermal fluctuations we assume the Brown hypothesis affirming that the effects of the temperature can be mimicked by an addictive random field acting on the magnetization. It means that we substitute $\frac{\partial\tilde{\vec{w}}}{\partial\tilde{\gamma}}$ with $\frac{\partial\tilde{\vec{w}}}{\partial\tilde{\gamma}}+\mathcal{D}\vec{n}$ in Eq.(4) of previous section, where n_i is a stochastic process with three main properties: its average value is zero at any time, it is completely uncorrelated (white), and it is Gaussian. The system obtained is a stochastic differential equation (SDE). The typical tool for studying SDEs is the Fokker-Planck methodology based on a partial differential equation describing the dynamic of the density probability of the state of the system. The obtained Fokker-Planck equation is particularly useful for obtaining a simplified version of the Langevin LLG system: in fact, a three-dimensional random vector has been added for introducing the fluctuations in a system with two variables (ϕ and ϑ). There is no need to embed the system in a three-dimensional space and, moreover, there are important reasons for not doing so. We therefore consider the following new version of the Langevin LLG system where only two noise terms are considered

$$\begin{aligned}\dot{\varphi} &= -\frac{\mathcal{G}}{M_s(1+\alpha^2)\sin\vartheta}\left[\frac{\partial\tilde{w}}{\partial\vartheta}+\frac{\alpha}{\sin\vartheta}\frac{\partial\tilde{w}}{\partial\varphi}\right]+\frac{1}{\sin\vartheta}\sqrt{\frac{1}{2\tau_N}}n_\phi,\\ \dot{\vartheta} &= -\frac{\mathcal{G}}{M_s(1+\alpha^2)}\left[-\frac{1}{\sin\vartheta}\frac{\partial\tilde{w}}{\partial\varphi}+\alpha\frac{\partial\tilde{w}}{\partial\vartheta}\right]+\frac{1}{2\tau_N}\frac{\cos\vartheta}{\sin\vartheta}+\sqrt{\frac{1}{2\tau_N}}n_\theta.\end{aligned} \tag{1}$$

Here we have introduced the so-called Néel time $\tau_N=\frac{M_s(1+\alpha^2)v}{2\alpha\mathcal{G}k_BT}$. From the theoretical point of view Eq. (1) is coherent and elegant since the SDE lives completely on the spherical surface without the need for a three-dimensional embedding (it represents the covariant formulation of the SDE on the spherical manifold). Moreover, from the computational point of view Eq.(1) is convenient since two random numbers must be generated, instead of the three ones needed for the implementation of the classical Brown scheme.

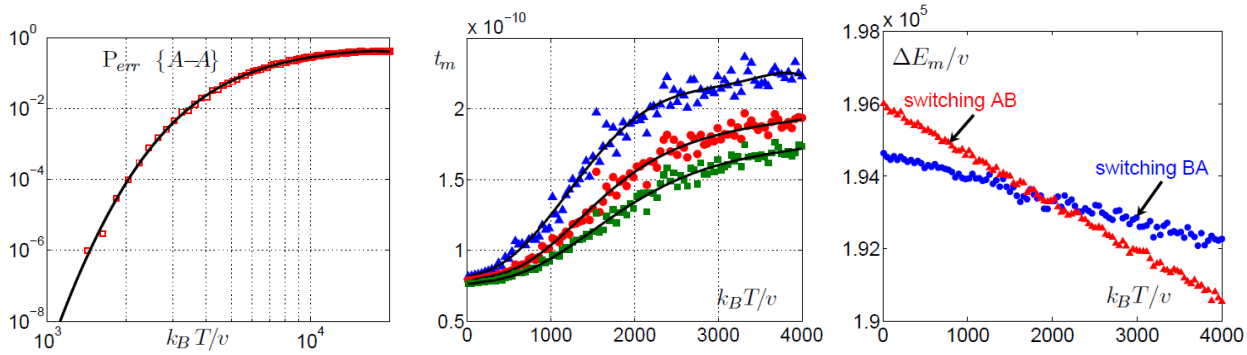

Fig.1. a) Stability analysis of the switching A (V = +0.5V) – A (V = 0V): error probability in terms of the ratio k_BT/v. b) Switching process between states A and B (traction, V =−0.5V): switching time t_m versus k_BT/v for three different values of the precision parameter. c) Energy dissipation during switching phases: magnetic dissipated energy $\Delta E_m/v$ in terms of k_BT/v for both transitions A-B and B-A.

For any value of k_BT/v we follow N_t trajectories for a long time and we determine the number of unwanted switching towards the other state. The error probability is given by the ratio between this number and the total number N_t of trajectories. Such a number N_t is dynamically adjusted and it corresponds to 10^4 for the higher values of k_BT/v (sizeable error probability) and to 5×10^6 for the lower values of k_BT/v (very low error probability). We obtained quite the same curve of P_{err} (Fig.1a) versus k_BT/v for both transitions A-A and B-B. It means that the error probability is a symmetric quantity for our system. Moreover, we observe that if $k_BT/v \rightarrow +\infty$ then $P_{err} \rightarrow 1/2$, a value exactly quantifying the total information loss. For any value of k_BT/v in the range from 10 J/m^3 to 4×10^3 J/m^3 we generate 10^4 trajectories of the magnetization and we evaluate their average values. In Fig.1b we show the results for the switching A-B corresponding to the applied traction at $V = -0.5$V. Of course, the switching times obtained (hundreds of ps) must be realistically augmented in order to consider different phenomena not contemplated in our model: response time of the piezoelectric matrix, time to transfer the stress to the magnetic particle, and delays of the electronic system generating the electric pulses. We can estimate a loss of velocity of about ten times, resulting in final switching times of some nanoseconds. However, the values of the writing time are in any case strongly competitive with other standard or spintronic memory technologies. To conclude, we show in Fig.1c the results concerning the energy consumption during the switching phases. It is calculated by taking into account two contributions. The first one ΔE_e represents the so-called CV^2 dissipation and it can be simply determined when the geometry of the system is given. The second contribution ΔE_m can be evaluated by determining the variation of the energy particle during the transitions phases. This procedure can be numerically implemented within the integration scheme of the Langevin system. As before, the average values are determined with the Monte Carlo technique. Interestingly enough, we note that the temperature effects are stronger in the transition A-B. The numerical integration leads to the results shown in the third panel of Fig.1, where $\Delta E_m/v$ is plotted versus k_BT/v for both transitions B-A and A-B. We observe that there is only a very slight (linear) dependence of $\Delta E_m/v$ on k_BT/v. In fact, we can approximate $\Delta E_m/v = 2 \times 10^5$J/m^3 for any value of k_BT/v. For a particle with v = 10^{-22}m^3 we obtain $\Delta E_m = 2 \times 10^{-17}$J and the total switching energy is therefore $\Delta E = \Delta E_e + \Delta E_m = 9.5 \times 10^{-17}$J.

2.2.3. Magneto-electro-elastic effective properties of multilayered laminated materials

(*S. Giordano, M. Goueygou, N. Tiercelin, A. Talbi, P. Pernod, and V. Preobrazhensky, Magneto-electro-elastic effective properties of multilayered artificial multiferroics with arbitrary lamination direction, International Journal of Engineering Science 78, 134-153, 2014, Stefano Giordano, Explicit nonlinear homogenization for magneto-electro-elastic laminated materials, Mechanics Research Communications 55, 18-29, 2014*)

This section deals with the determination of the effective response of a multilayered or laminated heterostructure composed of materials with an arbitrary coupled anisotropic behaviour. In particular, we elaborate a fully algebraic technique for obtaining the homogenized parameters of a magneto-electro-elastic system (artificial multiferroic). To do this, we load the system with an arbitrary electromagnetic/mechanical generalized action and we calculate the coupled physical fields within each layer. Then, we determine the average values of these fields, eventually obtaining the effective tensor response of the whole structure. The theory has been developed for an arbitrary lamination direction, taken into account by means of an *ad hoc* lamination tensor $\mathsf{P}_{\vec{n}}$ whose components are obtained in closed form. Its implementation is based on simple matrix algebra and does not require any extensive computation. Moreover, the formalism has been generalised to graded structures and to multiple-rank laminated materials.

Magneto-electro-elastic composites and multiferroic phases represent a new class of materials with several potential applications in modern nanoscience and nanotechnology. Their peculiar characteristic is the cross-coupling between electric polarization and magnetization. This interaction offers new possibilities for functional electronic devices, such as sensors, actuators, transducers and memories. Such materials can be realized through single phases or composite structures. However, because of the weak magneto-electric coupling (at very low temperature) of most single-phase systems, the introduction of composites offers a promising route for obtaining strong interactions at room temperature. In these materials, the magneto-electric coupling is strain or stress-mediated because of the magnetostrictive and piezoelectric properties of the components. From the historical point of view, one of the first sintered magnetoelectric composites was based on the combination $BaTiO_3$-$NiFe_2O_4$ with small additions of cobalt and manganese (van den Boomgaard, J., and Born, R. A. J., 1978, A sintered magnetoelectric composite material $BaTiO_3$-$Ni(Co,Mn)Fe_2O_4$, *J. Materials Science*, 13, 1538-1548). More recently, laminated structures with a significant magnetoelectric coupling have been proposed and fabricated (Fetisov, L. Y., Perov, N. S., Fetisov, Y. K., Srinivasan G., and Petrov, V. M., 2011, Resonance magnetoelectric interactions in an asymmetric ferromagnetic-ferroelectric layered structure. *J. Appl. Phys.*, 109, 053908, Tiercelin, N., Talbi, A., Preobrazhensky, V., Pernod, P., Mortet, V., Haenen, K., and Soltani, A., 2008, Magnetoelectric effect near spin reorientation transition in giant magnetostrictive-aluminum nitride thin film structure. *Appl. Phys. Lett.*, 93, 162902, Tiercelin, N., Preobrazhensky, V., Pernod, P., and Ostaschenko, A., 2008, Enhanced magnetoelectric effect in nanostructured magnetostrictive thin film resonant actuator with field induced spin reorientation transition. *Appl. Phys. Lett.*, 92, 062904). An exhaustive analysis of the theoretical modelling of magnetostrictive-piezoelectric nanostructures has been recently developed (Bichurin, M. I., Petrov, V. M., Averkin, S. V., and Liverts, E., 2010, Present status of theoretical modeling the magnetoelectric effect in magnetostrictive-piezoelectric nanostructures. Part I: Low frequency and electromechanical resonance ranges. *J. Appl. Phys.*, 107, 053904, Bichurin, M. I., Petrov, V. M., Averkin, S. V., and Liverts, E., 2010, Present status of theoretical modeling the magnetoelectric effect in magnetostrictive-piezoelectric nanostructures. Part II: Magnetic and magnetoacoustic resonance ranges. *J. Appl. Phys.*, 107, 053905). Although very efficient multi-scale computational techniques have been elaborated to homogenize the behaviour of composite structures (Brenner, R., 2009, Numerical computation of the response of piezoelectric composites using Fourier transform. *Phys. Rev. B*, 79, 184106), there is a great interest in working out analytical procedures providing their effective physical properties. In fact, these theoretical approaches are not only stimulating for the encountered mathematical challenges, but also extremely competitive with numerical methods from the computational point of view. Another advantage of these approaches is the possibility to directly optimize some effective properties in terms of microstructural features, e.g. crystallographic orientations and volume fractions of constituents. Here, we elaborate a theoretical methodology for determining the effective properties of multilayered magneto-electro-elastic

heterostructures with an arbitrary lamination direction. This geometry is largely used in modern nanotechnology since, compared to a particulate composite, it exhibits much higher magneto-electric couplings. As for the history of the analysis of laminates, the first pioneering results were obtained by Postma (Postma G. W., 1955, Waves propagation in a stratified medium. *Geophysics* 20, 780-806) and Backus (Backus, G. E., 1962, Long-wave elastic anisotropy produced by horizontal layering. *J. Geophys. Res.*, 67, 4427-4440) for the purely elastic case and by Tartar (Tartar, L., 1979, Estimation de coefficients homogénéisés, *Computing Methods in Applied Sciences and Engineering* ed R Glowinski and J L Lions, Berlin, Springer-Verlag, pp. 364-373) for the purely dielectric one. They developed a general method for determining the effective tensors in the absence of physical couplings and for a fixed lamination direction. Furthermore, other techniques for dealing with piezoelectric and/or magnetoelastic laminated materials were introduced as well (Avellaneda, M., and Olson, T., Effective medium theories and effective electromechanical coupling factors for piezoelectric composites. *J. Intell. Mater. Syst. Struct.*, 4, 82-88, Avellaneda, M., and Harshé, G., 1994, Magnetoelectric effect piezoelectric/magnetostrictive multilayer 2-2 composites. *J. Intell. Mater. Syst. Struct.*, 5, 501-513, Gibiansky, L. V., and Torquato, S., 1999, Matrix laminate composites: Realizable approximations for the effective moduli of piezoelectric dispersions. *J. Mat. Res.*, 14, 49-63). The so-called multiple-rank laminates (i.e. laminates of laminates) were introduced by Maxwell (Maxwell, J. C., 1881, *A Treatise on Electricity and Magnetism,* Oxford, Clarendon), who provided explicit expressions for the conductivities of some third-rank laminates composed of isotropic constituents. A comprehensive analysis of this complex microstructure was performed by Tartar (Tartar, L., 2009, *The General Theory of Homogenization: A Personalized Introduction,* Berlin: Springer-Verlag), who proved a famous equation giving the permittivity tensor of a two-component rank-m laminate in terms of m arbitrary lamination directions. More recently, some approaches have been proposed to deal with fully coupled magneto-electro-elastic laminates (Kim, J. Y., 2011, Micromechanical analysis of effective properties of magneto-electro-thermo-elastic multilayer composites. *Int. J. Eng. Sci.*, 49, 1001-1018, Challagulla, K. S., and Georgiades, A. V., 2011, Micromechanical analysis of magneto-electro-thermo-elastic composite materials with applications to multilayered structures. *Int. J. Eng. Sci.*, 49, 85-104, Bravo-Castillero, J., Rodríguez-Ramos, R., Mechkour, H., Otero, J. A., and Sabina, F. J., 2008, Homogenization of magneto-electro-elastic multilaminated materials. *Q. J. Mech. Appl. Math.*, 61, 311-332, Sixto-Camacho, L. M., Bravo-Castillero, J., Brenner, R., Guinovart-Díaz, R., Mechkourd, H., Rodríguez-Ramos, R., and Sabina, F. J., 2013, Asymptotic homogenization of periodic thermo-magneto-electro-elastic heterogeneous media. Computers and Mathematics with Applications, 66, 2056-2074). Since these formalisms have been elaborated for a fixed lamination direction, here we study the general case concerning an arbitrary lamination direction, which is an important point to thoroughly exploit the anisotropic character of the involved components. We develop a self-consistent fully algebraic technique based on the definition of an *ad hoc* operator $\mathsf{P}_{\vec{n}}$, which allows us to explore the effects of the orientation (indicated by $\vec{n}$) of the interfaces on the overall response of the system. The main result is given by a single exact tensor expression furnishing all effective properties of the laminated material. Typically, for developing a homogenization scheme, one needs to consider the differential equation describing the distribution of physical fields. In contrast, we solved the problem by means of the continuity conditions at the interfaces. This alternative approach is justified by the uniformity of the fields induced in each layer. Finally, the definition of tensor $\mathsf{P}_{\vec{n}}$ allows us to further extend our theory in order to consider (i) graded structures with an arbitrary lamination direction and (ii) rank-m laminates with m arbitrary lamination directions. This is a generalization of the Tartar formula to the magneto-electro-elastic coupling.

In order to take into account all possible couplings among electric, magnetic and elastic quantities, we consider the following generalized relation giving the time variation of the total energy density

$$\frac{\mathrm{d}u}{\mathrm{d}t} = T_{ij}\frac{\mathrm{d}\varepsilon_{ij}}{\mathrm{d}t} + E_i\frac{\mathrm{d}D_i}{\mathrm{d}t} + H_i\frac{\mathrm{d}B_i}{\mathrm{d}t}, \qquad (1)$$

where we have supposed an arbitrarily nonlinear energy function $u = u(\hat{\varepsilon}, \vec{D}, \vec{B})$. Here T_{ij} represents the Cauchy stress tensor, ε_{ij} the infinitesimal strain tensor, E_i and H_i the electric and magnetic fields and, finally, D_i and B_i the electric and magnetic inductions. From Eq.(1), we immediately obtain the constitutive equations in terms of the energy function

$$T_{ij} = \frac{\partial u(\hat{\varepsilon}, \vec{D}, \vec{B})}{\partial \varepsilon_{ij}}, E_i = \frac{\partial u(\hat{\varepsilon}, \vec{D}, \vec{B})}{\partial D_i} \text{ and } H_i = \frac{\partial u(\hat{\varepsilon}, \vec{D}, \vec{B})}{\partial B_i}. \quad (2)$$

In the case of a linear material, we can introduce a tensor relationship

$$\mathsf{K}_0 = \mathsf{L}_0 \mathsf{Z}_0, \quad (3)$$

where we adopted the generalized Voigt notation

$$\mathsf{K}_0^T = \left(T_{11}, T_{22}, T_{33}, T_{23}, T_{13}, T_{12}, E_1, E_2, E_3, H_1, H_2, H_3\right), \quad (4)$$

$$\mathsf{Z}_0^T = \left(\varepsilon_{11}, \varepsilon_{22}, \varepsilon_{33}, 2\varepsilon_{23}, 2\varepsilon_{13}, 2\varepsilon_{12}, D_1, D_2, D_3, B_1, B_2, B_3\right), \quad (5)$$

and we may prove the symmetry $\mathsf{L}_0 = \mathsf{L}_0^T$ (T means matrix transposition).

In addition, we can adopt an alternative version of the generalized Voigt notation leading to the following linear constitutive equation

$$\mathsf{K} = \mathsf{L}\mathsf{Z}, \quad (6)$$

where

$$\mathsf{K}^T = \left(T_{11}, T_{22}, T_{33}, T_{23}, T_{13}, T_{12}, D_1, D_2, D_3, B_1, B_2, B_3\right), \quad (7)$$

$$\mathsf{Z}^T = \left(\varepsilon_{11}, \varepsilon_{22}, \varepsilon_{33}, 2\varepsilon_{23}, 2\varepsilon_{13}, 2\varepsilon_{12}, -E_1, -E_2, -E_3, -H_1, -H_2, -H_3\right), \quad (8)$$

and the symmetry $\mathsf{L} = \mathsf{L}^T$ is still preserved. In this work, we use this latter representation where the quantity L contains the elastic stiffness tensor, the magnetic permeability tensor, the electric permittivity tensor, the piezoelectric tensor, the magnetostrictive tensor and the magnetoelectric tensor. Of course, L may represent any form of anisotropy, i.e. any kind of crystal symmetry.

We consider a single layer composed of a linear material L_1 embedded in a homogeneous space L_0. We consider the system remotely loaded by Z_0 and K_0, which are uniform fields generated by remote sources. These fields are those existing in the entire space L_0 before introducing the layer L_1. We suppose that the interfaces are perpendicular to the axis x_3 (see Fig.1a for details). Moreover, we assume that there is no free electric charge and no electric current distributed on the interfaces and we study the continuity of the physical fields across them. As well known, the continuous components of K across the interface are T_{13}, T_{23}, T_{33}, D_3 and B_3. Similarly, the continuous components of Z are ε_{11}, ε_{12}, ε_{22}, E_1, E_2, H_1 and H_2. We observe that these two sets of continuous components are complementary in the structure of vectors Z and K. It means that the i-th component of Z is continuous if and only if the i-th component of K suffers a discontinuity. This property allows us to build up the following formalism. Since K and $\mathsf{Z} \in \Re^{12}$ we define a first simple set $\mathbf{C}$ containing the integer numbers from 1 to 12: $\mathbf{C} = \{1,2,3,...,12\}$. Then, we can define $\mathbf{C}_\mathsf{K} = \{3,4,5,9,12\} \subset \mathbf{C}$ as the subset containing the positions of continuous components of K. Of course, we have $\text{card}(\mathbf{C}_\mathsf{K}) = n$ having defined $n = 5$. Similarly, we can define $\mathbf{C}_\mathsf{Z} = \mathbf{C} \setminus \mathbf{C}_\mathsf{K} \subset \mathbf{C}$ as the subset containing the positions of continuous components of Z. As before, we have $\text{card}(\mathbf{C}_\mathsf{Z}) = m$ having defined $m = 7$. We introduce now the following matrices

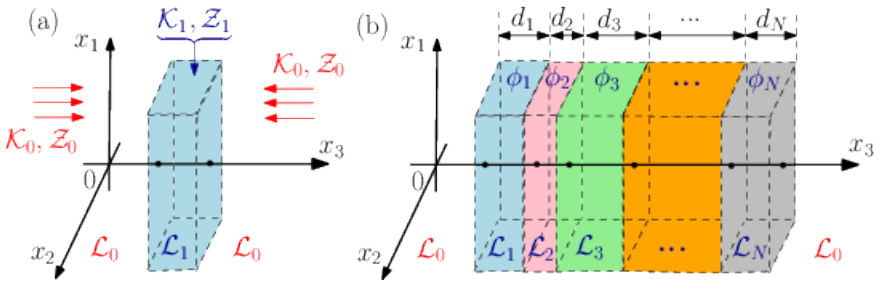

Figure 1: Schematic representation of a single layer embedded in a homogeneous space (a) and a multilayered structure composed of N different components (b).

$$\mathsf{P}=\sum_{i=1}^{n}\sum_{j\in \mathbf{C}_{\mathsf{K}}}\mathsf{F}_{i,j}^{n,n+m}\in \mathbf{M}_{n,n+m}(\Re)\ \textit{and}\ \mathsf{Q}=\sum_{i=1}^{m}\sum_{j\in \mathbf{C}_{\mathsf{Z}}}\mathsf{F}_{i,j}^{m,n+m}\in \mathbf{M}_{m,n+m}(\Re), \tag{9}$$

where $\mathsf{F}_{i,j}^{a,b}\in \mathbf{M}_{a,b}(\Re)$ is an elementary matrix with a rows and b columns with the element (i,j) equal to one and all the others equal to zero. The set $\mathbf{M}_{a,b}(\Re)$ represents the linear space of real matrices with a rows and b columns. Moreover, the symbol $\mathsf{I}_r\in \mathbf{M}_{r,r}(\Re)$ represents the identity matrix of order r and $\mathsf{O}_{ab}\in \mathbf{M}_{a,b}(\Re)$ is the null matrix. The following properties hold on

$$\mathsf{P}\mathsf{P}^T=\mathsf{I}_n\ \textit{and}\ \mathsf{Q}\mathsf{Q}^T=\mathsf{I}_m, \tag{10}$$

$$\mathsf{P}\mathsf{Q}^T=\mathsf{O}_{nm}\ \textit{and}\ \mathsf{Q}\mathsf{P}^T=\mathsf{O}_{mn}, \tag{11}$$

$$\mathsf{P}^T\mathsf{P}+\mathsf{Q}^T\mathsf{Q}=\mathsf{I}_{n+m}, \tag{12}$$

as one can easily verify. The physical meaning of the matrices P and Q becomes evident by considering the following statements. The vector $\mathsf{P}\mathsf{K}\in\Re^n$ contains the continuous components of $\mathsf{K}\in\Re^{n+m}$ across the interface. Similarly, the vector $\mathsf{Q}\mathsf{Z}\in\Re^m$ contains the continuous components of $\mathsf{Z}\in\Re^{n+m}$. Furthermore, other properties will be used in the following developments: the vector $\mathsf{P}^T\mathsf{P}\mathsf{K}\in\Re^{n+m}$ has the same structure as K, but all the discontinuous components are imposed to zero. In other words, we have $(\mathsf{P}^T\mathsf{P}\mathsf{K})_i=\mathsf{K}_i$ if $i\in\mathbf{C}_{\mathsf{K}}$ and $(\mathsf{P}^T\mathsf{P}\mathsf{K})_i=0$ if $i\in\mathbf{C}_{\mathsf{Z}}$. Similarly, $\mathsf{Q}^T\mathsf{Q}\mathsf{Z}\in\Re^{n+m}$ has the same structure as Z, but all the discontinuous components are imposed to zero. It means that $(\mathsf{Q}^T\mathsf{Q}\mathsf{Z})_i=\mathsf{Z}_i$ if $i\in\mathbf{C}_{\mathsf{Z}}$ and $(\mathsf{Q}^T\mathsf{Q}\mathsf{K})_i=0$ if $i\in\mathbf{C}_{\mathsf{K}}$. We remark that this formalism can be adopted to analyse any linear physical coupling described by two dual sets of variables (here K and $\mathsf{Z}\in\Re^{n+m}$) exhibiting the continuity of the complementary components (n components of K and m complementary components of Z) across a given interface. We present here the theory for the magneto-electro-elastic case, but it can be easily generalized to more complex situations, e.g. with thermal and/or other transport properties.

We can now consider a single layer perpendicular to the axis x_3 (Fig.1a). The internal generalized stress K_1 is constituted by the n continuous components of K_0 and by a set of arbitrary components $\mathsf{X}\in\Re^m$. Similarly, the internal generalized strain Z_1 is constituted by the m continuous components of Z_0 and by a set of arbitrary components $\mathsf{Y}\in\Re^n$. Explicitly, we have

$$\mathsf{K}_1=\mathsf{P}^T\mathsf{P}\mathsf{K}_0+\mathsf{Q}^T\mathsf{X}, \tag{13}$$

$$\mathsf{Z}_1=\mathsf{Q}^T\mathsf{Q}\mathsf{Z}_0+\mathsf{P}^T\mathsf{Y}, \tag{14}$$

with the conditions $\mathsf{K}_1=\mathsf{L}_1\mathsf{Z}_1$ and $\mathsf{K}_0=\mathsf{L}_0\mathsf{Z}_0$. We must solve previous equations to find $\mathsf{X}\in\Re^m$ and $\mathsf{Y}\in\Re^n$. By substituting Eqs.(13) and (14) in the constitutive relation of the layer we obtain

$$\mathsf{P}^T\mathsf{P}\mathsf{K}_0+\mathsf{Q}^T\mathsf{X}=\mathsf{L}_1\mathsf{Q}^T\mathsf{Q}\mathsf{Z}_0+\mathsf{L}_1\mathsf{P}^T\mathsf{Y}. \tag{15}$$

Now, we apply the operator P and, by using the properties $\mathsf{P}\mathsf{Q}^T=0$ and $\mathsf{P}\mathsf{P}^T=\mathsf{I}_n$, we easily obtain the vector Y

$$\mathsf{Y}=\left(\mathsf{P}\mathsf{L}_1\mathsf{P}^T\right)^{-1}\left(\mathsf{P}\mathsf{K}_0-\mathsf{P}\mathsf{L}_1\mathsf{Q}^T\mathsf{Q}\mathsf{Z}_0\right). \tag{16}$$

The resulting expression for Z_1 follows

$$\mathsf{Z}_1=\left[\mathsf{Q}^T\mathsf{Q}+\mathsf{P}^T\left(\mathsf{P}\mathsf{L}_1\mathsf{P}^T\right)^{-1}\mathsf{P}\left(\mathsf{L}_0-\mathsf{L}_1\mathsf{Q}^T\mathsf{Q}\right)\right]\mathsf{Z}_0. \tag{17}$$

Finally, by using the property $\mathsf{P}^T\mathsf{P}+\mathsf{Q}^T\mathsf{Q}=\mathsf{I}_{n+m}$, Eq.(17) can be elaborated, eventually obtaining

$$\mathsf{Z}_1=\left[\mathsf{I}_{n+m}+\mathsf{P}^T\left(\mathsf{P}\mathsf{L}_1\mathsf{P}^T\right)^{-1}\mathsf{P}\left(\mathsf{L}_0-\mathsf{L}_1\right)\right]\mathsf{Z}_0. \tag{18}$$

Of course, the generalized stress can be directly calculated through the relation $\mathsf{K}_1=\mathsf{L}_1\mathsf{Z}_1$. We have therefore obtained the solutions giving the internal physical fields when the externally applied ones are known. Interestingly enough, these results are independent of the layer thickness. We also note that only a

single auxiliary matrix $\mathbf{P}$ is sufficient to write the internal fields in closed form (i.e. $\mathbf{Q}$ is not necessary in final equations). As expected, the physical fields are uniform in the whole space (i.e. $\mathbf{K}_1 = \mathbf{K}_0$ and $\mathbf{Z}_1 = \mathbf{Z}_0$) if $\mathbf{L}_0 = \mathbf{L}_1$. The usefulness of the lamination operator $\mathbf{P}$ will be even more evident when we consider an arbitrary lamination direction.

We consider now a laminated structure composed of N different layers, each described by a tensor $\mathbf{L}_i$ and having a thickness d_i, $i = 1,...,N$ (Fig.1b). We can define the volume fraction of each component as $\phi_i = d_i/D$ where $D = \sum_{i=1}^{N} d_i$ is the total length of the heterostructure. As before, the external material is described by $\mathbf{L}_0$ and the system is loaded by remotely applied uniform fields $\mathbf{Z}_0$ and $\mathbf{K}_0 = \mathbf{L}_0\mathbf{Z}_0$. All interfaces are perpendicular to axis x_3. Because of the geometry of the system, the determination of the internal fields performed in the previous Section is valid for each layer of the present composite structure. Therefore, the local generalized stress $\mathbf{K}_i$ and the local generalized strains $\mathbf{Z}_i$ are given by

$$\mathbf{K}_i = \mathbf{L}_i\mathbf{A}_i\mathbf{Z}_0 \;\; and \;\; \mathbf{Z}_i = \mathbf{A}_i\mathbf{Z}_0, \tag{19}$$

for any $i = 1,...,N$, where $\mathbf{A}_i$ represents the layer concentration tensor (see Eq.(18)) given by

$$\mathbf{A}_i = \mathbf{I}_{n+m} + \mathbf{P}^T\left(\mathbf{P}\mathbf{L}_i\mathbf{P}^T\right)^{-1}\mathbf{P}\left(\mathbf{L}_0 - \mathbf{L}_i\right). \tag{20}$$

In order to obtain the effective response of the multilayered structure we evaluate the average value of the physical fields over the whole system

$$\langle\mathbf{K}\rangle = \sum_{i=1}^{N}\phi_i\mathbf{K}_i = \left(\sum_{i=1}^{N}\phi_i\mathbf{L}_i\mathbf{A}_i\right)\mathbf{Z}_0, \tag{21}$$

$$\langle\mathbf{Z}\rangle = \sum_{i=1}^{N}\phi_i\mathbf{Z}_i = \left(\sum_{i=1}^{N}\phi_i\mathbf{A}_i\right)\mathbf{Z}_0. \tag{22}$$

By determining $\mathbf{Z}_0$ from Eq.(22) and substituting the result in Eq.(21) we obtain the effective tensor of the structure defined through the relation $\langle\mathbf{K}\rangle = \mathbf{L}_{eff}\langle\mathbf{Z}\rangle$; we simply have

$$\mathbf{L}_{eff} = \left(\sum_{i=1}^{N}\phi_i\mathbf{L}_i\mathbf{A}_i\right)\left(\sum_{i=1}^{N}\phi_i\mathbf{A}_i\right)^{-1}, \tag{23}$$

or, more explicitly using Eq.(20)

$$\mathbf{L}_{eff} = \left[\sum_{i=1}^{N}\phi_i\mathbf{L}_i + \sum_{i=1}^{N}\phi_i\mathbf{L}_i\mathbf{P}^T\left(\mathbf{P}\mathbf{L}_i\mathbf{P}^T\right)^{-1}\mathbf{P}\left(\mathbf{L}_0 - \mathbf{L}_i\right)\right]$$
$$\times\left[\mathbf{I}_{n+m} + \sum_{i=1}^{N}\phi_i\mathbf{P}^T\left(\mathbf{P}\mathbf{L}_i\mathbf{P}^T\right)^{-1}\mathbf{P}\left(\mathbf{L}_0 - \mathbf{L}_i\right)\right]^{-1}. \tag{24}$$

The last expression represents the effective tensor of the laminated material. However, in order to prove the coherence of this result, we must show that $\mathbf{L}_{eff}$ does not depend on tensor $\mathbf{L}_0$ describing the behavior of the external medium. As a matter of fact, we demonstrate that the effective tensor $\mathbf{L}_{eff}$ depends only on the components tensors $\mathbf{L}_i$ and on the stoichiometric coefficients ϕ_i with $i = 1,...,N$. The proposed proof consists in obtaining a new form of Eq.(24) where $\mathbf{L}_0$ is not present. To this aim, we introduce a theorem valid for any matrix $\mathbf{S} \in \mathbf{M}_{n+m,n}(\Re)$ and $\mathbf{R} \in \mathbf{M}_{n,n+m}(\Re)$ such that $\left(\mathbf{I}_{n+m} + \mathbf{SR}\right)$ and $\left(\mathbf{I}_{n+m} + \mathbf{RS}\right)$ are not singular

$$\left(\mathbf{I}_{n+m} + \mathbf{SR}\right)^{-1} = \mathbf{I}_{n+m} - \mathbf{S}\left(\mathbf{I}_{n+m} + \mathbf{RS}\right)^{-1}\mathbf{R}. \tag{25}$$

It can be easily proved by considering $\left[\mathbf{I}_{n+m} - \mathbf{S}\left(\mathbf{I}_{n+m} + \mathbf{RS}\right)^{-1}\mathbf{R}\right]\left(\mathbf{I}_{n+m} + \mathbf{SR}\right)$, by using the relation $\mathbf{R}\mathbf{I}_{n+m} = \mathbf{I}_n\mathbf{R}$ and by obtaining the result $\mathbf{I}_{n+m}$, as requested. We can now use this property for elaborating the inverse matrix appearing in the second line of Eq.(24) by letting $\mathbf{S} = \mathbf{P}^T$ and

$\mathbf{R} = \sum_{i=1}^{N} \phi_i \left(\mathbf{P}\mathbf{L}_i\mathbf{P}^T\right)^{-1} \mathbf{P}\left(\mathbf{L}_0 - \mathbf{L}_i\right)$. So doing, the term $\mathbf{I}_{n+m} + \mathbf{R}\mathbf{S}$ in the right hand side of Eq.(25) reads $\mathbf{I}_{n+m} + \mathbf{R}\mathbf{S} = \sum_{i=1}^{N} \phi_i \left(\mathbf{P}\mathbf{L}_i\mathbf{P}^T\right)^{-1} \mathbf{P}\mathbf{L}_0\mathbf{P}^T$, where we used the condition $\sum_{i=1}^{N} \phi_i = 1$. Hence, the effective tensor assumes the following form

$$\begin{aligned}
\mathbf{L}_{eff} &= \sum_{i=1}^{N} \phi_i \mathbf{L}_i + \sum_{i=1}^{N} \phi_i \mathbf{L}_i \mathbf{P}^T \left(\mathbf{P}\mathbf{L}_i\mathbf{P}^T\right)^{-1} \mathbf{P}\left(\mathbf{L}_0 - \mathbf{L}_i\right) \\
&- \sum_{k=1}^{N} \phi_k \mathbf{L}_k \mathbf{P}^T \left(\mathbf{P}\mathbf{L}_0\mathbf{P}^T\right)^{-1} \left[\sum_{i=1}^{N} \phi_i \left(\mathbf{P}\mathbf{L}_i\mathbf{P}^T\right)^{-1}\right]^{-1} \sum_{j=1}^{N} \phi_j \left(\mathbf{P}\mathbf{L}_j\mathbf{P}^T\right)^{-1} \mathbf{P}\left(\mathbf{L}_0 - \mathbf{L}_j\right) \\
&- \sum_{k=1}^{N} \phi_k \mathbf{L}_k \mathbf{P}^T \left(\mathbf{P}\mathbf{L}_k\mathbf{P}^T\right)^{-1} \mathbf{P}\left(\mathbf{L}_0 - \mathbf{L}_k\right) \mathbf{P}^T \left(\mathbf{P}\mathbf{L}_0\mathbf{P}^T\right)^{-1} \left[\sum_{i=1}^{N} \phi_i \left(\mathbf{P}\mathbf{L}_i\mathbf{P}^T\right)^{-1}\right]^{-1} \\
&\times \sum_{j=1}^{N} \phi_j \left(\mathbf{P}\mathbf{L}_j\mathbf{P}^T\right)^{-1} \mathbf{P}\left(\mathbf{L}_0 - \mathbf{L}_j\right). \qquad (26)
\end{aligned}$$

Now, we can expand the terms $\mathbf{L}_0 - \mathbf{L}_i$, $\mathbf{L}_0 - \mathbf{L}_j$ and $\mathbf{L}_0 - \mathbf{L}_k$ and, after a very long but straightforward calculation, we can prove that all terms containing $\mathbf{L}_0$ disappear. We eventually find the final result

$$\begin{aligned}
\mathbf{L}_{eff} &= \sum_{i=1}^{N} \phi_i \mathbf{L}_i - \sum_{i=1}^{N} \phi_i \mathbf{L}_i \mathbf{P}^T \left(\mathbf{P}\mathbf{L}_i\mathbf{P}^T\right)^{-1} \mathbf{P}\mathbf{L}_i \\
&+ \sum_{k=1}^{N} \phi_k \mathbf{L}_k \mathbf{P}^T \left(\mathbf{P}\mathbf{L}_k\mathbf{P}^T\right)^{-1} \left[\sum_{i=1}^{N} \phi_i \left(\mathbf{P}\mathbf{L}_i\mathbf{P}^T\right)^{-1}\right]^{-1} \sum_{j=1}^{N} \phi_j \left(\mathbf{P}\mathbf{L}_j\mathbf{P}^T\right)^{-1} \mathbf{P}\mathbf{L}_j, \qquad (27)
\end{aligned}$$

where the matrix $\mathbf{P}$ defined in Eq.(9) can be given explicitly as

$$\mathbf{P} = \begin{pmatrix}
0 & 0 & 1 & 0 & 0 & 0 & 0 & 0 & 0 & 0 & 0 & 0 \\
0 & 0 & 0 & 1 & 0 & 0 & 0 & 0 & 0 & 0 & 0 & 0 \\
0 & 0 & 0 & 0 & 1 & 0 & 0 & 0 & 0 & 0 & 0 & 0 \\
0 & 0 & 0 & 0 & 0 & 0 & 0 & 0 & 1 & 0 & 0 & 0 \\
0 & 0 & 0 & 0 & 0 & 0 & 0 & 0 & 0 & 0 & 0 & 1
\end{pmatrix}. \qquad (28)$$

Eq.(27) represents a closed-form expression of the effective tensor of the structure. We briefly summarize here the practical application of Eq.(27): each layer is characterized by tensor $\mathbf{L}_i$ and by volume fraction ϕ_i, which is simply proportional to the thickness of the layer (with $\sum_{i=1}^{N} \phi_i = 1$). The tensor $\mathbf{P}$ given in Eq.(28) indicates that the lamination direction corresponds to x_3. Below, we will prove that Eq.(27) remains valid when we consider an arbitrary lamination direction $\vec{n}$, provided that we use the operator $\mathbf{P}_{\vec{n}}$ defined in Eq. (65) in place of $\mathbf{P}$. The result obtained through Eq.(27) represents the overall average response of the multilayer system. Therefore, we can write $\mathbf{L}_{eff} = \mathbf{L}_{eff}(\mathbf{L}_1,...,\mathbf{L}_N;\phi_1,...,\phi_N)$, for a given lamination tensor $\mathbf{P}$ (or $\mathbf{P}_{\vec{n}}$). Interestingly enough, a single matrix expression provides all the effective coupling properties of the whole structure. This points is very convenient from the computational point of view. We underline in fact that Eq.(27) can be simply implemented in a software code through the basic operations of matrix algebra. In particular, we need to calculate $N+1$ inverse matrices, where N is the number of layers. The result in Eq. (27) fulfils a series of rules with a simple physical meaning:

• *homogeneity*: it means that we can rescale the units of measurement without loosing the structure of the formula

$$\mathbf{L}_{eff}(\lambda\mathbf{L}_1,...,\lambda\mathbf{L}_N;\phi_1,...,\phi_N) = \lambda\,\mathbf{L}_{eff}(\mathbf{L}_1,...,\mathbf{L}_N;\phi_1,...,\phi_N) \;\forall\, \lambda \in \Re\,; \qquad (29)$$

• *boundary conditions*: when only one component is present we must have the effective tensor properties coinciding with its specific tensor

$$\mathbb{L}_{eff}(\mathbb{L}_1,...,\mathbb{L}_N;\phi_j = 0 \forall\, j \neq i, \phi_i = 1) = \mathbb{L}_i \;\forall\; i = 1,...,N; \tag{30}$$

• *undistinguishability*: for a two-phase laminated material the components are undistinguishable (it is also true for the N -phase structure if we apply an arbitrary permutation of constituents)

$$\mathbb{L}_{eff}(\mathbb{L}_1,\mathbb{L}_2;\phi_1,\phi_2) = \mathbb{L}_{eff}(\mathbb{L}_2,\mathbb{L}_1;\phi_2,\phi_1); \tag{31}$$

• *two-step calculability*: if we deal with a three-phase system we can determine the effective response either directly with the expression for three components or by using iteratively (twice) the expression for two components

$$\mathbb{L}_{eff}(\mathbb{L}_1,\mathbb{L}_2,\mathbb{L}_3;\phi_1,\phi_2,\phi_3) = \mathbb{L}_{eff}\left(\mathbb{L}_{eff}\left(\mathbb{L}_1,\mathbb{L}_2;\frac{\phi_1}{\phi_1+\phi_2},\frac{\phi_2}{\phi_1+\phi_2}\right),\mathbb{L}_3;\phi_1+\phi_2,\phi_3\right). \tag{32}$$

Of course, the final tensor $\mathbb{L}_{eff}$ exhibits the standard symmetry $\mathbb{L}_{eff} = \mathbb{L}_{eff}^T$.

In order to show the applicability of the general theory to realistic problems, we present in this Section the analysis of simple specific cases (uncoupled systems) and we use the general formalism for some more advanced multiferroic structures. The following situations will be considered:

1. linear analysis of purely electric (or magnetic) isotropic systems: we prove that the classical results reported in the literature can be obtained as a particular case of our general formalism;
2. linear analysis of purely elastic isotropic systems: again, we obtain the classical results for the linear response as specific cases of our theory;
3. analysis of artificial multiferroics: we apply the general solution to numerically determine the magnetoelectric response of piezoelectric/magnetoelastic laminates. We will stress the good agreement with some results published in recent papers;
4. analysis of more realistic artificial multiferroics with a pure elastic interphase between the piezoelectric and magnetoelastic layers. We will study the degradation of the magnetoelectric response in terms of interphase properties;
5. linear properties of coupled magnetoelectric isotropic systems: we perform a theoretical analysis providing the complete effective constitutive equation of a laminated system composed of different magnetoelectric layers (intrinsic multiferroics).

We consider the particular case corresponding to the homogenization of purely dielectric structures. To begin, we suppose to deal with a sequence of anisotropic layers having permittivity tensors $\hat{\varepsilon}_i$, volume fractions ϕ_i and an effective permittivity tensor $\hat{\varepsilon}_{eff}$ (the lamination direction is x_3 as before). It is simple to prove that Eq.(27) reduces to the following simpler version

$$\hat{\varepsilon}_{eff} = \sum_{i=1}^{N}\phi_i\hat{\varepsilon}_i - \sum_{i=1}^{N}\phi_i\frac{(\hat{\varepsilon}_i\vec{e}_3)\otimes(\hat{\varepsilon}_i\vec{e}_3)}{\vec{e}_3\cdot\hat{\varepsilon}_i\vec{e}_3} + \sum_{k=1}^{N}\sum_{j=1}^{N}\phi_k\phi_j\frac{(\hat{\varepsilon}_k\vec{e}_3)\otimes(\hat{\varepsilon}_j\vec{e}_3)}{(\vec{e}_3\cdot\hat{\varepsilon}_k\vec{e}_3)(\vec{e}_3\cdot\hat{\varepsilon}_j\vec{e}_3)}\frac{1}{\sum_{i=1}^{N}\frac{\phi_i}{\vec{e}_3\cdot\hat{\varepsilon}_i\vec{e}_3}} \tag{33}$$

where $\vec{e}_i$ is the unit vector in direction x_i, $\hat{\varepsilon}_i\vec{v}$ represents the standard matrix-vector product (here $\vec{v}$ is an arbitrary vector) and, finally, $\hat{A} = \vec{b}\otimes\vec{c}$ represents the tensor product, i.e. $A_{ij} = b_i c_j$. In order to explicitly prove Eq.(33), one can entirely repeat, step by step, the whole proof given in Section 4, considering only the terms related to the electric permittivity. Alternatively, it is simple to observe that Eq.(33) is formally identical to Eq.(27) provided that we substitute operator $\mathbb{P}$ with the scalar product with the unit vector $\vec{e}_3$, representing the actual lamination direction. Moreover, according to the analysis performed in Section 6, we also remark that Eq.(33) remains valid for an arbitrary lamination direction if we substitute $\vec{e}_3$ with a given unit vector $\vec{n}$. Interestingly enough, we underline that the result given in Eq.(33) (or the version with an arbitrary $\vec{n}$ in place of $\vec{e}_3$) can be equally applied to homogenize other physical properties such as the

magnetic permeability tensor, the electric or thermal conductivity tensor and the diffusion tensor in a given transport process. Although Eq.(33) is an explicit result of direct applicability for homogenizing arbitrarily anisotropic structures, it is interesting to study the case with isotropic layers described by $\hat{\varepsilon}_i = \varepsilon_i \hat{I}$ (where ε_i is the scalar permittivity and $\hat{I}$ is the 3×3 identity matrix). In this case we can simplify Eq.(33), as follows

$$\hat{\varepsilon}_{eff} = \sum_{i=1}^{N} \phi_i \varepsilon_i \hat{I} - \sum_{i=1}^{N} \phi_i \frac{\varepsilon_i^2 \vec{e}_3 \otimes \vec{e}_3}{\varepsilon_i} + \sum_{k=1}^{N} \sum_{j=1}^{N} \phi_k \phi_j \frac{\varepsilon_k \varepsilon_j \vec{e}_3 \otimes \vec{e}_3}{\varepsilon_k \varepsilon_j} \frac{1}{\sum_{i=1}^{N} \frac{\phi_i}{\varepsilon_i}}. \tag{34}$$

Since $\sum_{k=1}^{N} \phi_k = 1$ we further obtain

$$\hat{\varepsilon}_{eff} = \sum_{i=1}^{N} \phi_i \varepsilon_i \hat{I} - \sum_{i=1}^{N} \phi_i \varepsilon_i \vec{e}_3 \otimes \vec{e}_3 + \frac{1}{\sum_{i=1}^{N} \frac{\phi_i}{\varepsilon_i}} \vec{e}_3 \otimes \vec{e}_3, \tag{35}$$

or, recalling that $\hat{I} = \vec{e}_1 \otimes \vec{e}_1 + \vec{e}_2 \otimes \vec{e}_2 + \vec{e}_3 \otimes \vec{e}_3$, we have

$$\hat{\varepsilon}_{eff} = \sum_{i=1}^{N} \phi_i \varepsilon_i \left(\vec{e}_1 \otimes \vec{e}_1 + \vec{e}_2 \otimes \vec{e}_2 \right) + \frac{1}{\sum_{i=1}^{N} \frac{\phi_i}{\varepsilon_i}} \vec{e}_3 \otimes \vec{e}_3. \tag{36}$$

Now, it is easy to identify the longitudinal (P) and the transverse ($\perp$) components of the effective permittivity tensor, defined through $\hat{\varepsilon}_{eff} = \varepsilon_{eff,\perp} \left(\vec{e}_1 \otimes \vec{e}_1 + \vec{e}_2 \otimes \vec{e}_2 \right) + \varepsilon_{eff,\mathsf{P}} \vec{e}_3 \otimes \vec{e}_3$; we have

$$\varepsilon_{eff,\perp} = \sum_{i=1}^{N} \phi_i \varepsilon_i = \langle \varepsilon \rangle \ \textit{and} \ \varepsilon_{eff,\mathsf{P}} = \frac{1}{\sum_{i=1}^{N} \frac{\phi_i}{\varepsilon_i}} = \frac{1}{\left\langle \frac{1}{\varepsilon} \right\rangle}, \tag{37}$$

which are the classical results for the dielectric constant of layers connected in parallel and in series, respectively. Here $\langle z \rangle = \sum_{i=1}^{N} \phi_i z_i$ is the weighted arithmetic mean over the sequence of layers. Of course, the same analysis can be simply conducted with an arbitrary unit vector $\vec{n}$ in place of $\vec{e}_3$. In the light of this result, we can say that our general solution given in Eq.(33) (or Eq.(27)) is a tensor generalization of the standard rules for determining the equivalent behavior of components connected in series (longitudinal direction) and in parallel (transverse direction).

Now, we analyse the mechanical behavior of multilayered structures. Since we are dealing with a pure elastic system, we can adopt the following simplified quantities

$$\mathsf{T} = \left(T_{11}, T_{22}, T_{33}, T_{23}, T_{13}, T_{12} \right)^T, \mathsf{E} = \left(\varepsilon_{11}, \varepsilon_{22}, \varepsilon_{33}, 2\varepsilon_{23}, 2\varepsilon_{13}, 2\varepsilon_{12} \right)^T, \tag{38}$$

leading to the constitutive equations $\mathsf{T} = \mathsf{C}_i \mathsf{E}$ in each layer (the 6×6 matrix C_i contains all the elastic constants of the materials). The general analysis conducted in the previous Section remains valid with minor modifications: the effective elastic tensor is in fact given by the following expression

$$\begin{aligned} \mathsf{C}_{eff} = & \sum_{i=1}^{N} \phi_i \mathsf{C}_i - \sum_{i=1}^{N} \phi_i \mathsf{C}_i \mathsf{P}_e^T \left(\mathsf{P}_e \mathsf{C}_i \mathsf{P}_e^T \right)^{-1} \mathsf{P}_e \mathsf{C}_i \\ & + \sum_{k=1}^{N} \phi_k \mathsf{C}_k \mathsf{P}_e^T \left(\mathsf{P}_e \mathsf{C}_k \mathsf{P}_e^T \right)^{-1} \left[\sum_{i=1}^{N} \phi_i \left(\mathsf{P}_e \mathsf{C}_i \mathsf{P}_e^T \right)^{-1} \right]^{-1} \sum_{j=1}^{N} \phi_j \left(\mathsf{P}_e \mathsf{C}_j \mathsf{P}_e^T \right)^{-1} \mathsf{P}_e \mathsf{C}_j, \end{aligned} \tag{39}$$

where the elastic version P_e of the lamination tensor (along the axis x_3) assumes the simpler form

$$\mathsf{P}_e = \begin{pmatrix} 0 & 0 & 1 & 0 & 0 & 0 \\ 0 & 0 & 0 & 1 & 0 & 0 \\ 0 & 0 & 0 & 0 & 1 & 0 \end{pmatrix}. \tag{40}$$

This result can be easily implemented in order to study laminated materials with an arbitrary elastic anisotropy. Nevertheless, it is interesting to analyse isotropic structures. We introduce the constitutive equation for an isotropic linear elastic material, which is valid in each layer ($i = 1...N$)

$$T_{kh} = 2\mu_i \varepsilon_{kh} + \lambda_i \varepsilon_{qq} \delta_{kh}, \tag{41}$$

where λ_i and μ_i are the standard Lamé coefficients of the i-th layer, T_{kh} the components of the stress, ε_{kh} the components of the strain and $\varepsilon_{qq} = Tr(\hat{\varepsilon})$. It means that now $\mathsf{T} = \mathsf{C}_i(\lambda_i, \mu_i)\mathsf{E}$, where the structure of $\mathsf{C}_i(\lambda_i, \mu_i)$ is standard within the context of the Voigt notation. After a long but straightforward application of Eq.(39), we can obtain the effective elastic properties of the multilayered structure in the form

$$\mathsf{T} = \mathsf{C}_{eff}\mathsf{E} = \begin{pmatrix} k+m & k-m & l & 0 & 0 & 0 \\ k-m & k+m & l & 0 & 0 & 0 \\ l & l & n & 0 & 0 & 0 \\ 0 & 0 & 0 & m & 0 & 0 \\ 0 & 0 & 0 & 0 & p & 0 \\ 0 & 0 & 0 & 0 & 0 & p \end{pmatrix} \mathsf{E}. \tag{42}$$

The resulting transversely isotropic material is described by the so called Hill parameters defined as follows

$$k = \sum_{i=1}^{N} \frac{\phi_i \mu_i (2\mu_i + 3\lambda_i)}{2\mu_i + \lambda_i} + \left(\sum_{i=1}^{N} \frac{\phi_i \lambda_i}{2\mu_i + \lambda_i} \right)^2 \left(\sum_{i=1}^{N} \frac{\phi_i}{2\mu_i + \lambda_i} \right)^{-1} \tag{43}$$

$$= \left\langle \frac{\mu(2\mu + 3\lambda)}{2\mu + \lambda} \right\rangle + \left\langle \frac{\lambda}{2\mu + \lambda} \right\rangle^2 \left\langle \frac{1}{2\mu + \lambda} \right\rangle^{-1},$$

$$m = \sum_{i=1}^{N} \phi_i \mu_i = \langle \mu \rangle, \tag{44}$$

$$l = \left(\sum_{i=1}^{N} \frac{\phi_i \lambda_i}{2\mu_i + \lambda_i} \right) \left(\sum_{i=1}^{N} \frac{\phi_i}{2\mu_i + \lambda_i} \right)^{-1} = \left\langle \frac{\lambda}{2\mu + \lambda} \right\rangle \left\langle \frac{1}{2\mu + \lambda} \right\rangle^{-1}, \tag{45}$$

$$n = \left(\sum_{i=1}^{N} \frac{\phi_i}{2\mu_i + \lambda_i} \right)^{-1} = \left\langle \frac{1}{2\mu + \lambda} \right\rangle^{-1}, \tag{46}$$

$$p = \left(\sum_{i=1}^{N} \frac{\phi_i}{\mu_i} \right)^{-1} = \left\langle \frac{1}{\mu} \right\rangle^{-1}. \tag{47}$$

These results are in perfect agreement with classical findings Postma and Backus. They can be used to determine the velocities of elastic waves propagating in stratified media under the long wavelength assumption; this point plays a central role in several geophysics investigations.

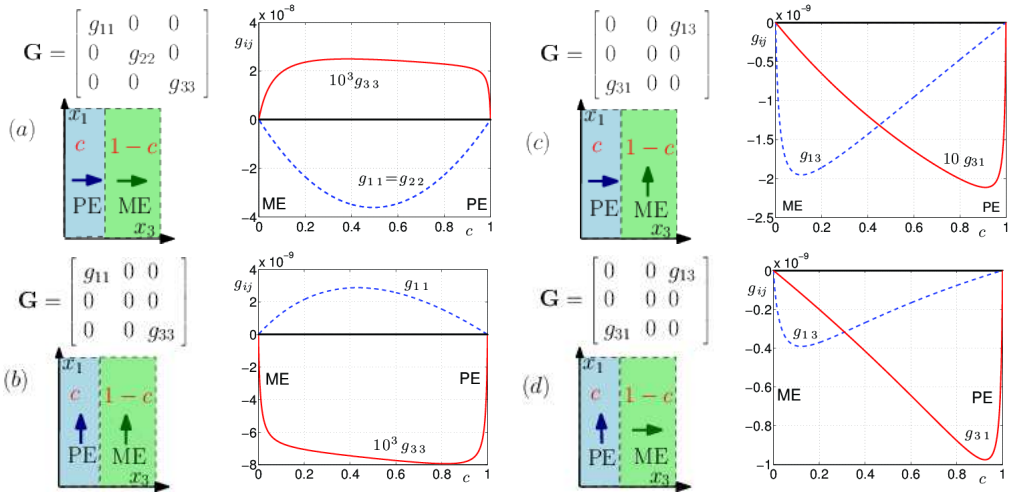

Figure 2: Magneto-electric response of simple combinations of piezoelectric (PE) and magnetoelastic (ME) layers. We considered four cases representing the parallel and orthogonal configurations of the poling directions. For each case we represented only the magnetoelectric components different from zero as function of the volume fraction c of the PE material.

We consider here the simplest configurations of multilayers composed of piezoelectric (PE) and magnetoelastic (ME) phases. In particular, we utilize the PE ceramic $BaTiO_3$ and the ME ferrite $CoFe_2O_4$. Both materials exhibit a transversely isotropic symmetry (corresponding to an uniaxial behavior) and therefore their crystal orientation can be defined through a given poling direction, as indicated in Fig.2. We consider the four geometries obtained with parallel and orthogonal alignement of the poling directions of the two components. We present here the results concerning the magneto-electric properties. It is indeed interesting to observe the emergence of the magneto-electric response generated by the combination of piezoelectric and magnetoelastic properties of two materials that have no intrinsic magneto-electric coupling. The result is given by tensor $\mathbf{G}=\{g_{ij}\}$, in general non symmetric, describing the relation $\vec{D}=\mathbf{G}\vec{H}$ (with $\hat{\varepsilon}=0$ and $\vec{E}=0$) or, equivalently, $\vec{B}=\mathbf{G}^T\vec{E}$ (with $\hat{\varepsilon}=0$ and $\vec{H}=0$). The form of these two relations is simply obtained through the general symmetry of matrix $\mathbf{L}$. In Fig.2, the components g_{ij} are represented in terms of volume fraction c of the PE phase. Of course, we always have $g_{ij}=0$ if $c=0$ (pure ME response) or $c=1$ (pure PE response). The first case (Fig.2a) is the only one described by an effective behavior corresponding to a transversely isotropic symmetry, similarly to the single phases composing the system. From a quantitative point of view, we observe that the largest magneto-electric response is obtained in the first system where $g_{11}=g_{22}\cong -3.5\times 10^{-8}$ s/m for $c=1/2$, while g_{33} is quite negligible. In the second structure (Fig.2b), we find a component g_{11} ten times lower than the previous value. We also note that, in the third case (Fig.2c), we have $|g_{13}|>|g_{31}|$, while in the fourth one (Fig.2d), we obtained $|g_{13}|<|g_{31}|$.

We consider a configuration involving piezoelectric (PE) and magnetoelastic (ME) phases with a purely elastic interphase. This corresponds to realistic situation where PE and ME materials are assembled with a glue layer. We utilize, as before, the PE ceramic $BaTiO_3$ and the ME compound $CoFe_2O_4$. For simplicity, we consider here the case with both the poling directions aligned to the lamination axis x_3. We suppose to have a purely elastic isotropic layer (EL) between the PE and the ME ones. It has a shear modulus $\mu_{in}=40\times 10^9$ Pa and a Poisson ratio $\nu_{in}=0.37$. The volume fractions are defined as follows: $\phi_{PE}=cx$, $\phi_{ME}=x(1-c)$ and $\phi_{EL}=1-x$, where the stoichiometric coefficients c and x vary in the range (0,1).
In Fig.3, the components g_{ij} are represented in terms of x and c. We can observe the absence of magneto-

electric effect for $x=0$ (pure elastic system EL) and the strongest magneto-electric effect for $x=1$ (absence of elastic interphase between ME and PE subsystems). Moreover, we always have $g_{ij}=0$ if $c=0$ (pure ME response) or $c=1$ (pure PE response). Note that we have represented g_{33} in logarithmic scale because of its very small values. The results for $x=1$ are in perfect agreement with the first case discussed in the previous example (see Fig.2a). We observe in fact that the largest magneto-electric response $g_{11}=g_{22}\cong -3.5\times 10^{-8}$ s/m is obtained for $x=1$ and $c=1/2$ (however, g_{33} is quite negligible).
In Fig.4, we investigated the effects of the elastic properties of the interphase on the overall magneto-electric behavior of the system. We considered an elastic layer with a fixed Poisson ratio $\nu_{in}=0.37$, but with a variable shear modulus μ_{in} in the range $10^6 - 10^{12}$ Pa. In Fig.4a, we show $g_{11}=g_{22}$ versus x and $\log_{10}\mu_{in}$ for $c=1/2$; similarly, in Fig.4b, the same quantity is shown versus c and $\log_{10}\mu_{in}$ for $x=1/2$. We observe that for small values of μ_{in}, we obtain a very weak magneto-electric interaction since the elastic layer is too soft to transmit the needed mechanical stress. On the other hand, for higher values of μ_{in}, we find a stronger magneto-electric coupling caused by a more intense elastic interaction. In the limiting case of a completely rigid interphase, we do not observe any degradation of the effective magneto-electric response.

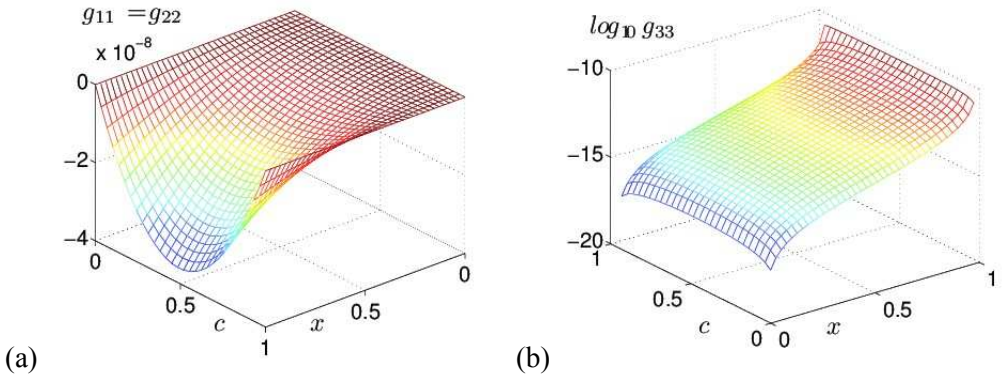

(a) (b)

Figure 3: Magneto-electric response of the structure PE/EL/ME: a) $g_{11}=g_{22}$ is shown versus x and c, b) similarly, g_{33} is shown versus x and c. In both cases we used an elastic intephase with a shear modulus $\mu_{in}=40\times 10^9$ Pa and a Poisson ratio $\nu_{in}=0.37$.

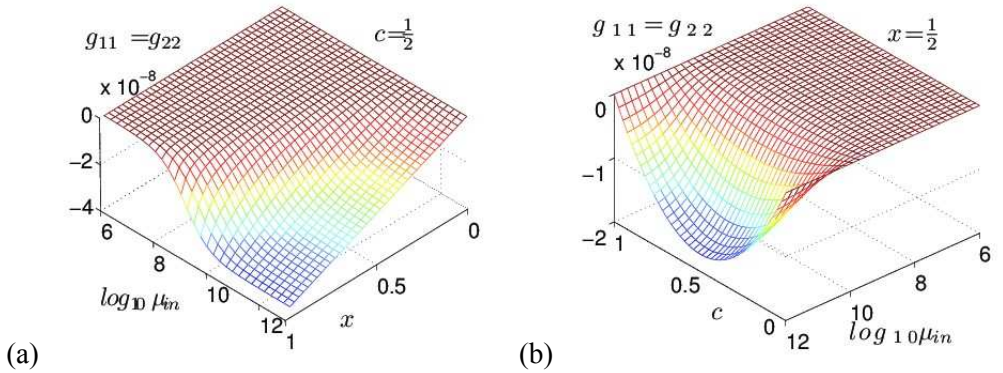

(a) (b)

Figure 4: Magneto-electric response of the structure PE/EL/ME: a) $g_{11}=g_{22}$ is shown versus x and $\log_{10}\mu_{in}$ for $c=1/2$, b) similarly, $g_{11}=g_{22}$ is shown versus c and $\log_{10}\mu_{in}$ for $x=1/2$. In both cases we used an elastic intephase with a Poisson ratio $\nu_{in}=0.37$.

We introduce a simple isotropic magneto-electric laminated system (along x_3) where each layer is described by the following constitutive equations

$$\vec{D} = \varepsilon_i \vec{E} + g_i \vec{H} \tag{48}$$

$$\vec{B} = g_i \vec{E} + \mu_i \vec{H}. \tag{49}$$

It means that each layer ($i = 1...N$) is made of an intrinsic multiferroic where there is a direct coupling between the magnetic and the electric response. In such a case, the coupling is intrinsic to the material and not mediated by any mechanical interaction. This kind of material is a so-called Tellegen medium where ε_i, μ_i and g_i are real parameters.

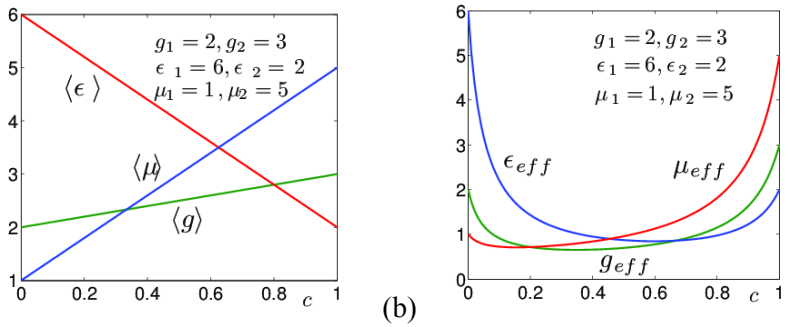

(a) (b)

Figure 5: Electromagnetic response of a two-layer system composed of intrinsic magneto-electric layers as function of the volume fraction c of the second layer: (a) transverse properties given by the simple averages $\langle \varepsilon \rangle$, $\langle \mu \rangle$ and $\langle g \rangle$, (b) longitudinal properties given by ε_{eff}, μ_{eff} and g_{eff}.

In order to apply the homogenization procedure, we can adopt the general solution given in Eq.(27) by neglecting the elastic components. We obtain, after long but straightforward calculations, the homogenized relation in the final form

$$\langle D_1 \rangle = \langle \varepsilon \rangle \langle E_1 \rangle + \langle g \rangle \langle H_1 \rangle, \tag{50}$$

$$\langle D_2 \rangle = \langle \varepsilon \rangle \langle E_2 \rangle + \langle g \rangle \langle H_2 \rangle, \tag{51}$$

$$\langle D_3 \rangle = \varepsilon_{eff} \langle E_3 \rangle + g_{eff} \langle H_3 \rangle, \tag{52}$$

$$\langle B_1 \rangle = \langle \mu \rangle \langle H_1 \rangle + \langle g \rangle \langle E_1 \rangle, \tag{53}$$

$$\langle B_2 \rangle = \langle \mu \rangle \langle H_2 \rangle + \langle g \rangle \langle E_2 \rangle, \tag{54}$$

$$\langle B_3 \rangle = \mu_{eff} \langle H_3 \rangle + g_{eff} \langle E_3 \rangle, \tag{55}$$

where the linear effective parameters ε_{eff}, μ_{eff} and g_{eff} are given by

$$\varepsilon_{eff} = \frac{\left\langle \frac{\varepsilon}{\varepsilon\mu - g^2} \right\rangle}{\left\langle \frac{\varepsilon}{\varepsilon\mu - g^2} \right\rangle \left\langle \frac{\mu}{\varepsilon\mu - g^2} \right\rangle - \left\langle \frac{g}{\varepsilon\mu - g^2} \right\rangle^2}, \tag{56}$$

$$\mu_{eff} = \frac{\left\langle \frac{\mu}{\varepsilon\mu - g^2} \right\rangle}{\left\langle \frac{\varepsilon}{\varepsilon\mu - g^2} \right\rangle \left\langle \frac{\mu}{\varepsilon\mu - g^2} \right\rangle - \left\langle \frac{g}{\varepsilon\mu - g^2} \right\rangle^2}, \tag{57}$$

$$g_{eff} = \frac{\left\langle \frac{g}{\varepsilon\mu - g^2} \right\rangle}{\left\langle \frac{\varepsilon}{\varepsilon\mu - g^2} \right\rangle \left\langle \frac{\mu}{\varepsilon\mu - g^2} \right\rangle - \left\langle \frac{g}{\varepsilon\mu - g^2} \right\rangle^2}. \qquad (58)$$

As before, $\langle z \rangle = \sum_{i=1}^{N} \phi_i z_i$ is the average value calculated over the sequence of layers. We observe that Eqs. (50)-(55) correspond to a transversely isotropic material where the transverse properties are given by the simple averages $\langle \varepsilon \rangle$, $\langle \mu \rangle$ and $\langle g \rangle$, while the longitudinal ones are given by ε_{eff}, μ_{eff} and g_{eff}, as reported in Eqs.(56)-(58). It is interesting to note that if $g_i = 0$ in each layer, then we have $\mu_{eff} = 1/\langle 1/\mu \rangle$, $\varepsilon_{eff} = 1/\langle 1/\varepsilon \rangle$ and $g_{eff} = 0$, in perfect agreement with previous results. It is also important to remember that the energy density stored in a Tellegen medium (i.e. $1/2\,\mu_i \vec{H}\cdot\vec{H} + 1/2\,\varepsilon_i \vec{E}\cdot\vec{E} + g_i \vec{E}\cdot\vec{H}$ within the i-th layer) is positive definite if $\mu_i > 0$, $\varepsilon_i > 0$ and $g_i \le \sqrt{\mu_i \varepsilon_i}$. These three conditions must be verified in any real layer. It is not difficult to prove that if the conditions $\mu_i > 0$, $\varepsilon_i > 0$ and $g_i \le \sqrt{\mu_i \varepsilon_i}$ are verified for any $i = 1...N$, then the same conditions are verified for the effective longitudinal quantities ε_{eff}, μ_{eff} and g_{eff} given in Eqs.(56)-(58), and for the effective transverse quantities $\langle \varepsilon \rangle$, $\langle \mu \rangle$ and $\langle g \rangle$. To conclude, we also underline that Eqs.(56)-(58) exhibit a curious unusual behavior: if we consider a two-layer system, we can obtain, for some combinations of parameters ε_i, μ_i and g_i ($i = 1,2$), results for ε_{eff}, μ_{eff} and g_{eff} out of the intervals $(\varepsilon_1, \varepsilon_1)$, (μ_1, μ_2) and (g_1, g_2), contrarily to most of standard homogenization rules. An example is given in Fig.5.

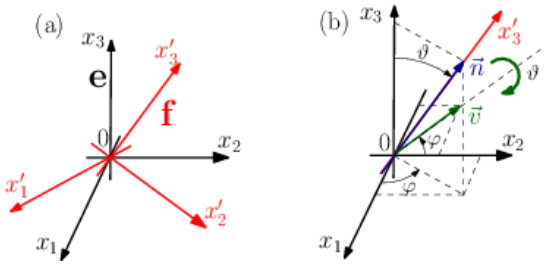

Figure 6: Couple of coordinate systems $\mathbf{e}$ (x_1, x_2, x_3) *and* $\mathbf{f}$ (x_1', x_2', x_3') *rotated through an orthogonal matrix* $\hat{\mathsf{R}}(\theta, \phi)$ *(a); the new axis* x_3' *is directed along the unit vector* $\vec{n} = (\cos\varphi \sin\vartheta, \sin\varphi \sin\vartheta, \cos\vartheta)$. *The transformation can be obtained by a rotation of an angle* ϑ *around the unit vector* $\vec{v} = (-\sin\varphi, \cos\varphi, 0)$ *(with the right-hand grip rule) lying on the plane* (x_1, x_2) *(b).*

We prove that the previous formalism can be generalized in order to consider an arbitrary direction $\vec{n}$ of lamination. We suppose to have N different materials described by tensor L_i in a given coordinate system $\mathbf{e}$ (x_1, x_2, x_3). We consider another system $\mathbf{f}$ (x_1', x_2', x_3'), rotated with respect to $\mathbf{e}$ in order to get the axis x_3' oriented along the unit vector $\vec{n} = (\cos\varphi \sin\vartheta, \sin\varphi \sin\vartheta, \cos\vartheta)$ on the base $\mathbf{e}$ (see Fig.6a). It means that we must rotate the system $\mathbf{e}$ of an angle ϑ along the unit vector $\vec{v} = (-\sin\varphi, \cos\varphi, 0)$ (with the right-hand grip rule) (see Fig.6b). To do this, we can use a rotation matrix given by the following expression

$$\hat{\mathsf{R}}(\vartheta, \varphi) = \exp(\hat{\mathsf{V}}\vartheta) = \mathsf{I}_3 + \hat{\mathsf{V}}\sin\vartheta + \hat{\mathsf{V}}^2(1 - \cos\vartheta) \qquad (59)$$

where $\hat{\mathsf{V}}$ is the antisymmetric matrix generated by the unit vector $\vec{v}$ (it means that $\mathsf{V}_{ij} = -\varepsilon_{ijk} v_k$ where ε_{ijk} is the Levi-Civita permutation symbol). For an arbitrary vector $\vec{w}$ we have $\vec{w}^{\mathbf{e}} = \hat{\mathsf{R}}(\vartheta, \varphi)\vec{w}^{\mathbf{f}}$ where $\vec{w}^{\mathbf{e}}$ are the coordinates of $\vec{w}$ on the base $\mathbf{e}$ and $\vec{w}^{\mathbf{f}}$ are those on the base $\mathbf{f}$. This is the law of transformation of all

the electric and magnetic vector fields. Explicitly, we find $\hat{\mathsf{R}}(\vartheta,\varphi)$ in the following form

$$\hat{\mathsf{R}}(\vartheta,\varphi)=\begin{pmatrix} \sin^2\varphi+\cos\vartheta\cos^2\varphi & \sin\varphi\cos\varphi(\cos\vartheta-1) & \cos\varphi\sin\vartheta \\ \sin\varphi\cos\varphi(\cos\vartheta-1) & \cos^2\varphi+\cos\vartheta\sin^2\varphi & \sin\varphi\sin\vartheta \\ -\cos\varphi\sin\vartheta & -\sin\varphi\sin\vartheta & \cos\vartheta \end{pmatrix}. \tag{60}$$

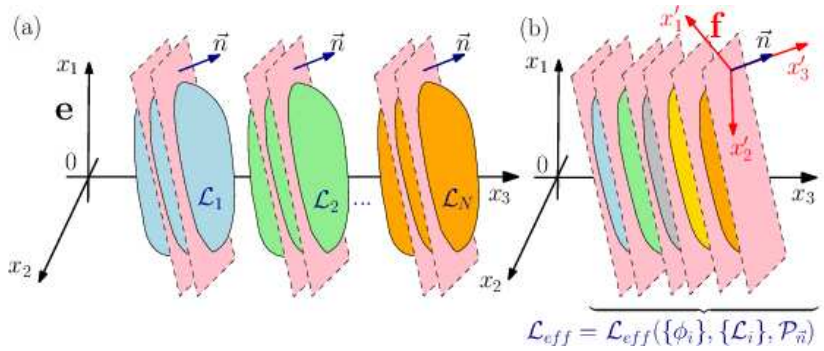

Figure 7: Series of monocrystalline materials with properties L_i (measured in the base $\mathbf{e}$) sliced (or cut) by planes perpendicular to the unit vector $\vec{n}$ (a). They are later assembled to compose a multilayered structure (with effective properties L_{eff}) with an arbitrary lamination direction (b). The base $\mathbf{f}$ with x_3' aligned with $\vec{n}$ is also represented.

Concerning the strain and stress tensors we have to introduce a more complicated procedure. The following relations hold on between different frames: $\hat{\varepsilon}^{\mathbf{e}}=\hat{\mathsf{R}}(\vartheta,\varphi)\hat{\varepsilon}^{\mathbf{f}}\hat{\mathsf{R}}(\vartheta,\varphi)^T$ for the strain and, similarly, $\hat{T}^{\mathbf{e}}=\hat{\mathsf{R}}(\vartheta,\varphi)\hat{T}^{\mathbf{f}}\hat{\mathsf{R}}(\vartheta,\varphi)^T$ for the stress. Such expressions can be converted in Voigt notation defining two matrices ω_{T} and ω_{E}, sometimes called Bond matrices, which acts as a rotation matrix on vectors $\mathsf{T}^T=(T_{11},T_{22},T_{33},T_{23},T_{13},T_{12})$ and $\mathsf{E}^T=(\varepsilon_{11},\varepsilon_{22},\varepsilon_{33},2\varepsilon_{23},2\varepsilon_{13},2\varepsilon_{12})$. In other words, we can write $\mathsf{T}^{\mathbf{e}}=\omega_{\mathsf{T}}\mathsf{T}^{\mathbf{f}}$ and $\mathsf{E}^{\mathbf{e}}=\omega_{\mathsf{E}}\mathsf{E}^{\mathbf{f}}$. The entries of the matrices ω_{T} and ω_{E} can be easily identified by comparing $\hat{T}^{\mathbf{e}}=\hat{\mathsf{R}}(\theta,\phi)\hat{T}^{\mathbf{f}}\hat{\mathsf{R}}(\theta,\phi)^T$ and $\mathsf{T}^{\mathbf{e}}=\omega_{\mathsf{T}}\mathsf{T}^{\mathbf{f}}$ for the stress (and similar relations for the strain). Summing up, we can write the laws of transformation of the generalized stress

$$\mathsf{K}^{\mathbf{e}}=\begin{pmatrix}\mathsf{T}^{\mathbf{e}}\\ \vec{D}^{\mathbf{e}}\\ \vec{B}^{\mathbf{e}}\end{pmatrix}=\begin{pmatrix}\omega_{\mathsf{T}} & 0 & 0\\ 0 & \hat{\mathsf{R}} & 0\\ 0 & 0 & \hat{\mathsf{R}}\end{pmatrix}\begin{pmatrix}\mathsf{T}^{\mathbf{f}}\\ \vec{D}^{\mathbf{f}}\\ \vec{B}^{\mathbf{f}}\end{pmatrix}=\Omega_{\mathsf{K}}\mathsf{K}^{\mathbf{f}}, \tag{61}$$

and strain

$$\mathsf{Z}^{\mathbf{e}}=\begin{pmatrix}\mathsf{E}^{\mathbf{e}}\\ -\vec{E}^{\mathbf{e}}\\ -\vec{H}^{\mathbf{e}}\end{pmatrix}=\begin{pmatrix}\omega_{\mathsf{E}} & 0 & 0\\ 0 & \hat{\mathsf{R}} & 0\\ 0 & 0 & \hat{\mathsf{R}}\end{pmatrix}\begin{pmatrix}\mathsf{E}^{\mathbf{f}}\\ -\vec{E}^{\mathbf{f}}\\ -\vec{H}^{\mathbf{f}}\end{pmatrix}=\Omega_{\mathsf{Z}}\mathsf{Z}^{\mathbf{f}}, \tag{62}$$

where we have introduced two generalized rotation matrices Ω_{K} and Ω_{Z}. Finally, we obtain the transformation rule $\mathsf{L}_i^{\mathbf{f}}=\Omega_{\mathsf{K}}^{-1}\mathsf{L}_i^{\mathbf{e}}\Omega_{\mathsf{Z}}$ for the matrix L_i describing the coupled response of each material.

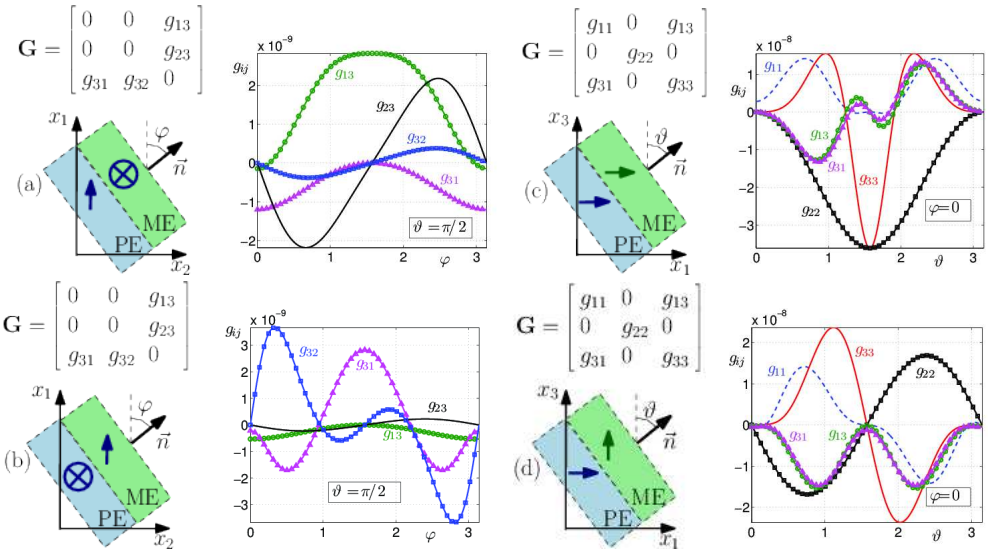

Figure 8: Magneto-electric response of PE/ME bilayer structures as function of the lamination direction (volume fractions $\phi_1 = \phi_2 = 1/2$). In panels (a) and (b) we used $\vec{n} = (\cos\varphi, \sin\varphi, 0)$, $0 < \varphi < \pi$ (rad), and orthogonal poling directions aligned to x_1 and x_3. In panels (c) and (d) we adopted $\vec{n} = (\sin\vartheta, 0, \cos\vartheta)$, $0 < \vartheta < \pi$ (rad), and parallel or orthogonal poling directions in the plane (x_1, x_3).

Now, we consider the laminated structure represented in Fig.7. While we observe in Fig.7a the cross section of each body with planes perpendicular to $\vec{n}$, we find in Fig.7b the multilayer assemblage with an arbitrary lamination direction. On base $\mathbf{f}$, the direction of lamination is x_3' (see Fig.7b for details) and, therefore, we can use Eq.(27) where L_i is substituted with $\Omega\,{}_{\mathsf{K}}^{-1}\mathsf{L}_i^{\mathbf{e}}\Omega\,{}_{\mathsf{Z}}$ (for any i) and L_{eff} with $\Omega\,{}_{\mathsf{K}}^{-1}\mathsf{L}_{eff}^{\mathbf{e}}\Omega\,{}_{\mathsf{Z}}$. We therefore obtain the following expression

$$\Omega\,{}_{\mathsf{K}}^{-1}\mathsf{L}_{eff}^{\mathbf{e}}\Omega\,{}_{\mathsf{Z}} = \sum_{i=1}^{N}\phi_i\,\Omega\,{}_{\mathsf{K}}^{-1}\mathsf{L}_i^{\mathbf{e}}\Omega\,{}_{\mathsf{Z}} - \sum_{i=1}^{N}\phi_i\,\Omega\,{}_{\mathsf{K}}^{-1}\mathsf{L}_i^{\mathbf{e}}\Omega\,{}_{\mathsf{Z}}\mathsf{P}^T\left(\mathsf{P}\Omega\,{}_{\mathsf{K}}^{-1}\mathsf{L}_i^{\mathbf{e}}\Omega\,{}_{\mathsf{Z}}\mathsf{P}^T\right)^{-1}\mathsf{P}\Omega\,{}_{\mathsf{K}}^{-1}\mathsf{L}_i^{\mathbf{e}}\Omega\,{}_{\mathsf{Z}}$$
$$+\sum_{k=1}^{N}\phi_k\,\Omega\,{}_{\mathsf{K}}^{-1}\mathsf{L}_k^{\mathbf{e}}\Omega\,{}_{\mathsf{Z}}\mathsf{P}^T\left(\mathsf{P}\Omega\,{}_{\mathsf{K}}^{-1}\mathsf{L}_k^{\mathbf{e}}\Omega\,{}_{\mathsf{Z}}\mathsf{P}^T\right)^{-1}\left[\sum_{i=1}^{N}\phi_i\left(\mathsf{P}\Omega\,{}_{\mathsf{K}}^{-1}\mathsf{L}_i^{\mathbf{e}}\Omega\,{}_{\mathsf{Z}}\mathsf{P}^T\right)^{-1}\right]^{-1}$$
$$\times\sum_{j=1}^{N}\phi_j\left(\mathsf{P}\Omega\,{}_{\mathsf{K}}^{-1}\mathsf{L}_j^{\mathbf{e}}\Omega\,{}_{\mathsf{Z}}\mathsf{P}^T\right)^{-1}\mathsf{P}\Omega\,{}_{\mathsf{K}}^{-1}\mathsf{L}_j^{\mathbf{e}}\Omega\,{}_{\mathsf{Z}}. \qquad (63)$$

Now, we introduce the operator $\mathsf{P}_{\vec{n}}$ defined through the relations $\mathsf{P}_{\vec{n}} = \mathsf{P}\Omega\,{}_{\mathsf{K}}^{-1}$ and $\mathsf{P}_{\vec{n}}^T = \Omega\,{}_{\mathsf{Z}}\mathsf{P}^T$. We therefore obtain the final result on the original base $\mathbf{e}$

$$\mathsf{L}_{eff}^{\mathbf{e}} = \sum_{i=1}^{N}\phi_i\mathsf{L}_i^{\mathbf{e}} - \sum_{i=1}^{N}\phi_i\mathsf{L}_i^{\mathbf{e}}\mathsf{P}_{\vec{n}}^T\left(\mathsf{P}_{\vec{n}}\mathsf{L}_i^{\mathbf{e}}\mathsf{P}_{\vec{n}}^T\right)^{-1}\mathsf{P}_{\vec{n}}\mathsf{L}_i^{\mathbf{e}}$$
$$+\sum_{k=1}^{N}\phi_k\mathsf{L}_k^{\mathbf{e}}\mathsf{P}_{\vec{n}}^T\left(\mathsf{P}_{\vec{n}}\mathsf{L}_k^{\mathbf{e}}\mathsf{P}_{\vec{n}}^T\right)^{-1}\left[\sum_{i=1}^{N}\phi_i\left(\mathsf{P}_{\vec{n}}\mathsf{L}_i^{\mathbf{e}}\mathsf{P}_{\vec{n}}^T\right)^{-1}\right]^{-1}\sum_{j=1}^{N}\phi_j\left(\mathsf{P}_{\vec{n}}\mathsf{L}_j^{\mathbf{e}}\mathsf{P}_{\vec{n}}^T\right)^{-1}\mathsf{P}_{\vec{n}}\mathsf{L}_j^{\mathbf{e}}, \qquad (64)$$

which is formally identical to Eq.(27).
We therefore proved that, with an arbitrary lamination direction, Eq.(27) remains unchanged provided that we use $\mathsf{P}_{\vec{n}}$ (lamination operator along $\vec{n}$) in place of P (lamination operator along x_3). We eventually obtain the following explicit form

$$\mathbf{P}_{\vec{n}}^{T} = \begin{pmatrix} c_\varphi^2 s_\vartheta^2 & -s_\varphi c_\varphi^2 s_\vartheta (1-c_\vartheta) & c_\varphi s_\vartheta \left(s_\varphi^2 + c_\varphi^2 c_\vartheta\right) & 0 & 0 \\ s_\varphi^2 s_\vartheta^2 & s_\varphi s_\vartheta \left(c_\varphi^2 + s_\varphi^2 c_\vartheta\right) & -s_\varphi^2 c_\varphi s_\vartheta (1-c_\vartheta) & 0 & 0 \\ c_\vartheta^2 & -s_\varphi s_\vartheta c_\vartheta & -c_\varphi s_\vartheta c_\vartheta & 0 & 0 \\ 2 s_\varphi s_\vartheta c_\vartheta & s_\varphi^2 \left(c_\vartheta^2 - s_\vartheta^2\right) + c_\varphi^2 c_\vartheta & s_\varphi c_\varphi \left(2c_\vartheta^2 - c_\vartheta - 1\right) & 0 & 0 \\ 2 c_\varphi s_\vartheta c_\vartheta & s_\varphi c_\varphi \left(2c_\vartheta^2 - c_\vartheta - 1\right) & c_\varphi^2 \left(c_\vartheta^2 - s_\vartheta^2\right) + s_\varphi^2 c_\vartheta & 0 & 0 \\ 2 s_\varphi c_\varphi s_\vartheta^2 & c_\varphi s_\vartheta \left(c_\varphi^2 - s_\varphi^2 + 2c_\vartheta s_\varphi^2\right) & s_\varphi s_\vartheta \left(s_\varphi^2 - c_\varphi^2 + 2c_\vartheta c_\varphi^2\right) & 0 & 0 \\ 0 & 0 & 0 & c_\varphi s_\vartheta & 0 \\ 0 & 0 & 0 & s_\varphi s_\vartheta & 0 \\ 0 & 0 & 0 & c_\vartheta & 0 \\ 0 & 0 & 0 & 0 & c_\varphi s_\vartheta \\ 0 & 0 & 0 & 0 & s_\varphi s_\vartheta \\ 0 & 0 & 0 & 0 & c_\vartheta \end{pmatrix} \tag{65}$$

where $c_\vartheta = \cos\vartheta$, $c_\varphi = \cos\varphi$, $s_\vartheta = \sin\vartheta$ and $s_\varphi = \sin\varphi$. We remark that the generalized homogenization rule in Eq.(64) satisfies the same properties as those described by Eqs.(29),(30),(31) and (32).

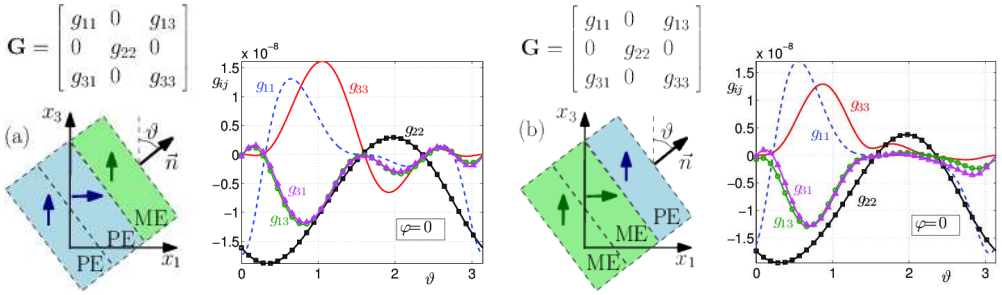

Figure 9: Magneto-electric response of PE/ME three-layer structures as function of the lamination direction with volume fractions $\phi_1 = \phi_2 = \phi_3 = 1/3$. *We adopted* $\vec{n} = (\sin\vartheta, 0, \cos\vartheta)$ *where* $0 < \vartheta < \pi$ *(rad).*

In Figs.8 and 9, we show some results obtained with the application of Eqs.(64) and (65). In Fig.8a-b, we consider configurations with two layers having orthogonal poling axes of PE and ME components in the plane (x_1, x_3). In this case, the lamination direction is orthogonal to one of the poling axes and makes a variable angle φ with the other one located in plane (x_1, x_2). In Fig.8c-d, we consider configurations with two parallel or orthogonal poling axes and a lamination direction lying in the same plane (x_1, x_3) (it makes an angle ϑ with the x_3-axis). It is interesting to note that each g_{ij} component exhibits maximum or minimum values at different specific angles φ or ϑ . This can be useful to optimize some effective properties of the overall material by changing the lamination direction. Finally, in Fig.9 we show two examples of three-layer materials. Here, we lose the symmetry (or antisymmetry) of the effective properties with respect to $\vartheta = \pi/2$; this point is clearly related to the fact that a transversely isotropic ME or PE material with a poling axis $\vec{v}$ is not coinciding with the same material with poling axis $-\vec{v}$.

The effective response of a multilayered structure obtained above (Eqs.(27) and (64)) can be written in a more general form by introducing the averaging operator $\langle \bullet \rangle$

$$\mathbf{L}_{eff} = \langle \mathbf{L} \rangle - \left\langle \mathbf{L}\mathbf{P}^T \left(\mathbf{P}\mathbf{L}\mathbf{P}^T\right)^{-1} \mathbf{P}\mathbf{L} \right\rangle + \left\langle \mathbf{L}\mathbf{P}^T \left(\mathbf{P}\mathbf{L}\mathbf{P}^T\right)^{-1} \right\rangle \left[\left\langle \left(\mathbf{P}\mathbf{L}\mathbf{P}^T\right)^{-1} \right\rangle \right]^{-1} \left\langle \left(\mathbf{P}\mathbf{L}\mathbf{P}^T\right)^{-1} \mathbf{P}\mathbf{L} \right\rangle. \tag{66}$$

Here, $\mathbf{P}$ can assume either the form given in Eq.(9) or in Eq.(65). Moreover, this expression can be simply interpreted for both discrete multilayered structures (as above) and continuous or planarly graded solids, which represent the subject of the present Section. Functionally graded materials are characterized by a smooth and continuous change of physical properties along a given direction. They are typically used for mechanical applications, but recently their use has been extended to sensors/actuators with magneto-electro-elastic layers. If we are dealing with a continuously stratified structure, we consider the dependence $\mathbf{L} = \mathbf{L}(x_s)$ along the lamination direction x_s corresponding to x_3, if we use $\mathbf{P}$, or to x_3' along $\vec{n}$, if we use $\mathbf{P}_{\vec{n}}$. It is not difficult to recognize that the effective tensor of a graded solid included between $x_s = 0$ and $x_s = x$ can be written in the following explicit form, where the average values of Eq.(66) are substituted by integrals

$$\mathbf{L}_{eff}(x) = \frac{1}{x}\int_0^x \mathbf{L}\,dx_s - \frac{1}{x}\int_0^x \mathbf{L}\mathbf{P}^T \left(\mathbf{P}\mathbf{L}\mathbf{P}^T\right)^{-1} \mathbf{P}\mathbf{L}\,dx_s + \frac{1}{x}\int_0^x \mathbf{L}\mathbf{P}^T \left(\mathbf{P}\mathbf{L}\mathbf{P}^T\right)^{-1} dx_s \left[\int_0^x \left(\mathbf{P}\mathbf{L}\mathbf{P}^T\right)^{-1} dx_s \right]^{-1} \int_0^x \left(\mathbf{P}\mathbf{L}\mathbf{P}^T\right)^{-1} \mathbf{P}\mathbf{L}\,dx_s. \tag{67}$$

In some numerical applications and theoretical developments, it can be useful to work with a differential equation describing the behavior of $\mathbf{L}_{eff}$ in terms of thickness x of the graded layer. To obtain this differential equation, we need three properties of Eq.(67):

1) if we multiply Eq.(67) by $\mathbf{P}$ on the left and by $\mathbf{P}^T$ on the right we obtain

$$\mathbf{G}_0(x) = \left[\int_0^x \left[\mathbf{P}\mathbf{L}(x_s)\mathbf{P}^T\right]^{-1} dx_s \right]^{-1} \Rightarrow \; x\mathbf{G}_0(x) = \mathbf{P}\mathbf{L}_{eff}(x)\mathbf{P}^T; \tag{68}$$

2) if we multiply Eq.(67) by $\mathbf{P}^T$ on the right we obtain

$$\mathbf{G}_1(x) = \int_0^x \mathbf{L}(x_s)\mathbf{P}^T \left[\mathbf{P}\mathbf{L}(x_s)\mathbf{P}^T\right]^{-1} dx_s \Rightarrow \; \frac{\mathbf{G}_1(x)}{x} = \mathbf{L}_{eff}(x)\mathbf{P}^T \left[\mathbf{P}\mathbf{L}_{eff}(x)\mathbf{P}^T\right]^{-1}; \tag{69}$$

3) if we multiply Eq.(67) by $\mathbf{P}$ on the left we obtain

$$\mathbf{G}_2(x) = \int_0^x \left[\mathbf{P}\mathbf{L}(x_s)\mathbf{P}^T\right]^{-1} \mathbf{P}\mathbf{L}(x_s)\,dx_s \Rightarrow \; \frac{\mathbf{G}_2(x)}{x} = \left[\mathbf{P}\mathbf{L}_{eff}(x)\mathbf{P}^T\right]^{-1} \mathbf{P}\mathbf{L}_{eff}(x). \tag{70}$$

Now, considering x as an independent variable, we determine $\frac{d}{dx}\mathbf{L}_{eff}(x)$ from Eq.(67)

$$\frac{d\mathbf{L}_{eff}}{dx} = -\frac{\mathbf{L}_{eff}}{x} + \frac{\mathbf{L}}{x} - \frac{1}{x}\mathbf{L}\mathbf{P}^T \left(\mathbf{P}\mathbf{L}\mathbf{P}^T\right)^{-1} \mathbf{P}\mathbf{L} + \frac{1}{x}\frac{d\mathbf{G}_1\mathbf{G}_0\mathbf{G}_2}{dx}, \tag{71}$$

where we have used the definitions in Eqs.(68), (69) and (70). Now, by differentiating the relation $\mathbf{G}_0(x)\mathbf{G}_0(x)^{-1} = \mathbf{I}_n$ we obtain $\frac{d}{dx}\mathbf{G}_0(x) = -\mathbf{G}_0(x)\frac{d}{dx}\left[\mathbf{G}_0(x)^{-1}\right]\mathbf{G}_0(x)$ and, after some straightforward calculations based on the properties in Eqs.(68), (69) and (70), we get the differential equation

$$x\frac{d\mathbf{L}_{eff}}{dx} = \mathbf{L} - \mathbf{L}_{eff} - \left(\mathbf{L} - \mathbf{L}_{eff}\right)\mathbf{P}^T \left(\mathbf{P}\mathbf{L}\mathbf{P}^T\right)^{-1} \mathbf{P}\left(\mathbf{L} - \mathbf{L}_{eff}\right), \tag{72}$$

which describes the effective properties of a continuously stratified layer of thickness x. Of course, we need to set the initial condition $\mathbf{L}_{eff}(0) = \mathbf{L}(0)$. We remark that a substitution $z = \log x$ transforms Eq.(72) into a Riccati equation.

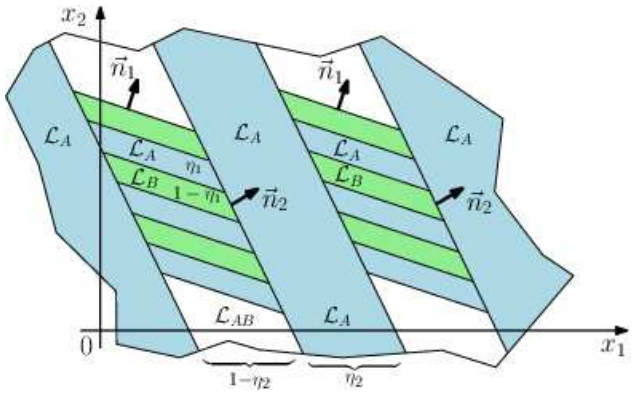

Figure 10: Scheme of a rank-two laminated material composed of components L_A and L_B. The first stage is described by the lamination direction $\vec{n}_1$ and the volume fraction η_1; the second one by $\vec{n}_2$ and η_2. The overall effective tensor $\mathsf{L}_{A(AB)}$ depends on L_A, L_B, $\vec{n}_1$, η_1, $\vec{n}_2$ and η_2, as explicitly shown in Eq.(80). Higher-rank laminations can be simply obtained by further iterations.

Multiple-rank laminated materials can be obtained by the following sequential process of lamination: dealing with two-phase materials characterized by matrices L_A and L_B, we start by creating a first layered structure (along a given direction $\vec{n}_1$) composed of these materials, resulting in an effective tensor L_{AB}. Next, we can use this composite material L_{AB} together with the original material L_A in order to obtain a rank-two laminated structure along another arbitrary direction $\vec{n}_2$. An example is shown in Fig.10. This process can be continued until we obtain a rank-m lamination. Of course, at any stage, the existing microstructure is sliced on a length scale much larger than the previous one, in order to have well defined physical properties, which can be calculated with the preceding homogenization theory. Here, we consider magneto-electro-elastic materials and m arbitrary sequential lamination directions. We start the analysis by observing that our initial result stated in Eq.(24) is also valid for an arbitrary lamination direction $\vec{n}$ if we adopt $\mathsf{P}_{\vec{n}}$ in place of P. We can use Eq.(24) with $\mathsf{L}_1 = \mathsf{L}_A$, $\mathsf{L}_2 = \mathsf{L}_B$, $\phi_1 = \eta$ and $\phi_2 = 1-\eta$. Since Eq.(24) does not effectively depend on L_0, we can adopt $\mathsf{L}_0 = \mathsf{L}_B$ in order to simplify the result. We simply obtain

$$\mathsf{L}_{AB} = \left[\eta\,\mathsf{L}_A + \eta\,\mathsf{L}_A\mathsf{P}_{\vec{n}}^T\left(\mathsf{P}_{\vec{n}}\mathsf{L}_A\mathsf{P}_{\vec{n}}^T\right)^{-1}\mathsf{P}_{\vec{n}}\left(\mathsf{L}_B-\mathsf{L}_A\right)+(1-\eta)\mathsf{L}_B\right] \times\left[\mathsf{I}_{n+m}+\eta\,\mathsf{P}_{\vec{n}}^T\left(\mathsf{P}_{\vec{n}}\mathsf{L}_A\mathsf{P}^T\right)^{-1}\mathsf{P}_{\vec{n}}\left(\mathsf{L}_B-\mathsf{L}_A\right)\right]^{-1}. \tag{73}$$

This expression can be elaborated as follows: defining the quantity $\Gamma_A = \mathsf{P}_{\vec{n}}^T\left(\mathsf{P}_{\vec{n}}\mathsf{L}_A\mathsf{P}_{\vec{n}}^T\right)^{-1}\mathsf{P}_{\vec{n}}$, we obtain

$$\left(\mathsf{L}_{AB}-\mathsf{L}_A\right)\left[\mathsf{I}_{n+m}+\eta\,\Gamma_A\left(\mathsf{L}_B-\mathsf{L}_A\right)\right]=(1-\eta)\left(\mathsf{L}_B-\mathsf{L}_A\right). \tag{74}$$

By inverting we have

$$\left(\mathsf{L}_{AB}-\mathsf{L}_A\right)^{-1}=\frac{1}{1-\eta}\left(\mathsf{L}_B-\mathsf{L}_A\right)^{-1}+\frac{\eta}{1-\eta}\mathsf{P}_{\vec{n}}^T\left(\mathsf{P}_{\vec{n}}\mathsf{L}_A\mathsf{P}_{\vec{n}}^T\right)^{-1}\mathsf{P}_{\vec{n}}. \tag{75}$$

This expression is perfectly suited for the generalization toward the sequential multiple-rank lamination. We consider a first lamination along $\vec{n}_1$ between materials L_A (concentration η_1) and L_B (concentration $1-\eta_1$), resulting in L_{AB}. Then, we perform a second lamination along $\vec{n}_2$ between materials L_A (concentration η_2) and L_{AB} (concentration $1-\eta_2$), resulting in $\mathsf{L}_{A(AB)}$. Next, we consider a third lamination along $\vec{n}_3$ between L_A (concentration η_3) and $\mathsf{L}_{A(AB)}$ (concentration $1-\eta_3$), resulting in $\mathsf{L}_{A(A(AB))}$, and so on until the m-th

step. We can write one homogenization rule for each lamination stage

$$\left(\mathbf{L}_{AB}-\mathbf{L}_{A}\right)^{-1}=\frac{1}{1-\eta_{1}}\left(\mathbf{L}_{B}-\mathbf{L}_{A}\right)^{-1}+\frac{\eta_{1}}{1-\eta_{1}}\mathbf{P}_{\vec{n}_{1}}^{T}\left(\mathbf{P}_{\vec{n}_{1}}\mathbf{L}_{A}\mathbf{P}_{\vec{n}_{1}}^{T}\right)^{-1}\mathbf{P}_{\vec{n}_{1}}, \tag{76}$$

$$\left(\mathbf{L}_{A(AB)}-\mathbf{L}_{A}\right)^{-1}=\frac{1}{1-\eta_{2}}\left(\mathbf{L}_{AB}-\mathbf{L}_{A}\right)^{-1}+\frac{\eta_{2}}{1-\eta_{2}}\mathbf{P}_{\vec{n}_{2}}^{T}\left(\mathbf{P}_{\vec{n}_{2}}\mathbf{L}_{A}\mathbf{P}_{\vec{n}_{2}}^{T}\right)^{-1}\mathbf{P}_{\vec{n}_{2}}, \tag{77}$$

$$\left(\mathbf{L}_{A(A(AB))}-\mathbf{L}_{A}\right)^{-1}=\frac{1}{1-\eta_{3}}\left(\mathbf{L}_{A(AB)}-\mathbf{L}_{A}\right)^{-1}+\frac{\eta_{3}}{1-\eta_{3}}\mathbf{P}_{\vec{n}_{3}}^{T}\left(\mathbf{P}_{\vec{n}_{3}}\mathbf{L}_{A}\mathbf{P}_{\vec{n}_{3}}^{T}\right)^{-1}\mathbf{P}_{\vec{n}_{3}}, \tag{78}$$

...

$$\left(\mathbf{L}_{\underbrace{A(A(...(AB)))}_{m\ times}}-\mathbf{L}_{A}\right)^{-1}=\frac{1}{1-\eta_{m}}\left(\mathbf{L}_{\underbrace{A(A(...(AB)))}_{(m-1)\ times}}-\mathbf{L}_{A}\right)^{-1}$$
$$+\frac{\eta_{m}}{1-\eta_{m}}\mathbf{P}_{\vec{n}_{m}}^{T}\left(\mathbf{P}_{\vec{n}_{m}}\mathbf{L}_{A}\mathbf{P}_{\vec{n}_{m}}^{T}\right)^{-1}\mathbf{P}_{\vec{n}_{m}}. \tag{79}$$

A simple iterative composition of these equations leads to the final result

$$\left(\mathbf{L}_{\underbrace{A(A(...(AB)))}_{m\ times}}-\mathbf{L}_{A}\right)^{-1}=\xi_{0}\left(\mathbf{L}_{B}-\mathbf{L}_{A}\right)^{-1}+\sum_{k=1}^{m}\xi_{k}\mathbf{P}_{\vec{n}_{k}}^{T}\left(\mathbf{P}_{\vec{n}_{k}}\mathbf{L}_{A}\mathbf{P}_{\vec{n}_{k}}^{T}\right)^{-1}\mathbf{P}_{\vec{n}_{k}}, \tag{80}$$

where

$$\xi_{0}=\prod_{k=1}^{m}\frac{1}{1-\eta_{k}}\ \ and\ \ \xi_{k}=\eta_{k}\prod_{j=k}^{m}\frac{1}{1-\eta_{j}}. \tag{81}$$

It is interesting to observe that the final volume fraction of $\mathbf{L}_{B}$ is given by $\eta_{B}=1/\xi_{0}$; similarly, the final volume fraction of $\mathbf{L}_{A}$ is $\eta_{A}=1-1/\xi_{0}$. To conclude, we have generalized the Tartar formula to magneto-electro-elastic multi-laminated systems with an arbitrary set of lamination directions $\vec{n}_{1},...,\vec{n}_{m}$. As before, the final result is ground on our definition of the arbitrary lamination tensor $\mathbf{P}_{\vec{n}}$, reported in Eq.(65).

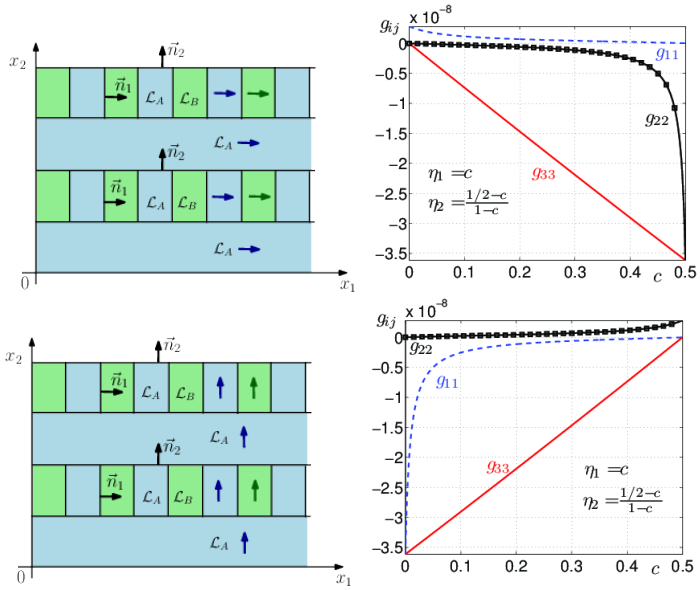

Figure 11: Rank-two multilayer materials with orthogonal lamination directions $\vec{n}_1 // x_1$ and $\vec{n}_2 // x_2$. Two configurations correspond to different alignment of the poling axes: PE ($\mathbf{L}_A$) and ME ($\mathbf{L}_B$) x_1 (top); PE ($\mathbf{L}_A$) and ME ($\mathbf{L}_B$) x_2 (bottom).

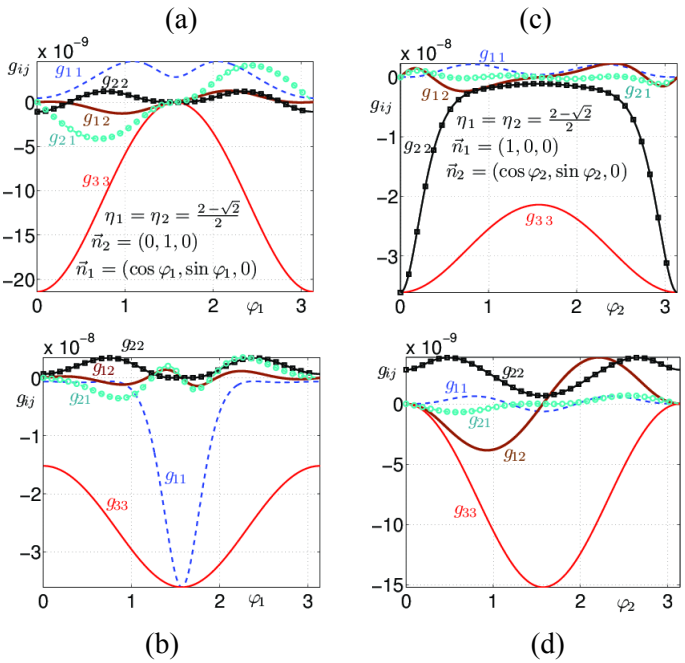

Figure 12: Effective magnetoelectric response of four configurations of rank-two multilayer materials with varying lamination directions: (a) $\vec{n}_1 = (\cos\varphi_1, \sin\varphi_1, 0)$, $\vec{n}_2 = (0,1,0)$, *PE* x_1 *and ME* x_1*; (b)* $\vec{n}_1 = (\cos\varphi_1, \sin\varphi_1, 0)$, $\vec{n}_2 = (0,1,0)$, *PE* x_2 *and ME* x_2*; (c)* $\vec{n}_1 = (1,0,0)$, $\vec{n}_2 = (\cos\varphi_2, \sin\varphi_2, 0)$, *PE* x_1 *and ME* x_1*; (d)* $\vec{n}_1 = (1,0,0)$, $\vec{n}_2 = (\cos\varphi_2, \sin\varphi_2, 0)$, *PE* x_2 *and ME* x_2*. Everywhere we adopted* $\eta_1 = \eta_2 = (2 - \sqrt{2})/2$ *and the angles are in radians.*

We describe a series of applications of the theory. We consider some two-dimensional structures with a rank-two lamination geometry. They can be found in Fig.11 where their diagram and the corresponding magneto-electric response are reported. For a rank-two configuration having volume fractions η_1 and η_2, the final volume fraction of the component A is given by $\eta_A = 1 - (1 - \eta_1)(1 - \eta_2) = \eta_1 + \eta_2 - \eta_1\eta_2$. If we impose $\eta_A = 1/2$ we have $\eta_1 = (1/2 - \eta_2)/(1 - \eta_2)$ or, equivalently, $\eta_2 = (1/2 - \eta_1)/(1 - \eta_1)$. Therefore, in Fig.11 we assumed $\eta_1 = c$ and $\eta_2 = (1/2 - c)/(1 - c)$ where $0 < c < 1/2$. Moreover, we used orthogonal lamination directions $\vec{n}_1$ along x_1 and $\vec{n}_2$ along x_2. The first configuration is characterized by poling directions along x_1 and the second one by poling directions along x_2. We note that the first structure for $c = 0$ and the second one for $c = 1/2$ correspond to the system in Fig.2b; similarly, the first structure for $c = 1/2$ and the second one for $c = 0$ correspond to the system in Fig.2a. Indeed, the values of the magneto-electric coefficients for $c = 0$ and $c = 1/2$ are in perfect agreement with Fig.2a and b. It is interesting to remark that such configurations exhibit a linear dependence of g_{33} as function of c. This property can be exploited to design a material with highly precise values of the magneto-electric parameter g_{33}. Now, we consider some examples with varying lamination directions. In Fig.12, four configurations have been shown: (a) $\vec{n}_1 = (\cos\varphi_1, \sin\varphi_1, 0)$, $\vec{n}_2 = (0,1,0)$, PE x_1 and ME x_1; (b) $\vec{n}_1 = (\cos\varphi_1, \sin\varphi_1, 0)$, $\vec{n}_2 = (0,1,0)$, PE x_2 and ME x_2; (c) $\vec{n}_1 = (1,0,0)$, $\vec{n}_2 = (\cos\varphi_2, \sin\varphi_2, 0)$, PE x_1 and ME x_1; (d) $\vec{n}_1 = (1,0,0)$, $\vec{n}_2 = (\cos\varphi_2, \sin\varphi_2, 0)$, PE x_2 and ME x_2. In all cases we imposed $\eta_A = 1/2$ and $\eta_1 = \eta_2$. Since $\eta_A = \eta_1 + \eta_2 - \eta_1\eta_2$ we obtained the volume fractions $\eta_1 = \eta_2 = (2 - \sqrt{2})/2$. Case (a) and (b) with $\varphi_1 = 0$ and case (c) and (d) with $\varphi_2 = \pi/2$ correspond to Fig.12 with $c = (2 - \sqrt{2})/2$. Case (a) with $\varphi_1 = \pi/2$ and case (d) with $\phi_2 = 0$ correspond to Fig.2b with $c = 1/2$. Finally, case (b) with $\varphi_1 = \pi/2$ and case (c) with $\phi_2 = 0$ correspond to Fig.2a with $c = 1/2$.

2.3.Thermo-elastic behaviour of polymer chains under stretching

The recent development of mechanical experiments on single molecules provided a deeper understanding of intermolecular and intramolecular forces, thereby introducing crucial additional information about the thermodynamics and kinetics of several molecular processes (F. Cleri, Sci. Model. Simul. 15, 369, 2008; K. R. Chaurasiya, T. Paramanathan, M. J. McCauley, and M. C. Williams, Phys. Life Rev. 7, 299, 2010). Single-molecule experimental methods can be typically based on laser optical tweezers (LOTs), magnetic tweezers (MTs) or atomic force microscope (AFM). These experimental techniques have been extensively applied to nucleic acids (DNA, RNA and DNA condensation), proteins (protein-protein interaction and protein folding), molecular motors and other long-chain polymers. Furthermore, in such experiments the determination of small energies and the detection of large deviations due to Brownian interactions offer a new method for analysing the basic foundations of statistical mechanics. In particular, the above techniques permit a clearer comprehension of the equilibrium and non-equilibrium thermodynamics of small systems and the experimental verification of fluctuation theorems. One of the most important single-molecule experiment concerns the stretching of a chain structure in order to measure its elastic features (see Fig.1 left below). The first famous investigation was performed on the double-stranded DNA and the results appeared in very good agreement with the worm-like chain (WLC) model (S. B. Smith, L. Finzi, and C. Bustamante, Science 258, 1122, 1992; J. F. Marko and E. D. Siggia, Macromolecules 28, 8759, 1995) while they were only in partial agreement with the freely jointed chain (FJC) model (the latter model typically providing, however, a better fit for single-stranded DNA and RNA, see J. M. Huguet, C. V. Bizarro, N. Forns, S. B. Smith, C. Bustamante, and F. Ritort, Proc. Natl. Acad. Sci. U.S.A. 107, 15341, 2010). This result and successive experimental evidences suggested that the mechanical properties of DNA, and in particular its flexibility (described by the persistence length), have a relevant role in many biological process (C. R. Calladine, H. R. Drew, B. F. Luisi, and A. A. Travers, *Understanding DNA: The Molecule and How it Works,* Elsevier/Academic, Amsterdam, 1992). The importance of understanding the force-extension relationship for macromolecules has therefore attracted the attention of physicists and mathematicians, who produced several models and relationships to explain the experimental results. In the following some results concerning chains stretched by forces and fields, chains undergoing conformational transitions and the corresponding equivalence ensembles will be discussed more in detail.

2.3.1.Polymer chains stretched by forces: Gibbs and Helmholtz ensembles

(*Fabio Manca, Stefano Giordano, Pier Luca Palla, Rinaldo Zucca, Fabrizio Cleri and Luciano Colombo, Elasticity of flexible and semiflexible polymers with extensible bonds in the Gibbs and Helmholtz ensembles, THE JOURNAL OF CHEMICAL PHYSICS 136, 154906, 2012, Fabio Manca, Stefano Giordano, Pier Luca Palla, Fabrizio Cleri and Luciano Colombo, Monte Carlo simulations of single polymer force-extension relations, Journal of Physics: Conference Series 383, 012016, 2012*)

Two main assumptions are typically considered in the analytical developments of the standard FJC and WLC models: (a) inextensibility, expressed as a fixed bond length between two adjacent monomers, and (b) the contour length (equal to N times the equilibrium bond length for a chain composed of N monomers) is supposed very large. The first assumption should not be adopted if we consider a large applied force. The second assumption is related to the concept of thermodynamic limit. In fact, the standard rules of equilibrium thermodynamics may not apply to experiments on individual, short-length polymer molecules. In such a case the results may depend on the boundary conditions imposed for stretching the polymer, namely: a fixed end-to-end distance, pertinent to the Helmholtz ensemble of statistical mechanics (see Fig. 1, centre), or a fixed force applied at one or both ends, rather representing a realization of the Gibbs ensemble (see Fig. 1, right). The differences between the two conditions should vanish in the thermodynamic limit (very large N). It is important to observe that from the experimental point of view both assumptions, inextensibility and attainment of thermodynamic limit, are often not fulfilled for many practical reasons (e.g. too large applied forces and force-rates, different configurations of the experimental devices, actual procedures for force and distance measurements, and so on). Therefore, we studied the effects of the superposition of the two aspects, by considering the mechanical stretching response of extensible polymer chains of arbitrary length. In particular, we considered the quantitative difference between the thermodynamic behaviour within either the Helmholtz or Gibbs ensemble, by investigating the statistical mechanics for small systems.

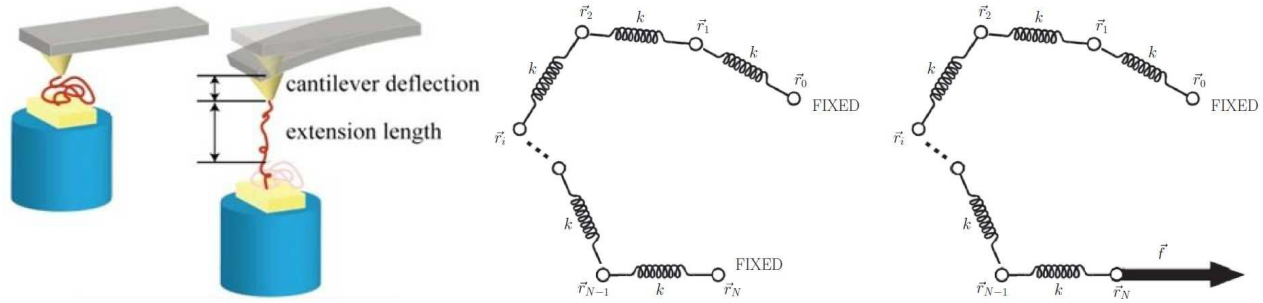

Fig.1. Left: paradigmatic single-molecule experiment conducted with a cantilever which applies a force to the polymer chain, varying its extension length. Centre: Helmholtz ensemble for a polymeric chain (we fix the end-terminals of the chain and we measure the force needed to maintain fixed their positions). Right: Gibbs ensemble for a polymeric chain (we fix one end-terminal of the chain and we apply a given force on the other extremity; so doing we can measure the induced extension of the molecule).

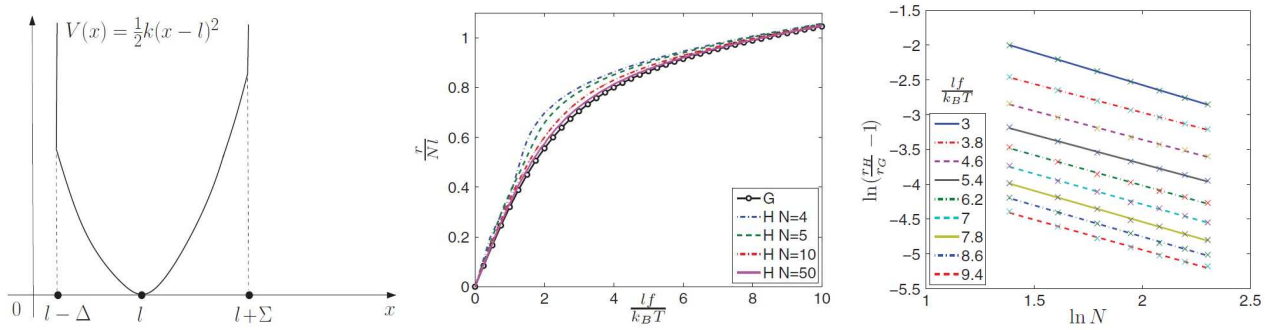

Fig.2. (left) Potential energy function for the stretching of a single bond in the polymer chain. (center) Constitutive relation provided by Monte Carlo simulations for a FJC model with elastic bonds between the monomers, both under Helmholtz (H) and Gibbs (G) boundary conditions. The elongation and the traction are reported on the vertical and horizontal axis. The Helmholtz constitutive relation is reported for different polymer lengths N. (right) Comparison between the elongations r_H and r_G for the FJC model with elastic bonds between the monomers. All sets of data are nicely fitted by $r_H(N)/r_G=1+a/N^{\alpha}$ with the same scaling exponent $\alpha = 0.80 \pm 0.05$.

We firstly consider a model in which each bond is represented by a harmonic spring with finite extension, while no potential is acting on bending or torsional degrees of freedom. Each spring is defined by the potential energy $V(x) = (1/2)k(x - l)^2$ for x in a given range specified in Fig.2 (left), where k is the spring constant, l is the equilibrium bond length, and x is the actual extension of the bond. As it can be seen in Fig. 2, the potential is set to infinity for x outside the previous range in order to impose a limited extension of the spring both for expansion and compression. The Monte Carlo approach simulates the stretching of the polymer under a force provided by a cantilever (mimicking, for instance, the loading by an atomic force microscope) with a proper adjustable elastic stiffness. In the limit of a soft cantilever the generalized ensemble of the coupled molecule/cantilever system reduces to the Gibbs ensemble for the isolated molecule subjected to a constant force. On the other hand, for a stiff cantilever we obtain the Helmholtz ensemble for the isolated molecule held at a fixed extension by the fluctuating force. The Monte Carlo simulation results for both the Helmholtz and Gibbs ensemble are shown in Fig. 2 (centre). As expected, we find a single curve for the Gibbs ensemble and a family of curves for the Helmholtz ensemble (corresponding to $N = 4$, 5, 10, and 50, from the top to the bottom). The curves in Fig.2 (centre) can be used to address the thermodynamic limit issue, as shown in Fig. 2 (right). We observe that the linear regression leads to the scaling exponent α=0.80±0.05 for any value of the normalized force $fl/(k_BT)$. We performed the same analysis on different polymer structures and we obtained different results concerning the scaling behaviour. This point suggests that different polymer models have different scaling exponents or, in other words, that they progress differently to reach the thermodynamic limit. The demonstration of different scaling laws may help to discriminate the response of polymers with different internal chemical structure, in the short-length limit.

2.3.2.Polymer chains stretched by fields: theory and MC simulations

(*Fabio Manca, Stefano Giordano, Pier Luca Palla, Fabrizio Cleri, and Luciano Colombo, Theory and Monte Carlo simulations for the stretching of flexible and semiflexible single polymer chains under external fields, Journal of Chemical Physics 137, 244907, 2012*)

Development of mechanical experiments allowed the manipulation of single polymer molecules in two main ways: uniform stretching by external forces (as above described) and non-uniform stretching by external fields. In this section we discuss our results on the non-uniform stretching of a single molecule via an external field (it can be a fluid in motion or an applied electric field). As before we adopted a statistical mechanics analysis and Monte Carlo simulations for the mechanical properties of flexible and semi-flexible polymer anchored at one end. While the analytical approach is useful to obtain the explicit partition function and the force-extension curve in some specific cases, Monte Carlo simulations are crucial to check the theoretical results and to study more generic situations, inaccessible to analytical treatments. In particular, while we developed our exact mathematical analysis starting from the more tractable FJC model, we considered some classical approximations to extend our theoretical study also to the WLC model. Finally, several comparisons have been drawn and more complex geometries have been analysed by taking full profit from the MC simulations.

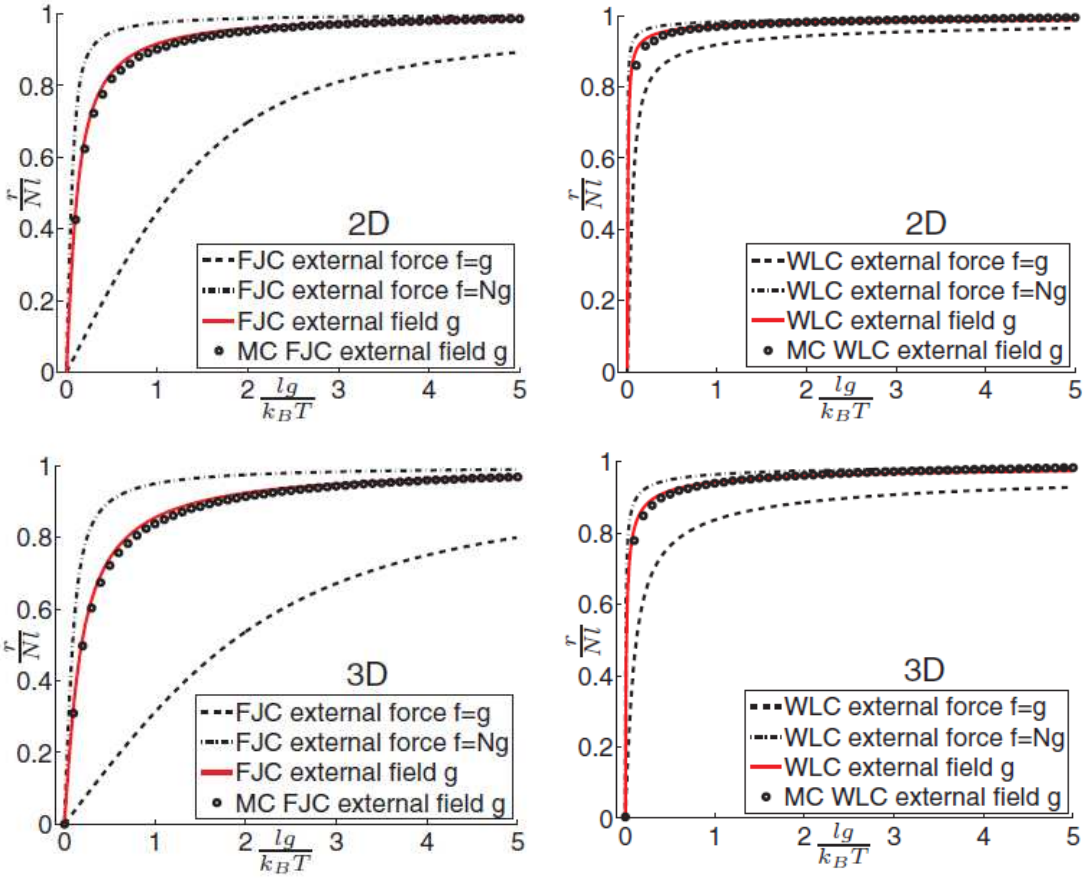

Fig. 1. (first column) Force-extension curves of a FJC polymer in an external field (or external force) with N = 20. The red line corresponds to the approximated expressions given in Eqs. (3) and (4) (see Table 1) while the black circles have been obtained through MC simulations. The 2D (Eq. (1)) and 3D (Eq. (2)) FJC expressions (without an external field) are plotted for comparison with f = g and f = Ng. (second column) Force-extension curves of a WLC polymer in an external field (or external force) with N = 20. The red line corresponds to the approximated expressions given in Eqs. (7) and (8) while the black circles have been obtained through MC simulations. The 2D (Eq. (5)) and 3D (Eq. (6)) WLC expressions (without an external field) are plotted for comparison with f = g and f = Ng. The value of the bending spring constant is $\kappa = 0.4 \times 10^{-19}$ *Nm=10*k_BT *at T = 293 K.*

1	$\frac{r}{lN} = \frac{I_1\left(\frac{lf}{k_BT}\right)}{I_0\left(\frac{lf}{k_BT}\right)}$	*2D-FJC with force f applied at one end*
2	$\frac{r}{lN} = \mathcal{L}\left(\frac{lf}{k_BT}\right)$	*3D-FJC with force f applied at one end*
3	$\frac{r}{lN} = \frac{1}{N}\frac{1}{\frac{lg}{k_BT}}\log\frac{I_0\left(\frac{lg}{k_BT}(N+1)\right)}{I_0\left(\frac{lg}{k_BT}\right)}$	*2D-FJC with field g applied at all monomers*
4	$\frac{r}{lN} = \frac{1}{N}\frac{1}{\frac{lg}{k_BT}}\log\frac{e^{2\frac{lg}{k_BT}(N+1)}-1}{(N+1)\left(e^{2\frac{lg}{k_BT}}-1\right)} - 1$	*3D-FJC with field g applied at all monomers*
5	$\frac{fl}{k_BT} = \frac{l}{L_p}\left[\frac{1}{16(1-\zeta)^2} - \frac{1}{16} + \frac{7}{8}\zeta\right]$	*2D-WLC with force f applied at one end*
6	$\frac{fl}{k_BT} = \frac{l}{L_p}\left[\frac{1}{4(1-\zeta)^2} - \frac{1}{4} + \zeta\right]$	*3D-WLC with force f applied at one end*
7	$N\frac{gl}{k_BT} = \frac{l}{L_p}\left[\frac{1}{4(1-\zeta)^2} - \frac{1}{4} + \frac{3}{2}\zeta\right]$	*2D-WLC with field g applied at all monomers*
8	$N\frac{gl}{k_BT} = \frac{l}{L_p}\left[\frac{1}{(1-\zeta)^2} - 1 + \zeta\right]$	*3D-WLC with field g applied at all monomers*

Table 1. Explicit expressions for the force-extension curves represented in Fig.1. The first four cases concern the FJC model (2D/3D, force/field). Here we defined l as the equilibrium length of each domain and N as the total number of domains. The other results concern the WLC model. We defined for convenience the dimensionless elongation $\zeta = r/(lN)$ *and the persistence length* $L_p = l\kappa/(k_BT)$*, where κ is the bending stiffness of the WLC model.*

It is interesting to compare the very different force-extension curves for a single molecule in the two cases of a uniform (only f applied) and non-uniform (only g applied) stretch. We can analyze the case of a FJC and a WLC polymer. The 2D and 3D FJC results are plotted in Fig. 1 (first column); on the other hand, the 2D and 3D WLC curves have been shown in Fig. 1 (second column). In any case, three curves have been reported for drawing all the possible comparisons: the response under the field g, the response under the force f = g and, finally, the response to an external force f = Ng. Interesting enough, we note that the curve corresponding to the field g is always comprised between the cases with only the force f = g and f = Ng. The response with the field g is clearly larger than that with the single force f = g since the field corresponds to a distribution of N forces (of intensity f) applied to all monomers; therefore, the total force applied is larger, generating a more intense effect. However, the case with a single force f = Ng shows a response larger than that of the field g. In this case, the total force applied in the two cases is the same but the single force Nf is applied entirely to the last terminal monomer, generating an overall stronger effect compared to the same force evenly distributed on the monomers. In fact, a force generates a stronger effect if it is placed in the region near the free polymer end (its effect is redistributed also to all preceding bonds). The curves in Figs. 1 have been obtained with a refined theoretical formulations (see Table 1) and confirmed by a series of MC simulations. In all cases, we obtained a quite perfect agreement between the two formulations.

In this activity, we investigated mechanical and conformational properties of flexible and semiflexible polymer chains in external fields. As for the FJC model, we developed a statistical theory, based on the exact analytical determination of the partition function, which generalizes previous results to the case where an external field is applied to the system. In particular, we obtained closed form expression for both the average conformation of the chain and its covariance distribution. For the sake of completeness, all calculations have been performed both in two-dimensional and three-dimensional geometry. On the other hand, as for the WLC model, we derived new approximate expressions describing the force-extension curve under the effect of an external field. They can be considered as the extensions of the classical Marko-Siggia relationships describing the polymer pulled by a single external force applied at the free end of the chain. All our analytical results, for both FJC and WLC models, have been confirmed by a series of Monte Carlo simulations, always found in very good agreement with the theory. The overall effects generated on the tethered polymer by the application of an external field can be summarized as follows. As for the average configuration of a chain, it is well known that a single pulling force generates a uniform deformation along the chain (for a homogeneous polymer with all monomers described by the same effective elastic stiffness). On the contrary, the application of an external field produces a non-uniform deformation along the chain, showing a larger deformation in the portion of the chain closest to the fixed end. Moreover, the variances of the positions increase linearly along the chain with a single force applied to the polymer. Conversely, the polymer subjected to an external field exhibits a non-linearly increasing behavior of the variances along the chain. More specifically, the variances assume the largest values nearby the last free monomers, where we can measure the highest fluctuations. To conclude, we underline that the use of the MC method, once validated against known analytical solutions, is crucial for analysing models conditions which are beyond reach of a full analytical calculation. We take full profit of this approach for analysing the effects of the combination of an applied force at the free end together with an external field, especially when the two are not aligned. We have analyzed the average configurational properties of the polymer, observing a very complex scenario concerning the behavior of the variances (not reported here for the sake of brevity).

2.3.3.Chains with conformational transitions
(*Fabio Manca, Stefano Giordano, Pier Luca Palla, Fabrizio Cleri, and Luciano Colombo, Two-state theory of single-molecule stretching experiments, Physical Review E 87, 032705, 2013*)

During the typical experiment of a mechanically-induced unfolding of a polymer made of N domains, different mechanical response regimes are observed as a function of increasing force level: the entropic unfolding of the polymer chain (now well understood in terms of worm-like chain (WLC) or freely-jointed chain (FJC) models); the linear-elastic extension of the straightened chain; the so-called overstretching, typically interpreted as a conformational transformation of the domain geometry; the eventual fracturing of the polymer. There is a great interest in understanding the behaviour of chains with force-induced domain transformations. Therefore, we will consider the statistical mechanics of chain polymers composed by domains with two stable states, subject to a pulling force by a molecular-scale mechanical device. We

learned from many experiments that for short chain length, or large stiffness of the device, the domain response is uncorrelated and originates the typical saw-tooth force-extension curve show in Fig. 1 (centre). On the other hand, upon increasing chain length, or vanishing device stiffness, the experimental response is cooperative and results in the plateau-like curve, also shown in Fig. 1 (right). Despite of the apparent contrasting experimental situations, we searched for a model able to explain all these dynamical mechanical responses. To do this we used again theoretical statistical mechanics techniques and numerical Monte Carlo simulations.

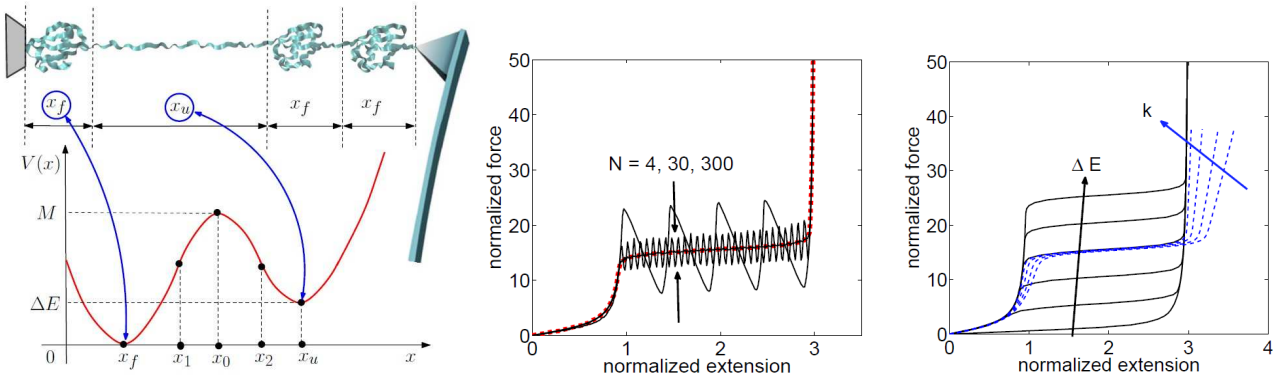

Figure 1. Left: polymer chain composed by domains with two stable states, subject to a pulling force by a molecular-scale mechanical device. Centre: response for short chains, or large stiffness of the device (Helmholtz ensemble, saw-tooth force-extension curve). Right: response for long chains, or vanishing device stiffness (Gibbs ensemble, plateau-like curve).

In this context, we provided a robust microscopic statistical mechanics foundation to the interpretation of the overstretching regime (or conformational transitions regime), which we represented in terms of the internal dynamics of a chain of two-state systems undergoing a conformational transformation, as described by the double-well potential in Fig. 1 (left). For the sake of argument we called "folded" and "unfolded" the two conformations; however, the transformation occurs, more generally, between two principal local minima of the domain free-energy hypersurface. We proved that this model is exactly capable of reproducing the two cooperative and non-cooperative responses observed in several experiments.

2.3.4.Statistical equivalence between isometric and isotensional ensembles
(*Fabio Manca, Stefano Giordano, Pier Luca Palla, and Fabrizio Cleri, On the equivalence of thermodynamics ensembles for flexible polymer chains, Physica A: Statistical Mechanics and its Applications 395, 154-170, 2014*)

The problem of ensembles equivalence plays a central role in the assessment of the basic foundations of statistical mechanics. It consists in determining whether, in the thermodynamic limit (number of degrees of freedom approaching infinity), two statistical ensembles are equivalent, i.e. they lead to the same mathematical form of the constitutive equation describing the system under investigation (at equilibrium). Similarly, the equivalence can be also characterized by a Legendre transformation between the thermodynamic potentials (free energies) of the conjugated variables or by a Laplace–Stieltjes transformation between the partition functions of the conjugated ensembles.
As an example, we can mention the microcanonical and canonical ensembles, representing the two most important statistical descriptions of many-particle systems. As initially observed by Gibbs, their definitions, in general, do not guarantee the equivalence in the thermodynamic limit (J.W. Gibbs, Elementary Principles in Statistical Mechanics, Charles Scribner's Sons, New York, 1902). Therefore, many theoretical studies have been conducted in order to understand how the equivalence property depends on the system considered, i.e. on the type of interaction acting among the particles.
The issue of the equivalence of statistical ensembles is notably important for one-dimensional systems. In particular, this concept plays a crucial role in the theory of single polymer chains, as above discussed. In this case, the deviation of the behaviour corresponding to different statistical ensembles is indeed easily observable at both theoretical and experimental level (for chains with a finite number N of domains). In other

words, short chains exhibit different physical responses (i.e. constitutive equations) when subjected to different boundary conditions (i.e. statistical ensembles). A large spectrum of single molecule manipulation techniques such as atomic force microscopy, optical and magnetic tweezers, have been recently developed and they allow to study these deviations for arbitrarily long molecules, such as DNA or proteins. For the case of single polymer chains under stretching (without confinement effects, i.e. free to fluctuate in the whole space), two ensembles are typically considered, as introduced in previous sections: the first one is the Gibbs (or isotensional) ensemble characterized by a deterministic force applied to the free end of the chain (being the other end clamped at the origin of the axes); the second one is the Helmholtz (or isometric) ensemble obtained with both the ends of the polymer tethered at two different points of the space. We remark that these two ensembles correspond to a couple of different canonical distributions, obtained with distinct boundary conditions. In this sense, we are dealing with the equivalence characterization between two dual versions of the canonical ensemble. On the one hand, when the thermodynamic limit is not satisfied (small number of monomers), these two situations are not equivalent, leading to different force–displacement curves. On the other hand, whenever N approaches infinity, it is important to elucidate if the equivalence of ensembles occurs or not. We rigorously proved the equivalence of the Helmholtz and the Gibbs ensembles in the thermodynamic limit for a specific class of polymer chains defined by the following assumptions:

• we suppose to study a non-branched single chain without confinements, i.e. freely fluctuating in the whole space;

• the only constraints consist in the punctual boundary conditions defining the Helmholtz and the Gibbs ensembles;

• we consider all polymer models characterized by an arbitrary pairing interaction between adjacent monomers, described by a continuous energy function $V(x)$;

• we always suppose that the integrals defining both Helmholtz and Gibbs partition functions are convergent everywhere.

The third hypothesis leads to a Gibbs partition function which can be exactly written as a power of N (always convergent for the fourth assumption). As a matter of fact, this form is particularly convenient because allows us to draw a thorough analytical comparison of the two ensembles. In particular, the equivalence between the Gibbs and the Helmholtz ensembles is proved by performing a direct asymptotic comparison ($N \to \infty$) of the two corresponding force–extension relations. Such an analysis is conducted by elaborating the integrals through the vector version of the stationary phase technique. The possibility to apply this method has been rigorously proved by investigating the sign of the eigenvalues of the Hessian matrix of the characteristic phase function. After having developed a general proof, valid for the entire class of potentials considered, the ensembles equivalence is further discussed for three particular systems, which are important for many applications: a freely jointed chain, a flexible polymer with extensible bonds and a chain with domains that exhibit conformational transitions between two stable states.

It is important to recall that a general criterion for the equivalence of thermodynamic ensembles exists and it is valid for a large class of physical systems: it affirms that the convexity of the Helmholtz free energy F is sufficient to assure the equivalence between the ensembles. This is a universal result largely utilized in general statistical mechanics since it can be applied to arbitrary systems and not only to polymer structures. Moreover, it is not only valid to characterize the equivalence between Helmholtz and Gibbs ensembles (which are two particular cases of canonical ensemble with different boundary conditions), but also the equivalence between microcanonical and canonical ensembles. This criterion is therefore of indubitable theoretical importance. However, although it has been largely used to infer the equivalence of Helmholtz and Gibbs ensembles of polymer systems, it has regrettably conducted to some controversies (R.G. Winkler, Soft Matter 6, 2010, 6183). In addition, while the convexity verification for F may be elementary for simple polymer structures, it can be rather complicated for polymers described by more elaborated Hamiltonians. As an example we can mention the interactions among monomers described by a potential energy exhibiting more than one minimum point, corresponding to different macroscopic states. Incidentally, we remark that there is a great interest in the polymer community in analysing complex chemical structures characterized by multiple-basin energy landscapes and multi-state conformational transitions. As a matter of fact, these structures are very important to understand the behaviour of biomolecules (proteins and nucleic acids) which often undergo folding and unfolding processes in order to execute their functions (e.g. binding or releasing ligands or signals transduction). For these reasons we searched for a more specific alternative equivalence criterion that is simpler from the mathematical point of view and more related to the quantities really measurable in standard single molecule manipulation techniques. We therefore analysed the equivalence by

directly examining the force–extension response in the two ensembles, for an increasing number of monomers. We are finally able to prove the following result. We consider a polymer chain with a pairing interaction between monomers described by the potential energy *V(x)* (being x the distance between two adjacent monomers). If we suppose (i) to avoid any form of confinement, (ii) to consider the Helmholtz and the Gibbs boundary conditions, (iii) to use a potential function *V(x)* continuous, and (iv) to assume partition functions convergent everywhere, then the ensembles are certainly statistically equivalent. Of course, this is a particular case of the more general result based on the convexity of the Helmholtz free energy F ; the new statement is indeed valid for a more restricted class of physical systems. Nevertheless, for the polymer community this result should be important since it is more easily applicable than the convexity of F , also for the case where *V(x)* exhibits more than one minimum point.
More specifically, the central result can be stated as follows; we define the following integrals depending on the energy potential *V(x)*:

$$B(\xi) = \text{const.} \times \int_0^{\infty} \exp\left[-\beta V(ly)\right] \frac{\sin(\xi y)}{\xi} y dy$$

Here, l is the equilibrium length between adjacent domains and $\beta=1/(k_B T)$. The equivalence between ensembles has been proved if the following eigenvalues are always positive (for any value of the force f):

$$\mu = -\frac{\beta l}{if}\left[\frac{1}{B(\xi)}\frac{\partial B(\xi)}{\partial \xi}\right]_{\xi=i\beta fl},$$

$$\lambda = \frac{(\beta l)^2}{B(\xi)}\left[\frac{1}{B(\xi)}\left(\frac{\partial B(\xi)}{\partial \xi}\right)^2 - \frac{\partial^2 B(\xi)}{\partial \xi^2}\right]_{\xi=i\beta fl}$$

It can be proved for any continuous energy function *V(x)* by means of the so-called Cauchy–Schwarz (or Cauchy–Bunyakovsky) inequality. Three examples are reported in Fig. 1 below.

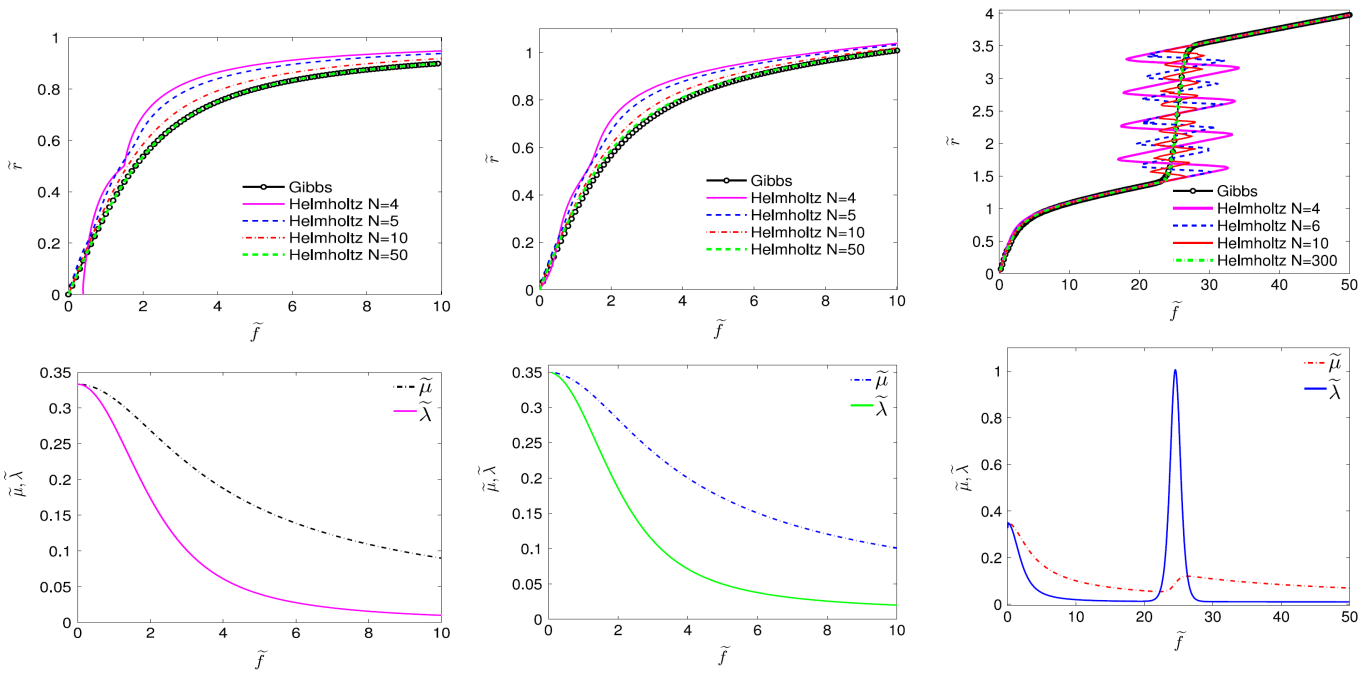

Fig.1 (left) Force–extension curves for Gibbs and Helmholtz ensembles (top panel) and dimensionless eigenvalues (bottom panel) for the freely jointed chain (FJC) model. (centre) Force–extension curves and dimensionless eigenvalues for the extendible bonds chain (EBC) model. (right) Force–extension curves and dimensionless eigenvalues for the two-state chain (TSC) model.

2.3.5.Scaling shift in multi-cracked fiber bundles

(*Fabio Manca, Stefano Giordano, Pier Luca Palla, and Fabrizio Cleri, Scaling Shift in Multicracked Fiber Bundles, PHYSICAL REVIEW LETTERS 113, 255501, 2014***)**

Bundles of fibers, wires or filaments are ubiquitous structures in both natural and artificial materials. We investigate the bundle degradation induced by an external damaging action through a theoretical model describing an assembly of parallel fibers, progressively damaged by a random population of cracks. Fibers in our model interact by means of a lateral linear coupling, thus retaining structural integrity even after substantial damage. Monte Carlo simulations of the Young's modulus degradation for increasing crack density, demonstrate a remarkable scaling shift between an exponential and a power-law regime. Analytical solutions of the model confirm this behavior, and provide a thorough understanding of the underlying physics.

Fiber bundle assemblies are structural elements largely present in both natural materials and technological applications. Nature has extensively exploited the mechanical properties of filamentary biopolymers, such as cytoskeletal proteins, F-actin or microtubules, for many crucial processes in eukaryotic cells. At the tissue length scale we find bundle structures like collagen, spider silk, bone, tendon, muscle, all exhibiting uncommon qualities, including the rare combination of large strength and high toughness. These materials take advantage of specific features, such as the hierarchical assemblage (M. Buehler, Nano Today **5**, 379, 2010), the twisted structure (G. M. Grason, Phys. Rev. Lett. **105**, 045502, 2010), and the degree of disorder that may increase the overall strength (S. W. Cranford, J. R. Soc. Interface **10**, 20130148, 2013). Artificial materials aiming at high mechanical performances have often taken inspiration from biomaterials, such as carbon nanotube that have been used as building blocks for novel assembled systems (L. Liu, W. Ma, and Z. Zhang, Small **7**, 1504, 2011; S. Kumar, *et al.*, Macromolecules **35**, 9039, 2002).
Given their interest as structural materials, mechanical failure in bundles is a major subject of study (S. Pradhan, A. Hansen, and B. K. Chakrabarti, Rev. Mod. Phys. **82**, 499, 2010; H. Kawamura, T. Hatano, N. Kato, S. Biswas, and B. K. Chakrabarti, Rev. Mod. Phys. **84**, 839, 2012). The "fiber-bundle model" (FBM), originally developed to study the failure of spun cotton yarns (F. T. Peirce, J. Text. Ind. **17**, 355, 1926), was extended to consider parallel fibers with statistically distributed strength (H. E. Daniels, Proc. R. Soc. London, Ser. A **183**, 405, 1945). There, when an external load produces the failure of a fiber, its fraction of load is equally redistributed among all the intact fibres (global load sharing). Another redistribution strategy is the so-called local load sharing, stating that the load of a broken fiber is carried only by the nearest intact fibers. It is well known that global and local rules lead to completely different statistical behaviors (S. Zapperi, P. Ray, H. E. Stanley, and A. Vespignani, Phys. Rev. Lett. **78**, 1408, 1997; M. Kloster, A. Hansen, and P. C. Hemmer, Phys. Rev. E **56**, 2615, 1997; P. Bhattacharyya, S. Pradhan, and B. K. Chakrabarti, Phys. Rev. E **67**, 046122, 2003; J. B. Gómez, D. Iñiguez, and A. F. Pacheco, Phys. Rev. Lett. **71**, 380, 1993; D. H. Kim, B. J. Kim, and H. Jeong, Phys. Rev. Lett. **94**, 025501, 2005). The FBM approach has been smartly modified in order to account for the matrix viscoelasticity with a power-law creep compliance, the plasticity, the nonlinear creeping matrix, the brittle-to-ductile transition, and the complexity of specific heterogeneous structures.
In this context, the mechanical degradation induced by external agents, such as chemicals or radiations, is crucial to understand the resistance of bundle materials to variable environmental constraints. As prominent examples, spanning widely different fields, one could cite: the degradation induced by some antibiotics in tendon collagen, or the lysis of muscle sarcomeres produced by some statins; damage in the form of single- and double-strand breaks in DNA irradiated by high-energy photons in cancer radiotherapy, or degraded by a restriction enzyme; at more macroscopic scales, corrosion of high-voltage power cable bundles, or suspended-bridge steel cables; corrosion of steel bundles and meshes in concrete structures; loss of cohesion in tree-root bundles with variable soil wetness, triggering shallow landslides.
In this Section, we investigate a fiber bundle assembly of arbitrary geometry, with M parallel fibers characterised by linear longitudinal response and lateral coupling; the fibers undergo localised damages, in the form of N random breaks affecting the overall Young's modulus. Notably, broken fibers in our model do not lose entirely their cohesion with the bundle, thanks to the lateral coupling k, an essential ingredient to model realistic structures. Although the progressive damage originated by the load redistribution is a relevant effect largely studied within the FBM, we have not included this feature in order to isolate the statistical behavior induced by the random fractures within the interacting fibers. Under this respect, the problem

belongs to the field of homogenization theories. In particular, our approach allows us to demonstrate the existence of a marked shift in the scaling law of the effective Young's modulus of the fiber bundle: the elastic modulus decays with an exponential scaling, $\exp(-N/M)$ at small N, and goes into a power-law scaling, $1/N^2$ at increasing values of N. The threshold N^* between the exponential and the power-law regime is a decreasing function of the lateral coupling k. This "slowing down" shift has therefore important practical implications, in that the yielding of a fiber-bundle material could be postponed to longer times upon increasing the amount of lateral coupling in the bundle.

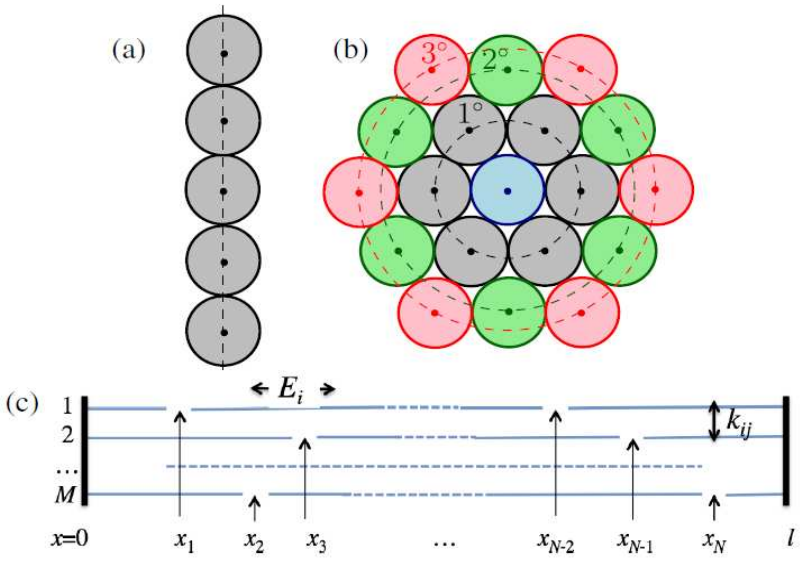

Fig. 1: Cross-sectional view of the bundle structures. In both the flat (a) and in the circular bundle (b), we considered M fibers with $7 \le M \le 19$ (note that $M = 7,13,19$ in the circular bundle correspond to exactly one, two or three shells of neighbours). In (c) the arrangement of M parallel fibers of length l with N breaks at $x_1,...x_N$ is shown; E_i is the longitudinal (Young) elastic modulus of the i-th fiber, and k_{ij} is the lateral coupling modulus of the pair ij.

Let us consider a bundle of M intact parallel fibers of length l, arbitrarily arranged on their cross section, for instance a flat (Fig.1a), or a circular bundle (Fig.1b). The system can be described by the balance equations

$$\frac{\partial T_i(x)}{\partial x} = -G_i(x), \quad \frac{\partial U_i(x)}{\partial x} = \frac{1}{E_i} T_i(x) \tag{1}$$

for $i = 1,...,M$ and $0 \le x \le l$, where

$$G_i(x) = \sum_{j=1}^{M} k_{ij}(U_j - U_i). \tag{2}$$

Here, $T_i(x)$ is the scalar stress, $U_i(x)$ the longitudinal displacement, E_i the Young modulus of the i-th fiber and k_{ij} are the lateral coupling coefficients (Fig.1c). The structure of the matrix k_{ij} introduces the most general coupling rule, being able to define the local, the global and all intermediate interaction schemes. Defining $\vec{\zeta}$ as the vector containing all the variables ($T_1, U_1, T_2, U_2, , T_M, U_M$), the system of equations can be written in the more compact form $d\vec{\zeta}/dx = \mathbf{A}\vec{\zeta}$, where $\mathbf{A}$ is a $2M \times 2M$ constant matrix. Therefore, the behavior of an intact bundle segment can be studied by means of the matrix exponential $\exp(\mathbf{A}x)$.

Let us now introduce a population of N breaks at the arbitrary positions x_i, $i = 1,...,N$. We assume that the fracture located at x_i is assigned to the j_i-th fiber of the bundle ($j_i \in \{1,2,...,M\}, \forall\, i = 1...N$). We also define for convenience $x_0 = 0$ (left end of the bundle) and $x_{N+1} = l$ (right end of the bundle). It is important to

remark that, when a fiber is broken in one or more points, it continues to contribute to the overall stiffness of the bundle through the lateral interactions with the other fibers. Under such assumptions, we can identify $N+1$ intact segments of the entire bundle, for any $x \in (x_i, x_{i+1}), \forall\, i = 0,...,N$. Hence, for each of the above intervals we can write: $\vec{\zeta}(x_{i+1}^-) = \exp[\mathbf{A}(x_{i+1} - x_i)]\vec{\zeta}(x_i^+)$. The fiber breaks are described by the following boundary conditions for $x = x_i$ $(i = 1...N)$: $U_k(x_i^-) = U_k(x_i^+) \forall\, k \neq j_i$ and $T_k(x_i^-) = T_k(x_i^+) \forall\, k \neq j_i$, representing respectively the continuity of displacement, and stress, in the intact fibers. Moreover, $T_{j_i}(x_i^-) = 0$ and $T_{j_i}(x_i^+) = 0$, meaning that there is no transmission of force across the broken fiber. We maintain fixed the left end of the bundle ($U_k(x_0) = 0$) and we prescribe a given displacement to its right end ($U_k(x_{N+1}) = \delta$ where δ is a parameter). If we rearrange the quantities $\vec{\zeta}(x_0)$, $\vec{\zeta}(x_1^-)$, $\vec{\zeta}(x_1^+)$, $\vec{\zeta}(x_2^-)$,..., $\vec{\zeta}(x_{N-1}^+)$, $\vec{\zeta}(x_N^-)$, $\vec{\zeta}(x_N^+)$, $\vec{\zeta}(x_{N+1})$ in a vector $\vec{\eta}$ we obtain a system $\mathbf{B}\vec{\eta} = \vec{b}$ with 4M(N+1) unknowns (it can be shown that $\mathbf{B}$ is always non-singular). For a given distribution of fiber breaks, the effective Young modulus of the overall bundle can be obtained as: $E_{eff} = \frac{l}{\delta}\sum_{k=1}^{M} T_k(l)$, which represents the effective modulus of a single fiber equivalent to the whole degraded bundle.

The most general problem dealing with M fibers and N randomly distributed breaks can only be solved numerically through Monte Carlo (MC) simulations. We generate a large number of break distributions for each given M, N and bundle geometry, from which we calculate the average Young modulus $\langle E_{eff} \rangle$ of the bundle. In the MC simulations we took $E_i = E$ for all fibers and $k_{ij} = k$ for each couple of neighbouring fibers (local coupling). The relative strength of the longitudinal vs. lateral interaction was set by the value of the reduced variable $\xi^2 = kl^2/E$, ranging from 0.045 to 8, to span almost three decades. For both the flat and the circular bundle we set $7 \leq M \leq 19$ (see Fig.1).

The degradation behaviour of $\langle E_{eff} \rangle$ as a function of N can be summarized by the MC results displayed in Fig.2 in which two specific degradation regimes can be clearly identified: for low values of N, the straight lines in the semi-log plot of Fig.2 correspond to an exponential scaling; for larger values of N, the straight lines in the log-log plot (inset) correspond to a power-law scaling (Fig.2 shows results only for the flat bundle and $\xi^2 = 0.045$, the results for other cases being entirely similar).

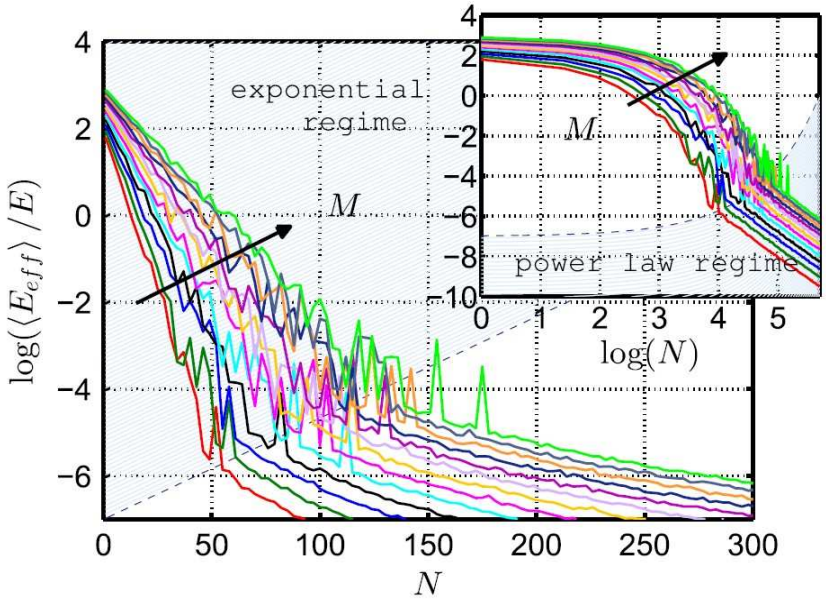

Figure 2: Monte Carlo results for $\langle E_{eff} \rangle / E$ versus N in semi-logarithmic (main plot) and bi-logarithmic (inset) scales. We considered $kl^2/E = 0.045$ and 13 values of M, from 7 to 19.

The shift between these two scaling regimes is, indeed, a very interesting feature, since it marks the passage from a very fast (exponential) decrease of $\langle E_{eff} \rangle (N)$ to a much slower degradation, in what may be called a "slowing-down" shift for the loss of structural integrity. In Fig.3 we report the results of MC simulations for the flat bundle with $M = 19$, for a discrete range of values of $\xi^2 = 0.045$ to 8. It can be seen that the shift at N^* is very sharp for the smallest values of k, and becomes smoother for higher values of the lateral coupling constant (increasing ξ^2). However, N^* decreases logarithmically upon increasing ξ^2, showing that an increase in the amount of lateral interaction between the fibers (even fragmented) anticipates the slowing-down shift to earlier stages of the degradation. We remark that we observed this shift behavior also with non-local couplings among the fibers. It is interesting to note that similar regimes were observed in multi-cracked bulk solid materials, for which it was separately found that randomly oriented cracks lead to an exponential degradation, while parallel cracks lead to a power-law decay of the effective properties.
The physics behind these two limiting regimes can be elucidated by looking at two extreme conditions for which a fully analytical solution to the model can be provided. Firstly, we consider just two interacting fibers, in which $N/2$ breaks are regularly and alternately distributed in each fiber of length l. In this simple, idealised case the model can be explicitly solved, obtaining

$$\frac{E_{eff}(N)}{2E} = \frac{1}{1 + 2 f_N(\sqrt{2}\xi)}, \tag{3}$$

where

$$f_N(z) = \frac{1}{z}\tanh\left(\frac{z}{N+1}\right) + \frac{N-1}{z}\coth\left(\frac{z}{N+1}\right) + \frac{N-1}{z}csch\left(\frac{z}{N+1}\right). \tag{4}$$

We observe that, for N approaching infinity, $E_{eff}(N)$ goes to zero with the power-law $E_{eff} : kl^2/N^2$. Moreover, it is important to recognize that, at large N, the decrease of E_{eff} does not depend on the Young modulus E of the fibers, but is dominated by the lateral interactions among the adjacent fragments of the broken fibers. This underscores the major role of the lateral interaction k, in determining the scaling shift at N^*.

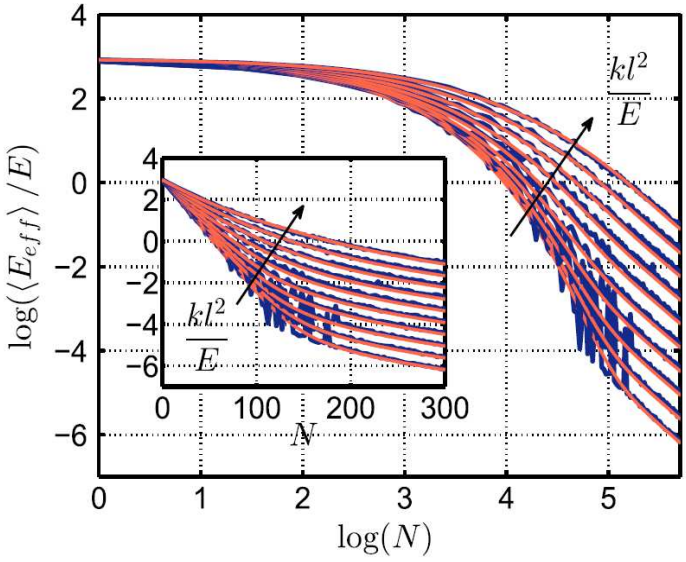

Figure 3: Monte Carlo results (noisy blue lines) and theoretical interpolation (continuous red lines) for $\langle E_{eff} \rangle / (ME)$ *versus* N *for different values of* kl^2/E *(0.045, 0.08, 0.14, 0.25, 0.45, 0.8, 1.4, 2.5, 4.5 and 8) and* $M = 19$ *(flat bundle).*

As a second, analytically solvable case, we consider the system composed of M non-interacting fibers ($k=0$), with N randomly distributed breaks among all the fibers with probability $1/M$. Since lateral interactions are now absent, when a fiber is broken at one or more sites its contribution to the effective stiffness $\langle E_{eff} \rangle$ is zero. We calculate the probability to have n_1 breaks on the first fiber, n_2 breaks on the second one, and so forth. Since there are $N!/(n_1!\cdot\ldots\cdot n_M!)$ sequences of N breaks yielding the particular distribution $\{n_1,\ldots,n_M\}$ (with $\sum_{i=1}^{M} n_i = N$), we find such a probability to be $Pr\{n_1,\ldots,n_M\} = N!/(n_1!\cdot\ldots\cdot n_M! M^N)$. We can therefore determine the probability $\mathsf{P}_s(N)$ to have s intact fibers after producing N random breaks in the bundle. If this is the case, in each distribution $\{n_1,\ldots,n_M\}$ there are s zeros and $M-s$ strictly positive numbers. Since there are $\binom{M}{s}$ combinations of such s zeros within the distribution $\{n_1,\ldots,n_M\}$, we eventually obtain

$$\mathsf{P}_s(N) = \binom{M}{s} \sum_{\substack{M-s \\ \sum_{i=1} n_i = N}}^{n_i>0} \frac{N!}{n_1!\cdot\ldots\cdot n_{M-s}!} \frac{1}{M^N}. \tag{5}$$

This expression for the probability can be summed, to obtain the following result in closed form

$$\mathsf{P}_s(N) = \frac{M!}{s!\,M^N} \mathsf{S}_N^{M-s}, \tag{6}$$

where S_n^m is the Stirling number of the second kind. This last equation can be used to prove that the probabilities $\mathsf{P}_s(N)$ generate a complete probability space, i.e. $\sum_{s=0}^{M} \mathsf{P}_s(N) = 1$. From the same equation, we obtain an explicit expression for the effective Young's modulus of the fiber bundle in the absence of lateral interactions

$$\frac{\langle E_{eff} \rangle}{ME} = \frac{1}{M} \sum_{s=0}^{M} s\mathsf{P}_s(N) = \left(\frac{M-1}{M} \right)^N \cong e^{-N/M}, \tag{7}$$

the last approximation being valid for large values of M . This second analytical result shows that the mechanical degradation in a bundle of non-interacting fibers follows an exponential law in the single variable N/M .

The above two limiting results allow to formulate appropriate scaling functions with free parameters, by which the whole results of MC simulations for any bundle geometry, size M , and interaction strength ξ^2 , can be represented. In fact, the exponential regime at small values of N is described by

$$\log \frac{\langle E_{eff}^{exp} \rangle}{ME} = -\varphi(\xi) \frac{N}{M^{\alpha}}, \tag{8}$$

with $\varphi(\xi)$ a function, to be determined by fitting the MC results, which describes the early-stage degradation of the bundle stiffness $\langle E_{eff} \rangle$ as a function of the relative interaction strength $\xi = \sqrt{kl^2/E}$. The shape of the function $\varphi(\xi)$ extracted from the MC simulations is shown in Fig.4, for the flat and circular bundle geometries. The value $\varphi(0) = 1$ is coherent with Eq.(7), when $k = 0$. The function is universal for a large enough M (in practice, already for M>10), and goes into the asymptotic behavior $\varphi(\xi) : c/\xi$ at large ξ , the value of c depending on the geometry ($c = 1.45$ for the flat, and $c = 0.85$ for the circular bundle, respectively).

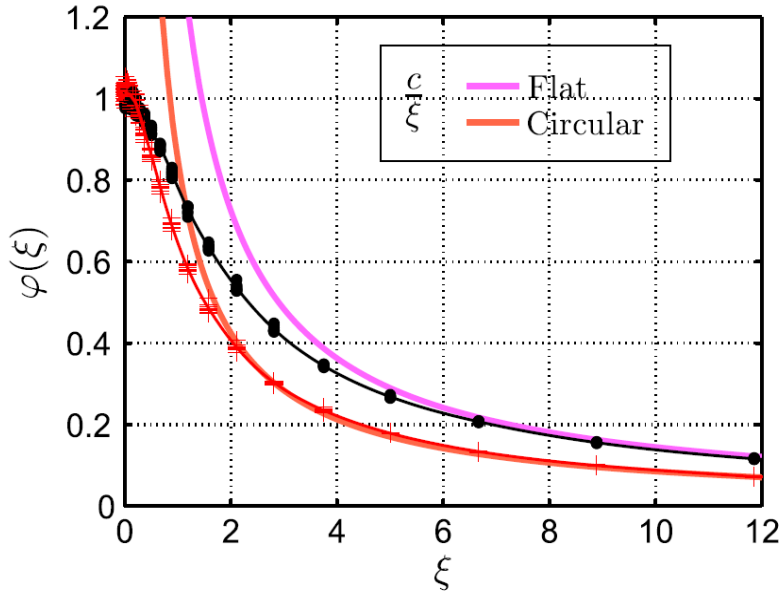

Figure 4: Numerical determination of the function $\varphi(\xi)$ defined in Eq.(8). The black curve (flat bundle) and the red curve (circular bundle) are asymptotically converging to $\varphi(\xi) = c/\xi$ with $c = 1.45$ (flat bundle) and $c = 0.85$ (circular bundle).

On the other hand, the power-law regime at larger N can be described by

$$\frac{\left\langle E_{eff}^{pow} \right\rangle}{ME} = a \frac{M^{\beta} \left(\sqrt{\frac{kl^2}{E}} \right)^{\nu}}{N^b}. \tag{9}$$

The best fit of the free parameters α, a, b, β and ν in Eqs. (8-9) from the numerical MC simulations are reported in Table 0. Coherently with Eq.(7), $\alpha = 1$, thus extending to any value of k the analytical result for $k = 0$, at small N. In the same way, the fitted value $b = 2$ confirms for any value of M the $1/N^2$ scaling, analytically obtained for $M = 2$. Furthermore, the value $\nu = 2$ obtained by the best fit allows to explain the loss of significance of E, and the parallel increase of importance of k, in determining the asymptotic effective stiffness $\left\langle E_{eff} \right\rangle$: indeed, for $\nu = 2$ the E appearing in the RHS and LHS of Eq.(9) cancel out each other. Therefore, the physical explanation of the shift towards a slower (power-law) degradation regime would be that increasingly small fiber fragments are only weakly deformed, and the effective Young modulus is eventually determined by their interactions.

Table 1: Parameters and scaling exponents characterizing the fast (exponential) and slow (power-law) degradation regimes.

	Parallel bundle	Circular bundle
α	0.97 ± 0.06	1.05 ± 0.12
a	0.40 ± 0.06	0.40 ± 0.07
b	2.09 ± 0.11	2.08 ± 0.21
β	2.29 ± 0.19	2.61 ± 0.35
ν	1.97 ± 0.25	1.91 ± 0.37

Finally, Eqs.(8) and (9) can be unified in a single function $\langle E_{eff} \rangle / ME = \mathsf{E} + 1/(r/N + 1/\mathsf{P})$, where $\mathsf{E} = \langle E_{eff}^{exp} \rangle / ME$ from Eq.(8), and $\mathsf{P} = \langle E_{eff}^{pow} \rangle / ME$ from Eq.(9). The switching between the two regimes is controlled by the coefficient r, which assumes the values 1.0×10^3 for the flat bundle and 3.0×10^3 for the circular one. This function is the origin of the continuous lines in Fig.3, nicely representing the MC simulations over the entire range of parameters.
In the present Section, we discussed a purely elastic system. Nevertheless, we have also studied a time-invariant viscoelastic coupling, described by a complex valued k under a permanent sinusoidal regime. Again, we observed the scaling shift between the exponential and power-law responses at N^*, which is now a decreasing function of the viscosity (further details will be published elsewhere). Other refined models for the viscoelastic behavior should be adopted to analyze more realistic structures, e.g. the power-law creep compliance, the plasticity and the nonlinear creeping.
In conclusion, we predicted the existence of an unprecedented exponential to power-law "slowing-down" shift in the degradation of a multi-cracked bundle. The lateral interaction among the fibers is the key ingredient in triggering this shift as a function of the crack density N. Notably, the critical value N^* can be lowered by increasing the interaction strength, a relevant feature for practical purposes. For example, in radiation (G. Perret, *et al.*, IEEE Conf. Eng. Med. Biol. 2013, 6820, 2013) or chemical (M. Kumemura, *et al.*, International Conference on Micro Electro Mechanical Systems MEMS, Cancún, IEEE, 2011) damage of DNA bundles for cancer radiotherapy, the knowledge of the degradation dynamics is useful to properly design therapy protocols. In related experiments an exponential degradation has been measured, which exactly corresponds to the first regime found in our investigation. Moreover, a strong dependence on the viscosity of the solution has been observed concerning the degradation velocity of the mechanical response. Although no quantitative results are presently available, there are indications that larger values of the viscosity in strongly degraded DNA bundles lead to a complex non-exponential dynamics, which could correspond to a scaling shift induced by denser buffer media.

3.Positioning the research in the laboratory context

Upon arrival at IEMN in October 2010, I joined the AIMAN group ("Acoustique Impulsionnelle et Magnéto-Acoustique Non-linéaire") coordinated by Prof. Philippe Pernod and the International Laboratory LICS, "Laboratoire International des phénomènes Critiques et Supercritiques", coordinated by Prof. Philippe Pernod (French side) and Prof. Vladmir Preobrazhensky (Russian side) (both at the "École Centrale de Lille", Cité Scientifique, 59651 Villeneuve-d'Ascq). This structure is the new version of the old International Laboratory LEMAC "Laboratoire International associé en Magnéto-ACoustique nonlinéaire de la matière condensée", closed in 2012 after 8 years of activity.

The AIMAN group of IEMN is composed of 32 researchers of which 11 are permanent (4 Professors, 4 "Maîtres de conférences", 3 Researcher CNRS). The activities mainly deal with: analysis of the multi-physics phenomena at the interface among wave propagation in electromagnetism and acoustics, magnetism, active and/or flexible nano-structures, micro-nano-technologies and microfluidics with the final aim of developing and realizing innovative applications in: ultrasound systems, electronic components and/or systems with special functionalities and microfluidics.

We can take into consideration four main lines of research for summing up the AIMAN group developments:

-Multistable nanostructures, very low power consumption components, towards the new paradigms for information processing

-Critical state materials, bosonic and composite nanostructures, towards the functional electronics and the theragnostic

-Flexible electronics and MEMS (micro electro-mechanical systems)

-Functional microfluidics, interface dynamics, MEMS for flow control.

My activity is integrated within the first line of the AIMAN group for the development of models for the magnetization control in ferromagnetic particles (with external actions such as electric fields or temperature) with the aim of developing new memory elements and, in the future, new implementations of memristive devices. In this line of research the studies concerning the properties of multiferroics (magneto-electro-elastic composites) are of vital importance in order to develop new structures with desired responses and properties. Also, I can give my contribution to the second research line of the AIMAN group for predicting the effective overall properties of heterogeneous or composite materials and structures largely used to realize components in functional electronics and theragnostic. Here, the aspect of the coupling between the physical properties and the possibility to consider imperfect interfaces among the constituents play a central role. The Eshelby theory and its generalizations find several applications in this field. My research activity on the elastic properties of polymeric chains has created interesting interactions with the second line of the AIMAN group (being the polymer domains with conformational transitions a good example of critical state systems) and with the third line where the elastic properties of polymeric materials are important to develop new sensors, actuators and flexible components (see for further details http://aiman.iemn.univ-lille1.fr).

As for the LICS international laboratory we give below a brief introduction on his history. The Joint International Laboratory LIA LICS results from more than 16-years scientific collaboration established since 1996 from French side by the Institute of Electronics, Microelectronics and Nanotechnology (IEMN-UMR CNRS 8520) / EC Lille and from Russian side by the Wave Research Center of A. M. Prokhorov General Physics Institute of Russian Academy of Sciences (WRC GPI RAS). The initial field of collaboration was focused on nonlinear magneto- acoustics of solids and applications in ultrasonics. In 2004 the collaboration was formed as the European Associated Laboratory on Nonlinear magneto-acoustics of condensed matter (LEA LEMAC). The domain of activity was extended on nonlinear ultrasonic imaging based on parametric wave phase conjugation and micro magneto-mechanical systems (MMMS). The new partners such as Moscow State Institute of Radio Engineering Electronics and Automation (Technical University MIREA) and Taurida National University (TNU, Ukraine) were involved in collaboration. Taking into account the partnership with the Ukrainian University, the Laboratory was reorganized in 2008 into the International Associated laboratory (LIA LEMAC). The activity on micro-systems was extended on micro-fluidics and nanostructured active films and multiferroics. The Joint International Laboratory LIA “LICS” between France, Russia and Ukraine on “Critical and supercritical phenomena in functional electronics, acoustics and fluidics” is a new LIA project for period 2013-2016, with enlarged and strongly renewed scientific scope. It is constructed on the core part of the partnership established during the 1995-2012 years, but presents slight evolutions of the members in accordance with the new scientific program.

The LICS composition is the following (see Fig.1 below):

1. Institute of Electronics, Microelectronics and Nanotechnology « IEMN », (UMR CNRS 8520), Villeneuve d’Ascq, France
2. Wave Research Center of A.M. Prokhorov General Physics Institute « WRC-GPI » (RAS), Moscow, Russia
3. V.A.Kotel’nikov Institute of RadioEngineering and Electronics « IRE » (RAS), Moscow, Russia
4. Moscow State Institute of Radio-Engineering, Electronics and Automation (MIREA, Technical University), Departments of Cybernetics and Electronics, Moscow, Russia
5. N.P.Ogarev Mordovia University, Department of Radio-Engineering, Saransk, Russia
6. V.I. Vernadsky University of Taurida, Department of experimental physics, Simferopol, Crimea, Ukraine

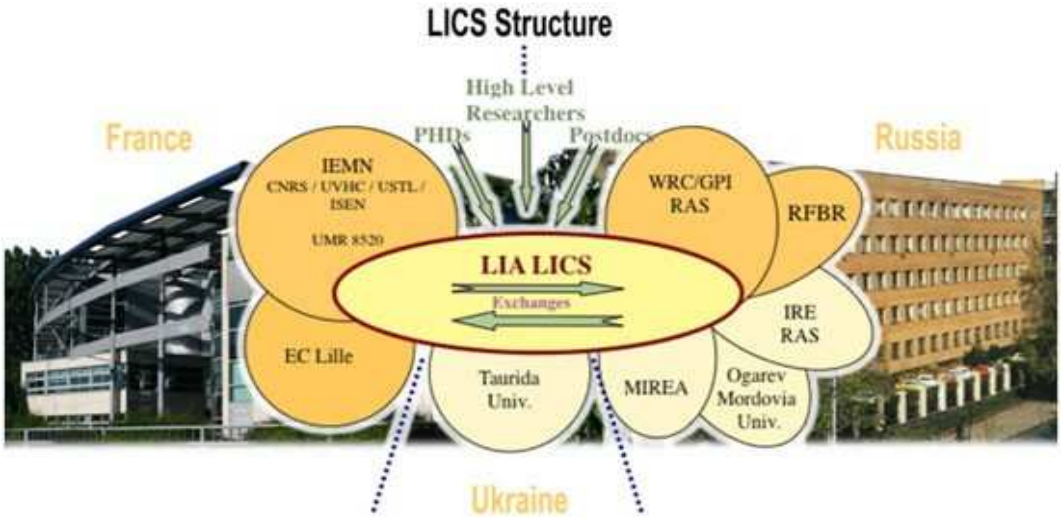

Fig.1. International structure of the LICS laboratory.

The laboratory is dedicated to studies of static, quasi-static and dynamic critical and supercritical phenomena in multi-physic fields of functional electronics, acoustics and fluidics. The fundamental investigations are focused on specific features of coupled nonlinear systems near equilibrium and non-equilibrium phase transitions. Taking into account prospective of innovative applications three hot topic objects of studies are defined (see Fig. 2):

1) Multistable & bosonic micro/nanostructures;

2) Critical State (CS) materials, composites & soft structures;

3) Functional micro-fluidics & interface dynamics.

Each of the three tasks can be subdivided in a series of subtasks described in Fig. 3 for the sake of completeness.

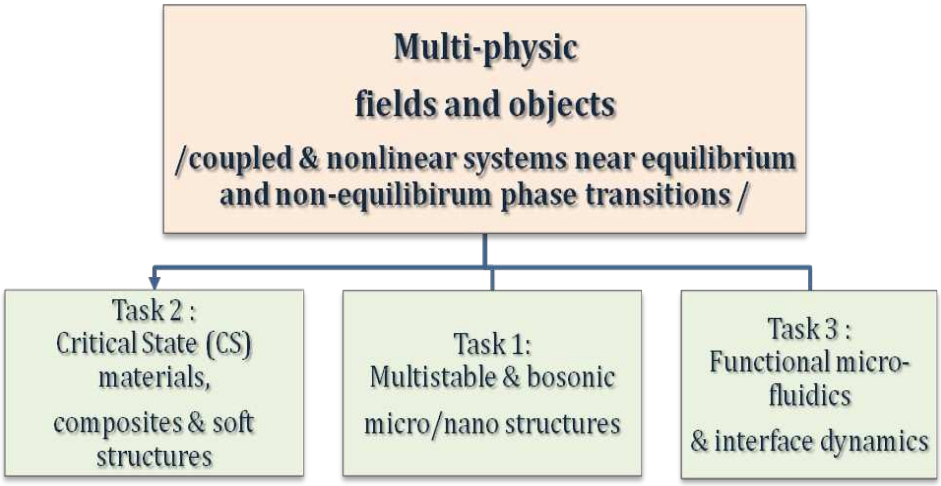

Fig.2. Three main tasks of the LICS laboratory.

My contributions can be therefore summed up as follows:

Subtask 1.1: development of theoretical models for the magnetization behaviour and switching (spin reorientation transition) in particles under the effect of external fields and temperature (applications to memory elements and memristor devices). Exploitation of the LLG equation and of the Langevin/Fokker-Planck methodology.
Subtask 2.2: analytical determination of the effective properties of multi-physics magneto-electro-elastic coupled materials with linear and nonlinear response (generalizations of the Eshelby theory, applications of the complex elastic potentials method, advanced homogenization techniques).
Subtask 2.1: analysis and design of artificial multiferroic structures (piezoelectric and magnetoelastic combined systems) with different components and microstructures (calculation of the effective magneto-electric response with the aim of realizing stress-mediated sensors and actuators).
Subtask 2.3: study of the thermo-mechanic response of polymer chain with conformational transition (application to molecules of biological interest) and generalization to bundles of chains.

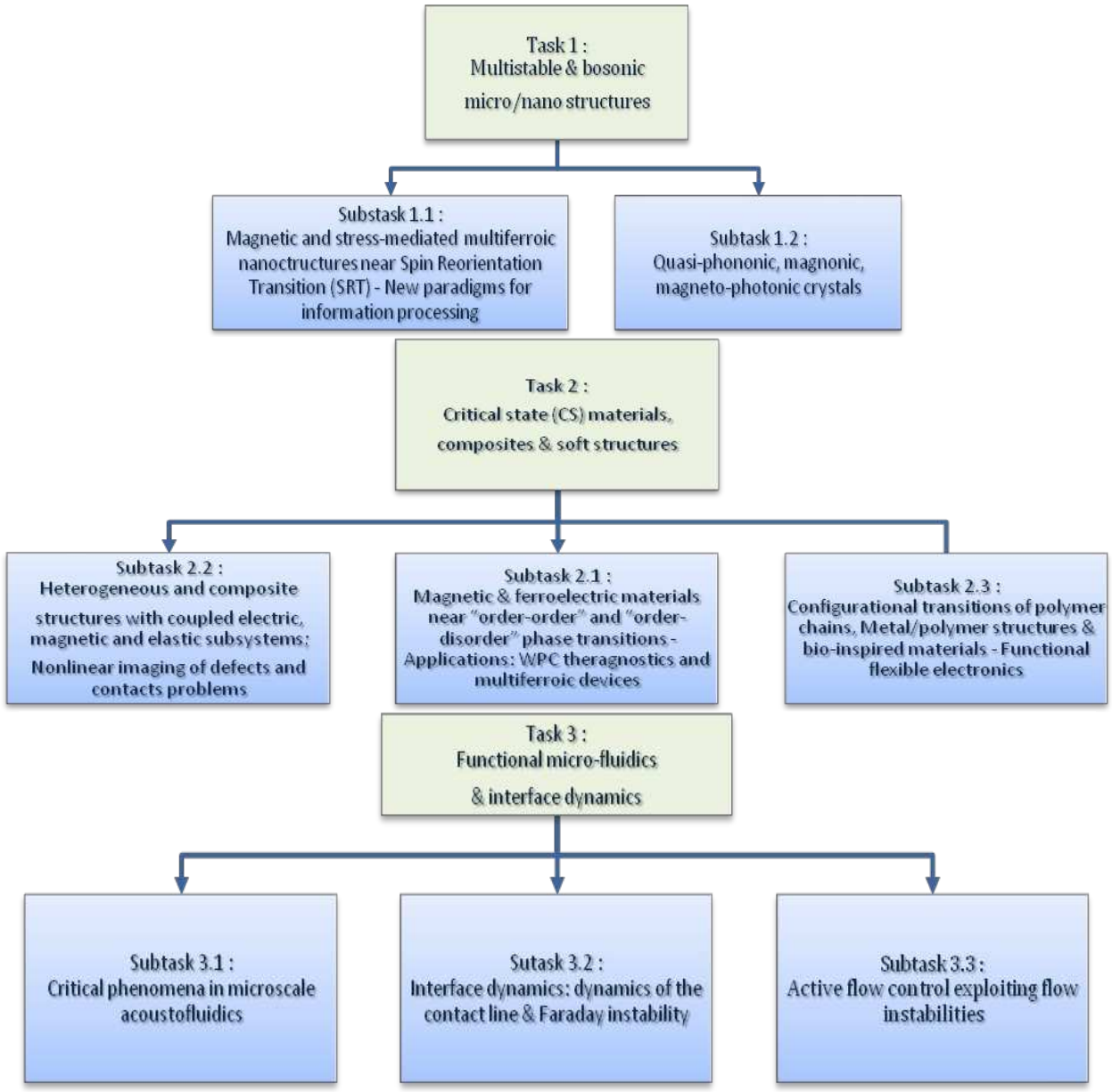

Fig. 3. Details of the three main scientific directions of the LICS laboratory.

4.Research project

I plan to work on the following topics in the near future.

a) Effects of an interphase between particles and matrix in magnetostrictive composites

In order to further explore the effects of imperfect interfaces in composite materials and structures we will also consider the case of the magnetostrictive composites (an introduction to the problem can be found in: International Journal of Solids and Structures 44, 2007, 18–33). In this case we suppose to deal with a population of mono-domain ferromagnetic particles embedded in a pure elastic matrix (some generalizations concerning a piezoelectric matrix can be contemplated in order to generate a sort of electric field induced artificial martensitic transformation: this is a possible extension of this research line). First of all, we will develop a procedure for homogenizing the behaviour of these heterogeneous materials without imperfect interfaces between particles and matrix. To do this, we consider the energy function of a single ferromagnetic domain given in Eq.(1) (pag.16) with a given anisotropic energy and a given magnetostriction (of course, they depend on the specific material utilised). We can assume the hypothesis of dilute dispersion and, therefore, we can determine the internal fields (elastic stress and magnetic field) inside the particles through the well-known Eshelby theories. Furthermore, we can determine the average of the fields over the whole structure in order to write the energy function for each particle in terms of these average quantities. The homogenization problem will be therefore reduced to a minimization problem, solvable with standard numerical techniques (a similar approach can be found in J. Mech. Phys. Sol. 54, 2006, 951-974). The same procedure will be developed for the case with an interphase between particles and matrix. In this case the important point is to determine the average values of the physical fields both inside the particles and in the coatings, representing the imperfect contacts. This problem will be approached with different methodologies depending on the dimensionality of the system. For two-dimensional systems we will use the Kolossov-Muskhelishvili complex potentials, which are able to describe any state of stress/strain in a planar system (Muskhelishvili, N.I., 1953. Some Basic Problems in the Mathematical Theory of Elasticity. Noordhoff, Groningen, Holland). With this technique we believe it is possible to obtain the exact average values of the important quantities both in the ferromagnetic cores and in the external shells. On the other hand, for the three-dimensional case we must adopt some approximated techniques in order to avoid the numerical full field approach (we will use the method described in International Journal of Solids and Structures 48, 2011, 2393–2401 and in Philosophical Magazine, 90:22, 3003-3026). The originality of this research should be the possibility to explore the effects of the imperfect contacts between particles and matrix in terms of all parameters describing the considered interphase. In fact, typically, the interfaces effects have been taken into consideration through some *ad hoc* jump equations for the physical fields (zero-thickness approach), which approximately represent a given interphase only under specific hypothesis. The consideration of a realistic interphase with a given finite thickness allows us to observe all the possible modifications of the overall effective magnetostriction induced by all the contacts features.

b) Memristive devices and spike-timing-dependent-plasticity

This line of research will deal with the possibility to combine piezoelectric phases with magnetoelastic ones in order to implement new devices with memristive behaviour, with applications to the emerging field of neurocomputing (Chua, L. O.,1971, Memristor - the missing circuit element. *IEEE Trans. Circuit Theory* 18, 507-519 ; Strukov, D. B., Snider, G. S., Stewart, D. R., and Williams, R. S., 2008, The missing memristor found. *Nature* 453, 80-83 ; Pershin, Y. V., and Di Ventra, M., 2010, Practical approach to programmable analog circuits with memristors. *IEEE Trans. Circuits Syst. I* 57, 1857-1864 ; Pershin, Y. V., and Di Ventra, M., 2010, Experimental demonstration of associative memory with memristive neural networks. *Neural Netw.* 23, 881). This approach represents a very exciting overlap between nanotechnology and neuroscience, which has been discovered and introduced by neuromorphic engineers (Mead, C., 1989, *Analog VLSI and Neural Systems*. Reading, MA: Addison Wesley and http://en.wikipedia.org/wiki/Neuromorphic). The idea is that of linking some types of memristor nanotechnology devices to the biological synaptic update rule known as spike-time-dependent-plasticity (STDP) found in real biological synapses (see e.g., Front. Neurosci., 17

March 2011, doi: 10.3389/fnins.2011.00026). Understanding this link may allow neuromorphic engineers to develop circuit architectures that use this type of memristors to artificially emulate parts of the visual cortex. The final result is the development of a complete elaboration system based on a new paradigm for the treatment of the information.

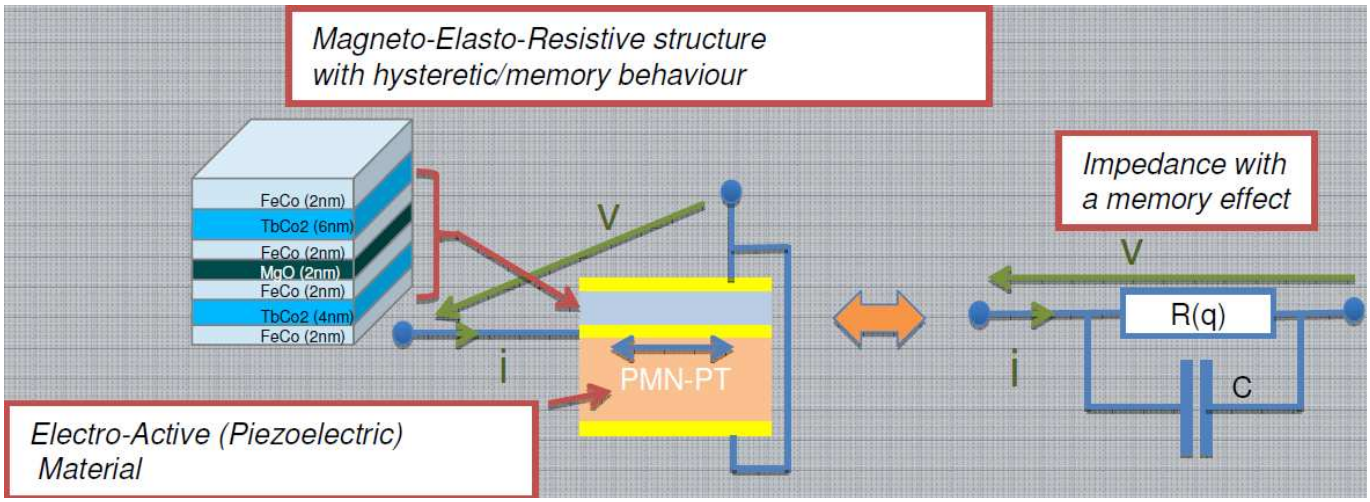

Fig.1. Scheme of a proposed memristive device implementing the spike-time-dependent-plasticity response. This analog 'memristive' component can be used for synapse implementation in neuromorphic architectures.

The planned activity concerns the design and the analysis of innovative memresistive devices, which can be used in neurocomputing structures. We believe that the combination of piezoelectric phases with magnetoelastic ones can lead to new interesting devices with memristive behaviour. We will primarily focus on ferroelectric relaxor, which is the base of our structures. In order to manipulate magnetization in the plane of the magnetoelastic layer, in-plane anisotropic stress is required. Commercially available single crystals PMN-PT (cut in the <011> direction) exhibit very large anisotropic deformations (typical values: d31 = -1900 pC/N, d32 = +1000 pC/N). With such a material, we evidenced the control of magnetization in a magnetoelastic layer at a large scale (see "Stress-mediated magnetoelectric memory effect with uni-axial TbCo2/FeCo multilayer on 011-cut PMN-PT ferroelectric relaxor", DUSCH Y., TIERCELIN N., KLIMOV A., GIORDANO S., PREOBRAZHENSKY V., PERNOD P., 12th Joint Magnetism and Magnetic Materials-Intermag Conference, MMM-Intermag 2013, Chicago, IL, USA, January 14-18, 2013, J. Appl. Phys., 113, 17, 2013, 17C719). In order to develop Magneto-Elasto-Resistive structures we will explore the embedding of magnetoelastic materials such as $TbCo_2$ or FeCo in magnetoresistive structures such as GMR (Giant Magneto Resistance) pillars or MTJs (Magnetic Tunnel Junctions). While the realization of these devices will be made at IEMN within the AIMAN group, I will be mainly involved in their modelling and analysis. A typical structure that will be taken into consideration is shown in Fig.1, where the piezoelectric substrate and the magnetoresistive multilayer are represented and coupled in a complete realistic structure. The magnetostrictive multilayer is composed of two regions separated by an oxide controlling the tunnelling effect. The first region (at the top) has a fixed (hard) magnetization, which remains constant during the working operations. On the other hand, the second region (at the bottom, near the ferroelectric relaxor), has a free (soft) magnetization, which can be easily oriented with external actions. It is well known that a current flowing in this device feels an electric resistance depending on the angle between the magnetization vectors in the two adjacent regions above (F. Montaigne, C. Tiusan, and M. Hehn, Angular dependence of tunnel magnetoresistance in magnetic tunnel junctions and specific aspects in spin-filtering devices, JOURNAL OF APPLIED PHYSICS 108, 063912, 2010). The elastic strain (deformation) imposed by the piezoelectric substrate interact with the magnetoresistive laminated material through the magnetoelastic coupling. Therefore, the corresponding magnetization (in the soft region) can be controlled through the electric charge accumulated in the electrodes across the piezoelectric substrate. It is therefore evident that we can obtain a Magneto-Elasto-Resistive structure with hysteretic memory behaviour. My activity will deal with the modelling of this device, by taking into account all the physical coupling occurring in the structure and the full dynamics of all components.

A second possibility that will be explored in order to obtain a continuous variation of a resistance generated by a tunnel junction concerns the use of a domain wall between two magnetic domains in a ferromagnetic sample. The idea is that of creating a continuous motion of the domain wall controlled by a mechanical stress, generated by a piezoelectric substrate as before.

c) Modelling of damage in bundles of DNA chains by therapeutic radiation beams

In the TWEEZ-RT Project (IEMN-LIMMS) and in recent literature quoted below, an experimental method is proposed to establish a direct correlation between the ionizing radiation and its damaging effects on DNA. Such a nanotechnology-based method is both revolutionary and straightforward, thanks to the unprecedented accuracy attainable and the extremely high technological level implied by the set up. We will employ a sophisticated nanoscale electromechanical device, the Electro-Mechanical Silicon Nanotweezer (SNT), to directly measure the rate of breaking of DNA placed under the radiation beam. DNA bundles of known sequence will be trapped and held straight in parallel strands between the tips of the SNT device (see Fig.1). Such nanoscale vibrating tips can measure with extreme accuracy the elastic modulus and viscosity of the DNA bundle immersed in physiological water in a sealed microfluidic chamber (C. Yamahata, D. Collard, B. Legrand, T. Takekawa, M. Kumemura, G. Hashiguchi, and H. Fujita, *J. Microelectromech. Syst.* 17, 623–631, 2008 and M. Kumemura, D. Collard, S. Yoshizawa, D. Fourmy, N. Lafitte, S. Takeuchi, T. Fujii, L. Jalabert and H. Fujita, *IEEE 23th Int Conf. on Micro Electro Mechanical Systems, MEMS 2010*, 915–918, 2010). During the irradiation, under well-known and fully characterized conditions by means of different machines typical of clinical radiotherapy, DNA strands will break, thus progressively reducing the bundle size (thickness). Correspondingly, the SNT device will measure the dynamical variation of the mechanical response of the bundle, with a time-constant characteristic of the type of damage, from which the crucial information about the rate (efficiency) of each damage mechanism can be directly assessed (C. Yamahata, D. Collard, T. Takekawa, M. Kumemura, G. Hashiguchi, H. Fujita, *Biophys. J.* 94, 63, 2008).

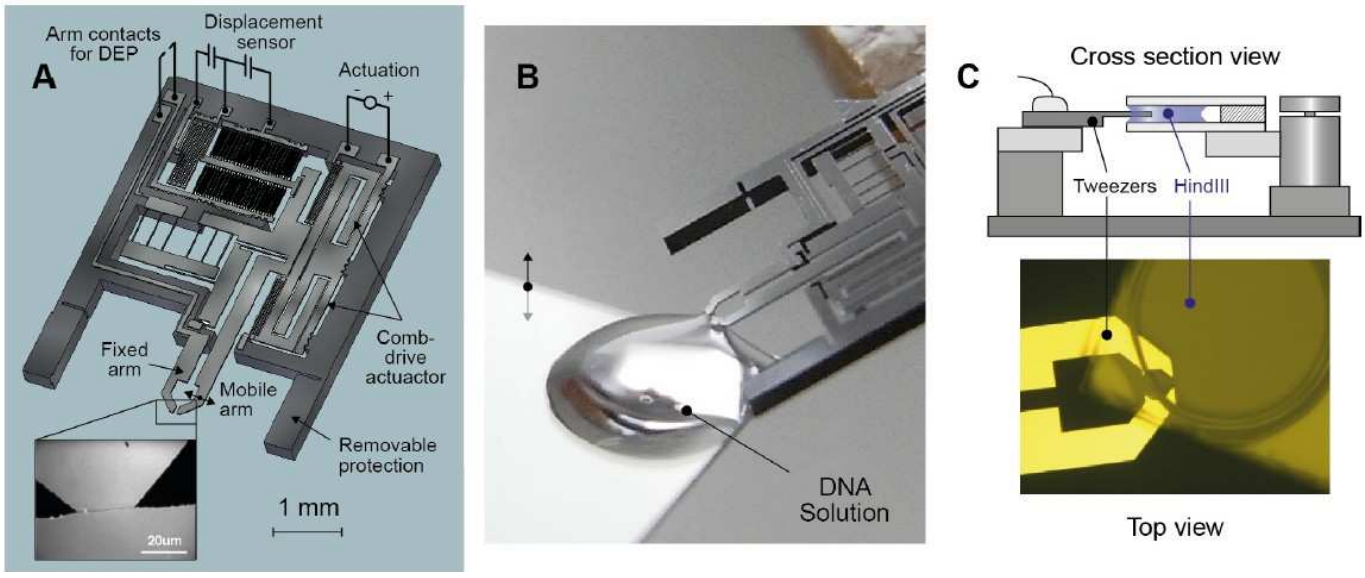

Fig. 1. Silicon Nanotweezers. A: Schematic plot showing the integrated functions. Insert: trapped DNA bundle between tips. B: DNA tapping procedure with Dielectrophoresis (DEP). C: Insertion of the SNT tips with the DNA in a microfluidic cavity for enzymatic reaction monitoring (the HIND-III is a restriction enzyme digesting the DNA and therefore mimicking the effects of the radiation in first experiments).

Evidently, the proposed DNA-bundle geometry with its parallel, fully extended strands, would be quite far from the tightly packed, coiled DNA inside a cell. However, this partial lack of realism is largely compensated by the qualitative homogeneity and quantitative reproducibility of our experiments (in the same spirit of, e.g., the irradiation experiments performed on crystallized DNA oligomers). In the attempt to compensate for such a limitation, in this activity we will also develop and use biophysics theoretical and numer-

ical models, to support the analysis of experiments and correlate the results with the in vivo DNA configurations.

In order to continue the activity described in Section 2.3.5, a range of biophysical theory and modelling studies will be developed, with the twofold aim of: (a) supporting the analysis and interpretation of the experimental results; and (b) attempting at a scale-up of the results from the *in vitro* experiments to some typical in vivo conditions. We propose to work on combined mesoscopic-Monte Carlo statistical modelling.

To correlate the results of SNT experiments with living-cell DNA, we will set up mesoscale coarse-grained models, complemented by Monte Carlo simulations, of the correlation between damage rate and mechanical response of parallel DNA bundles. We can envisage different models of increasing complexity as represented in Fig.2.

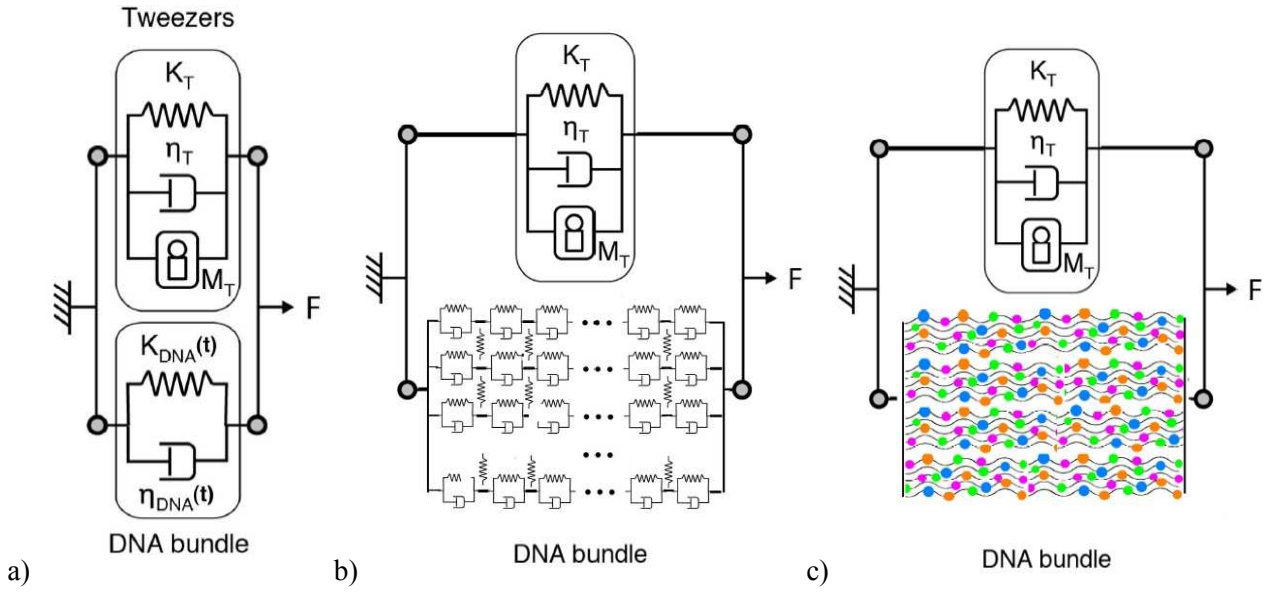

Fig.2. The models with increasing complexity: a) a forced–damped harmonic oscillator actuated by a harmonic force; b) a parallel/series bundle of many coupled forced–damped harmonic oscillators, actuated by a harmonic force; c) a coarse-grained molecular model of coupled flexible-extensible polymer chains, actuated by a harmonic force.

A brief description of these models follows:

a) a forced–damped harmonic oscillator actuated by a harmonic force ; we will consider double spring-and-dashpot with time evolving $K_{DNA}(t)$ and $\eta_{DNA}(t)$ describing the degradation of the DNA bundle. The system is simply described by a coupled system of partial differential equations (PDEs) with varying coefficients (analytical/numerical solution).

b) a parallel/series bundle of many coupled forced–damped harmonic oscillators, actuated by a harmonic force ; it is formed by double springs-and-dashpots with damageable properties, describing the degradation of the individual fibres in the DNA bundle. A similar structure can be realized with a series of coupled elastic chains. These systems are described by complex coupled systems of many PDEs with varying coefficients (analytical in simple cases/numerical solution for the full system).

c) a coarse-grained molecular model of coupled flexible-extensible polymer chains, actuated by a harmonic force; it is described by a molecular model of fully coupled individual DNA fibres in a bath, susceptible of various types of localized degradation. The PDE for the tweezers is coupled to a symbolic load with elastic and damping coefficients derived by the iterative solution of coarse-grained molecular dynamics simulations (numerical/Monte Carlo solution).

d) <u>Homogenization of composite or heterogeneous bundles with random or periodic structures</u>

We plan to work on the homogenization of elastic bundles composed of non-homogeneous and interacting fibers. These structures are very important in several biophysical developments being representative for collagen (main structural protein of the various connective tissues in animals, see Fig.1), sarcomere (the basic unit of a muscle, see Fig.2) and other molecular structures. The most important geometries correspond to periodic bundles. We will suppose that a given section of length L, which represents the "period" of the repetitive structure, is composed of S homogeneous sub-sections, by generating a piece-wise homogeneous bundle. The ideal mechanical link among the sub-sections is described by the continuity of the stress and the displacement. For a given sub-section ($i=1,...,N$) the system is described by $d\vec{\zeta}/dx = \mathbf{A}_i\vec{\zeta}$, where $\vec{\zeta}$ is composed of all stresses and displacements ($2M$ components for M fibers); $\mathbf{A}_i$ represents the viscoelasticity of fibers and their mechanical interactions (see Section 2.3.5 for details about the mathematical setting). The overall behavior of a "period" of bundle is given by $\vec{\zeta}(L) = \exp(\mathbf{A}_S l_S)\cdot\ldots\cdot\exp(\mathbf{A}_1 l_1)\vec{\zeta}(0)$ where l_i is the length of the sub-section i. For a sequence of N periods we can define the effective elastic properties with an isometric ensemble (prescribed displacement) and with an isotensional ensemble (prescribed stress). We expect that both results, for large N, converge to the solution for the periodic bundle. This point will be widely studied in detail by considering particular cases and the general Floquet theory.

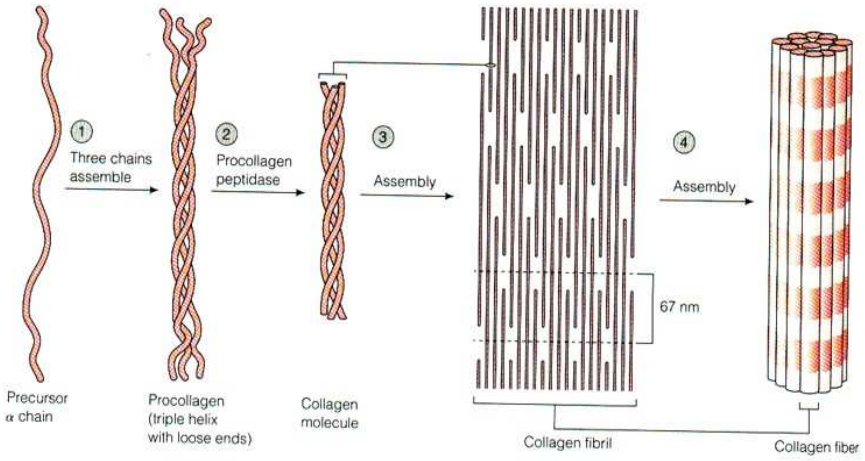

Figure 1. Collagen structure.

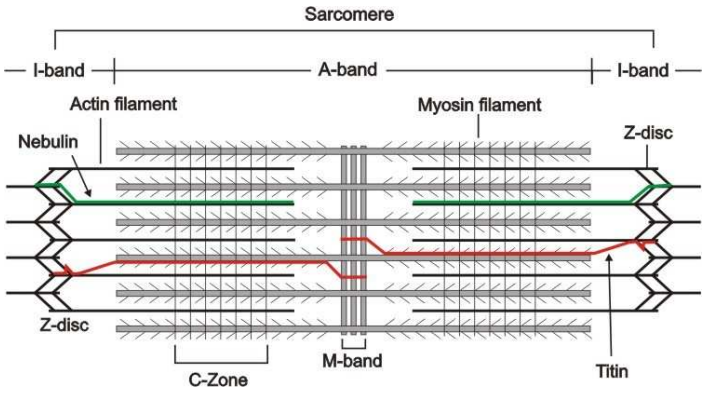

Figure 2. Sarcomere structure.

e) Nonequilibrium statistical mechanics for constrained systems

We will analyse an approach to the non-equilibrium statistical mechanics of arbitrary holonomic systems described in arbitrary coordinates and subjected to arbitrary external actions. We will try to generalize the classical Lagrange and Hamilton motion equations with friction and noise terms, representing the effects of a Langevin thermal bath (at a finite temperature T>0). Then, we will apply the Fokker-Planck methodology in order to obtain the generalized Klein-Kramers equation, describing the dynamics of the density probability in the phase space. Afterwards, we could analyse the over-damped behavior of the system and we eventually obtain the over-damped Langevin dynamics and the corresponding Smoluchowski equation, characterizing the stochastic motion in the configurational space.

Importantly, these equations will be written in a generally covariant form (within either the Ito or the Stratonovich formulations) and they will exhibit asymptotic solutions corresponding to the Gibbs distribution, being therefore coherent with standard thermodynamics. We also will try to prove that the over-damped Langevin dynamics of a free holonomic system exactly corresponds to the mathematical definition of the Brownian motion on a differentiable manifold. These results should find significant applications in the study of several statistical mechanics properties of constrained molecular assemblies (e.g. polymers) of interest in chemistry, physics and biology.

These examples typically concern molecular structures with stiff bonds and rigid constraints (e.g., freely-jointed polymer chains) or systems constrained to move on given surfaces (e.g., biopolymers on membranes). Therefore, these structures must be analysed through generalized coordinates, which lead to a very complex framework for the rigorous introduction of the non-equilibrium statistical mechanics.

We will start from the standards results of the analytical mechanics rewritten by taking into account the two additional terms above discussed, adopted to introduce the non-equilibrium statistical mechanics: a friction term and a noise term. They describe the interaction between the system and a thermal bath, introducing an energy exchange and a correct asymptotic thermodynamic equilibrium. Indeed, it is well known that for a single particle described with orthogonal coordinates this development leads to the standard Gibbs distribution for long time. The aim of the present activity is to obtain a statistical mechanics coherent formalism for a system described by an arbitrary set of generalized coordinates, describing the configuration of a constrained system in standard Lagrangian and Hamiltonian mechanics. The objective is to develop a Klein-Kramers equation for a general holonomic scleronomous system, to prove the coherence with the asymptotic Gibbs distribution and to perform the over-damped limit yielding the so-called Smoluchowski equation. Both the generally covariant versions of the Klein-Kramers and the Smoluchowski equations will be studied and they should describe the statistical mechanics of a system with arbitrary coordinates. In other words, we will try to prove that the non-equilibrium statistical mechanics can be interpreted through a Brownian motion on a Riemannian manifold.
We remark that this work will be performed simply by starting with the classical equations of mechanics generalized with the Langevin thermal bath and all results will be potentially derived without further assumptions. In particular, for a system with N particles, following Langevin, we have to introduce 3N noise terms to describe the fluctuations. However, the constrained system is represented by n<3N degrees of freedom. One of the crucial point, useful to obtain the non-equilibrium equations living on a given differentiable manifold of dimension n, corresponds to the reduction of the noise terms from 3N to n. So doing, the final dynamics will be naturally described on the manifold (dimension n) without the necessity for an embedding in a larger space (dimension 3N). As a result, we will obtain the generally covariant description of the system. Interestingly enough, for the over-damped case (high friction limit) we will obtain a motion equation, which could be compared with the equation postulated within the mathematical community for the description of Brownian motion on a manifold.
We remark that the Langevin equations for a constrained system can be adopted to develop an *ad hoc* Langevin molecular dynamics able to analyse the time behavior of holonomic structures. This is an important topic in computational physics, as largely described in recent literature (G. Ciccotti, R. Kapral, and E. Vanden-Eijnden, ChemPhysChem 6, 1809, 2005, T. Lelièvre, M. Rousset, and G. Stolz, Mathematics of computation 81, 2071, 2012). The problem of the constraints, which is crucial for these numerical applications, is automatically solved and it does not require any other particular expedient. The convergence proper-

ties of finite difference schemes for Stratonovich and Ito stochastic differential equations are indeed largely studied in literature. These methodologies play a central role in studying the out of equilibrium response of constrained molecular structures such as chains with rigid bonds or polymers confined over arbitrary surfaces.

f) Nonlinear effective behavior of a dispersion of randomly oriented coated ellipsoids with arbitrary temporal dispersion

This work deals with the determination of the linear and nonlinear effective properties of an heterogeneous material composed of a dispersion of coated ellipsoidal particles (core-shell structure). The particles are considered randomly oriented and positioned within the matrix. Moreover, all constitutive equations (matrix, cores, shells) exhibit an hereditary behavior, leading to an arbitrary temporal dispersion. While matrix and shell are considered linear, the particles core shows an additional third-order nonlinearity. We develop an effective medium theory, which allows us to calculate the linear and nonlinear response in terms of the microstructure features. In particular, we can investigate the effects of the inter-phase on the overall behavior, in combination with the randomness of the orientations and with the linear and nonlinear hereditary phenomena. The results may find relevant applications in material science and, more specifically, in nonlinear optics, bulk plasmonics and metamaterials.

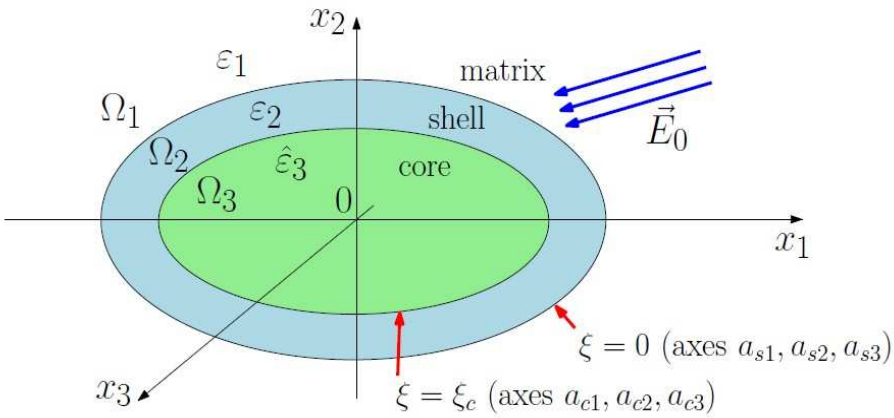

Figure 1. Confocal structure corresponding to the composite particle composed of a core and a shell embedded in an external matrix.

In this activity we develop an homogenization theory able to combine three specific aspects, separately considered in several investigations, namely: (i) the randomness of the orientations in a population of ellipsoidal particles embedded in a given matrix; (ii) the presence of a coating (or finite-thickness inter-phase or shell) between the core of each particle and the matrix (it can model all the intermediate cases between the low and the high conducting interface models); (iii) the specific constitutive equations of matrix, shells and cores, exhibiting an hereditary behavior leading to an arbitrary temporal dispersion; while matrix and shell are considered linear, the particles core shows an additional third-order nonlinearity.

The entire development will be performed for the dielectric behavior of the involved materials (described by their permittivities and nonlinear susceptibilities). However, it is well known that the solutions can be used to describe similar situations concerning the magnetic behavior of the composite material and the transport properties (diffusion, electric and thermal conduction), as well.
The first step of the proposed procedure deals with the determination of the electric field (or potential) in the coated ellipsoidal geometry, exposed to a uniform remotely applied field (see Fig. 1). To do this, to begin we suppose a linear behavior for the three phases (matrix, shells and cores). More specifically, we consider isotropic responses for matrix and shells, while the cores have to be considered anisotropic. We use these hypotheses since we prove that an isotropic nonlinear particle with temporal dispersion can be effectively represented by a frequency-dependent and field-dependent permittivity tensor, which is, in general, anisotropic. These properties of linear and nonlinear constitutive equations with temporal dispersion will be rigorously proved. We will also generalize previous results in order to contemplate the nonlinear cores. To

this aim we will use a general result, stating that the electric field inside an inclusion remains uniform even in the nonlinear case and it may be calculated by means of the same equations deduced for the linear case, which assume however an implicit form. Therefore, both the problems originated by the temporal dispersion and by the nonlinear behavior can be solved introducing the frequency and field dependent permittivity tensor describing the sinusoidal steady-state response of the nonlinear cores. The result is that we can finally obtain the internal electric field within the core and the average value of the electric field over the shell for the composite particle described by the properties summed up in the above point (iii). Since we have to analyse a population of random oriented particles, we average previous results over all the possible orientations of the particle itself. To do this, we use a rotational-averaging technique, largely used to calculate properties of a macroscopic bulk sample in terms of microscopic parameters. While this procedure is typically adopted to determine the statistical averages over the orientations of molecules in physical chemistry, here we use this approach at the scale of the dispersed particles (Andrews, S. S., 2004, Using rotational averaging to calculate the bulk response of isotropic and anisotropic samples from molecular parameters, Journal of Chemical Education, 81, 877-885).

Finally, we can elaborate the effective medium theory, which is based on the calculation of the average values of the electric field and electric induction over the whole structure (see Fig.2). Such an approach leads to the final expressions for the linear and nonlinear effective properties of the heterogeneous material. These results are correct for a low volume fraction of the particles in the matrix (dilute hypothesis). Conversely, the volume fraction of the core within each particle is completely arbitrary, and it can be modulated to fix the shell thickness. An additional hypothesis concerns the wavelength of the propagating fields, which must be much larger than the particles size.

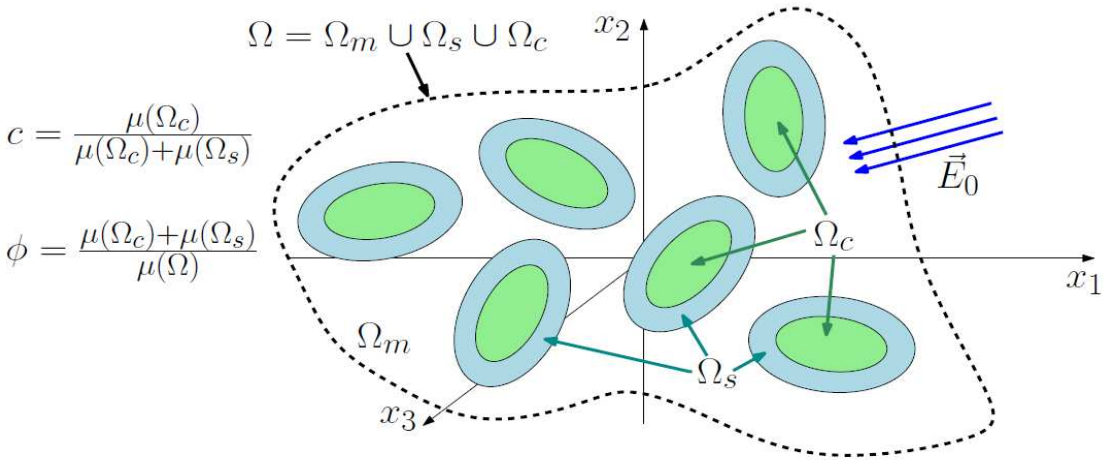

Figure 2. Composite structure formed by randomly oriented coated particles.